Design of High-Speed Railway Turnouts

Design of High-Speed Railway Turnouts

Theory and Applications

Ping Wang

Professor of Civil Engineering,
Southwest Jiaotong University, China

and

Director of the MOE,
Key Laboratory of High-Speed Railway
Engineering at the University

SWJTUP 西南交通大學出版社

ELSEVIER

AMSTERDAM • BOSTON • HEIDELBERG • LONDON
NEW YORK • OXFORD • PARIS • SAN DIEGO
SAN FRANCISCO • SINGAPORE • SYDNEY • TOKYO
Academic Press is an imprint of Elsevier

AP

Academic Press is an imprint of Elsevier
125 London Wall, London EC2Y 5AS
525 B Street, Suite 1800, San Diego, CA 92101-4495, USA
225 Wyman Street, Waltham, MA 02451, USA
The Boulevard, Langford Lane, Kidlington, Oxford OX5 1GB, UK

Notices
Knowledge and best practice in this field are constantly changing. As new research and experience broaden our understanding, changes in research methods, professional practices, or medical treatment may become necessary.

Practitioners and researchers must always rely on their own experience and knowledge in evaluating and using any information, methods, compounds, or experiments described herein. In using such information or methods they should be mindful of their own safety and the safety of others, including parties for whom they have a professional responsibility.

To the fullest extent of the law, neither the Publisher nor the authors, contributors, or editors, assume any liability for any injury and/or damage to persons or property as a matter of products liability, negligence or otherwise, or from any use or operation of any methods, products, instructions, or ideas contained in the material herein.

ISBN: 978-0-323-39617-2

British Library Cataloguing-in-Publication Data
A catalogue record for this book is available from the British Library.

Library of Congress Cataloging-in-Publication Data
A catalog record for this book is available from the Library of Congress.

Typeset by MPS Limited, Chennai, India
www.adi-mps.com

Printed and bound in the United States

Publisher: Joe Hayton
Acquisition Editor: Simon Tian
Editorial Project Manager: Naomi Robertson
Production Project Manager: Lisa Jones
Designer: Maria Ines Cruz

Preface

Since the publication of the first edition of *High-Speed Railway Turnouts: Design Theories and Application* in 2011, the book has been highly received by engineers in turnout design, manufacturing, and maintenance fields. The first edition was selected into "Three Hundred" Project of Originality Book Publication (held biennially, in which 100 outstanding books of originality will be selected respectively for the categories of humanities and social sciences, science and technology and literature, and children's books) by SAPPRFT of the P.R.C. in 2013. The first edition summarized the design theories for high-speed turnouts developed by China.

By the end of 2014, Chinese high-speed railways have covered an operating kilometrage of up to 16,000 km, with more than 5000 sets of high-speed turnouts for 250 km/h and above and the longest service time of 6 years. Chinese high-speed railway turnouts have suffered many difficulties in the past. Specifically, the turnouts were exposed to degraded manufacturing and laying quality due to short construction period. In face of this problem, relevant administration had taken corresponding measures to assure the quality, such as resident supervision system, field laying, and acceptance and accurate adjustment based on CPIII. Previously, degraded riding quality and safety also occurred when high-speed train traveled in certain turnout, so this problem had been temporarily controlled by speed restriction for a period as the maintainers failed to find out the causes in due time. The problem was finally settled through the demonstration and analysis of relevant experts. Rail cracks had been a concern in certain turnouts, which had been settled by improving the reliability and safety of the turnouts by enhancing rail detection, developing turnout monitoring system and introducing RAMS management. This new edition is produced based on above practices, so as to supplement the theories and technologies in the field of manufacturing, laying, maintenance, and management of high-speed turnouts, and elaborate the measures for maintaining high smoothness in the life cycle of high-speed turnouts. This edition aims at introducing the technical performance of high-speed turnouts in depth, analyzing relevant causes of defects and damages accurately, providing reasonable solutions to any technical problems, and contributing to the scientific management of high-speed turnouts. In addition, it hopes to provide theoretical and technical support for the safe operation of Chinese high-speed railways, and benefit the rest of the world anyhow.

High smoothness is the key and core technology to ensure the riding safety, quality, and comfort of high-speed train in high-speed turnouts. This feature shall be controlled in all sectors from design to manufacturing, laying, and maintenance. The smoothness of a turnout is mainly reflected by the low dynamic force, strong constraint, and high reliability while withstanding train load, transmitting temperature load, and during the conversion in the main/diverging line. There are mainly four types of irregularity: structural irregularity induced by complicated wheel−rail relation, geometry irregularity caused by poor status of rail, fastening, and bed, status irregularity caused by manufacturing and assembly error of parts and conversion failure, and dynamic irregularity caused by uneven track bearing stiffness. These irregularities will cooperate with train systems and impact the dynamic response and dynamic characteristics of turnout structure during the passage of trains in the turnout, thus affecting the riding safety, quality and comfort in the turnout, as well as influencing the stability, durability, and service life of the turnout. This book will introduce the theories, structural design, manufacturing and laying technologies, and maintenance policies centering around high

smoothness of the turnout. In addition to the contents in the first edition, the design theories of CWR turnouts, design methods for CWR turnouts on bridge, manufacturing and laying technologies for high-speed turnouts, typical cases of irregularity control for high-speed turnout in use, and the maintenance and management technologies for high-speed turnouts will be elaborated in this edition.

The book includes 14 chapters:

Chapter 1 introduces the structural type, main technological requirements, and structural characteristics of high-speed turnouts, and compares the technical characteristics of high-speed turnouts in China, Germany, French, etc.

Chapter 2 mainly describes the design and application conditions, plane line types, traditional fundamental parameter method for plane line type design and that based on particle motion, and introduces the turnout plane line type design methods and design software developed based on rigid body motion and wheel−rail vibration during the development process of Chinese high-speed turnouts.

Chapter 3 presents the structural type, principle and method for selection, and structural design and stress analysis of special rails in the turnout, and briefs the technical requirements and manufacturing process of the rails for Chinese high-speed railways.

Chapter 4 discusses the design theories and methods of turnout wheel−rail relation, which is a key and core point of the book. Vehicle-turnout system dynamics is a main tool for assessing the impacts of irregularities and the theoretical basis for the low dynamic force design of turnout structure, analysis of the cause of inordinate dynamic indicators during the passage of train in the turnout, and formulation of technical indicators related to turnout manufacturing, assembly, laying, and maintenance. This chapter also introduces the change rule of wheel−rail contact relation with train motion in the turnout area, 3D elastic body multi-point rolling contact analytical theory in the turnout, vehicle-turnout dynamics, and its application in assessment. Besides, the design methods for dynamic parameters based on single DOF wheelset is introduced in this chapter to help the designers to understand the impact rule of wheel−rail relation design on riding quality.

Chapter 5 tells about the track composition in the turnout area and its rule of longitudinal distribution, rational arrangement of track stiffness of the fastenings, and the methods and engineering methods for homogenous stiffness design along the track.

Chapters 6 and 7 are dealing with the calculation theories and design methods of high-speed turnouts in trans-sectional CWR line under the action of longitudinal temperature force. Specifically, Chapter 6 tells about the structural characteristics, analytical theories and methods and stress deformation rule of CWR turnouts, and the design verification method and layout principle for CWR turnouts in the design of trans-section CWR lines.

Chapter 7 introduces the rules of longitudinal interaction between CWR turnouts and bridges, and the rules of dynamic interactions of train-turnout-bridge system, and proposed recommended design requirements on relative position of the sleeper and bridge beam structure when laying a CWR turnout on bridge.

Chapter 8 introduces the traction and conversion devices and conversion principle for the conversion in the main/diverging line of the turnout, design methods for switching force and throws, as well as applicable engineering measures for reducing the switching force and easing scant displacement in Chinese high-speed railways.

Chapter 9 introduces the design methods for baseplates, fastenings, turnout sleepers, and other sub-rail components for turnouts.
Chapter 10 describes indoor and outdoor test technologies for justifying the above theories and methods.
Chapter 11 discusses the manufacturing equipment and process of high-speed turnouts, key production process for rails and baseplates, and assembly and acceptance technologies for high-speed turnouts.
Chapter 12 introduces the technologies for transportation, laying, inspection, and acceptance of high-speed turnouts.
Chapter 13 analyzes the impacts of poor wheel−rail relation, geometry and defective parts on the riding safety, and quality of high-speed turnout in the turnout with the example of several typical turnout defects occurred in the operation of Chinese high-speed railway, and provides with related improvement measures which may provide reference for maintaining personnel in analyzing the cause and formulating countermeasures in the future.
Chapter 14 introduces the management systems and maintenance standards of Chinese high-speed railways and turnouts, inspection and monitoring technology, and machines and methods for maintenance and repair. At last, the application and future prospect of certain leading technologies, such as RMAS, LCC, and informatization technology, in the management of Chinese high-speed turnouts are introduced.

This book is co-sponsored by “Critical theory and methods for the inspection of high-speed railway track structures” (U1234201), a key project supported by the joint fund for the fundamental research of high-speed railways of National Natural Science Foundation of China, and “Research on key scientific problems on operational safety of high-speed railway track structures” (51425804), a product supported by National Natural Science Funds for Distinguished Young Scholar.

My thanks go to Mr. Li Zhenting of Shanghai Railway Bureau, Mr. Wu Xishui and Mr. Liu Bingqiang of High-speed Railway Department, Infrastructure Division, Transportation Bureau of China Railway Cooperation, Mr. Wang Shuguo, assistant researcher of CARS for their contribution of a great number of references, field cases, and relevant data.

The compilation of the book is supported by my staff of railway engineering group of Southwest Jiaotong University. I am almost indebted to my PhD/graduate students: Dr. Xu Jingmang for his study on 3D elastic body multi-point rolling contact theory in the turnout zone, Dr. Chen Xiaoping for his research on homogenization of turnout stiffness, Dr. Chen Rong for his efforts on dynamics of train-turnout-bridge system, Dr. Yang Rongshan for the study on turnout-bridge longitudinal interactions, Dr. Ren Juanjuan for the study on turnout-bridge longitudinal interaction on tracks with longitudinally coupled base slabs, Dr. Cai Xiaopei for the analysis on turnout conversion, Mr. Zhou Wen for the analysis on turnout plane line type, Dr. Quan Shunxi for the dynamic analysis on track geometry irregularity in turnout zone, Dr. Cao Yang for the analysis on turnout plane line type, Dr. Zhao Weihua for the analysis on wheel−rail relation at the crossing, and Dr. Ma Xiaochuan for his analysis on turnout dynamic simulation. In addition, my postgraduate students, Zhang Mengnan, Sun Hongyou, etc. have made a great deal of effort in reviewing the text, drawing, tabulating, equation editing and translating, and proofreading.

This book will be published both in English and Chinese at the same time. I would like to express my gratitude to Southwest Jiaotong University Press and Elsevier B.V. of the Netherlands

for their help in the publishing work. My gratitude will also be given to my peers in railway engineering and relevant publishers who have helped and concerned about this book.

I would like to mention in particular Doctor Chen Rong, Doctor Zhao Caiyou and Doctor Xu Jingmang who helped a lot in proofreading the English draft.

The independent development of high-speed turnouts is relatively new in China. Therefore, relevant design theories and maintenance technologies need to be improved gradually in practice. Certain researches are still on the way. The book, which will be upgraded in the future, may not be satisfactory to every reader. Limited by time and knowledge of the author, the text, particularly some of the English expressions, might be inaccurate, or may not be rendered in-depth or in detail. For any inaccuracy, please oblige me with your valuable comments and active discussions.

Wang Ping
Southwest Jiaotong University,
Chengdu, China
2015

CHAPTER

TYPES AND STRUCTURE

1

A turnout is a trackside installation enabling railway vehicles to change tracks or crossover another track. It is an essential part of a railway track system. In fact, a turnout is an integrated system. It is difficult to maintain and critical to riding speed and safety. In addition, it is regarded as the weak point of a line and a main concern in high-speed railway (HSR) construction [1,2].

1.1 MAIN TYPES [3]

High-speed turnouts refer to the turnouts for 250 km/h and above in the main line. Among these turnouts, those for 160 km/h and above in the diverging line are known as high-speed turnouts in the diverging line, which have greater numbers and longer lengths than other turnouts.

1.1.1 COMPOSITION

A high-speed turnout is composed of rails, sub-rail foundations (e.g., fastenings, ties, and ballast or ballastless bed), conversion equipment, monitoring system, turnout heaters, and track stiffness transitions at two ends [4].

It is generally designed as a simple type crossing owing to the structural complexity, that is, consisting of a set of switches, crossing, and transition lead curve.

1.1.2 CLASSIFICATION

Main types:

1. Turnouts for 250 km/h and 350 km/h in the main line.
2. Turnouts for 80 km/h, 120 km/h, 160 km/h, and 220 km/h in the diverging line.
3. Turnouts in the main line, the crossover, and the connecting line (by function). The turnout in the main line lies at the throat of a station, enabling trains to access the receiving-departure track through the main line. The turnout in the crossover, as shown in Figure 1.1, lies away from the station throat and enables a train to switch routes between the up line and the down line. The turnout in the connecting line also lies outside the station throat and enables a train to change tracks between two HSR lines. The three types of turnouts are for 80 km/h, 80−160 km/h, and 120−220 km/h in the diverging line, respectively.

Design of High-Speed Railway Turnouts.

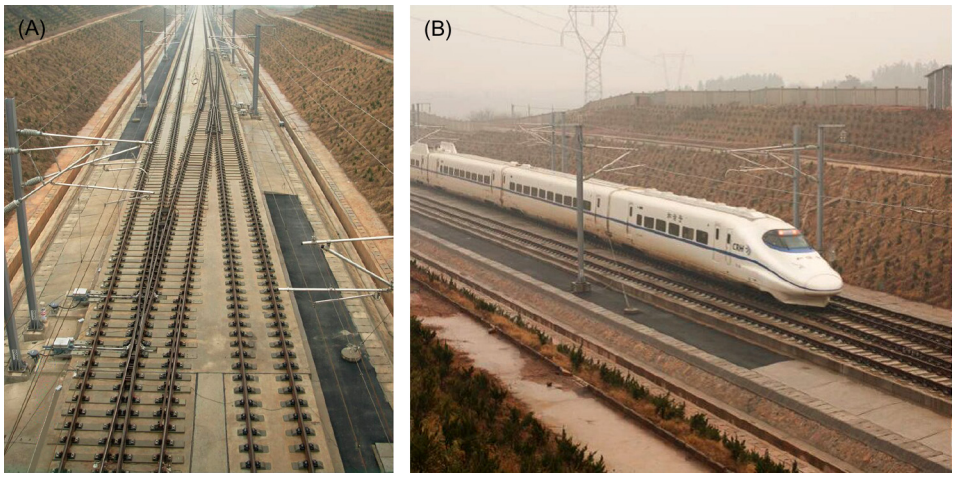

FIGURE 1.1

(A) Layout of crossover turnouts. (B) An EMU train changing tracks between the up line and the down line.

4. Ballasted turnouts and ballastless turnouts (by subfoundations). Ballasted turnout uses prestressed concrete ties; ballastless one may use embedded concrete ties or slabs. The two turnouts use the same rails.
5. No. 18, No. 30, No. 42, and No. 62 turnouts, etc. (by turnout number). In France and Germany, a high-speed turnout in the diverging line may have a nonintegral number (e.g., No. 39.113) when being laid in a line with varied track distances.
6. Turnouts with swing nose crossings or fixed crossings (by crossing type). All high-speed turnouts in China are provided with swing nose crossings, whereas in other countries, fixed crossings may be used in some turnouts for 250 km/h.
7. Turnouts with a rail cant of 1:40 or 1:20 (by rail cant). The rail cant of high-speed turnouts is 1:40 in both China and Germany, and 1:20 in France.
8. In addition, 60 kg/m rails, standard gauge, and trans-sectional continuously welded rail (CWR) track are quite common in HSRs, so high-speed turnouts are not classified by rail type, gauge, or joint.

Normally, a high-speed turnout is named after the combination of the rail type, the permissible speed in the main line, the sub-rail foundation, and the turnout number, such as No. 18 ballastless simple turnout with 60 kg/m rails for 350 km/h.

1.2 TECHNICAL REQUIREMENTS

A high-speed turnout is an intricate system. It involves the technologies of track structures (rails, fasteners, ties, and ballasted and ballastless bed, etc.), interface technologies of CWR track on embankments and bridges, the wheel−rail relation, electrical conversion, and track circuit, as well as interdisciplinary technologies of precision machinery manufacturing, mechanized track laying and maintenance, control survey, and informatized management [5].

1.2.1 EXCELLENT TECHNICAL PERFORMANCE

A high-speed turnout shall meet the following technical requirements:

1. High speed

   It shall have the same speed in the main line of the turnout as in a common railway section, and have a relatively high speed in the diverging line without affecting normal traffic. For safety considerations, the design speeds in the main line and the diverging line shall have safety margins of 10% and 10 km/h, respectively.
2. High safety

   For a high-speed turnout, the following requirements shall be satisfied when an Electric Multiple Unit (EMU) train travels at the design speed in the main/diverging line:
   - **a.** Indicators such as load reduction rate and derailment coefficient are the same as in a section
   - **b.** The spreads of switch rails and swing nose rails are sufficient to avoid collision against wheels
   - **c.** The conversion equipment functions normally, so that no defective insulation area (where all traffic lights are red) or signal abnormalities occur
   - **d.** Moveable rails are locked securely, so that no derailment takes place in case any inclusion appears in the closed zones, or the switch rod is distorted by the inclusion
   - **e.** The monitoring systems are integrated to identify faults and hidden dangers degrading riding safety, such as abnormal conversion, inordinate closure, and rail fracture; and
   - **f.** Turnout heaters are provided in cold areas to prevent snow or ice accumulating at the switches and crossings in cold weather, so as to ensure normal operation.
3. High stability

   When an EMU train travels at a normal speed in the main/diverging line of turnouts, the train will not shake significantly, thus providing the same passenger comfort in turnouts as in sections. The lateral carbody acceleration shall not have first-order inordinateness (i.e., 0.6 m/s^2 as per the criteria of the planned preventive maintenance for Chinese HSR) during the passage of comprehensive inspection trains or track geometry cars in the turnout.
4. Excellent comfort

   The same passenger comfort can be offered vertically as in a section, and no "jerking" (which may occur at bridge ends) occurs when an EMU train travels at a normal speed in the main/diverging line, nor does any inordinate vertical vibration appear due to inhomogeneous track integral stiffness in the turnout area. The vertical carbody acceleration shall not have first-order inordinateness (i.e., 1.0 m/s^2 as per the criteria of the planned preventive maintenance for Chinese HSR) during the passage of comprehensive inspection trains or track geometry cars in the turnout.
5. High reliability

   HSRs are in closed operation in the daytime, and occupied for "skylight" maintenance at nighttime. Therefore, high-speed turnouts shall have high reliability, without conversion faults or invalid closure detections, etc.
6. High smoothness

   All HSR track structures, including high-speed turnouts, shall have high performance in smoothness. Geometric deviation (alignment, longitudinal level, etc.) and closure clearances of a turnout shall be acceptable. The scant switching displacement shall not affect the deviation of the gauge, and structural irregularities induced by wheel−rail relation shall not affect riding quality.

7. High accuracy

   A turnout is composed of thousands of components; each component may have certain manufacturing errors. For high smoothness in assembly geometry and closure, the manufacture, assembly, and laying must be highly accurate (optimally 0.2 mm as per the criteria for planned preventive maintenance for Chinese HSRs).
8. High stability and less maintenance

   A high margin of strength is required under the action of high-speed trains and temperature, etc., so that turnouts are less susceptible to large residual deformation, featuring higher structural stability and less maintenance.
9. Easy maintenance

   With the increase in operation time, gross carrying tonnage, and deterioration of turnouts, tracks with inordinate irregularities or seriously damaged components shall be repaired or replaced immediately during the "skylight" period to resume normal operation in the shortest possible time. The structural design of high-speed turnouts shall facilitate future maintenance from practical and technical considerations.

1.2.2 HIGH COST-EFFECTIVENESS

The rails (switch rail, point rail, etc.) of a turnout will bear great wheel−rail force when guiding the wheels during conversion operations. Therefore, they are subject to wear or damage due to thin cross sections, resulting in short service life and frequent replacement. High-speed turnouts are used extensively. Generally for HSRs, one station shall be set every 30 km, and each station shall have at least 4−8 sets of high-speed turnouts. Therefore, to cut down the maintenance cost, high-speed turnouts shall be highly cost-effective.

1.2.3 OUTSTANDING ADAPTABILITY

High-speed turnouts may be laid on ballasted tracks, ballastless tracks with different geological conditions, or in cold regions, so they shall preferably agree with the climate and environment. In China, HSRs are mainly built on bridges rather than embankments. As there are lots of bridges, elevated stations are necessary. So turnouts may be laid on bridges, and certain stations may also lie in tunnels. This calls for adaptability of turnouts to different foundations.

1.3 TECHNICAL FEATURES [6]

1.3.1 SYSTEM INTEGRATION

High-speed turnouts have two major parts: engineering facilities (rails, fastenings, turnout ties, and sub-rail foundation) and electrical facilities (e.g., conversion system, monitoring system, and turnout heaters). Both are essential for operation and high technical performances of the turnouts. They must be high-precision electromechanical devices rather than simple civil structures.

In addition, high-speed turnouts integrate the latest technologies in track structures (e.g., rails and fastenings, ballastless tracks, and CWRs), and combine recent research achievements in design,

manufacture, transport, laying, and maintenance. Therefore, they mark the state of the art of high-speed track structures of a country to some extent.

1.3.2 THEORETICAL BASIS AND PRACTICAL TESTS

As the key equipment in terms of riding safety and quality of high-speed trains, high-speed turnouts shall be designed in line with the theories of wheel−rail relations, track stiffness, CWR lines, etc. Turnouts can be accepted for production and application only upon passing the stepwise speed-up dynamic tests with real cars and long-term running tests.

1.3.3 STATE-OF-THE-ART MANUFACTURE AND LAYING PROCESSES

For high technical performance, high-speed turnouts shall be manufactured with modern equipment (e.g., long and large CNC planer-type milling machines, high-precision CNC saw drills, large-tonnage press, advanced rail welding machines, large-scale hoisting machines, and high-precision assembly platforms), technologies, and detection equipment. Additionally, the concept "detail is everything" shall be borne in mind, and a strict quality management system for raw materials, purchased components, and production processes shall be formulated, thus forming a factory-centered integrated supply and resident supervision system.

Laying is a key process for ensuring high technical performance. Successful laying means that the permissible speed can be reached immediately after the high-speed turnouts are put into use. So mechanical, standard construction processes and professional construction teams are required.

1.3.4 SCIENTIFIC MAINTENANCE AND MANAGEMENT

HSRs are in closed operation in the daytime, inspected and maintained only during the "skylight" period at nighttime. Therefore, for high technical performance, less maintenance, and orderly operation of turnouts, informatized and scientific maintenance methods are required, and reliability-oriented modern maintenance facilities shall be developed for high-speed turnouts.

1.4 GLOBAL OVERVIEW OF HIGH-SPEED TURNOUTS

1.4.1 FRANCE

Cogifer has become the most intimate partner of SNCF since 1975. In 1981, the first generation of high-speed turnouts with timber ties was designed and manufactured. Meanwhile, single cubic parabola curve type No. 46 and No. 65 high-speed turnouts in the diverging line for 270 km/h were also developed. The second generation changed the single parabola curve to a "circular + easement" curve and adopted concrete ties and ballasted beds, creating a world speed record of 501 km/h in the main line in 1990. At present, the third generation is widely used in railways from Paris to Marseilles for up to 300 km/h. The fourth generation adopts NiCr antifriction coatings and adjustable rollers based on the third generation, which will be used in new railways for more than 330 km/h (Figure 1.2). After numerous tests, the technology of French high-speed turnouts has been

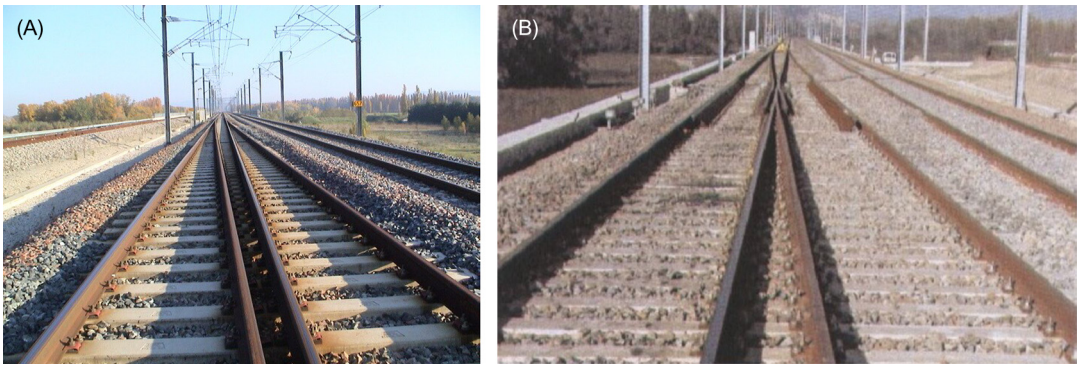

FIGURE 1.2

High-speed turnout in France: (A) Switch; (B) Crossing.

improved drastically. About 1200 sets of Cogifer high-speed turnouts have been used in railways around the world, of which more than 200 are used in Chinese railway lines (Zhengzhou−Xi'an, Hefei−Nanjing, and Hefei−Wuhan) [7,8].

1. Plane line type

   High-speed turnouts in France include No. 65, No. 46, No. 29, No. 26, No. 21, and No. 15.3 series, for 230 km/h, 170 km/h, 160 km/h, 130 km/h, 100 km/h, and 80 km/h in the diverging line, respectively. Normally, the "circular + easement" curve line type is adopted for high-speed turnouts in the diverging line, and circular curve for the rest.

   Design controlling indexes:

   If $V_{\text{diverging}} = 70-170$ km/h: the unbalanced centrifugal acceleration $\alpha \leq 0.65\ m/s^2$, the deficient superelevation ≤ 100 mm, and the variation rate of deficient superelevation ≤ 236 mm/s; or

   If $V_{\text{diverging}} = 170-230$ km/h: the unbalanced centrifugal acceleration $\alpha \leq 0.56\ m/s^2$, the maximum deficient superelevation ≤ 85 mm, and the variation rate of deficient superelevation ≤ 260 mm/s.

2. Switch

   In France, switch rails are made of monoblock flat-web-special section rails (AT rails in China), and mainly are untempered UIC60D rails (strength: 900 A). To reduce the expansion displacement of the switch rails of CWR turnouts, the following considerations shall apply: (a) the longitudinal resistance of turnout fasteners shall not be below track resistance; (b) the fastening force of a set of fasteners shall be greater than 12 kN; (c) the switch rail shall have the smallest movable length; and (d) modified Nabla fasteners (Figure 1.3A) or USK2/SKL24 clips of Vossloh (Figure 1.3B) shall be used at the narrow heel end of the switch rail.

   In France, the conversion of switch rails relies on the rolling friction, rather than sliding friction, with the provision of lubrication-free or rollered slide plates (Figure 1.4). Thus, it reduces switching resistance, scant displacement, and switching force; increases traction points; shortens the distance between the last traction point and the heel of the switch rail; and maintains the line type of switch rails by the connecting rods in between.

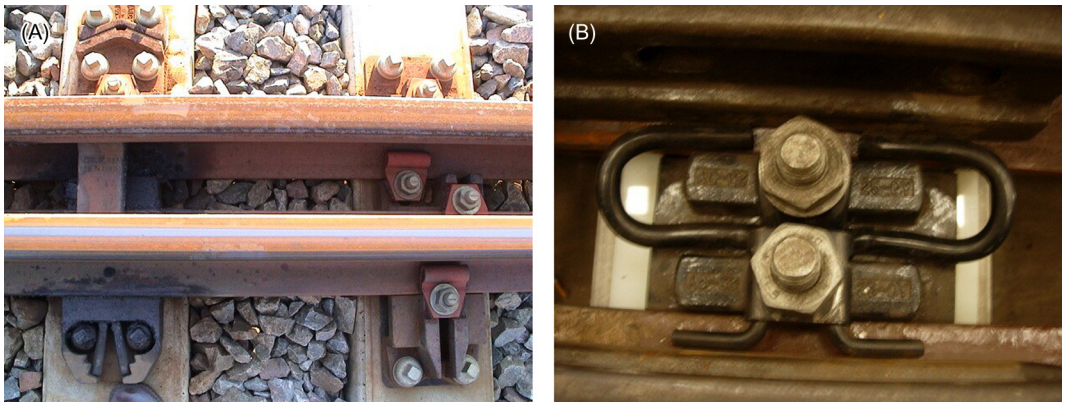

FIGURE 1.3

Compromise fasteners at the heel of the switch rail: (A) Nabla compromise fasteners; (B) Vossloh compromise fasteners.

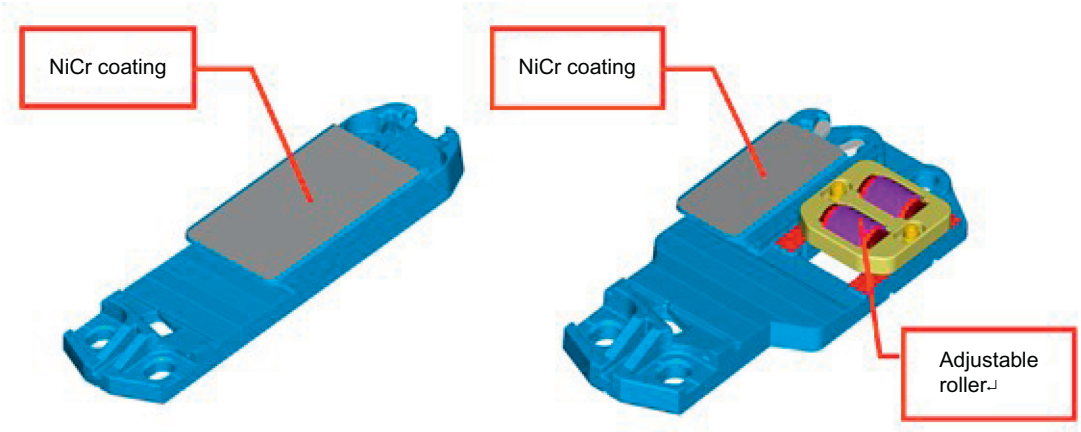

FIGURE 1.4

Antifriction slide plate.

French high-speed turnouts are fixed by approximately n-shaped elastic clips (Figure 1.5), whose fastening force is equivalent to that of ordinary fasteners. These clips can fix the inner side of stock rails reliably to prevent rail tilting. They are easy to handle with special tools.

In France, based on the relationship among the degree of hunting movement of trains, the cant at rail base and the critical speed, it is proposed according to wheelset dynamics that the rail cant of 1:20 is preferable for high-speed turnouts for more than 250 km/h. In this way, the design equivalent conicity of treads and the maximum equivalent conicity of the worn profile can be controlled within 0.1 and 0.15, respectively.

FIGURE 1.5

Elastic clips for French turnouts.

FIGURE 1.6

Horizontal hidden tip point structure of the point rail.

3. Crossing

In France, point rails and switch rails are made of the same materials. The point rails are constructed by embedding and assembling the long and short point rails with Huck bolts (in factory) or high-strength bolts (on site). To reduce lateral irregularity during passage at the crossing, a horizontal hidden tip point structure is adopted for the point rail, as shown in Figure 1.6.

Long fillers are set at the crossing heel. Specifically, three fillers are arranged on each side of the point rails and the wing rails and coupled with elastic sleeve-type locking bolts (Figure 1.7). The longitudinal forces distributed on the bolts of long rails in turnout rear are approximately the same, and can be transmitted to the rails in the transition lead curve through long wing rails.

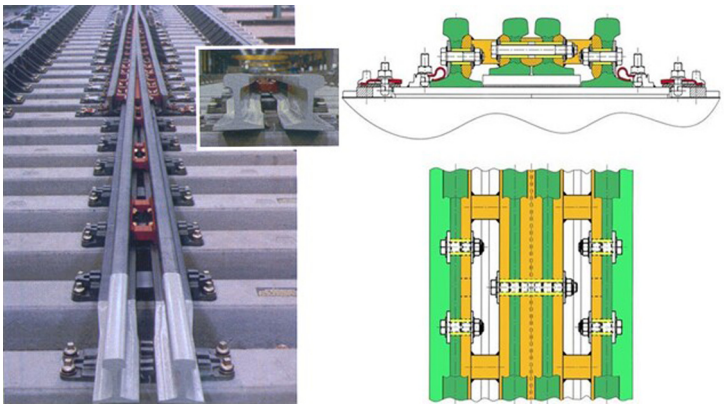

FIGURE 1.7

Crossing heel structure.

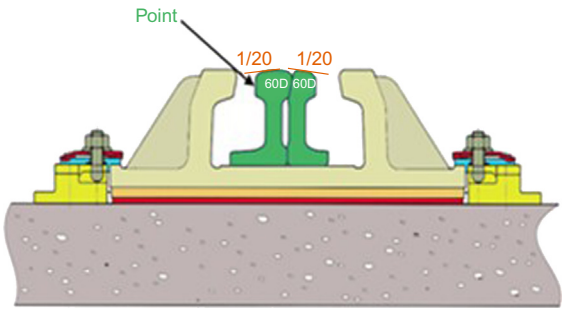

FIGURE 1.8

Solid "cradle-type" crossing.

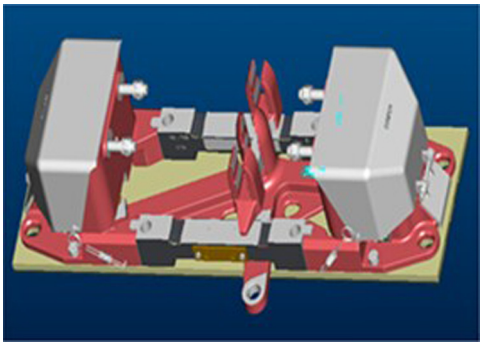

FIGURE 1.9

Bracket of the point rail.

The wing rails of French high-speed turnouts are of a "cradle" structure (monoblock wing rails, with point rail laid in between), made of solid high manganese steel, as shown in Figure 1.8. The front end is welded with common rails in the factory by flash welding, and the rear end is welded with A74 rails. This structure is stable, and the point rails and wing rails will not tilt. The electrical device at the first traction point on the point rail pokes out from the bottom to pull the point rail. Three U-shaped brackets for receiving the point rails are provided, which can slide on the slide bed (Figure 1.9), allowing greater expansion displacement of the point rails. The traction point on the point rail is relatively high, so the rail is unlikely to tilt.

4. Fastenings

French high-speed turnouts are mainly fastened with Nabla clips, the same as in sections. The gauge of a turnout may vary slightly owing to slight abrasion of rails in use, so it is nonadjustable.

FIGURE 1.10

Fastenings of ballasted turnout.

The ballasted turnouts in China designed by Cogifer adopt SKl-12 narrow clips of Vossloh, provided with a 9 mm rubber pad under the rail and a 4 mm rubber pad under the tie plate. At the slide bed, only a 9 mm rubber pad is provided beneath the plate (no rail pad). In the non-breathing length of the heel, both the rail and the plate are provided with a 4.5 mm rubber pad underneath. The tie plate is connected to the tie by double-row Φ24 high-strength bolts. A riser block may be arranged under the plate, with vertical adjustment capacity of 0−10 mm. A gauge block is not arranged. The track gauge is regulated by a quadrant block at the end of the tie plate with an adjustment range of −4 to +2 mm, as shown in Figure 1.10.

The ballastless turnouts in China designed by Cogifer adopt W300 fastenings and SKl-15 clips of Vossloh, provided with a 6 mm rubber pad under the rail and a 12 mm elastic pad under the plate. The cast iron shoulder cooperates with the V-shaped groove on the tie, and the stress point of the anchor bolts is relatively low. The riser block, with a vertical adjustment range of −4 to +26 mm, is installed under the plate. The insulated gauge block can adjust the gauge in collaboration with the spacer, with an adjustment range of −4 to +8 mm, as shown in Figure 1.11.

Unlike other countries, the ballasted turnouts in France are characterized by high stiffness of fastening and low stiffness in the bed. The pad stiffness of a turnout is determined as per the principle that the vertical displacement of the tie and the rail can be controlled within 0.5−0.7 mm and 1 mm, respectively. The turnout bed is made of uniformly graded premium granite ballasts (Figure 1.12), whose elasticity equals the tie support stiffness of 40−60 kN/mm. The static pad stiffness at the switch and the crossing is 200−250 kN/mm. The transition of track stiffness between a turnout and a section is about 5 m long, so the vertical displacement of the rail under static wheel load is 0.9 mm (Figure 1.13).

The stiffness setting of turnout fastenings in France has many advantages. It can control the displacement of switch rails and swing nose rails with respect to stock rails and wing rails, reduce rail stress, control the dynamic gauge widening in a turnout, and decrease the loss of fastening force of the fasteners. However, it is disadvantageous in the overlarge stiffness of the

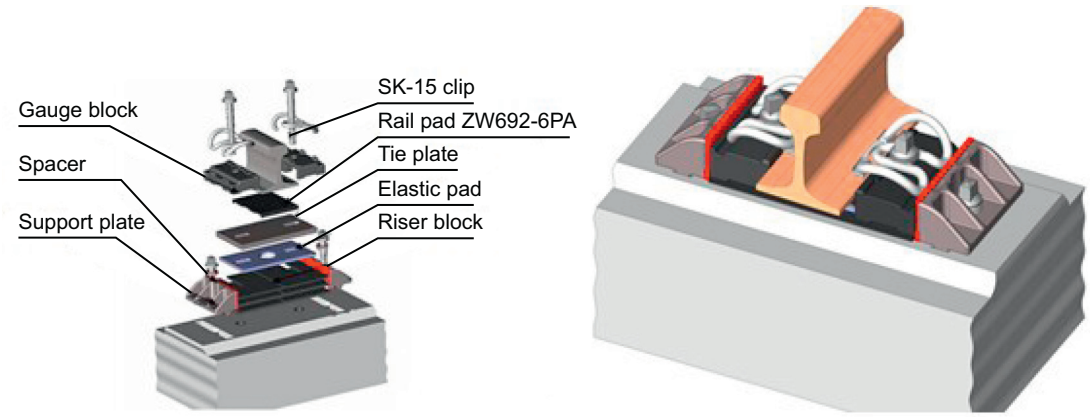

FIGURE 1.11

Fastening of ballastless turnout.

FIGURE 1.12

Uniformly graded ballasts in France.

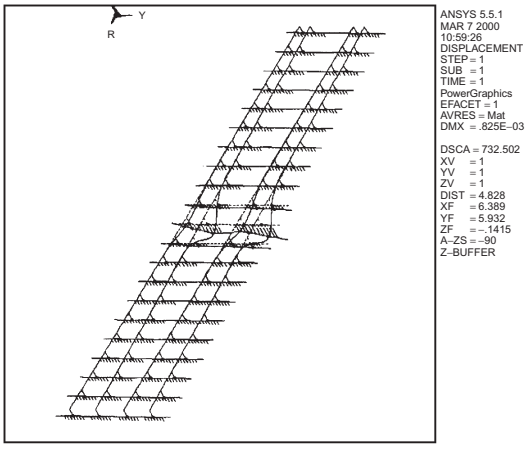

FIGURE 1.13

Track displacement.

rail pad. In view of dynamics, the track integral stiffness is directly proportional to the additional dynamic wheel load, contact fatigue damage to the rail, stress and displacement of the tie and the bed, train stress, and vibration acceleration. Overly large stiffness may jeopardize the maintenance of turnout rails.

5. Sub-rail foundation

Ballasted bed with monoblock prestressed concrete ties (Figure 1.14) is used with an allowable carrying capacity of ± 25 kN.m, and provided with unthreaded round rebars (ends

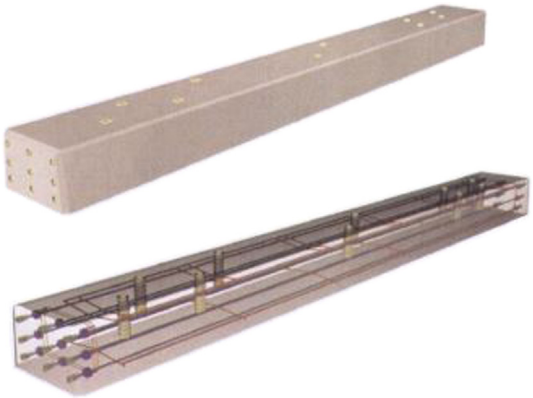

FIGURE 1.14

Solid tie.

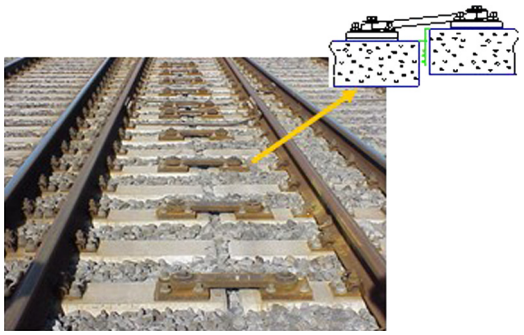

FIGURE 1.15

Hinged tie.

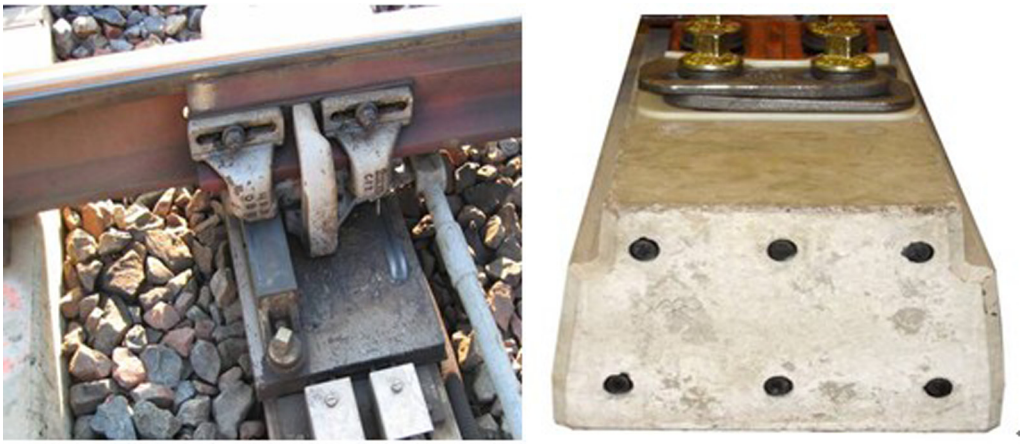

FIGURE 1.16

Compromise tie for installing electrical equipment.

anchored) and plastic sleeves embedded in the ties. To prevent the end of a long turnout tie on untraveled track tilting and beating the bed, a hinged tie (Figure 1.15) has been developed, but is seldom used; the problem is mainly solved by ballast tamping.

The rods and locking facilities of the conversion system are all installed on turnout ties to facilitate the operation of large maintenance machinery on ballasted tracks. Therefore, the ties accommodating electrical devices shall be in a special section or below the top of other ties, as shown in Figure 1.16. Ballastless turnouts in France adopt overshoe-type embedded long ties, having the same fastenings as ballasted turnouts, with the elasticity principally provided by

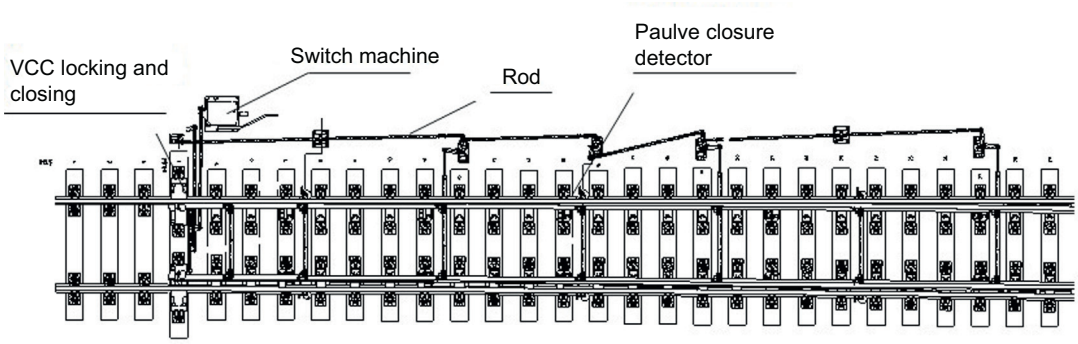

FIGURE 1.17

"One-machine multi-point" traction mode for French turnouts.

FIGURE 1.18

Closure detector.

elastic ties. The Zhengzhou−Xi'an railway in China uses embedded long concrete ties with steel trusses, with the elasticity provided mainly by the fastenings.

6. Conversion equipment

For French high-speed turnouts, "one-machine multi-point" traction mode (Figure 1.17) is adopted, wherein the two switch rails act simultaneously. Only the first traction point is provided with an external locking device; other traction points are indirectly locked by the switch machines via right-angle cranks and conduits. The switch machine has no indication rod, but an operating rod for conversion and locking. A built-in switch rail positioning and locking detector is used to detect closure between the actual points of the switch rail and the point rail. Closure between the switch rail and the point rail is detected by a closure detector arranged between two traction points, as shown in Figure 1.18.

The one-machine multi-point mechanical conduit mode is featured with good synchronization performance and small equipment investment. At the switch, the external locking device is connected with the belleville spring between the connecting irons of the switch rail as per the fixing moment by means of external locking. The device is highly adaptable to switch rail expansion (up to $\pm 30-40$ mm), which can secure the locking of the switch rail and allow its possible expansion, as shown in Figure 1.19. At the crossing, the point rail can move freely

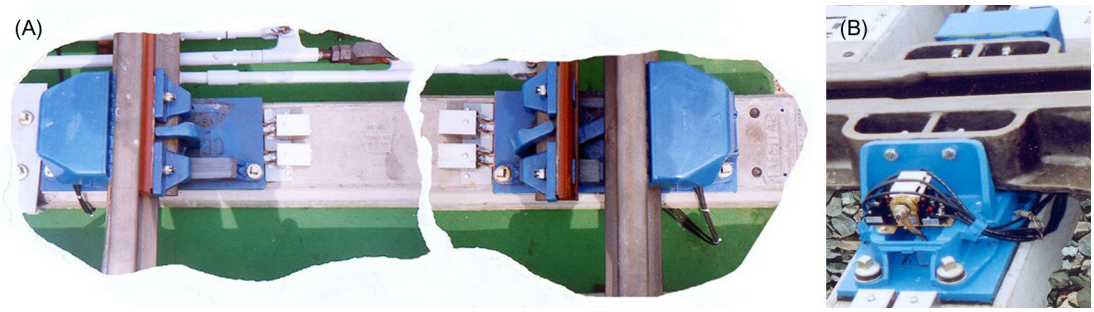

FIGURE 1.19

External locking device: (A) Switch; (B) Crossing.

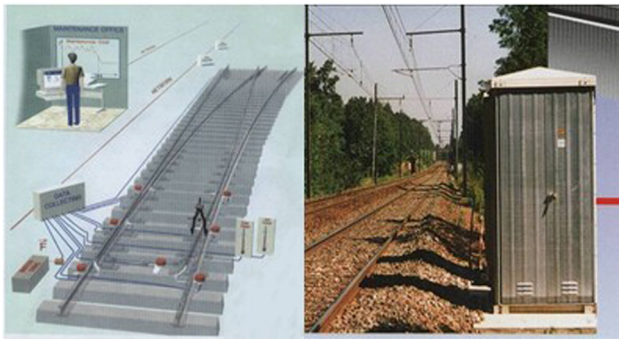

FIGURE 1.20

Monitoring system.

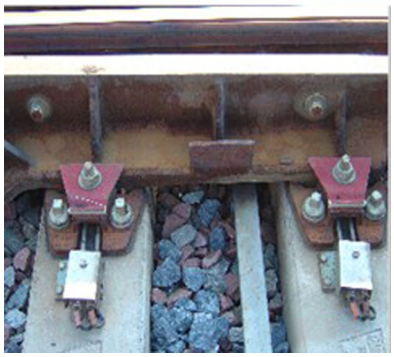

FIGURE 1.21

Heating components.

(range: $\pm 10-20$ mm) in the external locking device owing to the flexible connection between the two.

7. Other components

The monitoring systems for French turnouts are remote type. The system has a warning function and is used mainly for maintenance. The system monitors various turnout data and ambient data, such as electric signals (e.g., current, voltage, communication equipment, track circuit status, and switch machine). In support, special sensors are used to monitor wayside engineering equipment and key components. The system consists of a monitoring center, a server, and a field acquisition facility, as shown in Figure 1.20.

For safe and reliable operation, high-speed turnouts in France, regardless of numbers and ambient temperature, are provided with electrical heaters. The heaters can be manipulated by the control center or manually with wayside controllers, depending on the weather, temperature, and humidity. The heater is installed in two parts: a longitudinal part and a transverse part, as shown in Figure 1.21.

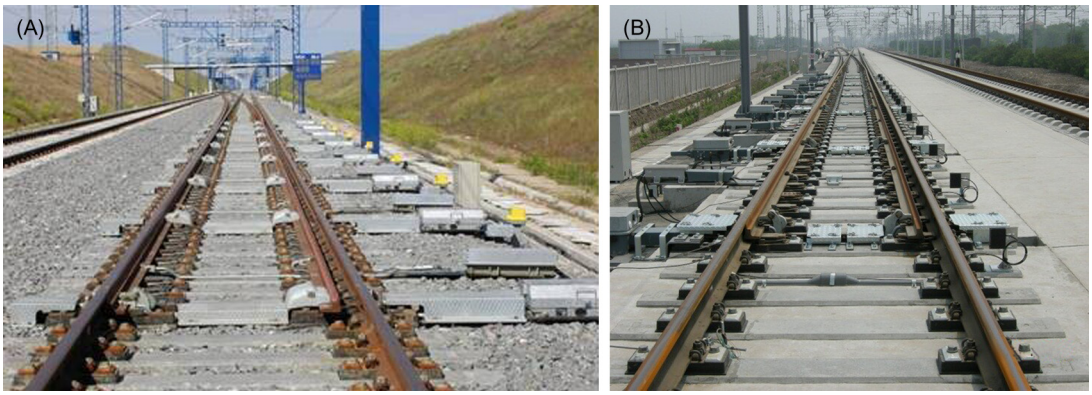

FIGURE 1.22

High-speed turnout in Germany: (A) Ballasted track; (B) Ballastless track.

The front halves of the switch rail and swing nose rail employ transverse heating, with the heating points arranged under the slide plates. The rear halves adopt longitudinal heating along the wing rail and the stock rail, with the heating point arranged at the web bottom on the inner side of the rails.

In France, the main and diverging lines of turnouts are provided with check rails. However, owing to large flangeway width, running trains will not come into contact with check rails, thus preventing derailment during railway maintenance and laying.

1.4.2 GERMANY

The BWG company is a specialized turnout manufacturer in Germany. Its first generation of high-speed turnouts was developed in the mid-1980s, employing a compound curve line and ballasted bed. With practices and further progress in R&D, tests, and dynamic simulation, the compound curve scheme of "small radius + large radius" was proven to cause serious abrasion to the switch rail. The second generation was eventually designed with an "easement + circular + easement" curve line and kinematic gauge optimization technology starting in 1996, and the highly elastic rubber pad system was developed, forming the complete technology of high-speed turnouts on ballastless track foundations and meeting the need for construction of 350 km/h HSRs in many countries (Spain, etc.). BWG has established a joint venture with China Railway Shanhaiguan Bridge Group Co., Ltd., which has produced thousands sets of high-speed turnouts for Chinese HSRs, as shown in Figure 1.22 [9].

1. Plane line type

   High-speed turnouts in Germany include No. 50, No. 42, No. 39.113, No. 23.7, No. 19.2, and No. 14 series, for 220 km/h, 160 km/h, 100 km/h, and 80 km/h in the diverging line, respectively. German high-speed turnouts have evolved from a compound curve line to the "easement + circular + easement" curve line used at present. The designed unbalanced centrifugal acceleration is not greater than 0.5 m/s^2, the design increment is less than 0.4 m/s^3, and that at the origin is less than 1.0 m/s^3. For this "three-curve" line type, the train shall run in each curve for 1 s at least to avoid superposition of vibration. The crossover turnout is designed with a

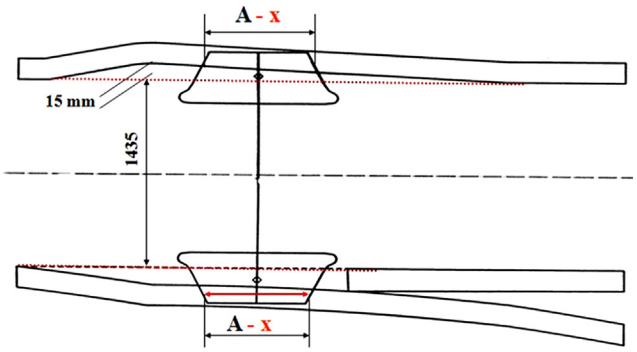

FIGURE 1.23

FAKOP technology for German turnouts.

FIGURE 1.24

Retainer at the heel of the switch rail.

track distance of 4 m, and may be provided with straight sections in areas with greater distance between two tracks. The length of the straight section equals 0.15 V for the turnout below 130 km/h and 0.4 V for turnouts above 130 km/h, thus providing enough regulation time for train suspension systems and guaranteeing passenger comfort.

2. Switch

Switch rails of German high-speed turnouts are made of monoblock 60E1A1 rails (R350HT head-hardened rails) with a tensile strength of 1175 MPa. The stock rail is provided with a 1:40 cant at the rail base; the switch rail is provided with a 1:40 cant at the rail top in the full length. The heel is not twisted, but welded flush with the working surface of the rail head in the transition lead curve.

German switches adopt the special kinematic gauge optimization (in German, *fahrkinematische Optimierung*, FAKOP for short) technology. The stock rail will bend 30 mm at the top width of the switch rail, thus widening the gauge by 15 mm, as shown in Figure 1.23. This design evens the lateral irregularity on the two rails of a track, effectively easing the hunting movement of trains traveling in the turnout and increasing the firmness and wear resistance of the switch rail.

To control the expansion displacement of the switch rail, German turnouts adopt Vossloh fasteners having a large fastening force and longitudinal resistance. The heel of the switch rail is fixed with narrow fasteners to shorten the movable length, and provided with one or more retainers to relieve expansion displacement, as shown in Figure 1.24.

Rollered antifriction slide plates (Figure 1.25) are used to reduce switching resistance, where clips are arranged on two sides of the slide plates to fasten the stock rail.

3. Crossing

For German point rails, the front part is an integrated structure machined with blooms (the same as for common rail), and the rear part is butt-welded with the two rails of crossing heel,

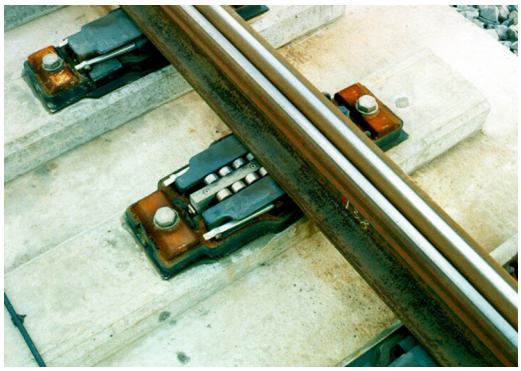

FIGURE 1.25

Rollered slide plate and elastic clips.

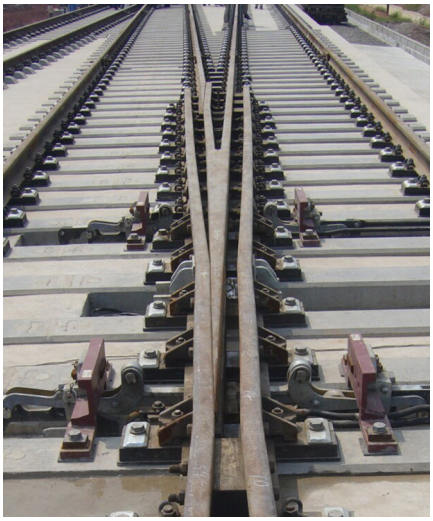

FIGURE 1.26

Point rail.

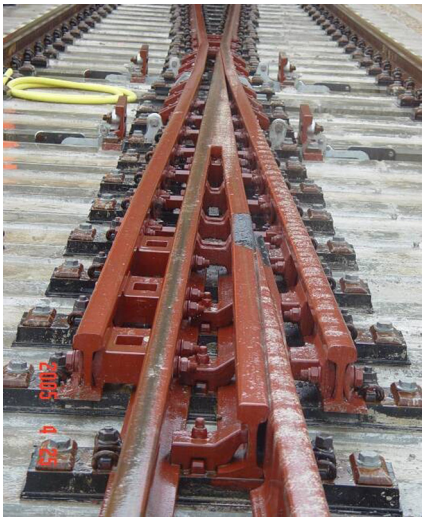

FIGURE 1.27

Crossing heel of No. 18 turnout.

as shown in Figure 1.26. For No. 18 turnouts, the fillers at the crossing heel are connected by high-strength bolts, as shown in Figure 1.27. For No. 42 turnouts, a full-length monoblock large plate is arranged beneath the crossing, bolted with the long and large fillers between point rails, as well as between the wing rail and the point rail. Additionally, transverse bolting is used to withstand the temperature force of CWR track in the section and preventing jamming between the switch rod and the hole on the wing rail web, as shown in Figure 1.28.

FIGURE 1.28

Crossing of No. 42 turnout.

FIGURE 1.29

Installation of traction rod for No. 18 turnout.

German wing rails are made of machined common rails, the outer side of which is fastened with clips. For No. 18 turnouts, the traction begins from the base of the wing rail, as shown in Figure 1.29. For No. 42 turnouts, the traction rod stretches out from the hole on the wing rail web (Figure 1.30); the wing rail will not be spliced at the base, and is simple in structure, and the traction point is located on the point rail web. This layout leads to desirable traction force on the point rail without risk of tilting. However, the oversized hole on the wing rail web reduces the rail's strength.

The swing nose crossing of German turnouts has a long moveable length. The point rails are provided with relevant devices (e.g., convex retaining block) to avoid jerking when the point rail and the wing rail come into contact. In addition, for antijerking purposes, the gap

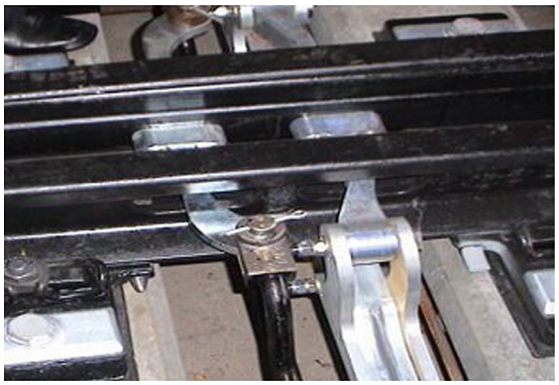

FIGURE 1.30

Installation of traction rod for No. 42 turnout.

FIGURE 1.31

Hydraulic antijerking device in the turnout.

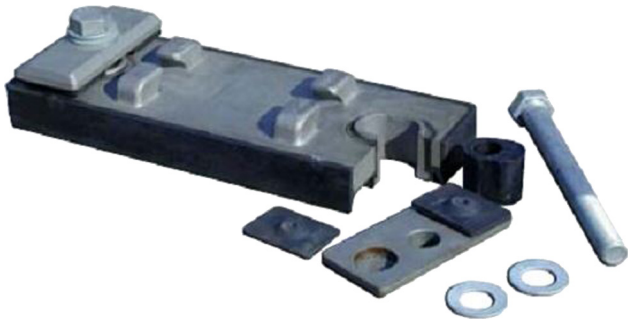

FIGURE 1.32

Fastening.

FIGURE 1.33

Elastic fastener.

between the fastening side of the jacking block and the upper slope of the point rail base is about 1 mm when the jacking block clings to the rail web. For ballastless turnouts, a hydraulic antijerking device, as shown in Figure 1.31, is also used, and has turned out to be effective. When the point rail is well converted, the device will cause the rod to pass through and fasten the point rail securely.

Swing nose turnouts have no check rails.

4. Fastening

The fastenings of German turnouts mainly use Vossloh clips (Figure 1.32). The gauge between the fastener and the rail is not adjustable. However, it can be regulated using an eccentric sleeve in the bolt hole of the tie plate (adjustment range: −12 to +12 mm). Two rubber springs (Figure 1.33) are used to securely fasten the bolts onto the highly elastic plate. The tie plate and the elastic pad are vulcanized into an integrated elastic substrate

FIGURE 1.34

Vulcanized elastic substrate.

structure. The pad under the plate is provided with a riser block capable of realizing a vertical adjustment of −4 to +26 mm on ballastless tracks.

For German turnouts, track stiffness is determined based on the principle that the maximum rail base stress is 75 MPa. The design vertical static stiffness of the fastening is 17.5 kN/mm. The vertical stiffness of a turnout is defined by the elastic substrate (vulcanized plate-pad structure). The substrate restricts the deformation of the rubber with a number of rigid bearing blocks of different shapes on the bottom of substrate, thereby homogenizing the track's integral stiffness and fastening support stiffness in a turnout (see Figure 1.34). The dynamic/static stiffness ratio of the elastic substrate is about 1.2−1.3. The elasticity of the plate remains stable at −15 to −20°C. In the case where the pad stiffness in a section is greater than that in a turnout, elastic transitions shall be provided in the front of the turnout and in the rear of the long turnout tie to mitigate the impact. The transitions may generally have an elasticity difference of 2−6 orders. The transition length equals the distance a train may travel in 0.5 s.

5. Sub-rail foundation

The foundation of ballasted turnouts in Germany mainly adopts hinged concrete ties. The tie longer than 3.2 m is flexibly hinged, as shown in Figure 1.35, thus solving the overload problem in delivering the whole set of a turnout, as well as the problem of ballast pulverization in case the untraveled side of the long tie tilts and beats the bed due to high-speed traffic. In China, as this tie may affect tamping performance, a long concrete tie is used instead.

Turnouts in Germany are also provided with steel ties to support the switch rod (Figure 1.36), so the electrical rod will not be removed during tamping. A stiff antislip rubber pad is attached to the tie bottom, which cooperates with the highly elastic fastening and stabilizes the tie. Thus the steel tie will produce no dynamic irregularity.

From the early track type (solid bed with embedded long ties at Rheda station in 1972) to Rheda2000 ballastless track at present, German tracks have developed substantially. Meanwhile, ties on concrete foundations have evolved from embedded type on subgrades to steel-trussed partially prestressed concrete type (Figure 1.37). The tie and the track bed slab constitute a stable foundation for a turnout. In China, a prefabricated slab-type ballastless track

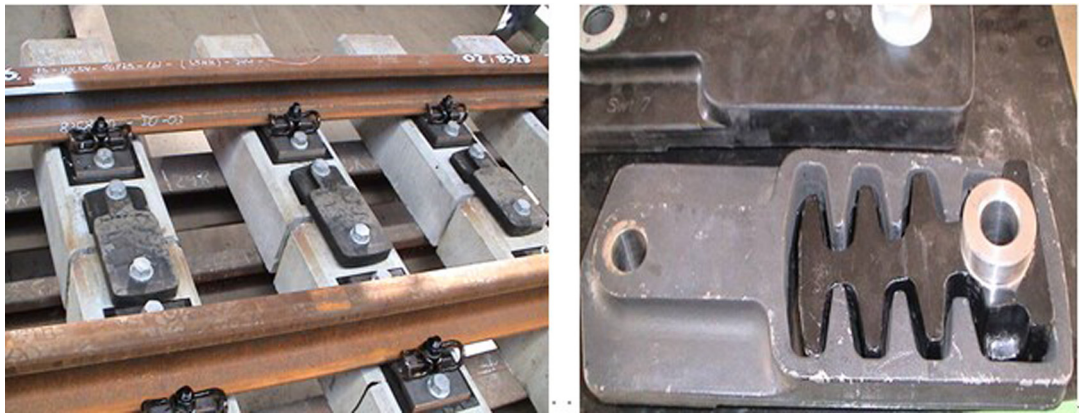

FIGURE 1.35

Hinged turnout tie.

FIGURE 1.36

Steel turnout tie.

FIGURE 1.37

Turnout with embedded long ties.

FIGURE 1.38

Slab turnout.

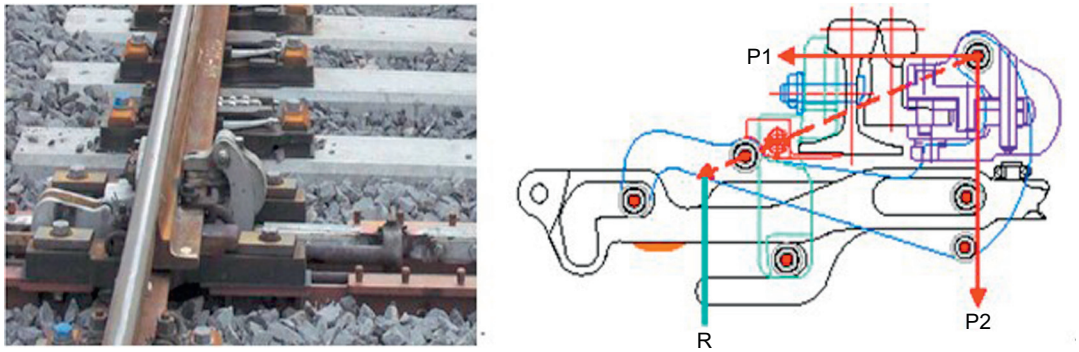

FIGURE 1.39

External locking device.

foundation has also been developed, where bolt holes are reserved for installing the fastening. This structure type is advantageous in a short construction period, but is quite demanding in terms of hole distance and bed slab smoothness, as shown in Figure 1.38.

6. Conversion equipment

High-speed turnouts in Germany adopt a "multi-point multi-switch" traction mode, with the external locking actuating separately. A Siemens S700K electric switch machine or L700H electro-hydraulic switch machine of Lorenz is used. A closure detector is arranged between each pair of traction points.

The external locking device transforms from the former swallow-tailed type into a rollered hook type, which can be adjusted automatically with the expansion of the switch rail, as shown in Figure 1.39. During locking, the resultant force of the locking hook will pass through the center of

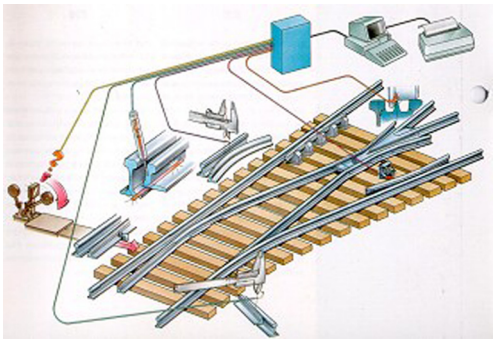

FIGURE 1.40

Turnout monitoring system.

FIGURE 1.41

Turnout heater.

the cross section of the switch rail; in this way, the switch rail and external locking hook are in a good stress state. Owing to rolling friction, switching resistance is reduced by using this device. For No. 18 turnouts, this device is applicable to expansion of ±30 mm in the switch rail.

For synchronous conversion at various traction points of a turnout, Germany takes many technical measures: Adopting switch machines of the same type in case the traction points on the front part of the switch rail have the same throw; setting the same action time for switch machines with different throws, and allowing the switch machines to be started up sequentially while circumventing the peak current within an extremely short time (ms) through the control circuit; and adjusting the throw of external locking depending on different switch machine throws and turnout spreads to guarantee synchronous unlocking and locking of switch rails and point rails.

7. Other components

In Germany, the Rodamaster2000 turnout monitoring system (Figure 1.40) is employed to monitor turnout data (location of the switch rail, current and voltage of the switch machine, switching force and conversion time at each traction point, minimum flangeway, longitudinal force of the rail, rail temperature, and heaters), the signal system, and the track circuit system. The system is not mechanically connected with the turnout, so it does not affect normal operation of the turnout. In addition, it can transmit the monitored turnout data to the maintenance center.

All German high-speed turnouts have electric heaters (Figure 1.41). For both the switch rail and the point rail, metallic heating bars are installed on the inner side of the stock rail with the aid of the clamping plate hooped at the rail base, and the terminal of the heating point is clamped on the base of the rail between two ties. Leads may be removed for mechanized maintenance of ballasted lines [10].

1.4.3 CHINA

According to the *Medium- and Long-term Railway Network Plan* of China (issued in January 2004), more than 18,000 km of HSRs will be constructed in China by 2020, so thousands of sets of high-speed turnouts are needed. The following efforts are being made to meet this demand: developing high-speed

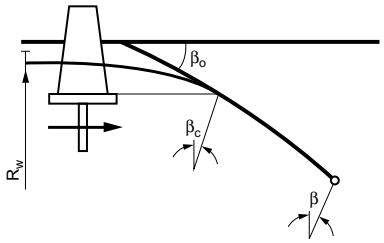

FIGURE 1.42

Separated line type at the front segment of the switch rail.

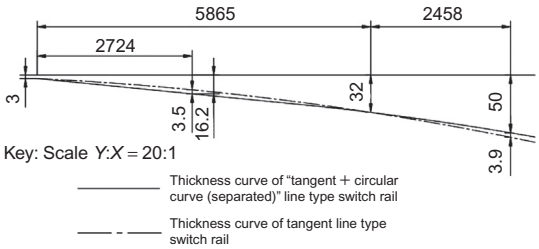

FIGURE 1.43

Thickness change of the switch rail.

turnouts independently, importing the technologies from France, and establishing joint ventures to manufacture German high-speed turnouts. In 2005, an R&D team for turnouts was set up by the former MOR of China. Through original innovation, China has overcome a series of technical problems in theoretical research, system design, structure comparison, standard formulation, in-plant trial production, assembly, acceptance inspection, field laying, and dynamic testing for No. 18, No. 42, and No. 62 turnouts in dedicated 250 km/h and 350 km/h passenger lines (PDLs). Certain products have been verified and approved for production. By 2014, nearly 5000 turnouts had been laid in Chinese HSRs (e.g., Wuhan−Guangzhou, Shanghai−Hangzhou, and Harbin−Dalian), with the longest expected time for safe and stable running of more than 5 years. Therefore, Chinese high-speed turnouts have been proven operationally feasible, but are technically different [11,12].

1. Plane line type

   To improve the riding quality of the diverging line, the design speed shall have a margin of 10 km/h maximum. For No. 18 turnouts for 80 km/h in the diverging line, 1100 m single circular curve line type is used; for No. 42 turnouts for 160 km/h in the diverging line, "5000 m circular + easement" curve line type is employed; and for No. 62 turnouts for 220 km/h in the diverging line, "8200 m circular + easement" curve line type is used. These are the high-speed turnout series in China. For the same turnout number, 250 km/h and 350 km/h high-speed turnouts have the same plane line type and dimensions. The front segment of the switch rail is a separated semi-tangent line, as shown in Figure 1.42. The circular curve of No. 18 turnouts is 11.95 mm away from the stock rail and obliquely tangent to the stock rail at a top width of 26 mm for the switch rail. This line type can greatly improve the firmness (thicken by 3.5 mm maximum, as shown in Figure 1.43) of the switch rail without impairing the riding quality in the straight and diverging lines, thus improving abrasion resistance and service life.
2. Switch

   UIC60D40 rails (i.e., 60E1A5 as per prEN13674-2) with small lateral bending stiffness are used as flat-web-special section rails (i.e., AT rail, as shown in Figure 1.44) for Chinese switch rails. This rail is made of U75V or U71MnK. Meanwhile, a rollered slide bedplate (Figure 1.45) is used to alleviate the switching force and scant displacement of the switch rail, and the approximately n-shaped elastic clips are used to fasten the rail base onto the inner side of the stock rail to prevent rail tilting.

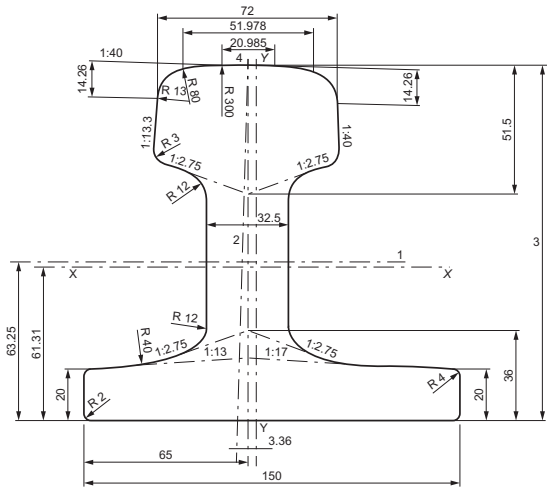

FIGURE 1.44

UIC60D40 rail.

FIGURE 1.45

Rollered slide bedplate.

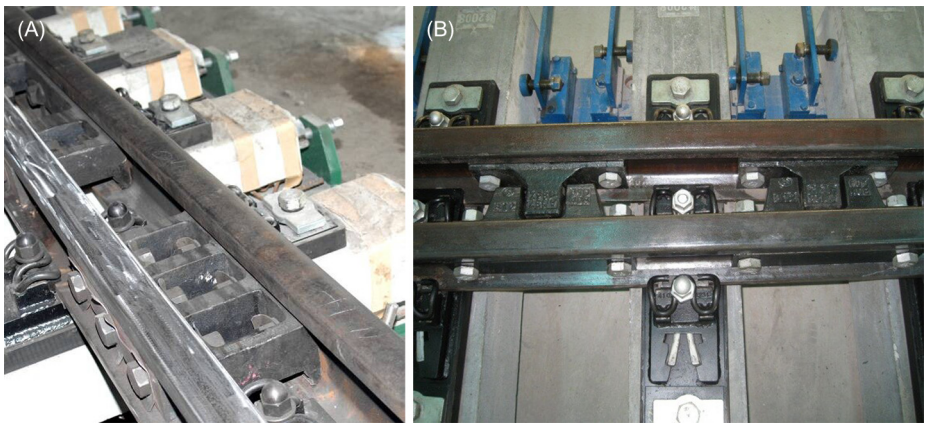

FIGURE 1.46

Force transmission components at the heel of the switch rail: (A) Fillers; (B) Retainers.

To improve wheel−rail relation in turnouts in China, the height difference of the switch rail is optimized, and the transition scope of the wheel load on the switch rail is shortened, shifting forward to the segment with a top width of 15−40 mm. This design, through dynamic simulation and operational practice, has been proven conductive to riding safety and quality in the main line. The heel of the switch rail is provided with various force transmission components (e.g., fillers and retainers, Figure 1.46) according to the temperature for laying rails, reducing

FIGURE 1.47

Crossing.

FIGURE 1.48

Special section wing rail.

the expansion displacement of the switch rail. This design is suitable for railways with great annual rail temperature difference in northern and southern China.

3. Crossing

Chinese turnouts adopt special section wing rails and swing nose rails made of UIC60D40 rails, as shown in Figure 1.47. A novel wide-head special section rail (i.e., special section wing

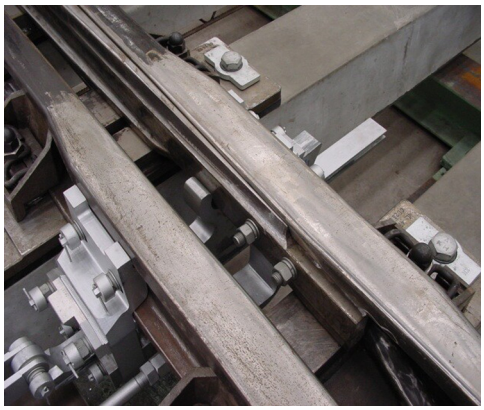

FIGURE 1.49

The first traction point of bracket-type point rail.

FIGURE 1.50

Horizontal hidden tip point structure of the point rail.

rail or TY rail in China, see Figure 1.48) has been developed. This wing rail has good lateral stability and leaves enough installation space for conversion equipment.

A bracket-type point rail locking hook is provided at the first traction point on the point rail. As the switching point rises, the closure status can be detected reliably, eliminating the detection failure of flange conversion mode due to tilted point rail and weakened wing rail resulting from excess machining on the rail web (Figure 1.49).

The horizontal hidden tip point structure (Figure 1.50) is adopted, which can reduce lateral wheel−rail force and improve riding safety and quality in the turnout.

4. Fastening

For turnouts in China, reasonable stiffnesses for different sub-rail foundations under different operation conditions are determined as per turnout dynamics. For instance, the vertical stiffness of the fastening is 25 ± 5 kN/mm for non freight ballastless track, 40 ± 10 kN/mm for freight ballastless tracks, 50 ± 10 kN/mm for non freight ballasted tracks, and 60 ± 10 kN/mm for freight ballasted tracks. Hence, the design principle of "high stiffness (rail pad) + low stiffness (plate pad)" is established.

The composition of the fastenings for turnouts in China is depicted in Figure 1.51. Gauge blocks and eccentric sleeves are employed to adjust the turnout gauge (adjustment range: −8 to +8 mm). The riser block is arranged under the plate (vertical adjustment range: −4 to +26 mm). Ballasted and ballastless turnouts use the same fastenings.

A turnout may have junction rails, shared plates, and shared ties, which will cause inhomogeneous track integral stiffness, affecting riding comfort. To solve this problem and realize uniform stiffness transition between a turnout and a section, a new graft-modified carbon black-filled rubber and blocky structure (Figure 1.52) are adopted. As per the design, all pads will have equal thickness, different stiffnesses, and low dynamic-static stiffness ratio ($\leq$1.35). Meanwhile, with the vulcanized plate-pad structure and buffering anchor bolt, the fastening can resist lateral deformation in case of low stiffness.

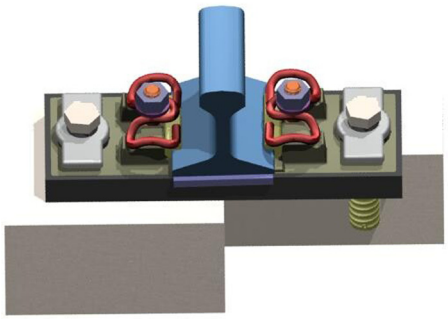

FIGURE 1.51

Fastening.

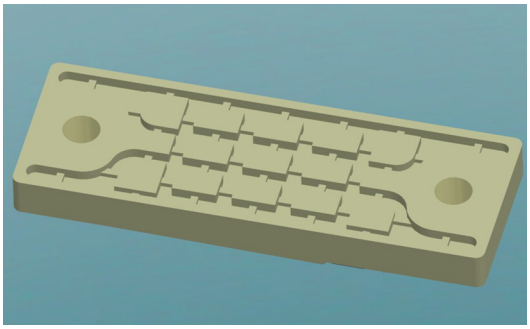

FIGURE 1.52

Blocky elastic pad.

5. Sub-rail foundation

   Chinese turnouts use prestressed long concrete ties on a ballasted track foundation. In addition, the quantity and arrangement of steel bars on cross sections of the ties of ballasted turnouts are optimized to make the centroids of steel bars overlap with those of the cross sections, alleviating the creepage of long ties. The ballastless track foundation is provided with steel-trussed embedded turnout ties (Figure 1.53) which can be reliably connected with the concrete bed, so that it is stable in structure and convenient for construction. Alternatively, the turnout slab (Figure 1.54) with embedded bolt sleeve is used, thus realizing high positioning accuracy and short construction period. The three turnout tie structures enable the high-speed turnout to be adaptable to different sub-rail foundations.

6. Conversion equipment

   "Multi-machine multi-point" traction (Figure 1.55) applies to the turnout in China, that is, switch machines with different throws are used and the traction points are actuated sequentially under the control, so as to realize synchronous conversion of the 54 m long switch rail of No. 62 turnouts. Hook-type external locking mode is employed for all traction points, characterized by powerful locking capability and high safety, capable of effectively maintaining reliable

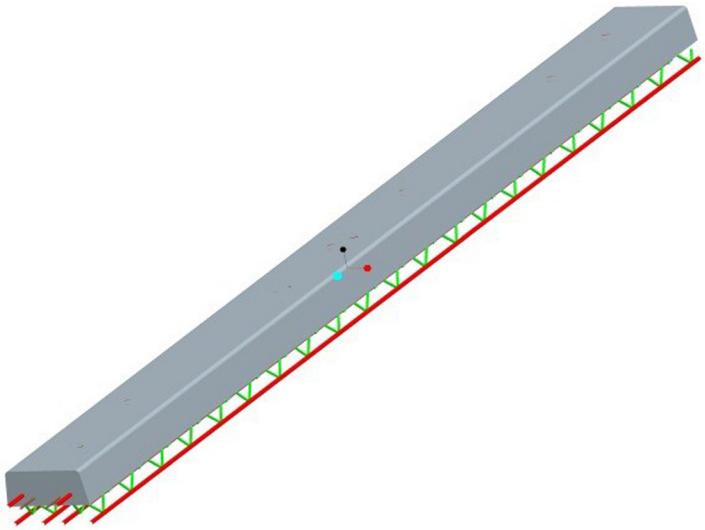

FIGURE 1.53

Embedded turnout tie.

FIGURE 1.54

Prefabricated turnout slab.

locking (Figure 1.56) between the switch rail and the stock rail as well as between the point rail and the wing rail, even when the switch rod is distorted by ice blocks, gravel, etc. brought about by high-speed train-induced wind in extreme cases. The permissible expansion displacement is 40 mm for switch rails, and 20 mm for point rails.

FIGURE 1.55

Multi-machine multi-point traction of ballasted and ballastless turnouts.

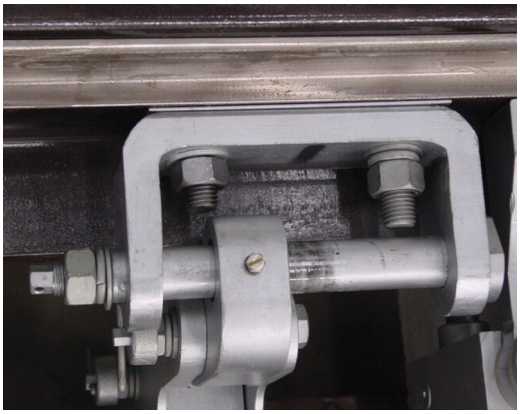

FIGURE 1.56

Hook-type external locking device.

A closure detector is mounted on the turnout tie to check the dynamic closure between the switch rail and the stock rail when a train travels in a turnout. The device will not occupy the free space of the tie and can provide information for turnout maintenance, as shown in Figure 1.57.

7. Other components

Turnouts in China are provided with turnout heating systems (Figure 1.58) characterized by high efficiency and simple installation. The heating system can automatically remove ice or snow from the slide bedplate on snowy or freezing days. Thus there will be no traffic interruption for manually removing snow or ice that causes conversion failure, guaranteeing normal operation in severe weather conditions.

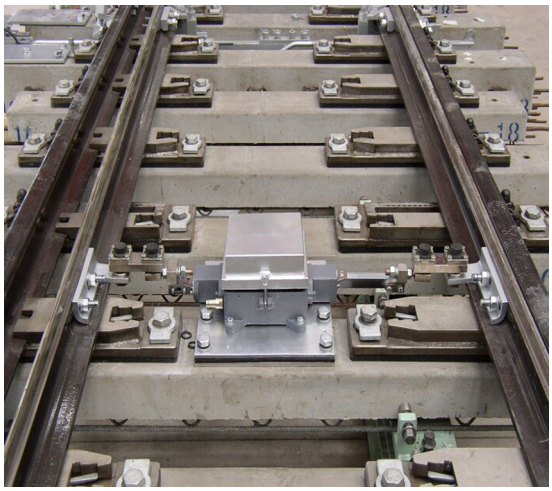

FIGURE 1.57

Closure detector.

FIGURE 1.58

Turnout heater.

FIGURE 1.59

Turnout monitoring system.

Turnout monitoring systems (Figure 1.59) are still under test, targeting at monitoring the defects and damages of switch rail/point rail, conversion parameters (i.e., rail closure, switching force of switch machine, dynamic force, vibration acceleration, working voltage, current, and oil pressure of the switch machine), and the turnout gauge, etc. The monitored data can be directly transmitted to a PDL comprehensive maintenance center, realizing informatized real-time monitoring, greatly reducing the workload of daily inspection, improving the performance of safety applications, and laying a foundation for reliability-centered maintenance for high-speed turnouts.

1.4.4 OTHER COUNTRIES

High-speed turnouts for 250 km/h or so have also been developed in other countries (such as Japan and the United Kingdom), but are less influential, lacking operational practice at 300 km/h or above [13,14].

1. Japan

   Japan began to develop No. 18 high-speed turnouts in 1964, and launched No. 38 turnouts in 1992. In Japan, the wing rail is of frame structure made of solid high manganese steel, and long/short point rails are also integrally cast with high manganese steel. This structure is rather stable, and a slip joint is arranged in the rear of short point rail, that is, the point rails are of a single flexible rail structure. The two switch rails are linked by a rod to retain the line type, and are provided with internal locking devices. Rigid clip and double-layer tie plate are adopted for variable gauge adjustment. Rubber pads are replaced by spring washers for elastic fastening. A plastic pad beneath the tie plate protects the timber tie from being cut.

   In many countries, turnout rails are continuously welded with section rails to reinforce turnout structures. On the other hand, Japan has developed an expansion joint at two ends of the throat, so that the longitudinal force on the CWR track in the section will not be transmitted to the turnout. Therefore, no long wing rail will be provided at the heel of the crossing, as shown in Figure 1.60. The point rail is somewhat like a common short rail with small expansion displacement. The switch rail is provided with fillers at the heel to reasonably restrict its expansion displacement. The turnout in Japan reduces the switching resistance of the switch rail with the rollered slide plate, as shown in Figure 1.61. Meanwhile, various types of turnout heaters (e.g., heating type, wind-warming type, and water-warming type) are used.

2. United Kingdom

   The CWR turnouts manufactured by Balfour Beatty of the United Kingdom mainly involve fixed crossings and swing nose crossings. These turnouts are widely applied to railways for mixed passenger and freight traffic, with a maximum design axle weight of 35 t and highest traveling speeds of 250 km/h. The CWR turnouts were once exported to the United States and other nations.

FIGURE 1.60

Crossing.

FIGURE 1.61

Rollered slide plate.

FIGURE 1.62

Fixed crossing.

The fixed crossing turnout is further classified into solid high manganese type (Figure 1.62) and common rail assembled type (Figure 1.63). The high manganese fixed crossing is welded with common rail at the heel via a chromium-based medium. It can be laid on CWR tracks.

FIGURE 1.63

Assembled crossing.

FIGURE 1.64

Swing nose crossing.

The swing nose crossing in the United Kingdom has a structure similar to its German counterpart, namely a monoblock alloy steel frog (Figure 1.64). A switching flange forged at the bottom is connected with the switch rod. A long wing rail structure is used to better transmit the longitudinal force of the rail. At the end of the wing rail, fillers are used to connect the two

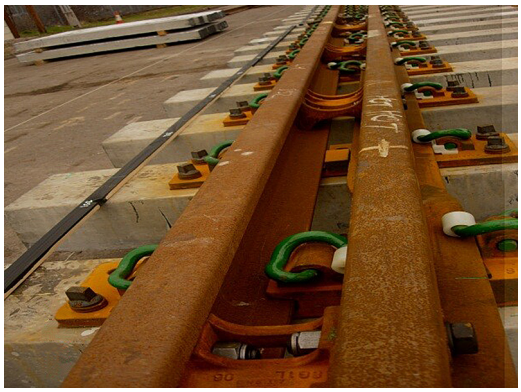

FIGURE 1.65

Porous filler.

bases of the point rail, as well as to connect the point rails with the wing rails. In addition, hinged turnout ties are used.

Generally, Pandrol e or Fast clips are adopted, which have the same fastening force as in a section. The switch rail is provided with fillers at the heel, exposed to the whole section of the rail web and fastened by four short bolts with small shearing deformation. To avoid shearing deformation of the bolts due to overlarge longitudinal force on each filler bolt, 4−5 pairs of fillers are normally arranged at the heel of the switch rail to share the longitudinal force transmitted by the rail of the transition lead curve, as shown in Figure 1.65. The switch rail is locked with the hook-type external locking device. The locking device has powerful locking capability, but it cannot expand freely in the locking state, so the fillers at the heel of the switch rail for transmitting force are reinforced to effectively control the expansion displacement of the switch rail.

CHAPTER

LAYOUT DESIGN

2

The design of turnouts falls into two aspects: general layout design and structural design. Normally, the general layout design comes first, followed by structural design of parts based on the main given dimensions. General layout design determines the main dimensions of turnouts, track gauges, layout and number of turnout ties, and track length.

In addition to meeting basic riding requirements, the design of a turnout shall follow the principles below:

1. In all cases, sufficient riding quality and comfort shall be ensured when a train travels in the turnout at a specified speed.
2. The track gauges and spacings of the turnout shall allow unrestricted passage of rolling stock under the most adverse conditions.
3. All parts and relevant accessories of the turnout shall in no case stretch into the construction clearance.
4. Conversion equipment shall be correctly installed. Insulated joints shall be arranged appropriately to correctly display the interlocking signals.
5. Turnout parts shall have adequate strength and stiffness, and the section type shall be maximally simple, reasonable, and economical, as well as feasible for mass production. Moreover, the interchangeability of turnout parts shall be enhanced for easy laying and maintenance.
6. The minimum length is preferred for smaller land occupation.

Moreover, high-speed turnouts shall have high-tech performance, good economic efficiency, applicability, etc. [16,17].

2.1 DESIGN CONDITIONS

In designing a high-speed turnout, the running conditions, vehicle structure, technical requirements for tracks, and laying conditions shall be taken into account, and the requirements of different loads, temperatures, and laying foundation shall be met. Moreover, turnout design shall match with the technical conditions of the whole line [18].

Design of High-Speed Railway Turnouts.

2.1.1 OPERATION

1. Permissible speeds

   In China, high-speed turnouts are for 250 and 350 km/h maximum in the main line portions, used in 250 km/h passenger lines (PDLs) and 350 km/h high-speed railways (HSRs), respectively.

   In China, there are turnouts for 80, 160, and 220 km/h in the diverging line portions, used in the main line turnouts for accessing the station, crossover turnouts, and connecting line turnouts, respectively.

   Thus, Chinese high-speed turnouts can be divided into six types as per the speeds in the main line and the diverging line.

   According to design safety requirements, the design calculation speed will add 10% for the main line, and 10 km/h for the diverging line, and the test speed shall be no less than the design calculation speed.

2. Design axle load

   The design axle load equals to the static axle load plus a margin of 10% (counterbalance). The power distributed high-speed EMU is used for 250 km/h nonfreight PDL and 350 km/h HSR, with an axle load of no more than 170 kN, taken as 187 kN considering a margin of 10% (equivalent to that of the power concentrated high-speed EMU with axle load of no more than 190 kN).

   For the 250 km/h mixed passenger and freight railway, the maximum speeds of EMU and freight cars are 250 and 120 km/h, respectively. The axle load of a freight car is the design control value, no more than 230 kN, taken as 250 kN considering a margin of 10%.

   Thus, the structure strength will be calculated with axle loads of 190 and 250 kN, respectively.

3. Transport volume

   Turnouts shall have an overall service life of at least 20 years, or with transport volume of more than 600 million tons. Considering the freight transport in 250 km/h mixed passenger and freight lines, turnouts shall have a service life equivalent to the speed-up turnouts based on total transport volume, that is, no less than 600 million tons. As nonfreight 250 km/h PDLs and 350 km/h HSRs are dedicated to passenger transport, generally, the total weight of annual transport volume is larger than 30 million tons. To this end, the service life of turnouts shall be no less than 20 years, equivalent to 600 million tons in transport volume.

   However, the switch rails and the point rails of turnouts are wear-prone, so their service life may be shorter than the overall service life.

2.1.2 ROLLING STOCK

Design parameters, such as train configuration and suspension, and dimensions of running gear and wheel treads, shall be included in the design of high-speed turnouts. In China, CRH EMU trains are adopted in HSRs, including CRH_1, CRH_2-200, CRH_2-300, CRH_3, CRH_5, and CRH380. The configuration of EMUs includes 5M + 3T, 4M + 4T, and 6M + 2T. LM_A worn profile tread is adopted, as shown in Figure 2.1, and the wheel back-to-back is 1353 mm.

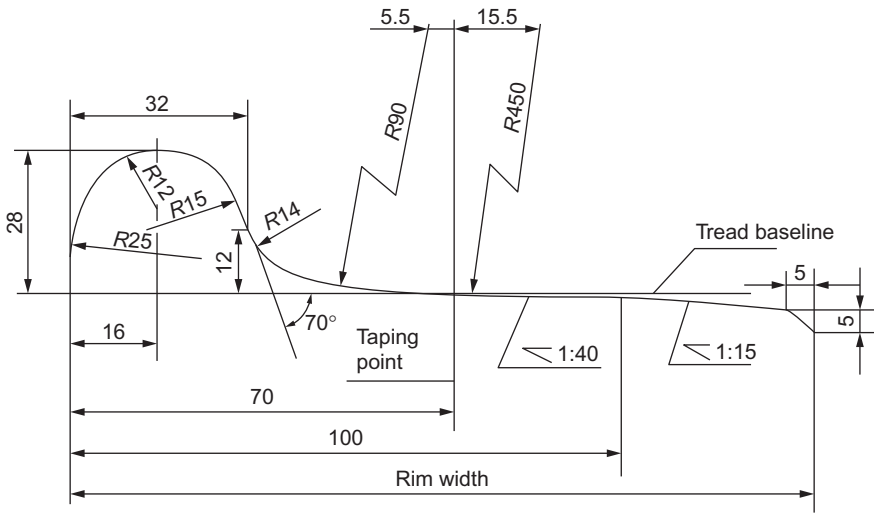

FIGURE 2.1

Profile of LM_A wheel tread.

2.1.3 TRACKS [19]

1. Track gauge

   The standard track gauge is 1435 mm, measured 16 mm below the rail top for Chinese railways (14 mm below the rail top for European railways). According to the inscribing requirements of the rolling stock in a turnout, the gauge shall allow the passage of a train in compulsory inscribing conditions. Wedging inscribing is not allowed. According to the design requirements for speed in the diverging line for Chinese high-speed turnouts, a large radius transition lead curve is used, so gauge widening is unnecessary. For German high-speed turnouts, in order to reduce the hunting motion of a running train, a 15 mm gauge widening is provided at top width 30 mm of the switch rail, and the change rate of track gauge for No. 18 turnouts is 2.67 mm/m. This has proven effective for improving the riding quality of high-speed EMU in a turnout.

2. Rail cant

   There are two rail cants: 1:40 and 1:20. Generally, the rail cant in a high-speed turnout is the same as in a section. As demonstrated, if the two areas are expected to have different rail cants, gentle transition measures shall be taken at turnout ends. In China, Germany, and Japan, high-speed railways and turnouts all employ 1:40 rail cant, with no transitions at the two ends of the turnouts. However, for switch rails and point rails to be switched, the 1:40 rail cant shall be arranged at the rail top.

3. Superelevation

   Superelevation on the transition lead curve can ease the deficient superelevation and enhance the riding quality in the diverging line. However, a series of difficulties must be solved beforehand for superelevation of turnouts:

   a. Limited by construction clearance when a train travels in the main line, the outer rail on the transition lead curve is generally superelevated by not more than 15 mm, so the reduction effect on deficient superelevation is insignificant
   b. Limited by height differences of rails (switch rail/stock rail, point rail/wing rail), the movable parts of the switch rail and the point rail cannot generally be superelevated, so there is no relieving effect on the deficient superelevation of curved switch rail and curved crossing; and
   c. As for the superelevated transition lead curve, superelevated transitions shall be arranged in the rear of the heel of the switch rail and in front of the crossing, fixed by the fastening. However, the fastening is relatively complex, so superelevated high-speed turnouts do not predominate.

4. Distance between two tracks

   The distance between centers of two tracks is 5 m for 350 km/h, and 4.6 m for 250 km/h in China. To simplify turnout types, the turnout numbers, line types, and main plane dimensions associated with the permissible speeds in the diverging line shall be consistent; accordingly, therefore, the distance of 4.6 m applies.

5. Rail materials and weight

   The rails for high-speed railways shall have high safety performance, straightness, and geometric precision. High safety performance requires pure steel, intact surfaces, low residual tensile stress at the rail base, excellent ductility and welding performance, easy production, stable quality, and high reliability. High geometric precision and high straightness of the rails are crucial for riding quality of HSR. The geometric tolerance, rail ends, straightness of the body, distortion, and other indicators are strictly specified in the technical specifications for HSR rails. To minimize welded joints, a 100 m steel rail shall be used for high-speed turnouts, but 25 or 50 m steel rails are available in special cases.

   The materials for HSR rails shall be of mature steel, consistent durability, pure quality, excellent welding quality, and adaptability to turnouts. The U71Mnk rails (tensile strength 880 MPa) are adopted for Chinese 350 km/h HSRs. Considering the needs of freight transport, U75V rails (tensile strength 980 MPa) are selected for 250 km/h HSRs. Turnout rails and section rails shall be of the same materials for ease of welding.

   The main lines of Chinese railways are mainly of 60 kg/m rails, along with some 50 and 75 kg/m rails. The 60 kg/m rails are also widely used for existing railways or railways under construction; therefore, it is preferred for high-speed turnouts. Research shows that UIC60 kg/m rails made of Chinese 60 kg/m (CHN60) steel have different railhead profiles, but exert small impact on the wheel−rail geometry contact, dynamic interaction, and wearing conditions, as well as service life of wheel rails. In view of the manufacturing conditions for rails in China, CHN60 rails are selected for both Chinese HSRs and turnouts.

   The materials of special section rails, such as 60D40 AT rails and TY rails, those used for a turnout shall be consistent with those for a section. Rails welded with common rails at both ends shall be machined or heat-treated into 60 kg/m rails of Chinese section type.

6. Fastening

HSRs pose demanding requirements for high speed, large traffic density, and excellent track smoothness, so rail fastenings should have the following properties:

a. Strong retainability of track gauges
b. Enough anticreeping resistance
c. Simple structure, good reliability, and less maintenance
d. Good damping performance
e. Good insulating performance
f. Good adjustability of vertical and lateral rail profile; and
g. High accuracy of parts and good smoothness of assembled tracks.

For a high-speed turnout, fastenings shall also meet some special technical requirements in addition to the above:

a. Considering the special structures (e.g., slide plate) in a high-speed turnout, double-elasticity positive fastenings are preferred
b. All turnout parts shall be reliably fixed with the elastic fasteners; and
c. The positions of the movable switch rail and the point rail without fastenings shall be capable of adjusting track gauge and vertical profile.

7. Continuously welded rail track

In a new HSR line, trans-sectional continuously welded rail (CWR) track will be laid at one time to achieve high track smoothness. Thus, high-speed turnouts will be continuously welded.

8. Conversion equipment

Conversion equipment shall have conversion, locking, and indication functions. For conversion function, the operational direction of a turnout is shifted by lining the switch rail or swing nose rail to guide the rolling stock to change track. Conversion equipment may have certain switching throws, so the throw of a turnout shall be consistent with the throw of the conversion equipment. Locking function relates to the fact that the conversion equipment, after turnout transition, shall lock the turnout to avoid false closure. Indication function refers to the fact that after turnout transition, the conversion equipment shall display normal position (main line in operation) and reverse position (diverging line in operation) of the turnout. Conversion equipment includes electrical, electrohydraulic, mechanical, and electro-pneumatic types. The first two types are commonly used.

a. Traction modes

The traction modes for turnout conversion include "multi-machine multi-point" and "one-machine multi-point" traction modes. For the one-machine multi-point traction mode, mechanical conduit is adopted for the traction of turnout conversion. This mode has good synchronization performance, fewer switch machines, and reduced failure. However, the conduit and crankshaft are prone to wear under vibration, resulting in difficult closure adjustment for the turnout. Moreover, only the first traction point is provided with an external locking device, so there are security risks in case of excess wear.

The multi-machine multi-point traction mode is generally of a separate movement external locking mode, that is, each traction point is provided with an external locking device, so it has high safety performance. However, it is unlikely to realize synchronized conversion for all switch machines due to the number and high failure frequency of switch machines. Based on the practice of former speed-up turnouts, the multi-machine multi-point traction mode is adopted in the design of high-speed turnouts in China.

b. Requirements for technical performance

Conversion equipment shall have a test life of more than 1 million times, and an actual life of no less than 20 years, so as to match with the overall service life of a turnout. The switch machine shall be equipped with a manual device to reliably shut off the motor power (3-phase 380 V AC). Controllers and adapters will not be arranged outdoors. The first traction point on the switch rail and the point rail will be locked with operating rod and locking rod.

After power on, the switch machine shall act correctly as per the following procedures: shutting off the original indication contact, unlocking, switching, locking, and connecting to a new indication contact.

c. Mechanical parameters

The throw of the operating rod: as per the turnout

Rated switching force: 3000−5000 N

Maximum traction force: 6000 N

Locking retention force of the locking rod: $\geq$20,000 N

Locking retention force of the operating rod (locking force): $\geq$90,000 N.

The throw of the switch machine operating rod depends on the throw of the switch rail to meet the synchronization and locking requirements for turnout conversion. The switching force of the switch machine shall be compatible with the actual lining force of the turnout.

d. Electrical parameters

Power supply: three-phase 380 V AC (allowable electric resistance for single line $\geq$54 Ω), 50 Hz

Operating time: $\leq$8 s.

The switch machine shall be circuited internally and marked properly. The operating time of the switch machine is a major indicator affecting route setting, and the minimum requirements are determined by use conditions.

e. Locking mode

The separate movement external locking device should be used for switch rails, and the position of its traction rod shall be readily accessible for tamping and maintenance operation. The locking capacity of an external locking device relates to the safety margin for reliable locking. It is no less than 35 mm at the first traction point of the switch rail and the point rail, with deviation of locking capacities on both sides no more than 2 mm. External locking devices shall be adaptive to the expansion requirements of the switch rail and the point rail of a CWR turnout, and have good insulation performance.

f. Closure detection

If there is a 4 mm or greater gap between the switch rail and the stock rail, or between the point rail and the wing rail at the external locking centerline of a traction point, the locking device shall have no locking or connection indication. At the contact area between the switch rail and the point rail, there shall be no turnout connection indication when there is a 5 mm or greater gap between two adjacent traction points. Therefore, the locking device at the traction point shall have a closure detection function. Closure detectors shall be provided among the traction points. The turnout connection indication shall be cut off reliably for a trailed turnout.

g. Installation device

The service life of an installation device for conversion equipment shall be no less than 20 years. The installation device shall be applicable to main and diverging lines.

9. Turnout heater

The device functions by means of gas heating, hot water circulation, hot air transmission in the pipeline, salt water injection, and electrical heating. In case of snowfall or temperature change, the turnout heater will be started either automatically or manually. In China, the electrical heating mode is mainly adopted for high-speed turnouts. The space for heating components shall be reserved in the design.

10. Monitoring system

Technologically mature and reliable turnout monitoring systems shall be adopted to monitor the current, voltage, conversion time, and switching force of the switch machine, closure status of the switch rail and the point rail, rail temperature, etc. Moreover, the monitoring system will be integrated into the comprehensive maintenance system of a PDL and can achieve remote test and diagnostic functions to provide real-time and accurate data for the maintenance of PDL turnouts.

11. Track circuit

At present, turnouts are generally circuited in parallel. According to the track circuit principle, insulated joints of the rails will be installed at certain parts in a turnout to make two rails have different polarities, capable of short-circuiting the rolling stock in any part of the turnout. The insulated joints can be arranged either in straight or curved track. In dividing the insulation sections, the rails at both ends of insulated joints shall have different polarities. If the polarities of adjacent rails are the same, the installation position of insulated joints on the rails shall be changed (from straight track to curved track, or vice versa) until the polarities are correct. In automatic blocking sections, for stations equipped with continuous cab signal, the insulation on turnout rails must be arranged in curved track of the turnout (for single turnout) to continuously send signals to locomotives from wayside facilities. The insulated joints on the two rails prefer the butted type. In case of staggered connection, the length of staggered parts shall not exceed 2.5 m (this area is called the dead section, as the two rails have the same polarity here). Otherwise, when a single carbody with the minimum wheel base stops in a dead section by accident, the car cannot be short-circuited, and the track circuit cannot display signals correctly, then accidents may take place. In the calculations for general turnout layout, it shall be considered that the insulated joints may be provided in both main and diverging lines. The parts of a circuited turnout, for example, rods, shall be provided with insulation devices. The insulated joints shall be glued for high-speed turnouts.

2.1.4 LAYING

1. Temperature

High-speed turnouts may be laid on the subgrade of ballast/ballastless tracks, tunnel portals, bridges, or slopes; therefore, they shall be highly adaptive. China has a big temperature difference between north and south. The annual track temperature difference is about 100°C in severely cold areas in the north, about 90°C in cold areas in the central plains, and about 80°C

in warm areas in the south. Therefore, high-speed turnouts shall adapt to the laying conditions in areas with varied temperature differences.

2. Station layout

   For the CWR turnout group in a station, the influence of the length of the intermediate straight line between two turnouts shall be taken into account. For two turnouts in the main line with fronts being connected, when trains travel in two diverging lines at the same time, the minimum length of the rail interpolated between two turnouts is 50 m. Limited by the length of the station site, it will be 33 m. If no trains travel in two diverging lines at the same time, or the front and rear of the turnouts are connected, it will be 25 m. For turnouts in a receiving-departure line with the front and rear being connected, the length will be 12.5 m, or it will be 25 m for the other layout.

3. Sub-rail foundation

   In China, the 250 km/h PDLs are mainly of ballasted tracks, and 350 km/h PDLs are mainly of ballastless tracks. Thus, high-speed turnouts shall be applicable to both track types. Metal parts (rail members and hardware) shall be consistent for ballast and ballastless turnouts, and the stiffness of the fastenings may be adjusted as per design requirements. To facilitate the operation of large maintenance and repair machines, the ballast turnouts may be provided with steel ties to accommodate the switch rod internally.

4. Track substructure

   High-speed turnouts are generally designed to be laid on subgrades (embankments). In an elevated station, if high-speed turnouts are to be laid on a bridge, the requirements for bridge structures, span, and turnout-bridge relative position shall be incorporated in the design to avoid impacts on riding safety and quality due to train−turnout−bridge resonance, and to avoid excessive stress and deformation of turnouts resulting from longitudinal interaction of the turnouts, bridge, and piers. Generally, high-speed turnouts should not be laid at tunnel portals or in transitions between the embankment and the bridge or other different structures to avoid poor geometry of turnouts due to drastic temperature changes and excessive differential settlement of the foundation.

5. Track gradient

   In general, ballast tracks should not be laid on slopes greater than 6‰, and ballastless tracks should not be laid on slopes greater than 12‰ to avoid inordinate stress and deformation of CWR turnouts due to excessive traction force or braking force of trains.

6. Other laying conditions

   High-speed turnouts generally should not be laid on circular curves, easement curves, or vertical curves. If requested through demonstration, the layout and structure shall be designed separately.

   For high-speed turnouts to be laid on foundations with a high degree of settlement (e.g., soft soil), sheet-pile subgrades will be adopted for reinforcement, and differential settlement in the longitudinal and transverse directions of the turnouts shall be controlled to avoid excessive geometric deviation of high-speed turnouts.

2.2 PLANE LINE TYPES

The plane line type design for a turnout shall determine the plane line type of connecting parts as per the speeds in the diverging line, and that of the switch rail as per its wear resistance and

traveling quality in the diverging line; it will also determine the plane line type of crossing based on that of connecting parts.

2.2.1 DESIGN REQUIREMENTS

The permissible speed in a turnout is governed by the strength, smoothness, and line types of turnout parts, so the geometry types of turnouts are essential for safe and stable running of trains and the comfort of passengers [20].

1. Speed in the diverging line

   The speed in the diverging line for single turnouts is mainly determined by the permissible traveling speeds on the switch and transition lead curve.

   a. Influential factors

      The speed in the diverging line may be impacted by many factors; in particular, as the transition lead curve is not superelevated and has small radius generally, trains may have large, unbalanced centrifugal acceleration. In addition, when a train approaches a diverging line from a main line, the train will collide with the rails at the moment when it is forced to change direction. In this moment, partial dynamic energy in the carbody will be converted into potential energy that leads to the compression of rails and lateral elastic deformation of the running gear of the rolling stock. This is known as dynamic energy loss. Excessive dynamic energy loss will influence traveling comfort and the stability of turnout structure and reduce the service life of the turnout. Thus, loss of dynamic energy shall be limited within the permissible range.

      In addition, some factors impacting the speeds in the main line, such as angle of attack of the check rail, wheel−rail relation, track stiffness, rail joints, turnout geometry, and structure strength, will have an impact on the speed in the diverging line.

   b. Measures for speedup

      The speed in the diverging line is increased mainly by enlarging the radius of the transition lead curve and reducing the angle of attack of the wheels to the turnout. An effective way is to increase the radius of the transition lead curve by using a large number turnout. However, larger turnout number means longer turnout and station site. Therefore, large number turnouts cannot be used at will. For a given turnout number, the radius of transition lead curve may be enlarged by optimizing the plane design, such as adopting a curved switch rail and curved crossing. The transition lead curve with variable curvature is able to ease the dynamic energy loss due to wheel−rail collision, as well as unbalanced centrifugal acceleration and change rate. However, this is only practical for large number turnouts.

      A superelevated transition lead curve can ease unbalanced centrifugal acceleration and its increment, but in fact, the superelevation value is very small, limited by the space of the turnout. Thus, this measure can improve running conditions (e.g., prevent reverse superelevation), but cannot enhance the speed in the diverging line.

      The speed in the diverging line can also be increased by reducing the angle of attack of wheels to rails in the diverging line, such as preventing unnecessary widening of track gauge, adopting a tangent curved switch rail, selecting switch rails, wing rails with the same

angle of attack as the buffer segment of check rails, and matching with the speed in the transition lead curve.

In addition, the speed in the diverging line may be increased by strengthening the turnout structure, such as removing the unions at the heel of the switch rail and common joints in the turnout, adopting external locking devices, optimizing wheel−rail relation at the switch and the crossing, optimizing track stiffness, mitigating the scant switching displacement of the switch rail and swing nose rail, using the point rails with double flexible rails and thus saving the diagonal joint at the heel of short point rail, enhancing the resistance of rails to tilting and the resistance of the track panel to lateral displacement (with elastic clips, rail braces, rods, anchors, etc.).

2. Speed in the main line

This speed is less impacted by the plane line type, but mainly determined by the wheel−rail relation at the switch and the crossing.

a. Influential factors

If the turnouts have check rails in the main line, the wheel flange will collide with the buffer segment working surface of the check rails at the crossing when a train approaches from the turnout front. Similarly, the buffer segment of the wing rail has a certain angle of attack. Thus, the same problem may occur in terms of the speed in the main line. In the design of the crossing, the wing rails in the main and diverging lines are designed as symmetrical, and have the same angle of attack as the check rails.

When the wheels move from wing rails to point rails at the crossing, as they leave the wing rails, the conical and worn profile treads will drop as the contact points move outward. Then the wheels will gradually return to the original level after moving onto the point rails. This is also applicable to passage in the reverse direction. Vertical and lateral structural irregularities shall be overcome when the wheels pass through the crossing, which will cause vibration and shaking of trains. When the wheels make transition from stock rails to switch rails, similar vibration on the wheels will occur, limiting the increase of speed in the turnout. Therefore, the design shall include optimized railhead profile, appropriate rail height difference of the switch rail and the point rail, and proper rail cant.

In a common railway section, if the structures and stiffnesses of the fastenings are equal, the track integral stiffnesses along the line are basically the same. However, in a turnout, as several rails may share one tie plate or one tie, or two rails may be connected by fillers, the track integral stiffness may vary along the line, resulting in extreme vibrations in trains and affecting riding quality and comfort in an irregular turnout track. Thus, the stiffnesses of the fastenings shall be adjusted in the design to homogenize the track integral stiffness along the longitudinal direction of the turnout.

As in a section, track gauge, alignment, and longitudinal and cross-level irregularity of a turnout will also affect riding quality and safety. In view of the special nature of the turnout structure, the following state irregularities influencing riding quality may exist in a turnout: gaps between the switch rail and point rail and slide bedplate due to poor manufacturing and assembling accuracy of the turnout; gaps in the closed area between the wing rail and the stock rail; and gaps with jacking blocks. To this end, the manufacturing, laying, and maintenance standards for turnouts shall be enhanced.

In recent years, turnout dynamics theory has been developed in China to determine the permissible speed in the main line. According to the structural design of the turnout, the

trains will travel in the turnout at the design speed plus 10% in the main line or at the design speed plus 10 km/h in the diverging line to model the indicators of riding quality (e.g., derailment coefficient, load reduction rate, rail stress, and spread of switch rails) and stability indicators (e.g., vertical and lateral vibration acceleration of the train), evaluate the conformity of turnout structure with design requirements, and, in addition, provide guidance for optimization of turnout structural design and compilation of relevant standards.

b. Measures for speedup

An effective way is to adopt new structure and materials for turnout parts, to gradually strengthen the structure, and to enhance manufacturing and assembly accuracy. Second, reasonable type and dimensions for the plane and structure of the turnouts shall be determined to reduce or eliminate the factors impacting speed in the main line. Finally, the stiffness of turnout track shall be homogenized to eliminate dynamic irregularities impacting speed in the main line.

2.2.2 TRANSITION LEAD CURVES

The line connecting the switch and the crossing is composed of straight connecting line and curved connecting line (transition lead curve). The structure of the straight connecting line is the same as that of the straight line in the section, but the curved connecting line differs from the curved line in the section in geometry type and structure [20,21].

The plane line type of transition lead curve is composed of a circular curve, an easement curve, and a compound curve.

1. Circular curve

The circular curve type may be used with straight switch rails and curved switch rails. It is commonly used as it is easy to design, manufacture, lay, and maintain [22].

When it is used with straight switch rail, the tangent point of the transition lead curve may be appropriately set at or in the rear of switch rail heel (Figure 2.2). This curve type is generally used in small number turnouts with low speed in the diverging line, typically for a straight crossing.

When it is used with curved switch rail, the radii of the transition lead curve and curved switch rail may be equal or unequal. The curve of the switch rail and the working surface of the stock rail may be in tangent, secant, or separated type. The crossing may be straight or curved, as shown in Figures 2.3 and 2.4. This curve type is used mainly in turnouts for high speed in the diverging line, such as No. 12 and 18 turnouts. The transition lead curves of the turnouts with curved switch rail and curved crossing may have relatively larger radii. If a transition lead curve ends near the heel of a straight crossing, the rear part of the transition lead curve will be intersected at a proper position in the front of the crossing, called rear-secant circular curve (Figure 2.5). It is commonly used in conjunction with the secant curved switch rail to increase curve radius. However, the transition lead curve has inclination angles, so it is mainly used in small number turnouts.

2. Easement curve

The easement curve may be quadratic and cubic parabola, spiral, or sinusoid. Considering the design, manufacture, laying, and maintenance difficulties, it is applicable to larger number

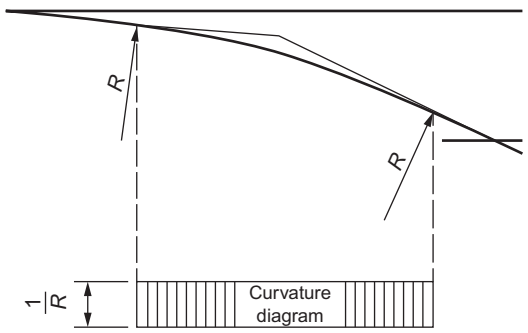

FIGURE 2.2

Circular curve type (straight switch rail).

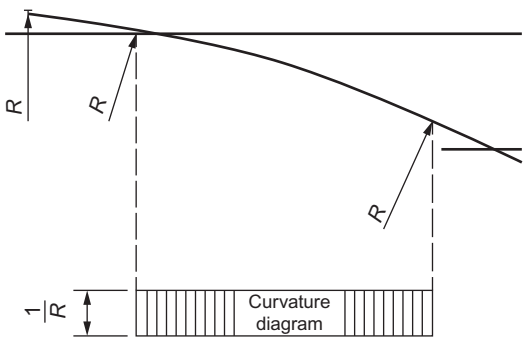

FIGURE 2.3

Circular curve type (curved switch rail and straight crossing).

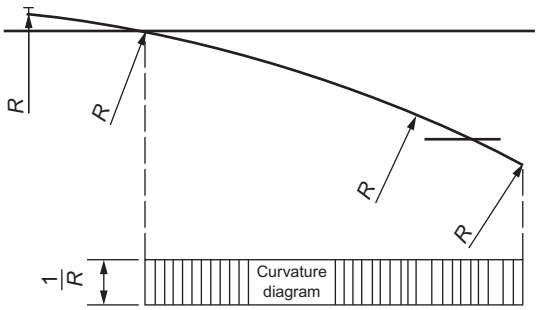

FIGURE 2.4

Circular curve type (curved switch rail and curved crossing).

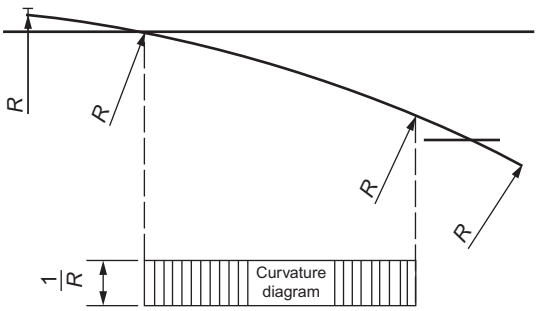

FIGURE 2.5

Circular curve type (curved switch rail, rear-secant).

turnouts where high-speed trains will travel in the diverging line. This curve type is advantageous in the gradual change of centrifugal acceleration and its incremental improvement of passengers' comfort. The cubic parabola is the simplest and most common form of easement curve [23,24].

Easement curves fall into single type and double type; the latter is a compound curve type. The single parabola involves the parabola originating from (Figure 2.6) or ending at (Figure 2.7) the front end of the switch rail. For the former type of easement curve, a straight crossing may be used. The switch rail is of the easement curve type, with a small angle of attack when a train travels from the turnout rear. However, the switch rail is susceptible to severe side wear and spalling due to the long weak section, so the curve is rarely used. For the latter easement curve type, either a straight or a curved crossing is available. When a crossover turnout connecting two turnouts is to be constructed, running stability may be improved by connecting the origins of two easement curves or interpolating a straight section.

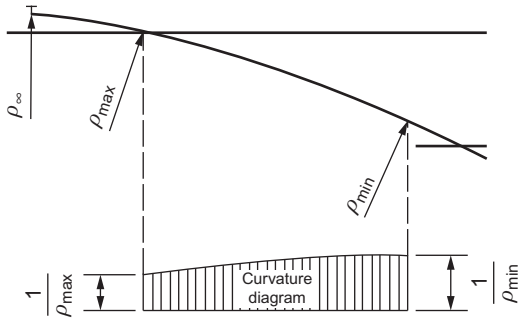

FIGURE 2.6

Single easement curve (origin at turnout front).

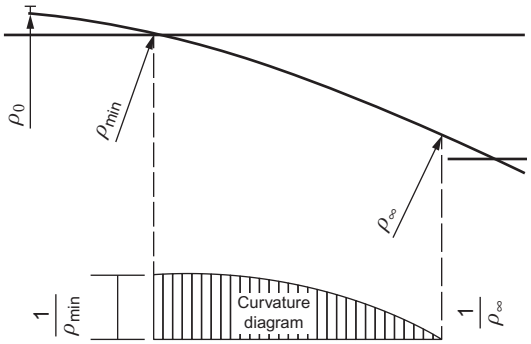

FIGURE 2.7

Single easement curve (origin at turnout rear).

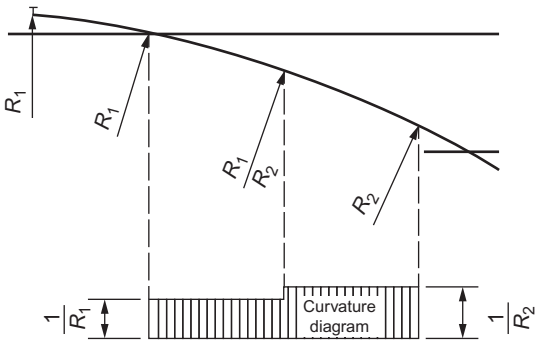

FIGURE 2.8

Compound circular curve type.

The wear resistance of the switch rail is better than the former easement curve. This single easement curve type is rarely used in switch rails due to design and manufacturing difficulties.

3. Compound curve type

The compound curve is composed of curves with different curvatures, generally including compound circular curve (Figure 2.8), double-easement curve type (Figure 2.9), "circular + easement" curve type (Figure 2.10), and "easement + circular + curve" type (Figure 2.11). The compound curve can be used in conjunction with straight or curved switch rails. If the common tangent points of a compound curve are set at or in the rear of the heel of the switch rail, turnouts of different numbers can be provided with the same switch structure. This line type is commonly used for German high-speed turnouts [25].

The compound circular curve is composed of several circular curves of different radii, mainly used in small number turnouts. Large radii circular curves are usually used for switches to reduce the angle of attack when a train travels from the turnout rear. Small radii circular

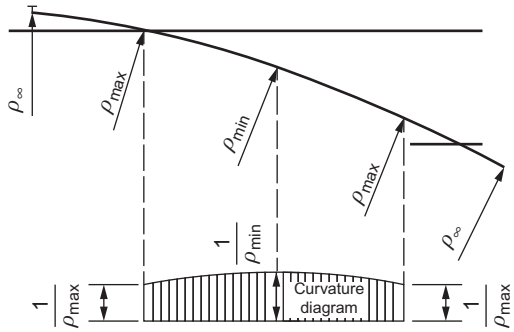

FIGURE 2.9

Double-easement curve type.

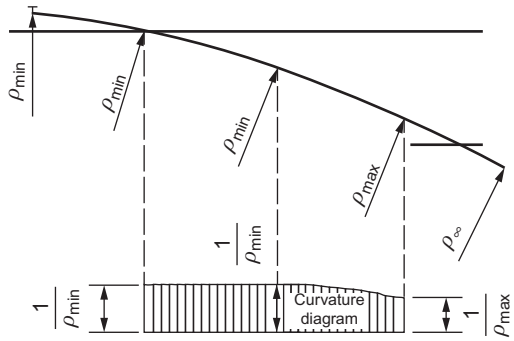

FIGURE 2.10

"Circular + easement" curve type.

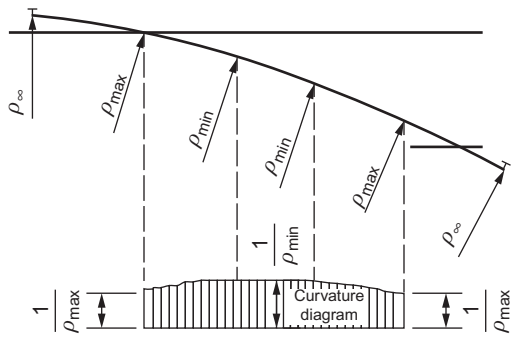

FIGURE 2.11

"Easement + circular + easement" curve type.

curves are usually used for switches to ease side wear and to enhance the firmness of the switch rail. As the regularity in the diverging line is poor, this line type is rarely used in high-speed turnouts.

Generally, the ending points of double easement curves are connected. The front easement curve originates from the switch, and the rear easement curve originates from the crossing. This curve type is able to reduce the angle of attack when a train accesses a turnout, and is commonly used in large number turnouts. Limited by the length of a turnout, design and manufacturing difficulties of the switch rail, and excessive long weak section at the front end, the origins of double easement curves will generally not be connected [26].

The "circular curve + easement curve" line type is used for the switch, wherein the switch rail features a simple design and easy manufacture, shorter weak section at the front end, and high wear resistance. The easement curve is adopted for a transition lead curve and crossing; it is able to improve the riding quality in the diverging line, and is mainly used for large number turnouts in China and France.

For the "easement curve + circular curve + easement curve" line type, easement curves are for the switch and the crossing, and the circular curve for transition lead curve. This line type is used mainly for large number high-speed turnouts in France; they may enhance the firmness and wear resistance of the switch rail in conjunction with gauge widening technology following the bending of stock rail. But it is rarely used in other countries.

In order to avoid vibration superposition on curves, the length of each component of compound curve should be larger than the distance that a train may travel in 1 s. Thus, the line types for a compound curve shall match with the length of turnouts and speeds in the diverging line.

2.2.3 SWITCH RAILS

Switch rail is an important component of the switch, which guides trains to the main line or the diverging line through lining. The plane line types of the switch rail fall into straight and curved types [27].

In the past, No. 12 and below turnouts used in Chinese railways were all of straight switch rails, as shown in Figure 2.12. Straight switch rails are characterized by easy manufacture and replacement, less cutting at front tips, large lateral stiffness, small swing and heel end flangeway, firm sections, and strong wear resistance, as well as compatibility with both left- and right-hand turnouts. However, the working surface of this kind of switch rail is in a straight line, and the angles of actual point, switch, and impact are equal. Thus, trains may produce a great impact force on switch rail, jeopardizing running quality in the diverging line.

Since the speedup of Chinese railways in 1996, straight switch rails have been applied to the main line of new No. 12 turnouts and above, and curved switch rails to the diverging line. The curved switch rail is conductive to high-speed traffic due to the small angle of attack, large radius of the transition lead curve, and stability of trains when accessing the diverging line. However, the curved switch rails are characterized by a complex manufacturing process, large cutting amount at front tips, and noninterchangeability of left- and right-hand turnouts. The line types for curved switch rail are tangent, semi-tangent, secant, semi-secant, and separated semi-tangent types, as shown in Figures 2.13–2.17 [28].

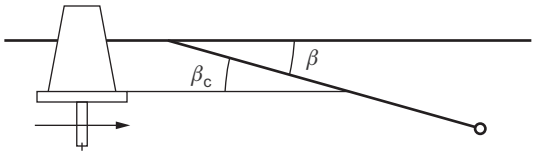

FIGURE 2.12

Straight switch rail.

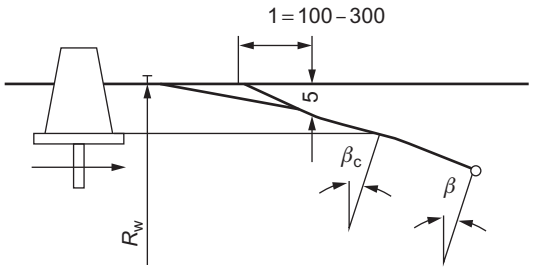

FIGURE 2.13

Tangent curved switch rail.

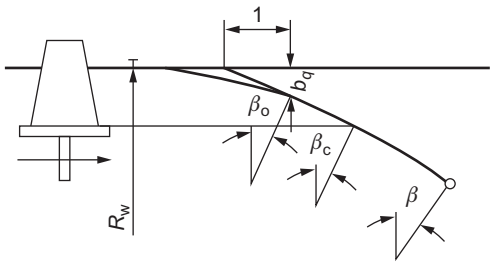

FIGURE 2.14

Semi-tangent curved switch rail.

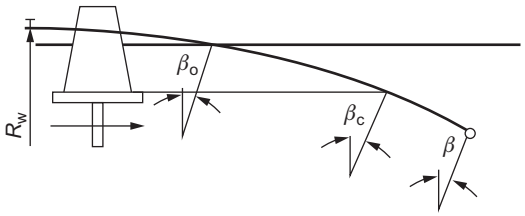

FIGURE 2.15

Secant curved switch rail.

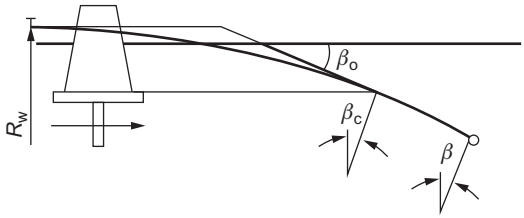

FIGURE 2.16

Semi-secant curved switch rail.

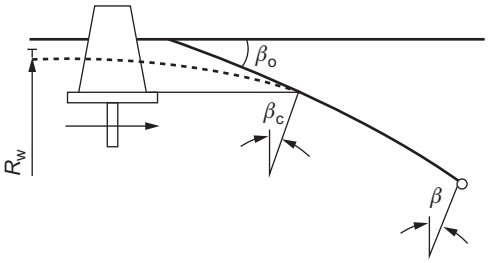

FIGURE 2.17

Separated semi-tangent curved switch rail.

The working surface of a tangent curved switch rail is tangent to the stock rail at the theoretical origin. In practice, in order to strengthen the actual point and shorten the switch rail, a 100−300 mm long straight section will be installed ahead of the 5 mm wide section of switch rail (the straight section is not tangent to the curved section). Compared with the single turnout adopting a straight switch rail with the same number, the radius of the transition lead curve for a tangent curved switch rail may be significantly increased, and the full length of a turnout can be significantly shortened. For a normal clearance between wheel flange and gauge line (standard track

gauge, wheel flange thickness, and wheel back-to-back), a curved switch rail may have a smaller angle of attack and gauge widening amount at the actual point, providing better riding quality. However, this line type requires a longer switch rail and has longer weak parts, and the switch rails for the left- and right-hand turnouts cannot be interchanged. This line type was used in the early Chinese speed-up turnouts. However, if a train travels from the turnout front in the diverging line, the switch rail is prone to severe side wear and spalling due to the close contact between external wheels and the curved switch rail and the long weak section, which affects the normal service life. Consequently, this line type is less favored now.

The semi-tangent curved switch rail is also tangent to the stock rail at the theoretical origin. However, the tangent is set at a cross section (top width under 40 mm typically) of the switch rail, and the front tip will be straight. Similar to the tangent curved type, the radius of the transition lead curve may be increased, and the full length of a turnout may be shortened. The switch rail and cutting parts of the switch rail are shorter than those of the tangent type, but longer than those of the straight type. The track gauge at the switch rail's actual point is shorter than that at the straight switch rail, but longer than that at the tangent curved switch rail. The switch rails at the left- and right-hand turnouts cannot be interchanged. In normal conditions, the angle of attack of the switch rail is equal to that of the semi-tangent curved part, but larger than that of the tangent curved switch rail. Thus, this line type is characterized by poor riding quality, but favorable wear resistance owing to the firmer switch rail. In general, this line type outperforms the tangent curved switch rail, so it is widely used in China.

The secant curved switch rail is tangent (negatively secant) to a straight line outside the stock rail at the theoretical origin. Compared with the tangent or semi-tangent types with the same number, it has a relatively larger radius in the transition lead curve, and shorter full length in a turnout. The track gauge at the switch rail's actual point is smaller than that at the straight switch rail and semi-tangent curved switch rail, but larger than that at the tangent curved switch rail. The actual point of the switch rail is easy to wear, owing to the small actual point angle and large angle of attack. Moreover, trains are easy to shake when traveling from the turnout rear in the diverging line. The switch rails at the left- and right-hand turnouts cannot be interchanged. This curved switch rail was applied in China's early conventional turnouts, but through comprehensive comparison, such switch rails have no prominent advantages, and are rarely used now.

The semi-secant curved switch rail is secant to the stock rail. The tangent is set at a part of the switch rail, and the straight line is adopted at the front tip, the same as for the semi-tangent curved switch rail. This line type has the following features: shortest switch rail and weak parts, and minimum theoretical full length of the turnout among these types. Compared with the secant switch rail, the angle of attack and firmness of semi-secant curved switch rails are increased. The line type is usually used in small number turnouts for slower speeds in the diverging line to maximally increase the radius of the transition lead curve, improve the internal inscribing conditions for large locomotives, or minimize the full length of turnouts.

The separated semi-tangent curved switch rail is tangent to a straight line on the inner side of the stock rail at the theoretical origin. The tangent is set at a part of the switch rail, and the straight line is adopted at the front tip. Compared with the curved switch rails of other line types, this line type has a smaller radius in the transition lead curve and a larger angle of attack; nevertheless, it has maximum firmness and wear capacity. This switch rail has a longer service life in the mixed passenger and freight railways of China, and is widely used.

The selection of plane line type of switch rail is determined by turnout geometry control, riding quality, wear resistance of the switch rail, simple processing and manufacturing techniques, easy maintenance, repair, and supply of raw materials, etc. If there are no limitations on turnout dimensions and radius of the transition lead curve, and trains travel stably, the separated semi-tangent curved switch rail is more suitable to the running conditions of mixed passenger and freight railways. Therefore, this line type is used for curved switch rails of Chinese high-speed turnouts.

2.2.4 CLEARANCES [29]

In a turnout, certain structural spaces (clearances) shall be reserved to ensure unrestricted passage of vehicles. If clearances are incorrect, the wheels may collide with the rails or rail wear may be worsened; even derailment may occur.

1. Calculation methods and parameters

   The most unfavorable combination method is adopted for calculating turnout clearances, that is, in calculating the clearances of a turnout, the most unfavorable conditions of the influential factors will be taken into account. The calculation method can ensure the safe passage of the wheelset at this part under the worst conditions; however, in this case, the clearances may be too large or small, so that trains may shake significantly when passing through the turnouts. In this case, turnout clearances may be determined by probabilistic methods.

   In calculating the turnout clearances, the impacts of elastic deformation of gauge or wheelset under dynamic load may also be considered, in addition to the upper/lower limits of the gauge and wheelset dimensions.

   For Chinese rolling stock and standard gauge, the parameters used for clearance calculation are given in Table 2.1.

   The above parameters are not all practical for HSRs, as EMU wheels require higher manufacturing precision than the average wheelset and shorter maintenance periods, but may hardly exhibit the worst values as shown in the table above. Moreover, high-speed turnouts outperform common ones in structural stability, follow stricter maintenance standards, and have smaller dynamic and static gauge deviations. Therefore, it takes time to obtain and improve the recommended values of parameters for calculating turnout clearances.

2. Clearances at the switch

   Clearances at the switch include flangeways at switch heels in main/diverging lines, the minimum flangeway of curved switch rails, and throw of switch.

   a. Flangeway at switch heel

   The flangeway at the switch heel in the main line shall ensure safe traveling of the wheelset under the most unfavorable conditions, that is, the flange on one side can pass through the rail smoothly without impacting the heel of the switch rail in the diverging line when the opposite flange clings to the switch rail in the main line, as shown in Figure 2.18. This is expressed by:

$$t_h \geq (S_h + \varepsilon_3 + \varepsilon_4) - (T_{min} - \varepsilon_2) - d_{min} \tag{2.1}$$

   where S_h is the gauge at the switch heel in the main line given a standard gauge, $t_h = 70$ mm.

Table 2.1 Parameters for Calculation of Turnout Clearances

SN	Parameter		Symbol	Calculated Value (mm)
1	Maximum gauge		S_{max}	1456
2	Minimum gauge		S_{min}	1433
3	Maximum wheel back-to-back		T_{max}	1356
4	Minimum wheel back-to-back		T_{min}	1350
5	Maximum flange thickness	Steam locomotives	d_{max}	33
		Other rolling stock		32
6	Minimum flange thickness	Rolling stock	d_{min}	23
		EMU driving wheel		22
7	Dynamic increment of wheel back-to-back when the wheelset bends under load	Steam locomotives	ε_1	2
		Other rolling stock		0
8	Dynamic decrement of wheel back-to-back when the wheelset bends under load	Steam locomotives	ε_2	0
		Other rolling stock		2
9	Dynamic widening amount of gauge		ε_3	2–4
10	Positive gauge tolerance		ε_4	3
11	Negative gauge tolerance		ε_5	2
12	Lateral wear value of check rail		δ_h	2

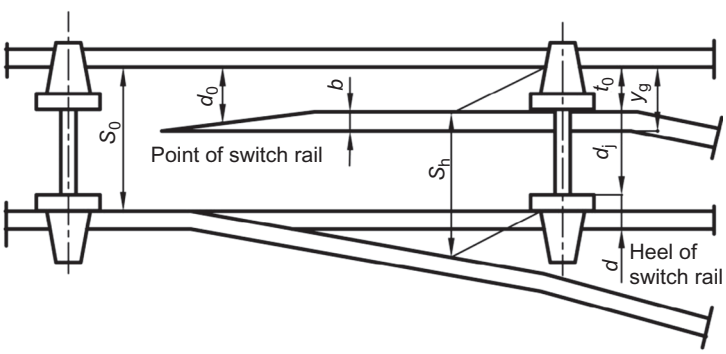

FIGURE 2.18

Clearances at the switch.

The flangeway at the switch heel for curved switch rails shall not be less than the flangeway at the switch heel for straight switch rails generally. The width of the flangeway at the switch heel is a control factor in determining the length of switch rails. Therefore, provided that the wheelset can travel safely, the flangeway shall not be too wide, so as not to unnecessarily increase the length of switch rails.

b. Throws of switch

Throws of switch shall ensure that the wheelset will not apply lateral stress on nonworking surfaces of the switch rail when the switch rail is in reverse position, that is,

$$d_0 \geq t_h + b_0 + (S_0 - S_h) \tag{2.2}$$

where b_0 is the railhead width of switch rails at rod center and S_0 is the track gauge at rod center.

The actual throw at the switch rod depends on the throw of the switch machine. The throw at the first traction point is taken as 160 mm. The throws at other traction points and the spread of the switch rail can be obtained based on the throw at the first rod of the switch rail and switch rail length, depending on the line type of the open switch rail.

c. Minimum flangeway of curved switch rails

The minimum flangeway of curved switch rails shall ensure safe traveling of the wheelset under the most unfavorable conditions, that is, the flange on one side can pass through the rail safely without impacting the nonworking surface of the switch rail when the opposite flange clings to the switch rail in the main line, that is,

$$t_{min} = (S + \varepsilon_3 + \varepsilon_4) - (T_{min} - \varepsilon_2) - d_{min} \tag{2.3}$$

where S is the gauge at the minimum flangeway. The minimum flangeway is a control factor in determining the length of the curved switch rail. Just as with the flangeway at the switch heel, the flangeway shall not be so wide as to shorten the switch rail length. Empirically, the minimum flangeway can be taken as 65 mm.

3. Clearances at the crossing and check rails

Clearances at the crossing and check rails include the check gauge of crossing, flangeways at the crossing throat, crossing, straight segment of check rails, and buffer segment of wing and check rails.

a. Crossing check gauges

Crossing check gauges shall ensure the distance between the working surfaces of the point rail and the check rail under the most unfavorable conditions for the wheelset. If the wheelset travels on the rail, the wheel on one side will not impact the frog when the opposite wheel is restricted by the check rail. Meanwhile, the check gauges shall ensure the distance between the working surfaces of the wing rail and the check rail under the most unfavorable conditions. The traveling wheelset will not be blocked between wing rails and check rails, as shown in Figure 2.19, that is,

$$\begin{aligned} D_1 &\geq (T_{max} + \varepsilon_1) + d_{max} \\ D_2 &\leq T_{min} - \varepsilon_2 \end{aligned} \tag{2.4}$$

$D_1 \geq 1391$ mm and $D_2 \leq 1348$ mm are obtained through calculation. The two values are the minimum and maximum allowable values for maintenance of turnouts, respectively, and have no positive or negative tolerances.

In case of gauge widening at the crossing, the straight section of the check rail shall be widened accordingly to maintain the check gauges and crossing flangeway.

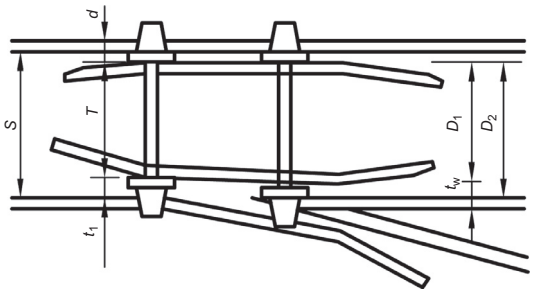

FIGURE 2.19

Check gauges (D_1, D_2).

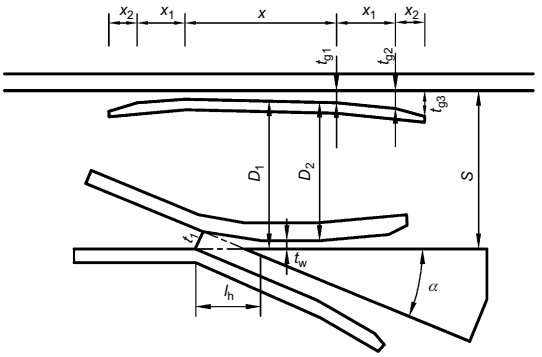

FIGURE 2.20

Geometry sizes of check rails.

b. Flangeway at straight section of check rails

The flangeway shall satisfy the requirement for check gauges at the crossing, $D_1 \geq 1391$ mm, as shown in Figure 2.20, that is,

$$t_{g1} \leq S - D_1 - \delta_h \tag{2.5}$$

The calculated value is 42 mm. In the case of gauge widening at the crossing, the flangeway at the straight segment of the check rail shall also be widened.

c. Flangeway at the crossing

For a given flangeway at the straight segment of the check rail, the crossing flangeway shall allow the unrestricted passage of the wheelset with minimum wheel back-to-back, and can satisfy the requirements for crossing check gauge $D_2 \leq 1348$ mm, that is,

$$t_w \geq S - (D_2 + t_{g1}) \tag{2.6}$$

The calculated value shall be greater than 45 mm, while 46 mm is generally taken in the design. The minimum crossing flangeway width shall be adopted to ease the wear of point rails and wing rails.

d. Flangeway at crossing throat

The flangeway shall ensure safe passage of the wheelset under the most unfavorable conditions, that is, the wheel on one side can pass through the rail safely without impacting the bending point at the throat of the wing rail when the opposite wheel is in close contact with the stock rail, that is,

$$t_1 \geq (S + \varepsilon_3 + \varepsilon_4) - (T_{min} - \varepsilon_2) - d_{min} \tag{2.7}$$

The calculation result is the same as that of the flangeway at the switch heel; however, the value is taken as 68 mm in practice. In the case of gauge widening at the crossing, the flangeway at the crossing throat shall be widened accordingly. For a swing nose crossing, this value is much greater than for a fixed crossing to ensure the throw at the first traction point on the point rail.

e. Flangeway at the end of buffer segments of wing and check rails

This flangeway shall allow the passage of the wheelset under the same conditions as with the flangeway at crossing throat, that is,

$$t_{g2} = t_1 \tag{2.8}$$

This value is also taken as 68 mm in practice. In the case of gauge widening at the crossing, the flangeway at buffer segments of wing rails and check rails shall be widened accordingly.

f. Flangeway at the end of spread sections of wing rails and check rails

This flangeway shall ensure the safe passage of the wheelset without impacting the spread at the end of wing rails and check rails at the maximum permissible track gauge, while taking all tolerances into consideration, that is,

$$t_{g3} \geq (S_{max} + \varepsilon_3) - (T_{min} - \varepsilon_2) - d_{min} \tag{2.9}$$

The calculated value is 88 mm, but the value is taken as 90 mm in practice. In the case of gauge widening at the crossing, this flangeway shall also be widened.

g. Throw of swing nose rails

The throw of swing nose rails shall ensure that sufficient flangeway is reserved at each part of the point rail to prevent the wheelset from impacting the working surface of the point rail. In addition, the actual throw of point rail shall be compatible with the throw of conversion equipment. Generally, the throw at the first traction point on the point rail is taken as 90 mm; however, this value has been increased to 120 mm to facilitate the installation of an external locking device.

2.2.5 GEOMETRIC SIZES

1. Switch

The geometric sizes of switches with curved switch rail mainly include lengths of curved switch rails and straight switch rails, lengths of the front end and rear end of the stock rail, and radii of curved switch rails.

a. Radii of curved switch rails

The radii of curved switch rails shall be determined in conjunction with the radii of transition lead curves, and the number and geometry type of the crossing as per the following procedures: First, determine the desired curve radius as per the required permissible speed in the diverging line and inscribing requirements for rolling stock, and round it off; second, obtain the number of a turnout with certain type of crossing (straight or curved) (note: Chinese prefer turnouts with integral numbers, while in other countries the turnouts may be expressed by the ratio or tangent value of the crossing angle, and therefore nonintegral numbers may be used); finally, check the feasibility of the radius. For a straight crossing, the straight segment in the front of the crossing shall meet:

$$K = \frac{S - R_w(1 - \cos\alpha) + f_1}{\sin\alpha} \geq K_{min} \tag{2.10}$$

where R_w is the radius of the circular curve, α is the crossing angle, f_1 is the secant distance of the switch rail (0 for the tangent type, and negative for the separated type), and K_{min} is the minimum straight segment required in the front of the crossing (requirements: must be capable of providing sufficient space for installing a fishplate at the toe end of the crossing for jointed turnout, provided that the end point of the transition lead curve does not extend to the check rail; in this way, rolling stock with the maximum rigid wheel base can pass through the crossing safely; moreover, must be capable of maintaining the straight segment in front of the crossing within the desired range by adjusting the curve radius).

For curved crossing, the heel spread shall satisfy:

$$P_m = R_w(1 - \cos\alpha) - f_1 - S \geq P_{m\,min} \tag{2.11}$$

where $P_{m\,min}$ is the heel spread of the curved crossing (requirements: must be capable of providing sufficient space for installing a fishplate at the heel of the jointed turnout or fillers for a jointed turnout; and must be capable of maintaining the spread at the heel of the crossing within the desired range by adjusting the curve radius or crossing angle).

If the turnout is not of the single circular curve type, the equation for computational check can also be derived with the above two equations. The relationship between turnout number (N) and crossing angle can be described by:

$$N = ctg\alpha \tag{2.12}$$

b. Angle of point of switch rail

To avoid an extremely thin point of switch rail and maintain proper stiffness, a curved switch rail may generally originate from a segment in the rear of the theoretical origin of the curve, wherein the longer the segment, the greater the angle of the point of switch rail, and the greater the stiffness. However, an oversized angle of point of the switch rail may lead to violent shaking of trains traveling from turnout rear, and in addition, may make it harder to keep the track gauge at the point of the switch rail and track alignment. Overall, the selected angle of the point of curved switch rail must ensure that for the wheelset with maximum wheel−rail clearance that travels from the turnout rear, the plane angle formed by wheel−rail collision shall not be larger than the permissible angle of attack; and the gauge widening at the point of the switch rail shall not be out of gauge.

To satisfy the above, the maximum secant distance (f_1) and the railhead width (b_q) at the actual origin of switch rail curve shall be controlled.

c. Length of curved switch rails

The minimum flangeway between the curved switch rail (open) and stock rail is not located at the heel, but in the middle of the switch rail.

The minimum flangeway shall be regarded as the controlling factor for calculating the length of a curved switch rail. Two calculation methods are generally accepted. One is to obtain the shortest length of curved switch rail based on the minimum flangeway t_{min}; the other is to calculate the length of the switch rail by assuming the offset of switch heel of the switch rail, obtain the position with the minimum flangeway, and check whether the minimum flangeway is desirable. The above two methods are based on the sub-triangular proportional relationship and are applicable to calculating the length of the switch rail of other curve types.

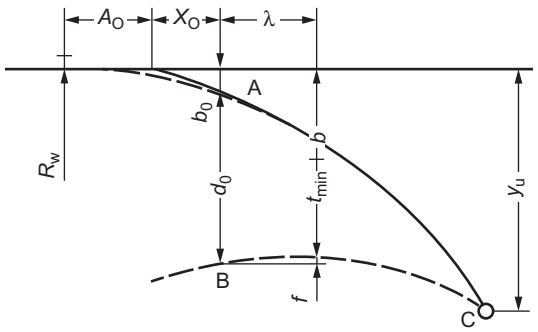

FIGURE 2.21

Semi-tangent circular-curved switch rail.

For the semi-tangent circular-curved switch rail shown in Figure 2.21, the switch angle at point of switch rail is

$$\beta_0 = \cos^{-1}\left(\frac{R_w - b_q}{R_w}\right) \tag{2.13}$$

The distance between the theoretical origin and actual point of curved switch rail is:

$$A_0 = R_w tg\beta_0/2 \tag{2.14}$$

Given that the top width of the switch rail at the minimum flangeway is b when the curved switch rail is in the open position, the rise of the curve at this part is:

$$f = (d_0 + b_0) - (t_{min} + b) \tag{2.15}$$

The distance between the minimum flangeway and the first traction point is approximated as:

$$\lambda \approx \sqrt{2R_w f} \tag{2.16}$$

Given $M = t_{min} + b - ((A_0 + x_0 + \lambda)^2/2R_w)$, the length of the shortest curved switch rail is:

$$l_{0\ min} = \frac{x_0 M - d_0(\lambda + x_0)}{M - d_0} \tag{2.17}$$

If the switch rail is of flexible heel structure, the length of the switch rail shall be 1.5−2.5 m longer than the calculated value. With the actual length, the actual switch angle of the switch rail can be obtained by:

$$\beta = \beta_0 + \frac{l_0 - A_0}{R_w} \cdot \frac{180}{\pi} \tag{2.18}$$

The actual offset y_u of the switch heel is thereby obtained, as shown by:

$$y_u = R_w(1 - \cos\beta) \tag{2.19}$$

For the switch of a curved switch rail, the length of horizontal projection of the curved switch rail from the actual point to the heel can be taken as the length of straight switch rail,

so that the actual points and heels of the two switch rails are aligned. The length of straight switch rail is:

$$l_0' = \frac{b_q}{tg\beta_0} + R_w(\sin\beta - \sin\beta_0) \tag{2.20}$$

d. Front length of stock rail

When an existing turnout is to be replaced with a new one with the same number, the two turnouts shall have equal total length. The new turnout with equivalent front length is preferred. If the new turnout has a longer front end, it is recommended to appropriately reduce the q value by easing the angle of point of the switch rail or enlarging the radius of transition lead curve, which is contributive to ride quality. Or, if the new turnout has a shorter front end, the front end cannot be shorter than 1/2 of the fishplate or the 10−15 mm expansion range reserved for the switch rail for a jointed turnout, nor can it be shorter than the heat-affected zone of a weld region and 20−25 mm expansion range reserved for the switch rail for CWR turnout.

The front length of the stock rail shall take the reasonable arrangement of turnout ties into consideration to avoid unexpected changes to tie spacings in the front end of the stock rail. Otherwise, the tamping and maintenance work may be affected. With regard to the stability of the line, a greater q value is conductive to the stability of joints in turnout front, maintaining turnout gauge and alignment, and closure between the switch rail and the stock rail.

All high-speed turnouts are applied to trans-sectional CWR tracks. The turnout rails will be welded with section rails; therefore, the stock rails at the turnout front can be shortened to about 600−1500 mm. Meanwhile, it shall be considered that the distance from the point of the switch rail to the tie immediately in the rear shall reserve sufficient space for the expansion of the switch rail and installation of rollered slide plate, which can be taken as 120 mm. Overall, the front length of the stock rail is taken as 1955 mm for Chinese high-speed turnouts.

e. Rear length of stock rail

The rear length of the stock rail q' shall satisfy the requirements for the heel structure of the switch rail, tie arrangement, and track distribution of a turnout. For a CWR turnout, since the maximum additional expansion force of the stock rail may occur at the corresponding part of switch rail heel, the rear length of the stock rail can be prolonged appropriately to avoid fracture of welded joints on stock rails at this part.

2. Swing nose crossing

The main dimensions of fixed crossings include the toe distance (n) and heel distance (m) of the crossing, while the main dimensions of swing nose crossings include throat width, lengths of long/short point rails, and the flangeway width of wing rails.

a. Crossing throat width

The throat width of acute crossing with a swing nose rail is the throw at the theoretical point of swing nose rail; therefore, it shall be within the permissible scope of the throw of switch machines (90−165 mm). An excessively wide throat may increase the crossing length unnecessarily. The position of the theoretical point of the point rail for high-speed turnouts is dependent on the spread throw and tie arrangement of electrical parts. The preferred value for the spread of the theoretical point of the point rail is about 100−120 mm. For No. 62 turnouts in China, to reduce railhead width at the traction point and avoid premature stress

on the point rail, the theoretical throat width of the crossing is taken as 117 mm, located within 100 mm of the center of the next turnout tie. Moreover, with horizontal hidden tip point structures, a 10 mm or so railhead width is reserved at the traction point, facilitating the inspection of electrical devices and reducing the cutting amount at the base of wing rails. The flangeway width at the end of a short wing rail (t_{g2}) (also the swing scope of a long point rail at this part) shall not be less than 68 mm, and the spread at the end of a short wing rail (t_{g3}) shall not be less than 90 mm. Considering the transmission of temperature force in CWR turnouts, a long wing rail will be used, which bends from the throat to the porous filler at the end of the point rail; in addition, the flangeway width at the end of wing rails is about 150 mm, limited by filler size.

b. Length of long point rail

Selection requirements for the length of long point rail are: The actual point of the point rail shall be set at a section with top width of 5−10 mm or at 100 mm away from the throat to prevent the switch rail extending beyond the throat due to the expansion and creep of the point rail; the distance between rod center and the flexible center of the point rail should not be shorter than 6 m to avoid excessive or reverse conversion; the length from the flexible center to the heel of the point rail shall be sufficient to install joints at the heel for jointed turnouts and to install porous stress-transferring fillers for CWR turnouts; the turnout ties must be reasonably arranged. The cutting amount for the flexible part of a long point rail can be calculated with reference to the flexible center of switch rails.

c. Length of short point rail

For point rails with a single flexible rail, if the front of the short point rail starts from the origin of cutting of the railhead of the long point rail, the distal end shall be aligned with the flexible center of the point rail. If the stock rail at the crossing heel serves as the diagonal joint, the angle at the end of the short point rail can be equivalent to the angle of the working surface of the point rail. If the pointed rail at the crossing heel is served as the diagonal joint, the bending angle at the end of the short point rail can be equivalent to the angle of the working surface of the point rail. The slippage at the end of short point rail is:

$$\Delta l \approx \frac{p'_{\mathrm{m}} t_1}{x_{\mathrm{m}}} \tag{2.21}$$

where p'_{m} is the offset distance at the flexible center of the long point rail, x_{m} is the distance between the flexible center of the long point rail and crossing throat, and t_1 is the width of the crossing throat.

d. Length of check rails

The length of the straight segment of check rails of straight crossing equals the length from the crossing throat to the frog, with a top width of 50 mm, plus 100−300 mm respectively on both ends.

The length of buffer segment shall be determined as per the flangeway width at both ends, and the length of spread section is about 100−150 mm. Generally, the angle of attack at the buffer segment of check rails (β_{c}) is equivalent to the angle of attack of switch rails.

For turnouts with speed in the main line far above the speed in the diverging line, long check rails with unequal lengths can be provided in both lines to reduce the angle of attack of straight check rails. The bending point at both ends of the straight segment of check rails

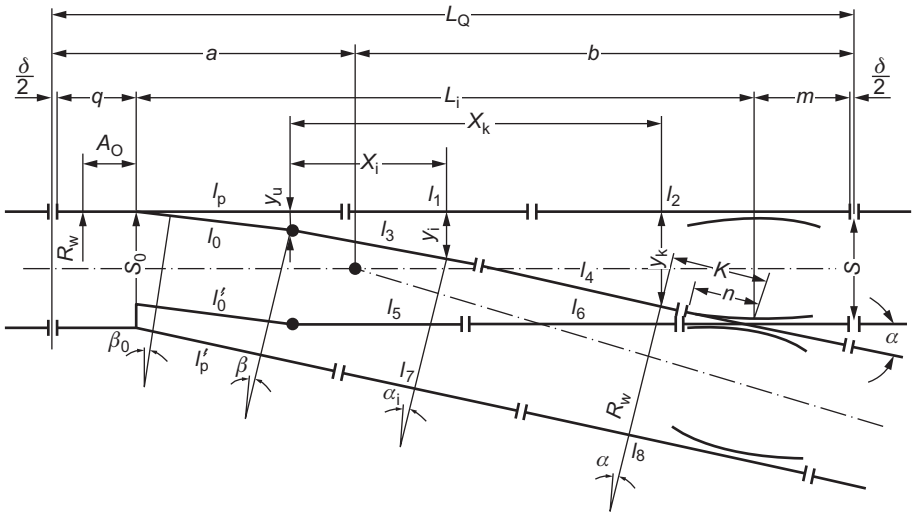

FIGURE 2.22

Calculation of sizes in general plan of turnout.

shall not be set on the turnout ties as far as possible to facilitate arrangement of rail braces. Both ends of check rails should be rested on the turnout ties instead of being unsupported. If the above requirements cannot be satisfied, the roundoff of the straight section may be adjusted, or the angle of attack at the buffer segment may be appropriately modified, or the length of the spread section may be altered.

3. General plan of turnout

The main dimensions in the general plan of turnouts include the front length of the turnout (a) (from the front rail-gap center of turnout to turnout center), rear length of turnout (b) (from turnout center to the rear rail-gap center of turnout), theoretical total length of turnout (L_t) (the distance between the theoretical points of switch rail and crossing), and actual total length of the turnout (L_Q) (the distance between front and rear rail-gap centers of turnout). See Figure 2.22 for calculation of the tangent and semi-tangent curved switch rails and straight crossings.

Projecting the working surface of the exterior track of transition lead curve onto the main line centerline, one gets:

$$L_t = R_w \sin\alpha + K\cos\alpha - A_0 \tag{2.22}$$

and, projecting it onto the vertical line of the main line centerline:

$$S = R_w(1-\cos\alpha) + K\sin\alpha \tag{2.23}$$

So, the main sizes of a turnout can be obtained by:

$$K = \frac{S - R_w(1-\cos\alpha)}{\sin\alpha} \geq K_{min} \tag{2.24}$$

$$R_w = \frac{s - K\sin\alpha}{1-\cos\alpha} \tag{2.25}$$

$$L_Q = q + L_t + m + \delta \tag{2.26}$$

$$b = \frac{S}{2tg(\alpha/2)} + m + \frac{\delta}{2} \tag{2.27}$$

$$a = L_Q - b \tag{2.28}$$

The equations can be selected as per given conditions. The calculations of sizes in the general plan of other plane line types are similar.

2.3 DESIGN OF PARAMETERS

For plane line type design of turnouts, the following three fundamental parameters can be used to define the adverse impacts of lateral forces produced by trains traveling in the diverging line: dynamic energy loss, unbalanced centrifugal acceleration, and its increment [1].

2.3.1 METHOD BASED ON PARTICLE MOTION

1. Dynamic energy loss

Assuming that the mass of the carbody is constant before and after collision, which can be approximated as a particle acting on the impact area, while the elastic deformation of the turnout after impact is ignored, the dynamic energy loss during vehicle−rail collision will be in direct proportion to the square of the speed loss of the carbody.

As shown in Figure 2.23, after the collision of the wheelset and straight switch rail at point C, the running direction is forced change from $\overrightarrow{AC}$ to $\overrightarrow{CB}$, and the running speed from V to $V\cos\beta'$ (where β' is the angle of attack), and the speed loss is $V\sin\beta'$. Therefore, the dynamic energy loss of collision is:

$$\Delta\omega = \frac{1}{2}V^2\sin^2\beta' \tag{2.29}$$

When a car approaches the switch with a straight switch rail from turnout rear, since the angle of attack (β') is equal to the switch angle (β), the dynamic energy loss is:

$$\omega = V^2\sin^2\beta \tag{2.30}$$

Figure 2.24 depicts how the clearance δ between the flange and gauge line relates to the curve radius R and angle of attack β' when a car collides with the tangent circular-curved switch rail from the straight segment.

$$\delta = R(1-\cos\beta') = 2R\sin^2\frac{\beta'}{2} \tag{2.31}$$

β' is generally small and can be approximated as:

$$\beta' = \sin^{-1}\sqrt{\frac{2\delta}{R}} \tag{2.32}$$

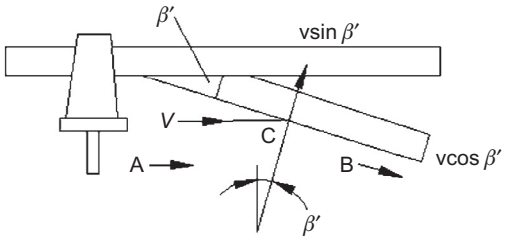

FIGURE 2.23

Angle of attack of straight switch rail.

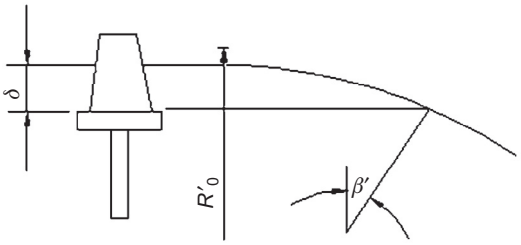

FIGURE 2.24

Angle of attack of curved switch rail.

Substituting the above into dynamic loss equation gives:

$$\omega = \frac{2\delta}{R} V^2 \tag{2.33}$$

For secant and separated tangent circular-curved switch rails, the correction of the secant or separation value f (positive for secant, negative for separation) shall be taken into account in calculating the angle of attack (with Eq. (2.34)). For a semi-tangent switch rail, if the clearance between the flange and gauge line is smaller than the top width of the switch rail at the origin of the semi-tangent curve, the angle of attack shall be calculated as per straight switch rail.

$$\beta = \sin^{-1}\sqrt{\frac{2\delta \pm f}{R}} \tag{2.34}$$

For the switch rail of a cubic parabola easement curve that originates from turnout front, given the clearance δ between the flange and gauge line, radius R at the end of the easement curve, and the length (l_0) of easement curve, β is:

$$\beta = \sqrt[3]{\frac{9\delta^2}{2Rl_0}} \tag{2.35}$$

For the switch rail of a cubic parabola easement curve that ends at turnout front:

$$\beta = \frac{l_0}{2R} - \sqrt[3]{\frac{9\delta^2}{2Rl_0}} \tag{2.36}$$

For secant or separated easement-curved switch rails, similar to circular-curved switch rails, the correction of secant and separation value shall be taken into account.

To avoid excessive dynamic energy loss in wheel−rail collision when a train travels in the diverging line, ω must be confined within the allowable value ω_0.

For Chinese turnouts, the allowable design dynamic energy loss is $\omega_0 = 0.65\ \text{km}^2/\text{h}^2$.

Since the clearance between wheel flange and gauge line is variable due to the hunting movement of trains, the measured dynamic energy loss is also variable. In particular, the calculation is more complicated compared to straight switch rails with the popularization of curved switch rails in turnouts. Dynamic energy loss is still included in the design for turnouts in

China. Nevertheless, it is insignificant and should not be seen as a control parameter. The parameter is basically excluded from the design for high-speed turnouts in Germany, France, and Japan.

The indicator of guidance force in switch rails is introduced in the design for turnouts in Austria to control the angle of attack and wear of switch rails. However, this parameter has not yet been adopted in turnout designs in other countries due to inaccurate calculation of the impact force of the switch rail.

2. Unbalanced centrifugal acceleration

Unbalanced centrifugal acceleration will be generated during passage on transition lead curves, calculated by:

$$\alpha = \frac{v^2}{R} = \frac{gh}{S}(\mathrm{m/s^2}) \tag{2.37}$$

where

v = riding speed (m/s)
R = radius of transition lead curve (m)
g = acceleration of gravity (m/s^2)
h = cant of transition lead curve (mm); and
S = gauge (mm).

When the transition lead curve is not superelevated, only the first term on the right side of the equation is taken during calculation.

To ensure riding quality and passenger comfort, α must be less than the allowable value of α_0.

$\alpha_0 = 0.5-0.65$ m/s^2 in China. This indicator creates a direct link between speed and radius of turnout transition lead curve, capable of reflecting the riding comfort on the circuit curve. Therefore, it is included in the plane design for turnouts in other countries. To improve passenger comfort, the unbalanced centrifugal acceleration for turnouts with high numbers can be taken as 0.5 m/s^2. Since the unbalanced centrifugal acceleration relates to the deficient superelevation Δh, the latter may be included in the design occasionally. For standard gauge turnout, the relationship between the deficient superelevation and the unbalanced centrifugal acceleration can be approximated as $\Delta h = 153\alpha$, and the allowable deficient superelevation is 75−100 mm (taken as 75 mm in China).

3. Increment of unbalanced centrifugal acceleration

The unbalanced centrifugal acceleration will change gradually when a car approaches the circular curve from a straight line; the increment rate is $\psi = \mathrm{d}\alpha/dt$. Meanwhile, ψ must be within the allowable value ψ_0, or $\psi_0 = 0.5$ m/s^3 in China. The variation of unbalanced centrifugal acceleration can be assumed to be completed within the approximate scope of the wheel base of the car. If the transition lead curve is not superelevated, ψ will be:

$$\psi = \frac{\mathrm{d}\alpha}{\mathrm{d}t} = \frac{v^2/R - gh/2}{l/v} = \frac{v^3}{Rl} - \frac{ghv}{ls}(\mathrm{m/s^3}) \tag{2.38}$$

where l is the wheel base of the car (the value differs by country, e.g., 17 m in France, 19 m in Germany, and 18 m in China for an all-metal passenger car), and v is train speed (m/s).

For the turnouts with high numbers, the variation of the unbalanced centrifugal acceleration may not be completed within the wheel base of a car since the switch rails are relatively long.

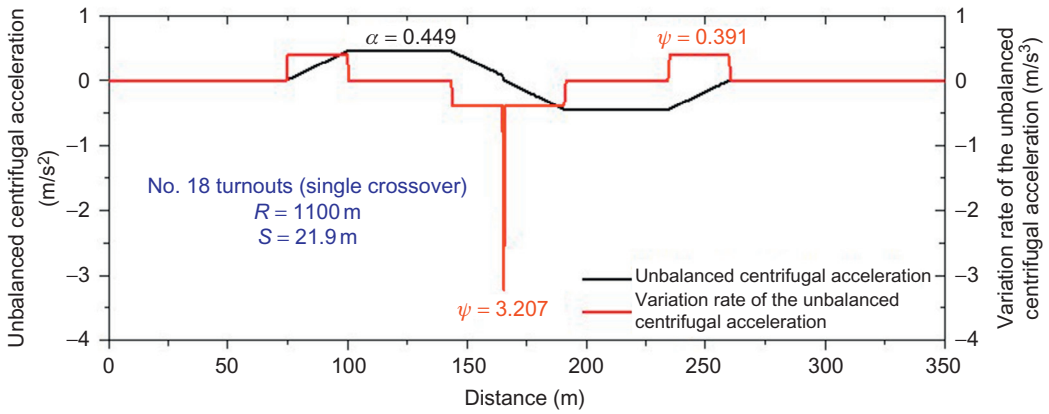

FIGURE 2.25

Circular curve with the intermediate straight line shorter than car length.

For this reason, the allowable limit of the variation rate of the unbalanced centrifugal acceleration can be up to 1.0 m/s^3.

For large number easement-curved turnouts (see Eq. (2.38)), l is the length of the easement curve. Under this circumstance, a stricter standard may be followed, and the allowable limit of the variation rate of the unbalanced centrifugal acceleration is specified as 0.4 m/s^3 in China.

2.3.2 METHOD BASED ON RIGID BODY MOTION

When a train travels in the diverging line, the wheelset may approach a curve from a straight line, or approach a component of compound curve from another component; during this process, α and ψ will change gradually as influenced by car length. Therefore, practically, the impact of car length will be embodied in the calculation result.

2.3.2.1 Application cases

Take No. 18 turnouts, for instance; given the radius of the circular transition lead curve of 1100 mm, car length of 25.5 m, and speed in the diverging line of 80 km/h, if the length of the intermediate straight line between two turnouts is shorter/longer than the car length, the unbalanced centrifugal acceleration and the variation rate of unbalanced centrifugal acceleration after considering the car length are reflected in Figures 2.25 and 2.26.

After considering the car length, while the maximum unbalanced centrifugal acceleration is identical to the calculation result with the fundamental parameter method based on particle motion, the unbalanced centrifugal acceleration is changed gradually when accessing the circular curve, and the variation rate of unbalanced centrifugal acceleration on the circular curve cannot be ignored. If the intermediate straight line is shorter than the car length and the car is traveling on

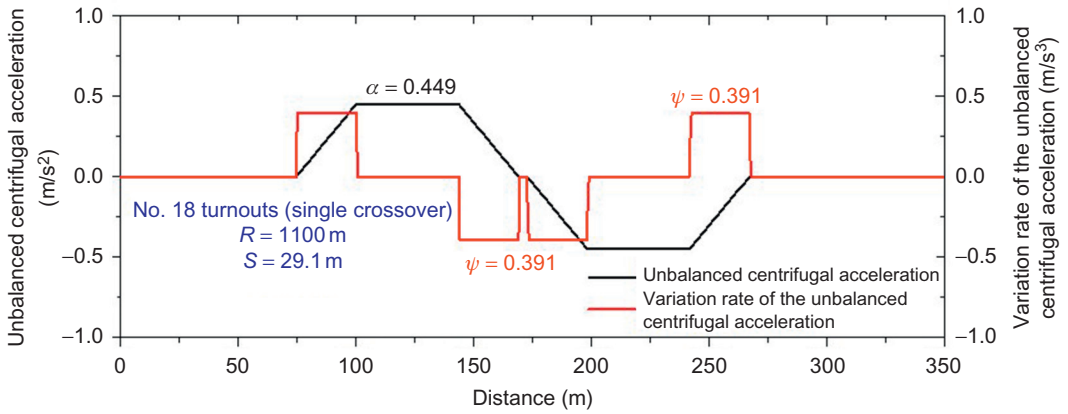

FIGURE 2.26

Circular curve with the intermediate straight line longer than car length.

two circular curves in opposite directions, the calculated variation rate of unbalanced centrifugal acceleration will exceed the allowable limit.

In conclusion, in plane line type designs of turnouts, to avoid vibration superposition of two turnouts, when the opposite curves of two crossover turnouts are connected, a straight segment may be connected directly with the origin of the two opposite easement curves, or interpolated between the two curves. The length of the interpolated straight segment will be determined by half the vibration period, at least $L \geq 0.4V_{\text{diverging}}$, or $L \geq 20$ m (i.e., the wheel base of a car) in unfavorable conditions.

2.3.3 DESIGN SOFTWARE [30]

Turnout plane line type calculation software (TPLCS), as shown in Figure 2.27, has been developed by Southwest Jiaotong University to design and calculate plane line type parameters for turnouts. With the calculated values, the turnout plane line type drawing software (TPLDS) will draw a series of diagrams (including turnout plane line type, corresponding unbalanced centrifugal acceleration, and variation rate, as well as tie arrangement).

Given the fundamental parameters, for a known or unknown turnout number (N), the turnout plane line types of single circular, compound circular, circular + easement, or easement + circular + easement can be calculated with this software based on the speed in the diverging line, distance of two tracks, radius of circular curve, preset length of certain parts of the curve, etc., provided that the unbalanced acceleration and the variation rate of unbalanced acceleration are within limits, and the curve is longer than the traveling distance of the train within the vibration period. This software is designed for circular-curved switch rails and easement-curved switch rails, including five cutting types of switch rails, namely semi-tangent, tangent, semi-secant, secant, and separated semi-tangent. Turnout ties can be laid vertically to the main line, in a fan shape or vertically to the angular bisector in front of and in the rear of the crossing.

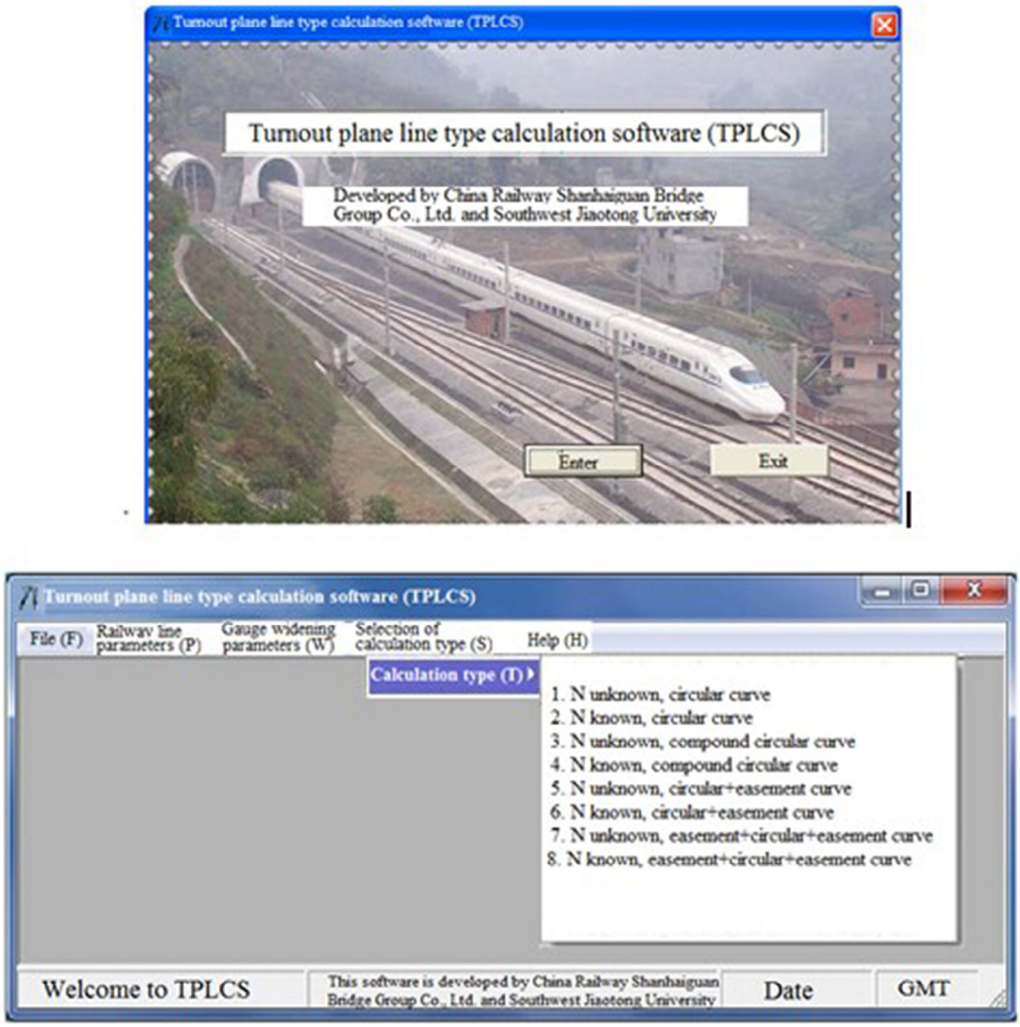

FIGURE 2.27

Turnout plane line type design software.

2.4 ASSESSMENT METHODS BASED ON WHEEL–RAIL SYSTEM VIBRATION [30,31]

2.4.1 THEORY OF WHEEL–RAIL SYSTEM DYNAMICS

The dynamics of wheel–rail system relates to the dynamic interactions between trains and tracks. It is at the core of basic science and technology for railways, providing a theoretical basis for

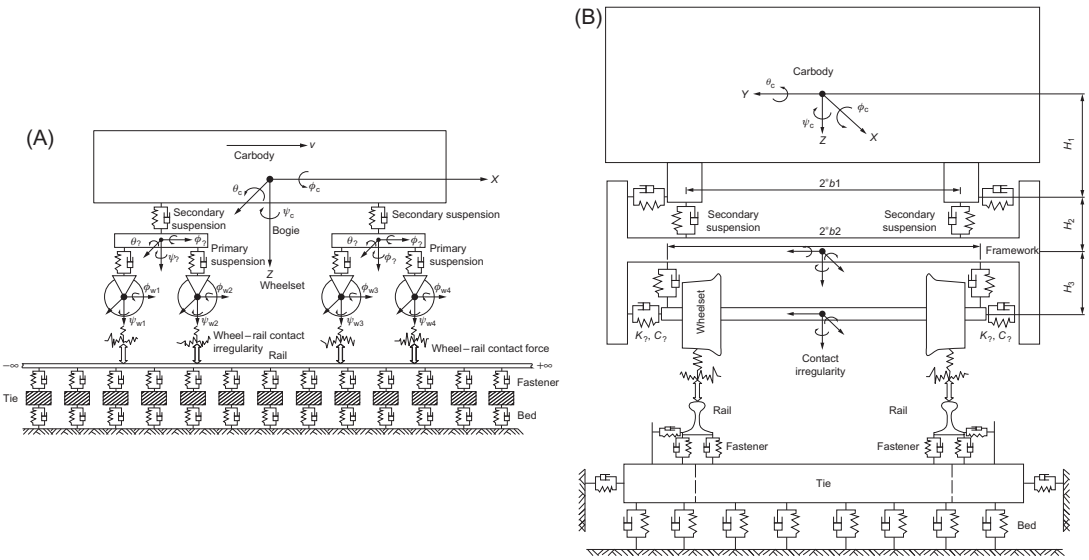

FIGURE 2.28

Model of wheel−rail system dynamics: (A) Longitudinal profile; (B) Transverse profile.

engineering vibration concerning ride safety and quality, reduction of maintenance load, improvement of service life of fixed and mobile equipment, and mitigation of building vibration and environmental noise.

Wheel−rail system dynamics studies the vertical, lateral, and longitudinal coupling vibrations of train and track systems based on wheel−rail interactions. With centuries of development and progress in computational technologies, wheel−rail system dynamics has witnessed the improvement of calculation theory and calculation models, expanding the scope of application. Wheel−rail system dynamics plays an important role in analyzing and assessing ride safety and quality, designing and optimizing trains and track structure, and directing the design and maintenance of track geometry. Undoubtedly, it can be used in directing the turnout plane line type design.

With regard to turnout plane line types, the line types of turnout transition lead curves and switch rails are the dominant factors impacting ride quality and safety. However, track stiffness, wheel−rail relations, geometry, and state irregularities of turnouts are insignificant and may be simplified appropriately in the calculation model; see Figure 2.28. The calculation model can be used to simulate the responses of the lateral vibration acceleration, etc., when a train travels in the diverging line, as well as to compare the advantages and disadvantages of various line types.

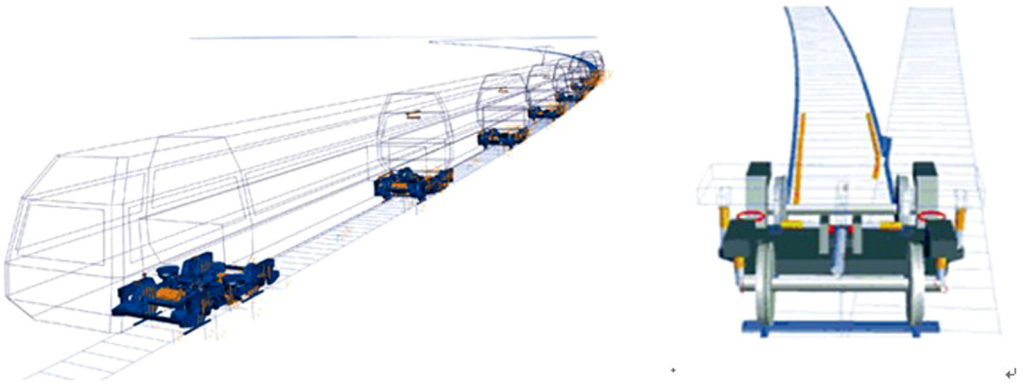

FIGURE 2.29

Application of SIMPACK software in turnout plane line type design.

2.4.2 MULTI-RIGID-BODY DYNAMICS ANALYSIS SOFTWARE

The rapid progress of computer software and hardware technology and the constant interaction of these technologies and application mathematics, multi-rigid-body dynamics, and computer graphics boost the constant innovation and improvement of theories and methods for structural design of modern products.

Since the middle 1960s, the multi-rigid-body system dynamics, based on classical mechanics, has developed into a new branch of dynamics. Multi-rigid-body system dynamics software (e.g., SIMPACK, MSC.ADAMS, DADS, and NUCARS) has been widely studied or applied in car kinematics and dynamics in many countries.

SIMPACK (renamed SIMPACK AG in 2009) is a multi-body dynamics analysis software package designed by INTEC GMBH for simulation analysis of mechanical and M&E system kinematics and dynamics. This software is widely applied in turnout plane line type design; see Figure 2.29.

ADAMS (Automatic Dynamic Analysis of Mechanical Systems) is a virtual prototype analysis software developed by MDI (which has merged with MSC) of the United States. The ADAMS/Rail (railway) module, as shown in Figure 2.30, is mainly used in wheel−rail system dynamics analysis, and was successfully applied in analyzing riding performance on curves or turnouts.

DADS (Dynamic Analysis and Design System) is a multi-body dynamics simulation software used worldwide.

NUCAR (New and Untried Car Analytic Regime Simulation) is a multi-body dynamics simulation calculation program designed to simulate the transient or steady-state responses of railway car models. To consolidate the dynamic performance validation techniques for new and untried cars, in

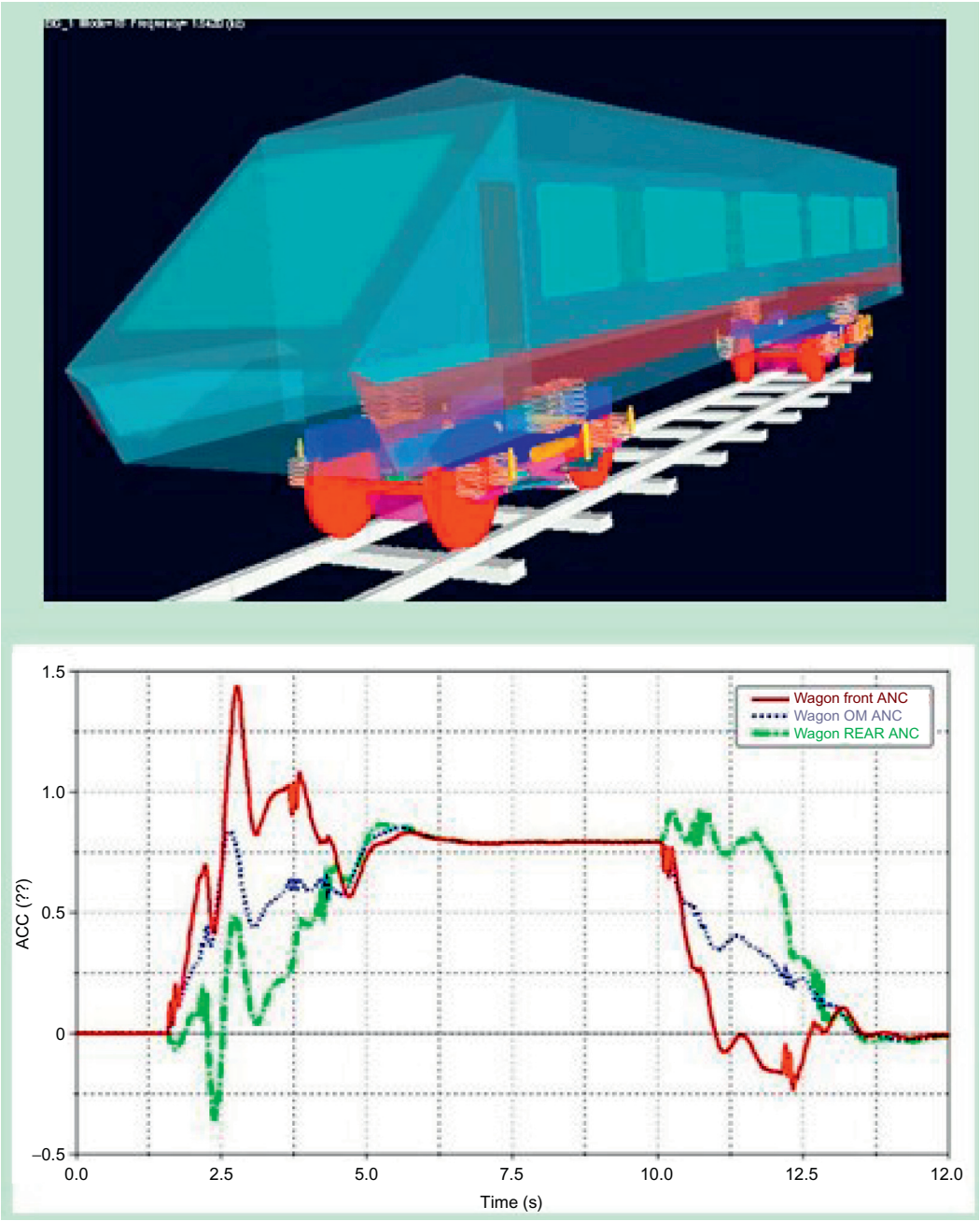

FIGURE 2.30

Application of ADAMS software in analyzing performance when traveling on curves.

Table 2.2 Design Schemes for Turnout Plane Line Types

Scheme	No. of Turnout	Line Type of Transition Lead Curve	Radius of Circular Curve (m)	Front Length of Turnout (m)	Rear Length of Turnout (m)
1	44	Circular + easement	4550	56.447	101.226
2	42	Circular + easement	5000	60.573	96.627
3	41	Circular + easement	4000	53.010	94.328
4	37	Easement + circular + easement	4000	68.052	85.134
5	36.3	Easement + circular + easement	4000	68.819	83.521
6	39	Easement + circular + easement	4550	71.336	89.732

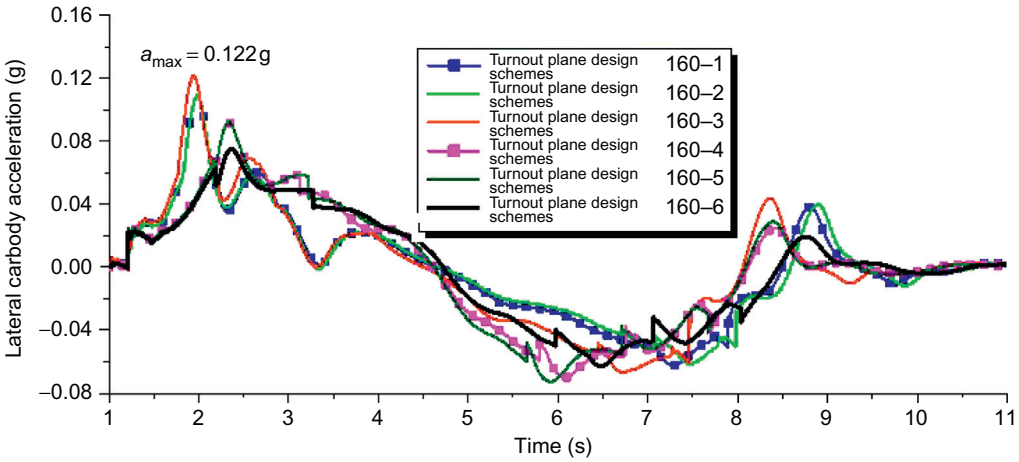

FIGURE 2.31

Impacts of turnout plane design schemes on lateral carbody acceleration.

1984, a special technical committee was set up by the research center of the Association of American Railroads (AAR) to study the dynamic properties of new cars with computer simulation technologies. The car dynamics simulation calculation program developed by the committee is called NUCARS.

2.4.3 APPLICATION CASES

1. Comparison of transition lead curve design schemes

   With the wheel−rail system dynamics model (Figure 2.28), six schemes, as given in Table 2.2, are compared in the plane line type design for high-speed turnouts (speed in the diverging line of 160 km/h) in China. The lateral carbody vibration accelerations are compared in Figure 2.31.

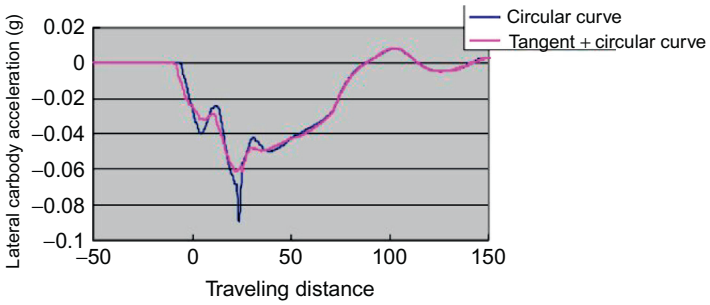

FIGURE 2.32

Impacts of line type schemes of switch rails on lateral carbody acceleration.

Safety indicators such as derailment coefficient and rate of wheel load reduction can also be compared in addition to lateral carbody acceleration. Through comparison, it is shown that lateral acceleration, derailment coefficient, and rate of wheel load reduction of the carbody for "easement + circular + easement" curves, after the interpolation of an easement curve between the straight section and circular curve, are less than those for "circular + easement" curves. The dynamic indicators, such as lateral carbody acceleration, derailment coefficient, and rate of wheel load reduction, of Scheme 6 are the lowest. From the point of dynamics, this design scheme for plane line type is the best. However, considering the abrasion performance of switch rails, Scheme 2 is selected for turnouts in China (speed of 160 km/h in the diverging line), that is, No. 42 turnouts.

2. Comparison of line type of switch rails

   Take No. 18 turnouts in China, for instance; two line types of switch rails are considered: tangent curved switch rails with radius of 1100 m, and semi-tangent curved switch rails with radius of 1100 m, having a separated distance of 11.95 mm and being semi-tangent at top width 26.8 mm of the switch rail. The lateral carbody accelerations for two line types are obtained through dynamic simulation with NUCARS software; see Figure 2.32 for comparison results.

   According to the calculated results, by comparing the lateral acceleration, rate of load reduction, wheel−rail lateral force, abrasion index, etc. of the carbody for the two switch rail line types, when an EMU train travels at 80 km/h in the diverging line from the rear of a No. 18 turnout, it turns out that the semi-tangent switch rail scheme outperforms the tangent scheme significantly. Moreover, the former scheme has been successfully applied to the existing No. 12 turnouts in China for long time; thus, this scheme is preferred for the switch rails of Chinese No. 18 high-speed turnouts.

3. Comparison of lengths of intermediate straight lines of turnouts

   Take No. 18 crossover turnouts, for instance; if the lengths of the intermediate straight lines between two turnouts are 21.9, 25.5, and 29.1 m, respectively, the lateral accelerations of the carbody when an EMU train travels at 80 km/h in the diverging line are obtained with NUCARS software. See Figure 2.33 for comparison results.

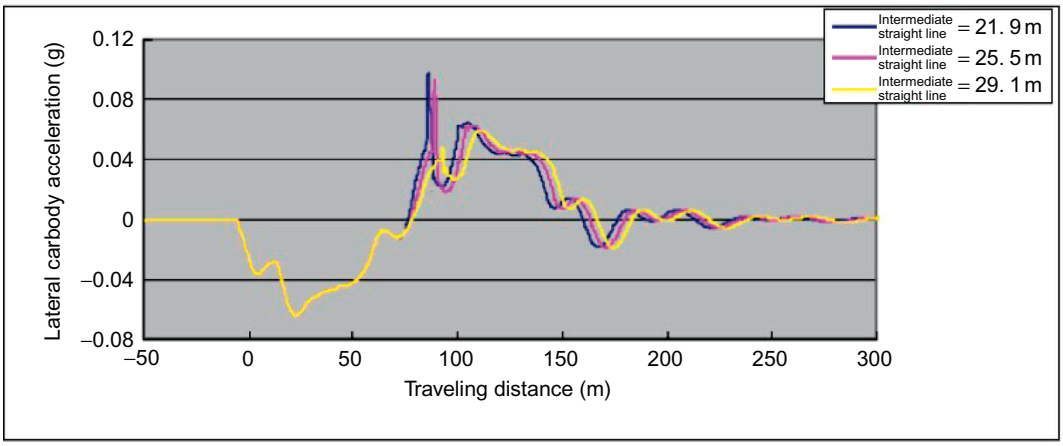

FIGURE 2.33

Impacts of length of intermediate straight lines on lateral carbody acceleration.

It is shown in Figure 2.33 that the greater the length of intermediate straight line L, the smaller the lateral carbody acceleration. When $L = 0.4V_{\text{diverging}}$ (32 m), the vibration of two turnouts can hardly be superposed. The absolute value of the reading on the carbody vibration accelerometer is also smaller when $L = 20$ m under unfavorable conditions.

CHAPTER

STRUCTURAL SELECTION AND RAIL DESIGN

3

The selection and design of turnout structure follow the layout design. The turnout structure design, including selection of component structure types, determination of component layout and quantity, section type, size, and materials, will be determined according to the running conditions of rolling stock, actual processing and manufacturing capacity, and maintenance requirements. As a turnout integrates various track systems, all new technologies and design theories around high-speed track structure shall be applied to the design of high-speed turnouts.

3.1 SELECTION PRINCIPLES [32]

First, the high-speed turnout structure shall ensure the riding quality and safety of high-speed train.

Turnout types shall be minimized, and the components adaptable to the same running conditions shall be interchangeable. The rail types of high-speed turnouts shall be consistent. In 350 and 250 km/h high-speed railways (HSRs), turnouts with the same speed in the diverging line (i.e., 80, 160, or 220 km/h), shall have identical numbers and main plane sizes. The parts for turnouts with the same speed in the main line should be interchangeable.

In addition, the selected turnout structures shall meet the requirements for manufacturing feasibility, laying convenience, and maintenance accessibility, and shall be technologically mature and reliable.

3.2 OVERALL STRUCTURE SELECTION

The following structure types are studied in the structural design for high-speed turnouts in China.

3.2.1 GUIDING-RAIL TURNOUTS

Turnouts where the wheelset is guided to the main or diverging line by switch rails and point rails are called guiding-rail turnouts. This is the dominant type of turnout in the world. The main line of the turnout with movable grade-separated crossings is the same as section line, so there's no speed limit in the main line; however, this turnout type has proven to be poor in riding safety and quality, as the train may climb the rails when traveling in the diverging line, as shown

Design of High-Speed Railway Turnouts.

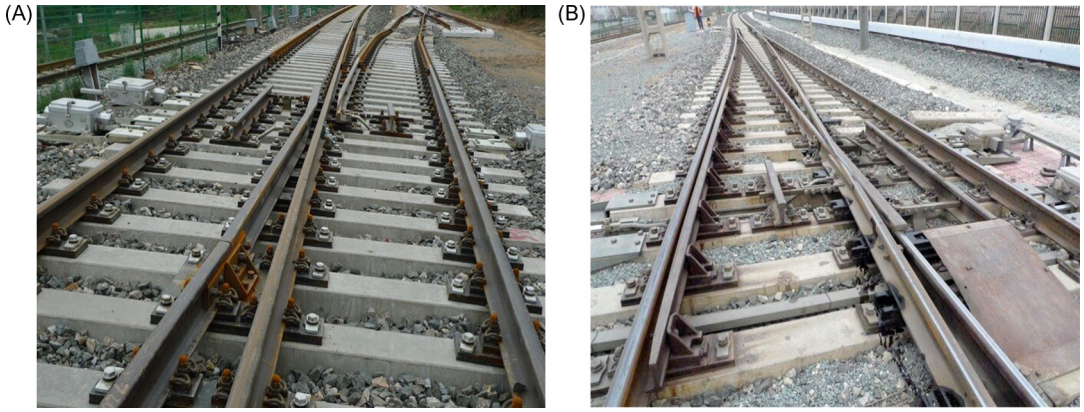

FIGURE 3.1

Turnout with movable grade-separated crossing; (A) Passage in the main line; (B) Passage in the diverging line.

in Figure 3.1. Therefore, it cannot be applied to high-speed turnouts in the diverging line. So guiding-rail turnouts will apply [33].

3.2.2 SWING NOSE CROSSING

There are gaps (gauge line interruptions) in the fixed crossing, which may cause significant vertical and lateral structural irregularities, seriously affecting the riding quality and safety in turnouts. In this case, movable crossings should be used for turnouts for more than 160 km/h in the main line to eliminate the gap. Fixed crossings may be used in 200 km/h railways in other countries. However, from the perspective of technological status, riding safety, and passenger comfort, a movable crossing is preferred for turnouts for 250 km/h or above [34].

Movable crossing falls into three types: swing nose crossings, movable-wing crossings, and movable-frog crossings. The swing nose crossing has fixed wing rails and swing nose rails; it is stable but requires a longer turnout for conversion of point rails. It is the most widely used movable crossing type in the world. The movable-wing crossing has fixed point rails and movable wing rails, which can be further categorized into crossings with a single movable wing rail and crossings with double movable wing rails, characterized by a shorter turnout (the same with the turnout with fixed crossing possible), and poor lateral stability of the wing rails and a complicated switch-and-lock mechanism. The movable-frog crossing has fixed rear ends of wing rails and point rails, movable point of point rails, and is characterized by shorter turnout and poorer front-end stability of point rails. The last two types are not adopted for high-speed turnouts due to poor structural stability.

3.2.3 FLEXIBLE POINT RAIL

In order to meet the conversion requirements of long and large switch rails and point rails, and to ease the switching force and scant switching displacement, generally, the rail base (about 1.2 m) in

FIGURE 3.2

Point rail with single flexible rail.

FIGURE 3.3

Point rail with double flexible rails.

front of the heels of switch rails and point rails will be machined to reduce the lateral bending stiffness and form a flexible center. Thus, the switch rails and long point rails are all flexible.

For a swing nose crossing, the short point rail in the diverging line will rotate with the long point rail. In small number turnouts, the diagonal joint (Figure 3.2) is generally arranged in the diverging line, and the short point rail will then rotate along the crossing heel rail, serving as the diagonal joint. This structure has smaller switching resistance, and is called the point rails with a single flexible rail. However, for high-speed turnout in the diverging line, in consideration of the requirements of high track smoothness for high-speed traffic in the diverging line, a flexible short point rail is preferred to constitute the point rails with double flexible rails, as shown in Figure 3.3, which has significant switching resistance.

3.2.4 LONG WING RAILS

The swing nose crossing has two wing rail types: long wing rail and short wing rail. The rear of the long wing rail extends to the heel of the point rail, as shown in Figure 3.4. The front of the point rail is in close contact with the rail head of the wing rail. Jacking blocks are arranged between the rear of the long and short point rails and the wing rails. In the end of the structure, the long and short point rails are connected with the wing rails by fillers. Advantages of this arrangement include good lateral stability, smaller expansion displacement of point rails, and capability of transferring the temperature force in the continuously welded rail (CWR) track in the turnout rear to the inner rail via the rear wing rail. Disadvantages include a complex wing rail structure and more material consumption. The rear of the short wing rail extends to the closed area at the front of point

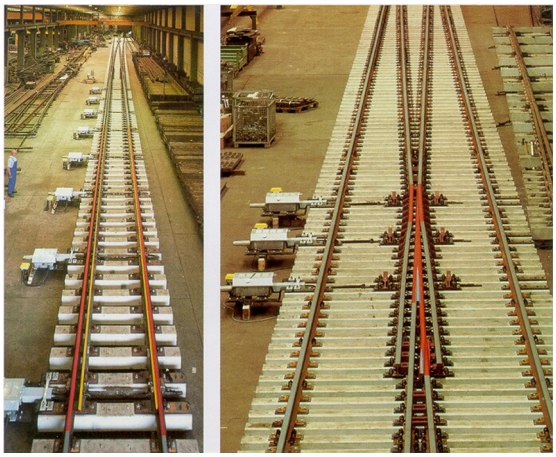

FIGURE 3.4

Long wing rails.

FIGURE 3.5

Assembled point rails.

rails, and the wing rail is relatively shorter. Crossing heel supports are provided at the end of point rails to keep the relative position of the two rails and convey the temperature force in the turnout rear to ties. Advantages include a simple structure and less material consumption. A disadvantage is the great expansion displacement of point rails as all the temperature force in the rear of a CWR turnout will be applied on the crossing. Short wing rails have been adopted in Japan, but long wing rails have been adopted for high-speed turnouts in other countries. Long wing rails have also been adopted for CWR turnouts in China and have achieved favorable results. To this end, this structure is preferred in the design of high-speed turnouts.

3.2.5 ASSEMBLED POINT RAILS

Point rails have two kinds of structures: assembled type and solid frog type. The long and short point rails of assembled point rails are made of flat-web-special section rails (i.e., AT rail) or other equivalent section rails. As shown in Figure 3.5, the long and short point rails are spliced by high-strength bolts at the full section (or in front of the section) of the long point rail. The ends of point rails are forged into a common rail section. An advantage is the simple manufacturing process. A disadvantage is poorer integrity as compared with the solid frog type. This structure has been adopted for French high-speed turnouts and speed-up turnouts in China. The point rails with solid frog are forged with the same blooms as the wing rails, where the sections with top width of 250 mm are machined into two common rail sections and welded with long and short point rails. This structure has been adopted for high-speed turnouts in Germany and Japan. An advantage is good structural stability. A disadvantage is the complicated manufacturing process. In view of technological conditions and manufacturing feasibility, assembled point rails have been adopted for high-speed turnouts in China.

3.2.6 ROLLED SPECIAL SECTION WING RAILS

In looking at the history of turnouts with the swing nose rail in China, the technological process of wing rails has witnessed an evolution from common rail machining to high manganese steel casting, AT rail die forging, and special section rolling. Wing rails made of machined common rails were used in early speed-up turnouts in China. This type of wing rail is characterized by a simple manufacturing process, great amount of cutting at the rail base, inadequate strength margin (reinforcing bars are required at the rail web of outer rails), small spacing for conversion equipment, and poor lateral stability. It has been adopted for high-speed turnouts in Germany. Notwithstanding the stable point rails of this structure, however, as demonstrated by dynamic tests with real cars in China, the wing rails have great lateral displacement. High manganese steel cast wing rails were used for high-speed turnouts in Japan and France, as well as for early swing nose crossings in China. Advantages include the ability to providing sufficient spacing for electrical conversion equipment and good structural stability (in particular, strong integrity). Disadvantages include rapid early wear at the top of wing rails under freight traffic conditions and poor performance when being welded with common rails on site. Research on this type of wing rail was suspended as it failed to meet operating conditions in China. The technology of producing special section wing rails with AT rails by die forging is a unique technology in China, which has been widely used in speed-up turnouts over the last decade, as shown in Figure 3.6. Advantages include good structural stability and capability of providing sufficient spacing for electrical facilities. Disadvantages include lower strength and hardness of wing rails after heat treatment, higher risk of vertical wear at the top of wing rails, and risk of brittle fractures.

For the three types of wing rails, the switch rod at the first traction point on the swing nose rail can extend from the rail web or rail base. For the early speed-up turnouts in China, the switch rod would pass through the holes on the rail web. However, great vibration may occur in case of poor turnout status, which may lead to vertical collisions of wing rail holes. In addition, in case of great expansion displacement of point rails for CWR turnouts, the switch rod might collide with the wall of rail web holes, leading to cracks or holes. Therefore, this technology was rejected later. This installation mode has also been adopted for high-speed turnouts in the diverging line in Germany. It is proven that by using this installation mode, the turnout is in good condition and has smaller vibration, and the expansion displacement of the point rail is reduced with the effective coupling structure in the crossing end. However, the holes on the rail web may also be cracked. Based on the die-forged wing rails, China has developed the conversion flange-type point rails for speed-up turnouts. For this type of point rail, a flange plate is hot-forged at the base of the point rail, the switch rod extends from the rail base and connects to the flange plate, driving the conversion of point rails. This structure features a strong locking capacity, stable structure, and simple manufacturing process. However, under operating conditions of great axle weight, high speed, and large traffic volume and density in China, some point rails are fractured along the conversion flange, as shown in Figure 3.6. In addition, since the coupling position of the switch rod and flange is relatively low, the point rail is prone to deformation during conversion, and the electrical indication rod cannot detect the correct rail closure. Thus, closure detection failure jeopardizes the safety of turnouts.

To solve the structural reliability problem at the first traction point on the point rail, China has developed the rolled special section wing rail (TY rail for short), using the same materials as other

FIGURE 3.6

Forged special section wing rail and fracture of point rail.

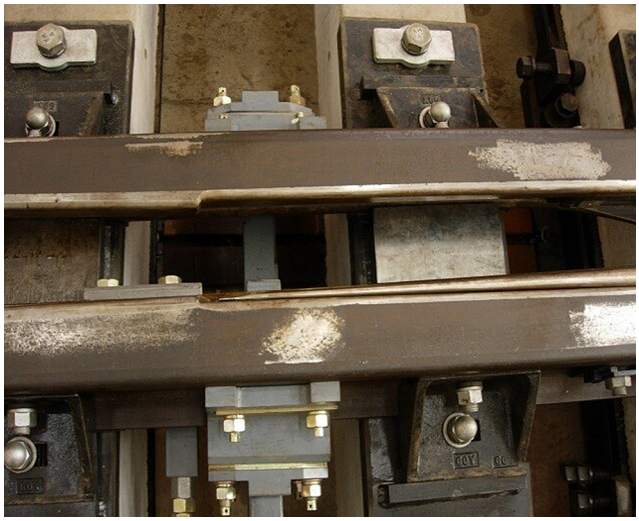

FIGURE 3.7

Rolled special section wing rail.

turnout rails, as shown in Figure 3.7. This type of rail improves the strength and stability of the wing rail on the one hand, while on the other it reserves enough space for electrical locking block and lock hook, saves the conversion flange, lifts the coupling point of the lock hook and point rail, solves the problem of detection failure, and simplifies the manufacturing process by abolishing the heat treatment process (only the machining process is required). Therefore, the rolled special section wing rail applies to high-speed turnouts in China through comprehensive comparison.

3.2.7 AT RAIL HOT-FORGED HEEL ENDS OF SWITCH RAILS AND POINT RAILS

The rolled flat-web-special section rail (i.e., AT rail in China) is characterized by firm section and superior stability compared to common section rail. The AT forged switch rails, when placed on the slide bedplate, can be flushed with the top of stock rails without the necessity of cutting the base of stock rails, thus ensuring the strength of switch rails and stock rails. In addition, the asymmetric flat-web-special section rail may improve the lateral stability of switch rails. Therefore, this rail type is widely used in turnouts all over the world. Since rail cant is required for high-speed switch rails, superelevated AT rail may be used to reduce the amount of processing. In order to facilitate the linkage between the heel end of the switch rail and the rail on the transition lead curve, the heel end of the switch rail is hot-forged into the shape as shown in Figure 3.8. The forged section for 60 kg/m standard rail shall not be shorter than 450 mm, and that for transition shall not be shorter than 150 mm. For a superelevated switch rail, the forged section can be deflected at a deflection angle of 1:40, and the allowed deviation of the deflection angle is $\pm$ 1:320. In another case, the heel of the switch rail may not be twisted as with German high-speed

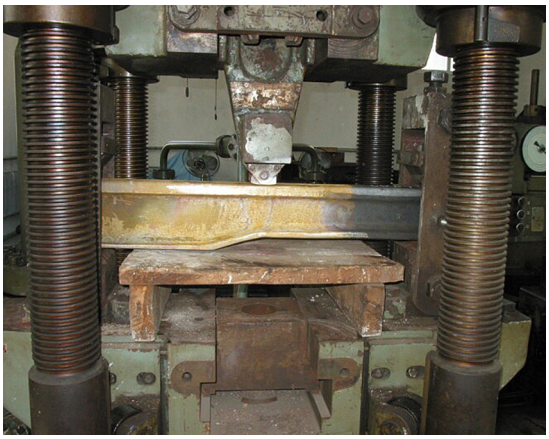

FIGURE 3.8

Hot-forged heel end of the switch rail.

FIGURE 3.9

Anti wear check rail in the diverging line.

turnouts; instead, it shall be aligned with the rail head and then welded with a transition lead curve at a deflection angle of 1:40. For AT rail assembled point rails, the heel shall be processed as that of the switch rail.

3.2.8 CHECK RAIL MADE OF GROOVED RAIL

Check rails are not required in swing nose turnouts as there is no gap in the fixed crossing, and the gauge line of the point rail is continuous. For the turnout with a small radius of curve, when a train travels in the diverging line, if the running wheelset clings to the working surface of the point rail in the diverging line, the point rail may be susceptible to severe side wear under the long-term effect of great lateral wheel−rail force, whereas when the main line is in operation, the point rail cannot be in close contact with the wing rail, affecting the riding quality for high speed in the main line. Therefore, anti wear check rail shall be provided in the diverging line. As shown in Figure 3.9, check rail is provided for No. 18 and below turnouts with swing nose rails in the diverging line in China. No check rail is installed in the main line as the wheelset will not come into contact with the point rail. Large number (No. 18 and above) turnouts have no check rails.

The top surface of the check rail shall be 12 mm above the stock rail to prevent the wheel mounting the check rail. In the past, Chinese turnouts adopted check rails made of machined common rails and welded rail pads, with the stock rails being fastened by pin-type elastic pads (similar to the slide bed). However, this structure is susceptible to sealing off, pad fracture, unstable fastening of stock rails, etc.

As shown in Figure 3.10, the UIC33kg/m rolled groove rail has been used in recent years as it occupies less space, coordinates with the solid check rail pad (see Figure 3.11), and allows installing elastic clips on the inner side of stock rails, enhancing the strength of check rail pads and lateral stability of stock rails. However, it is difficult to inspect and re-screw the bolts on the elastic

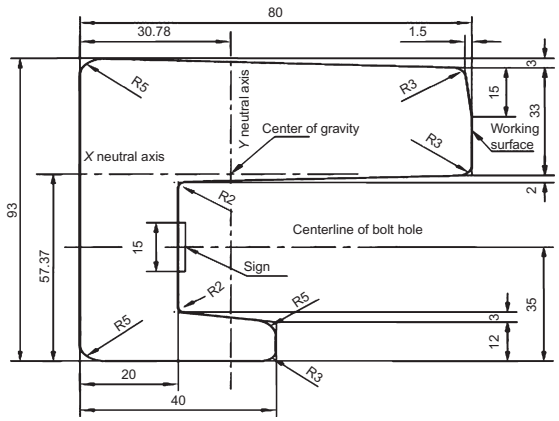

FIGURE 3.10

33 kg/m grooved rail.

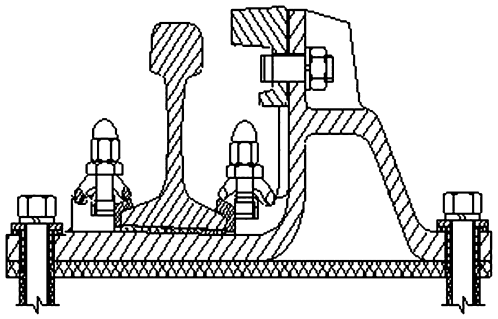

FIGURE 3.11

Solid check rail.

clips during routine maintenance and repair, so the locking device or the approximately n-shaped elastic clips (similar to the slide bedplate) will be used.

So the grooved check rails, solid check rail pads, and elastic clips are used for turnouts in China.

3.3 DESIGN OF RAIL MEMBERS

The special rail members of high-speed turnouts include switch rail, point rail, pointed rail at crossing heel, and wing rail. These rails are processed into thin sections or transition sections by machining or hot treatment. To avoid fatigue fracture under the action of high-speed trains, special designs and calculations are necessary.

3.3.1 SELECTION OF AT RAIL [35]

1. Selection principles

   Selection principles for AT rail of high-speed turnouts include:

   - **a.** having sufficient strength and vertical bending stiffness capable of meeting strength requirements when the switch rail section with smaller top width is under full load
   - **b.** having low occurrence of buckling and less maintenance work
   - **c.** having appropriate lateral bending stiffness which is able to meet strength requirements to reduce side buckling and deformation, as well as to reduce switching resistance and scant switching displacement
   - **d.** having enough height difference (preferably greater than 30 mm) with the stock rail to achieve the design of hidden tip point and elastic fastening on the inner side of the stock rail, and to allow the installation of anti wear structures (e.g., rollers) and use of thickened slide bedplate

Table 3.1 Comparison of Section Parameters of Three AT Rails

Type of Rail	CHN60AT	UIC60D	Zul-60
Sectional area (m^2)	104	89	93
Unit weight (kg/m)	82	70	73
Height difference with stock rail (mm)	24	30	38
I_x (cm^4)	2539	2040	1728
I_y (cm^4)	901	764	744

e. having enough sectional area to allow the heel end to be forged into common section rail (the larger the difference in sectional area, the greater the processing difficulties; AT rail which is able to be forged into 60 kg/m common rail is called as 60AT rail); and

f. having the capacity to produce 50 or 100 m rails and meet the design requirements for welding-free switch rail of large number high-speed turnouts in the diverging line.

2. Structure type

The CHN60AT rail has been adopted for speed-up turnouts in China. The UIC60A symmetrical cross-section rail (or 60E1T2 in EN standard, with height equivalent to the stock rail) was adopted for the first high-speed railway (east−south line) turnouts in France, later replaced with the UIC60D20AT rail (or 60E1A4 in EN standard, with 1:20 rail cant). The Zul-60 rail (or 60E1A1 in EN standard, unsuperelevated) is adopted for railway (including HSR) turnouts in Germany. Initially, the 70S rail applicable to the 50 kg/m rail type was used for Japanese Tokaido Shinkansen turnouts, but was replaced with 80S rail applicable to 60 kg/m rail later. The height differences of the two rails with stock rails are 15 mm, which are not applicable to the installation of elastic fasteners of stock rails. Through comprehensive analysis, in China, the AT rail of high-speed turnouts will be selected from among CHN60AT, UIC60D40, and Zul-60. A comparison of section parameters is shown in Table 3.1.

Compared with UIC60D and Zul-60, CHN60AT rail has a larger sectional area, unit weight, height, and moment of inertia in the x-axis and y-axis. The Chinese CHN60AT rail was developed for the existing railways for mixed passenger and freight traffic and for heavy haul railways, and it is also widely used in speed-up turnouts. Advantages include strength and resistance to deformation, and applicability to the operational requirements of heavy haul railways and speed-up railways for mixed passenger and freight traffic. Disadvantages include inadequate height difference with the stock rail (which limits the use of elastic clips on the slide plate in fastening the inner side of stock rails); great switching resistance of the switch rail and point rail; and large scant switching displacement and large bending stiffness. Moreover, the deformation occurring during use is difficult to rectify.

At present, the UIC60D rail is widely used in France to manufacture switch rails and point rails. This rail is provided with 1:20 rail cant, a height difference of 30 mm with UIC60 rail (34 mm with CHN60 stock rail), which is able to solve scant switching displacement (combined with the antifriction measures of slide bedplate and rollers) of the switch rail and swing nose rail.

German Zul-60 rail is used for the switch rails and swing nose rails of high-speed turnouts, and is also commonly used for existing railway turnouts applicable to 225 kN axle loads in freight cars.

3. Strength calculation

Three vertical loads have been considered in the track structural design of the Japanese Shinkansen: design load, fatigue load, and abnormal load. For the axle load of a high-speed train of 170 kN, the design wheel load also includes the increased dynamic wheel load due to wheel flats; given the velocity coefficient of 2.0, the design load will be 255 kN (three times the static wheel load). Fatigue load refers to the load including the fluctuating coefficient of wheel load, taken as 124 kN allowing for three times wheel load fluctuation ($3 \times 15\%$). Abnormal load refers to the maximum wheel load measured in practice, taken as 340 kN (four times the dynamic wheel load). Different check methods and safety factors will be adopted for different loads. For instance, fatigue load is adopted for fatigue calculation, and the safety factor for design load is larger than that for abnormal load.

China mainly adopts the allowable stress method; that is, certain safety factors will be used to calculate the strength of rails and track components. The quasi-static continuous, resiliently supported track model is employed for strength calculation. The vertical dynamic load and vertical bending moment of the rail can be obtained by:

$$P_{\mathrm{d}} = P_0(1 + \alpha + \beta) \tag{3.1}$$

where α is the velocity coefficient, taken as 2.0 for 250 km/h and above HSRs; β is the eccentric load coefficient, determined by deficient superelevation, taken as 2‰ of the deficient superelevation (in millimeter) for trains in China; and P_0 and P_{d} are the static wheel load and dynamic wheel load, respectively. When considering only the vertical load in calculating rail stress, a lateral horizontal force amplification factor may be multiplied, which is taken as 1.25 when the curve radius is larger than 2000 m.

For fixed crossing and other components with special structural irregularity, the abnormal load may be taken as four to five times static wheel load in calculation.

At present, there is no universal method to calculate the lateral load of rails. In the Japanese Shinkansen, the design lateral load is taken as 68 kN, which is the product of the derailment coefficient allowable limit of 0.8 and static wheel load. According to turnout dynamics simulation, when a train travels in the main line, the lateral wheel−rail dynamic action is mainly the impact load produced by the hunting movement of the wheelset, characterized by short times and variable position with the lateral movement of the wheelset. When a train travels in the diverging line, under the action of unbalanced centrifugal force, the outer wheel will cling to the curved switch rail and transition lead curve. Combined with the results of mass dynamic tests and simulations on site, it is recommended that the lateral fore on the rail be taken as 70 kN when a freight car travels in a turnout, and 50 kN for an EMU train. For the lateral force on the check rail, the value is taken as 100 kN for a freight or passenger car with axle load of 23 t, and 120 kN for a freight car with axle load of 25 t.

The longitudinal rail force mainly includes the braking force (or starting force) of trains, temperature force of CWR line, and its additional force. In China, the braking force on rails is generally taken as 10 MPa in calculating rail strength, which will be superimposed on the temperature force and dynamic force of the rail. The nonbreathing length of CWR line will bear the temperature compressive force or tensile force, which is directly proportional to the temperature variation range and rail section; that is, $F = EA\alpha\Delta t$, where E, A, α, and Δt denote elasticity modulus, sectional area, expansion coefficient, and temperature variation range of

Table 3.2 Comparison of Strengths and Conversion Impacts of Three AT Rails

Type of Rail	CHN60AT	UIC60D	Zul-60
Dynamic stress on rail head (MPa)	180.3	199.6	211.1
Dynamic stress on rail base (MPa)	136.5	151.5	165.2
Stress on tie (kN)	124.7	132.5	138.8
Dynamic displacement of rail (mm)	1.56	1.66	1.73
Total switching force (N)	7452	6260	6334
Scant displacement (mm)	2.4	2.1	2.3

rails, respectively. For CWR turnouts on subgrades and bridges, additional temperature force may be applied on stock rails adjacent to the heel of switch rails due to the thermal expansion of inner rails of turnouts and bridges. This force is approximated as 30−40% of the temperature force of the nonbreathing length. Therefore, in calculating the strength of turnout rails, for the heel of stock rails, the temperature force of the nonbreathing length and additional force shall be considered. For the movable part of the switch rail and the point rail, the temperature force may be ignored. For other parts, only the temperature force of the nonbreathing length will be considered.

The allowable stress method is adopted to calculate rail strength. Under the joint actions of vertical, lateral, and longitudinal loads, the stress shall meet $\sigma \leq [\sigma] = \sigma_s/K$, where K is the safety factor (for new rail $K = 1.3$, for secondhand rail $K = 1.35$), σ_s is the yield limit of rail (MPa) (for U71Mnk and other low-alloy rail $\sigma_s = 457$ MPa; for U75V and other high-strength rail $\sigma_s = 550$ MPa).

4. Selection comparison

A comparison of the strengths of three AT rails and their impacts on switching force and scant switching displacement is shown in Table 3.2. Given that the support stiffness of the slide bed of ballast turnouts is 60 MN/m, and riding speed is 350 km/h, the speed coefficient is 2.0, the static axle load of EMU is 170 kN, and the lateral force factor is 1.25, and the two-axle bogie is used. For No. 18 turnouts, three traction points are selected on the switch rail, at intervals of 4.2 and 4.2 m, respectively, and the friction coefficient of the slide bed is taken as 0.25.

From Table 3.2, under the most unfavorable load combination, switch rails made of CHN60AT, UIC60D, and Zul-60 rails are within the allowable strength range, so all three rails are applicable to HSRs. UIC60D and Zul-60 switch rails have a small difference in switching resistance, but their switching resistance is less than that of CHN60AT switch rails by more than 15%. The scant switching displacement of the three switch rails exceeds 2 mm, but there is no obvious difference.

For reducing stress and deformation of rails and sub-rail foundation, CHN60AT and UIC60D are preferred. For controlling the scant displacement of turnout blades, UIC60D and Zul-60 are preferred. For reducing switching resistance and facilitating the design of the point rail with double flexible rails, UIC60D and Zul-60 are preferred. For reserving sufficient installation space for reasonably arranging fasteners on the inner side of the stock rail, Zul-60 and UIC60D are preferred.

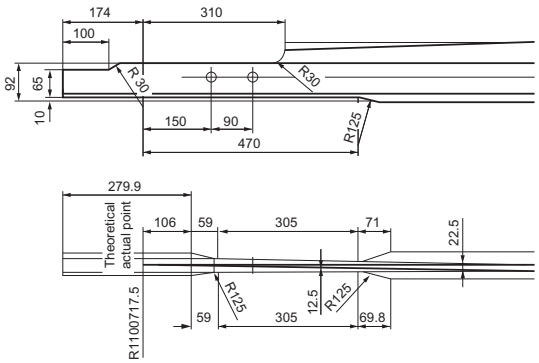

FIGURE 3.12

Structure of actual point of point rail.

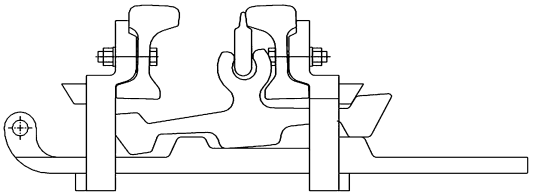

FIGURE 3.13

Lock hook bracket and point rail locking point.

By comparison, UIC60D section rails have been adopted to manufacture switch rails and swing nose rails for high-speed turnouts in China. UIC60D40 section rails may be selected to be compatible with the 1:40 rail cant in a turnout. The 25 and 50 m rails can be produced by upgrading the production equipment and processes of steel plants. U75V or U71Mnk [used for passenger line (PDL) rails] may be adopted.

3.3.2 DESIGN OF COMPONENTS AT THE FIRST TRACTION POINT ON SWING NOSE RAIL

The engineering and electrical design at the first traction point on a swing nose rail is the most intricate, as it must allow the conversion of point rails within the narrow space of the crossing throat and maintain the strength of point rails, wing rails, and the switch locking device, while ensuring reliable locking and detection of the entire engineering and electrical structure.

1. Structure at the first traction point on the point rail

   Chinese high-speed turnouts are made of machined, specially rolled section rails. The rail base at the actual point of the point rail will be machined, as shown in Figure 3.12, before being installed in the bracket of the electrical conversion lock hook, as shown in Figure 3.13.
2. Analysis of gap between point rail top and wing rail

   In order to understand the stress status of the point rail, the wing rail, and conversion structure of high-speed turnouts, and to assess the reliability of closure detection (point rail and wing rail closure), the torsion of the point rail must be analyzed. During the conversion of the point rail, in order to make the point rail actual point cling to the wing rail, generally, the switch rod will keep moving until the lock hook and locking frame are reliably locked when the point rail is in place. Under this circumstance, although the point rail and wing rail are closely contacted, the point rail may be twisted by the eccentric action of the switching force, forming a gap between the point rail top and wing rail. In the technical conditions of Chinese high-speed turnouts, the gap between point rail top and wing rail at the first traction point shall not exceed 0.2 mm. Given the maximum switching force on the locking point of 6000 N, the change in the

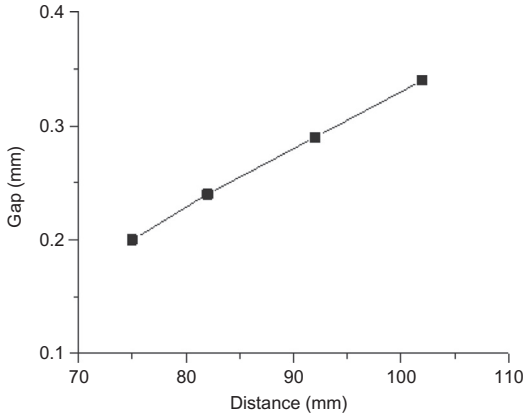

FIGURE 3.14

Change of gap between point rail top and wing rail.

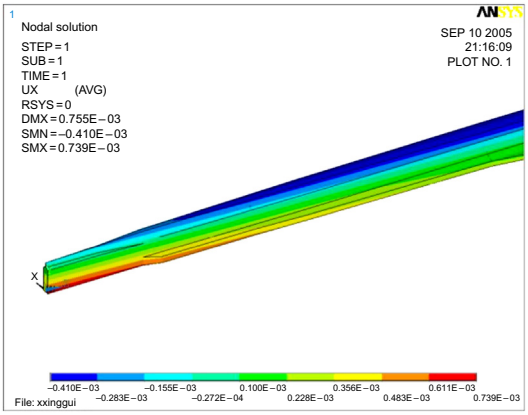

FIGURE 3.15

Lateral displacement of point rail.

gap value with the distance between locking point and point rail top can be obtained, as shown in Figure 3.14. The distribution of lateral displacement of the point rail is shown in Figure 3.15.

From Figure 3.14, when the locking point gets closer to the point rail top, the gap becomes smaller, and the two are in an approximate linear relationship. With the rising of the locking point, the torsion of the point rail is greatly eased, which is how the gap is controlled. In order to meet the 0.2 mm gap requirement, the distance between the locking point and point rail top must not exceed 75 mm. The stress of the point rail during conversion is small, about 5.4 MPa.

3. Analysis of strength of wing rails and lock hook

Under the most unfavorable conditions (i.e., wing rails bear all vertical and lateral loads applied on the cutting section at the base of the wing rail), the stress distribution is shown in Figure 3.16 when taking into consideration the vertical and lateral supporting actions of fastening at the support points of fasteners.

In analyzing the stress of the lock hook, the switching force and dynamic action of trains shall be taken into account at the same time. During conversion and locking, the external force on the lock hook is small, mainly involving the tension of the lock rod and the bounce of the point rail. In locking status, the external load on the lock hook mainly involves the locking force and elastic force. Locking force refers to the force on the lock hook due to elastic deformation of the point rail when the conversion is in place, which may be taken as the maximum switching force. The elastic force mainly refers to the stress on the lock hook at the traction point due to elastic deformation of the point rail caused by the lateral force acting on the point rail between the first and second traction points when a train travels in a turnout. This force can be obtained with the analytic model of point rail stress. The vertical force on the lock hook will be transmitted to the locking rod, and then to the wing rail via the locking frame. Thus, the vertical supporting stiffness of the locking system can be regarded as the integral vertical stiffness of the wing rail. The lateral force on the lock hook is transmitted to the locking block, and then to the locking frame, and finally to the wing rail. Thus, the lateral supporting stiffness of the locking system can be

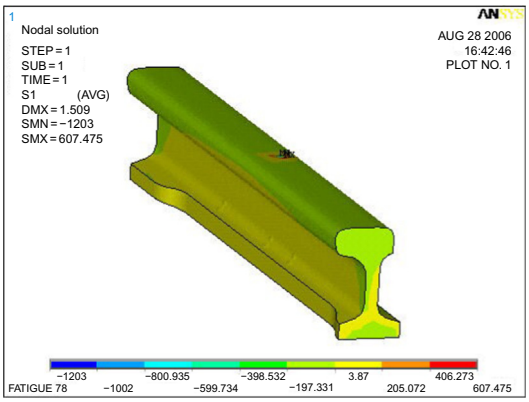

FIGURE 3.16

Stress on the wing rail.

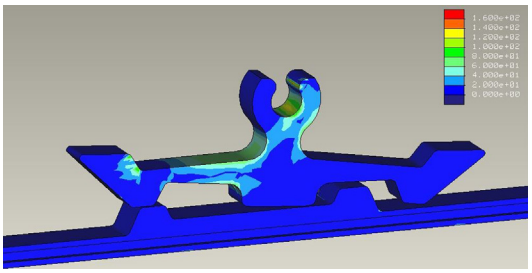

FIGURE 3.17

Stress on the locking hook at the first traction point on the point rail.

regarded as the integral lateral supporting stiffness of the wing rail. The distribution of the calculated stresses of lock hook is depicted in Figure 3.17.

Under the most unfavorable load, it is calculated that the strength of the wing rail and lock hook is within allowable limits, but the calculated value is larger than the test value, about 1.5−1.8 times the latter, thus showing that the calculated value as per the most unfavorable load is safer. A test was performed on a Chinese HSR (Wuhan−Guangzhou). According to the test, under the action of an EMU train, the maximum stresses on the point rail, wing rail, lock hook, and locking rod are about 83.8, 80.7, 68, and 31 MPa, respectively, within the allowable strength limit of U71MNk rail and A3 steel; see Figure 3.18 for the test results.

4. Strength analysis of pointed rail at crossing heel

The 60D40 rail adopted for high-speed turnouts in China has a 1:40 rail cant, so the longer portion of the base of AT rail is laid outward. By doing so, the longer portion of the base of AT rail in the rear of the short point rail must be cut by 57 mm. Owing to the large cutting amounts on rail sections, strength shall be verified by calculation (see Figure 3.19 for calculation model). The vertical and lateral supports are arranged according to the supports of fasteners. The calculated vertical and lateral loads of trains traveling in the diverging line at 80 km/h are shown in Figure 3.20, where the maximum stress is about 194 MPa, within the allowable strength limit of rails.

3.4 TECHNICAL REQUIREMENTS FOR RAILS [36]

Rails for HSR shall have high safety performance, straightness, and geometric precision. High safety performance requires pure steel, intact surfaces, low residual tensile stress at the rail base, excellent ductility and welding performance, easy production, stable quality, and high reliability.

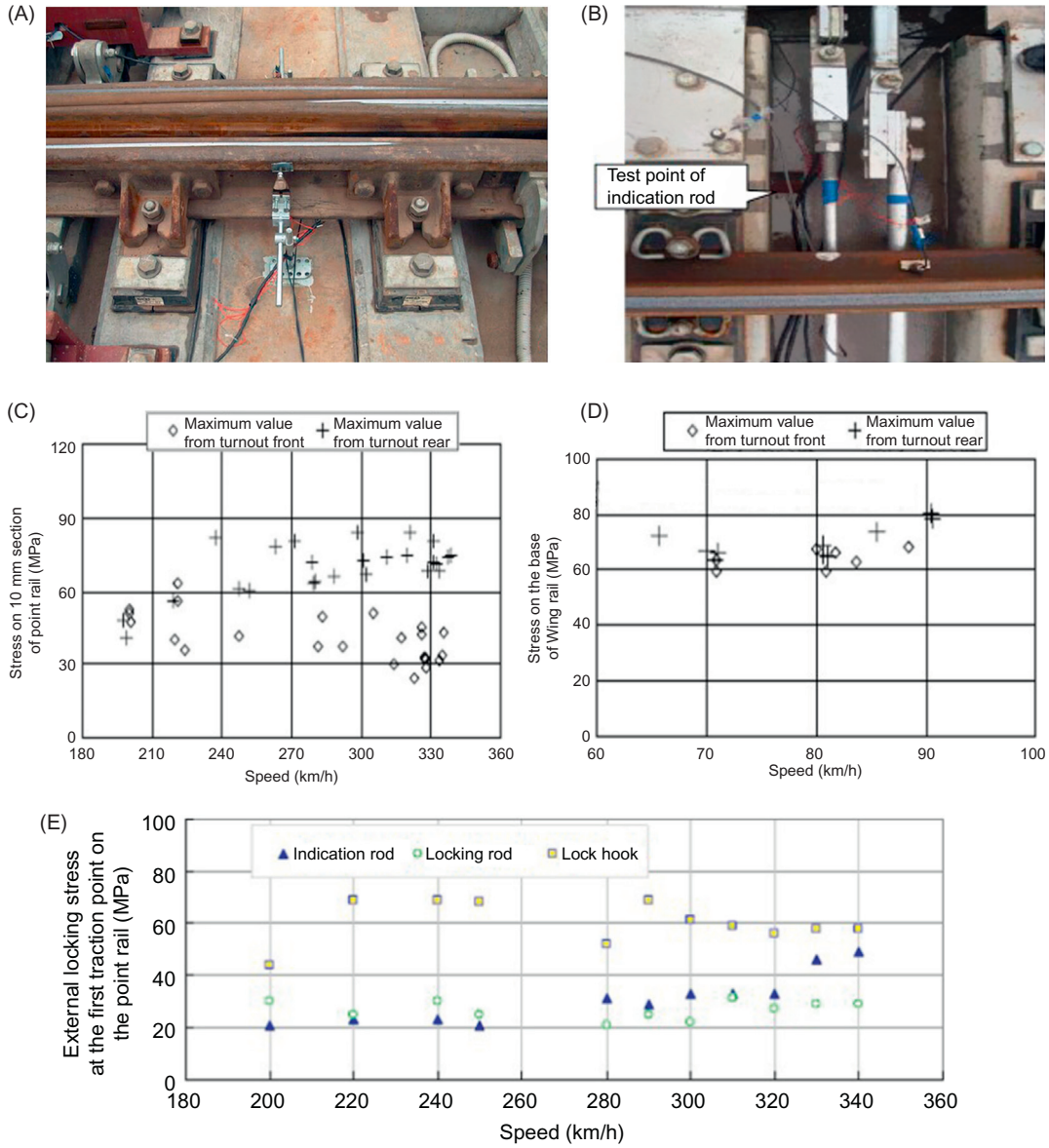

FIGURE 3.18

Tests on a high-speed turnout in the Wuhan−Guangzhou line: (A) Stress on wing rail; (B) Stress on switch/indication rod; (C) Point rail stress test values; (D) Wing rail stress test values; (E) Stress test values of lock hook, locking rod, and indication rod.

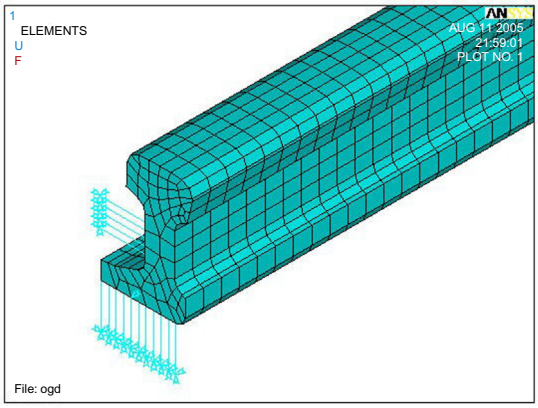

FIGURE 3.19

Calculation model of pointed rail at crossing heel.

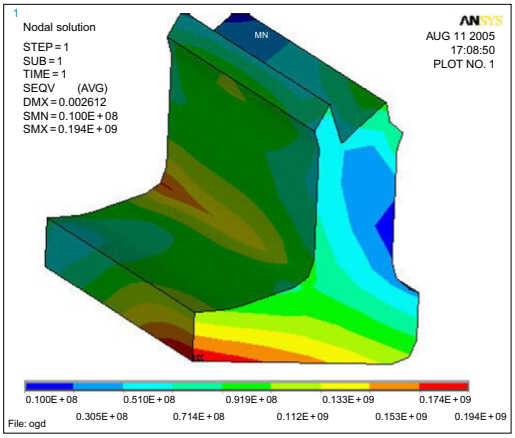

FIGURE 3.20

Stress distribution on pointed rail at crossing heel.

3.4.1 REQUIREMENTS

1. Pure steel

   For the rails of HSR, harmful elements in steel must be strictly controlled; for example, the content of *P* and *S* must not exceed 0.025%. The gas content in steel must be strictly controlled; for example, the content of hydrogen and oxygen must be less than $(2.5 \times 10^{-4})\%$ and $(20 \times 10^{-4})\%$, and the hydrogen content in finished rails must be less than $(2.0 \times 10^{-4})\%$. The content of residual elements, such as Mo, N, Cr, Cu, Ti, Sb, and Sn, in the steel must not exceed certain limits. To effectively reduce alumina in steel, Al-free deoxidation is adopted, and the Al content in steel must be $\leq 0.004\%$. The content of impurities in steel must be strictly controlled: Category A (sulfide) impurities must not exceed 2−2.5 orders; Category B (oxide), Category C (silicate), and Category D (spherical oxide) impurities must not exceed 1.0−1.5 orders.
2. Intact surface

   It is specified that the maximum allowable depths of scratches, abrasion marks, thermal scratches, longitudinal cracks, and indentations of roll scale on the rail surface under heat conditions are 0.35 mm on the tread and 0.5 mm on other parts; the maximum allowable depth of a longitudinal crack on rail surface under cold conditions is 0.3 mm on the tread and lower surface of rail base, and 0.5 mm on other parts.
3. Thinner decarburized layer

   Surface decarburation of rails will reduce the hardness and abrasion and peeling resistance of rail surface, resulting in premature rail corrugation. Thus, rails shall be ground with grinding trains before the line is open to traffic. Generally, each feed of the rail grinding train will not exceed 0.20−0.3 mm, so the decarburized depth of the rail must not exceed 0.3 mm.
4. Low residual tensile stress on rail base

   For traffic safety, it is necessary to limit the residual tensile stress on the rail base, especially for HSR rails. According to the technical specifications for rails of Chinese HSR, the maximum longitudinal residual tensile stress on the rail base shall be no more than 250 MPa.

5. High fracture toughness and low fatigue crack growth rate

   Under a test temperature of −20°C, the measured minimum and average values of fracture toughness K_{IC} are no less than 26 and 29 MPa $m^{1/2}$, respectively. The fatigue crack growth rate da/dN meets the specifications: when $\Delta K = 10$ MPa $m^{1/2}$, $da/dN \leq 17$ m/Gc; when $\Delta K = 13.5$ MPa $m^{1/2}$, $da/dN \leq 55$ m/Gc.

6. High geometric precision and smoothness

   High geometric precision and smoothness are essential to the riding quality of speed-up railways. Technical specifications have included the strict geometric tolerance, smoothness of the rail head and the body, distortion, and other indicators for rails used for PDLs and speed-up railways.

3.4.2 TYPE, SECTION, AND LENGTH OF RAILS

1. Types of rails

   Heavy rails and light rails (by unit weight). At present, mainly 60 kg/m heavy rails have been adopted for Chinese HSRs.

   Symmetrical and asymmetrical section rails (by section type). Asymmetrical section rails are mainly used to manufacture turnout rails (switch rail, point rail, wing rail, etc.), such as 60AT, 60D40, and 60TY.

   Carbon rails (no alloying elements, also called common rail), **micro-alloy rails** (trace alloy elements allowed, such as V, Nb, and Ti), and **low-alloy rails** (e.g., EN320Cr, containing 0.80−1.20% Cr in the steel) (by chemical compositions).

   Hot-rolled rails and **heat-treated rails** (by delivery status). Regardless of the strength of rails, rails delivered in hot-rolled status are called hot-rolled rails. Heat-treated rails are further subdivided into off-line heat-treated rails (reheat-treating after cooling) and online heat-treated rails (heat-treating using the residual rolling heat) according to the process conditions.

   Grade 780 MPa (e.g., U74), **Grade 880 MPa** (e.g., U71Mnk), **Grade 980 MPa** (e.g., U75V hot-rolled rail), **Grade 1080 MPa** (e.g., EN320Cr alloy rail, Japanese HH340 online heat-treated rail), **Grade 1180 MPa**, and **Grade 1280 MPa heat-treated rails** (by strength). Generally, rails with a strength grade of 1080 MPa and above are called wear-resistance rails or high-strength rails. At present, U75V and U71Mnk rails and their heat-treated equivalents are commonly used for railways in China. The minimum tensile strength of U75V hot-rolled steel rail is 980 MPa, which can increase to 1230 MPa after heat treatment; the minimum tensile strength of U71Mnk hot-rolled steel rail is 880 MPa; this rail is used for 350 km/h HSRs in China.

2. Rail section

   For HSRs, the rails must have considerable stiffness and wear resistance. To ensure adequate stiffness in the rails, I-shaped rails are generally adopted. In addition, rail height may be increased to achieve a desired horizontal moment of inertia, and a wider rail base may be selected to guarantee the required stability. In order to match the stiffness with stability, in designing the rail section, the ratio of rail height (H) to base width (B), that is, H/B, shall be 1.15−1.248.

   In all countries, the design of the rail head tread follows the principles below:

   a. The arc of the rail head tread shall be consistent with the dimensions of wheel tread, that is, the dimensions of the arc of approximately worn rail head tread

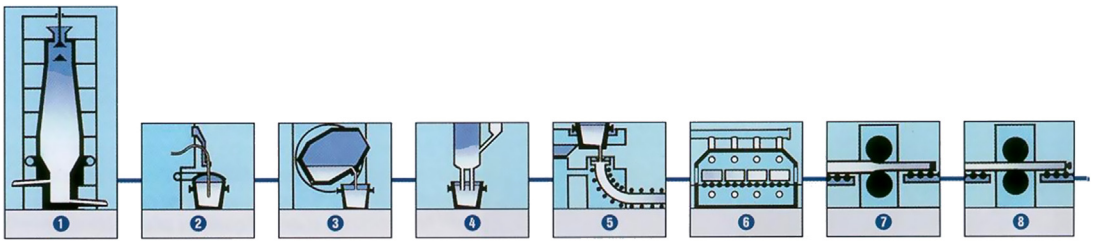

FIGURE 3.21

Bloom smelting and continuous casting system.

b. A large radius compound curve will be designed at the transitional area of the rail head and rail web to reduce cracks caused by stress concentration in this area

c. A compound curve will also be designed to achieve stable transition of the section at the transitional area of the rail head and rail web and to guarantee smooth connection with the rail base slope; and

d. A flat-bottom rail will be adopted to ensure stability of the section.

China makes no changes to the rail section of HSRs, and adopts a section of 60 kg/m rail, which is also used for speed-up railways. The above design principles are taken into account for new TY rails [37].

3. Rail length

Long cut-to-length rail features few welding joints, high smoothness of the rail end, no NDT blind area at the rail end, and capability to enhance track smoothness. It is an important symbol of HSR construction technology. The 100 m rails are commonly used in Chinese HSRs, and 50 and 55 m AT rails are used in turnouts.

3.5 MANUFACTURING OF RAILS

Rails produced with traditional manufacturing technologies (open-hearth process, die casting, rolling in passes, etc.) can hardly meet the desired purity of steel, geometry, smoothness, and appearance quality, and therefore cannot be used in HSR [38]. With the development of modern manufacturing technologies (e.g., converter smelting, continuous casting, rolling with universal mill, and horizontal−vertical combined straightening), the refining, finishing, conditioning, automatic quality detection, and long-length production for rails are realized, improving the interior and exterior quality of rails necessary for manufacturing rails for HSR.

3.5.1 REFINING

The refining technology for rail steel includes the following processes (as shown in Figure 3.21): pig iron desulfurization pretreatment → top-blown converter steelmaking → LF secondary refining → VD (vacuum degassing) or RH → bloom continuous casting. The processes of desulfurization pretreatment,

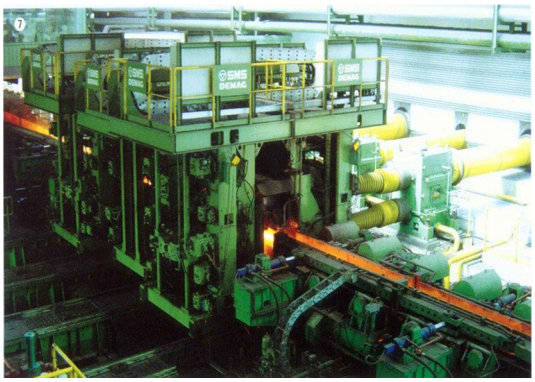

FIGURE 3.22

Rolling rails with compact universal mill.

FIGURE 3.23

Horizontal–vertical combined straightener.

secondary refining, and vacuum degassing are designed to purify the steel, improve the interior quality, and prolong the service life of rails. The processes of soft press and electromagnetic stirring are aimed at improving the quality of cast blooms; bloom continuous casting increases the yield of steel, and more importantly, enhances the uniformity of rail steel (unlike die casting blooms, which have a good middle section but poor ends).

3.5.2 FINISHING

Rail finishing technology includes the processes of heating in a walking-beam furnace, multi-pass descaling with HP water, rolling with a universal mill, and hot pre-bending of rails. The walking-beam furnace can uniformly heat the blooms to ensure dimensional uniformity of rails. Multi-pass descaling with HP water can guarantee the quality of appearance of rails. Rolling with a universal mill (as shown in Figure 3.22) can enhance the geometric accuracy of rails, and is one of the symbols of modern rail production. Hot pre-bending can reduce the residual stress and kinked rail straightening noises, and improve the working environment.

3.5.3 CONDITIONING

Rail conditioning technology includes horizontal–vertical combined straightening (as shown in Figure 3.23), quadrilateral hydraulic restraightening, cutting to length, and drilling with a combined sawing and drilling machine.

3.5.4 CENTRALIZED DETECTION

Rail detection technologies include ultrasonic detection, eddy current detection, laser-assisted automatic smoothness detection, and automatic detection of rail geometry.

3.5.5 LONG RAIL PRODUCTION

During the production of long rails, the processes of straightening of long kinked rails and cutting to length with a cooling saw are used, wherein the straightened and intermediate zones are obtained by cutting off the excess ends of hot-rolled metal, which realizes a high uniformity of dimensions in the entire rail, and significantly improves the overall smoothness of the rail. Additionally, the production of large-length rails facilitates the hot pre-bending of rails and eases the bending of rails before straightening, which reduces the residual stress and surface damage to rails due to straightening, and also improves the yield rate. Finally, the interior quality of rail ends can be ensured since no NDT blind areas exist after NDT. More importantly, using longer cut-to-length rails decreases the number of welding joints, which in turn improves riding safety and quality. Therefore, long cut-to-length rails have been adopted for HSR in many countries, for example 80 m in France, 50 m in Japan, and 120 m in Germany and by VAI.

CHAPTER

WHEEL–RAIL RELATION DESIGN

4

A track is connected with a traveling train through wheel–rail contact. Therefore, the wheel–rail relation links the railway vehicle and the track and enables their interaction in a wheel–track system. This relation defines the running characteristics of a train. Broadly, it is composed of wheel–rail contact geometry relation and wheel–rail creep relation.

The wheelset is guided by switch rails and point rails in a turnout. Since the rail top width and height change gradually, the wheel–rail contact will change accordingly, influencing the running characteristics of a traveling train. The design of the wheel–rail relation is crucial to riding quality and safety in high-speed turnouts.

4.1 WHEEL–RAIL CONTACT GEOMETRY RELATION

4.1.1 CALCULATION METHODS [39,40]

Different wheel–rail profiles reflect different wheel–rail contact geometry relations and parameters. These parameters are essential to the study of dynamic interactions in a wheel–rail system.

The wheel–rail contact geometry relation is affected by railhead profile, track height, rail cant, track gauge, lateral/vertical displacement and torsion angle of rails, tread profile, wheel back-to-back and radius of tread rolling circle of wheels, and lateral distance from axle center to nominal tread rolling circle, as well as the lateral displacement, yaw, and longitudinal displacement difference of the wheelset.

In the calculation, the input parameters include lateral displacement and yaw angle of the wheelset, and the output parameters include vertical displacement of center of gravity of the wheelset, curvature radius of tread, radii of tread rolling circles and their difference at right-left wheel contact points, right-left wheel contact angles and their difference, roll angle of the wheelset, and curvature radii at right and left track contact points. All the wheel–rail contact geometry parameters are functions of the lateral displacement and yaw of the wheelset.

There are many wheel–rail profiles, which can be expressed by a fitting curve based on a set of discrete coordinate points when a simple analytical expression is unavailable. Given the coordinate of any point on the wheel and rail, the wheel–rail contact point can be determined by the trace method. The basic assumptions are as follows:

1. The wheel and rail are approximated as a rigid body, and no points on the wheel surface may be embedded in the rail

Design of High-Speed Railway Turnouts.

2. The two wheels of a wheelset contact the rails of a track at the same time, and no wheel–rail detachment occurs
3. The contact points of the wheelset and rails are spatially identical
4. There is a common tangent plane at the wheel–rail contact point (between the wheel and the rail); and
5. The wheelset contacts the rail at a point or spot, and there is no collinear or coplanar contact between the wheel tread and the rail.

The wheel–rail contact geometry relation will be a spatial issue when referring to the yaw or lateral displacement of the wheelset. However, it will become a planar issue when setting aside yaw angle of the wheelset, as this relation may only change in a plane. As the wheel–rail contact geometry parameters are functions of the lateral displacement of a wheelset, the positions of the contact points can be calculated with the following geometric conditions: (i) the wheel–rail vertical distance is zero at the contact points, and greater than zero at other points; and (ii) the wheel–rail profiles at the contact points have the same slope, that is, they have a common tangent. The two conditions are equivalent. The wheel–rail contact point is defined by the former and verified by the latter.

When lateral displacement and yaw occur at the same time, the wheel–rail contact points are determined by scanning the points on the wheel–rail profiles, determining the points with the minimum vertical distance, comparing the minimum distances between the wheelset and rails, and adjusting the roll angles of the wheelset to meet the wheel–rail contact conditions. This method corresponds to that for the plane issue. With these contact points, the contact parameters can be determined.

4.1.2 RAIL PROFILES

1. Switch rail

   The switch rail is provided with a pointed tip by horizontally cutting the railhead and horizontally and vertically cutting the rail base. In this way, the wheelset can make a transition between stock rails and switch rails easily, and two rails can be properly closed. Additionally, the top of the switch rail will be vertically cut to make the switch rail lower than the stock rail, so as to prevent the actual point of the switch rail being damaged or bearing excess vertical wheel load.

   The hidden tip point structure is applied to prevent collision between the point of the switch rail and wheels traveling from turnout rear. In this structure, the point of the switch rail is about 16–23 mm lower than the stock rail, “hidden” by about 3 mm within the jaw of the stock railhead. Therefore, the wheelset will not impact the actual point, even at the maximum vertical wear of the wheelset and stock rail top, as shown in Figure 4.1A. However, the height difference shall not exceed 25 mm, that is, the switch rail shall not be below the flange; otherwise, the flange may mount the switch rail when the switch rail and stock rail are separated (traveling from turnout rear).

   The tools for vertically cutting the switch rail top shall have the same profile as the stock rail top. The switch rail top is vertically cut as per the longitudinal gradient formed by the height differences of theoretical center lines on the control section. This process directly affects the traffic conditions and service life of switch rails. In designing a common turnout, the height difference of the switch rail top shall follow the following rules: The wheelset may make a

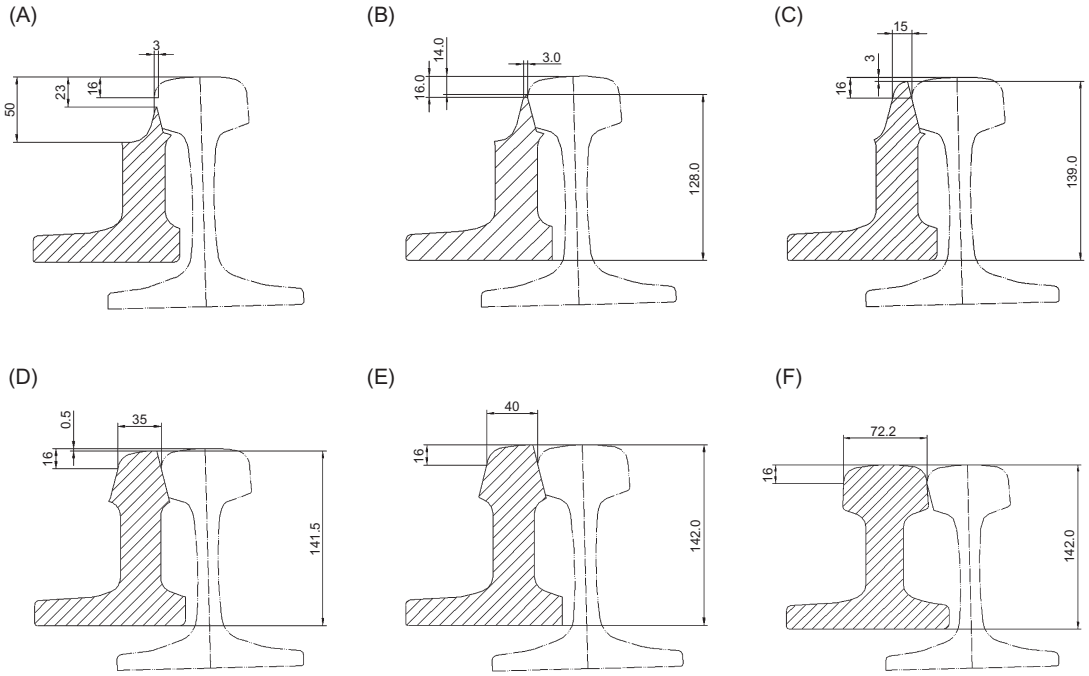

FIGURE 4.1

Profiles of straight switch rail: (A) Point of switch rail; (B) Top width 3 mm; (C) Top width 15 mm; (D) Top width 35 mm; (E) Top width 40 mm; (F) Top width 71.2 mm.

transition from the switch rail section with top width of 20 mm, and then the switch rail and the stock rail will share the vertical wheel load. Before approaching this section, there is no load on the switch rail, and the switch rail top will be depressed from the section with 50 mm top width (the same level as the stock rail). The stock rail is relieved of the load after this section; at the same time, one wheel of the wheelset with the minimum wheel back-to-back and flange wear can cling to a rail, and the arc of the outer tire of the opposite wheel may overlap with the side connecting arc of the stock railhead, so that the tire will not press the gauge or turn the stock rail. For Chinese high-speed turnouts, considering the riding quality and smaller deviation of the wheel profile, the "rules" do not prevail, and the wheelset may make a transition within 15−40 mm.

The processes of cutting and bending are combined to make the railhead at the point of cut switch rail be supported by the rail web, forming the curved working surface on a curved switch rail. A curved stock rail may also be bent if required to maintain the gauge, alignment, and closure between straight switch rail and curved stock rail at the switch.

Figure 4.1 shows the profiles of the control sections of the straight switch rail of a No. 18 high-speed turnout for 350 km/h in China. The profiles of curved switch rail and straight switch rail may differ slightly due to height differences.

2. Point rail

In China, the swing nose rails are assembled by long and short point rails (made of flat-web-special section). The head and base of the two rails shall be cut for better attachment and pointed working surface. The process is as follows: Horizontally cut the railhead and horizontally and vertically cut the rail base on the nonworking surface of the short point rail (apply to the nonworking surface of long point rail occasionally); assemble with the long point rail into an "inverted V shape"; and horizontally cut the railhead and rail base on the working surface.

The selection principle for the cut arc of a rail section is as follows. The radius of the cut arc on the working surface contacting with the flange shall be the same as that of the side connecting arc of the original railhead. Smaller arc radii are preferable for the two railhead profiles at a narrow section (free from vertical wheel load). For the part contacting the flange top surface, the radius of the cut arc shall be consistent with the arc of the flange top. For the working surface contacting the wheel back, the radius of the cut arc is generally taken as 3–5 mm to leave a larger contact area for rail side and wheel back.

As with the switch rail, the wheel tread will contact the point rail top from the section with a top width of 20 mm, and leave the wing rail at the section with a top width of about 50 mm.

The point of the long point rail, like the switch rail, may be hidden vertically. For special section wing rail, the horizontal hidden tip point structure may be used if the railhead is wide enough. In this case, the head of the wing rail is partially cut to hide the point of the closed point rail within the profile of the wing railhead (rather than the jaw), so that the height difference of the point may be properly reduced. Figures 4.2 and 4.3 show the profiles of the control sections of the long point rail and wing rail of a No. 18 high-speed turnout for 350 km/h in China. About 9 mm of the point of a point rail is hidden.

The assembled short and long point rails may adopt fitted points or a closed point structure. For the fitted point structure, a groove will be cut on the assembled head of the long point rail to fit the corresponding convex form on the head of the short point rail. This structure makes the working surface of the point rail a continuous straight line in the diverging line. However, it increases the risk of rail fracture at the fitting section due to excess cut of the long point rail. Moreover, the process is rather complex. For the closed point structure, the point of the short point rail will be sharpened and close with the side of the head of the long point rail. This process is simple, as the head of the long point rail will not be cut. However, structural irregularities similar to those in the front of switch rail and long point rail may occur.

For point rails with a single flexible rail that adopts the pointed rail at the heel of a crossing as a diagonal joint, the front of the pointed rail at the heel of the crossing will be sharpened and come into contact with the heel of the short point rail when the diverging line is in operation. The pointed rail at the heel of the crossing is generally made of common rail.

4.1.3 WHEEL–RAIL CONTACT GEOMETRY (WITHOUT WHEELSET LATERAL DISPLACEMENT)

Switch rails and point rails have special profiles, and they bear no load before the transition of the wheelset (when the wheelset is in contact with the stock rail or wing rail). The stock rail and wing rail will bend depending on the top width of the switch rail and point rail. Therefore, the wheel–rail contact geometry relation will change longitudinally regardless of the lateral displacement of the wheelset. With the transition of the wheelset, the switch rails and point rails are under full load. As the rail profile

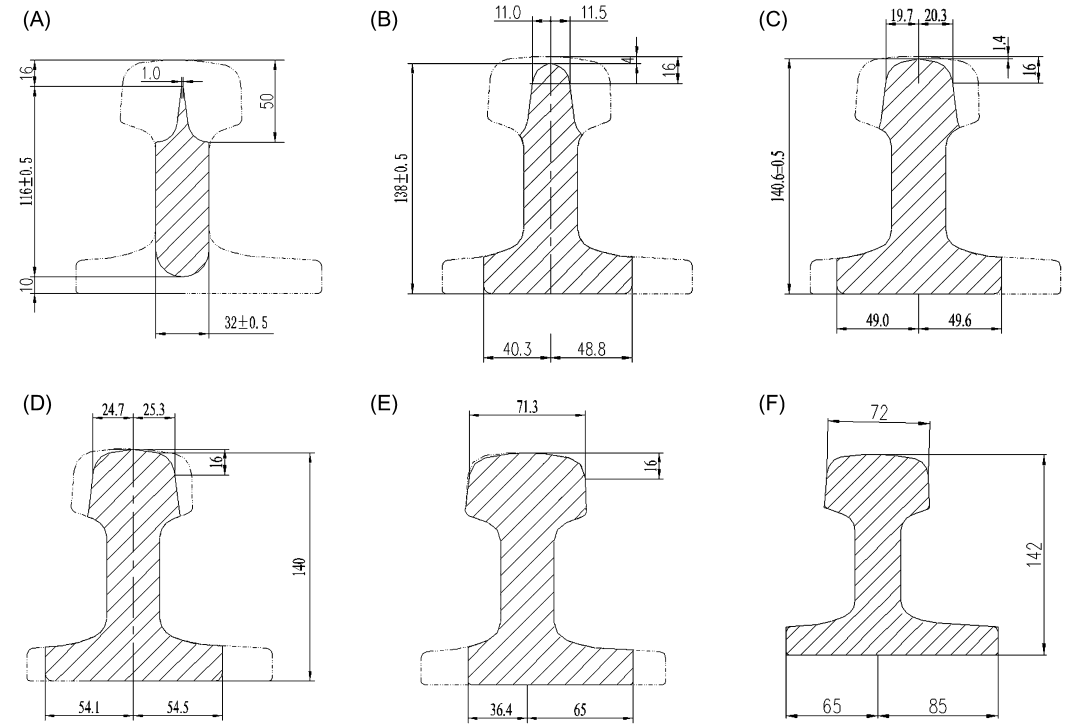

FIGURE 4.2

Profiles of long point rail: (A) Point of point rail; (B) Top width 22.5 mm; (C) Top width 40 mm; (D) Top width 50 mm; (E) Top width 71.3 mm; (F) Top width 72 mm.

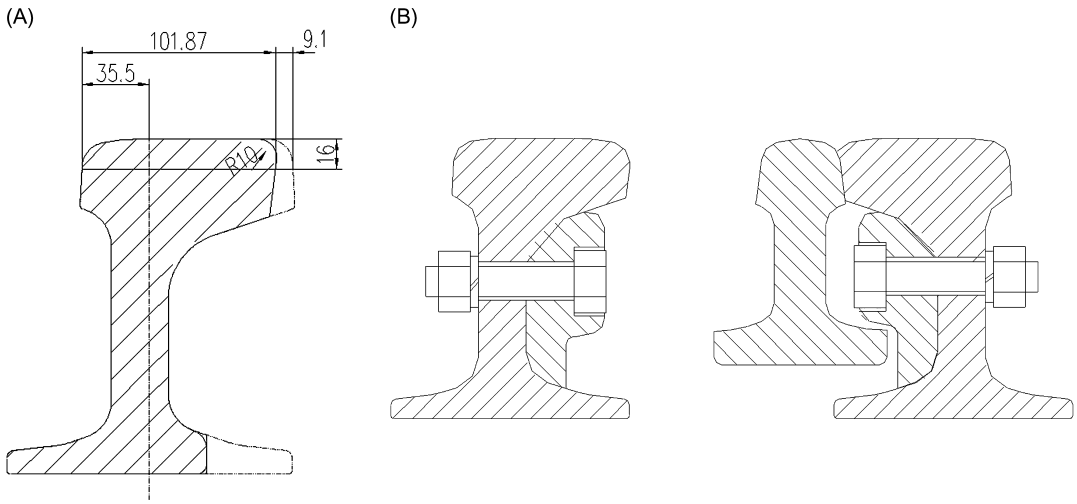

FIGURE 4.3

Wing rail profile: (A) Wing rail profile at the point of point rail; (B) Relative positions of point rails and wing rails.

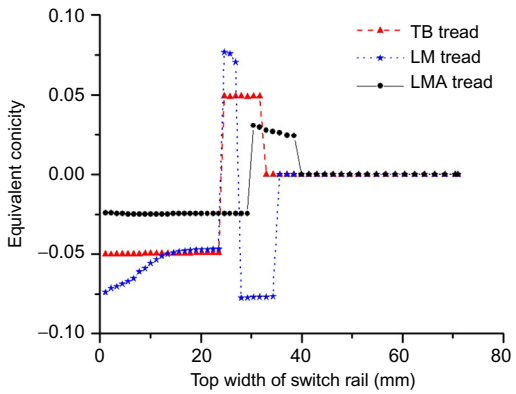

FIGURE 4.4

Equivalent tread conicity at the switch.

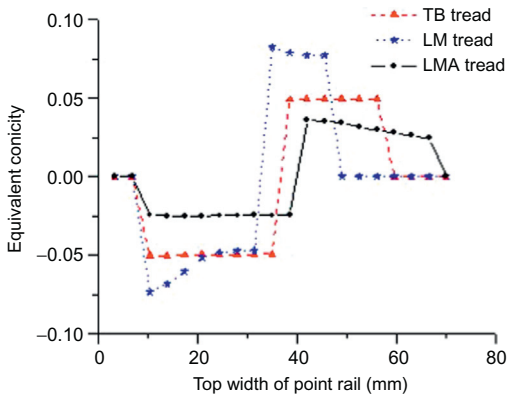

FIGURE 4.5

Equivalent tread conicity at the crossing.

changes (the two rails have different profiles from stock rail), the wheel–rail contact geometry relation will also change.

In studying the static wheel–rail contact geometry relation, ignoring the rail displacement and assuming that the switch rails and stock rails, point rails and wing rails, long/short point rail, pointed rail at the heel of the crossing, and short point rail are closed, the profile of top of the closed rails may be deemed as one specially shaped profile. Figure 4.1 shows a "combined" profile of closed switch rail and stock rail.

1. Equivalent tread conicity [41]

   When a train travels in the main line, the left wheel will contact the rail at r_0 of the nominal tread rolling circle. The contact point between the right wheel and the rail will change with the top widths of the switch rail and the point rail. Given the distance from right wheel–rail contact point to nominal tread rolling circle of d_R, d_R equals the top width of the switch rail and the point rail before wheel transition, which may be deemed as that the right wheel shifts about d_R to the left. After wheel transition, the contact point shifts from a place near the gauge corner to the nominal tread rolling circle, the radii of the actual tread rolling circles of the left and right wheels traveling in main/diverging line can be calculated by:

$$\begin{cases} \text{Main line: } r_L = r_0 - \lambda y_w \quad r_R = r_0 + \lambda(y_w - d_R) \\ \text{Diverging line: } r_L = r_0 - \lambda(y_w + d_R) \quad r_R = r_0 + \lambda y_w \end{cases} \tag{4.1}$$

   where y_w is the lateral displacement of the wheelset. With the above equations, the relationship between the equivalent tread conicity and lateral displacement of the wheelset, and the switch rail–point rails relation in a turnout can be expressed as:

$$\begin{cases} \Delta P/\overline{P} \le 0.65 \quad \text{(Limit 1, acceptable)} \\ \Delta P/\overline{P} \le 0.60 \quad \text{(Limit 2, increased safety margin)} \end{cases} \tag{4.2}$$

   Figures 4.4 and 4.5 depict the changes in the equivalent conicity of TB, LM, and LMA wheel treads with the top widths of switch rails and point rails when a train travels in a No. 18 turnout for 350 km/h (rail cant 1:40, CHN 60 kg/m rail, no check rail in the main line) in the main line.

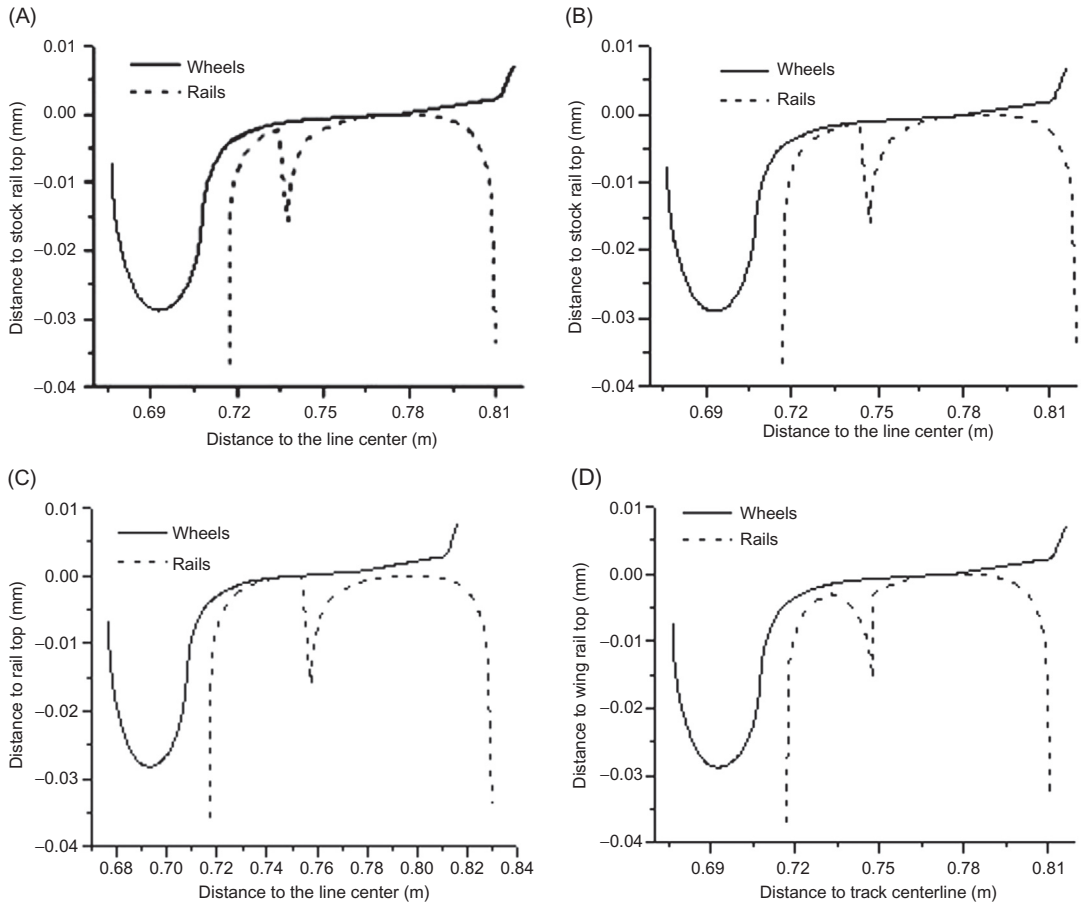

FIGURE 4.6

(A) Contact at top width 20 mm of switch rail. (B) Contact at top width 30 mm of switch rail. (C) Contact at top width 40 mm of switch rail. (D) Contact at top width 30 mm of point rail.

In these figures, regardless of the lateral displacement of the wheelset, the equivalent tread conicity will fluctuate with widening of the top width of switch rails and point rails when the wheelset advances in the main line. The maximum equivalent conicity is about 0.08 for LM tread, 0.05 for TB tread, and 0.025 (at the switch) and 0.035 (at the crossing) for LMA tread. From the above, LMA tread involves minimum irregularity when traveling in the turnout. It is the preferable tread type.

As the switch rail and the point rail differ in top profile and height difference, the variation trend of equivalent conicity with the top width may also vary between the two. The contact information between LMA tread and switch rail at top widths of 20, 30, and 40 mm, as well as between LMA tread and point rail at top widths of 30, 40, and 50 mm, are shown in Figures 4.6 and 4.7.

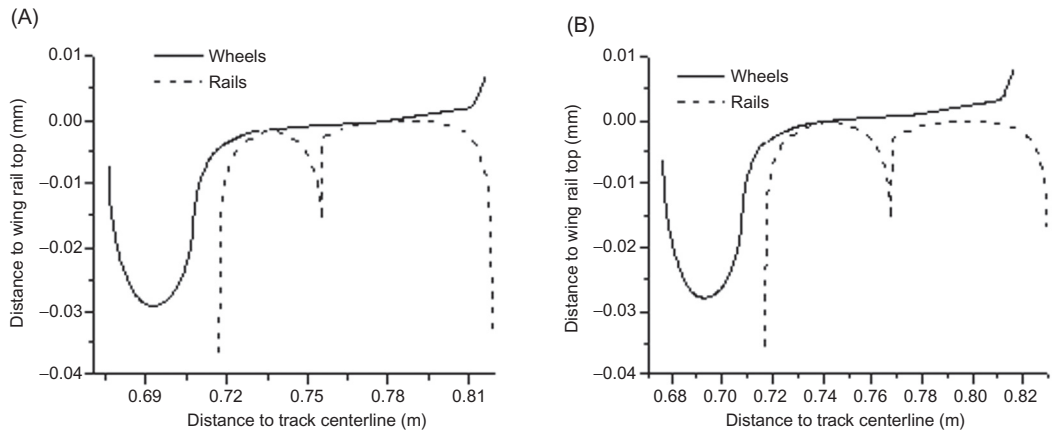

FIGURE 4.7

(A) Contact at top width 40 mm of point rail. (B) Contact at top width 50 mm of point rail.

The wheel tread will simultaneously come into contact with the top surfaces of switch rails and stock rails, and point rails and wing rails at the critical point of wheel-load transition, where the wheel load will be shared by two rails. In consideration of the wheel–rail rigid body displacement and elastic compressive deformation at the contact point, the wheel-load transition will no longer be limited to a critical point, but a certain range. In this case, the wheel load distributed to each rail can be obtained with the displacement coordination conditions.

For wheels with different treads, the wheel load will transfer at different sections on the switch rail and the point rail. LM tread is the foremost, and LMA tread is the backmost. For wheels with the same tread, the wheel load will transfer at different points on the switch rail and the point rail. The reason lies in the different top profile and height difference of the two rails, cutting of wing railhead, and so on.

2. Roll angle coefficient

As with equivalent conicity, in consideration of the lateral displacement of the wheelset and top widths of switch rails and point rails, the roll angle coefficient can be defined as:

$$\Gamma = \frac{\theta_w}{2y_w \mu d_R} = \frac{\text{Wheelset roll angle}}{\text{The sum of the distances from the left and right contact points to the nominal contact points}} \tag{4.3}$$

where θ_w is the roll angle of the wheelset.

When a train travels in a Chinese No. 18 turnout for 350 km/h in the main line, the changes of roll angles and roll angle coefficients of TB, LM, and LMA treads with top widths of switch rails and point rails at the switch and the crossing are shown in Figures 4.8 and 4.9. With the change of wheel–rail contact points, the wheelset will roll at the switch and the crossing even if there is no lateral displacement. The greater the roll angle, the worse the riding quality. The roll angles are different for different treads. TB tread is the greatest, followed by LM tread and

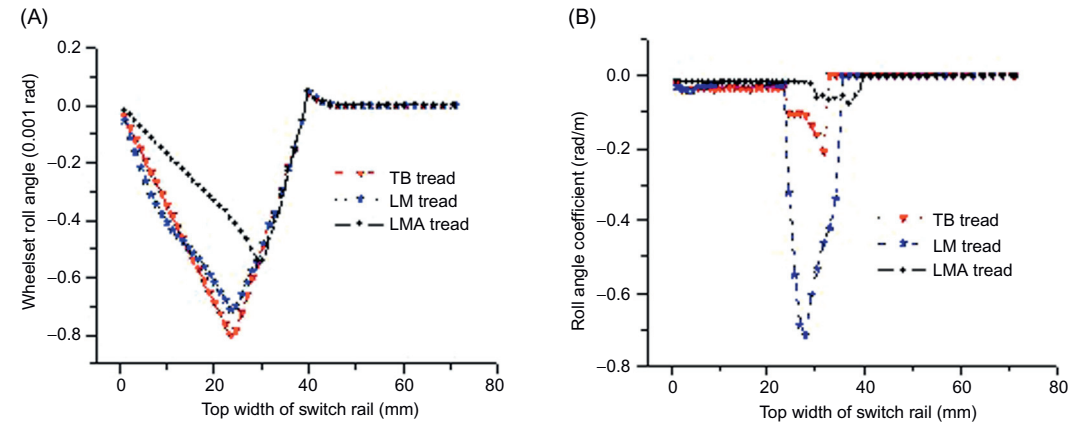

FIGURE 4.8

(A) Change of wheelset roll angle with the top width of switch rail. (B) Change of roll angle coefficient with the top width of switch rail.

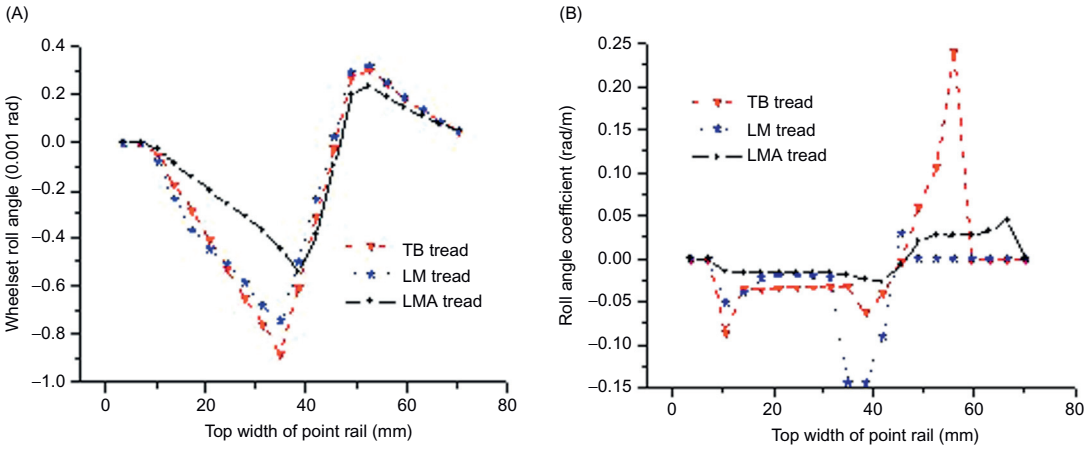

FIGURE 4.9

(A) Change of wheelset roll angle with the top width of point rail. (B) Change of roll angle coefficient with the top width of point rail.

LMA tread in order. The roll angle coefficients reflect the change rate of roll angle of the wheelset with wheel–rail contact points. In view of the different top profiles of the switch rail and point rail, LM tread is greatest at the switch, TB tread is greatest at the point rail. However, LMA tread is smallest at both points. The roll angle of the wheelset is controlled within 4/1000 rad for high-speed turnouts for 300 km/h in France.

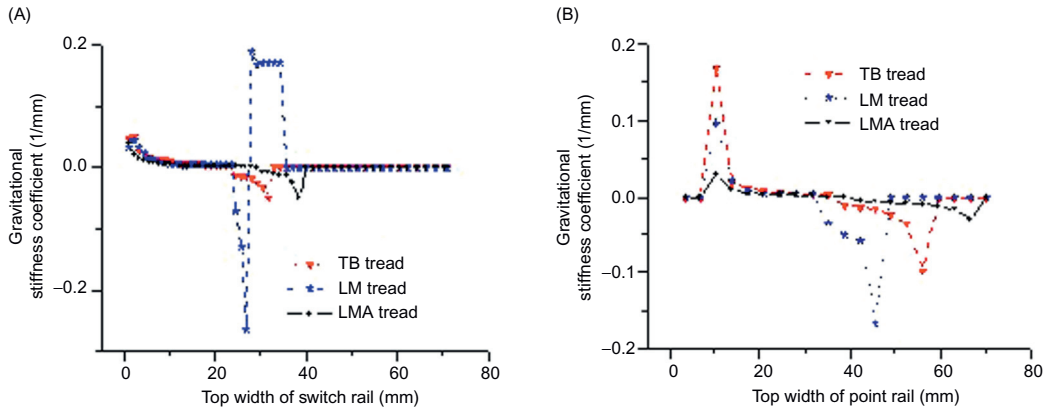

FIGURE 4.10

(A) Change of gravitational stiffness coefficient with the top width of switch rail. (B) Change of gravitational stiffness coefficient with the top width of point rail.

3. Gravitational stiffness of the wheelset

As with equivalent conicity, in consideration of the lateral displacement of the wheelset and top widths of switch rails and point rails, the gravitational stiffness of the wheelset can be defined as:

$$K_{gy} = \frac{W}{2y_w \mu d_R}[tg(\delta_R + \theta_w) - tg(\delta_L - \theta_w)] = \frac{\text{Resiliency of the wheelset}}{\text{The sum of the distances from the left and right contact points to the nominal contact points}} \tag{4.4}$$

where W is the weight of the wheelset and δ_L and δ_R are the contact angles of right and left wheels.

When a train travels in a Chinese No. 18 turnout for 350 km/h in the main line, the changes of gravitational stiffness coefficient of the wheelset of TB, LM, and LMA treads with top widths of switch rails and point rails at the switch and the crossing are shown in Figure 4.10. Given the same top widths of the switch rail and the point rail, the smaller the gravitational stiffness of the wheelset, the less the resiliency, and the better the riding quality. From the figures, LMA tread is ideal for Chinese high-speed turnouts.

Similarly, the contact angle difference coefficients between different treads and the switch rail and point rail, gravitational angular stiffness of the wheelset, and other contact geometry parameters can also be obtained. Comprehensively, LMA tread is compatible with the wheel–rail relation in Chinese high-speed turnouts.

4. Structural irregularities

Figure 4.11 shows the changes in the wheel–rail contact points on the tread between the wheel and straight switch rail/stock rail with the top width of the switch rail at the switch. Figure 4.12 shows the changes in the wheel–rail contact points on the tread between the wheel and long point rail/wing rail with the top width of the point rail. Before the wheel-load transition, the contact points will move outward, increasing the top width of the switch rail and the

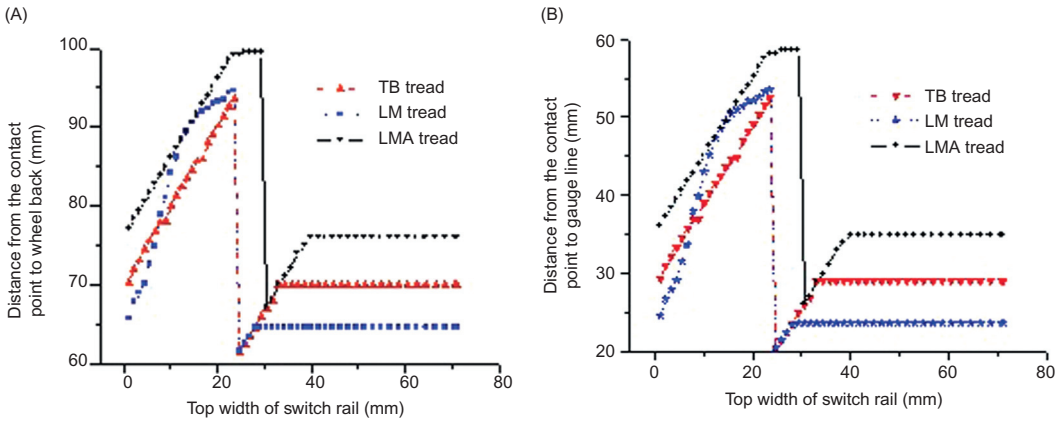

FIGURE 4.11

(A) Change of contact point on the wheel with the top width of switch rail. (B) Change of contact point on the rail with the top width of switch rail.

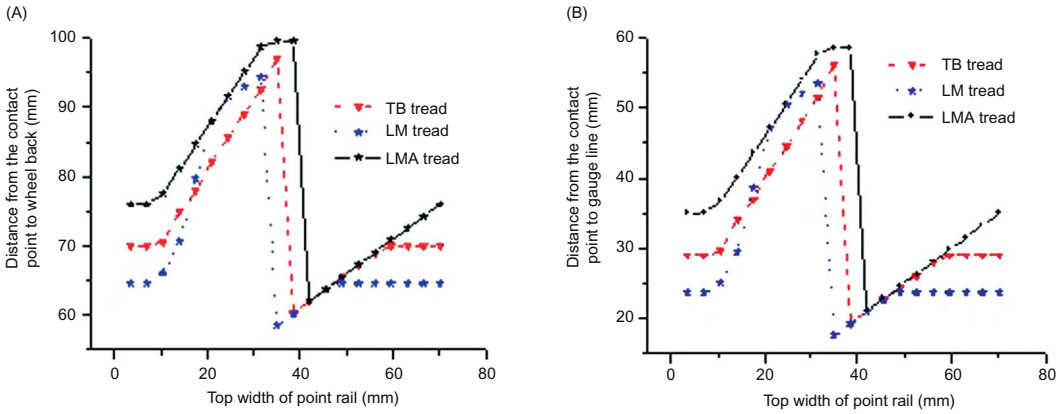

FIGURE 4.12

(A) Change of contact point on the wheel with the top width of point rail. (B) Change of contact point on the rail with the top width of point rail.

point rail. After that, the contact points will shift significantly, moving outward from the gauge line, increasing the top width of the switch rail and the point rail. The change of wheel–rail contact points on the wheel and the rail follows the same rule. The only difference is in the initial coordinate, regardless of the lateral displacement of the wheelset. The wheel–rail contact points on the opposite wheel and stock rail are slightly different (within 1 mm) due to the change of wheelset roll angle.

This change rule is determined by the characteristics of turnout structure, corresponding to a case in a section, where the right rail has vertical profile and alignment irregularities as shown

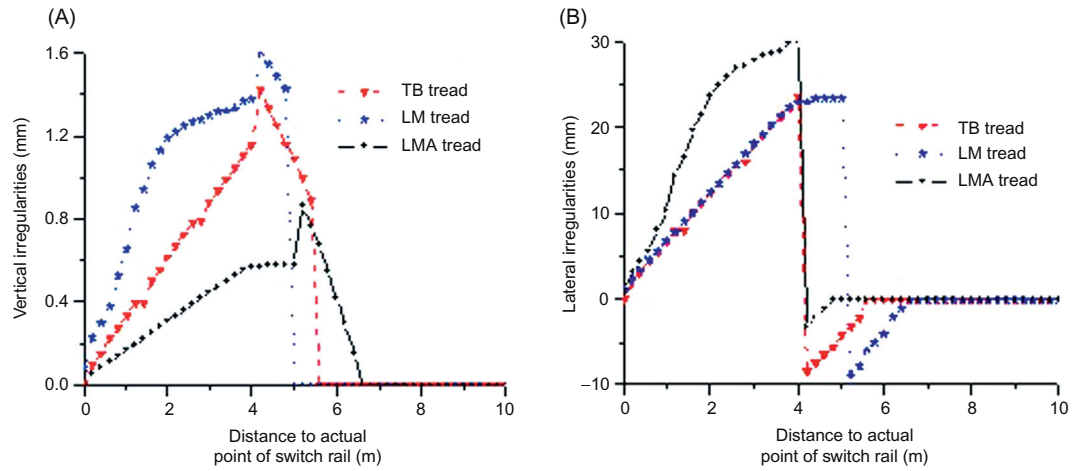

FIGURE 4.13

(A) Vertical irregularities at the switch. (B) Lateral irregularities at the switch.

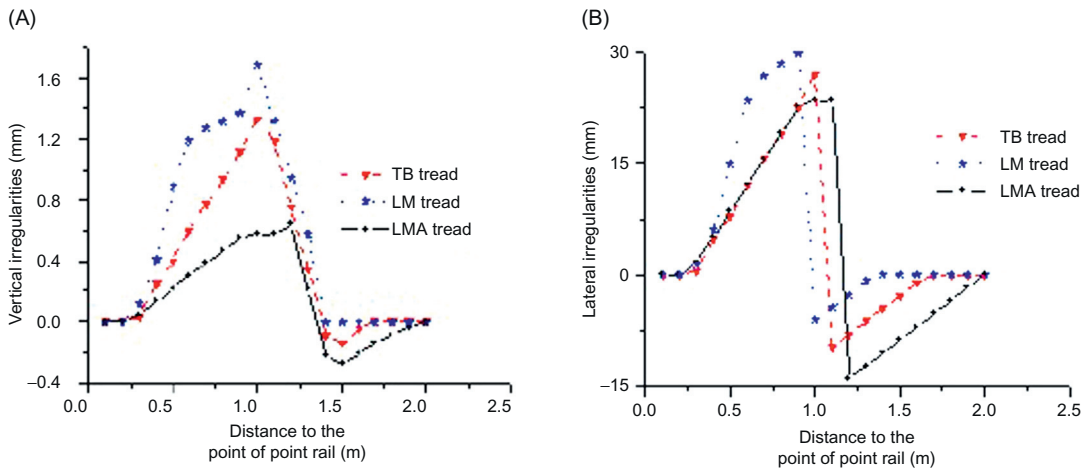

FIGURE 4.14

(A) Vertical irregularities at the crossing. (B) Lateral irregularities at the crossing.

in Figures 4.13 and 4.14. These irregularities, or structural irregularities, as an impact source of train-turnout vibration, may be unavoidable with the use of gradually widened and risen switch rail and point rail.

In these figures, the lateral irregularities are great and vertical irregularities are minor in the turnout. LM tread produces the greatest irregularities, followed by TB tread and then LMA

tread. The wavelength of the vertical and lateral irregularities at the crossing is about 2 m due to rapid change of the top width of point rails, much less than 5–7 m at the switch. However, the irregularity amplitude at the crossing is equivalent to that at the switch, so the wheel–rail vertical impact at the crossing will be much greater. To reduce wheel–rail dynamic interaction and improve riding quality and safety, the top profiles of the switch rail and the point rail should be reasonably designed as per the wheel tread.

4.1.4 WHEEL–RAIL CONTACT GEOMETRY IN THE DIVERGING LINE

The wheel–rail contact geometry relation follows the same change rule when a train passes through the switch in the diverging line, as the curved switch rail and straight switch rail have similar top profiles, differing only slightly in top height. When a train passes through the crossing in the diverging line, if the point rail is assembled with short and long point rails (the point of a short point rail is hidden below the jaw of the long point railhead), new structural irregularities may be produced with the transition of wheel load (from long point rail to short point rail). Taking LMA tread, for example, a comparison of wheel–rail contact geometry relations when the wheelset passes through the crossing in the diverging line and in the main line is shown in Figure 4.15.

Figure 4.15 shows that the vertical and lateral structural irregularities are greater and broader when a train travels in the diverging line than in the main line, due to changes in the top profiles of the long and short point rails and pointed rail at the heel of crossing. The structural irregularities limit the speed in the diverging line. To reduce wheel–rail dynamic interaction when a train travels in the diverging line, point rails with double flexible rails and solid frog may be used.

4.1.5 WHEEL–RAIL CONTACT GEOMETRY (WITH WHEELSET LATERAL DISPLACEMENT)

When the wheelset of LMA tread travels in a Chinese No. 18 turnout for 350 km/h, considering a wheelset lateral displacement of 0 – ±12 mm, the changes of wheel–rail contact geometry relations with the lateral displacement of the wheelset at top widths (measured at gauge line) of 20, 30, and 40 mm of straight switch rail, as well as 30, 40, and 50 mm of long point rail, are shown in the following pages.

1. Equivalent tread conicity

   Figure 4.16 shows the changes of equivalent conicity at typical sections at the switch and the crossing with the lateral displacement of the wheelset. Figure 4.17 shows the changes in wheel–rail contact point at the sections of switch rails and point rails with top width of 30 mm with the lateral displacement of the wheelset.

   The equivalent conicity is smaller when the flange is not in contact with the switch rail and the point rail. The equivalent conicity is about 0.04 when the wheel–rail contact points are on the stock rails and wing rails, and slightly bigger than 0.025 in a section, as the points shift outward due to the impact of top widths of switch rails and point rails. When the wheel–rail contact points move to the switch rail and the point rail, the equivalent conicity is about 0.022, equal to that in a section. When the wheel contacts with the gauge corner on the

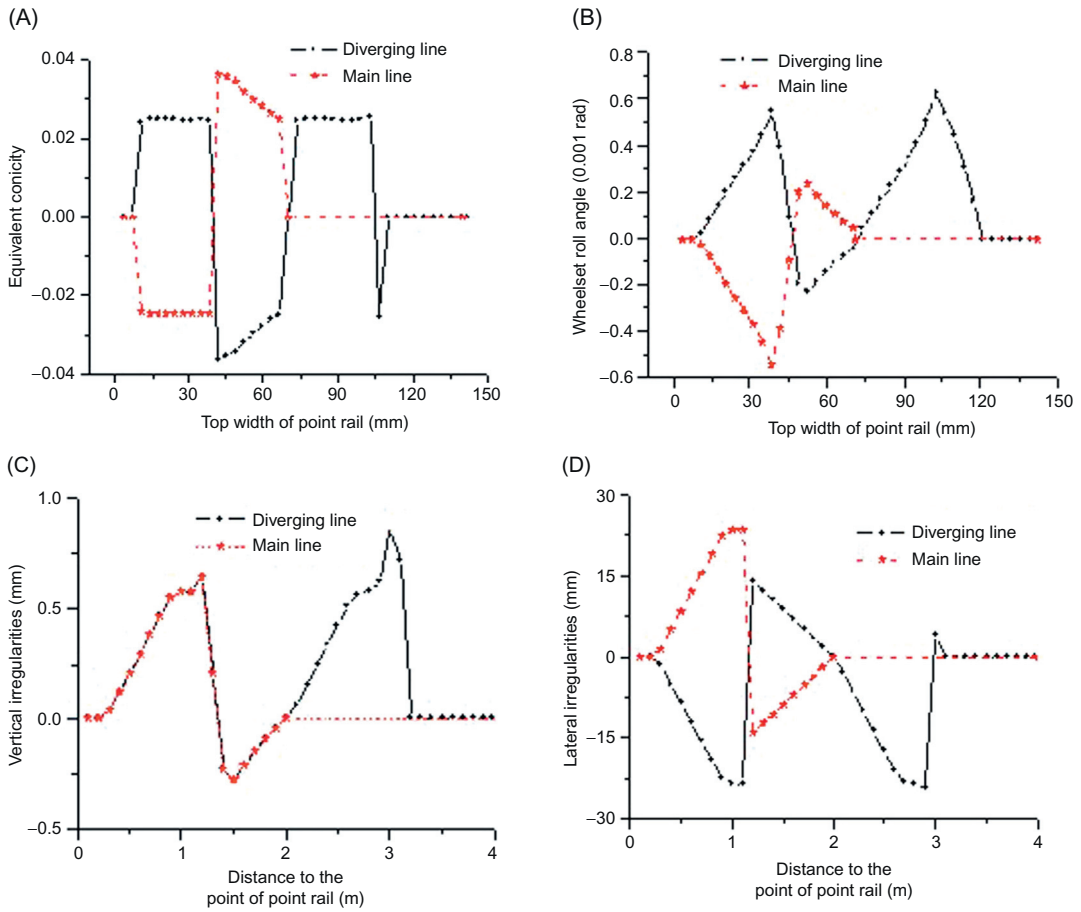

FIGURE 4.15

(A) Change of equivalent conicity with top width of point rail. (B) Change of roll angle with top width of point rail. (C) Distribution of vertical irregularities at the crossing. (D) Distribution of lateral irregularities at the crossing.

switch rail and the point rail, the equivalent conicity is larger. When the lateral displacement of the wheelset exceeds the clearance between flange and gauge line, the wheel will climb on the rail.

The wheel-load transfer points are in a dynamic state when taking the lateral displacement of the wheelset into consideration. The larger the wheelset lateral displacement toward the switch rail and the point rail, the greater the advancement of wheel-load transfer points. If lateral movement occurs before approaching a turnout, the lateral vibration will be intensified when the train travels the turnout.

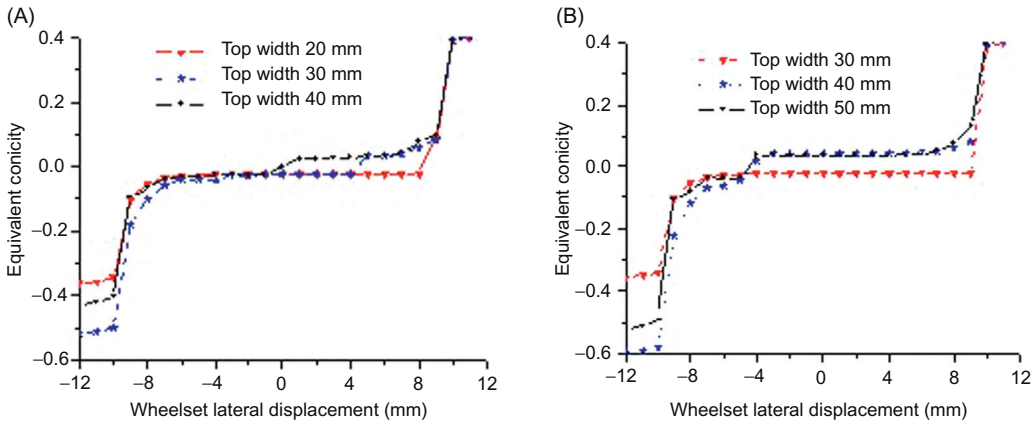

FIGURE 4.16

(A) Equivalent conicity at typical sections of switch rail. (B) Equivalent conicity at typical sections of point rail.

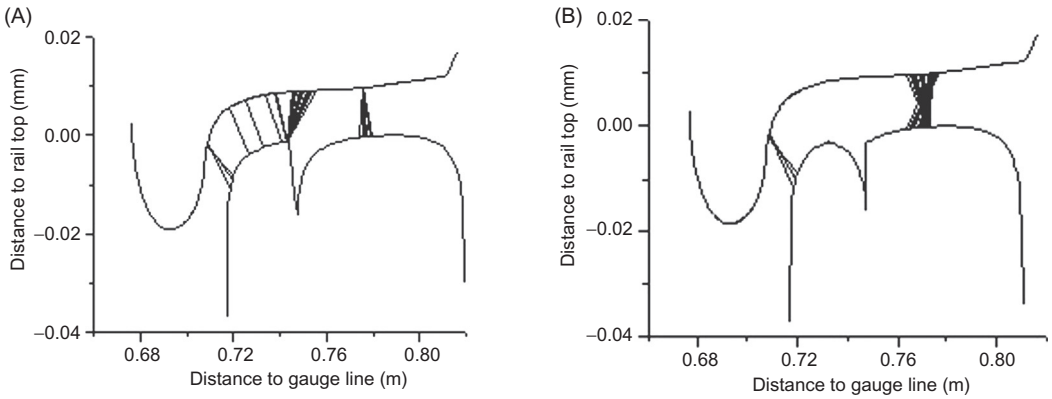

FIGURE 4.17

(A) Change of wheel–rail contact point at top width 30 mm of switch rail. (B) Change of wheel–rail contact point at top width 30 mm of point rail.

2. Structural irregularities

Figures 4.18 and 4.19 show the changes in the vertical and lateral structural irregularities on right and left rails at typical sections at the switch and the crossing with lateral displacement of the wheelset.

When the flange clings to and tends to mount the rail, vertical structural irregularity is great and negative, indicating that the rail top surface is detached from the wheel tread. The vertical structural irregularity is small when the flange and rail are detached. The vertical structural irregularities on the stock rail change slightly with lateral displacement of the wheelset. Owing

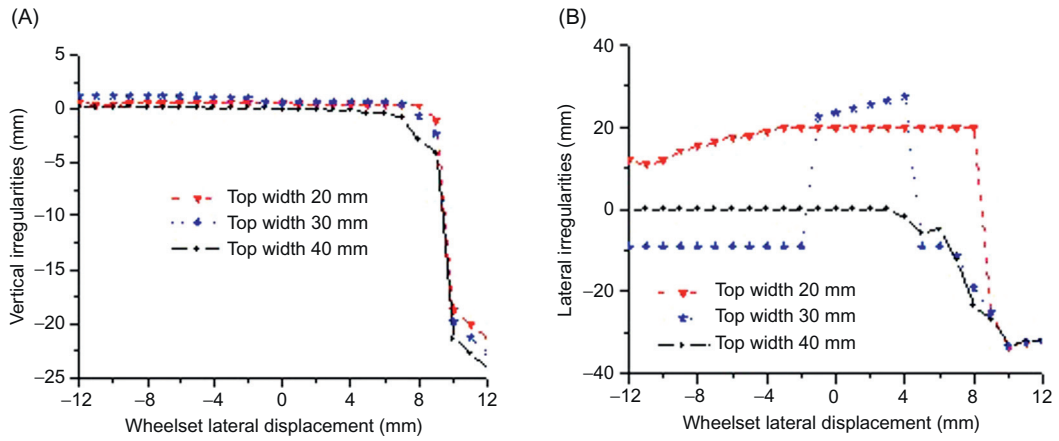

FIGURE 4.18

(A) Change of vertical irregularities at typical sections of switch rail. (B) Change of lateral irregularities at typical sections of switch rail.

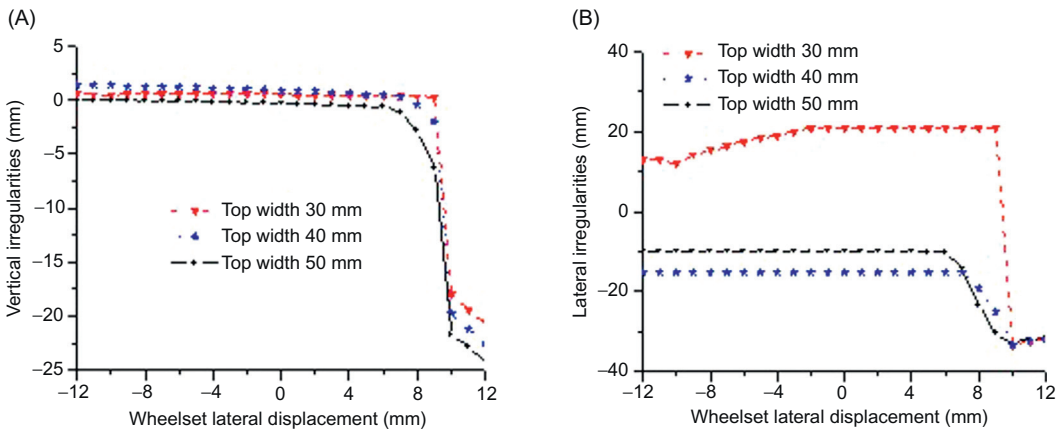

FIGURE 4.19

(A) Change of vertical irregularities at typical sections of point rail. (B) Change of lateral irregularities at typical sections of point rail.

to the roll angle variation, the vertical irregularities on the left rail are about 0.2 mm; those on the switch rail and the point rail may be more than 1.3 mm due to the height differences of the switch rail and point rail and the change of wheel–rail contact points.

In the vicinity of the wheel-load transition section on the switch rail and the point rail (e.g., at top width 30 mm of the switch rail), if the wheelset lateral displacement is large, the wheel–rail contact point will lie on the switch rail and the point rail, and the lateral structural

irregularity is negative. If the wheelset lateral displacement is small, the wheel–rail contact point will lie on the stock rail and the wing rail, and the lateral structural irregularity is positive. In this case, the irregularity severely fluctuates with the lateral displacement of the wheelset, as shown in Figure 4.18B.

If the crossing has a check rail (the clearance at straight flangeway of the check rail is 42 mm) in the diverging line, when the wheelset moves transversely toward the point rail, the maximum left-lateral displacement is only 1 mm due to the limitation of the check rail on the wheel back. When the wheelset moves transversely toward the check rail, there is no limitation on the lateral displacement of the wheelset. Therefore, the flange will not come in contact with the gauge corner of the point rail. In addition, the wheel–rail contact geometry relation is the same as in the case where the lateral displacement of the wheelset is −12 to +1 mm.

4.1.6 LONGITUDINAL CHANGE ALONG THE TURNOUT (WITH WHEELSET LATERAL DISPLACEMENT)

1. Switch

When the wheelset of LMA tread travels in a Chinese No. 18 turnout for 350 km/h, considering different wheelset lateral displacements, the longitudinal changes in equivalent tread conicity and roll angle at the switch are shown in Figure 4.20.

Since the top profile of the switch rail changes longitudinally along the line and the tread profile varies with the wheelset lateral displacement, the wheel–rail contact geometry distribution in the turnout area constitutes a spatially curved surface, which changes with line position

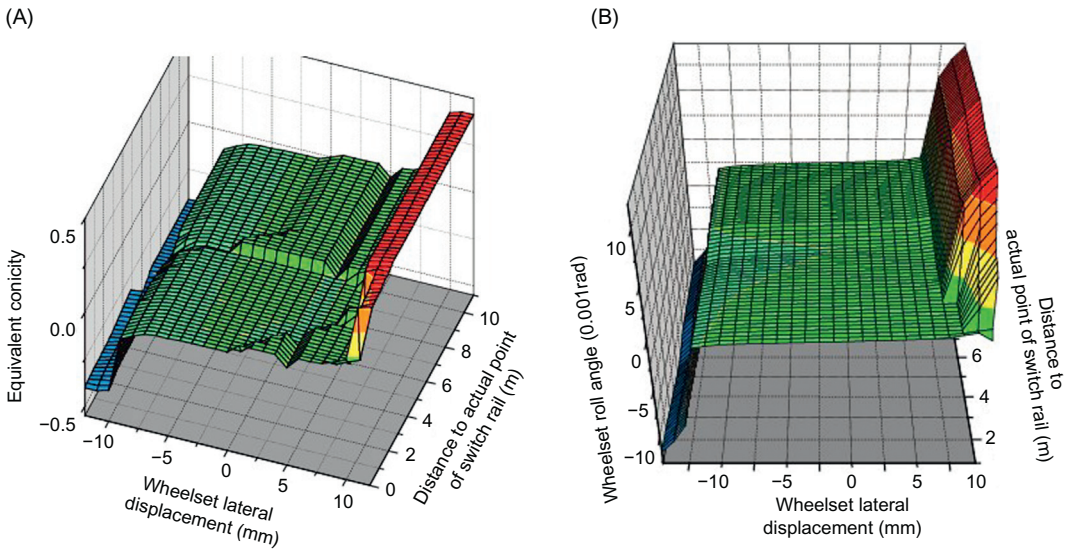

FIGURE 4.20

(A) Distribution of equivalent conicity at the switch. (B) Distribution of roll angle at the switch.

and wheelset lateral displacement. If the wheelset lateral displacement is great and the flange is in contact with the gauge corner of the rail, the wheel–rail contact geometry relation will change dramatically. The maximum roll angle and vertical and lateral structural irregularities will occur near the wheel-load transition position. As shown in Figure 4.21, the larger the wheelset lateral displacement, the more severe the vertical and lateral structural irregularities, and the greater the wheel–rail system vibration. Riding quality and safety may be enhanced by reducing the wheelset lateral displacement of a running car. Therefore, the geometric

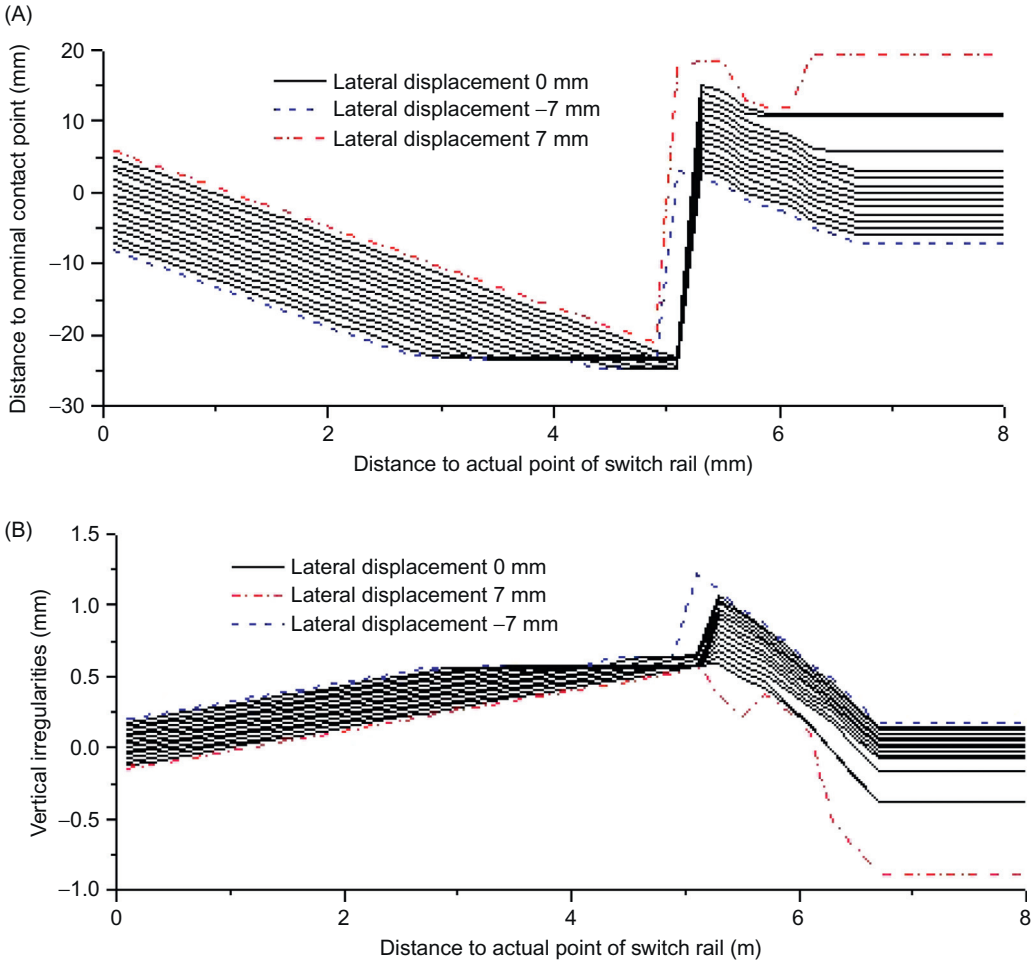

FIGURE 4.21

(A) Change of wheel–rail contact point with wheelset lateral displacement and line position at the switch.
(B) Change of vertical structure irregularities with wheelset lateral displacement and line position at the switch.

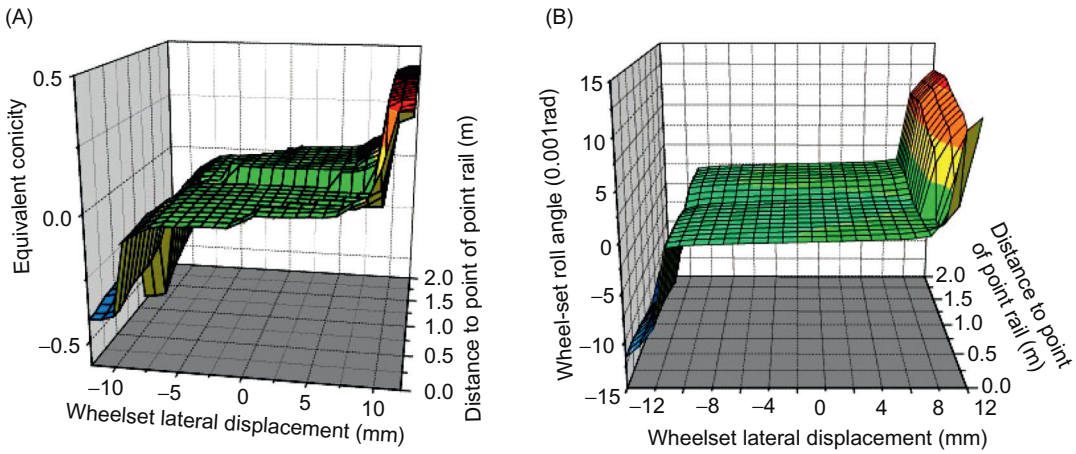

FIGURE 4.22

(A) Distribution of equivalent conicity at the crossing. (B) Distribution of roll angle at the crossing.

irregularities should be controlled in the transition area between a section and a turnout during maintenance.

2. Crossing

When the wheelset of LMA tread travels in a Chinese No. 18 turnout for 350 km/h, considering different wheelset lateral displacements, the longitudinal changes of equivalent tread conicity and roll angle at the crossing are shown in Figure 4.22, and the change of structural irregularities with wheelset lateral displacement at the crossing is shown in Figure 4.23.

The change rule for the wheel–rail contact geometry relation at a crossing is similar to that at the switch. However, the values of contact geometry parameters are different due to the different top profiles of the two types of rails (the point rails are approximately symmetrical) and the rapid change rate of top width of the point rail along the line. All these values change sharply near the wheel-load transfer point after the contact between the flange and gauge corner of the rail.

The wheel–rail contact relation at the switch changes from the actual point of the switch rail to the origin of the depressed rail top. At a crossing, as the top profile of the point rail is approximately symmetrical, the wheel–rail contact relation will change within a short distance, that is, from the actual point to the full section of the point rail (top width: 71 mm). In this case, structural irregularities at the crossing are featured with short wavelength but equivalent amplitude, as at the switch. Therefore, it is imperative to control the geometric irregularities, closure status of the point rail, slide bedplate, wing rail, jacking block, and the stability of sub-rail foundation at this area, so as to avoid superposition of static and dynamic irregularities, which may intensify train-turnout coupled vibration and affect the riding quality and safety.

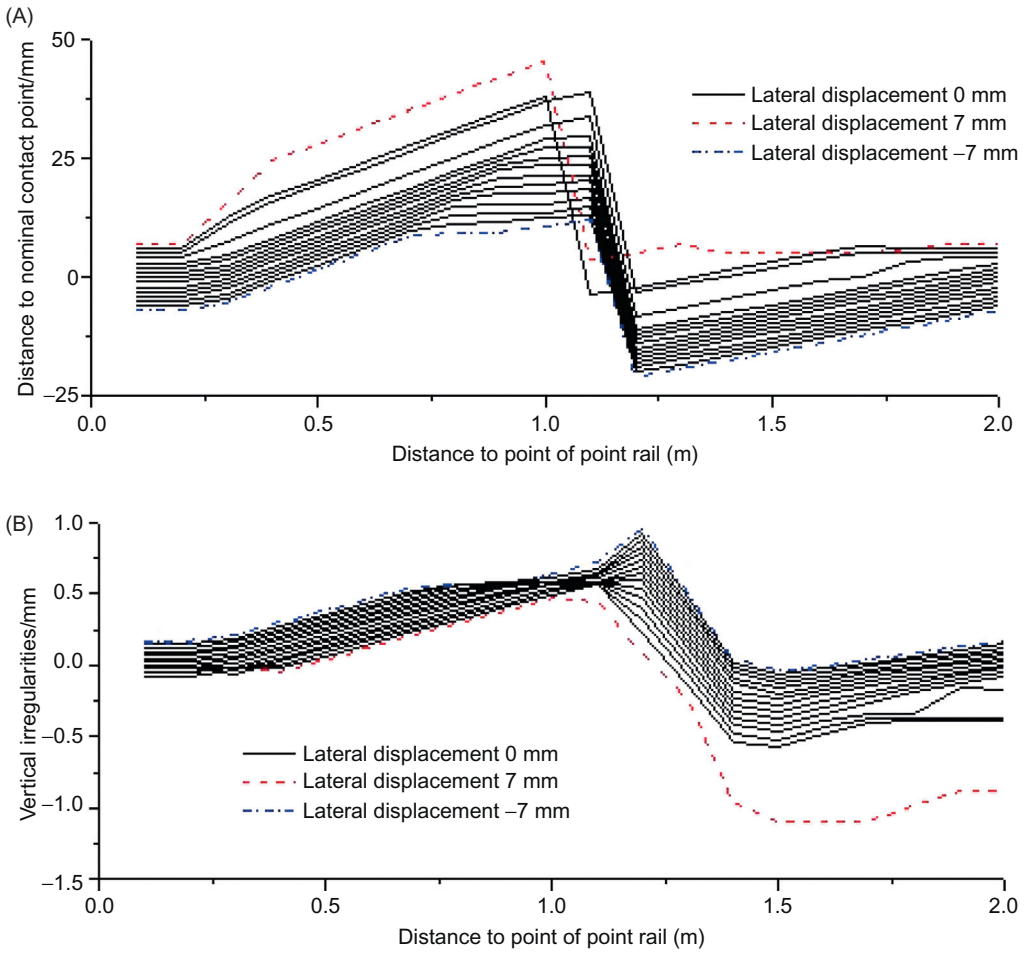

FIGURE 4.23

(A) Change of wheel–rail contact point with wheelset lateral displacement and line position at the crossing.
(B) Change of vertical structural irregularities with wheelset lateral displacement and line position at the crossing.

4.2 WHEEL–RAIL ROLLING CONTACT THEORIES IN TURNOUT ZONE [42]

Wheel–rail rolling contact is the unique behavior of a wheel–rail system, linking the dynamic interaction between the vehicle system and the turnout system. The rolling contact between the wheelset and the section rails has been well studied, and certain theories have gone beyond the assumption of traditional Hertzian contact theory and can be effectively applied to the simulation of wheel–rail conformal contact, flange contact, two-point contact, etc. The theories of wheel–rail rolling contact in the turnout area will be analyzed in detail to accurately simulate the complicated wheel–rail two-point contact relation in the turnout area.

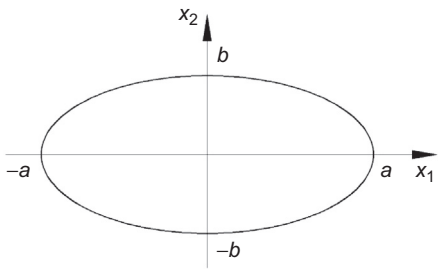

FIGURE 4.24

Shape of elliptical contact area.

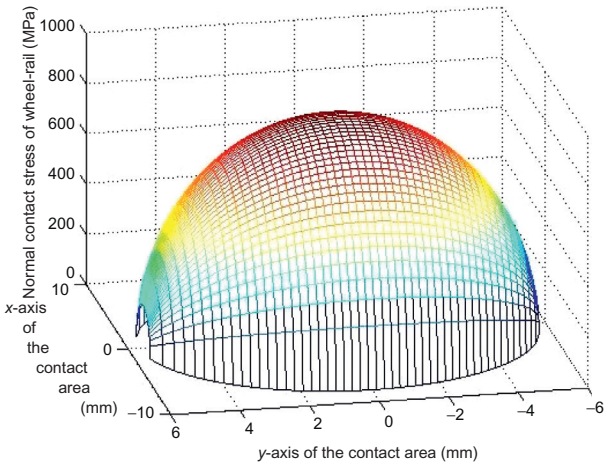

FIGURE 4.25

Distribution of normal contact stress in the contact area.

4.2.1 HERTZIAN THEORY

Hertzian contact theory was initiated by Heinrich Hertz in the late nineteenth century. He was studying the possible influence of elastic deformation of the surfaces of two cylindrical lenses due to the contact pressure between them and was concerned with the ellipse interference fringes in the gap between two glass lenses before and after deformation. Assumptions about the elliptical contact area were put forward. Hertzian theory is founded on the assumption that the contact pressure on the contact surfaces between two elastic solids is semi-elliptical, by analogy with the height distributing feature of charge density on a conductor surface, supported by detailed theoretical derivation. The theory has stood the test of time for over a century and has been widely applied to the solution of normal force in wheel–rail dynamics owing to its high performance in calculation efficiency and accuracy. In addition, most models of rolling contact mechanics for solving tangential force have been developed based on Hertzian theory.

1. Normal contact [43]

   According to Hertzian contact mechanics, the dimensions of the contact area must be much smaller compared with the relative principal radii of curvature of the surfaces. In other words, according to the hypothesis of elastic half-spaces, the contact surfaces are frictionless so that only normal contact pressure is transmitted between them. In addition, Hertz believed that the contact area is, in general, elliptical (Figure 4.24), and the contact curvature in the contact area of the two bodies is a constant.

   With the calculated longitudinal half-axial length a and lateral half-axial length b, the distribution of normal contact stress p_z in the contact area will be as shown in Figure 4.25 under the assumptions of Hertzian contact mechanics. The normal contact stress can be defined by:

$$p_z(x,y) = \frac{3}{2}\frac{N}{\pi ab}\sqrt{1-\left(\frac{x}{a}\right)^2-\left(\frac{y}{b}\right)^2} \tag{4.5}$$

   where N denotes normal stress in wheel–rail contact area.

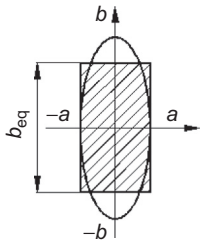

FIGURE 4.26

Shape of equivalent rectangular contact area.

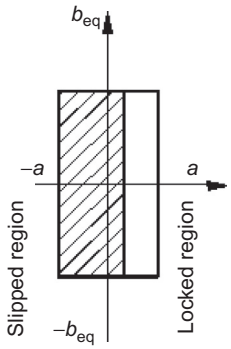

FIGURE 4.27

Division of the rectangular contact area.

2. Tangential contact

Solution methods based on Hertzian contact theory for wheel–rail tangential contact problems are referred to as wheel–rail creep theory, which is composed of Carter 2D rolling contact theory, Johnson–Vermeulen 3D rolling contact theory, Kalker linear creep theory, Shen–Hedrick–Elkins creep theory, and Kalker simplified theory.

a. Carter 2D rolling contact theory [44]

Carter introduced two cylinders with perpendicular axes to simulate the rolling contact behavior of the wheel–rail system. To make the assumption of the half-space elastic bodies in Hertzian contact theory available, Carter assumed that the radii of the cylinders modeling the rails were infinitely long, and a wheel rolling on the rails was regarded as the rolling of the cylinders on the surfaces of half-space bodies. In this case, the wheel–rail contact area was slender. The width of the contact area along the wheel rolling direction was generally constant; therefore the elliptical contact area may be replaced with equivalent rectangular contact area $2a \times b_{eq}$ (Figure 4.26), where a represents the longitudinal half-axial length of the contact ellipse, and b_{eq} represents the equivalent lateral width of the rectangular contact area. Thus the normal stress distribution of the rectangular contact area, per Hertzian contact theory, can be expressed by:

$$p_z(x,y) = \frac{2N}{\pi a b_{eq}} \sqrt{1 - \left(\frac{x}{a}\right)^2} \tag{4.6}$$

To study the distribution of tangential force in the contact area, Carter assumed that the contact area fell into two parts: a front part (locked region) and a rear part (slipped region), as shown in Figure 4.26. The tangential force is zero in the front part of the contact area, but will increase along the opposite direction of rolling. By Coulomb's friction law, slip may occur when tangential force increases to a certain value. Based on the above, Carter further assumed that the contact area was in a slipped state on the whole. Therefore, as shown in Figure 4.27, the distribution of tangential force in the contact area in such circumstances could be obtained by reducing that in the slipped region, expressed by:

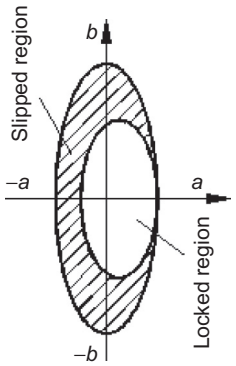

FIGURE 4.28

Division of the elliptical contact area in Johnson–Vermeulen theory.

$$p_1(x) = \begin{cases} -\operatorname{sgn}(s_1)(2\mu N/\pi a^2)\sqrt{(a^2 - x^2)} & x \in \{S\} \\ -\operatorname{sgn}(s_1)(2\mu N/\pi a^2)\left[\sqrt{(a^2 - x^2)} - \sqrt{(a_1^2 - x^2)}\right] & x \in \{A\} \end{cases} \tag{4.7}$$

where S represents the slipped region, A represents the locked region, μ is the friction coefficient, and a_1 is the half-width of the locked region, given by $a_1 = a\sqrt{1 - (P_x/fP_z)^2}$, in which P_x is the total tangential force per lateral unit length. The division of the rectangular contact area depends mainly on the value of the total tangential force P_x. When $P_x = fP_z$, the contact area is in a slipped state on the whole; when $P_x = 0$, the contact area is completely in a locked state. The Carter rolling contact model is feasible for solving 2D rolling contact issues only; however, it provides a reference for future studies on rolling contact models.

b. Johnson–Vermeulen 3D rolling contact theory [45]

In this theory, the application of the Carter 2D rolling theory is extended from a rectangular contact area to an elliptical contact area, and the locked region is assumed to be elliptical, as shown in Figure 4.28, with the axial length ratio being:

$$\left(\frac{a_A}{a}\right)^3 = \left(\frac{b_A}{b}\right)^3 = 1 - \frac{P_x}{fP_z} \tag{4.8}$$

where a_A and b_A denote the long and short half-axial lengths of the ellipse in the locked region, respectively, P_x is the total tangential force on the contact area, and P_z is the total normal load on the contact area.

Knowing the tangential elastic displacement equation in the locked region of the elliptical contact area, the relationship between the total tangential force and creepage in the contact area can be expressed by:

$$T_J = \mu N \begin{cases} [(1 - \xi^*/3)^3 - 1](\xi_1^* + \xi_2^*)/\xi^* & |\xi^*| < 3 \\ (\xi_1^* + \xi_2^*)/\xi^* & |\xi^*| \geq 3 \end{cases} \tag{4.9}$$

where ξ_1^* and ξ_2^* denote longitudinal and lateral creepages after normalization, respectively, with $\xi_1^* = \pi abG\xi_1/\mu N\phi_1$ and $\xi_2^* = \pi abG\xi_2/\mu N\psi_1$. ξ^* refers to the total creepage after normalizing, and $\xi^* = \sqrt{\xi_1^{*2} + \xi_2^{*2}}$.

Johnson–Vermeulen rolling contact theory disregards the spin of the rolling object, and takes only longitudinal and lateral creep into account. In addition, the division of the contact area is unsatisfactory in the theory, and may even be wrong.

c. Kalker linear creeping theory and its revision [46]

In this theory, the influence of longitudinal and lateral creepages and spin creepage on the creep force are included. Given that the wheel–rail rolling contact is a uniform Hertzian rolling contact in a quasi-stable state, and with Boussinesq–Cerruti force/displacement equations and the gradient of elastic displacement difference, the creepage/creep force relation can be defined as:

$$\begin{cases} F_1 = -Gc^2C_{11}\xi_1 \\ F_2 = -Gc^2(C_{22}\xi_2 + C_{23}c\xi_3) \\ F_3 = -Gc^3(C_{32}\xi_2 + C_{33}c\xi_3) \end{cases} \tag{4.10}$$

where F_1, F_2, and F_3 denote the creep forces in the directions of x_1, x_2, and creep moment, respectively; C_{ij} is the Kalker creep coefficient; and ξ_i represents creepage in the direction of x_i; in addition, $c = (ab)^{1/2}$ $(i, j = 1,2,3)$.

In this theory, the limit sliding friction has not been determined by Coulomb's friction law; therefore, the theory is applicable to the calculation of small creep or vehicle dynamics simulation under small spin. The creep coefficient and expression for creepage/creep force in Vermeulen–Johnson 3D rolling contact theory have been revised by Shen Zhiyun, J. K. Hedrick, and J. A. Elkins with Kalker linear theory, specifically:

$$\begin{cases} \xi_1^* = -c^2GC_{11}\xi_1/3\mu N \\ \xi_2^* = -(c^2GC_{22}\xi_2 + c^2GC_{23}\xi_3)/3\mu N \end{cases} \tag{4.11}$$

After the revision, the effect of spin creepage ξ_3 can be included in the normalized creepage ξ_2^*; therefore, the total creepage and creep force read:

$$\xi^* = \sqrt{\xi_1^* + \xi_2^*} \tag{4.12}$$

$$F^* = \sqrt{F_1^2 + F_2^2} \tag{4.13}$$

Substituting Eqs (4.12) and (4.13) into the creepage/creep force equation of Vermeulen–Johnson 3D rolling contact gives:

$$F^* = \begin{cases} \mu N\left[\left(\dfrac{F}{\mu N}\right) - \dfrac{1}{3}\left(\dfrac{F}{\mu N}\right)^2 + \dfrac{1}{27}\left(\dfrac{F}{\mu N}\right)^3\right] & \dfrac{F}{\mu N} < 3 \\ \mu N & \dfrac{F}{\mu N} \geq 3 \end{cases} \tag{4.14}$$

The Shen–Hedrick–Elkins rolling contact model has introduced spin creepage into the calculation; however, it is applicable to calculating the creep force under small spin creeping, but not large spin creeping, through extensive calculations [47].

d. Kalker simplified theory and its numerical program FASTSIM [48]

Kalker linear creep theory has a restricted application as it is not applicable to the contact area with any slip. In the regard, Kalker put forward a more advanced and effective model based on the former linear creep theory in 1973, that is, the simplified theory. In this theory, it is assumed that the elastic displacement at any point in the contact area correlates to the tangential force at this point only, and only the tangential force of the same direction matters. Therefore, the contact ellipse can be divided into $n_x \times n_y$ cells. The lengths of each cell in the x- and y-axes are Δx and Δy, respectively. In each cell, the slippage s is composed of elastic displacement u_F and rigid slippage w_F, that is,

$$s(x,y)\Delta x = u_F(x,y) - u_F(x-\Delta x,y) + w_F(x,y)\Delta x \tag{4.15}$$

where $(x-\Delta x)$ represents the location of the previous cell in the x-axis.

The cell (x,y) is in the locked region, which means its slippage $s(x,y)=0$. Thus the surface force p_A in this cell is:

$$p_A(x,y) = p_F(x-\Delta x,y) - w_F\Delta x/L \tag{4.16}$$

where L is the flexibility coefficient obtained from the creepage/creep force relation in the linear theory.

According to Hertzian contact theory and Coulomb's friction law, the limit surface force p_L in the cell (x,y) will be:

$$p_L(x,y) = 2\mu N(1-x^2/a^2-y^2/b^2)/\pi ab \tag{4.17}$$

When $p_A < p_L$, there is a locked region in the contact area and vice versa. The surface force in the slipped region is:

$$p_S(x,y) = p_L(x,y)p_A(x,y)/|p_A(x,y)| \tag{4.18}$$

With the above equations, the distribution of locked and slipped regions in the contact area and the creep force in the cells for calculation of wheel wear can be obtained.

The creep force and creep moment under any creepage and spin can be solved only by the numerical method. First, the elliptical contact area will be converted into unit circle contact area with dimensionlessness, as shown in Figure 4.29. The numerical calculation of the

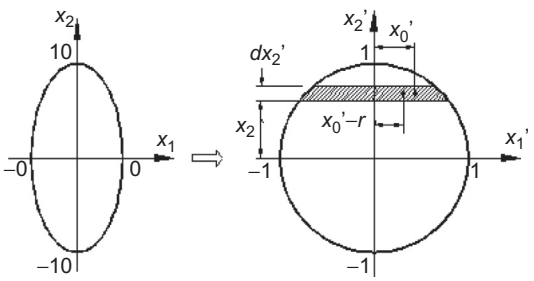

FIGURE 4.29

Converting elliptical contact area into unit circle contact area.

simplified theory is realized by the FASTSIM program, developed by Kalker. This program is capable of solving tangential force and slippage in general cases. However, it is confined to the Hertzian contact area.

4.2.2 NON-HERTZIAN ROLLING CONTACT THEORIES

Researchers began to shift their interests to the true shape and stress distribution of wheel–rail contact area with the progress of the studies on wheel–rail rolling contact, aiming at forecasting wheel–rail wear and rolling contact fatigue. In particular, if a worn wheelset and the rails are in contact, the radii of curvature of the two bodies in contact in the contact area are not constant. In this case, the assumptions of Hertzian contact theory will not apply, and a more accurate contact theory is required to model the contact between the worn wheelset and the rails. Applicable non-Hertzian rolling contact theories include Kalker 3D non-Hertzian rolling contact theory, rolling contact theory based on theoretical penetration, and finite element contact theory.

1. Kalker 3D non-Hertzian rolling contact theory [49]

   In the 1990s, Kalker derived the complementary virtual work principle for problems of rolling contact using the virtual work principle of continuum mechanics and its dual form based on the assumption of elastic half-space, and solved this unconstrained convex function by quadratic programming. The 3D elastic bodies of non-Hertzian contact theory and the relevant solver CONTACT were then established.

   Kalker 3D non-Hertzian rolling contact theory with the solver CONTACT has been proved to be the most practical theory of rolling contact so far, applicable to accurate calculation of the shape of the contact area, distribution of normal stress, division of slipped and locked regions, and distribution of relative slip displacement of the contact surfaces. Nevertheless, CONTACT is not an efficient solver and cannot be directly used in vehicle dynamic simulation; therefore, the theory is most frequently used in verifying other engineering approximation methods. In addition, Kalker 3D non-Hertzian rolling theory applies only to 2D contact areas, and can derive approximate solution in cases of flange contact that may induce conformal contact. For this, Mr Jin Xuesong (Southwest Jiaotong University) has had the solver CONTACT improved to include the influence of boundary condition on contact behavior, as well as taking the relative slippage of each pair of contact points on the contact surfaces and relevant complementary virtual work method into consideration. With these efforts, the wheel–rail two-point contact and conformal contact can be calculated accurately.

2. Finite element wheel–rail rolling contact theory [50,51]

   Kalker's accurate theory goes beyond the assumptions of Hertzian contact theory, yet it will still satisfy the assumption of elastic half-space, that is, the dimensions of contact area will be much smaller than the characteristic dimensions of the contact bodies. The assumption of elastic half-space is satisfied when the standard wheel treads and rails are brought into contact, and the calculated results with the accurate theory are close to the actual stress distribution. However, when a worn wheelset and the rails are in conformal contact, this assumption does not apply, and the results produced with this theory may have great errors. Additionally, conventional wheel–rail rolling contact theories are based on classic elastic theories and do not apply to plastic deformation induced by inordinate contact stress. Therefore, overcoming the limitations of classic theories must await the development of improved rolling contact theories.

The advance of computer technology boosts the spreading of finite element software to engineering numerical simulation. The finite element method can solve the wheel–rail rolling contact problems satisfactorily as it can simulate the true geometry profile, boundary constraints, and elastic-plastic deformation of materials of the contact bodies.

At present, the successful application of finite element contact theory in analyzing wheel–-rail rolling contact can be represented by the finite element quadratic programming method based on the parametric variational principle and the rolling contact theory based on the arbitrary Lagrangian Eulerian (ALE) method. The finite element parametric quadratic programming method was proposed by Prof. Zhong Wanxie of Dalian University of Technology, applicable to analyzing elastoplastic frictional contact problems. The ALE method was put forward by Prof. Udo (University of Federal Defense Munich) and has been introduced in general commercial finite element software (such as ANSYS/LSDYNA and ABUQUS), widely used in analyzing the wheel–rail rolling contact behaviors. Martin built an explicit dynamic analysis model using a single wheel rolling on a fixed crossing based on ABUQUS, to analyze the factors (e.g., wheel–rail impact force, wheel–rail contact stress, internal stress, and equivalent plastic deformation) when the wheel passes through the crossing from turnout front/rear at different speeds, so as to provide a theoretical basis for predicating the wear status of the fixed crossing and contact fatigue failures.

Wheel–rail rolling contact is a highly linear dynamic issue, demanding more computational resources compared with static contact analysis. In this process, reasonable models and fine grids are critical for effective computation. When dozens of tons of alternating load of the train is applied on a contact area of about 100 mm^2, stress concentration and plastic strain will take place in the contact area, leading to great stress gradient between the contact area and the noncontact area. In this case, computational accuracy relies on the fineness of the finite element grid; that is, finer grids relate to computational results of higher accuracy. Solving the problems of wheel–rail rolling contact by this method will be accompanied by huge calculation models, low efficiency, and unpredictable errors. These difficulties may be eliminated by employing ALE methods. The ALE method breaks down the wheel–rail rolling contact into rigid motion and elastoplastic deformation of the wheel (as shown in Figure 4.30). The rigid motion of the

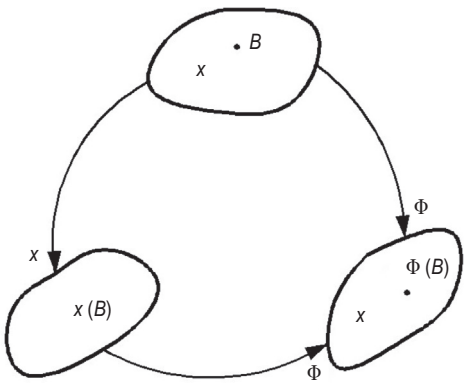

FIGURE 4.30

Breakdown of ALE method.

wheel can be further divided into rolling and lateral displacement, which can be modeled with Eulerian equations. The elastoplastic deformation of the wheel can be modeled with classic Lagrangian equations.

Figure 4.30 shows the process of the ALE method: $x = \phi(X, t)$, establishing a reference domain $\hat{\Omega}$ while mapping the initial form Ω_0 of the subject of the study to current form Ω; $\chi = \chi(X, t)$, mapping the initial form Ω_0 of the subject of the study to the form of reference domain $\hat{\Omega}$, where χ is the coordinate of ALE; and describing the rigid motion (independent from the motion of material) of the grid cell with the reference domain $\hat{\Omega}$.

In addition, point χ in the reference domain is mapped to point x in the spatial domain by the mapping of $\hat{\phi}$; then the deformation of the finite element grid cell can be expressed by:

$$x = \hat{\phi}(\chi, t) \tag{4.19}$$

With this deformation and the mapping of χ in the reference domain, the motion of the material of the studied subject may be defined by:

$$x = \phi(X, t) = \hat{\phi}(\chi(X, t), t) \tag{4.20}$$

The rigid motion of the wheel is modeled as the combination of rolling and lateral displacement of the wheel by Eulerian equations, defined as the relation between rigid displacement and time, where the total derivative of particle motion may be determined as per the rule of relative chain:

$$\frac{\mathrm{D}f}{\mathrm{D}t} = \dot{f}(\chi, t) = \frac{\partial f(\chi, t)}{\partial t} + \frac{\partial f(\chi, t)}{\partial \chi_i} \frac{\partial \chi_i(X, t)}{\partial t} = f_{t[\chi]} + \frac{\partial f}{\partial \chi_i} \frac{\partial \chi_i}{\partial t} \tag{4.21}$$

where the velocity of rigid lateral displacement of the wheel (v) and the angular velocity of the axle (ω) can be defined as:

$$v = \frac{\partial \phi(X, t)}{\partial t} = \frac{\partial \hat{\phi}(\chi, t)}{\partial t} + \frac{\partial \hat{\phi}(\chi, t)}{\partial \chi_i} \frac{\partial \chi_i(\chi, t)}{\partial t} \tag{4.22}$$

$$\dot{\chi} = \frac{\partial \chi(X, t)}{\partial t} = \frac{\partial \chi}{\partial t}\Big|_{\chi} + \omega \times \chi \tag{4.23}$$

The law of conservation of momentum will be followed in the reference domain $\hat{\Omega}$:

$$\hat{\rho} \frac{\mathrm{D}v}{\mathrm{D}t} - \hat{\rho} b - \nabla \hat{\sigma} = 0 \tag{4.24}$$

Based on the impulse theorem and boundary conditions for surface force and internal force equilibrium theory, the equilibrium equation can be obtained with the variational principle of virtual work:

$$\int_{\hat{\Omega}} \delta\eta \cdot \hat{\rho} \frac{\mathrm{D}v}{\mathrm{D}t} d\Omega + \int_{\hat{\Omega}} \delta \mathrm{D} : \hat{\sigma}\, d\Omega - \int_{\hat{\Omega}} \delta\eta \cdot \hat{\rho}\, d\Omega - \int_{\hat{\Gamma}_t} \delta\eta \cdot t\, d\Gamma = 0 \tag{4.25}$$

Including the virtual work done by the contact force, one gets:

$$\int_{\hat{\Omega}} \delta\eta \cdot \hat{\rho} \frac{\mathrm{D}v}{\mathrm{D}t} d\Omega + \int_{\hat{\Omega}} \delta \mathrm{D} : \hat{\sigma}\, d\Omega - \int_{\hat{\Omega}} \delta\eta \cdot \hat{\rho}\, d\Omega - \int_{\hat{\Gamma}_t} \delta\eta \cdot t\, d\Gamma - \delta \int_{\hat{\Gamma}_t} (pd + \tau s) d\Gamma = 0 \tag{4.26}$$

And the virtual work done by the normal force and tangential force of wheel–rail contact is:

$$W_c = -\delta\int_{\hat{\Gamma}_t}(pd)d\Gamma - \delta\int_{\hat{\Gamma}_t}(\tau s)d\Gamma = -\delta\int_{\hat{\Gamma}_t}(pd+\tau s)d\Gamma \tag{4.27}$$

Combining Eqs (4.26) and (4.27), one obtains:

$$\int_{\hat{\Omega}}\delta\eta\cdot\hat{\rho}\frac{\mathrm{D}v}{\mathrm{D}t}d\Omega + \int_{\hat{\Omega}}\delta\mathrm{D}:\hat{\sigma}\,d\Omega - \int_{\hat{\Omega}}\delta\eta\cdot\hat{\rho}\,d\Omega - \int_{\hat{\Gamma}_t}\delta\eta\cdot t\,d\Gamma - \delta\int_{\hat{\Gamma}_t}(pd+\tau s)d\Gamma = 0 \tag{4.28}$$

The adhesion problem in wheel–rail rolling contact may be solved by the penalty function method. The distribution and degree of the stress of the wheel–rail rolling contact under any state may be obtained with the above equation.

3. Wheel–rail contact theory based on theoretical penetration principle [52–54]

Hertzian contact theory saves computational time but produces less accurate results in calculating the contact of a worn wheel profile and a rail. Finite element contact theory and Kalker 3D non-Hertzian rolling contact theory can model the wheel–rail contact behavior more accurately, including the shape and division of contact area, and stress distribution, but they are time-consuming and cannot be applied to the simulation of vehicle–track system dynamics and wheel–rail wear. Therefore, for effective and accurate solution of the contact area, both the computational efficiency and the accuracy must be taken into account in exploring the optimal rolling contact theory. Sauvage derived the penetration δ of the contact body for the first time, based on Hertzian contact theory. This parameter is obtained with the normal force N, relative curvatures A and B, and the material properties of the contact body; it is capable of determining the dimensions of the contact area of the bodies in contact. However, it is widely believed that the dimensions of the contact area obtained by this method are greater than the actual dimensions; the theoretical penetration area needs to be modified generally to obtain the true shape of the contact area. By including the influence of the variation of contact profile on the normal clearance, the Ayasse–Chollet (AC) modification method can be applied to the contact area on a curved surface, which is closer to true shape.

In the theoretical penetration method, to simplify this process, it is assumed that the elastic deformation produced by wheel–rail contact is zero, that is, the wheel and rail penetrate into each other in rigid form, and produce a corresponding penetration area. As the elastic compression of the wheel–rail is disregarded in the process of theoretical penetration, the penetration area determined is greater than the actual case. Therefore, the reasonable penetration δ_0 is generally obtained by iteration to determine the true contact area, as shown in Figure 4.31.

Suppose the wheel is a solid of revolution with the radius of turn equaling the rolling radius R_w, the rolling surface of the rail is an infinitely long cylinder, and the requirement of elastic half-space is met. Then the elastic deformation in the contact area of the wheel–rail can be obtained with the Boussinesq influence function. At the beginning of the contact of two elastic bodies, when no compressive deformation occurs, the contact position is the rigid contact point o, defined as the origin of local coordinates $oxyz_1$ and $oxyz_2$ of the wheel–rail profile. The wheel profile is represented by $z_1(y)$ and the rail profile is expressed by $z_2(y)$. The wheel–rail

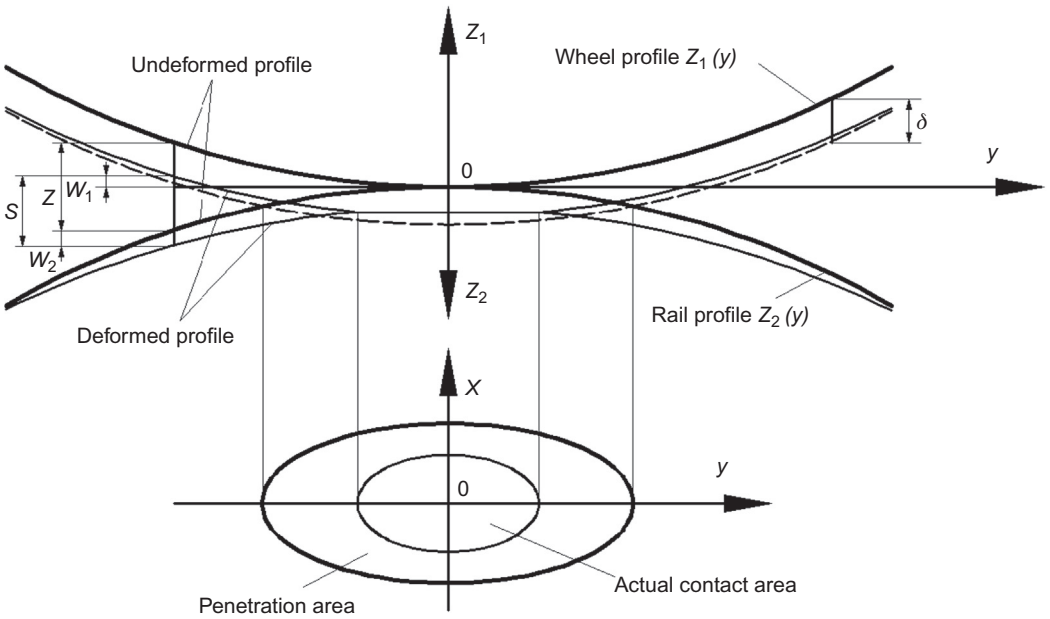

FIGURE 4.31

Diagram of theoretical penetration method.

normal clearance in the plane oyz can be expressed by $f(y) = z_1(y) + z_2(y)$. Further, the normal clearance at any point on the wheel–rail profile will be:

$$z(x, y) = f(y) + \frac{x^2}{2R} \tag{4.29}$$

The theoretical penetration method is based on the following assumptions: The rail profile is fixed; the wheel profile displaces laterally by δ along the z-axis and brings about the rigid penetration of wheel and rail profile, producing a penetration area correspondingly on the plane oxy. The displacement δ is taken as the penetration. In a practical situation, however, there is no penetration, but compressive elastic deformation between two elastic bodies in contact, and the resulting contact area lies in the theoretical penetration area. In this case, the normal clearance at any point on the wheel–rail profile will be:

$$s(x, y) = z(x, y) - \delta_0 + w_1(x, y) + w_2(x, y) \tag{4.30}$$

where $w_1(x, y)$ and $w_2(x, y)$ denote the deformation at any point on the wheel–rail profile with elastic deformation, respectively, and δ_0 is the mutual approach of the two bodies in contact. It can be obtained from the assumption of elastic half-space that $w_1(x, y) = w_2(x, y) = w(x, y)$. Therefore, Eq. (4.30) can be converted to:

$$s(x, y) = z(x, y) - \delta_0 + 2w(x, y) \tag{4.31}$$

Given $s(x,y)=0$ at any point on the wheel–rail profile at the contact boundary, $\delta_0 = z(x,y) + 2w(x,y)$. As for the rigid contact point, $z(0,0)=0$, so:

$$\delta_0 = 2w(0,0) = 2w_0 \tag{4.32}$$

where the elastic deformation $w(x,y)$ is determined by the normal force on the contact area. Given the normal force N, the elastic deformation $w(x,y)$ can be obtained with the Boussinesq influence function by integration, specifically:

$$w(x,y) = \frac{1-\nu^2}{\pi E}\iint_C \frac{p(x',y')}{\sqrt{(x-x')^2+(y-y')^2}}\mathrm{d}x'\,\mathrm{d}y' \tag{4.33}$$

where

$p(x',y')$ = normal force at the coordinate point (x',y')

ν = Poisson's ratio of wheel–rail material

E = elastic modulus of wheel–rail material.

It can be found by summarizing Eqs (4.31)–(4.33) that the normal force $p(x,y)\geq 0$ in the contact area and at the boundary. This means the points on the wheel–rail profile are in contact, that is,

$$\begin{cases} p(x,y)\geq 0 \\ p(x,y)\cdot s(x,y)=0 \end{cases} \tag{4.34}$$

The region C in the contact area and the normal stress distribution $p(x,y)$ can be obtained with Eq. (4.34). While for arbitrary an wheel–rail profile, the iteration method may be employed to solve the problems of normal contact.

The long/short half-axial length of the contact area obtained with classic Hertzian contact theory depends on the relative curvature ratio at the contact point of rigid bodies, that is, $\lambda = A/B$. But for the theoretical penetration method, the long/short half-axial length (a_p and b_p) of the contact area is determined by penetration h_0. As shown in Figure 4.32, $h_0 = a_\mathrm{p}^2 A = b_\mathrm{p}^2 B$. It can be found that the ratios of the long/short half-axial lengths of the contact area are not identical for the two methods. The reason lies in the fact that the influence of local elastic compressive deformation of the bodies in contact is disregarded in calculating the contact area for the theoretical penetration method, that is,

$$\frac{b_\mathrm{p}}{a_\mathrm{p}} = \sqrt{\frac{A}{B}} = \sqrt{\lambda} \neq \frac{b_\mathrm{h}}{a_\mathrm{h}} = \frac{n}{m} \tag{4.35}$$

Two French scholars, Ayasse and Chollet, put forward modified methods for the relative curvature ratio at the contact point, revising the initial relative curvature of two bodies in contact. Suppose that the revised relative curvatures are A_c and B_c; then, the condition below shall be met:

$$\frac{A_\mathrm{c}}{B}\,\mathrm{or}\,\frac{A_\mathrm{c}}{B_\mathrm{c}}\,\mathrm{or}\,\frac{A}{B_\mathrm{c}} = \left(\frac{b}{a}\right)^2 = \left(\frac{n}{m}\right)^2 \tag{4.36}$$

They put forward two modification methods based on the above equation: modifying only the relative curvature A and modifying relative curvatures A and B at the same time. The derivation processes of the two methods are described in detail below.

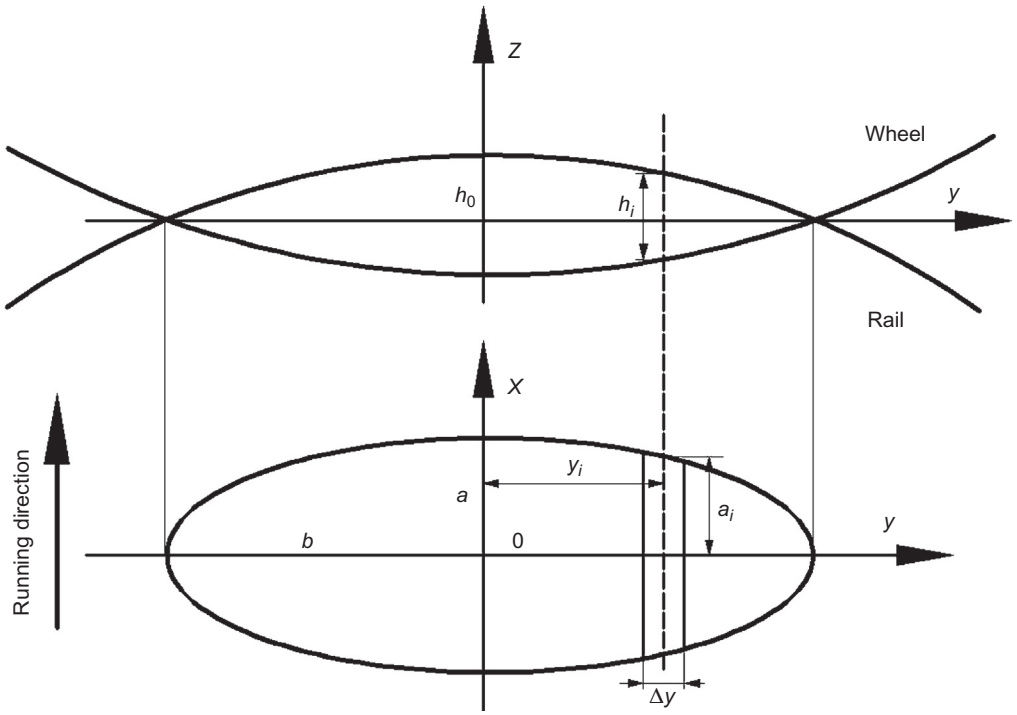

FIGURE 4.32

Diagram of semi-Hertzian contact.

Modifying only the relative curvature A is the simplest modification method, as the relative curvature A concerns only the rolling radius of the wheel; with Eqs (4.35) and (4.36), one obtains:

$$\frac{A_c}{A} = \left(\frac{b_h}{a_h}\right)^2 \frac{B}{A} = \left(\frac{n}{m}\right)^2 \frac{B}{A} = \left(\frac{b_h}{a_h}\right)^2 \frac{1}{\lambda} = \left(\frac{n}{m}\right)^2 \frac{1}{\lambda} \tag{4.37}$$

Then the ratio of long/short half-axial lengths of the contact area after modification will be:

$$\frac{b_p}{a_p} = \sqrt{\frac{A_c}{B}} = \frac{b_h}{a_h} = \frac{n}{m} \tag{4.38}$$

In combination with Hertzian contact theory, the penetration of the two bodies in contact after modification can be expressed by:

$$h_0 = a_h^2 A_c = b_h^2 B = \frac{n^2}{r} \frac{\delta}{1+\lambda} \tag{4.39}$$

where h_0 is the modified theoretical penetration; a_h and b_h denote the long and short half-axial length of the elliptical contact area obtained with Hertzian contact theory; A_c is the modified

relative curvature; $A_c = (n^2/m^2)B$, where B is the unmodified relative curvature and n, r, and λ are coefficients relating to relative curvature A and B; and δ is the penetration obtained with Hertzian contact theory, defined by:

$$\delta = r\left(\left(\frac{3}{2}N\frac{1-\nu^2}{E}\right)^2(A+B)\right)^{1/3} \tag{4.40}$$

When modifying relative curvatures A and B at the same time, the condition $A_c + B_c = A + B$ must be met. With Eq. (4.37) and $\lambda = A/B$, one gets:

$$\frac{A_c}{A} = \frac{1+\lambda}{\lambda}\frac{\nu^2}{1+\nu^2} \tag{4.41}$$

$$\frac{B_c}{B} = \frac{1+\lambda}{1+\nu^2} \tag{4.42}$$

where $\nu = n/m$. Similarly, with Eqs (4.40)–(4.42), the modified penetration of the bodies in contact can be obtained:

$$h_0 = a_h^2 A_c = b_h^2 B = \frac{n^2}{r}\frac{\delta}{1+\nu^2} \tag{4.43}$$

In normal cases, the principal radii of curvature of the wheel and the rail may not be constant in the wheel–rail contact area. Particularly for a worn wheel–rail profile, the principal radii of curvature are not constant, the assumptions in Hertzian contact theory do not apply, and the calculated shape of the contact area differs significantly with the actual shape. In the AC method, the possible wheel–rail contact area is broken down into several long strips with width Δy along the direction perpendicular to the running direction of the vehicle, as shown in Figure 4.32. This method assumes that the principal radius of curvature of the body in contact in each individual strip is a constant; therefore, the length of the strip can be obtained if the penetration on the strip is known. In addition, the penetration on the strip can also be obtained with the modified total penetration and wheel–rail profile. The AC method also assumes that the assumptions of Hertzian contact are satisfied for the wheel–rail contact along the running direction, but these assumptions do not apply in the direction vertical to the running direction. In this case, the calculated contact area is not elliptical. Thus, the AC method is also termed the semi-Hertzian method, or SH method.

The derivation process of the normal force and creep force in semi-Hertzian contact theory will be explained with the example of modifying only relative curvature A. According to Eqs (4.39) and (4.40), the rigidity K of the wheel–rail contact surface concerning penetration will be:

$$K = \frac{N}{h_0} = \frac{2Eb}{3(1-\nu^2)}\frac{1+\lambda}{n^3} \tag{4.44}$$

where the contact rigidity K relates to coefficients λ and n only. Therefore, the above equation can be applied to the contact rigidity of all strips. Given that the contact rigidity at strip centers is 1.5 times the rigidity of the contact surface, the contact rigidity at the strip center K_i will be:

$$K_i = \frac{E\Delta y}{2(1-\nu^2)}\frac{1+\lambda_i}{n_i^3} \tag{4.45}$$

The sum of the normal forces at all strip centers in the contact area follows:

$$N = \sum_{i=1}^{t} K_i h_i \tag{4.46}$$

Generally, a reasonable penetration h_{s0} is determined by iterating Eq. (4.46) so as to attain the equilibrium of initial normal force. The true shape of the contact area and distribution of normal stress can be obtained with penetration h_{s0}. In case of multi-point contact, the rigid contact point of the wheel–rail can be obtained first with the rigid wheel–rail contact geometry relation, which will then be used as the main contact point for determining initial penetration. The positions of the contact points and dimensions of the contact area can be found by iteration of the normal force and normal clearance of a wheel–rail.

All strips in the wheel–rail contact area can satisfy Hertzian contact conditions partially. Therefore, the distribution and magnitude of the tangential force on each strip may be obtained with the modified FASTSIM of Kalker, and the creep force in semi-Hertzian contact area can be found by adding up the results. As the assumptions of Hertzian theory are available for each strip only in the running direction, the FASTSIM method will be modified, particularly in terms of flexibility coefficient L_i and spin creep. Specifically, among the flexibility coefficients, L_1 is modified, L_2 remains the same, and L_3 is disregarded, as shown below:

$$L_1 = \frac{8a}{3C_{11}G} = \frac{8a_i}{3C_{11}G(a_i/a)} = \frac{8a_i}{3C_{11}Gk_i} \tag{4.47}$$

The major difference of the modified FASTSIM method in solving the tangential force on the strip lies in the handling of the spin creep. Specifically, spin creepage is not taken into consideration in the running direction. Instead, its effect is analyzed by the difference in longitudinal creepage among the strips. The derivation process can be expressed by:

$$\nu_x - y_i\varphi\frac{32}{3\pi}\frac{C_{23}}{C_{11}}\sqrt{\frac{n}{m}} \approx \nu_x - \frac{\delta r}{R_{22}}\frac{32}{3\pi}\frac{C_{23}}{C_{11}}\sqrt{\frac{n}{m}} \approx \nu_x - \frac{\delta r}{R_{22}} = \nu_{xi} \tag{4.48}$$

The normal stress and tangential stress on each strip in the semi-Hertzian contact area will be obtained with Eqs (4.47) and (4.48):

$$\begin{cases} \sigma_{zi}(x, y_i) = \dfrac{2N}{\pi ab}\left(1 - \dfrac{x^2}{a_i^2}\right)\dfrac{a_i^2}{a^2} \\ \sigma_{xi}(x, y_i) = \left(\dfrac{3}{8}GC_{11}\nu_x - \dfrac{4}{\pi}\sqrt{\dfrac{n}{m}}GC_{23}\varphi y_i\right)\left(\dfrac{a_i - x}{a}\right) \\ \sigma_{yi}(x, y_i) = \left(\dfrac{3}{8}GC_{22}\nu_y + \dfrac{2}{\pi}\sqrt{\dfrac{n}{m}}GC_{23}\varphi(a_i + x)\right)\left(\dfrac{a_i - x}{a}\right) \end{cases} \tag{4.49}$$

When modifying relative curvature A only, the above equation becomes:

$$\begin{cases} \sigma_{zi}(x,y_i) = \dfrac{4E(1+\lambda)}{3\pi n^3(1-\nu^2)}\dfrac{h_i}{a_i}\left(1-\dfrac{x^2}{a_i^2}\right)k_i^2 \\ \sigma_{xi}(x,y_i) = \dfrac{3}{8}GC_{11}\nu_{xi}\left(\dfrac{a_i-x}{a_i}\right)k_i \\ \sigma_{yi}(x,y_i) = \left(\dfrac{3}{8}GC_{22}\nu_y + \dfrac{2}{\pi}\sqrt{\dfrac{n}{m}}GC_{23}\varphi_i(a_i+x)\right)\left(\dfrac{a_i-x}{a_i}\right)k_i \end{cases} \tag{4.50}$$

The shape of the contact area, distribution, and magnitude of normal and tangential stress under semi-Hertzian contact can be obtained with the above equations. These results may be included in vehicle–track system dynamics to indicate the wheel–rail interaction and describe the coupling relation of wheel–rail system accurately.

4.2.3 WHEEL–RAIL ROLLING CONTACT IN TURNOUT AREA [42]

1. Wheel–rail normal contact

Wheel–rail normal contact focuses on the actual shape and magnitude of the contact area, as well as the distribution of normal stress in the contact area when two elastic bodies are in contact under the action of normal force. The normal contact between LMA tread and the design profile of switch rails with top width of 35 mm is analyzed with Hertzian contact theory, semi-Hertzian contact theory, Kalker 3D non-Hertzian contact theory, and finite element contact theory. Tables 4.1 and 4.2 show the results of the shape and size of the wheel–rail contact area and the distribution of normal stress under different lateral displacements of the wheelset.

It can be seen from Table 4.1 that the shape of the contact area of LMA wheel tread and a turnout rail changes with wheelset lateral displacement. For Hertzian theory, the contact areas are elliptical under all lateral displacements, while the long and short half-axial lengths are determined by the radii of curvature at the contact point. Specifically, when the wheelset lateral displacement is 0, the contact ellipse is slender; and when the wheelset lateral displacement is 3–9 mm, the change in the shape of the contact ellipse is insignificant, as there is no major change in the location of the contact point during lateral displacement. For semi-Hertzian contact theory, Kalker non-Hertzian contact theory, and finite element contact theory, as the actual contact profile of the wheel–rail has been taken into account in defining the contact area, the resulting contact area is no longer elliptical. In this regard, when the lateral displacement of the wheelset is 3 mm, the shape of the contact area obtained with semi-Hertzian contact area and Kalker non-Hertzian contact area are somewhat similar to the results of finite element contact theory. When the lateral displacement of the wheelset is 9 mm, the calculation results of the three theories indicate that the wheel and rail are in two-point contact, that is, the right wheel is in contact with the switch rail and the stock rail at the same time, and the shapes of the contact

Table 4.1 Shapes of Contact Area of LMA Tread and Turnout Rail in Contact

Wheels and Lateral Displacement	Hertzian Contact Theory	Semi-Hertzian Contact Theory	CONTACT Theory	Finite Element Contact Theory
0 mm	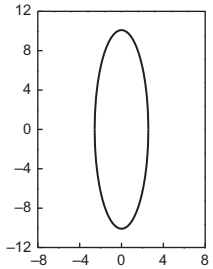	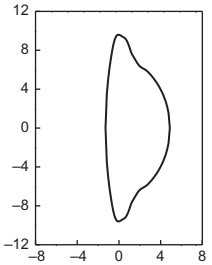	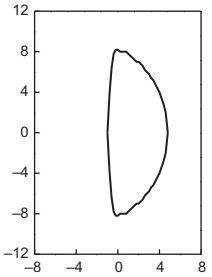	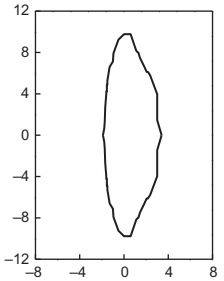
3 mm	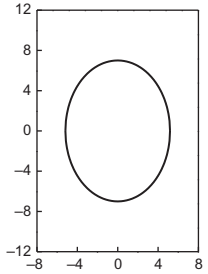	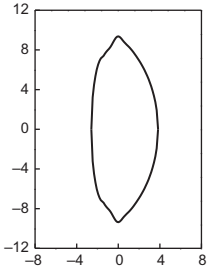	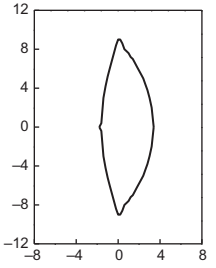	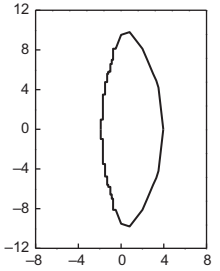
6 mm	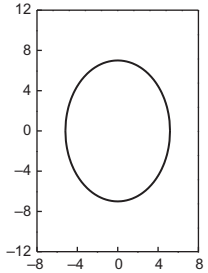	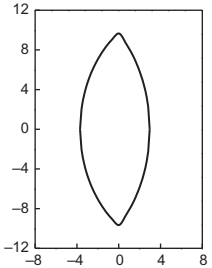	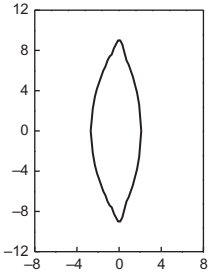	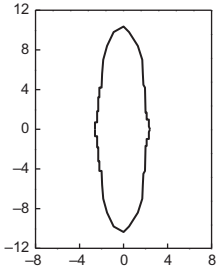
9 mm	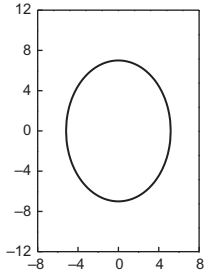	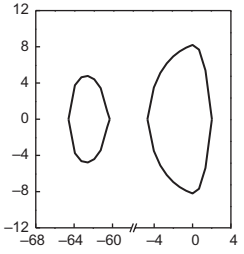	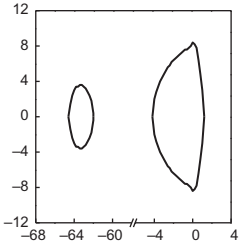	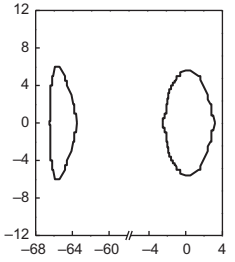

Table 4.2 Size of Contact Area and Contact Stress of the LMA Tread and Turnout Rail in Contact

Wheelset Lateral Displacement		Hertzian Contact Theory	Semi-Hertzian Contact Theory	CONTACT Theory	Finite Element Contact Theory
0 mm	Size of contact area (mm^2)	81.3	76.0	69.5	71.3
	Maximum contact stress (MPa)	1788.2	2042.7	2121.2	2053.5
3 mm	Size of contact area (mm^2)	114.0	87.4	59.2	81.0
	Maximum contact stress (MPa)	1118.1	1495.5	2527.4	1610.5
6 mm	Size of contact area (mm^2)	114.0	79.9	56.6	73.5
	Maximum contact stress (MPa)	1118.1	1542.8	2564.6	1739.5
9 mm	Size of contact area (mm^2)	114.0	83.9	76.0	78.6
	Maximum contact stress (MPa)	1118.1	1430.1	1695.4	1854.53

area are alike. Therefore, the three theories can be used to model the multi-point contact between the wheel and the switch rail, as well as between the wheel and stock rail.

Table 4.2 shows that, given the same lateral displacement, the size of contact area obtained with Hertzian contact theory is the biggest, followed by semi-Hertzian contact area, finite element contact theory, and Kalker 3D non-Hertzian contact theory in order. However, the rule of maximum contact stress in the contact area is just the opposite. Under different wheelset lateral displacements, the calculation results of semi-Hertzian contact theory and finite element contact theory are alike, but those of Kalker 3D non-Hertzian contact theory and finite element contact theory differ greatly.

In conclusion, when LMA wheel tread and turnout rail are in contact, semi-Hertzian contact theory and finite element contact theory produce closer results in the shape and size of the contact area, as well as contact stress. This shows that the two theories are more suitable for solving the wheel–rail force in vehicle–turnout coupled dynamics.

2. Wheel–rail tangential contact

A number of rolling contact theories, including the Shen–Hedrick–Elkins theory, Kalker simplified theory, Kalker 3D non-Hertzian contact theory (CONTACT theory), and semi-Hertzian contact theory (SH theory), are employed to compare and analyze the tangential contact behavior of wheel–rail in the turnout area. In the comparative analysis, the wheel is of LMA tread, the profile of the switch rail and the stock rail at top width 35 mm of the switch rail are taken as the rail section, and the wheelset lateral displacement is 0 mm.

a. Comparison of calculation of creep force

The four theories are introduced to study the influences of longitudinal creep, lateral creep, simple creep without spinning, and simple spin creep on creep force and moment,

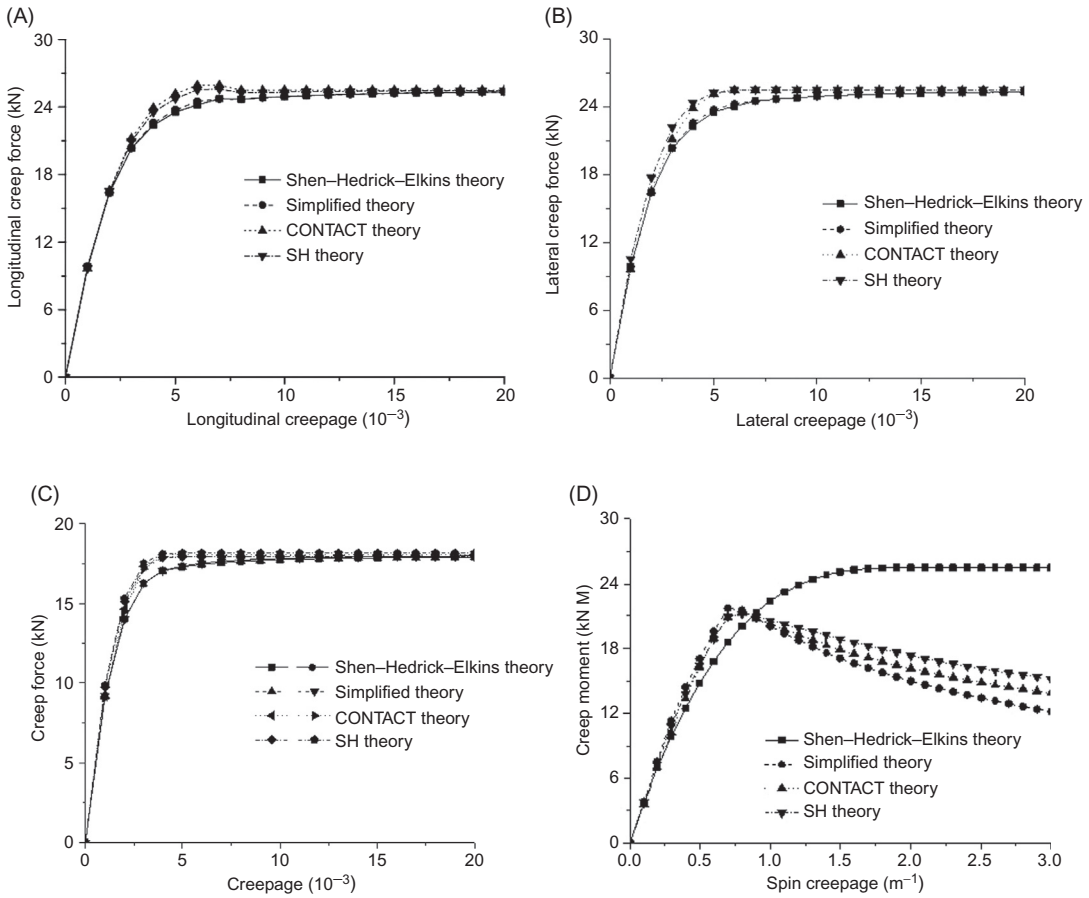

FIGURE 4.33

(A) Longitudinal creep force. (B) Lateral creep force. (C) Simple creep force without spinning. (D) Simple spin creep moment.

respectively. Figure 4.33 presents calculation results under different cases. In the analysis, simple creep means that the longitudinal creepage f_x and lateral creepage f_y are equal.

It can be found from Figure 4.33 that, when the spinning is disregarded, the creep forces obtained from the four theories follow similar rules. While in the case of simple spin creep, the simplified theory, CONTACT theory, and semi-Hertzian theory reflect the same distribution rule as the creep force, when the spin creepage is beyond 0.7 m^{-1}, the creep force will drop with increasing the creepage. However, for Shen−Hedrick−Elkins theory, the creep force may increase with increasing the creepage, which may become saturated at spin creepage of 1.6 m^{-1}, as the distribution of slipped and locked regions in the actual contact area is not included in the theory.

b. Distribution of locked and slipped regions

As the Shen–Hedrick–Elkins theory cannot produce the distribution of locked and slipped regions in the actual contact area, the other three theories are studied to analyze the distribution of locked and slipped regions in the contact area in the cases of simple creep and simple spin creep. Relevant calculation results are reflected in Figures 4.34–4.36. In these figures, the shadow region in the contact area symbolizes the slipped region, and the clear region represents the locked region.

It may be seen from Figures 4.34–4.36 that, with small creep without spinning, the slipped region is at the end of the contact area for all theories, that is, opposite to the running direction. Due to the absence of spin creep, the simplified theory produces a slipped region symmetric with respect to the longitudinal axis of the contact area, whereas semi-Hertzian contact area and CONTACT theory produce an asymmetric contact area. For the size of the slipped region in the contact area predicated by these theories, simplified theory predicts 5.7 mm^2, accounting for 8.0% of the total size of the contact area; semi-Hertzian

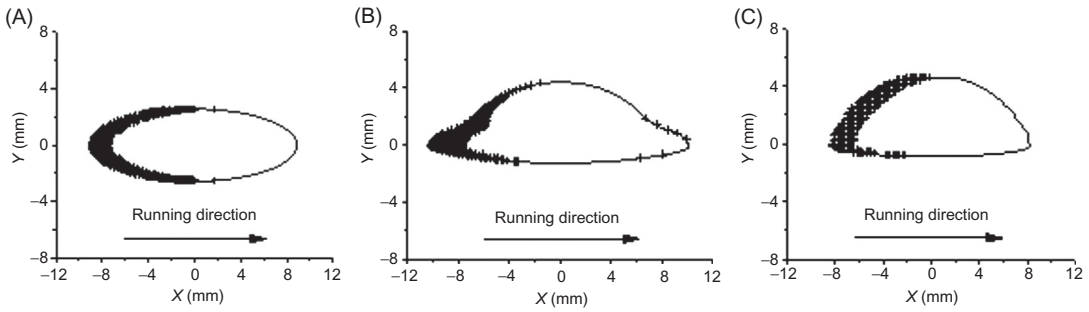

FIGURE 4.34

Simple creep (small creepage, $f_x = f_y = 1.5e-4, fin = 0$): (A) Simplified theory; (B) SH theory; (C) Accurate theory.

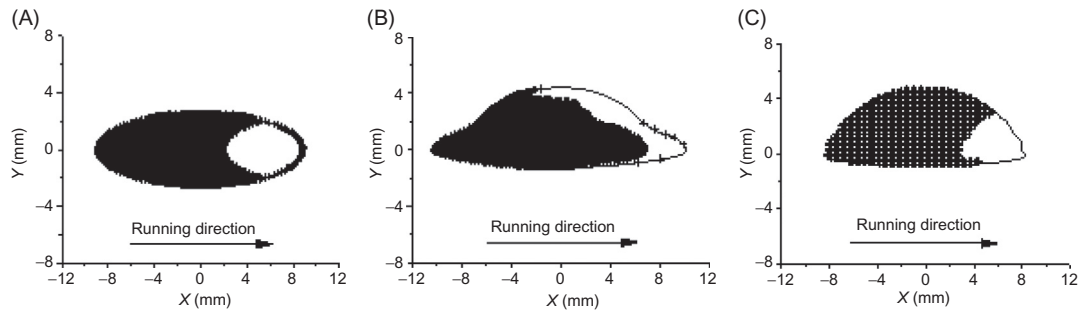

FIGURE 4.35

Simple creep (great creepage, $f_x = f_y = 3e-3, fin = 0$): (A) Simplified theory; (B) SH theory; (C) Accurate theory.

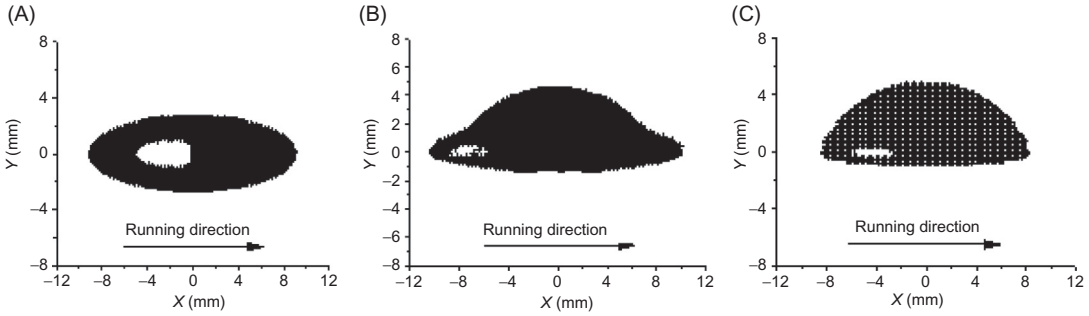

FIGURE 4.36

Simple spin creep ($f_x = f_y = 0, fin = 1.5$): (A) Simplified theory; (B) SH theory; (C) Accurate theory.

contact theory predicts 7.4 mm^2, accounting for 9.7% of the total size of the contact area; CONTACT theory predicts 9.1 mm^2, accounting for 13.8% of the total size of the contact area. For great creep without spinning, the slipped region grows in size significantly in the contact area, and the shapes obtained with the three theories show great discrepancy. For simple spin creep, the slipped region moves to the interior from the front end of the contact area; the calculated slipped region in the simplified theory is symmetric with respect to the longitudinal axis of the contact area, while the contact area in semi-Hertzian contact theory and CONTACT theory is asymmetric, with the locked region lying at the rear bottom of the contact area. Therefore, for the size of the slipped region in the contact area predicted by these theories, simplified theory shows 63.1 mm^2, accounting for 87.8% of the total size of the contact area; semi-Hertzian contact theory predicts 70.8 mm^2, accounting for 93.2% of the total size of the contact area; and CONTACT theory predicts 67.2 mm^2, accounting for 96.7% of the total size of the contact area. Overall, the size and distribution of the slipped region obtained with semi-Hertzian contact theory are closer to the results of Kalker 3D non-Hertzian contact theory.

c. Comparison of calculation efficiency

The Shen–Hedrick–Elkins theory is characterized by the minimum calculation time, disregarding the division of the contact area. The simplified theory has a relatively shorter calculation process because it saves the calculation of the shape of the contact area, as the shape may be determined upon defining the location of the wheel–rail contact point, and the creep force can be found easily by dividing the slipped/locked regions. Semi-Hertzian contact theory needs to obtain the shape of the contact area by balance and iteration of the normal force, followed by calculating the contact parameters and slipped/locked distribution of each strip; therefore, it is time-consuming. As for Kalker 3D non-Hertzian contact theory, the process of identifying the contact area and slipped/locked distribution is rather complex, further complicated by the calculation of boundary elements and programming; thus, this theory has the most time-consuming process.

In conclusion, semi-Hertzian contact theory outperforms the simplified theory in calculation accuracy and is more efficient than Kalker 3D non-Hertzian contact theory; therefore, it

can be used as the wheel–rail coupled contact model in the vehicle–turnout dynamics and simulation of the wear of turnout rails.

4.2.4 CALCULATION METHOD FOR 3D ELASTIC BODY SEMI-HERTZIAN ROLLING CONTACT OF THE WHEEL–RAIL SYSTEM IN TURNOUT AREA

At present, the influence of sub-rail elastic bearing cannot be taken into account for all rolling contact theories (except finite element contact theory, which is excluded from the calculation of wheel–rail dynamics due to inefficiency). However, little impact may be produced on the contact between single wheel and single rail in common tracks, as this contact case satisfies Saint-Venant's principle; the information for solving the wheel–rail contact area is independent of rail support conditions. However, it may affect the contact between the wheel and multiple rails in the turnout area. Actually, the stock rail and the switch rail are supported by slide bedplate, where an elastic pad is laid between the stock rail and the slide bedplate, while the switch rail and the slide bedplate are in rigid contact. In this case, when the wheel and turnout rails are brought into contact, the stock rail and the switch rail may displace vertically out of step, producing a relative displacement discrepancy. The discrepancy prevents wheel–rail contact, satisfying Saint-Venant's principle. In addition, lateral displacement discrepancy may occur between the two rails. These factors may alter the wheel–rail contact behavior to a great extent, including the number of contact points, the shape of the contact area, and stress distribution. Based on the above, a 3D elastic body rolling contact theory should be developed to include sub-rail elastic bearing and lateral relative displacement, so as to solve the contact problems in the turnout area where the wheel and a number of rails are in contact.

The solution process for 3D elastic body rolling contact behavior is as follows: assuming that the stock rail and the switch rail are provided with rigid constraint; defining the position of the principal contact point; defining the position of the principal contact point of wheel–rail with the principle of trace line method (taking the stock rail as the main contact rail) and calculating the minimum distance between the wheel tread and the profile of the switch rail h_{cs}; and either (i) at wheel load P, when the sum of the compressive distance of the pad under the stock rail d_{cs} and wheel–rail elastic compression w_{cs} is smaller than h_{cs}, that is, $d_{cs} + w_{cs} < h_{cs}$, the wheel is in single-point contact with the rail in the turnout area, the method for common single wheel–rail contact may apply; or (ii) at wheel load P, when the sum of the compressive distance of the pad under the stock rail d_{cs} and wheel–rail elastic compression w_{cs} is greater than or equal to h_{cs}, $d_{cs} + w_{cs} \geq h_{cs}$, the wheel will be in contact with two turnout rails at the same time. In the latter case, the point with the minimum distance between the wheel tread and the profile of the switch rail is defined as the second contact point. When the wheel and the switch rail are just brought into contact, partial wheel load will be borne by compressive deformation of the pad under the stock rail, and the rest by the stock rail and the switch rail, that is, $P_{sy} = P - P_{cs}$. In addition, the elastic compression between the wheel and the switch rail w_1 equals the sum of compressive displacement of the pad under the stock rail d_{sy} and the elastic compression between the wheel and the stock rail w_{sy}. After performing multiple iterations based on the above process until equilibrium is attained, the elastic compression between the wheel and the switch rail and between the wheel and the stock rail can be obtained. The results can aid the determination of the shape of stress distribution of each contact area. After that, the improved FASTSIM solver can be employed to obtain the

distribution and magnitude of the creep force on each contact area. This is the solution process for contact between the wheel and multiple turnout rails. When the principal contact point is located on the switch rail, the solution process for the wheel–rail rolling contact behavior is the same.

4.3 ASSESSMENT OF SIMPLIFIED MODELS [55]

The design optimization for wheel–rail relation in the turnout aims to control the structural irregularities and mitigate their impact on train vibration. During the maintenance, the irregularity amplitude and variation rate are regarded as the control factors. However, the dynamic effects may also be interfered by irregularity shape and wavelength. Thus, a complete theory of train-turnout system dynamics shall be established to reveal the dynamic impacts of irregularities on train-turnout system. This method is accurate, but time-consuming. It is unable to figure out the strengths and weaknesses of a design in a vivid and rapid means. Moreover, it is difficult to use.

To properly evaluate the designs of wheel–rail relation, a simple single degree of freedom (DOF) model (making an independent wheel travel in a turnout with vertical irregularities) is used to analyze the additional dynamic load when a train runs in an uneven track. Moreover, a two-DOF model (making a free wheelset travel in a turnout with lateral irregularities) is used to evaluate the rule of hunting motion.

4.3.1 VERTICAL IRREGULARITIES

1. Unsprung weight vibration equation

A uniform rail settlement y_0 may be produced when a train runs in a completely smooth track. In this case, there is no additional rail settlement or dynamic wheel load. However, the dynamic equilibrium conditions are different when a train travels in a line with vertical irregularities. Before that, the wheel gravity center remains parallel to the original rail surface. Then the gravity center suddenly drops (the amount equals to the irregularity depth η_r) when traveling in an uneven track, which forces the unsprung part of the wheel and partial track to vibrate, resulting in an additional rail settlement y_d and additional dynamic wheel load P_d. The forced vibration will last till the irregularity ends. After finishing the uneven track, free vibration may exist in a certain range due to the residual vertical vibration acceleration and displacement. However, this irregularity-induced vibration will die finally under the damping effect. Then the rail settlement will resume to y_0 and the dynamic wheel load will disappear. According to D'Alembert's principle, dynamic equilibrium can be attained when:

$$R + I - T = 0 \tag{4.51}$$

where, R is the counterforce induced by additional settlement, equals to dynamic wheel load P_d. $P_d = (2k/\beta)y_d$. Where k is the elastic modulus of rail supporting, which is the ratio of elastic modulus of rail support D to tie spacing a (i.e., $k = D/a$); β is track-rail stiffness ratio, $\beta = (k/4EI)^{\frac{1}{4}}$, where EI is the vertical flexural stiffness of the rail.

I is the inertia force produced by the vibration of unsprung part of wheel and partial track. $I = m_0(d^2(y_d + \eta_r)/dt^2)$. Where m_0 is the vibrating weight, approximated as unsprung weight q.

T is the damping force of the whole vibration system. $T = c(dy_d/dt)$, where, c is damping coefficient. To simplify the calculation process, the damping term can be omitted.

So:

$$\frac{2k}{\beta}y_{\mathrm{d}} + q\frac{d^2(y_{\mathrm{d}}+\eta_{\mathrm{r}})}{\mathrm{d}t^2} = 0 \tag{4.52}$$

Given $K_{\mathrm{r}} = (2k/\beta)$, one gets:

$$q\frac{d^2y_{\mathrm{d}}}{\mathrm{d}t^2} + k_{\mathrm{r}}y_{\mathrm{d}} = -q\frac{d^2\eta_{\mathrm{r}}}{\mathrm{d}t^2} = f(t) \tag{4.53}$$

Given $\omega_0 = \sqrt{(K_{\mathrm{r}}/q)}$, the transient vibration can be obtained by:

$$y_d(t) = \frac{1}{q\omega_0}\int_0^t f(t)\sin\omega_0(t-\tau)\mathrm{d}\tau \tag{4.54}$$

2. Calculation parameters

The wheel−rail dynamics research shows that the unsprung weight shall be minimized for low dynamic high-speed bogie, so as to ease the increase of low frequency (LF) wheel−rail force with accelerating the speed. This can be realized by the use of light alloy axle box, solid wheel and hollow axle. In China, high-speed EMU adopts solid rolled wheel and hollow axle. The diameter of wheel rolling circle is 860 mm and the unsprung weight of the wheelset is about 2400 kg. The unsprung weight of a single wheel is taken as 1200 kg for calculation. The stiffness of fastening support is 25 kN/mm, and tie spacing is 600 mm for Chinese high-speed turnout.

3. Additional dynamic force

When a CRH EMU train passes through No. 18 turnout for 350 km/h in the main line, taking no account of wheelset lateral displacement, the vertical irregularities induced by LMA tread at the switch and the crossing are shown in Figures 4.13 and 4.14. The rail dynamic displacement and additional dynamic force of the wheel at the switch and the crossing are calculated with single DOF model, as shown in Figures 4.37 and 4.38.

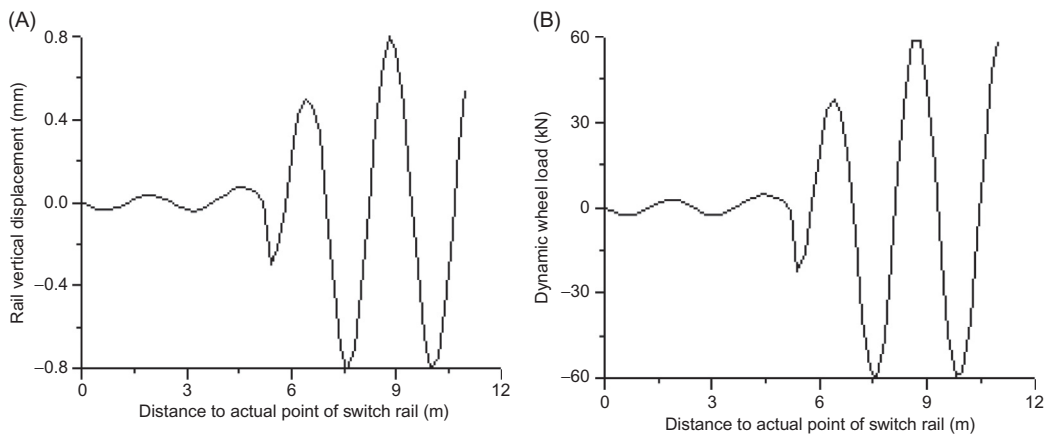

FIGURE 4.37

(A) Rail dynamic displacement at the switch. (B) Dynamic wheel load at the switch.

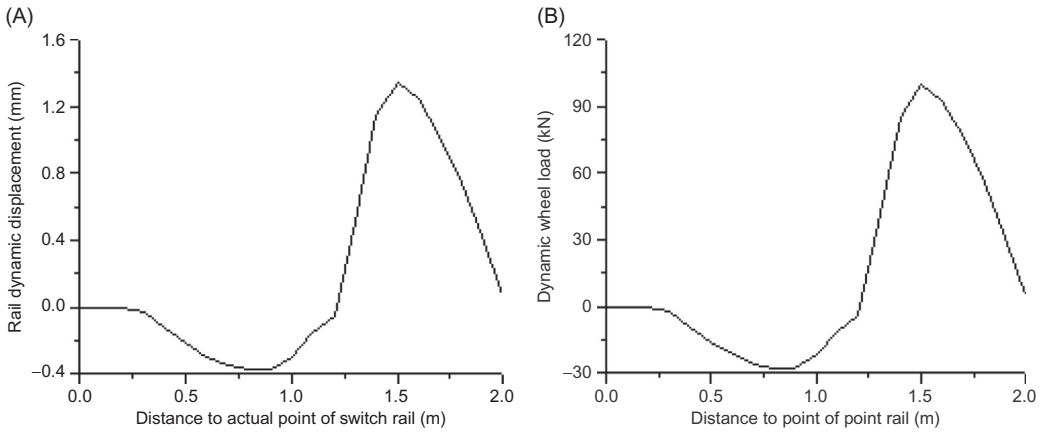

FIGURE 4.38

(A) Rail dynamic displacement at the crossing. (B) Dynamic wheel load at the crossing.

In the above figures, the vertical structure irregularities at the switch and the crossing result in severe wheel–rail vibration. The vibration is much more severe at the crossing due to the short wavelength of the structural irregularity. At the switch, the maximum rail dynamic displacement is 0.81 mm, the maximum dynamic wheel load is about 60.0 kN. At the crossing, the maximum rail dynamic displacement is about 1.32 mm, the maximum dynamic wheel load is about 98.4 kN, and the maximum wheel vibration acceleration is about 59.2 *g*. It indicates that the structural irregularities have been transformed to wheel–rail dynamic response, which may be used to evaluate the design of wheel–rail relation. The wheel dynamic load is directly proportional to rail dynamic displacement, so they follow the same change rule that may be evaluated with additional wheel dynamic force. The vertical irregularities at the switch will act from the actual point of the switch rail to a segment 6.6 m in the rear. Ignoring suspension damping, the wheel will vibrate freely without attenuation beyond that range.

4.3.2 LATERAL IRREGULARITIES

A wheelset is composed of two wheels press-fitted on one axle. The wheel tread is tapered. Hence, the geometric center of the wheelset can move straightly along the track provided that the wheelset geometric center is vertical to the longitudinal track centerline and the two wheels of a wheelset have the same radii of rolling circles. However, lateral displacement of the wheelset may occur due to other interferences in practice. For example, at the switch and the crossing, the wheel–rail contact points will shift to the stock rail and the wing rail as the tops of switch rails and point rails are depressed, which may move laterally with widening the tops of switch rails and point rails, leading to wheelset lateral movement toward switch rails and point rails under the effect of creep force. When the central position of the wheelset is off the track centerline and the two wheels of the wheelset have different rolling circle radii, the geometric center of the wheelset will move in a

zigzag. Such motion of the wheelset is called hunting motion. The rule of hunting motion in the turnout area can be used to evaluate the lateral structural irregularities of a turnout.

1. Wheelset creep force

   To accurately analyze the motions of vehicle system in a turnout, a rigorous nonlinear motion equation is required. However, a simple linear motion equation may be adopted to fully describe the impacts of lateral structural irregularities on vibration excitation of the wheelset. In a simplified model, the error produced therefrom is acceptable. The motion equation of the wheelset is linearized based on the following assumptions:

   a. The free wheelset moves at constant velocity along the straight rails with constant gauge on rigid subgrade

   b. The wheelset is regarded as a rigid body with the two wheels in contact with the rails continuously

   c. As the wheelset vibrates slightly, the linear creep force theory is true. In addition, the spin effect is disregarded, longitudinal and lateral creep forces are considered, and longitudinal and lateral creep coefficients are equal

   d. In view of small equivalent tread conicity and minor change, the tread of the free wheelset can be deemed as conical. Then the wheel radius is proportional to the lateral displacement of contact point. The gravitational stiffness-induced force and the torque produced by gravitational angular stiffness are disregarded; and

   e. The two wheels of a wheelset have the same weight.

   Given that: the wheelset has two degrees of freedom, that is, lateral displacement y_w (positive = right) and yaw ψ_w (positive = clockwise). The nominal rolling radius is r_0. The rotation angular velocity ω of the wheel is a constant. The advance velocity of the wheelset is v, $v = \omega r_0$. The equivalent tread conicity is λ. The half distance between the right and left rolling circles is b. The lateral irregularity under the right wheel is ξ_r when traveling in the main line. The creep coefficient is f. Hence, the creep ratio and creep force induced by lateral displacements y_w and $\dot{y}_w$ and yaws ψ_w and $\dot{\psi}_w$ can be expressed with corresponding expressions in Tables 4.3 and 4.4.

Table 4.3 Equations of Wheel–Rail Creep Ratio

Factors	Direction	Variables	Left Wheel	Right Wheel
Lateral displacement	Longitudinal	Rolling circle radius	$r_0 - \lambda y_w$	$r_0 + \lambda(y_w - \xi_r)$
		Theoretical velocity	$\omega(r_0 - \lambda y_w)$	$\omega(r_0 + \lambda y_w - \lambda\xi_r)$
		Sliding velocity	$v - \omega(r_0 - \lambda y_w) = \omega\lambda y_w$	$\omega\lambda(\xi_r - y_w)$
		Creep ratio	$\omega\lambda y_w/\varpi r_0 = \lambda y_w/r_0$	$\lambda(\xi_r - y_w)/r_0$
	Lateral	Sliding velocity	$\dot{y}_w$	$\dot{y}_w - \dot{\xi}_r$
		Creep ratio	$\dot{y}_w/v$	$(\dot{y}_w - \dot{\xi}_r)/v$
Yaw	Longitudinal	Sliding velocity	$b\dot{\psi}_w$	$-b\dot{\psi}_w$
		Creep ratio	$b\dot{\psi}_w/v$	$-b\dot{\psi}_w/v$
	Lateral	Sliding velocity	$-v\tan\psi_w = -v\psi_w$	$-v\psi_w$
		Creep ratio	$-\psi_w$	$-\psi_w$

Table 4.4 Creep Ratio and Creep Force of Wheel–Rail

	Creep Ratio		Creep Force	
Wheel	**Longitudinal**	**Lateral**	**Longitudinal**	**Lateral**
Left wheel	$\lambda y_w/r_0 + b\dot{\psi}_w/v$	$\dot{y}_w/v - \psi_w$	$-f(\lambda y_w/r_0 + b\dot{\psi}_w/v)$	$f\psi_w - f\dot{y}_w/v$
Right wheel	$\lambda(\xi_r - y_w)/r_0 - b\dot{\psi}_w/v$	$(\dot{y}_w - \dot{\xi}_r)/v - \psi_w$	$f\lambda(y_w - \xi_r)/r_0 + fb\dot{\psi}_w/v$	$f(\dot{\xi}_r - \dot{y}_w)/v + f\psi_w$

2. Wheelset vibration equation and its solution

Given that the wheelset weight is M_w and the moment of inertia is J_w, according to Newton's laws of motion, one gets:

$$\begin{cases} M_w\ddot{y}_w = -2f\dot{y}_w/v + 2f\psi_w + f\dot{\xi}_r/v \\ J_w\ddot{\psi}_w = -2fb^2\dot{\psi}_w/v - 2fb\lambda y_w/r_0 + fb\lambda\xi_r/r_0 \end{cases} \tag{4.55}$$

Equation (4.55) is the second order nonhomogeneous linear differential equation with constant coefficients. The lateral irregularity is an excitation source of train-track system vibration, however, it cannot be expressed with any simple equation, let alone obtain the solutions. The approximate solutions may be obtained with Newmark-β numerical integration method, etc.

The frequency of wheelset hunting motion is $\omega_w = \sqrt{(\lambda/br_0)}v$, and the wavelength is $L_w = 2\pi\sqrt{(br_0/\lambda)}$.

3. Wheelset hunting motion in turnout area

The wheelset weight of an EMU train is 2400 kg and the inertia of yaw is 1350 kg m; $r_0 = 0.43$ m, $b = S/2 = 0.75$ m; the creep coefficient is $f = 9.57 \times 10^6$ N; equivalent conicity is 0.1; the lateral irregularity the turnout is taken as per LMA tread as shown in Figures 4.13 and 4.14. Through the calculation, the distribution results of the hunting motion and yaw of the wheelset at the switch and the crossing are shown in Figures 4.39 and 4.40.

In the above figures, the lateral structural irregularities at the switch and the crossing will induce obvious hunting motion during the passage in a turnout. The wheelset is subject to forced vibration within the scope of irregularity. After that, it will vibrate freely. The lateral irregularity has a longer action range at the switch, the maximum wheelset lateral displacement is 18.6 mm (this value is greater than the clearance between flange and gauge line as the effect of flange–rail contact is neglected) and the max lateral vibration acceleration is about 5.5 g. The lateral irregularity amplitude at the crossing is equal to that at the switch. However, the action range is short. Therefore, the maximum wheelset lateral displacement is 9.5 mm and maximum lateral vibration acceleration in the irregularity range is about 12.1 g, and about 2.8 g during free vibration. In conclusion, the lateral stability of the wheelset at the switch is much poorer than that at the crossing, so the flange will cling to the rail, leading to great wheelset lateral displacement that exert significant lateral impact on the rail. To this end, the hunting motion amplitude of the wheelset can be used to evaluate the lateral irregularities of the turnout.

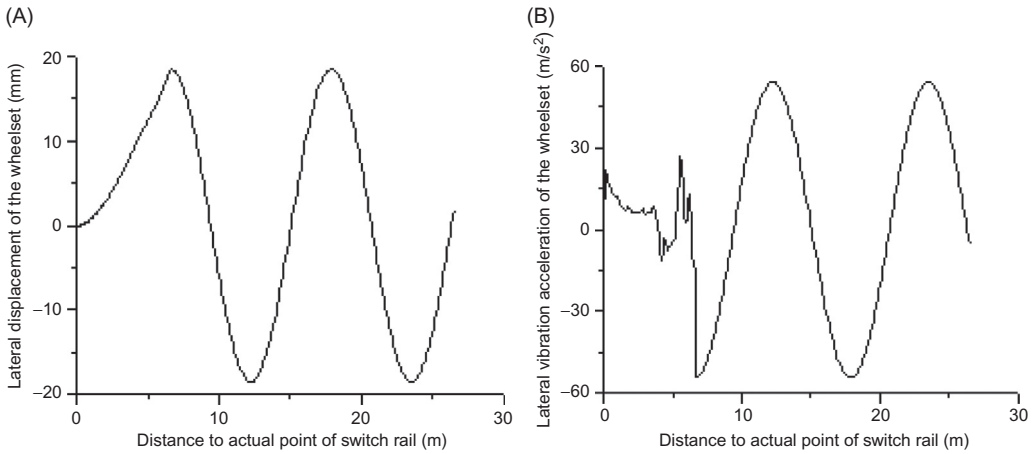

FIGURE 4.39

(A) Lateral displacement of the wheelset at the switch. (B) Lateral vibration acceleration of the wheelset at the switch.

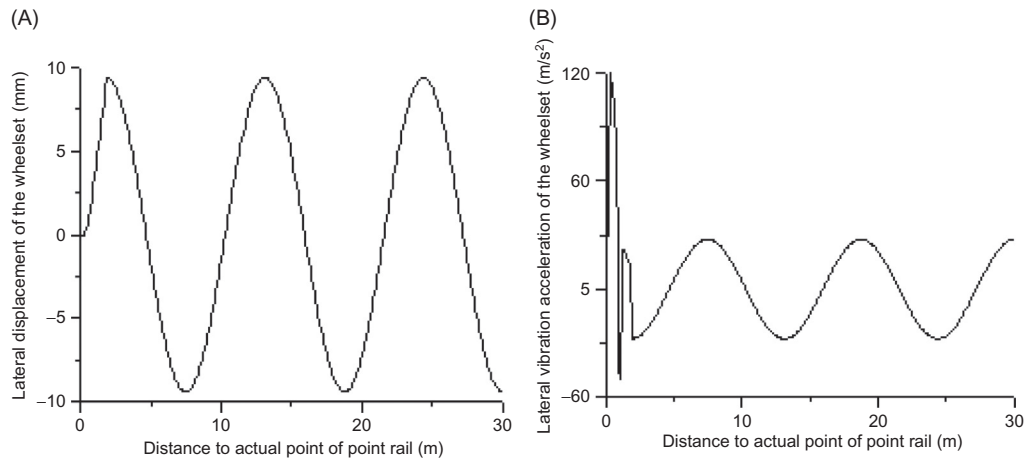

FIGURE 4.40

(A) Lateral displacement of the wheelset at the crossing. (B) Lateral vibration acceleration of the wheelset at the switch.

Table 4.5 Comparison of Design Schemes of Wheel–Rail Relation at the Switch

Scheme	Initial Load-Bearing Section (mm)	Full Load-Bearing Section (mm)	Depressed Amount of Switch Rail at the Initial Load-Bearing Section (mm)	Wheel Dynamic Load (kN)	Wheelset Lateral Displacement (mm)
1	20	50	3	100.8	17.7
2	20	50	4	74.6	18.0
3	20	50	5	83.9	19.6
4	15	50	4	84.7	17.9
5	25	50	4	82.3	18.9
6	20	40	4	78.5	17.9
7	20	60	4	110.8	20.8

4.3.3 APPLICATION CASES

1. Forward-shifting and shortening of wheel-load transition range at the switch

   For common turnouts, the section of the switch rail with top width of 20 mm will bear the load first, where height difference with the stock rail is 3–5 mm; the section with top width of 50 mm will fully bear the load, where the two types of rails are at the same level. For high-speed turnout, the wheel–rail relation at the switch may be optimized by altering the height difference or position of the initial load-bearing section, or shifting the position of full load-bearing section. In addition, the design schemes may be evaluated by wheel dynamic load and wheelset lateral displacement. Table 4.5 presents the comparison results of certain design schemes.

   As given in Table 4.5, the wider the initial and full load-bearing sections and the greater the depressed amount, the farther the wheel-load transition section shifting backward, the greater the wheelset lateral displacement, and the poorer the riding quality. However, the vertical additional dynamic force of the wheel changes slightly with the backward shifting of the wheel load transition point. For high-speed turnouts in China, the riding quality in the main line is mainly improved by: controlling the wheelset lateral displacement and depressing the straight switch rail by 3 and 0 mm at top widths of 15 and 40 mm, respectively. The strength of the switch rail when a train travels in the diverging line is maintained by: controlling wheel dynamic load, and depressing the curved switch rail by 4 and 0 mm at top widths of 20 and 50 mm, respectively.

2. Gauge widening design at the switch

   For German high-speed turnouts, the gauge widening technology as shown in Figure 1.22 is adopted. In the design, the switch rail is depressed by 5.8, 0.3, and 0 mm at top widths of 20, 34, and 50 mm, respectively. In this design, the wheel load transition point will move forward. Given the gauge is widened by 0, 5, 10, and 15 mm, respectively at top width 15 mm of the switch rail (these segments of the switch rail will be thickened by 15, 20, 25, and 30 mm correspondingly), the comparison results of design parameters, such as equivalent conicity, wheelset inclination, additional dynamic force, and amplitude of hunting motion during the passage of LMA tread wheel are given in Table 4.6. The comparison results of additional dynamic pressure and wheelset hunting motion are shown in Figure 4.41.

   When the stock rail bends outward, the wheel–rail contact points at the bending side will also move outward. The resulting lateral structural irregularity offsets the lateral force on the

Table 4.6 Effect of Gauge Widening Amount on Design Parameters of Turnouts

Gauge Widening Amount (mm)	0 mm	5 mm	10 mm	15 mm
Top width of switch rail at wheel-load transfer point (mm)	30.4	31.2	30.8	31.4
Equivalent conicity	0.030	0.028	0.027	0.026
Inclination of the wheelset (0.001 rad)	0.60	0.50	0.42	0.36
Additional dynamic force (kN)	42.0	32.3	42.9	30.8
Wheelset lateral displacement (mm)	18.3	16.5	12.2	7.9

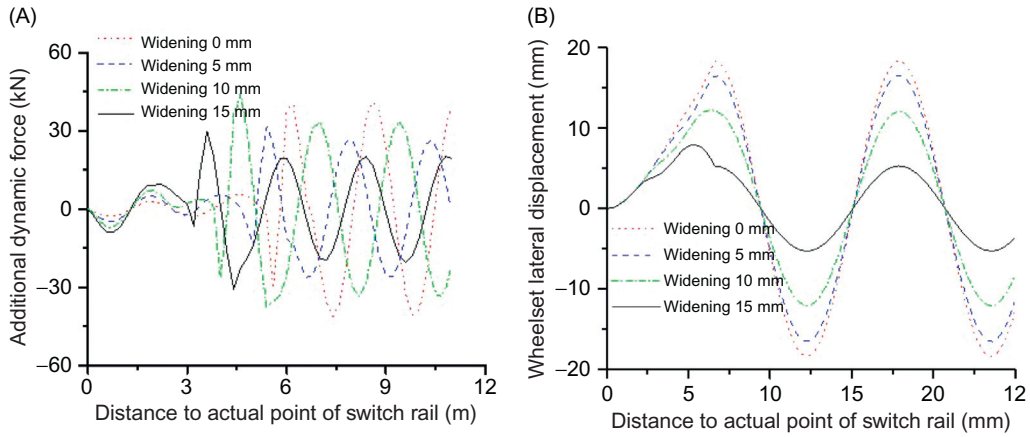

FIGURE 4.41

(A) Additional dynamic force. (B) Hunting motion of the wheelset.

wheelset induced by the lateral irregularity at the switch rail. Therefore, the greater the gauge widening amount, the smaller the wheelset lateral displacement. It is the same with equivalent tread conicity, wheelset inclination, and other geometry parameters. The vertical wheel dynamic load changes insignificantly with gauge widening. The values are much smaller than those included in Table 4.6. Therefore, for German high-speed turnouts, the wheel−rail relation is optimized by widening the gauge by 15 mm, which is realized through bending the stock rail by 15 mm at the top width 15 mm of the switch rail.

3. Wheel−rail relation design for the point rail at the crossing

In designing the wheel−rail relation for the point rail at the crossing, the height difference of rail top may be optimized as with the switch rail. In addition, the horizontal hidden tip point structure and heightening of the wing rail are available, as shown in Figure 1.48. Given the point rail is depressed by 16, 4, and 0 mm at top widths of 5, 20, and 50 mm, respectively, the comparison results of hidden tip point structure (hidden amounts of 5, 7.5, and, 10 mm, respectively), heightening of the wing rail (heightening amounts of 0.5, 1.0, and 1.5 mm, respectively) for different wheel−rail relation design schemes are given in Table 4.7.

As shown in Table 4.7, the greater the horizontal hidden tip point amount of the point rail, the smaller the wheel dynamic force and wheelset lateral displacement. Restricted by the crossing

Table 4.7 Comparison of Design Schemes of Wheel–Rail Relation at the Crossing

Scheme	Description		Wheel Dynamic Force (kN)	Wheelset Lateral Displacement (mm)
1	Optimization of height difference of the point rail		118.2	9.7
2	Horizontal hidden tip point amount of the point rail (mm)	5	116.7	10.2
3		7.5	100.3	9.5
4		10	95.1	9.2
5	Heightening amount of the wing rail (mm)	0.5	62.8	10.2
6		1.0	17.4	10.3
7		1.5	23.6	10.6

structure, China's high-speed turnout adopts the structural design with a hidden tip point amount of 9 mm. This design is also used in France. The greater the heightening amount of the wing rail, the smaller the vertical wheel dynamic force. Yet the lateral displacement of the wheelset slightly increases. Germany adopts the wing rail with a heightening amount of 2.3 mm.

4.4 DYNAMIC EVALUATION BASED ON WHEEL–RAIL DYNAMICS IN TURNOUT AREA [56]

Based on the above analysis, the dynamic wheel–rail contact geometry relation shall be further explored and specific train-turnout dynamics models and relevant calculation theories shall be developed to accurately reveal the vibration rules of train-turnout system.

4.4.1 DYNAMICS MODELS OF TRAIN-TURNOUT SYSTEM

Turnout models aim to present the structural features of a turnout, tell the vibration characteristics of turnout components and solve problems of concern. Different from the simplified single-rail track structure for common railway section, a 3D bilayer beam structure shall be applied to a turnout. So the analytical models for wheel–rail system must be 3D coupled vibration models.

1. Vehicle model

   There is no special requirement on the vehicle models in turnout area, existing ones are applicable. The commonly used vehicle models include the full-vehicle model and bogie model. Full-vehicle model, as shown in Figure 2.28, is adopted to better simulate the dynamic characteristics of a train traveling in a turnout.

   In the modeling, the main concerns for the carbody and bogie are the same, that is, vertical and lateral movement, rolling, pitch, and yaw; the main concerns for wheelset are similar excluding the omission of pitch. The wheel tread is tapered or worn profiled. The wheel and rail are vertically coupled by nonlinear Hertzian contact force, and transversely linked by creep force of the tread and flange force.

2. Full model of a single turnout with swing nose rail [57,58]

Figure 4.42 presents a full model of a turnout with swing nose rail.

The model is based on the following assumptions and structural features of the turnout:

a. The vibration of each rail is considered in the model. The rails are regarded as bi-directionally (laterally and vertically) flexible Euler beams. The switch rail, swing nose rail, and wing rail are regarded as nonuniform beams, while other rails are uniform beams

b. For ballast turnout, the eccentric loading and bending deformation of the tie are considered, the tie is deemed as a vertically flexible Euler beam, or a rigid body in lateral direction. For ballastless turnout, the vibration of the monolithic bed shall be considered, and the track slab is regarded as bi-directionally flexible; and

c. Fasteners are regarded as the spring-damping devices connecting the rail and the tie. The elasticity and damping differ in various bearing conditions. The bed support is also regarded as the spring-damping device with the bed bearing elasticity and damping uniformly distributed on the tie in the longitudinal direction.

3. Detailed model at the switch

The detailed model at the switch of the swing-nose turnout is shown in Figure 4.43.

The model is based on the following assumptions and structural features of the turnout:

a. The nonlinear vertical force between the switch rail and the stock rail is considered. At the actual point of the switch rail, the jaw of the switch railhead is hidden beneath the head of

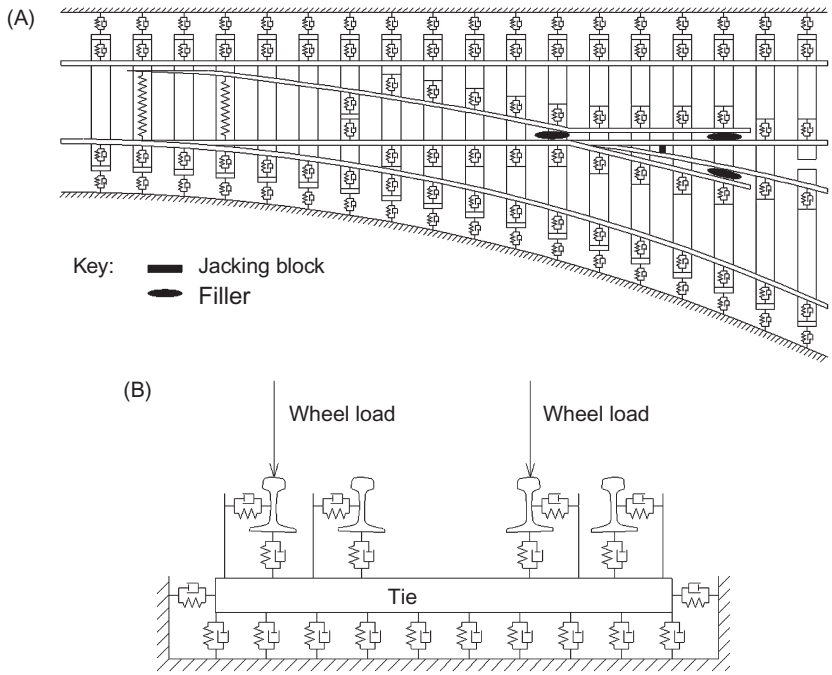

FIGURE 4.42

(A) Plan of a swing-nose turnout. (B) Elevation of a swing-nose turnout.

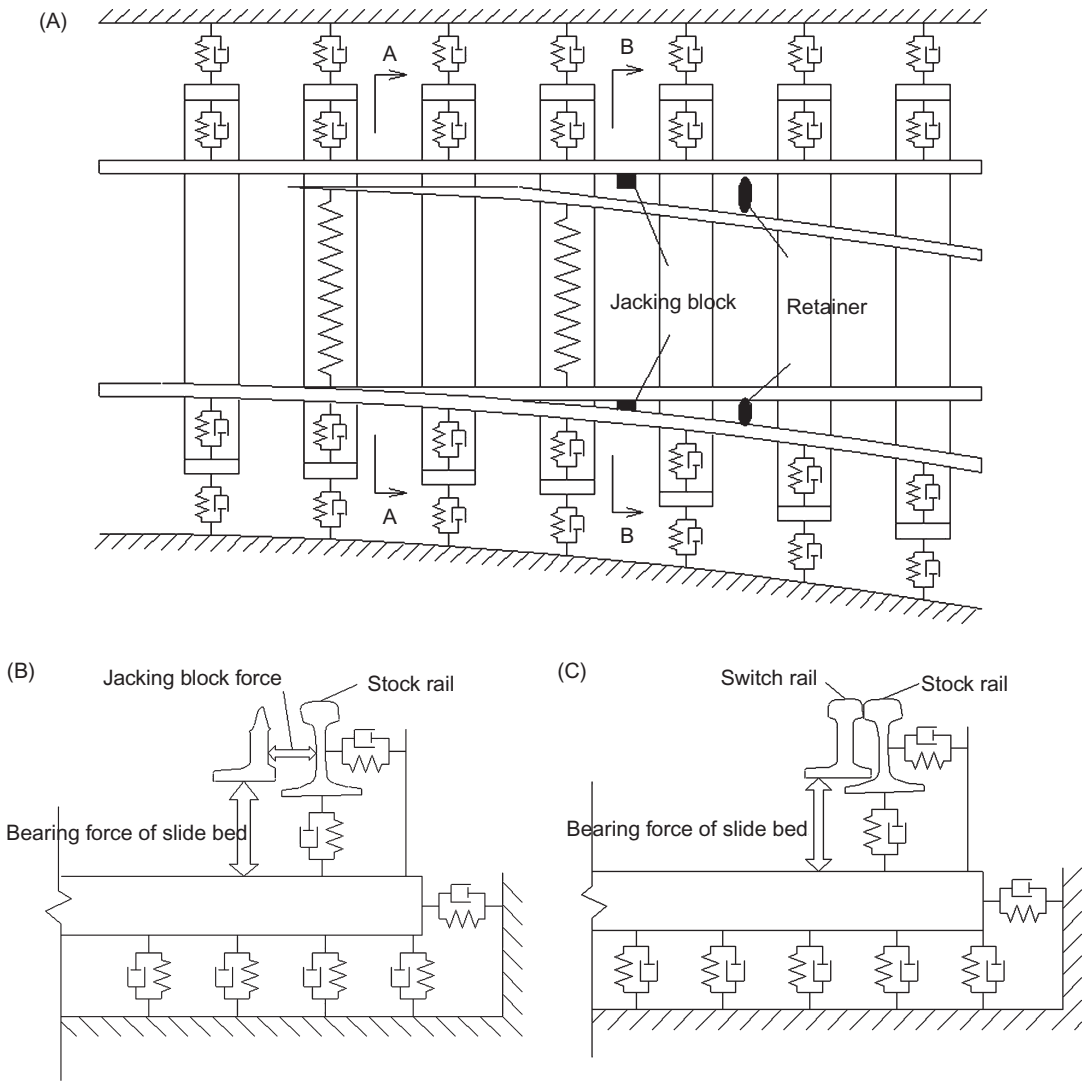

FIGURE 4.43

(A) Plan of an analytical model at the switch. (B) Section A-A. (C) Section B-B.

the stock rail, and there is gap between the jaws of two rails (3 mm typically). When the switch rail jerks while it clings to the stock rail, the vertical displacement of switch rail will be constrained by the stock rail under a vertical force. The action range of the force will vary with the section profile of the switch rail, and may be affected by the lateral relative position between the heads of the switch rail and the stock rail. The force may appear when the jaw of switch railhead moves beyond the head of the stock rail

b. The nonlinear lateral force of the heads of the closed switch rails and stock rails is considered. For a closed switch rail, the lateral force from the wheel will be transmitted to the stock rail. Similarly, the lateral displacement of the switch rail will be limited by the stock rail

c. The effect of the jacking block restricting the lateral relative displacement at the noncontact area of the switch rail and stock rail is considered. The lateral jacking block force exists when the stock rail is in close contact with the jacking block. This force will transfer the lateral force and restrict the lateral displacement of the switch rail with respect to the stock rail

d. The restriction of electrical switch rod on the lateral vibration of nonworking switch rail, as well as the restriction of locking device on switch rails and stock rails vertical and lateral displacement is considered; and

e. Nonlinear supporting action of the slide plate on the switch rail is considered. When the switch rail clings to the slide bedplate, the vertical force on the switch rail will be transferred to the slide bedplate. In this way, the vertical displacement of the switch rail is constrained.

4. Detailed model of the connecting part

The detailed model of the connecting part of a swing-nose turnout is shown in Figure 4.44.

The model is based on the following structural features of the turnout and other specifications:

a. The operating conditions when a train travels in the main and diverging lines are considered; and

b. The load-transfer effect of the jacking block between two rails and the effects of the flexural stiffness of the big plate supporting the two rails are considered.

5. Detailed model of the crossing [59]

Figure 4.45 shows the detailed model of the crossing of a swing-nose turnout. The model is based on the following structural features of the crossing and other specifications:

a. The point rails and wing rails vertical coupling relationship is considered, including the vertical force of the external locking device there-between, nonlinear vertical force between the heads of point rails and wing rails and the vertical filler force at the end of the long wing rail

b. The point rails and wing rails lateral coupling relationship is considered, including the lateral force of the external locking device there-between, nonlinear lateral force transferred between the heads of the closed point rails and wing rails, the lateral jacking block force there-between, and the lateral filler force at the end of the long wing rail; and

c. The vertical supporting effects of the slide bedplate on the point rail and the effects of the flexural stiffness of the big plate supporting the track rails are considered.

4.4.2 VIBRATION EQUATION OF TRAIN-TURNOUT SYSTEM

1. Contact mechanism of 3D elastic bodies

The wheel experiences three states during wheel load transition. First, the wheel acts on the stock rail or wing rail. In this case, the wheel tread comes into contact with the rail top at one point, the load is completely applied on the stock rail/wing rail (no load on the switch rail/point rail). Second, the wheel transfers the load. The wheel will act on stock rail/switch rail or wing rail/point rail at the same time with two contact points between the tread and rail top. The load is shared by the stock rail and the switch rail or the wing rail and the point rail. The normal forces and creep forces at the two contact points can be calculated separately. Third, the wheel acts on

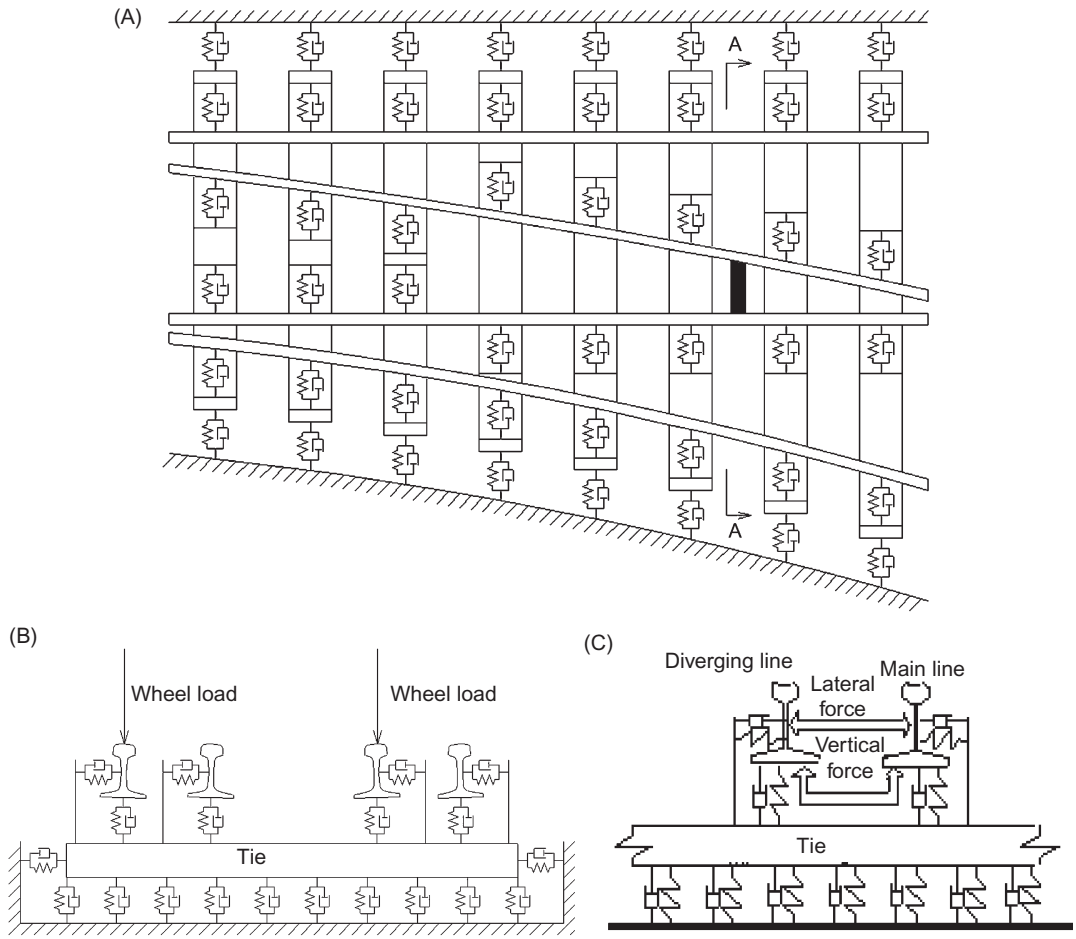

FIGURE 4.44

(A) Plan of an analytical model of turnout connecting part. (B) Elevation. (C) Section A-A.

the switch rail and the point rail. The tread comes into contact with rail top at one point, the load is completely applied on the switch rail/point rail (no load on the stock rail/wing rail) [60].

In the second state, the distribution ratio of the wheel load on the two rails is unknown, so the displacement coordination condition of the wheel–rail contact points on two rails shall be provided, as shown in Figure 4.46. Given the height difference of two rails is Z, with the vertical displacement Z_{2r} of stock rail/wing rail, vertical displacement Z_{1r} of the switch rail/point rail, and the height difference Z_{12} between the front part of the switch rail and the stock rail (or between the point rail and the wing rail), one gets:

$$Z = Z_{12} + Z_{1r} - Z_{2r} \tag{4.56}$$

Given the rolling circle radii at the contact points between the wheel and the switch rail/point rail and between the wheel and the stock rail/wing rail are r_1 and r_2, respectively, when

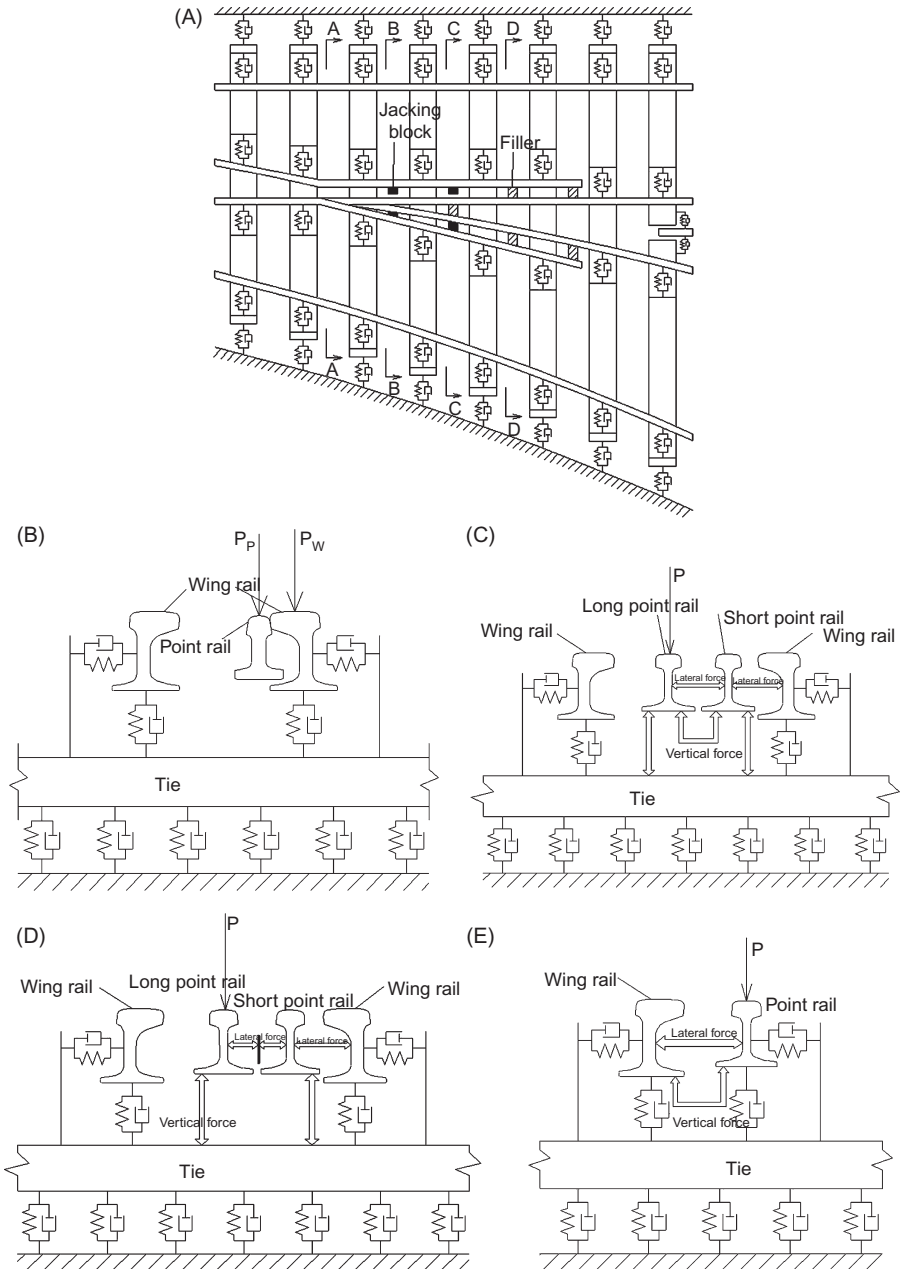

FIGURE 4.45

(A) Top view of an analytical model of the crossing of a swing-nose turnout. (B) Elevation A-A of the crossing. (C) Elevation B-B of the crossing. (D) Elevation C-C of the crossing. (E) Elevation D-D of the crossing.

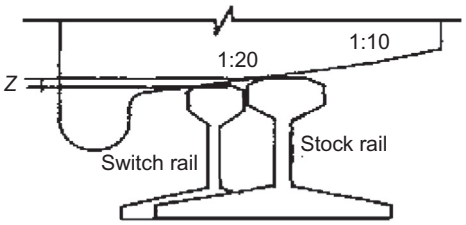

FIGURE 4.46

Diagram of wheel load transition calculation.

$Z \leq r_1 - r_2$, the load will be applied on the switch rail/point rail. In this case, the elastic compression displacement between the wheel and the switch rail/point rail is $\Delta Z_1 = Z_w + r_1 - r_0 - Z_{12} - Z_{1r}$, and that between the wheel and the stock rail/wing rail is $\Delta Z_2 = Z_w + r_2 - r_0 - Z_{2r}$; where Z_w is the vertical displacement of the wheel and r_0 is the nominal rolling circle radius. Then the wheel distribution at both contact points can be obtained.

The wheel load transition is finished when the load on the stock rail/wing rail disappears.

2. Excitation load

Four types of irregularities may exist in the turnout system:

a. Structural irregularities

When a train runs in a turnout, the wheel does not move straightly. At the switch rail and the point rail, the gravity center of the wheel drops as the contact point on the tread moves outward, producing vertical and lateral structural irregularities. These irregularities are the main source of vibration excitation when a train travels in a turnout, as reflected in the change of dynamic wheel–rail contact relation.

b. Dynamic irregularities

The vibration of one rail will be constrained by another rail with the use of filler, jacking block and the big plate in the turnout. Any dimensional change of the elastic pad is directly related to stiffness change of the fastening, which may lead to the uneven distribution of track stiffness in the longitudinal direction of a line, even result in the change of wheel–rail interaction. The irregularities are a source of vibration excitation, which may be expressed with the effects of connecting parts, different stiffnesses of different fastenings, the change of bed bearing stiffness with tie length, etc. in the model.

c. State irregularities

According to the field application state of a turnout, common turnout irregularities, including the scant switching displacement of the switch rail and the point rail, gap between the switch rail/point rail and slide bed, unsupported tie at the switch rod, and the switch rail and the point rail height difference, are considered. The state irregularities can be modeled by setting the initial states of nonlinear forces.

d. Geometry irregularities

As with a section, geometry irregularities including gauge, alignment, and longitudinal and cross level irregularities as well as shortwave irregularity of welding joint may exist in the turnout area. The irregularities are a source of vibration excitation of train-turnout system and can be modeled by inputting the track irregularity.

3. Vibration equation of train-turnout system

The vibration differential equation of wheel−rail system in a turnout can be developed according to the principle of minimum potential energy in variation form:

$$[M]\{\ddot{u}(t)\} + [C]\{\dot{u}(t)\} + \{F(t,u)\} = \{P(t,u,\dot{u})\} \tag{4.57}$$

The contact state of flange and jacking block and the supporting effect of tie on the switch rail will change with the time, position or even integration step. In this sense, the stiffness matrix and load array are time dependent.

4. Solution of vibration equation

a. Integration method

As Eq. (4.57) is nonlinearly time varying with higher order, it is better to use a direct integration method to solve the equation. In this method, the riding time is discretized. Assuming that the vibration displacement, speed, and acceleration of the system change as per a certain rule in a given time, the response of the system at a given moment will be a combination of the response values at the discrete points of time before that moment, obtained as per the change rule. So the vibration equations for all discrete points of time can be solved with the given initial conditions.

Different integration methods are followed according to different change rules assumed. The Park method is chosen for its good LF precision and unconditional stability in nonlinear problems without overshoot.

Given the displacements and velocities at three previous points of time, the response of the system at point $n+1$ can be obtained with this method. Therefore, the Newmark-β method is used to obtain the preconditions (displacement, velocity, and acceleration) in advance.

b. Reduced DOF

As dynamic analysis is a laborious process, the exploration of a more effective and labor-saving solution or method will be an important direction of dynamic studies. In this regard, reduced DOF is widely applied, where master−slave DOF and modal synthesis methods are most common. For the master−slave DOF, the DOF (displacement vector) of the system falls into two parts, namely master DOF and slave DOF, where the latter is dependent on the former.

c. Iteration

The solution of the vibration equation is complex, as it involves the iteration of nonlinear contact force and nonlinear creep force, iteration of integration time steps, and determination of closed flange, closed jacking block, contact between the switch rail/point rail with ties, and switch rails' and stock rails' contact in the lateral plane. To simplify the process and maintain the stability and convergence of iteration, it is important to find a way to reasonably construct multiple iteration structures.

In the direct integration method, iteration of the integration time step is the outermost. In the 3D wheel−rail coupling vibration system, lateral vibration is seriously affected by vertical vibration, but has small impact on the latter. For this, the iteration of wheel−rail contact force (innermost) is carried out first. Following the convergence of this iteration, the convergence of creep force may be easier and less impacted by the closure status of the flange or jacking block. Then iteration of the nonlinear creep force will be carried out.

According to the dynamics studies, when a train travels in a curved line, guidance is totally supported by creep force in a large radius curve, and may be supported by flange force only in a tight curve. Given the creep force, it is easier to determine the necessity of flange force for guidance, or flange–rail contact. Therefore, the determination of flange–rail contact will be carried out immediately for creep force iteration. After that, determination of the closed jacking block, the contact status of all bearing points beneath the switch rail, and switch rail and stock rail contact can be performed in one iteration structure (the second outermost). This iteration structure has been justified. All iterations may be converged after six or so iterations.

d. Programming

The computer-aided solver Spatial Interactions between Cars and Turnout (SICT) was developed with FORTRAN language for a 3D wheel–rail system coupling vibration model. To save the memory during programming, one-dimension variable-bandwidth compression storage is adopted. Moreover, the improved advancing front method is used to solve large sparse matrixes.

4.4.3 EVALUATION INDICATORS

1. Safety

Derailment coefficient and rate of wheel load reduction are generally used to evaluate riding safety in the dynamics of railway vehicles.

The derailment coefficient is the ratio of lateral force Q to vertical force P on the wheel at a specific time. As stipulated in *Railway Vehicles—Specification for Dynamic Performance Evaluation and Accreditation Test* (GB 5599-85), the derailment coefficient of the wheel on the rail-mounting side shall meet:

$$\begin{cases} O/P \le 1.2 & \text{(Limit 1, acceptable)} \\ Q/P \le 1.0 & \text{(Limit 2, increased safety margin)} \end{cases} \tag{4.58}$$

The above equation applies to the rail-mounting condition with action time of lateral force longer than 0.05 s.

The rate of wheel load reduction is a safety indicator for evaluating whether a derailment will occur due to drastic load reduction on one wheel given that the wheelset lateral force is zero or close to zero. As per GB 5599-85, the rate of wheel load reduction shall meet:

$$K_{gy} = \frac{W}{2y_w \mu d_R}[tg(\delta_R + \theta_w) - tg(\delta_L - \theta_w)] = \frac{\text{Resiliency of the wheelset}}{\text{The sum of the distances from the left and right contact points to the nominal contact points}} \tag{4.59}$$

It should be noted that, as determined by equilibrium conditions of wheel stress, the derailment coefficient and the rate of wheel-load reduction will function under two different conditions, respectively: wheelset lateral force $H > 0$ and $H = 0$. Generally, the derailment coefficient is taken as an indicator of riding safety and the rate of wheel-load reduction is regarded as an evaluation indicator in static or quasi-static conditions. To ensure high-speed traffic safety, the rate of wheel load reduction should not exceed 0.8 when a car travels at more than 30 km/h.

Table 4.8 Rating of Vibration Acceleration Stabilities of Railway Vehicles in China

	$A_{max}(m/s^2)$		$A_w(m/s^2)$	
Ratings	**Vertical**	**Lateral**	**Vertical**	**Lateral**
Excellent	2.45	1.47	0.393	0.273
Good	2.95	1.96	0.586	0.407
Acceptable	3.63	2.45	0.840	0.580

2. Riding quality

Riding comfort, or riding quality, can be determined by carbody vibration acceleration. For accuracy, vibration frequency may also be considered. Evaluation indicators may differ by country. Normally, carbody vibration acceleration is the dominant indicator in analyzing the riding comfort over a short period. For a longer period, the amplitude, frequency, duration, etc. of the acceleration will be taken into account. In China, riding quality (passenger comfort) is determined by carbody vibration acceleration and riding quality indicators.

The maximum vibration acceleration A_{max} and the effective value of weighted vibration acceleration of the cab A_w are used in two Chinese codes: *Test Evaluation Method and Standard for Dynamic Performance of Railway Locomotive* (TB/T 2360-93) and *Specifications for Power Car Strength and Dynamic Performance of High-Speed Testing Train* (95J01-L), See Table 4.8 for details.

In the table, $A_{max} = \overline{A} + 3\sigma_a$, where $\overline{A}$ and σ_a denote the average and mean square error of the absolute values of all peak accelerations, respectively.

$A_w = \sqrt{2\int_1^{80} G(f)\cdot B^2(f)\mathrm{d}f}$; f represents the frequency and $G(f)$ is the average power spectral density of the acceleration.

$$B(f) = \begin{cases} 0.5\sqrt{f} & (f = 1-4\ \text{Hz}) \\ 1 & (f = 4-8\ \text{Hz}) \\ 8/f & (f = 8-80\ \text{Hz}) \end{cases} \quad \text{(Frequency weighting function of vertical acceleration)}$$

$$B(f) = \begin{cases} 1 & (f = 1-2\ \text{Hz}) \\ 2/f & (f = 2-80\ \text{Hz}) \end{cases} \quad \text{(Frequency weighting function of lateral acceleration)}$$

The rating of riding quality in *Test Evaluation Method and Standard for Dynamic Performance of Railway Locomotive* (TB/T 2360-93) and *Railway Vehicles—Specification for Dynamic Performance Evaluation and Accreditation Test* (GB 5599-85) are given in Table 4.9. The rating of vertical and lateral stabilities is the same.

The indicator W is expressed as:

$$W = 7.08\sqrt[10]{\frac{A^3}{f}F(f)} \tag{4.60}$$

where W, A, f, and $F(f)$ refer to riding quality indicator, vibration acceleration (g), vibration frequency (Hz, taken as 0.5−40 Hz), and frequency correction coefficient, respectively, as shown in Table 4.10.

Table 4.9 Rating of Riding Quality of Railway Vehicles in China

Rating	Evaluation Result	Locomotives	Passenger Car	Freight Car
Level 1	Excellent	<2.75	<2.5	<3.5
Level 2	Good	2.75–3.10	2.5–2.75	3.5–4.0
Level 3	Acceptable	3.10–3.45	2.75–3.0	4.0–4.25

Table 4.10 Frequency Correction Coefficients for Riding Quality Indicator Calculation

Vertical Vibration		Lateral Vibration	
0.5–5.9 Hz	$F(f) = 0.325f^2$	0.5–5.4 Hz	$F(f) = 0.8f^2$
5.9–20 Hz	$F(f) = 400/f^2$	5.4–26 Hz	$F(f) = 650/f^2$
> 20 Hz	$F(f) = 1$	> 26 Hz	$F(f) = 1$

3. Track force

a. Wheel–rail vertical force

In the specification for speed-up tests for existing lines in Japan, the maximum wheel load shall be less than the design load (including the dynamic wheel–rail impact due to wheel flats) of rail parts. In China, based on the specification, the maximum allowable dynamic load in the turnout is determined as:

$$P_{\max} = 300 \text{ kN} \tag{4.61}$$

b. Wheel–rail lateral force

The railway track structure may have a certain margin of strength in the vertical direction, but its lateral strength is determined empirically under the premise of a smooth line layout. However, in a degraded line, excess wheel–rail lateral force may lead to fastening damage and track irregularities, or even derailment induced by rail tilting. The limit of this force is determined mainly by the design lateral load of elastic rail fastenings.

The limit of the lateral design load of the fasteners used in the Japanese Shinkanshen is taken as a multiple of axle load. According to different curve radii, the coefficients adopted in existing railway lines are, respectively, 0.4 ($R \geq 800$), 0.6 ($800 > R \geq 600$), and 0.8 ($R < 600$). For European and American railways, the limit of wheel–rail lateral force is taken as 0.4 times the axle load according to test results, that is,

$$Q \leq 0.4(P_{st1} + P_{st2}) \tag{4.62}$$

where P_{st1} and P_{st2} are the wheel static loads.

Considering the unbalanced superelevation on the unsuperelevated transition lead curve, the wheel–rail lateral force when a train travels in a No. 18 turnout (radius: 1100 m) in the diverging line at 80 km/h is the same as in a section (radius: 600 m). In this text, the limit of wheel–rail lateral force is taken as 120 kN, and is regarded as a reference for the flange force and impact force of the check rail.

c. Wheel−axle lateral force

A study on the stability of continuously welded rail (CWR) line shows that excessive wheel−axle lateral force is the major cause of the lateral displacement of track panel and dynamic instability of the CWR line, which may lead to track buckling. Therefore, the wheelset lateral force must also be controlled, in addition to wheel−rail lateral and vertical stresses.

The limit of wheelset lateral force is initially obtained by SNCF from the derailment test of a freight car. A study on the limit of lateral force of a single wheelset was carried out by Prudhomme. His calculation equations are still used in the United States, Europe, and by UIC.

$$\begin{cases} Q \le 10 + \dfrac{P}{3} & \text{(Limit value)} \\ Q \le 0.85\left(10 + \dfrac{P}{3}\right) & \text{(Recommended value)} \end{cases} \tag{4.63}$$

where P is axle load (in kilonewton).

4. Track deformation

a. Spreads of switch rails and point rails

To prevent the train wheel from colliding with the actual points of the switch rail and the point rail when traveling from turnout rear, the dynamic spreads of switch rails and point rails must be less than 4 mm in China.

b. Dynamic displacement of track

Track vertical displacement: $\le \pm 3$ mm (traveling in the main and diverging lines).

Lateral elastic displacement of rail members: $\le \pm 1.5$ mm (traveling in the main line).

4.4.4 SIMULATION EVALUATION

The essence of turnout dynamics simulation evaluation is to simulate the dynamic behaviors of a train traveling in a turnout and the dynamic impacts thereof on turnout structures based on computer simulation. As in other industries, a simulation system is essential to the study of complex systems throughout the whole life cycle; it is an effective means for safety evaluation. Nowadays, it has become an indispensable tool for research on turnout, together with theoretical analysis and experimental study.

Simulation has the following functions: predicting the traffic safety and stability of a turnout, determining permissible speeds in the turnout (replacing the stepwise acceleration test); detecting weak parts of turnout structures and providing suggestions; providing a reference for the design of wheel−rail relation, track stiffness, and critical components; providing a reference for the formulation of fabrication, assembly, laying, and maintenance specifications, as well as test protocols and methods; and analyzing causes of turnout defects and shaking of trains and provide remedies.

For No. 18 ballastless high-speed turnouts for 350 km/h in China, the results of dynamic simulation evaluation on an EMU train traveling in the main and diverging lines are given below.

1. Main line

The dynamic responses of a CRH2 train traveling in the main line at 385 km/h (the calculation speed is 110% of the design speed) are shown in Figure 4.47. The plain line type

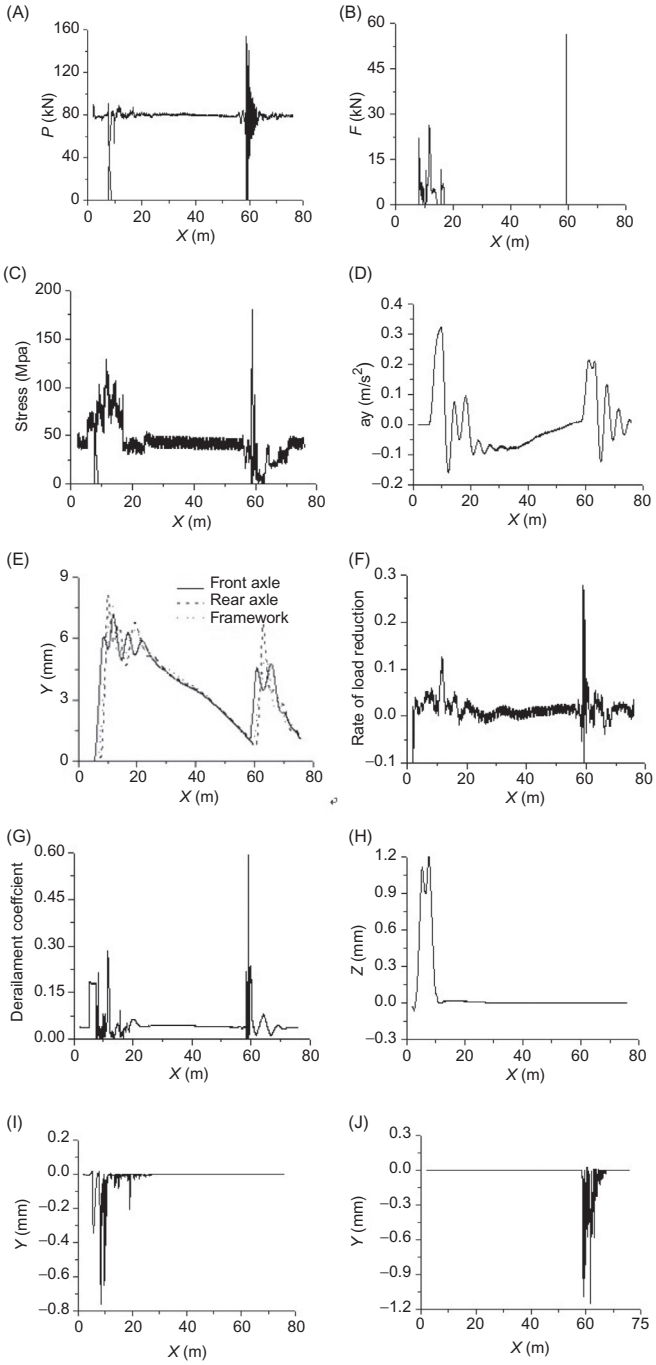

FIGURE 4.47

Results of dynamic simulation on an EMU train traveling in No. 18 turnout for 350 km/h in the main line: (A) Dynamic wheel load of front axle; (B) Flange force of front axle; (C) Dynamic stress on the rail; (D) Lateral vibration acceleration of the wheel; (E) Hunting motion; (F) Rate of front-axle load reduction; (G) Derailment coefficient; (H) Jerk of point of switch rail; (I) Spread of point of switch rail; (J) Spread of point of point rail.

wheel−rail relation and track stiffness are taken as per the design drawing, and the state and geometric irregularities based on laying conditions are taken into account in the simulation. The *x*-axis represents the distance from the wheel to the beginning of turnout.

Figure 4.47 shows that intensive fluctuation of the wheel load occurs at the point rail. The maximum dynamic wheel load is 155.3 kN, below the required limit (300 kN). The inner wheel on the front axle will cling to the switch rail in a certain range, with a maximum impact force of about 26.4 kN. The point rail has a maximum impact force of 56.4 kN, as an instant impact force may act on the top width 35.9 mm for about 0.4 ms. The maximum dynamic stresses on switch rails and point rails are 128.7 and 81.8 MPa, respectively, within the allowable range of rail strength. The lateral acceleration amplitude of the carbody is less than 0.05 *g* at the switch rail and the point rail, meeting the requirements for lateral stability. The hunting motion is minor. The rate of load reduction is small at the switch, up to 0.28 (max) at the crossing, within the allowable limit of 0.8. The derailment coefficient is small at the switch and about 0.58 (maximum instant value) at the crossing, within the allowable limit of 1.0. The maximum spreads of the points of the switch rail and the point rail are about 0.78 and 1.17 mm, respectively, within the allowable limit of 4.0 mm. Given the above, desired riding safety and quality can be attained when a high-speed train travels at 385 km/h in a No. 18 ballastless turnout for 350 km/h in the main line.

2. Diverging line

The dynamic responses of a CRH2 train traveling in the diverging line at 90 km/h (the calculation speed is 110% of the design speed) are shown in Figure 4.48. The plain line type wheel−rail relation and track stiffness are taken as per the design drawing, and the state and geometric irregularities (gaps, etc.) based on laying conditions are taken into account in the simulation.

When a train travels in the diverging line, the fluctuation of wheel load is small, about 21.3 kN maximally, much less than in the main line. The switch rail and point rail will bear the load at top widths of 25.1 and 23.3 mm, respectively. The maximum flange force at the switch is about 26.9 kN, within the allowable limit of lateral force. The maximum instant lateral impact force at the crossing is about 49.6 kN. The amplitude of lateral carbody vibration acceleration at the switch is -0.67 to $+0.40$ m/s^2, beyond 0.5 m/s^2 as in the main line; however, it is acceptable due to the low traveling speed in the diverging line. The lateral carbody vibration acceleration at the crossing is small. The maximum rates of load reduction at the switch and the crossing are 0.27 and 0.47, respectively, within the allowable limit of 0.8. The maximum derailment coefficient is about 0.36, within the allowable limit of 1.0. The lateral impact force of the check rail is smaller than the bearing capacity of the check rail tie plate.

Given the above, desired riding safety and quality can be attained when a high-speed train travels at 90 km/h in a No. 18 high-speed turnout in the diverging line.

4.4.5 EVALUATION OF WHEEL−RAIL RELATION DESIGN

1. Forward-shifting and shortening of wheel-load transition range at the switch

As mentioned above, riding quality can be improved by forward-shifting and shortening the wheel-load transition range at the switch. The design scheme can be refined through evaluation based on turnout dynamics, as given in Table 4.11.

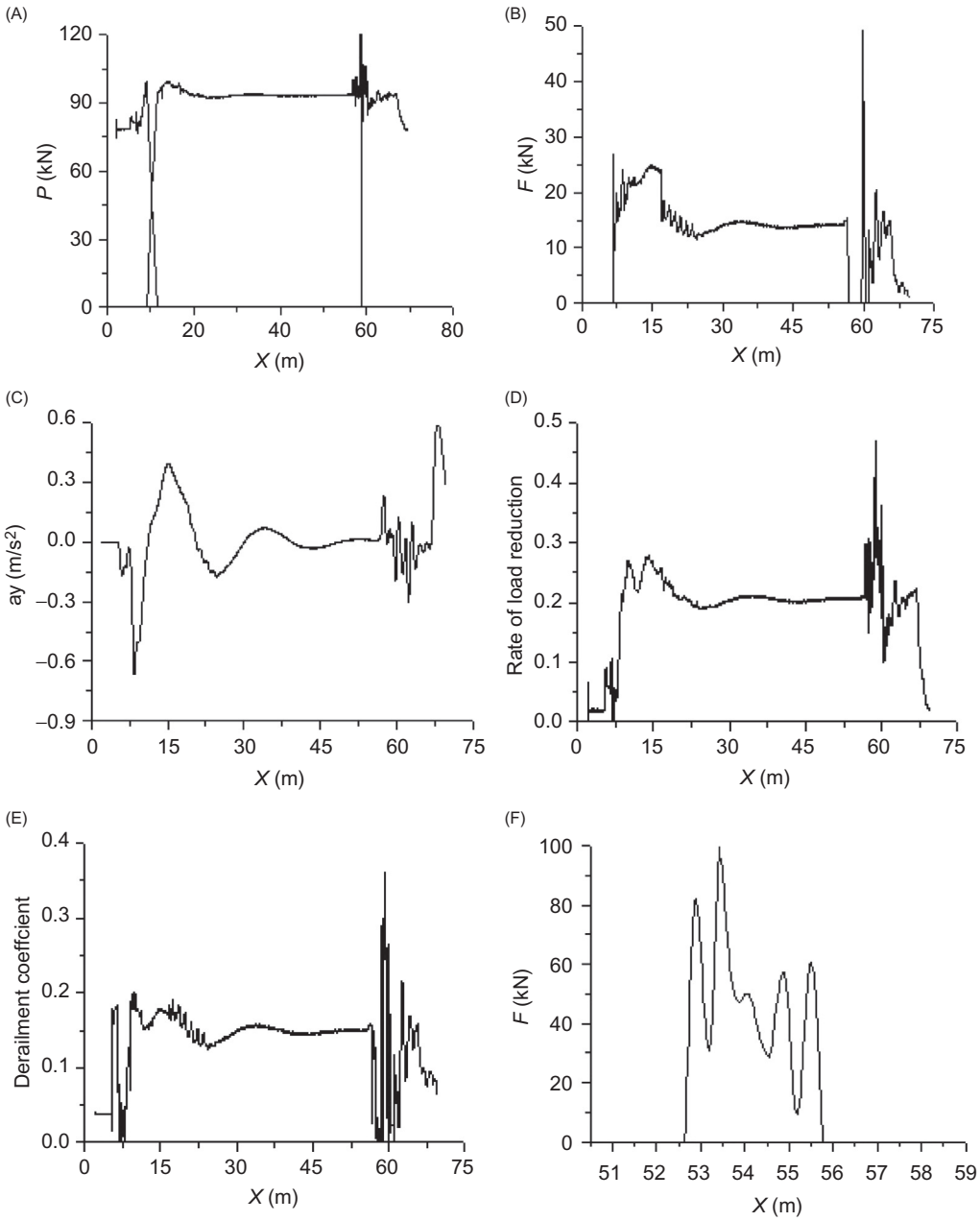

FIGURE 4.48

Results of dynamic simulation on an EMU train traveling in No. 18 turnout for 350 km/h in the diverging line: (A) Dynamic wheel load of front axle; (B) Flange force of front axle; (C) Lateral carbody vibration acceleration; (D) Rate of front-axle load reduction; (E) Derailment coefficient of front axle; (F) Lateral impact force of check rail.

Table 4.11 Dynamic Evaluation of Design Scheme of Wheel–Rail Relation

Scheme	1	2	3	4	5	6	7
Design initial load-bearing section (mm)	15	15	15	15	18	18	18
Depressed amount at the initial load-bearing section (mm)	3	3	3	4	3	3	4
Full load-bearing section (mm)	35	40	45	40	35	40	35
Maximum dynamic wheel load at the switch (kN)	97.5	90.1	87.5	93.7	102.9	95.3	100.2
Initial load-bearing section at the switch rail (mm)	13.3	15.1	17.0	18.1	14.4	16.3	16.3
Maximum flange force at the switch (kN)	33.1	25.9	23.8	25.6	29.9	27.2	29.8
Maximum dynamic stress at the switch rail (MPa)	125.0	114.8	119.9	116.7	126.3	112.2	116.7
Maximum lateral carbody vibration acceleration at the switch (m/s^2)	0.42	0.50	0.57	0.56	0.45	0.53	0.50
Maximum rate of load reduction at the switch	0.13	0.12	0.13	0.12	0.14	0.12	0.13
Maximum derailment coefficient at the switch	0.31	0.28	0.24	0.27	0.30	0.27	0.31
Maximum spread of switch rails (mm)	1.21	0.53	0.61	0.40	0.87	0.66	0.44

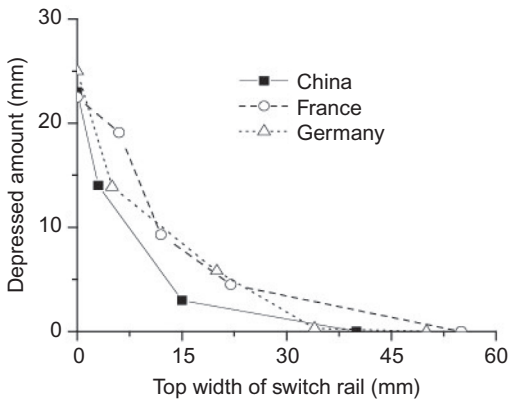

FIGURE 4.49

Depressed amount of switch rail.

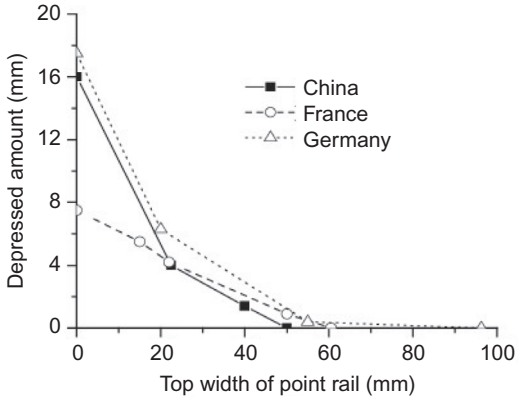

FIGURE 4.50

Depressed amount of point rail.

Table 4.11 shows that different design schemes at the switch correspond to different dynamic responses of the wheel–rail system. The design indicators of all schemes are acceptable; however, scheme 1 is the best in regard to riding quality, scheme 3 is preferred from the standpoint of wheel–rail vertical and lateral dynamic forces, and scheme 6 is the most ideal in regard to strength of the switch rail. After comparing the riding quality, wheel–rail dynamic interaction, strength of the switch rail, fabrication and dimension inspection of the switch rail, and other factors, scheme 2 has been adopted in China.

2. Comparison of wheel–rail relations of high-speed turnouts in China, Germany, and France

The designs for wheel–rail relation of No. 18 high-speed turnouts are different in the three countries. Figure 4.49 shows the changes in the depressed amounts with the top widths of the switch rail at the switch. Figure 4.50 shows the depressed amounts of the point rail at the crossing.

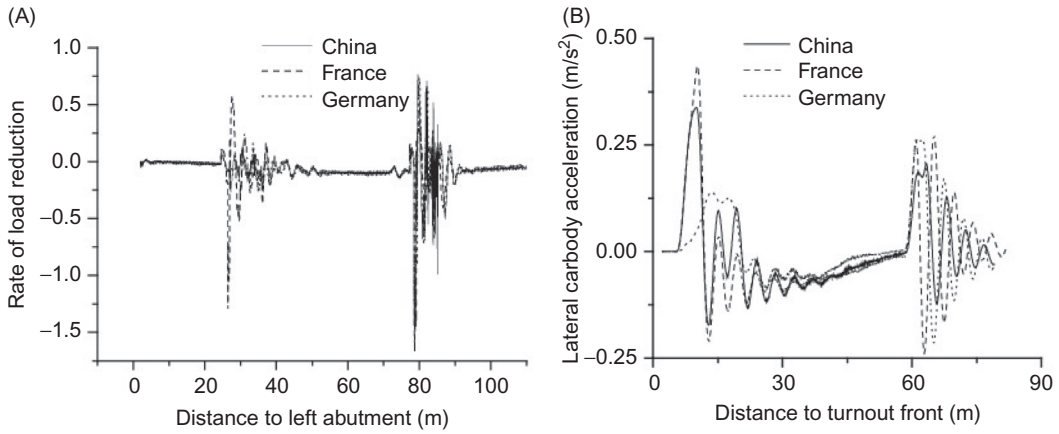

FIGURE 4.51

Lateral carbody vibration accelerations: (A) Comparison of load reduction rates; (B) Comparison of lateral carbody vibration acceleration.

In the figures, the wheel-load transition range at the switch is the shortest and foremost in China and the longest and backmost in France. At the crossing, China and French adopt similar designs, but the wheel-load transition range is the longest and backmost in Germany. The wheel–rail relation designs for high-speed turnouts in the three nations are evaluated based on turnout dynamics; comparative results of load reduction rate and lateral carbody vibration acceleration are shown in Figure 4.51.

Figure 4.51 shows that, for all three countries, the load reduction rate is great at the crossing and small at the switch, yet within the allowable range. The amplitudes of lateral carbody vibration acceleration at the switch in the three countries are, respectively, -0.21 to $+0.45\ \text{m/s}^2$ in France, -0.17 to $+0.33\ \text{m/s}^2$ in China, and -0.1 to $+0.14\ \text{m/s}^2$ in Germany. Of these, Germany has the best riding quality in the main line using wheel-load forward-shifting and a gauge widening design, followed by China (wheel-load forward-shifting design). The three nations have similar riding quality at crossings; however, China is the best, using wheel-load forward-shifting and a horizontal hidden tip point design. Other dynamic responses may also differ among three nations, but are all acceptable in terms of riding safety and quality in turnouts for 350 km/h.

CHAPTER

TRACK STIFFNESS DESIGN

5

Track stiffness is a major influential factor in the structural load, wheel−track interaction, and structural vibration of a track. It involves both track integral stiffness and track component stiffness. Track integral stiffness is measured by the ratio of the force acting on rail surfaces to the displacement of a corresponding point, which can be further classified into vertical and lateral stiffness. Track component stiffness refers to the stiffness of track components (i.e., rail, ties, fasteners, bed, and subgrade).

Track stiffness may be static or dynamic, but generally refers to the static stiffness of a track. Dynamic stiffness refers to track stiffness under certain frequency excitations. Static stiffness is a constant, while dynamic stiffness varies with excitation frequency if nonlinear factors are ignored.

Main features:

1. Directivity
2. Discreteness
3. Longitudinal variability along the track
4. Time-variability
5. Nonlinearity

In the design of track stiffness, the reasonable stiffness of the fastening will be defined for a given support stiffness in the bed. As there are slide bedplates and other structures in a turnout, a fastening includes the elastic pads beneath the rail and plate; therefore, the two pads must be compatible. In a turnout, certain rails are connected by long tie plates, fillers, etc., which may cause longitudinal variation of the integral stiffness along the line; therefore, the stiffnesses of fastenings at all parts must be adjusted to even the integral track stiffness along the longitudinal direction of a line, so as to ease the impact of dynamic irregularities. In addition, track stiffness transitions must be provided at two ends of a turnout for smooth transition of stiffness.

5.1 COMPOSITION [61]

Track integral stiffness in a turnout consists mainly of rail flexural stiffness and stiffness of fastening, bed, and subgrade. Track integral stiffness in a turnout is different from that in a section due to the nature of the turnout structure. It is not simply a linear combination of the stiffnesses of various parts, but may be affected by rail sections, length of pad and tie, linkage of filler, and other structural factors.

Design of High-Speed Railway Turnouts.

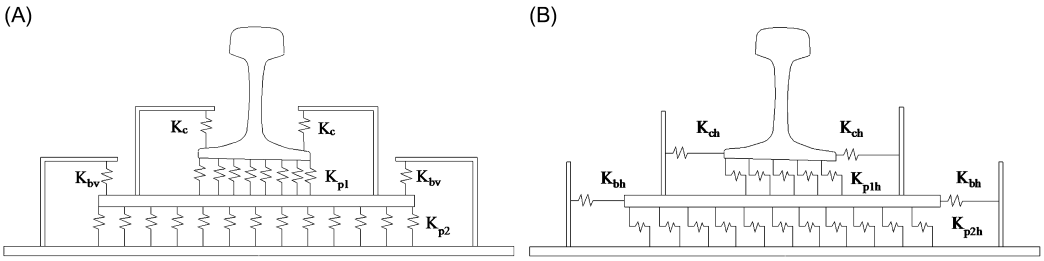

FIGURE 5.1

(A)Vertical stiffness of fastening; (B) Lateral stiffness of fastening.

5.1.1 FASTENING STIFFNESS

Turnout and railway sections are different in structure. In a turnout, indirect fixation fastening with a tie plate (or slide plate) is used, and two elastic layers (one each beneath the rail and plate) are provided. The fastener connects the rail and the tie plate, and the bolt connects the tie and the tie plate, as shown in Figure 5.1.

The vertical stiffness of a fastening consists mainly of the vertical stiffnesses of the fastener, pads beneath the rail and plate, anchor bolts, and cover plate. It can be calculated by:

$$k_{\mathrm{f}} = \frac{(2k_{\mathrm{bv}} + k_{\mathrm{p2}})(2k_{\mathrm{c}} + k_{\mathrm{p1}})}{2k_{\mathrm{c}} + k_{\mathrm{p1}} + 2k_{\mathrm{bv}} + k_{\mathrm{p2}}} \tag{5.1}$$

where

k_{f} is the vertical stiffness of the fastening (N/m)
k_{c} is the vertical stiffness of an individual fastener (the initial fastening force P_{c} is about 10 kN, and the spring coefficient is about 1 kN/mm)
k_{p1} is the vertical stiffness of the rail pad
k_{p2} is the vertical stiffness of the plate pad; and
k_{bv} is the vertical stiffness of anchor bolts and cover plate.

The lateral stiffness of a fastening consists mainly of the shear stiffnesses of the pads beneath the rail and plate, the lateral compressive stiffness of gauge blocks and stoppers, and the lateral anti thrust stiffness of anchor bolts. It can be calculated by:

$$k_{\mathrm{fh}} = \frac{(k_{\mathrm{p1h}} + 2k_{\mathrm{ch}})(k_{\mathrm{p2h}} + 2k_{\mathrm{bh}})}{k_{\mathrm{p1h}} + k_{\mathrm{p2h}} + 2k_{\mathrm{ch}} + 2k_{\mathrm{bh}}} \tag{5.2}$$

where

k_{fh} is the lateral stiffness of the fastening
k_{p1h} is the lateral shear stiffness of rail pad
k_{p2h} is the lateral shear stiffness of the pad under the plate
k_{ch} is the lateral compressive stiffness of gauge blocks and stoppers; and

k_{bh} is the lateral anti thrust stiffness of anchor bolts, which can be approximated with a cantilever beam equation: $k_{bh} = 3E_bI_b/l_b^3$, where E_bI_b is the lateral flexural stiffness of bolts and l_b is the cantilever distance at the action point of the bolt.

The impacts of bending stiffness of the tie plate on fastening stiffness must be considered when one tie plate is shared by several rails. For a rigid tie plate, the stiffness of the fastening will increase approximately linearly with tie plate length.

5.1.2 SUB-RAIL FOUNDATION STIFFNESS

The sub-rail foundation of a high-speed turnout may be a ballast or ballastless track. Concrete tie or slab is generally regarded as inelastic. Therefore, the stiffness of the sub-rail foundation of a ballast track is the series of the stiffnesses of bed and subgrade, while for a ballastless track, it equals the subgrade stiffness.

1. Bed stiffness [62]

   In the dynamic analysis of a train−track system, the vibration mass of the bed can be viewed as the total mass of the platform constructed by stress dispersion lines at the bottom of a tie, as shown in Figure 5.2. Therefore, the bed stiffness equals the bearing stiffness of the vibration platform against the tie. This platform is divided into an upper part and a lower part in calculations. Bed stiffness is the series of the stiffnesses of the two parts. In Figure 5.2, the upper part is represented by BCDE, and the lower part is represented by ABEF. The bed vertical stiffness (vertical bearing stiffness) can be derived based on the stress−strain relationship inside the bed platform, as shown in Figure 5.2.

   The vertical stiffness of the upper platform is:

$$k_{s1} = \frac{2(l-b)E_s tg\phi}{\ln(la/(b(l+2h_1 tg\phi)))} \tag{5.3}$$

   where

   l is the length of the tie, which increases gradually along the length of a turnout
   a is the space of two adjacent fastening supports
   b is the bottom width of the tie
   h_1 is the distance from the intersection point of bed stress dispersion lines to the tie bottom
   E_s is the elasticity modulus of the bed, generally taken as 150 MPa; and
   ϕ is the bed stress dispersion angle, generally taken as 35°.

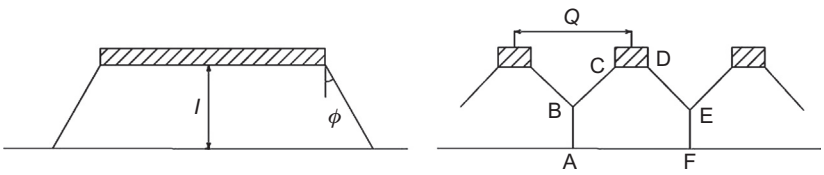

FIGURE 5.2

Vibration platform of a ballast bed.

The vertical stiffness of the lower platform is expressed as:

$$k_{s2} = \frac{2aE_s tg\phi}{\ln(l + 2Htg\phi/l + 2h_1 tg\phi)} \tag{5.4}$$

where H is the bed thickness, generally designed as 35 cm. If there is ballast, half-thickness of the ballast will be considered. Thus, the vertical stiffness of the bed under a long tie can be expressed as (N/m):

$$k_s = \frac{k_{s1}k_{s2}}{k_{s1} + k_{s2}} \tag{5.5}$$

The lateral stiffness of the bed can be determined as per its lateral resistance, with $Q = k_{sh}y = qa$, where Q is the lateral resistance of an individual tie. This resistance is composed of the frictional resistances between tie sides/bottom and the contact surface of ballast, as well as the resistance of the ballast shoulder at the tie end against lateral displacement (composition ratio: 30% for bed shoulder, 20−30% for tie sides, and 50% for tie bottom). k_{sh} is the lateral stiffness of the bed, y is the lateral displacement of the tie, a is the tie spacing. q is the unit lateral resistance of the bed, normally expressed as $q = q_0 - By^z + cy^{1/N}$, where q_0 is the initial lateral resistance of the bed, and B, c, z, and N are resistance coefficients. Owing to the nonlinear relation between the lateral resistance of the bed and the lateral displacement of the tie, the relationship between the lateral stiffness of the bed and the lateral displacement of the tie is also nonlinear. The resistance increases and the lateral stiffness reduces with increasing displacement. When the displacement reaches a certain value, the resistance is close to a constant and the stiffness is close to zero. If the displacement continues to increase, the bed will be damaged.

2. Subgrade stiffness [63]

Subgrade vertical stiffness (N/m) can be calculated by two methods. Given the subgrade indicator K_{30},

$$k_b = a(l + 2Htg\phi)K_{30} \tag{5.6}$$

Given the subgrade elasticity modulus E_b,

$$k_b = \frac{2(l - a + 2Htg\phi)tg\phi_1}{\ln((l + 2Htg\phi)/a)}E_b \tag{5.7}$$

where ϕ_1 denotes the inner friction angle of subgrade soil, generally taken as 45°.

The subgrade lateral stiffness is not generally considered in the mechanical calculation of tracks.

In addition, the vertical elasticity characteristics of the ballast bed and subgrade may be expressed by bed coefficient C (N/m^3), defined as the pressure acting on the unit area of the bed top for unit settlement of the bed top. Assuming that the vertical displacement of the tie at rail support is y_s, the average settlement of the tie is αy_s, where α is the bending coefficient of the tie, taken as 1 for concrete tie and 0.81−0.92 for timber tie; R is the vertical force at the rail support. For a section, the relationship between the bed coefficient and sub-rail foundation stiffness is expressed by:

$$2R = Clb\alpha y_s = \frac{k_s k_b}{k_s + k_b}y_s \tag{5.8}$$

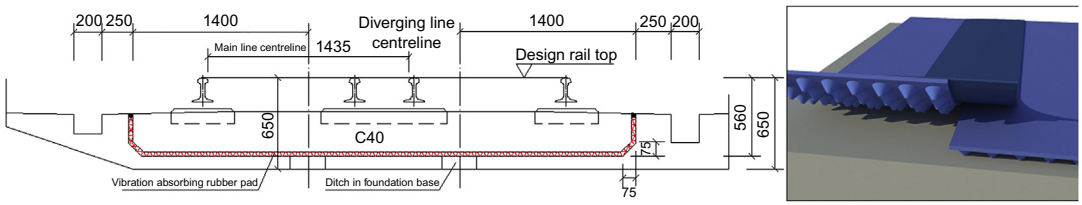

FIGURE 5.3

Elastic pad under a ballastless turnout.

For a heavy track, the bed coefficient C is usually taken as 0.6−0.8 MPa/cm, and the sub-rail foundation stiffness (for a half-length of the tie) under a rail is generally taken as 100−140 kN/mm. For a cemented bed, the sub-rail foundation stiffness will increase significantly, to more than 400 kN/mm or by an order.

3. Vibration-absorbing pad stiffness

If a vibration-absorbing pad is provided under the slab of a ballastless track or tie of a ballast track, as shown in Figure 5.3, the bearing stiffness can be expressed by the deformation quantity of the unit area under unit load. Impacted by the bending resistance and other factors of the track slab, no equivalent equation is available for the pad stiffness under the fastening support. Yet the deformation at the fastening support under unit load can be obtained by the finite element method (FEM). The numerical solution of the pad stiffness can thus be obtained.

5.1.3 TRACK INTEGRAL STIFFNESS

The track integral stiffness relates to the flexural stiffness of the rail in addition to the stiffnesses of the fastenings and sub-rail foundation. For lateral integral stiffness, the anti heeling stiffness of the rail also matters. The relationship between the flexural stiffness of the rail and sub-foundation stiffness can be described by rail support stiffness, elasticity modulus of rail foundation, track−rail stiffness ratio, etc.

1. Vertical stiffness of the rail support

The vertical stiffness of a rail support represents its vertical elasticity, defined as the force acting on the support top for unit settlement of the rail support (N/m). This concept is widely used in the elastically supported beam model in track mechanics. In a section, this stiffness can be regarded as the series of the vertical stiffnesses of the fastenings and sub-rail foundation. It can be expressed by:

$$\frac{1}{k_{\mathrm{D}}} = \frac{1}{k_{\mathrm{f}}} + \frac{1}{k_{\mathrm{s}}/2} + \frac{1}{k_{\mathrm{b}}/2} \tag{5.9}$$

where k_{D} is the stiffness of the rail supports; for a ballastless track, k_{s} can be infinite. In a turnout, as k_{f} varies with the tie plate length, and k_{s} and k_{b} vary with the tie length, k_{D} will change longitudinally along the turnout.

2. Vertical elasticity modulus of rail supporting

The vertical elasticity modulus of rail supporting k represents its vertical elasticity, defined as the force acting on a rail supporting unit settlement of rail support (N/m^2). This concept is widely used in the continuous foundation beam model in track mechanics. The relationship between this factor and the vertical stiffness of rail support is expressed by:

$$k = \frac{k_D}{a} \tag{5.10}$$

3. Track−rail stiffness ratio

The characteristic coefficient of a track system can be expressed by the stiffness ratio β between rail support and the rail, taken as $0.009-0.020\ cm^{-1}$ and defined as:

$$\beta = \sqrt[4]{\frac{k}{4EI}} = \sqrt[4]{\frac{k_D}{4EIa}} \tag{5.11}$$

where EI is the vertical flexural stiffness of the rail. β integrates all mechanic parameters of a track and their relationships, as it may change with any track parameter; at the same time, the change of β will affect the distribution of interior force on the track and stress of components. The rail bending moment and support pressure are not determined by k and EI solely, but by the ratio k/EI. If k is large and the foundation is rigid, the support pressure will be great, and the rail bending moment will be small and attenuate laterally at a fast speed. In this case, the load will act in a small scope. When EI is great and the foundation is less rigid, the reverse applies.

Assuming that the rail is an infinitely long beam on a continuous elastic foundation, given the vertical load on the rail P, the vertical force acting on rail support or tie can be expressed by $R = Pa\beta/2 = \gamma P$, where γ is the load distribution coefficient, normally taken as 0.3−0.6. The greater the stiffness ratio, the greater the load distribution coefficient.

4. Equivalent anti-heeling stiffness of the rail

Given the elastic modulus of continuous torsional support of the rail k_R, rail angle of inclination θ_R, and rail torsional stiffness C_R (taken as 16.1×10^7 kN mm^2 for 60 kg/m rail), the rail angle of inclination under the action of inclination torque T (produced under the combined action of vertical eccentric load P and lateral load H of the rail) is:

$$\theta_R = \frac{T}{2\sqrt{k_R C_R / a}} \tag{5.12}$$

The equivalent anti heeling stiffness of the rail is:

$$k_\theta = \frac{H_R}{h_R \theta_R} \tag{5.13}$$

where h_R is the rail height and H_R is the lateral load of the rail at the support point of the fastener.

The elastic modulus of continuous torsional support of the rail with a single elastic pad can be obtained with the vertical stiffness of rail support:

$$k_R = 2\int_0^{b_R/2} \frac{k_D}{b_R} y^2 \, dy = \frac{b_R^2 k_D}{12} \tag{5.14}$$

where b_R is the width of rail base.

5. Vertical track integral stiffness

The vertical integral stiffness of the rail is defined as the vertical load for unit settlement of the rail (N/m). In a section, it can be expressed by:

$$K_{\mathrm{t}} = \frac{P}{y_{\mathrm{R}}} = \frac{2k}{\beta} = 2\sqrt[4]{4EIk^3} \tag{5.15}$$

where y_{R} is the vertical displacement of the rail under load action point. In a turnout, since the vertical elastic modulus of rail support varies longitudinally along the turnout, and the equivalent flexural stiffness EI of the two rails bonded by fillers is variable, the vertical integral stiffness will also change along the turnout length. Therefore, the simple equation for a section will no longer apply, but may be substituted by a complex computation model for the overall turnout.

6. Lateral track integral stiffness

The two rails of a track have similar vertical stress, but differ greatly in lateral stress. The lateral stress difference is exceptionally large when the running flange clings to a rail. Therefore, the gauge widening (lateral displacement of single railhead) and lateral displacement of track panel will be the main concerns in calculating the lateral stress and deformation of a track. For gauge widening, the angles of inclination and lateral displacement of two rails will be calculated separately, and the lateral displacement of the track panel can be ignored. Therefore, the lateral stiffness of rail support is:

$$k_{\mathrm{Dh}} = \frac{k_\theta k_{\mathrm{fh}}}{k_\theta + k_{\mathrm{fh}}} \tag{5.16}$$

Given the lateral force of the wheel axle H_{w} (the sum of the lateral stresses on two rails) and the lateral displacement of the centerline of two rails y_{Rh}, the equivalent lateral track integral stiffness in a section is:

$$K_{\mathrm{th}} = \frac{H_{\mathrm{w}}}{y_{\mathrm{Rh}}} = \frac{(k_{\mathrm{Dh1}} + k_{\mathrm{Dh2}})k_{\mathrm{sh}}}{k_{\mathrm{Dh1}} + k_{\mathrm{Dh2}} + k_{\mathrm{sh}}} \tag{5.17}$$

where k_{Dh1} and k_{Dh2} denote the lateral stiffnesses of the supports of the two rails, respectively. In a turnout, the cooperation of rails and the actions of fillers contribute to the great lateral integral stiffness of a track and the longitudinal vibration along the turnout.

5.2 TRACK STIFFNESS DESIGN [64–67]

Reasonable design of track stiffness in a high-speed turnout can effectively ease the wheel–rail dynamic interaction, while improving the riding comfort, attenuating vibration, prolonging the service life of parts, and reducing maintenance workload. It includes the design of vertical and lateral track integral stiffness, coordinating the stiffnesses of the fastening and sub-rail foundation, and coordinating the stiffnesses of pads under the rail and plate.

In a fastening, since the lateral compressive stiffness of gauge blocks and stoppers and the lateral anti thrust stiffness of bolts are relatively large, the changes of lateral sheer stiffness of pads under the rail and plate may exert little influence on the lateral stiffness of the fastening, and the stiffnesses of bed and subgrade may vary slightly. Hence, the track stiffness design in a turnout should focus on the vertical stiffness of the fastening and its impact on gauge widening.

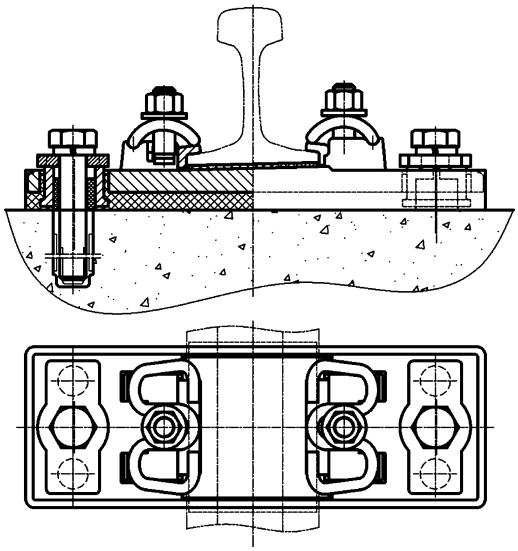

FIGURE 5.4

Fastening for high-speed turnouts in China.

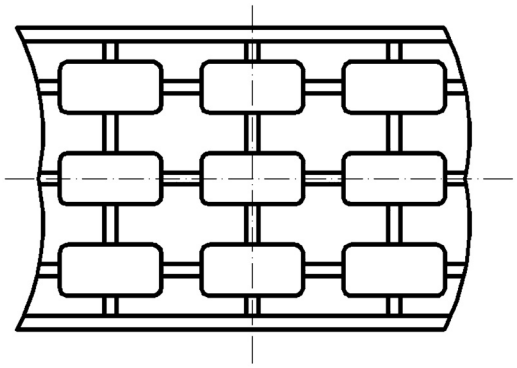

FIGURE 5.5

Blocky plate pad.

5.2.1 STRUCTURE OF A FASTENING FOR HIGH-SPEED TURNOUTS IN CHINA

The structure of a fastening for high-speed turnouts in China is shown in Figure 5.4, which shows the following features:

1. The elastic fastening is in direct fixation structure with tie plate
2. The upper structure of the tie plate may be bolted or boltless fastening
3. A gauge block is arranged between the shoulder and the rail base to adjust and maintain the gauge
4. A rail pad is provided between the rail and elastic tie plate for buffering
5. The tie plate is provided with an elastic pad underneath to reduce vibration
6. The tie plate and concrete tie are fastened with bolts and embedded sleeves
7. A buffering distance-adjusting block is arranged between the tie plate and bolt to buffer the lateral impact of the tie plate on the bolt and adjust the gauge by regulating the tie plate position; and
8. The bolt fastens the elastic tie plate through a cover plate. The cover plate is provided with a reasonably elastic rubber cushion to ease tie plate stress and prevent tie plate turning.

A blocky pad, as shown in Figure 5.5, is provided under the tie plate to reduce and homogenize the track stiffness. By modifying the end structure and rubber quality, the low stiffness under normal load and high stiffness under large load are ensured; in this way, rail tilting can be effectively controlled. To ensure the bonding performance between the tie plate edge and pad and to prevent

the bonded part being damaged by the tie plate during handling, a 5-mm-thick glue is applied to the plate edge. The rubber profile is ribbed to enhance bonding performance and stability, so as to prevent it from buckling.

5.2.2 VERTICAL STIFFNESS OF RAIL PAD

1. Design principles

   In a turnout, switch rails, stock rails, point rails, and wing rails are all rested on the slide plate. Elastic pads are arranged beneath the slide plate as well as between the stock rail/wing rail and slide plate, fastened with the fasteners. The switch rail and point rail are movable on the slide bed (slide beds are integrally welded or cast with the slide plate).

   The stiffness design of rail pads follows several principles: (i) The strength of switch rails and point rails can be ensured; (ii) The dynamic height differences between switch rail and stock rail, as well as between point rail and wing rail, can be controlled within a reasonable range, so that the backward-shifting of wheel-load transition will not seriously impact riding quality in a turnout JRS (iii) The pad has a buffering effect between the rail and tie plate.

   In conclusion, the stiffness of the fastening must coordinate with the height difference between switch rails and point rails. The design follows the principle of "high stiffness + low stiffness"; that is, the rail pad will adopt a high stiffness design to maintain the dynamic height differences between rails, and the plate pad will use a low stiffness design to ensure proper elasticity of the fastening.

2. Rail pad stiffness for high-speed turnouts in China

   As mentioned in Chapter 4, when an EMU train with LMA tread travels in a ballastless turnout in the main line, the wheel load will be transferred to the switch rail when the height difference of the stock rail and the switch rail is smaller than about 1.25 mm. To ensure the strength of weak sections of the switch rail, in Chinese and French high-speed turnouts, the dynamic height difference with the stock rail at top width 20 mm of the switch rail must be greater than 1.0 mm. Since the height difference at top width 15 mm of the switch rail may have a tolerance of 1 mm during fabrication and assembly, and the actual height difference at top width 20 mm of the switch rail may be 1.6 mm, the vertical dynamic displacement difference between the switch rail and the stock rail should not be greater than 0.6 mm.

   The vertical loads on two rails can be obtained with Eq. (4.10), and the vertical displacement can be calculated with Eq. (5.15). Thus, one can get the rail pad stiffness under different plate pad stiffnesses, as given in Table 5.1. The smaller the plate pad stiffness, the greater the required rail pad stiffness. Given a plate pad stiffness of 25 kN/mm, the rail pad stiffness is taken as 250 kN/mm for a ballastless turnout. If the rail pad is a 5-mm-thick rubber pad, the stiffness can be attained by grooving on one side.

Table 5.1 Required Minimum Stiffness of Rail Pad

Plate pad stiffness (kN/mm)	20	25	30	35
Required rail pad stiffness (kN/mm)	294	242	211	196

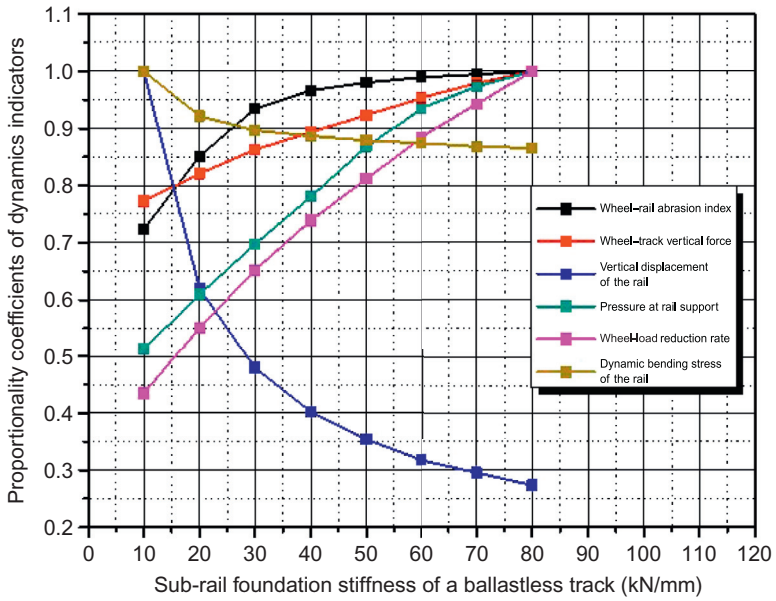

FIGURE 5.6

Impacts of fastening stiffness on wheel−rail dynamic interaction.

For a ballast turnout, given a plate pad stiffness of 60 kN/mm, the rail pad stiffness will be 180 kN/mm. For a 5-mm-thick rubber pad, the stiffness can be attained by grooving on both sides.

3. Vertical plate pad stiffness

Plate pad stiffness is a major influential factor in the elasticity of the fastening. Therefore, the following issues must be considered in the design.

a. Coordination of fastening and bed stiffness

Since the subgrade is rather rigid and not very elastic in a track system, the fastening and bed are the main contributors to track elasticity. When the bed stiffness k_s approaches infinity (i.e., solid bed), the stiffness of the track support is simply the stiffness of the fastening. In a ballast track, k_s is relevant to bed density and the supporting area of the tie. The denser the bed and the larger the supporting area of the tie, the greater the value of k_s and the poorer the bed elasticity.

The vertical stiffness (k_f) of the fastening must match with the bearing stiffness (k_s) of the bed. The smaller the value of k_f, the greater the elasticity. In this case, the dynamic effect of a vehicle can be reduced, yet the rail stress will increase, which leads to unstable track layout and comfort degradation. However, k_s drops with increasing k_f. In a ballast turnout, this may cause serious bed deformation and increase maintenance load. For a shoulder-free fastening, k_f may increase the angle of rail inclination or result in excessive dynamic gauge widening. Dynamic studies of train−track systems (see Figure 5.6) show

that, with reduced fastening stiffness, the wheel−rail dynamic interaction and the accelerations of bed and concrete tie decrease accordingly, but dynamic displacement of the rail will increase. This indicates that a reduction in the stiffness of the fastening can ease wheel−rail dynamic interaction and sub-rail foundation vibration. They are in a monotonic relation, that is, the smaller the former, the smaller the latter. On the other hand, dynamic displacement of the rail will increase with decreasing fastening stiffness. When the fastening stiffness drops to a certain value, any further drop may lead to a drastic increase in dynamic displacement of the rail. Excessive increase in dynamic displacement of the rail will in turn cause elasticity failure of the fastener and a significant loss of fastening force, which may lead to rail inclination and creeping, as well as inordinate lateral displacement of the railhead and violent fluctuation of rail deflection, or even shorter service life of the pad. Generally, the low stiffness of the fastening should not be lower than 20 kN/mm.

b. Vertical stiffness of pad cover plate

In Figure 5.4, the vertical stiffness (k_{bv}) of the anchor bolt and cover plate may have effects similar to the elastic fastening. It pre-tightens the plate pad to prevent plate suspension under the action of lifting force; however, the pre-tension applied on the pad must not be so great as to affect the elasticity. In this regard, a location sleeve will be arranged between the bolt and tie plate to withstand a majority of the tension, leaving a small portion of tension on the plate and plate pad transferred via the cover plate.

The plate pad may be pre-compressed under the pre-tension. Under normal load, the stress on the pad cannot exceed the strength, or no severe groove deformation is allowed. As specified by JRS of Japan, the plate pad shall meet the following requirements: (i) The average compressive stress under normal load is smaller than 2 MPa; (ii) the maximum compressive stress (at the ends of plate pad) under normal load is under 4 MPa, and the average compressive deformation is under 10%; (iii) The grooves on the pad will deform drastically and the stiffness will increase sharply under excessive load. The performance of the plate pad is shown in Figure 5.7.

The vertical stiffness (k_{bv}) of the bolt and cover plates consists of the tensile stiffness (k_l) of the bolt and the stiffness of cushion (k_g) under the cover plate. It is expressed by:

$$\frac{1}{k_{bv}} = \frac{1}{k_l} + \frac{1}{k_g} \tag{5.18}$$

The tensile spring coefficient of bolts and the bolt length are related; that is, $k_l = E_l A_l / l$, where E_l is the elasticity modulus of the bolt and A_l is the cross sectional area of the bolt (Φ 30 bolt is preferred). Given the effective tensile length of the bolt of 50 mm, k_l will be about 2914 kN/mm.

Two rubber cushions (size: L 60 × W 60 × H 6 mm) under the cover plate are arranged on two sides of the bolt, buried in the locating slot (burial depth 1 mm). The cushion stiffness k_g can be obtained by:

$$\frac{1}{k_g} = \frac{h_1}{2E_r A_r} + \frac{h_2}{2E_r A_r (1 - \nu_r^2)} \tag{5.19}$$

where h_1 is the free deformation height (5 mm); h_2 is the constrained deformation height (1 mm), that is, the depth buried in the locating slot; ν_r is the Poisson ratio of the rubber,

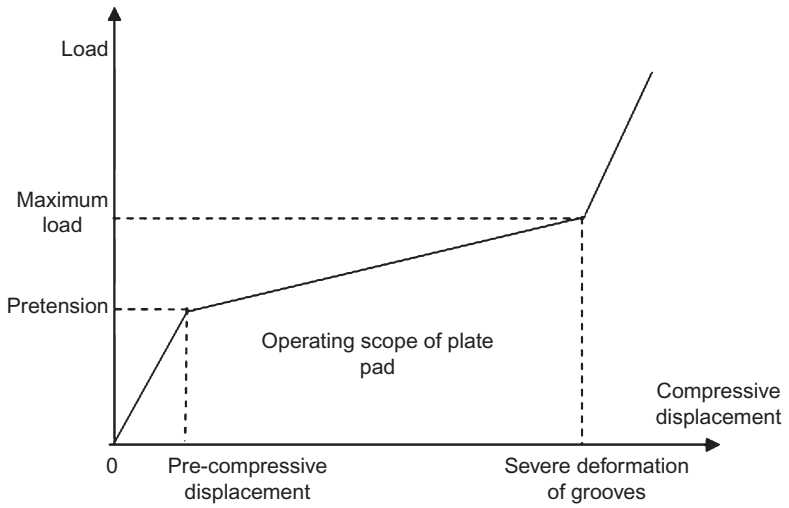

FIGURE 5.7

Stiffness change of plate pad.

taken as 0.5; E_r is the elasticity modulus of the rubber, taken as 1 MPa. It reads: $k_g = 1.12$ kN/mm. Round fastening cushions have been adopted for high-speed turnouts in China, and the measured cushion stiffness is nearly 1.2 kN/mm. Considering the maximum compression of the plate pad of 1.5 mm, the amount of pre-compression of the cushion is taken as 2−3 mm in the design.

c. Impacts of plate pad stiffness on gauge widening

As shown in Figure 5.4, given that the vertical force on the rail is W, the offset of the action point from the rail center is e (approximated as 30 mm as per wheel−rail contact relation), the lateral force on railhead is H, and the lateral pressure action height of the rail is h (approximated as 160 mm for 60 kg/m rail); therefore, the inclination torque of the rail is $T = Hh - We$. With the load distribution coefficient obtained by the theory of continuous bearing beam, the vertical load of the fastening support can be obtained by $P_R = \gamma_P W$ and the lateral load is obtained by $H_R = \gamma_H H$. Given that the inclination angles of the rail and tie plate are θ_1 and θ_2, respectively, the lateral distance between two fasteners is b_1, the rail base width is b_2, the lateral distance between two anchor bolts is b_3, and the tie plate length is b_4, when a rail clines, the resistance moment of the rail pad will be:

$$M_1 = 2\int_0^{b_2} \frac{b_2}{2}\cdot(\theta_1 - \theta_2)\cdot\frac{x}{b_2/2}\cdot x\cdot\frac{K_{p1}}{b_2}\mathrm{d}x = \frac{K_{p1}b_2^2}{12}(\theta_1 - \theta_2) \tag{5.20}$$

and the resistance moment of the elastic fastening will be:

$$M_2 = \frac{1}{2}K_c b_1^2(\theta_1 - \theta_2) \tag{5.21}$$

If a tie plate inclines, the impact of the bolt spring at one side on inclination resistance must be considered. Then the resistance moments of plate pad and bolt spring will be:

$$M_3 = \frac{K_{p2} b_4^2}{12}\theta_2 + \frac{1}{2}K_{bv} b_3^2 \theta_2 \tag{5.22}$$

According to the equilibrium conditions of the tie plate,

$$M_3 = M_1 + M_2 \tag{5.23}$$

one gets:

$$\theta_2 = \frac{(K_{p1} b_2^2/12) + (K_c b_1^2/2)}{(K_{p1} b_2^2/12) + (K_c b_1^2/2) + (K_{p2} b_4^2/12) + (K_{bv} b_3^2/2)}\theta_1 = K_q \theta_1 \tag{5.24}$$

and the elastic modulus of continuous torsional support of the rail with double elastic pads is:

$$k_R = \left(\frac{K_{p1} b_2^2}{12} + \frac{K_c b_1^2}{2}\right)(1 - K_q) \tag{5.25}$$

Then the equivalent anti heeling stiffness (k_θ) of the rail can be calculated with the rail inclination angle obtained from Eq. (5.25). The lateral stiffness of the fastening when a rail inclines will be:

$$\frac{1}{k_{fh}} = \frac{1}{k_\theta} + \frac{1}{k_{p1h} + k_{cp}} + \frac{1}{k_{p2h} + k_{bh}} \tag{5.26}$$

and the rail pad compression will be:

$$\delta_1 = \frac{2P_c}{K_{p1}} + \frac{P_R}{K_{p1} + 2K_c} \pm \frac{1}{2} b_2 \theta_1 (1 - K_q) \tag{5.27}$$

where P_c is the fastening force of a single fastener. The rail pad stress is:

$$\sigma_1 = \frac{K_{p1}\delta_1}{A_1} \tag{5.28}$$

where A_1 is the area of the rail pad. The plate pad compression is:

$$\delta_2 = \frac{2P_b}{K_{p2}} + \frac{P_R}{K_{p2} + 2K_{bv}} \pm \frac{1}{2} b_4 K_q \theta_1 \tag{5.29}$$

and the plate pad stress is:

$$\sigma_2 = \frac{K_{p2}\delta_2}{A_2} \tag{5.30}$$

In calculating gauge widening, the vertical and lateral loads of the rail are taken as 85 and 50 kN, respectively, when an EMU train travels in a turnout. Under the most unfavorable conditions, when a flange clings to a rail, the opposite flange will not cling to the

Table 5.2 Impacts of Plate Pad Stiffness on Gauge Widening

Plate Pad Stiffness (kN/mm)	10	20	30	40	50	60	70	80
Rail tilting amount under flange force (mm)	2.45	2.31	2.21	2.13	2.07	2.01	1.97	1.94
Tilting amount of the opposite rail (mm)	0.92	0.87	0.83	0.80	0.78	0.76	0.74	0.73
Gauge widening amount (mm)	3.37	3.18	3.04	2.93	2.85	2.77	2.71	2.67

Table 5.3 Impacts of Vertical Stiffness on a High-Speed Train Traveling in a Turnout in the Main Line

Vertical Stiffness of the Fastening (kN/mm)	15	20	25	30	35	40
Maximum dynamic wheel load (kN)	154.4	155.3	156.2	151.0	148.9	148.4
Initial load-bearing section of switch rail (mm)	13.5	14.5	15.2	15.7	16.2	16.4
Initial load-bearing section of point rail (mm)	20.1	21.5	23.2	23.6	24.0	24.4
Maximum flange force at the switch (kN)	27.2	26.4	25.5	27.2	26.8	27.1
Maximum flange force at the crossing (kN)	41.0	56.4	46.6	73.0	80.0	75.5
Maximum dynamic stress of switch rail (MPa)	130.2	128.7	127.4	127.6	124.5	113.2
Maximum dynamic stress of point rail (MPa)	174.7	181.1	171.8	170.0	172.8	175.6
Maximum lateral carbody vibration acceleration (m/s^2)	0.47	0.48	0.49	0.50	0.51	0.52
Maximum load reduction rate	0.26	0.28	0.27	0.26	0.27	0.28
Maximum derailment coefficient	0.65	0.58	0.42	0.49	0.53	1.07
Maximum spread of switch rail (mm)	1.0	0.78	0.66	0.61	0.58	0.59
Maximum spread of point rail (mm)	1.33	1.17	1.41	1.33	1.21	1.08
Vertical displacement of stock rail at the point of switch rail (mm)	2.03	1.88	1.77	1.68	1.62	1.57

opposite rail. In this case, the maximum wheel−rail lateral load (taken as 17.0 kN) applied on the rail top is the product of the wheel load and friction coefficient of the tread (taken as 0.20). The distance between the load action point and rail base is 176 mm. Thus, the impacts of plate pad stiffness on gauge widening are given in Table 5.2.

From the table it can be found that the smaller the pad stiffness, the greater the rail tilting, that is, the greater the dynamic gauge expansion. The plate pad will be specifically designed to make the stiffness at two sides greater than the middle part, so as to control rail tilting under low stiffness. For Chinese high-speed turnouts, the middle part of the plate pad is of a blocky structure, as shown in Figure 5.5, and the two sides are of integral structure. In this way, the lateral displacement of the rail is within 1.5 mm.

d. Impacts of vertical stiffness of the fastening on wheel−rail dynamic interaction [68−70]

For a Chinese No. 18 ballastless turnout for 350 km/h, the impacts of vertical stiffness of the fastening support on wheel−rail dynamic interaction are analyzed with train-turnout system dynamics theory. See Table 5.3 for dynamic responses.

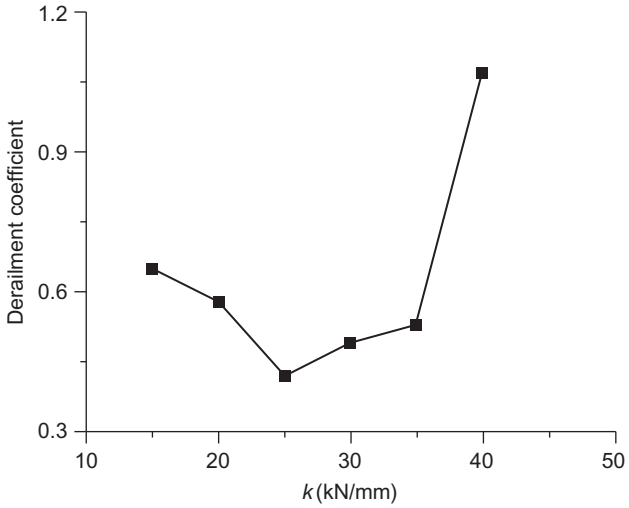

FIGURE 5.8

Impacts of fastening stiffness in a turnout on derailment coefficient.

It is shown in Table 5.3 that the stiffness of the fastening in a turnout will exert significant impacts on the wheel−rail dynamic responses:

- The greater the fastening stiffness and the firmer the initial load-bearing sections of switch rails and point rails, the smaller the dynamic stress of the switch rail. For the given height difference of the switch rail, the vertical stiffness of the fastening should not be lower than 20 kN/mm to make the switch rail withstand the load at top width of more than 15 mm.
- As the fastening stiffness increases, the wheel−rail lateral forces may change slightly at the switch. However, the wheel−rail lateral force at the crossing will increase.
- The greater the fastening stiffness, the greater the lateral carbody vibration acceleration, and the poorer the riding quality in the main line. Hence, lower fastening stiffness is preferred in a ballastless turnout for better riding comfort.
- The greater the fastening stiffness, the greater the derailment coefficient. Therefore, the fastening stiffness must not be greater than 40 kN/mm to maintain the derailment coefficient within the safety margin of 1.0. The impacts of fastening stiffness on derailment coefficient are shown in Figure 5.8. The minimum derailment coefficient appears when the fastening stiffness is 25 kN/mm. Fastening stiffness has a minor impact on the rate of wheel load reduction.
- The greater the fastening stiffness, the smaller the spread at the point of the switch rail. The change of the spread at the point of the point rail is insignificant.

In conclusion, the vertical fastening stiffness in high-speed turnouts in China is designed as 25 ± 5 kN/mm for ballastless turnouts and 50 ± 10 kN/mm for ballast turnouts. The plate pad stiffness is designed as per Eq. (5.1).

5.3 DISTRIBUTION RULES OF TRACK INTEGRAL STIFFNESS

5.3.1 INFLUENTIAL FACTORS

The track in a section is composed of standard rails, ties, fasteners, and bed. Owing to the sophisticated calculation models and methods for track stiffness, and with the use of the same ties, fasteners, etc. in a line, the track stiffness in a section is evenly distributed in the longitudinal direction of the line. However, the track structure is much more complex in a turnout. In a turnout, the track is made up of several types of rails, ties, and tie plates of variable lengths, plate pads of variable stiffness, as well as such unique parts as fillers, retainers, and slide beds. Therefore, track stiffness may vary significantly longitudinally. Specifically, the track stiffness in a turnout may be impacted by the following factors:

1. Tie: The tie is long in a ballast turnout, supporting the main and diverging lines simultaneously. When a train travels in the turnout, the load on one track can be distributed to another track via the ties. For a turnout with a slab track, as a number of rails may be laid on one slab, vertical displacement of the latter may lead to vertical deformation of several rails.
2. Fasteners and rail pads: The stiffnesses of the fasteners and rail pads are the major components of rail support stiffness; the two are directly related. The movable parts are not provided with fasteners and rail pads. However, the integral stiffness of other parts will be directly affected by the stiffnesses of fasteners and rail pads.
3. Tie plate and plate pad: Two or more rails may share one tie plate at the switch, the crossing, and the rear of the transition lead curve. In this respect, the wheel load on one track can be effectively distributed to another. Furthermore, as the length of the shared plate may vary greatly to accommodate the rails, the pad stiffness is also subject to significant change, leading to inhomogeneous distribution of track stiffness.
4. Rail types: The rails in a turnout include stock rail, switch rail, wing rail, point rail, and check rail. These rails differ in section profile and flexural stiffness. Moreover, the sections of the switch rail and swing nose rail are variable.
5. Filler: In a turnout, fillers are installed between two check rails in front of the point rails, between the long and short point rails, as well as between the wing rail and point rail, to transfer load and maintain track geometry. The fillers link two rails and enable the wheel load on one rail to be distributed to another (Figure 5.9).

5.3.2 CALCULATION MODELS

Given the above factors, a FEM is used for modeling the track integral stiffness in a turnout. Stock rails, check rails, and tie plates are modeled with uniform beams; switch rails and points rail are modeled with long nonuniform beams; the fasteners, rail pads, and plate pads are simplified into linear springs; fillers are modeled with short beams; ties are modeled with finite long beams on an elastic foundation; the bonding between switch rail and slide bed is modeled with nonlinear springs,

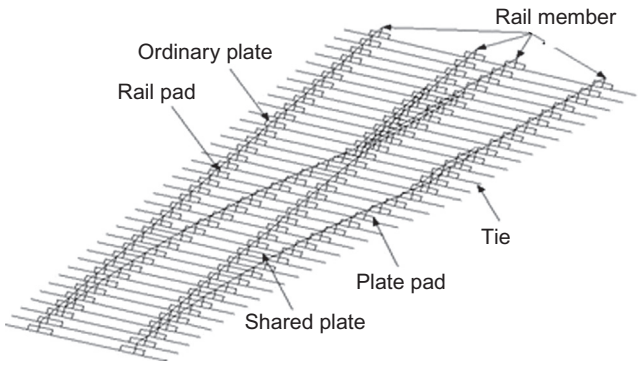

FIGURE 5.9

Calculation model for integral stiffness of a turnout.

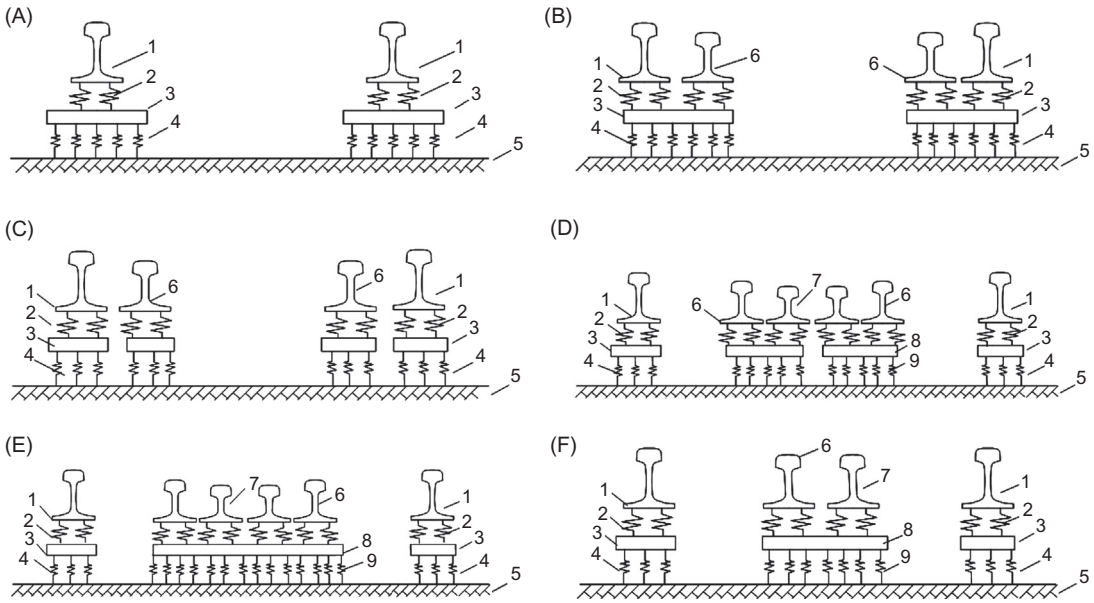

FIGURE 5.10

(A) Submodel A: front part of the actual point of switch rail (1, stock rail; 2, rail pad; 3, tie plate; 4, plate pad; 5, foundation). (B) Submodel B: switch (1, stock rail; 2, rail pad; 3, tie plate; 4, plate pad; 5, foundation; 6, switch rail). (C) Submodel C: transition lead curve (1, stock rail; 2, rail pad; 3, tie plate; 4, plate pad; 5, foundation; 6, check rail). (D) Submodel D: shared tie plate of transition lead curve (1, stock rail; 2, rail pad; 3, ordinary tie plate; 4, ordinary plate pad; 5, foundation; 6, wing rail; 7, check rail; 8, shared tie plate; 9, shared plate pad). (E) Submodel E: tie plate shared by two point rails and two wing rails of crossing (1, stock rail; 2, rail pad; 3, ordinary tie plate; 4, ordinary plate pad; 5, foundation; 6, wing rail; 7, point rail; 8, shared tie plate; 9, shared plate pad). (F) Submodel F: tie plate shared by point rail and wing rail of crossing (1, stock rail; 2, rail pad; 3, ordinary tie plate; 4, ordinary plate pad; 5, foundation; 6, long point rail; 7, short point rail; 8, shared tie plate; 9, shared plate pad).

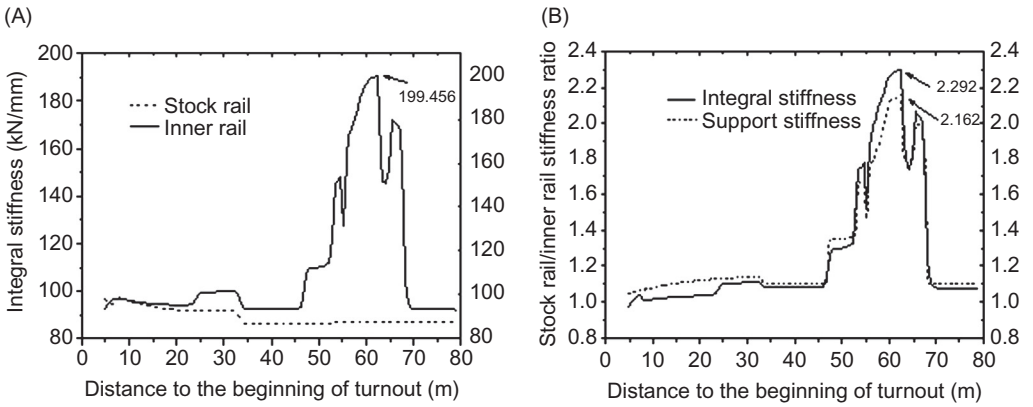

FIGURE 5.11

(A) Distribution of integral stiffnesses in the main line. (B) Stock rail/inner rail stiffness ratio in the main line.

which transfer load under compressive force (not under tensile force). The model includes six submodels, as shown in Figure 5.10:

1. Submodel A (for modeling the front part of the actual point of the switch rail): Composed of the stock rail, spring-modeled elastic fastening, tie plate, spring-modeled plate pad and tie. Linear springs and uniform beams are used in the model.
2. Submodel B (for modeling the switch): The switch rail and the stock rail share one tie plate. Four rails are laid on one tie. The switch rail is connected to the tie plate with nonlinear springs. The load applied on the switch rail can be distributed to the stock rail.
3. Submodel C (for modeling the transition lead curve): Four rails are laid on one tie: straight and curved stock rails and check rails. Each check rail is provided with one tie plate. The load can be distributed to four rails through the tie.
4. Submodel D (for modeling the tie plate shared by two check rails near the point rail in the transition lead curve): The straight and curved check rails share one tie plate. The wheel load applied on the check rail in the main or diverging line can be distributed to another through the shared tie plate.
5. Submodel E (for modeling the tie plate shared by two wing rails and two point rails): This tie plate is rather long, enabling the wheel load on one point rail to be distributed to another point rail and two wing rails.
6. Submodel F (for modeling the tie plate shared by the wing rail and point rail): The tie plate enables the wheel load on the point rail to be distributed to the wing rail.

5.3.3 DISTRIBUTION RULE IN BALLASTED TURNOUT

For a Chinese No. 18 ballast turnout, the distributions of integral stiffnesses of stock rail and inner rail in the main and diverging lines as well as the stock rail/inner rail stiffness ratio are shown in Figures 5.11 and 5.12; comparative results of integral stiffness, support stiffness, and vertical displacement of the rail are depicted in Table 5.4.

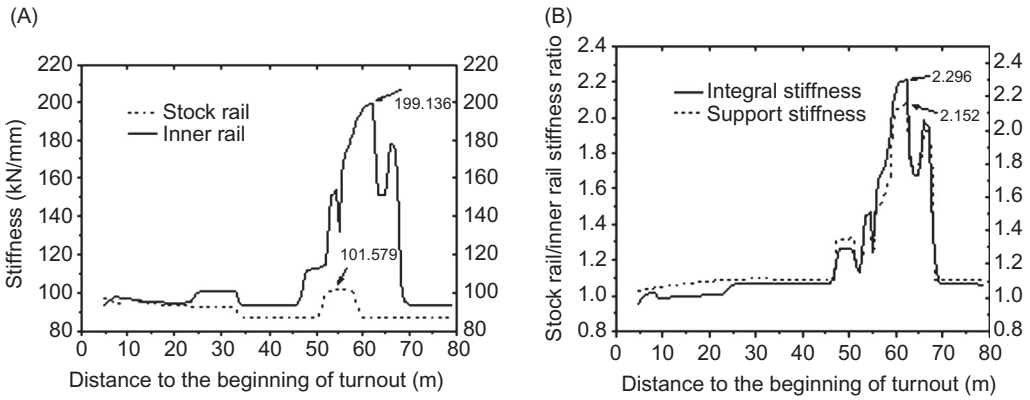

FIGURE 5.12

(A) Distribution of integral stiffnesses in the diverging line. (B) Stock rail/inner rail stiffness ratio in the diverging line.

Table 5.4 Comparison of Calculated Results of Ballasted Turnouts

Types of Rails		Items					
		Integral Stiffness (kN/mm)		Support Stiffness (kN/mm)		Vertical Displacement (mm)	
		Max	Min	Max	Min	Max	Min
Main line	Stock rail	97.4	85.9	34.1	21.7	1.49	1.31
	Inner rail	199.5	92.5	66.2	23.2	1.38	0.64
Diverging line	Stock rail	101.6	85.8	35.4	21.7	1.48	1.26
	Inner rail	199.1	92.5	66.2	23.3	1.37	0.64

Note: *The vertical displacement in the table refers to that of the rail surface under static wheel load of a train.*

From Figures 5.11 and 5.12 and Table 5.4, it can be found that the integral stiffness is unevenly distributed in the longitudinal direction of the turnout. The integral stiffness of a crossing is much greater than that of other parts. Different rails have different integral stiffnesses. The integral stiffness of stock rails shows little change longitudinally. However, in a turnout, the integral stiffness of one stock rail may vary greatly as affected by the switch rail, point rail, and other special rail members. The same change rule applies in main and diverging lines. The maximum and minimum vertical displacements of the rail are 1.49 and 0.64 mm, respectively, with a ratio of about 2.3.

In all, the integral stiffness, support stiffness, and vertical displacement of rails are unevenly distributed in main and diverging lines of the turnout, which can lead to serious dynamic irregularities, degrading the riding comfort and stability. Therefore, track stiffness must be homogenized.

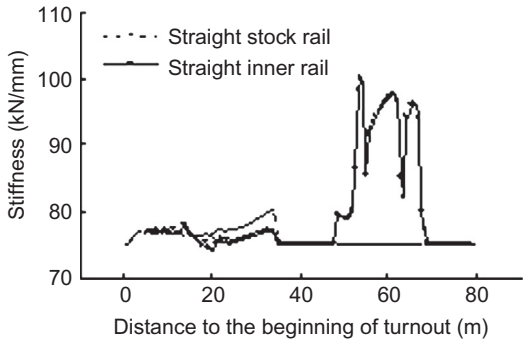

FIGURE 5.13

Distribution of integral stiffnesses of stock rail and inner rails.

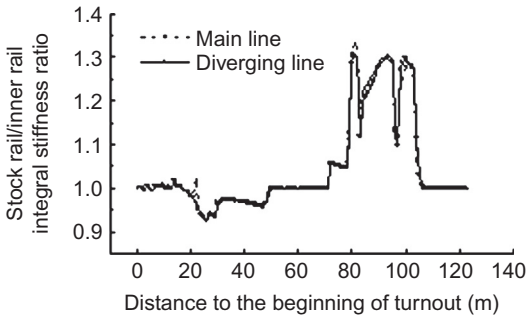

FIGURE 5.14

Stock rail/inner rail integral stiffness ratio.

5.3.4 DISTRIBUTION RULE IN BALLASTLESS TURNOUT

Taking a Chinese No. 18 ballastless turnout for 350 km/h, for example, the distribution of integral stiffnesses of the stock rail and the inner rail in the main and diverging lines are shown in Figure 5.13, and the stock rail/inner rail stiffness ratio is shown in Figure 5.14.

Owing to the considerable stiffness of the sub-rail foundation, the integral stiffness of ballastless track along the longitudinal direction of a turnout varies mildly as compared with ballast track. The crossing has much greater stiffness than other parts due to the interaction of rails. The maximum ratio of inner rail/stock rail integral stiffness is about 1.33, which may lead to dynamic irregularities and affect riding comfort.

5.4 HOMOGENIZATION DESIGN FOR TRACK STIFFNESS IN A TURNOUT [71]

5.4.1 DYNAMIC ANALYSIS AT TRACK STIFFNESS TRANSITION

The analytical model and theory of train−track coupling dynamics, as shown in Figure 5.15, is used to explore the dynamic responses of a train traveling in an inhomogeneous part of a turnout, the change rules, and the reasonable design parameters for stiffness transition. The sub-rail foundation stiffnesses at the stiffness transitions of ballast and ballast tracks are the same, making the model applicable to both track types. Additionally, the rail support stiffnesses under two rails of a track are longitudinally and laterally variable.

The model is composed of the submodels of vehicle, track, and the wheel−rail coupling relation. The wheel and the rail will interact dynamically when a train travels in the track stiffness transition of a turnout. Thus, the riding safety and comfort and structural strength of the line must be included in designing this section. In addition, the design should ease the vibration of track structure, maximize the service life of wayside equipment, and reduce maintenance costs. Wheel−rail

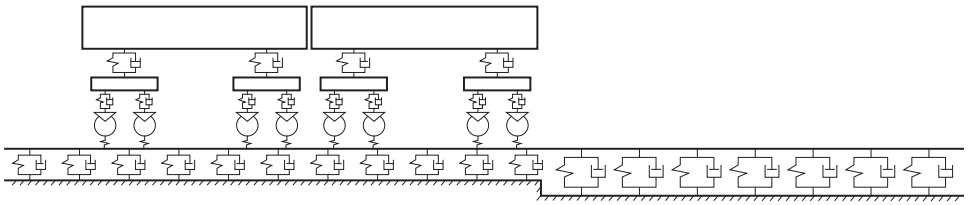

FIGURE 5.15

Dynamic model of track stiffness transition of a turnout.

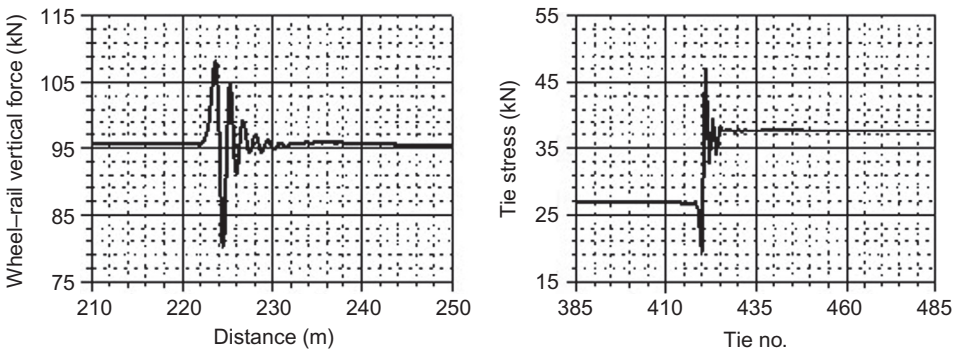

FIGURE 5.16

Changes of wheel−rail vertical force and tie stress caused by stiffness difference of sub-rail foundation.

dynamic force, tie stress, dynamic bending stress of the rail, rate of wheel load reduction, and vertical carbody acceleration are dynamic performance indicators in evaluating this section.

5.4.2 RELATION BETWEEN VARIATION RATE OF RAIL DEFLECTION AND LENGTH OF TRACK STIFFNESS TRANSITION [72−73]

The wheel−rail dynamic performance induced by a sub-rail foundation stiffness difference is studied by exploring the connecting performance of two tracks with different sub-rail foundation stiffnesses. The sub-rail foundation supporting stiffnesses of high-stiffness track and low-stiffness track are taken as 60 and 15 MN/m, respectively. A CRH2 EMU train is used. The traveling speed is taken as 300 km/h.

The dynamic responses, that is, wheel−rail vertical force, tie stress, vertical displacement of the rail, and vertical carbody vibration acceleration caused by sub-rail foundation stiffness difference when a train travels in the connecting parts of two tracks, are shown in Figures 5.16 and 5.17.

The results show that the stiffness difference of sub-rail foundation leads to the deflection difference of the rail under wheel load, thus resulting in wheel−rail dynamic impact and leading to train vibration. The tie stress changes sharply at the connecting part of two tracks. This part is susceptible to fastener failure, unsupported or damaged ties, bed settlement, and other track defects

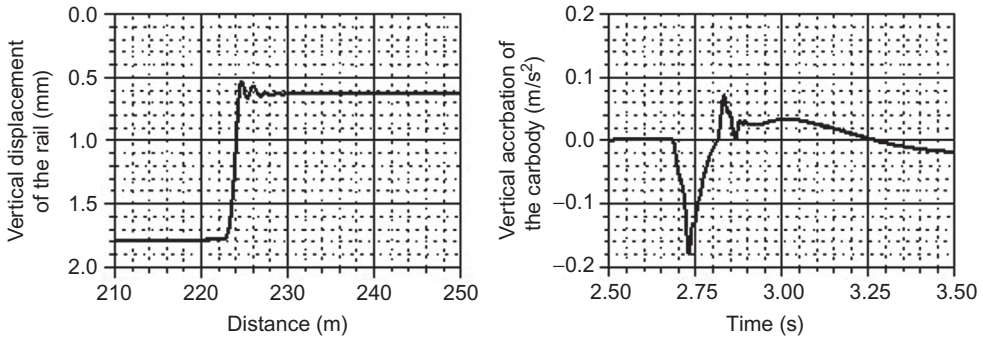

FIGURE 5.17

Changes of vertical displacement of the rail and vertical carbody acceleration caused by stiffness difference of sub-rail foundation.

Table 5.5 Comparison of Rail Deflection Variation Rates for the Same Stiffness Ratio of Sub-Rail Foundation

Condition	Stiffness Ratio	Stiffness Difference (MN/mm)	Wheel−Rail Force (kN)	Carbody Acceleration (m/s^2)	Rail Deflection Difference (mm)	Rail Deflection Variation Rate (mm/m)
1	4	15	112.5	0.41	2.92	2.08
2	4	60	107.4	0.15	0.93	1.08

under long-term traffic load. Once any defect occurs, the wheel−rail dynamic interaction will deteriorate rapidly, seriously affecting driving safety and comfort. Therefore, track stiffness transition must be provided in the area with large stiffness differences in the sub-rail foundation. In the absence of this transition measure, the effective attenuation distance of wheel−rail force caused by the stiffness difference in the sub-rail foundation is about 8 m, and the effective attenuation time of carbody acceleration is about 0.5 s.

In view of the length of this section, the indicator "rail deflection variation rate" is employed to explore the effects of wheel−rail dynamic interaction caused by the stiffness difference of sub-rail foundation and transition length. This indicator is defined as the gradient of the dynamic deflection curve of the rail.

Stiffness difference or "stiffness ratio" was used in previous studies. In fact, the two indicators cannot correctly reflect stiffness difference-induced wheel−rail dynamic interaction. The study was carried out under two conditions: (i) sub-rail foundation stiffnesses of 5 and 20 MN/m and (ii) sub-rail foundation stiffnesses of 20 and 80 MN/m. Table 5.5 shows the wheel−rail dynamic interaction and rail deflection variation rate under the two conditions.

As shown in Table 5.5, the wheel−rail dynamic interaction in condition (i) is much greater than that in condition (ii); the reverse may apply to stiffness difference. However, this rule does not apply to stiffness ratio. Therefore, only "rail deflection variation rate" can clearly mirror this rule.

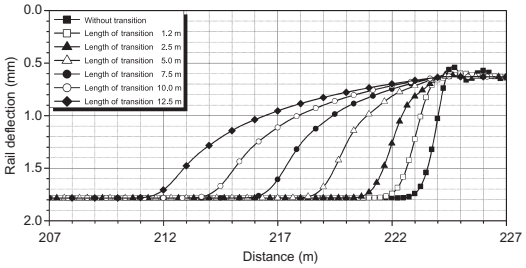

FIGURE 5.18

Rail deflections for different transition lengths.

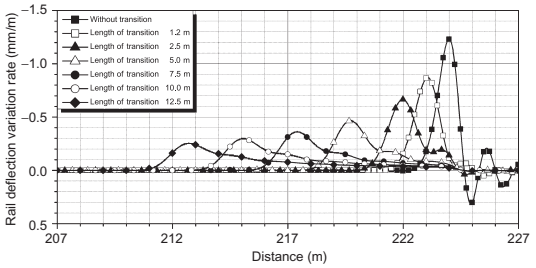

FIGURE 5.19

Rail deflection variation rates for different transition lengths.

Table 5.6 Effects of Transition Length on Wheel–Rail Dynamic Interaction

Length of Transition (m)	0	1.2	2.5	5.0	7.5	10.0	12.5
Rail deflection variation rate (mm/m)	1.24	0.87	0.67	0.47	0.36	0.30	0.26
Wheel–rail force (kN)	108.2	103.5	101.4	99.4	98.5	97.7	97.6
Tie stress (kN)	47.1	41.3	39.5	38.7	38.3	37.8	37.6
Carbody acceleration (m/s^2)	0.18	0.16	0.14	0.12	0.10	0.09	0.08

In what follows, rail deflection variation rate is used for evaluating the effects of the length of track stiffness transition on wheel–rail dynamic interaction. Figures 5.18 and 5.19 show the deflection curve and deflection variation rate curve of the rail at the connecting parts of two tracks with different transition lengths. Table 5.6 shows the change rules of rail deflection variation rate, carbody vibration acceleration, wheel–rail dynamic interaction, and tie stress for different transition lengths.

The results show that, in areas with large stiffness difference in the sub-rail foundation, the stiffness transition must be provided in line with stricter requirements, so as to ensure high smoothness of the track structure for the high-speed railways (HSRs). In view of the performance in reducing wheel–rail interaction, this section should be about 10 m long. In another sense, the rail deflection variation rate induced by the stiffness difference of sub-rail foundation should be under 0.3 mm/m. This indicator can be used to evaluate the homogenization performance of track stiffness in a turnout.

5.4.3 HOMOGENIZATION DESIGN OF TRACK STIFFNESS IN A TURNOUT

1. Measures

   Track integral stiffness is affected by flexural stiffness of the rail as well as the supporting stiffnesses of fillers, rail pad, plate pad, and bed. For this, the strength, service life, process, etc. of the rail must be taken into consideration in selecting rail types. After selection, the flexural stiffness is determined and cannot be changed during stiffness optimization.

Table 5.7 Design Values of Plate Pad Stiffness

Pad Code	Stiffness (kN/mm)	Applicable Tie No.	Shared Rails
ZZ-A	66	1−14	Stock rail and switch rail
ZZ-B	80	15−19	Stock rail and switch rail
ZZ-C	92	20−58	Stock rail and switch rail
DW-A	70	80−88	Two check rails
DW-B	40	89−92	Two check rails
ZC-A	50	93−94, 105−107, 111−114	Two point rails and two wing rails
ZC-B	40	95−104, 108−110	Two point rails and two wing rails
HG-A	60	85−98	Curved stock rail and check rail

Notes:
1. *For a pad code "XX-X," "XX" represents the area where the pad is laid, and "X" represents the pad type. For example, "ZZ-A" refers to an A-typed shared pad laid at the switch, the stiffness of which is 66 kN/mm.*
2. *ZZ, switch; DW, rear of transition lead curve; ZC, crossing; HG, check rail.*

The elasticity of a fastening is determined mainly by the plate pad. Rail pads are relatively stiff to maintain the dynamic height difference between movable rail parts and the stock rail/wing rail. In this regard, the homogenization effect cannot be realized by changing the stiffness of a rail pad.

The support stiffness of a ballast bed may be changed by modifying ballast grading and materials. If the track stiffness is homogenized by changing the support stiffness of the bed, the ballast grading will differ in different sections, leading to construction and maintenance difficulties. For a ballastless bed, its high stiffness may be altered by providing rubber pads under the plate, which is costly and hard to repair. In conclusion, track stiffness cannot be homogenized by modifying the stiffness of the bed for both ballast and ballastless tracks.

As the plate pad is the main donor of the elasticity of a fastening, track stiffness will change with plate pad stiffness. Thus, track stiffness in a turnout may be homogenized by optimizing the stiffness of the plate pad. More importantly, plate pad stiffness may be changed easily by cutting grooves or adopting blocky or split designs. Modifying the thickness of a plate pad is not recommended, to ensure consistent height of a track. In addition, the pads under a shared plate must be provided with specific stiffness grades (minimally) to facilitate laying and replacement.

2. Homogenization of track stiffness for No. 18 ballast turnout in China

By analyzing the designs of rail pad stiffness, the design values of rail pad stiffness for No. 18 ballast turnout in China are obtained, as given in Table 5.7.

Figures 5.20−5.23, respectively, present the distribution rule of integral stiffness of stock rail and inner rail in the main line, stock rail/inner rail integral stiffness ratio, deflection variation rate of inner rail, and vertical vibration acceleration change of a train after stiffness homogenization.

The results show that, except for minor fluctuations in the middle of a crossing, track integral stiffness is basically stable in the longitudinal direction of the line after homogenization, about 93 kN/mm. The maximum inner stock rail integral stiffness ratio drops from 2.29 to 1.28

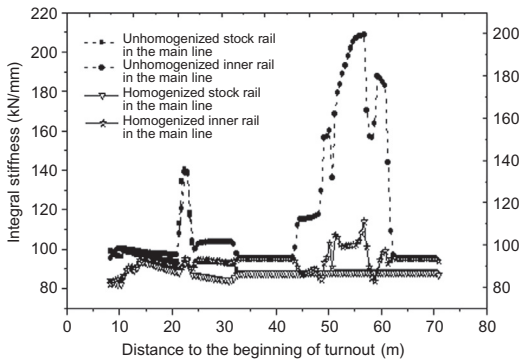

FIGURE 5.20

Distribution change of integral stiffness.

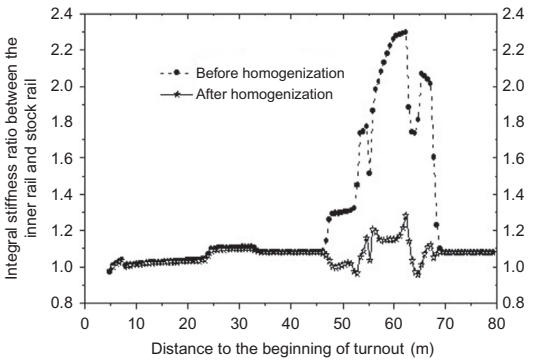

FIGURE 5.21

Change of inner stock rail integral stiffness ratio.

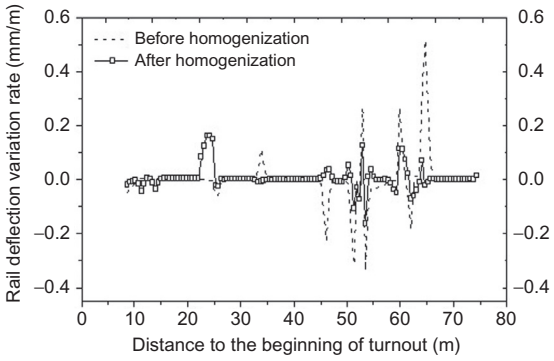

FIGURE 5.22

Change of rail deflection variation rate.

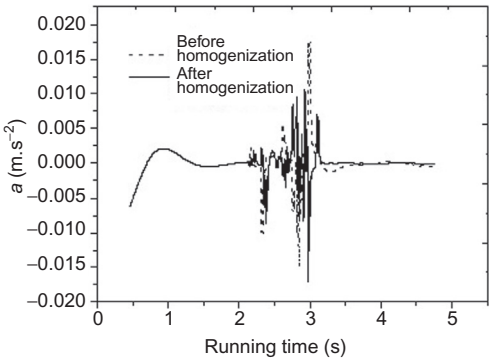

FIGURE 5.23

Change of carbody vibration acceleration.

after homogenization. The deflection variation of the rail slows down significantly after this stiffness treatment. The deflection variation rate of the inner rail in the main direction changes from 0.517 to 0.125 mm/m, below the limit of 0.3 mm/m. After treatment, the amplitudes and scope of carbody vibration acceleration, wheel−rail interaction, and tie stress are reduced, and the vertical displacement of the rail increases, but at a slower speed longitudinally along the line. This reveals that the stiffness homogenization measures improve the elasticity of the track system and make the stiffness uniform in the longitudinal and transverse directions, thereby effectively improving the wheel−rail dynamic interaction and running comfort of the train, and reducing the vibration intensity of the track structure.

3. Homogenization of track stiffness for No. 18 ballastless turnouts in China

Similarly, by analyzing the designs of rail pad stiffness in Chinese No. 18 ballastless turnouts for 350 km/h, the distribution rule of integral stiffness of stock rail and inner rail and the

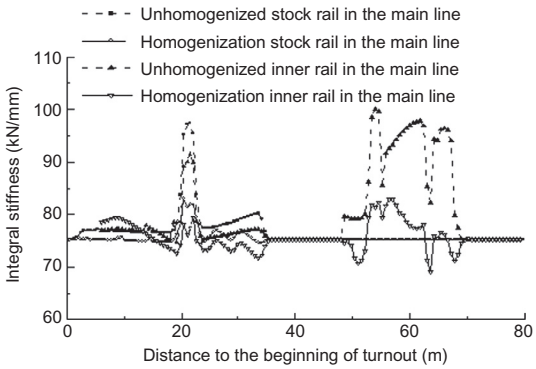

FIGURE 5.24

Distribution change of integral stiffness.

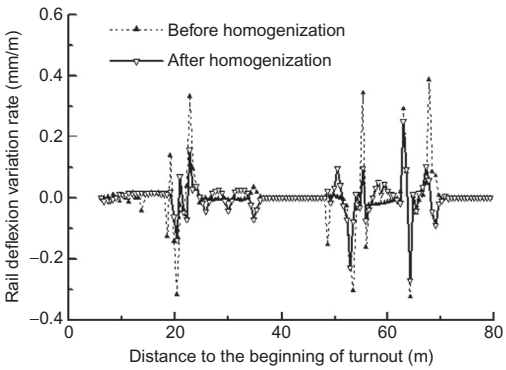

FIGURE 5.25

Distribution of deflection variation rates of inner rail.

deflection variation rate of the inner rail in the main line after stiffness homogenization are shown in Figures 5.24 and 5.25.

The results show that the dynamic irregularities caused by track stiffness are obviously reduced after the measures. With the homogenization measures, the maximum inner rail/stock rail stiffness ratio is reduced from 1.33 to 1.11 and the rail deflection variation rate of the inner rail in the main line from 0.35 to 0.19 mm/m, below the limit of 0.3 mm/m.

5.4.4 DESIGN OF PLATE PAD

The fastening of a high-speed turnout should have low stiffness; this is determined by the material and profile of the elastic pads. Based on the dynamic/static stiffness and fatigue performance of the pad and numerous practices, *in situ* graft-modified carbon black-filling technology is used to manufacture the rubber pad: Polar white carbon black is graft-modified on the surface with nonpolar *in situ* grafting modification agent. This technology is applied to elastic tie plate production, which is capable of reducing the rigidity of rubber while maintaining the proper stiffness. Moreover, it improves the tensile stress at a given elongation at 300% and reduces the compression set significantly. With this technology, the static stiffness deviation of the product is $\pm 20\%$ of the design value, and the dynamic/static stiffness ratio is not greater than 1.5; the pad will not break or crack after 3,000,000 cycles of fatigue tests, with the change rate of static stiffness not greater than 20% after fatigue tests.

The blocky design, as shown in Figure 5.26, has been adopted for the pad to meet the stiffness requirements. The blocky structure should be compatible with the stiffness requirements of a turnout, which can be verified with the Mooney−Rivlin constitutive mode and ABAQUS analytical software (see Figure 5.27). The pad should reach the design stiffness (25 kN/mm) and desired strength in the end.

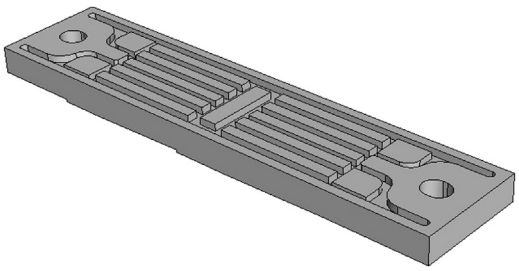

FIGURE 5.26

Structure of the pad.

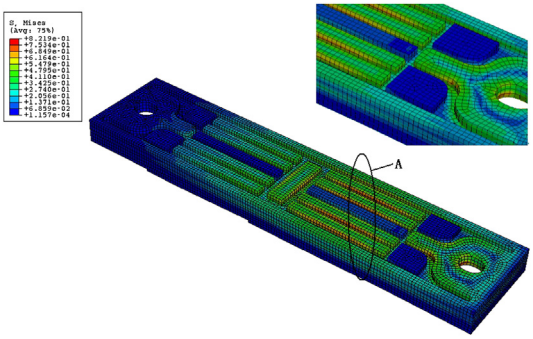

FIGURE 5.27

Calculated results of pad stiffness.

5.5 DESIGN OF TRACK STIFFNESS TRANSITION FOR A TURNOUT

The stiffness of the fastening and tie spacing may be different between a turnout and a section, so track stiffness transitions may be provided between the two, so as not to affect riding comfort and quality in the turnout.

According to dynamic simulation analysis, track stiffness transitions are required at both ends of the turnout to ease wheel−rail interaction and keep the variation rate of rail deflection induced by the stiffness difference of the sub-rail foundation within 0.3 mm/m. This section should not be shorter than the distance a train may travel in 0.5 s. The section may include two stiffness grades after stiffness homogenization. In stiffness-graded transition schemes, the stiffness grade difference may differ, and may be smaller in low areas and greater in high stiffness areas.

Taking the No. 18 ballasted turnout in China as an example, the support stiffnesses of the fastening and the bed are, respectively, 50 and 100 kN/mm; therefore, the rail node stiffness in the turnout is 33.3 kN/mm. In the section, if the stiffness of the fastening is 80 kN/mm, the rail node stiffness will be 44.4 kN/mm. Since the difference of vertical displacement of the rails in two sections is 0.44 mm, exceeding the allowable value of 0.3 mm/m, transitions are required. The transition may have two stiffness grades, each grade covering about 18 m (equals 30 tie spans). In addition, the design stiffnesses of the fastenings adjacent to the turnout and the section are 55−65 and 65−75 kN/mm, respectively.

CHAPTER

STRUCTURAL DESIGN OF CWR TURNOUTS

6

Continuously welded rail (CWR) turnouts mark the trend of global railway tracks, as they save rail joints and reduce wheel−rail dynamic interaction considerably. Under the mechanical principle for CWR track, theoretically, the rails of a CWR track can be infinitely long. However, in a common CWR track, particularly in a turnout or on a bridge where the rails cannot be welded, the rail length may be constrained to about 1500 m. The provision of transitional jointed track at two ends of a CWR track unavoidably leads to rail joints, limiting the performance of the CWR railway line.

In a trans-section CWR track, if all rail joints of a turnout are welded or glued, and the rails at two ends of the turnout are welded with long rail strings of CWR track in both straight and diverging directions, this turnout is called a CWR turnout. Trans-sectional CWR track minimizes rail joints (continuous weld) and the impact of transitions and breathing areas. It marks a big leap for modern CWR railway lines.

A CWR turnout is an integral part of a trans-section CWR track, withstanding the same temperature force in the CWR track as rail strings. In addition, the inner rails of a CWR turnout may be under different stresses at two ends; thus the temperature force in the turnout is unbalanced. This unbalanced force makes the rail stress and deformation displacement unstable; therefore, it is the main concern in the design, laying, and maintenance of CWR turnouts [74].

6.1 STRUCTURAL FEATURES

Engineering and electrical parts must be coordinated and compatible in designing a CWR turnout. The electrical parts must ensure normal conversion and locking performance of a turnout on one hand, and maintain the normal operation layout of switch rail and point rail after conversion on the other. Engineering parts shall provide proper operational environment and installation space for electrical facilities, but also can cooperate with electrical system structurally to overcome scant switching displacements, and control expansion displacements (switch rail/point rail) within the allowable scope, so as to avoid conversion failure, that is, blockage.

6.1.1 BASIC REQUIREMENTS

A CWR turnout will be exposed to dynamic loads from rolling stock (as with common turnouts) and gigantic temperature forces. Therefore, the prerequisites below must be met before construction.

Design of High-Speed Railway Turnouts.

1. The rails at two ends of the turnout must be weldable, so as to be welded with long rail strings of CWR track. Or, alternatively, freezing or gluing processes may apply.
2. Rail fastenings for the turnout must have proper elasticity; displacement resistance must be greater than the longitudinal resistance of the turnout bed. The inner rails of the turnout should be locked from creeping, preferably with elastic clips. The fastening bolts shall be tightened as per required torque.
3. Fillers, retainers, or the like should be arranged at the heel of the switch rail and point rail to transmit the longitudinal force between two rails. High-strength bolts must be used to couple these force transmission components and increase the frictional resistance and shear strength. The bolts will be tightened as per required torque.
4. The ties of the CWR turnout must have proper lateral bending stiffness. RC ties with type II or III clips may meet the requirements for desired rail longitudinal resistance.
5. The bed of a ballast turnout should be well filled and compacted, especially in the tie box. The ballast shoulder should be widened as specified for a CWR track.
6. Conversion, locking, and closure detection devices, etc. must be compatible with the great expansion displacement of the switch rail/point rail. No rail expansion−induced conversion failure is allowed.
7. The impacts of rail expansion must be considered in designing turnout components (including positions of bolt holes), so as to avoid misplacement of bolt holes, parts jamming, or other defects.

6.1.2 TRANSMISSION PATH OF TEMPERATURE FORCE [75]

Figure 6.1 represents the transmission path of temperature force in a CWR turnout after taking away all the isolators (the turnout rails are continuously welded in both straight and diverging directions). From the figure, the temperature force of long and short point rails at turnout rear will be transferred to the wing rail and guiding rail (the rail connecting the curved or straight switch rail) via the structure at the heel of the crossing, and then to the stock rail via the structure at the heel of the switch. The expansion of the guiding rail will lead to longitudinal displacement of ties, and distribute partial temperature force to the stock rail via the guiding rail. As a result, the proper design of the force transmission structure is critical to reasonable stress and deformation of a CWR turnout and even the construction of a trans-section CWR track.

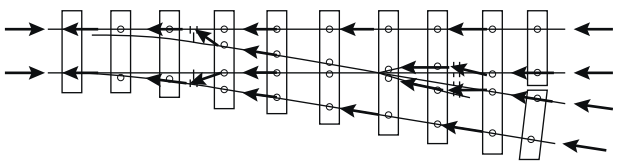

FIGURE 6.1

Path for temperature force transmission in a CWR turnout (arrows represent the transmission direction at temperature rise).

6.1.3 FORCE TRANSMISSION STRUCTURE

From Figure 6.1, when the turnout rails are welded with section rails, the unbalanced longitudinal temperature force at turnout rear and front will cause longitudinal displacement of rails in the turnout. A new balance can be attained when the temperature force is partially released. The outer stock rails of a turnout are part of the trans-section CWR track, which can be regarded as the fixed area in the line. In case the two outer rails move longitudinally, there will be no additional temperature force in displacement variation area except for redistribution of longitudinal force of rail strings. The rail strings have the same temperature force as in the fixed area, and follow the same change rule in longitudinal force for long rail strings of a CWR track on a bridge.

With the connection of force transmission components, the inner rails of a turnout become two long rails under temperature force. However, the movable switch rail and point rail at the front part of the rail string will not be constrained by a locking device and can expand freely. So the inner rails of the turnout can be regarded as the breathing area of the CWR track. In the absence of restrictions, the longitudinal movement of long rails will impact the inner geometry of the turnout. If the expansion displacement of conversion equipment is out of gauge, the locking device will be choked by the switch rail/point rail with variable top width, thus causing blockage. Therefore, the displacement of inner rails must be restricted by distributing partial temperature force to outer stock rails via force transmission components.

The main force transmission structures in a CWR turnout are composed of the heel of crossing, heel of switch, fastening, and tie. The operational principles of these parts are given below.

1. Heel of crossing [76]

   CWR turnouts can be classified into turnouts with fixed crossing and swing nose crossing. The swing nose crossing has two structural types: one with fillers and long wing rail, and one with crossing heel supports and short wing rail. The fixed crossing will bear the rail temperature force transmitted from the heel end, and then transmit the force evenly to two rails at the toe end after overcoming the longitudinal resistance of crossing fasteners and frictional resistance of the crossing plate. The fixed crossing is normally short; therefore, the resistance to longitudinal temperature force is limited. For swing nose crossings, the heels of the point rail and wing rail are connected by fillers. In this way, the temperature force on the point rail can be transferred to the wing rail through the frictional resistance of fillers. Given excessive longitudinal displacement of fillers, the longitudinal horizontal bolt may bend under shear, and the horizontal bolt may transfer partial longitudinal force. The fillers may be glued with point rail/wing rail (see Figure 6.2) to enhance transmission capacity. After that, the displacement of the point of the point rail is related mainly to breathing length and temperature change, not the displacement of the heel of the point rail, to prevent blockage of the point of the point rail and creeping of a flange-type point rail. For crossings with long wing rails and swing nose rails, the longitudinal stress is borne by fasteners in a certain range and will be distributed to outer stock rails via ties. This structure is preferable and has been applied to swing nose CWR turnouts since the emergence of speed-up turnouts in China. The structure with crossing heel support and short wing rail is rarely used because of its transmission inefficiency.
2. Heel of switch

   The heel of switch consists of three types: heel without force transmission components, heel with retainers, and heel with fillers. Normally, the temperature force on the wing rail will be

FIGURE 6.2

Glued structure at heel of crossing.

FIGURE 6.3

Fillers at heel of switch rail.

transferred to the heel of switch rail via the rails of the transition lead curve, during which process the longitudinal resistance of fastenings involved must be overcome. Thus, notwithstanding the significantly lowered longitudinal resistance, the rails adjacent to the heel of switch rail are subject to great longitudinal displacement. If not constrained, with the superposition of expansion displacement, excessive displacement will lead to conversion failure. Except for the conversion equipment with considerably large allowable expansion displacement, force transmission components are required at the heel of switch rail to limit the displacement. Fillers and retainers are commonly used for force transmission at the switch. The force transmission principle for the fillers resembles that for the heel of crossing. Glued structures are not feasible for the frequent replacement of switch rails. Too many long and large fillers are not preferred, considering the limited space (see Figure 6.3). Fillers are capable of withstanding a great part of the rail temperature force and transferring the temperature force on the transition lead curve to stock rail; however, a certain longitudinal displacement may occur, particularly for less refined fillers. In serious cases, the longitudinal displacement of wedge-shaped fillers may lead to local minor bendings at the heel of switch, and inordinate temperature force on stock rail may cause rail fracture or breakage. For this circumstance, Germany has developed a retainer structure (equivalent to filler structure) to release partial temperature force. This structure is composed of separated combination blocks mounted on the webs of the switch rail and stock rail, respectively. When longitudinal displacement occurs at the heel of switch rail, the two blocks of the retainer will come into contact, and then the longitudinal force can be transferred with the frictional resistance between the blocks and rail web and the shear and bending resistance of horizontal bolts. Owing to partial expansion displacement of rails, less longitudinal force may be transferred to stock rails with this structure, but the displacement at the heel of switch rail is greater. The geometrical centers of retainer blocks are not aligned; thus torsion may take place during force transfer. In view of the poor torsional resistance of the switch rail, the shorter block of the retainer will be mounted on the switch rail. However, minor bends may appear at local areas of the switch rail in use.

Constrained by allowable expandability of the switch rail and the strength of stock rail as required by conversion equipment, as well as the stability requirements, the retainer structure applies in colder regions, and filler structure prevails in warmer regions.

3. Fasteners

   Fasteners are an important part of a CWR track. In a common CWR track, the longitudinal resistance of fasteners must be greater than that of the bed, so the displacement of rails with respect to ties can be controlled under the considerable resistance of the line. The fasteners in a CWR turnout should have enough resistance to transmit the temperature force of the inner rails to the ties, and then to stock rails, where the longitudinal resistance of fasteners on two inner rails is the sum of longitudinal bed stress on ties and the longitudinal resistance of two stock rails. Therefore, the direction of resistance of inner rail fasteners and that of stock rails are opposite, the same as with the gradient of temperature force.

4. Ties

   Under the longitudinal force from fasteners of inner rails, the turnout ties may be subject to longitudinal displacement, shifting, or even horizontal bending, which causes displacement of stock rails. This is how the temperature force is transmitted from the inner rails to outer stock rails. As the compactness of the ballast bed and the cross section of tie increase, the longitudinal resistance of the bed rises, but that of fasteners of stock rails drops, and thus the stress and deformation of stock rail are eased.

6.2 CALCULATION THEORIES AND APPROACHES

The welded stock rails of a CWR turnout can be compared to a fixed area in a line, where no expansion displacement may occur under stress. The welded inner rails of the CWR turnout can be viewed as the breathing area in the line, where the relieved temperature force will be converted to expansion displacement. In a turnout, as stock rails are connected to inner rails via ties and fillers at the heel of switch, they will also resist the expansion displacement under temperature force, and thus share the temperature force transmitted from inner rails. The additional temperature force on the outer stock rails of a turnout will be calculated by summing the calculated value and initial temperature of the stock rail, the strength of stock rails, and the stability of common CWR track in front of the turnout. This is an important aspect of designing a CWR turnout.

There is a diversity of calculation theories for CWR turnout in China, mainly including "double-rail interaction method," "equivalent resistance coefficient method," "generalized variational method," and "finite element method (FEM)" [76–77].

6.2.1 EQUIVALENT RESISTANCE COEFFICIENT METHOD

For this method, the filler structure is obtained first, followed by stress transferred to stock rail per tie. Adding the resistance force of the bed under the stock rail gives additional temperature force on the calculated stock rail. Figure 6.4 represents the stress on the tie in a turnout welded in both straight and diverging directions and in a turnout welded in straight direction only. Figure 6.5 shows the calculation principle of superposition of additional temperature forces on stock rails.

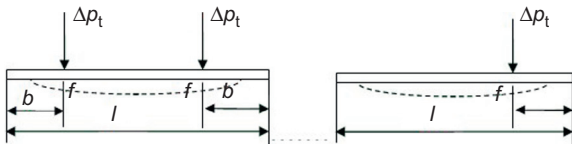

FIGURE 6.4

Stress and deformation of a turnout tie.

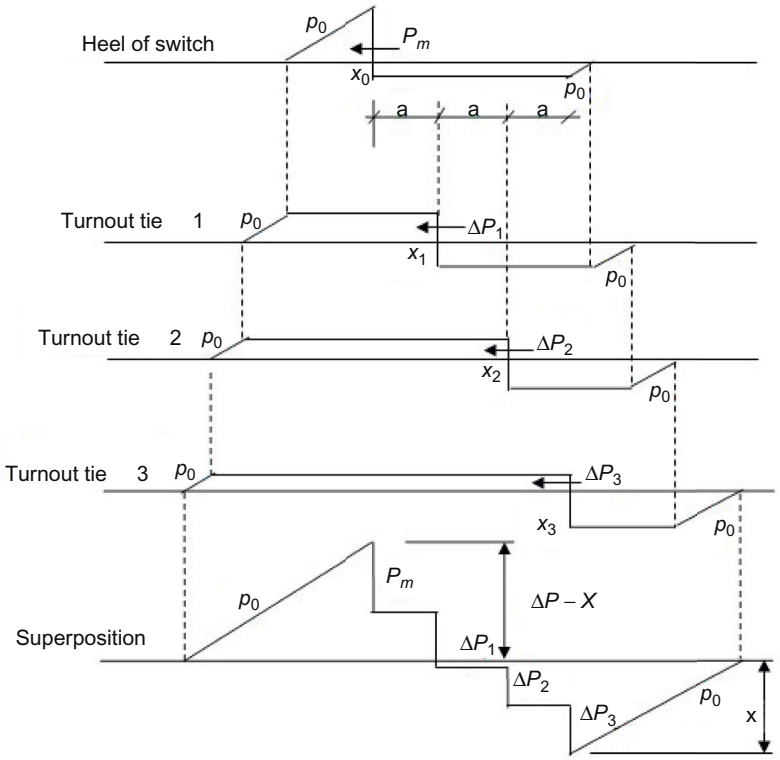

FIGURE 6.5

Schematic diagram of additional temperature force, superposition of stock rail.

As the stock rails of a CWR turnout lie in the nonbreathing area of a CWR track, no expansion displacement exists in a certain length of rails at two ends of the turnout. When the stock rails expand under additional temperature force, the resulting rail tensile deformation and compressive deformation are equal; as shown in the figure, the area of tension equals the area of compression. Thus, the rails at two ends of the turnout can remain stable in position within a certain length. The calculation is analogous to that for the additional expansion force of CWR track on a bridge. Superposing the

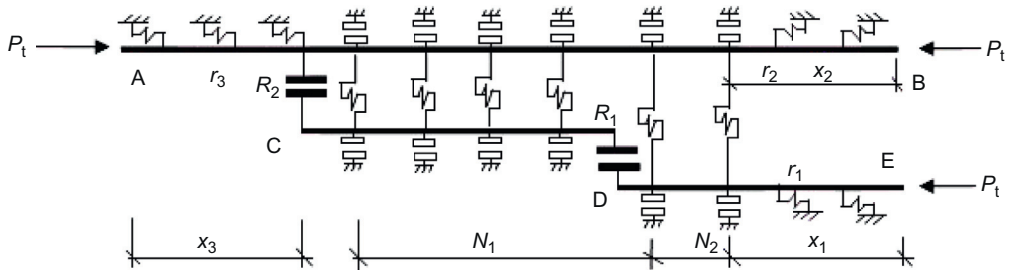

FIGURE 6.6

Calculation model of guiding rail−stock rail interaction.

components of the force transmission direction yields the diagram of additional temperature force on the stock rail of a CWR turnout.

6.2.2 DOUBLE-RAIL INTERACTION METHOD

As the turnout connects to the CWR line directly, the guiding rail will expand against resistance in case the rail temperature changes. Linked by bolts, fillers or ties, fasteners, or other coupling means, the guiding rail and stock rail form an equilibrium system. Thus, expansion of the guiding rail will introduce longitudinal force on the stock rail via coupling parts and ties, leading to displacement of stock rails and changes in the longitudinal force of rails in the turnout, and finally attaining equilibrium of forces in the system. In this process, the guiding rail must conquer such resistance forces as the longitudinal force of the line, the interaction between guiding rail and stock rail, and resistance from the retainer, filler, and crossing. The stock rail will be exposed to such forces as longitudinal force of the line and interaction between guiding rail and stock rail, as well as resistance from the retainer and filler. The model of guiding rail−stock rail interaction is depicted in Figure 6.6.

6.2.3 GENERALIZED VARIATIONAL METHOD

According to the energy variational principle based on structural analysis, the first-order variation is zero when a CWR turnout is in the equilibrium state. In other circumstances, the energy variation can be solved with the energy equations, boundary conditions of structure, and deformation compatibility conditions by assuming the longitudinal displacement function of rails. From field results, the shape function of rail longitudinal forces can be developed. After that, the rail displacement function can be derived based on the differential relation between displacement and longitudinal force, as shown in Figure 6.7. In the figures, (A) and (B) represent the curves of longitudinal force and displacement of the stock rail of a CWR swing nose turnout continuously welded in both straight and diverging directions; (C) and (D) are the curves of temperature force function and displacement of the guiding rail.

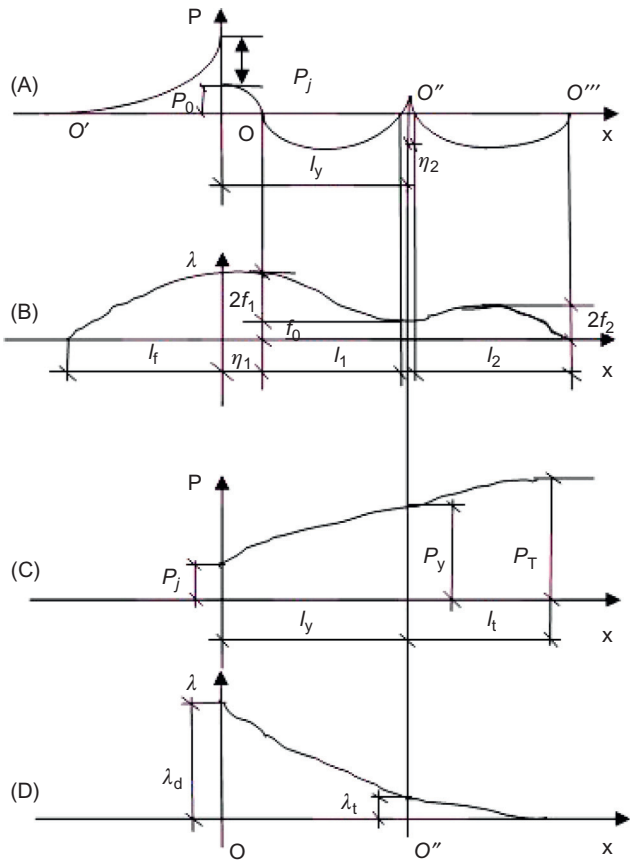

FIGURE 6.7

Function of rail longitudinal force and displacement.

6.2.4 FINITE ELEMENT METHOD [78,79]

The FEM is a generalized method for CWR turnout calculation, applicable to analyzing the effects of influential factors on turnout stress and deformation.

1. Calculation models
   a. Single CWR turnout

      In FEM, the rail and tie elements are divided by tie supporting points; the nodal displacement of the nodal temperature of rails is considered to be a variable. The longitudinal force at two ends of the rail node is balanced with the longitudinal resistance of fastening. The displacement difference of two adjacent rail nodes is proportional to the temperature force relieved by a rail element. The turnout tie is considered to be a finite long beam laterally supported on an elastic foundation, the fastening resistance on which equals the longitudinal

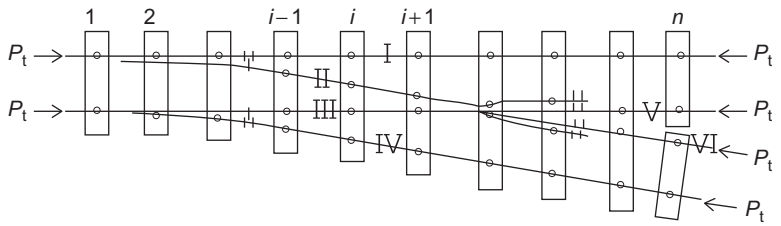

FIGURE 6.8

Calculation model of a single CWR swing nose turnout.

resistance of the bed. The retainer or filler at heel of switch rail and the filler at the end of long wing rail are all important force transmission aspects in a CWR turnout; actual values will be used to describe the relations between the resistances of those aspects and the relative displacement of the rail in calculation. Moreover, those resistances are viewed as concentrated forces applied on the rail center. The calculation model of a single swing nose turnout is plotted in Figure 6.8.

b. CWR turnout group [80]

The calculation of a CWR turnout group composed of two or more turnouts can be developed further. Practically, two single turnouts may be joined in various modes, as shown in Figure 6.9.

2. Equilibrium equation of temperature force and displacement

a. Temperature force of rail node

In a CWR turnout, each rail is divided into finite beam elements by supporting points of the ties. The finite beam element will move longitudinally under the combined action of temperature force and fastening resistance. The length of the beam element equals tie spacing. Longitudinal displacement and the temperature force of the rail node are two unknown variables of the node of the rail beam element. The temperature force is taken as the temperature force of the beam element on the left of rail node.

The stress beside the rail node is depicted in Figure 6.10. The temperature force on the left of node i is P_i, and that on the right refers to the temperature force of node $i-1$, marked as $P_{i\text{-}1}$. Given that the rail node moves to the left with respect to the tie, the direction of rail fastening resistance R_{ci} is right. Thus, the equilibrium equation for rail temperature force at node i is:

$$P_i = P_{i-1} - R_{ci} \tag{6.1}$$

When the fastening resistance is constant, R_{ci} is a fixed value. If the fastening resistance is nonlinear, it can be obtained from the displacements of rail node and tie node u_{ri} and u_{si} and the characteristic function of fastening displacement and resistance:

$$R_{ci} = f_{rc}(u_{ri} - u_{si}) \tag{6.2}$$

Considering the resistance of retainer and filler as the concentrated force acting upon the center of a beam element, given that the beam element on the right of rail node i is under

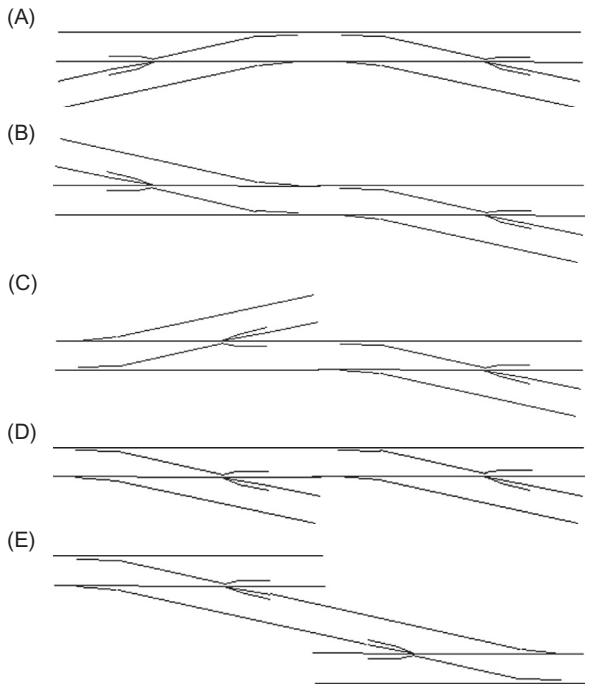

FIGURE 6.9

(A) Two turnouts with the diverging lines on one side and the fronts of turnouts connected. (B) Two turnouts with the diverging lines on opposite sides and the fronts of turnouts connected. (C) Two turnouts with the diverging lines on opposite sides and the front and rear of turnouts connected. (D) Two turnouts with the diverging lines on side and the front and rear of turnouts connected. (E) Two crossover turnouts.

some concentrated force, as shown in Figure 6.11, the equilibrium equation for the rail temperature force of rail node i is:

$$P_i = P_{i-1} - R_{ci} + F \tag{6.3}$$

For the initial rail node:

$$P_1 = P_0 - R_{ci} \tag{6.4}$$

where P_0 is the temperature force on the right of the initial node, determined as per the status of the node end and displacement compatibility conditions when the rails are welded with the section rails.

b. Displacement of rail node

Adding the displacement of node $i-1$ and the expansion displacement of the beam element on the right of rail node i gives the displacement of rail node i. Assuming that the temperature force of the rail is P_t before expansion displacement of the beam element, and $P_{i\text{-}1}$

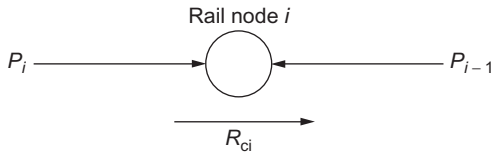

FIGURE 6.10

Stress on rail node under no concentrated force.

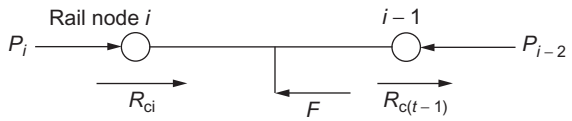

FIGURE 6.11

Stress on rail node under concentrated force.

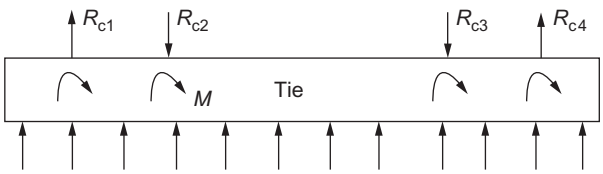

FIGURE 6.12

Stress on the tie.

after expansion displacement, according to the calculation principle of expansion displacement for CWR track, the displacement of rail node i is:

$$u_{ri} = u_{r(i-1)} + \frac{(P_t - P_{i-1})l_r}{EA} \tag{6.5}$$

where E is the elastic modulus or rail, A is the cross section area of rail, and l_r is the length of the beam element.Given that some concentrated force is applied on the center of the beam element, the displacement of node i is:

$$u_{ri} = u_{r(i-1)} + \frac{(P_t - P_{i-1} - F/2)l_r}{EA} \tag{6.6}$$

As the displacement of the initial rail node is unknown, the compatibility conditions for temperature force of the last rail node should be provided to obtain the solution.

c. Tie displacement

The tie is regarded as a finite long beam supported on an elastic foundation in a plane, divided into several finite elements by supporting points of rail. Each element node may be subject to longitudinal or angular displacement. The stress on the tie is depicted in Figure 6.12.

R_c and M denote fastening resistance and its moment on the tie top in the longitudinal direction of rail; Q is the resistance of the gravel ballast bed to the bottom and side of the tie. The resistance moment M will restrict the deflection displacement of the tie node. Given that the moment is a constant, the moment can be superposed in a load column matrix. If the resistance is nonlinear, the moment may be related to the deflection angle φ_s of the tie node:

$$M_s = f_{Mc}(\varphi_s) \tag{6.7}$$

d. Calculation equation of CWR turnout

Given the temperature force and displacement compatibility conditions, the nonlinear equation below can be developed with the equations of temperature force and displacement of the rail node and tie displacement.

$$\boldsymbol{F}(\boldsymbol{u}) = \boldsymbol{P} \tag{6.8}$$

where $\boldsymbol{u}$ is an unknown variable, $\boldsymbol{P}$ is the load column matrix.

e. Solutions

As Eq. (6.8) is strongly nonlinear, the load increment approach and newton iteration approach are adopted in solving the equation. Specifically, based on the rail laying temperature, an increase of 5°C in rail temperature is taken as a calculation step, and the initial value of each step equals the calculated result of the last step, so in the turnout, the status of a force of each step equals that of the last step. The newton iteration approach is applied. During iteration, the contact status of the combination blocks of a retainer is taken into consideration. If contacted, a new nonlinear equation is required; meanwhile, one must determine whether the fastening resistance and joint resistance are within the allowable range. The iteration may proceed only when all acting forces are stable. In this sense, the load increment approach, newton iteration, and status determination of acting forces will be performed throughout the calculation.

6.3 REGULARITY OF STRESS AND DEFORMATION OF CWR TURNOUT

6.3.1 DISTRIBUTION REGULARITY

The distribution regularities of rail temperature force and expansion displacement of a CWR turnout are explained with the example of a No. 18 CWR swing nose turnout of CHN60 rail. In the turnout, both the straight and diverting directions, as well as all joints at two ends of the turnouts, are welded. A pair of retainers (clearance between the combination blocks is 7 mm) is arranged at the heel of the switch rail. Four pairs of fillers are arranged at the end of the long wing rail with a swing nose rail. The stress and deformation of rails in straight and diverting directions are symmetric. Therefore, the distribution of rail temperature force and displacement of the turnout are as shown in Figures 6.13 and 6.14.

The point rail lies in the breathing area of the CWR turnout rear, which expands under temperature force while overcoming the frictional resistance of two groups of fillers and the longitudinal resistance of the line. The filler resistance is P_F, the displacement of the heel of point rail is u_F, so the sum of heel displacement and expansion displacement of the movable section gives the displacement of the actual point of point rail. During this process, partial force on the point rail will be transmitted to the stock rail through the longitudinal displacement and lateral bending of long ties. In this case, a small additional force will occur at position C at the heel of point rail, that is, P_C.

The heel of switch rail and end of wing rail lie, respectively, in the front and rear of the guiding rail. The filler resistance P_E acting on the end of the wing rail equals P_F, but has a different direction. The displacement of the end of the wing rail is u_E. The difference between u_E and

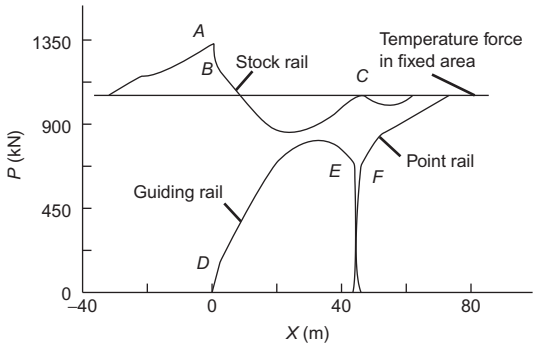

FIGURE 6.13

Distribution of rail longitudinal force in CWR turnout.

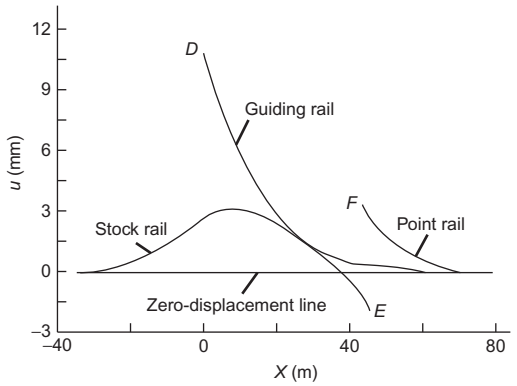

FIGURE 6.14

Distribution of rail displacement in CWR turnout.

displacement of the heel of point rail conforms to the displacement resistance characteristics of four sets of fillers. The guiding rail can be regarded as a short rail string, provided with retainer resistance P_D at the front. As the combination blocks of the retainer are mounted on the webs of the stock rail and switch rail, respectively, the stock rail will be subject to a force $P_A - P_B$, which equals but is opposite to P_D. The expansion displacements at front and rear of the guiding rail are in opposite directions. The displacement of the heel of switch rail is u_D. The difference between u_D and the displacement of stock rail at point A at the heel of switch rail is larger than the retainer clearance (7 mm), indicating that the combination blocks of the retainer will come into contact. The relative displacements of two blocks $u_D - u_A - 7$ and the retainer force P_D conform to the resistance displacement characteristics of the retainer. The displacement of the actual point of the switch rail is the sum of heel displacement u_D and displacement of the movable section.

In the process of expansion, the front of the guiding rail transfers partial longitudinal force to the long tie via fastening. Afterward, the tie will transfer part of the longitudinal force to stock rails via the fastening of stock rails against the bed resistance during the course of longitudinal displacement and lateral deformation of the tie. In this way, the stock rail will be exposed to additional temperature force. Since the resistance of fastenings under the guiding rail is smaller than the combination of resistances of the bed and outer stock rail fastening, the variation gradient of temperature force in front of the transition lead curve is approximated as fastening resistance. The maximum additional compressive temperature force of the stock rail occurs in the vicinity of the heel of switch rail, exceeding that in the fixed area by about 25−35%, or even above 40% in the most unfavorable cases.

To conclude, the resistances of bed, fastening, filler, and retainer are the major determining factors of stress and deformation of CWR turnout. Moreover, the strength and stability of stock rail, strength of filler and retainer, and the displacement verification of the switch rail and point rail form the core of CWR turnout design.

6.3.2 INFLUENTIAL FACTORS

In addition to rail temperature change and resistance characteristics of above four force transmission components (i.e., bed, fastening, filler, and retainer), turnout number, crossing and welding type, junction modes of the turnout group, rail laying temperature difference between adjacent rail links, etc. may also exert a certain influence on the deformation and stress of CWR turnout. See below for details.

1. Welding type

   Three welding types may be used for rails of a CWR turnout: fully welded type, semi-welded type, and welded turnout type. For the first type, all turnout rails are welded and the rails at turnout ends are welded to section rails. For the second type, only the rails in the straight direction of the turnout are welded, and at turnout ends, only the rails in the straight direction are welded with section rails, while those in the diverging direction are simply jointed. The last type is an intermediate, where the rails in both straight and diverting directions of the turnout are welded in the turnout area, and at turnout ends only the rails in the straight direction are welded with section rails, while those in the diverging direction are simply jointed.

   Given a rail temperature change of 50°C and ballast track, the three welding types are compared with the example of a No. 18 CWR swing nose single turnout of CHN60 rail. For the semi-welded type, common joints are used in the vicinities of heel of switch rail in the diverting direction and the actual point and heel of point rail; the 30th tie span in the rear of a long tie is connected with section rails with common joints, where the joint resistance is a constant 588 kN.

   The comparative results of deformation and stress of CWR turnout parts for the three welding types are given in Table 6.1. The distributions of rail temperature force for semi-welded and welded turnout types are plotted in Figures 6.15 and 6.16.

   For fully welded turnouts, rail stress and displacement in both straight and diverting directions are symmetric. As a considerable part of the temperature force is transmitted to CWR turnouts by the transition lead curve in the diverting direction at turnout rear, the deformation and stress of parts are significant. The rails in the diverging direction are welded. This type prevails in high-speed turnouts. For semi-welded turnouts, rail temperature changes moderately, but the retainer in the diverging direction may bear significant stress; therefore, this type is not preferable. Welded turnouts can ease the stress and deformation of turnout parts, and the stress and displacement in both straight and diverging directions are approximately symmetric. This type, jointless in the main line but jointed in the station line, is widely used in common turnouts.

2. Junction modes of turnout group

   Turnout groups exist in practice. When a group of turnouts are continuously welded, the rail stress and deformation will spread, complicating the variation regularities. Three types of turnout groups, shown in Figure 6.9, are compared with a single turnout with the example of a No. 18 swing nose single ballast turnout of CHN60 rail. In the figure, the length of the intermediate straight line between two turnouts is zero, and the turnout is of the fully welded type. In the turnout group, the single turnout on the left is referred to as a left turnout, and the right-handed one as a right turnout.

Table 6.1 Comparison of Additional Temperature Force and Expansion Displacement of Stock Rail for Different Welding Types

Additional Temperature Force	Fully Welded Type	Semi-Welded Type	Welded Turnout
Maximum additional compressive temperature force of straight stock rail (kN)	263.0	241.1	258.2
Maximum additional tensile temperature force of straight stock rail (kN)	195.7	165.4	194.5
Increase rate of additional temperature force of straight stock rail (%)	24.9	22.8	24.5
Maximum additional compressive temperature force of curved stock rail (kN)	270.7	0.0	255.6
Maximum additional tensile temperature force of curved stock rail (kN)	200.1	135.1	215.8
Increase rate of additional temperature force of curved stock rail (%)	25.6	0.0	24.2
Maximum displacement of straight stock rail (mm)	3.1	2.5	3.0
Maximum displacement of curved stock rail (mm)	3.2	−0.9	3.0
Displacement of heel of curved switch rail (mm)	10.8	10.1	10.7
Displacement of heel of straight switch rail (mm)	10.8	9.5	10.6
Displacement of heel of long point rail (mm)	2.9	2.9	2.6
Retainer resistance on straight stock rail (kN)	85.3	65.3	81.5
Retainer resistance on curved stock rail (kN)	84.4	274.4	79.8
Filler resistance on long point rail (kN)	175.2	178.0	173.8
Filler resistance on short point rail (kN)	202.9	169.4	188.4

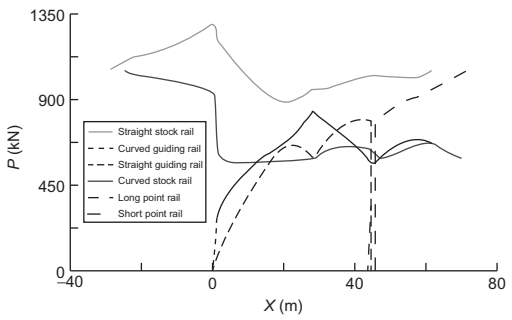

FIGURE 6.15

Rail temperature force for semi-welded type.

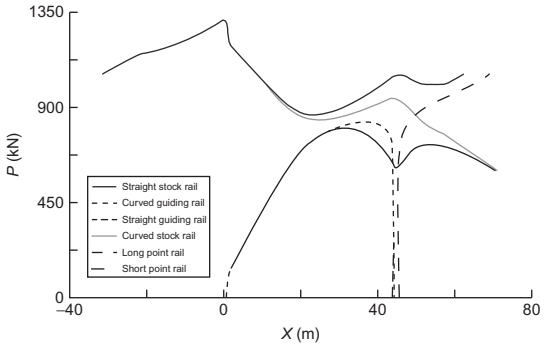

FIGURE 6.16

Rail temperature force for welded turnout type.

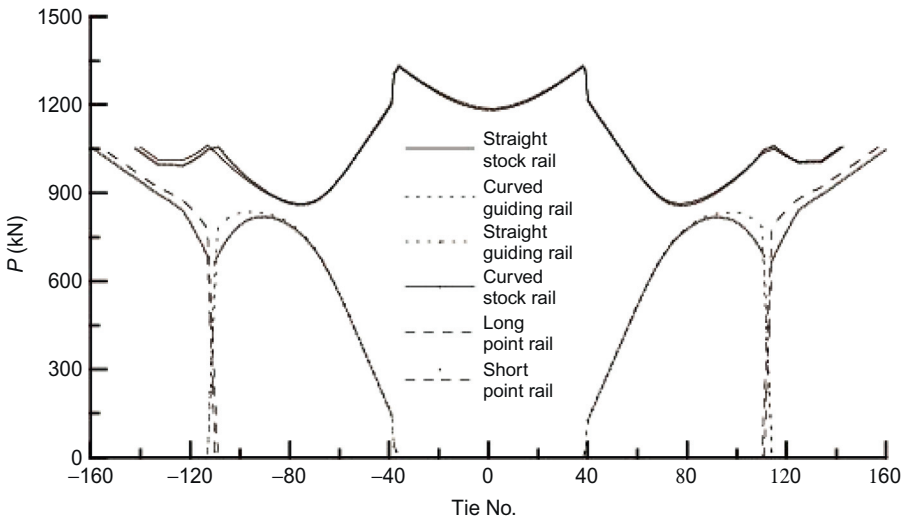

FIGURE 6.17

Rail temperature force of turnouts with diverging lines on one side and the fronts of turnouts connected.

The comparative results of additional temperature force of stock rails for turnouts of different junction modes are given in Figures 6.17–6.19, where the *x*-axis represents tie number, the zero point represents the intersection of two turnouts, " + " refers to the tie number of the right turnout (increasing from zero point to right), and "–" refers to the tie number of the left turnout (increasing from zero point to left).

According to the calculation, for the turnout group with the fronts of turnouts connected, the longitudinal force on the stock rail increases due to force superposition; for the turnout group with the front and rear of turnouts connected, the additional temperature force of stock rail, expansion displacement of switch rail and point rail, and the forces on transmission parts of the front turnout increase significantly, as additional temperature force is transmitted from the rear turnout to the front one. In conclusion, with regard to the impact degree of CWR turnouts, the turnout group with the front and rear of turnouts connected is the largest, followed by the turnout group with the fronts of turnouts connected, and then the crossover type.

3. Rail laying temperature difference of CWR turnout [81]

A CWR turnout is regarded as a rail link in a trans-section CWR track. Rail laying temperature difference occurs when two neighboring links with different rail laying temperatures are welded, which may impact the stress and deformation of the turnout.

The rail laying temperature differences between a CWR turnout and the adjacent section line are taken as 5°C, 10°C, and 15°C, and general calculation parameters apply. Table 6.2 gives the impact of rail laying temperature difference on turnout stress and deformation for a rise of 55°C in turnout rail temperature. Figures 6.20–6.23, respectively, depict the comparison of rail temperature and displacement of straight stock rail, and the variation of the maximum additional temperature force and displacement of heel of point rail with rail temperature.

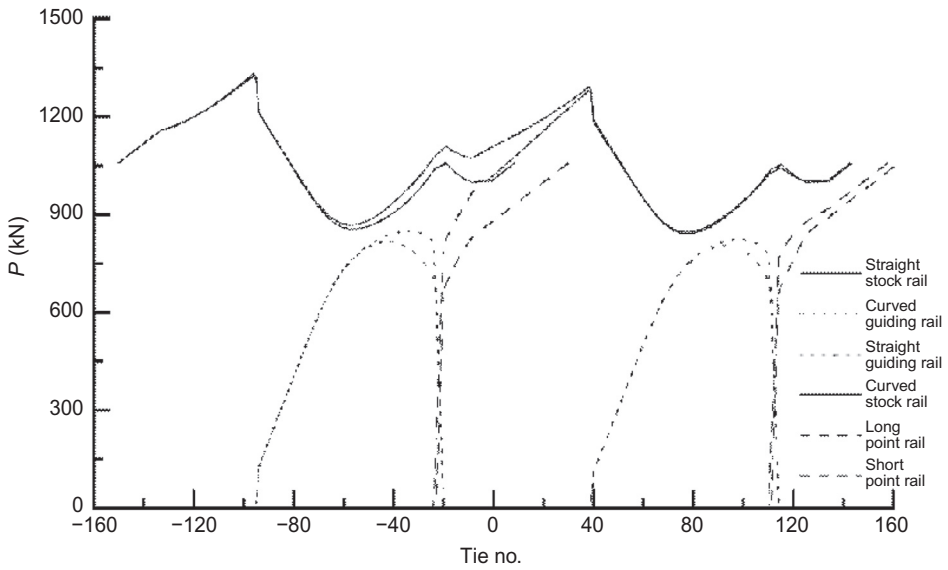

FIGURE 6.18

Rail temperature force of turnouts with the diverging lines on opposite sides and the front and rear of turnouts connected.

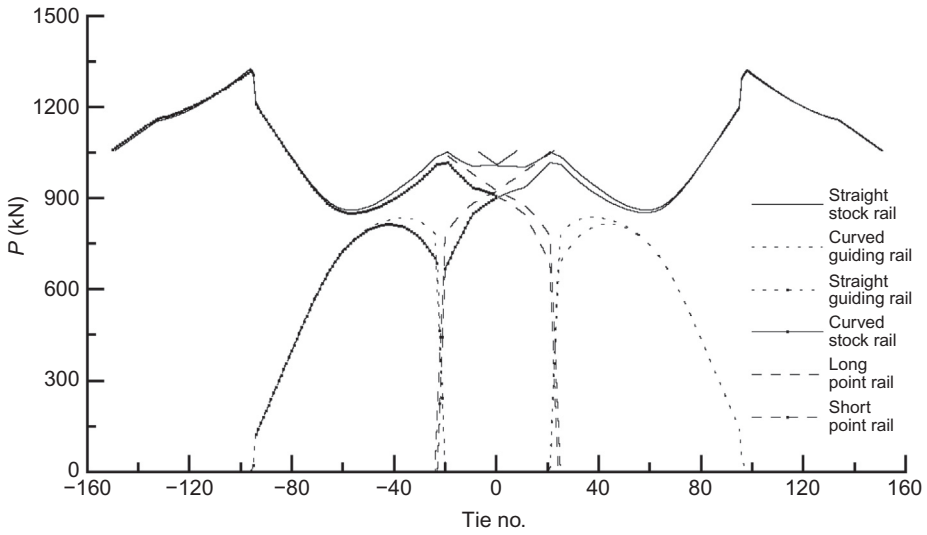

FIGURE 6.19

Rail temperature force on crossover turnouts.

Table 6.2 Comparison of Impact of Rail Laying Temperature Difference on CWR Turnout

Rail Laying Temperature Difference	0°C	5°C	10°C	15°C
Additional temperature force of straight stock rail (kN)	263.0	275.4	285.3	301.6
Increase rate of additional temperature force (%)	24.9	26.1	27.0	28.6
Maximum displacement of straight stock rail (mm)	3.1	3.1	3.2	3.2
Displacement of heel of curved switch rail (mm)	10.8	10.8	10.8	10.9
Displacement of heel of long point rail (mm)	2.9	3.2	3.6	4.2
Maximum retainer resistance (kN)	85.3	90.9	95.3	102.9
Maximum filler resistance (kN)	202.9	209.7	218.5	229.2

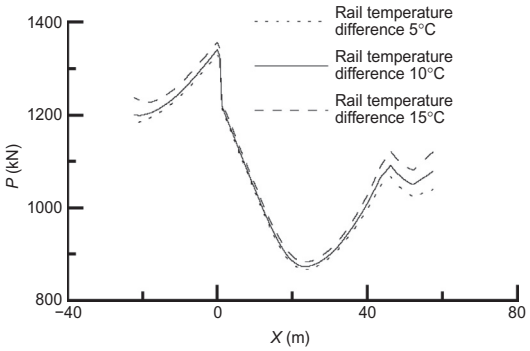

FIGURE 6.20

Distribution of temperature force of straight stock rail.

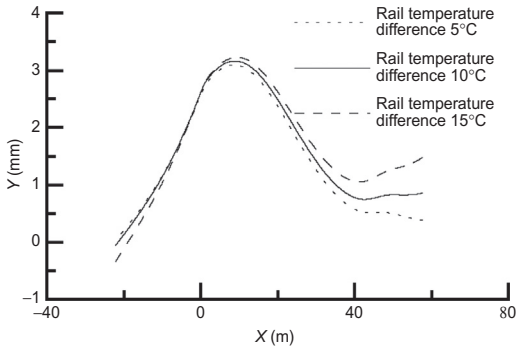

FIGURE 6.21

Distribution of displacement of straight stock rail.

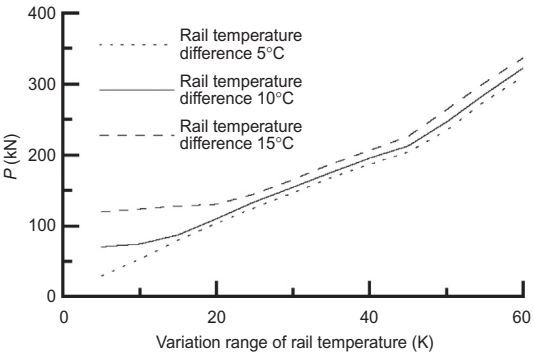

FIGURE 6.22

Variation of additional temperature force with rail temperature.

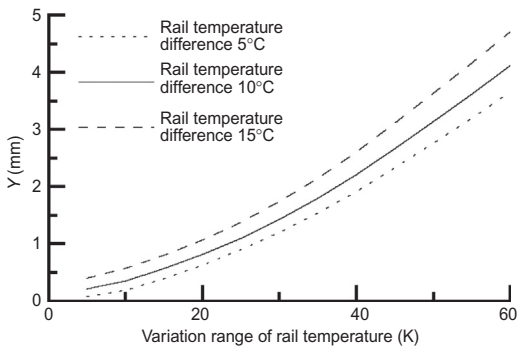

FIGURE 6.23

Variation of displacement of heel of point rail with rail temperature.

It turns out that greater rail laying temperature difference between CWR turnout and adjoining section leads to greater amounts of temperature force transmitted to the turnout. Therefore, the additional temperature force and displacement of stock rail, displacement of heel of point rail, and resistance of retainer and filler will increase with the rail temperature difference. Moreover, the displacement of the heel of switch rail will increase slightly. If the rail laying temperature of a CWR turnout is lower than that of the adjoining section, the additional temperature force of the stock rail and expansion displacement of rails will still increase despite the temperature drop. Thus, the rail laying temperature difference between CWR turnout and the adjoining section must be restricted to ease deformation and stress in the turnout.

4. Longitudinal resistance of bed [82]

Assuming that the longitudinal resistance of the 2.6-m-long tie in a section resembles that in a turnout, the tie spacing is 0.6 m, the longitudinal resistance of section bed is r, and the longitudinal resistance of bed per unit length of tie is $0.46r$. The longitudinal resistances of five types of concrete tie bed are analyzed: $r = 6.1$ kN/m (=resistance of timber tie line), $r = 7.6$ kN/m (=resistance of type-I tie line), $r = 9.9$ kN/m (test value for No. 38 turnout laid on trial in Langwopu Station of Beijing District, uncompacted bed), $r = 12.2$ kN/m (=resistance of type-II tie line), and $r = 15.2$ kN/m (=resistance of type-III tie line). Other calculation parameters are the same.

The comparative results of additional temperature force of straight stock rail under different bed resistances are given in Table 6.3; the distributions of additional temperature force of stock rail and temperature forces of curved guiding rail and long point rail are given in Figures 6.24 and 6.25, respectively.

According to the calculation, the smaller the bed longitudinal resistance, the greater the additional temperature force of stock rail. The reason lies in the fact that, when the fastening resistance of the inner rail attains slippage value, more temperature force will be transmitted to the stock rail to maintain the force balance of the tie. It can be seen that smaller bed resistance

Table 6.3 Comparison of Additional Temperature Force of Stock Rail Under Different Bed Resistances

Additional Temperature Force	$r = 6.1$ kN/m	$r = 7.6$ kN/m	$r = 9.9$ kN/m	$r = 12.2$ kN/m	$r = 15.2$ kN/m
Maximum additional compressive temperature force (kN)	276.0	274.2	263.0	244.5	219.0
Maximum additional tensile temperature force (kN)	225.9	216.8	195.7	172.0	144.2
Increase rate of additional temperature force (%)	26.1	26.0	24.9	23.2	20.7
Impact scope of additional temperature force in the front of heel of switch rail (m)	45.6	38.4	32.4	28.2	25.2
Impact scope of additional temperature force in the rear of heel of point rail (m)	26.0	20.6	16.7	14.8	13.5

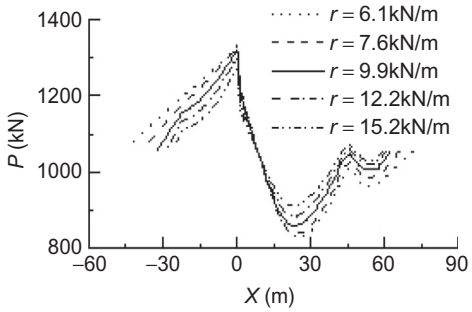

FIGURE 6.24

Temperature force of straight stock rail.

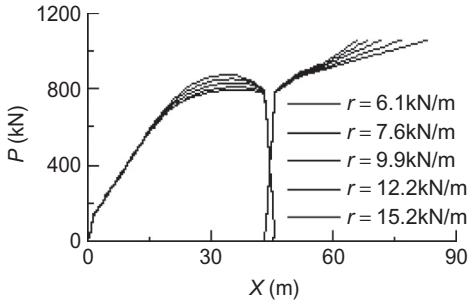

FIGURE 6.25

Temperature force of inner rail.

relates to greater effective scope of additional temperature force. Bed longitudinal force has a minor effect on the distribution of temperature force of the guiding rail and point rail, where the rail longitudinal force is mainly affected by fastening resistance.

6.4 DESIGN AND VERIFICATION

6.4.1 CONTENTS

Rail expansion displacement, strength, and turnout stability are verified by calculation in designing a CWR turnout.

1. Expansion displacement
   - **a.** Absolute displacement of switch rail

     The expansion displacement of the actual point of switch rail is the sum of displacement of heel and flexible displacement of switch rail, expressed by:

     $$\delta_1 = \delta_{10} + L_1 \alpha \Delta t \tag{6.9}$$

     where δ_{10} = displacement of heel of switch rail and L_1 = length of switch rail.
   - **b.** Absolute displacement of point rail

     The expansion displacement of the actual point of a swing nose rail is the sum of displacement of the heel and flexible displacement of the swing nose rail, expressed by:

     $$\delta_2 = \delta_{20} + L_2 \alpha \Delta t \tag{6.10}$$

     where δ_{20} = displacement of heel of swing nose rail and L_2 = length of swing nose rail.
   - **c.** Relative displacement

     For normal conversion of a CWR turnout, the relative displacements between the actual point of switch rail and stock rail, left and right switch rail, as well as between the actual point of swing nose rail and wing rail must meet the requirements of turnout structure and mechanical properties for conversion, and must meet:

     $$\delta_k - \delta_g \leq [\delta] \tag{6.11}$$

where δ_k = displacement of actual point of switch rail or swing nose rail, δ_g = displacement of stock rail or wing rail corresponding to the actual point of switch rail or swing nose rail, and $[\delta]$ = allowable displacement of the external locking device, taken as 40 mm for No. 18 turnouts in China.

2. Strength
   a. Force transmission components

      As mentioned above, in a CWR turnout, force transmission components are composed of retainers at the heel of switch rail and fillers at the end of long wing rail. The shear stress on coupling bolts of force transmission components must meet:

$$\tau = \frac{4Q}{n_1 \pi D_1^2} \leq [\tau] \tag{6.12}$$

      where Q = longitudinal force of force transmission components, n_1 = number of coupling bolts, and D_1 = diameter of coupling bolt.

   b. Rails

      Peak additional temperature force occurs at the stock rail corresponding to the switch heel and flexible center of a swing nose rail, therefore; the rail strength at this location must be verified. If a CWR turnout fails to meet rail strength requirements, the rails must be consolidated; special attention must be paid to the weld joints of a stock rail. If this does not work out, the rail laying temperature of the turnout must be adjusted.

      The verification method for rail strength is the same as that for common CWR track. The load combination of dynamic stress, temperature stress, and the additional stress of stock rail is used in verification calculation.

3. Turnout stability
   a. Turnout front

      The calculation equation of stability for common CWR track may apply to stability of the turnout front. However, it must be noted that the temperature force is evenly distributed at the turnout front; thus, a proper position must be selected for calculation verification. Generally, this place is about 4 m ahead of the actual point of switch rail. If the turnout front fails to meet stability requirements, stability may be enhanced by making sure that the bed is well filled and compacted, and the ballast shoulder is wide enough; increasing the ballast thickness properly at shoulder; or tightening the rail fastening. If these measures fail, the rail laying temperature of the CWR turnout and section may be increased appropriately.

   b. Turnout area

      When verifying the stability in the turnout area, only the switch is considered. This is because the transition lead curve has greater lateral bending stiffness, and no track buckling may occur. The calculation of stability in common CWR track may apply to stability of the turnout rear, but it does not apply to a switch that has one curved rail only. The equation for compressive temperature force of a CWR turnout can be derived based on the fundamental theory of uniform equations for the stability of CWR track, where the load combination of temperature force and additional compressive temperature force of stock rail is employed. When the turnout rails are welded in both straight and diverting directions, the allowable temperature pressure is expressed by:

$$P = \frac{(EI_y(\pi^2/l^2) + (3lr/2))(f + f_{0e}) + (4/\pi^3)Ql^2 + (2l^3 r/\pi^3)((1/R_c) + (1/R_{0p}))}{2(f + f_{0e}) + (4l^2/\pi^3)((1/R_c) + (1/R_{0p}))} \tag{6.13}$$

where

R_c = radius of transition lead curve
r = gradient of longitudinal resistance of the line
f = allowable lateral deformation of turnout rail, taken as 0.2 cm
f_{0e} = rise of initial elastic bending, taken as 0.3 cm
l = length of deformed curve, the initial value of which is 400 cm; and
f_{0p} = rise of initial plastic bending, taken as 0.3 cm.

Q is the equivalent lateral resistance of bed, $Q = q_0 - (\pi C_1/4)f + (\pi/2)C_1C_nf^n$, where $C_nl_0 = \int_0^1 \sin^{n+1}(\pi X/l)\mathrm{dX}$. The lateral bed resistance is expressed by $q = q_0 - C_1y + C_2y^n$ $(n < 1)$. Given that 1760 pieces of Chinese type-II reinforced concrete ties are laid per kilometer of ballast bed, $Q = 85$ N/cm, but $Q = 89$ N/cm when 1840 pieces are laid per kilometer. Moreover, $Q = 115$ N/cm when 1667 pieces of Chinese type-II reinforced concrete ties are laid per kilometer of ballast bed. Substituting the calculated extreme value of l into Eq. (6.13) gives the critical compressive temperature force of instability at the switch heel of a CWR turnout. The allowable temperature rise in the turnout area can be obtained after considering a safety factor of 1.3.

6.4.2 DESIGN OF RAIL LAYING TEMPERATURE OF CWR TURNOUT

A CWR turnout is a rail link whose design rail laying temperature should be consistent with that of the adjoining rail link to facilitate field management.

The actual rail laying temperature equals the design value $\pm 3{-}5$°C. When the verified items fail to meet the requirements, the actual rail laying temperature will be adjusted.

The rail laying temperature difference between two adjoining rail links must not be greater than 5°C. In a trans-section CWR track, the difference between the maximum and minimum rail laying temperatures in a railway line must not be greater than 10°C.

6.4.3 ARRANGEMENT OF CREEP OBSERVATION STAKES

The rail displacement of a CWR track should be observed periodically to detect any displacement abnormality, locking performance after repeated maintenance and repair, and the condition of original rail laying temperature after construction operations. With the analysis of observation data, any abnormal displacement detected must be corrected immediately.

Observation stakes are used to measure displacement. Different numbers of creep observation stakes are arranged at the breathing area and fixing area of a CWR track. These stakes divide the long rail into several fixed observation areas, which will be observed periodically. Generally, the creep of a CWR track is observed on a monthly basis (semi-monthly in the hot season). Observation is to be performed on the same day for all track subdivisions. Otherwise, discrepancies may exist among observation results, as certain trans-section long rails are not observed at the same time, which will further affect calculation accuracy.

The provision of creep observation stakes in a CWR turnout aims to control the rail laying temperature of the turnout, preventing track buckling, inordinate flexible displacement of actual point of switch rail and swing nose rail, and conversion failure. Limited by turnout length, inhomogeneous temperature force and displacement of rails, different operating conditions, and differential

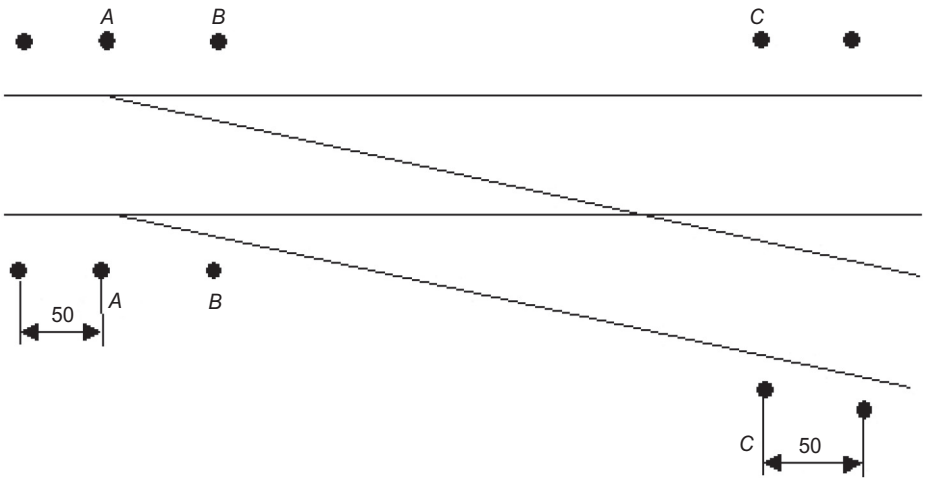

FIGURE 6.26

Arrangement of observation stakes for tracing the displacement of a single turnout (m). *Note*: In the figure, "•" represents a displacement observation stake; *A*, *B*, and *C* denote the observation stakes arranged at turnout front, retainer, and turnout rear, respectively.

change regularity and impact of rail laying temperature as compared with a section, the observation stakes will be arranged in a special way.

A CWR turnout is an important part of a CWR track, whose stress and deformation regularity is rather complex. During construction, welding is performed first in the turnout area, and then between turnout rails and long rail strings of the section under proper rail laying temperature. In this process, the turnout is regarded as a special rail link. Additionally, a CWR turnout is a major subject of observation in trans-section CWR track, provided with displacement observation stakes at the turnout front, turnout rear, and switch heel, notwithstanding it is less than 200 m long. Consequently, a CWR turnout is seen as a rail link in designing a trans-section CWR railway line.

For a trans-section CWR track, it is vital to determine any change in rail laying temperature and distribution of rail longitudinal force with the data from creep observation stakes and relevant calculation results. The arrangement of observation stakes for tracing the displacement of rail links in the section and turnout must follow the requirements as shown in Figure 6.26.

The arrangement of observation stakes must meet the requirements as specified in *Rules for Maintenance of Railway Line*. Specifically:

1. Observation stakes may be installed at the shoulder in a section or at the platform in a station
2. Clearance between observation stakes and ballast toe/shoulder edge shall be not greater than 0.3 m
3. At a narrow shoulder, observation stakes may be installed in the middle of the shoulder
4. At subgrade, observation stakes shall be buried at least 0.5 m below the maximum freezing depth line; and
5. On a bridge, observation stakes may be installed on the stable ballast retaining wall on the deck in the vicinity of a fixed bridge support (or installed on a protecting wall for ballastless track).

The observation stakes shall be securely buried and marked immediately after being placed at two ends of a rail link. The marks shall be prominent, durable, and reliable.

6.4.4 WELDING SEQUENCE FOR LARGE NUMBER TURNOUT

The following requirements shall be met in welding a CWR turnout:

1. Facilitating the geometrical adjustment of turnout rails to ensure laying accuracy
2. Controlling the displacement of turnout parts to ensure installation accuracy
3. Facilitating the destressing of inhomogeneous stress on rails produced during welding
4. Preventing the force transmission structure at the heel of switch rail from excessive load; and
5. Maintaining the integrity and geometrical smoothness of turnout structure.

Welding principles for large number CWR turnouts (e.g., Chinese No. 62 turnout): Welding is performed first in the turnout area, and then between the turnout and section; when welding the turnout, welding is performed from turnout rear to front, from straight to curved rails, and from outer to inner; when welding with the section, welding is performed from front to rear, and from outer to inner at turnout rear. During this process, straight and curved stock rails or guiding rails shall be welded simultaneously (i.e., the rails of the same type, such as ① and ②, or ③ and ④ as shown in Figure 6.27, shall be welded simultaneously). In addition, the temperature difference between two adjoining weldings shall be lower than 2°C.

As the speed is higher in a straight line than in a diverging line, welding from straight rails to curved rails can ensure greater smoothness in the straight direction of the turnout.

By welding from turnout rear to front, the rail stress produced in welding can be effectively relieved to mitigate related deformation.

By welding from outer to inner, that is, welding the stock rails before the guiding rails, the high integrity and stability of the turnout can be ensured. Moreover, this sequence facilitates positioning in welding the inner rails, conducive to maintaining geometrical accuracy of the turnout.

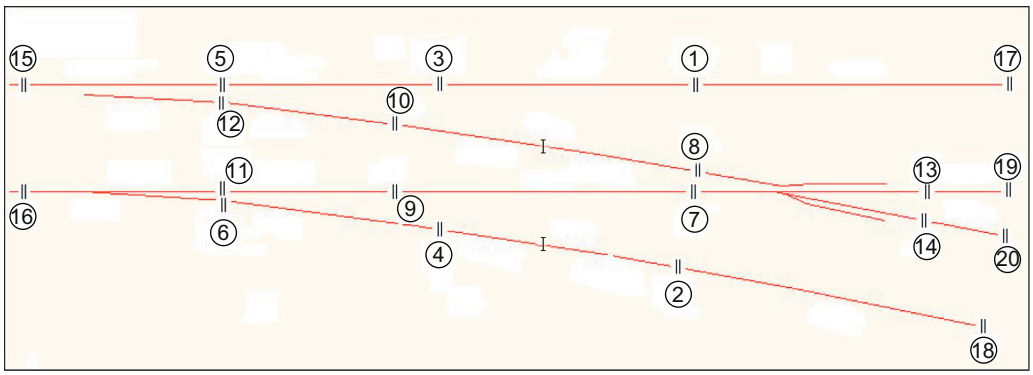

FIGURE 6.27

Welding sequence of rail joints for No. 62 CWR turnout in China.

By welding the rails of the same type simultaneously while keeping the temperature difference of two consecutive weldings under 2°C, the stress and deformation of straight and curved rails are consistent, conducive to maintaining turnout integrity.

Welding the rails in the turnout before joining with section rails is conducive to the accuracy of integral geometry of the turnout and rail destressing.

6.4.5 LAYOUT PRINCIPLE FOR TURNOUT GROUP

As shown above, smaller turnout numbers and spacing between two turnouts correspond to greater impact of the layout of a turnout group on stress and deformation of CWR turnouts. Further, for smaller longitudinal resistance of the bed, the layout of a turnout group may impact the stress and deformation of the turnout significantly.

In verifying the CWR turnout group in a station, the influence of the length of the intermediate straight line between two turnouts must be taken into account. Suppose the turnouts in the main line are arranged with fronts connected; when trains travel in two diverging lines at the same time, the minimum length of the rail interpolated between two turnouts is 50 m. Limited by the length of the station site, it will be 33 m. If no trains travel in two diverging lines at the same time, or the turnouts are arranged with front and rear being connected, it will be 25 m. If the turnouts in a receiving-departure line are arranged with front and rear connected, the length will be 12.5 m, or it will be 25 m if they are arranged with fronts connected.

6.4.6 LAYOUT PRINCIPLE FOR CWR TURNOUT IN TUNNEL

Operations are rather challenging in tunnels with confined space, bad ventilation and lighting, and even harmful gas in some long tunnels, as well as inconvenient maintenance and unfavorable working conditions. In this regard, section or trans-section CWR tracks may have some advantages in reducing maintenance load and improving working conditions and efficiency. The temperature change in the tunnel will not be directly affected by sunlight, demonstrating a much milder annual temperature change than general sections (about 20°C lower). This is very conductive to laying CWR tracks.

Observations show that the rail temperature of CWR tracks and ambient temperature in tunnels may follow certain rules. The ambient and rail temperature in tunnels is basically the same in summer and winter. In summer, the ambient and rail temperature is 20−30°C lower than that outside, while in winter, it is 3−8°C higher than that outside. There is a temperature transition between the tunnel and the outside, whose length is dependent on the length, direction, and ventilation conditions of the tunnel, generally taken as 10−50 m.

The great temperature differences and significant differences in rail temperature force between the tunnel and outside lead to inhomogeneous temperature force in fixed areas of CWR track. There is a rail temperature transition between the tunnel and outside. The greater the rail temperature difference between the tunnel and outside, the greater the gradient of rail temperature change. According to the principle of temperature, different rail temperatures correspond to different temperature forces, so a temperature force transition exists. However, this temperature force change involves an inconsistent change of rail temperatures, different from that in the breathing area of CWR track. In addition, the conditions of rail displacement are also different. In a rail temperature

transition in a trans-section CWR track, the gradient of temperature force change relates to longitudinal resistance of the bed and the change range of rail temperature at corresponding positions. In another sense, those factors are correlated as per certain rules. The gradient change of temperature may be controlled within an allowable range by dividing the rail into several rail links.

6.4.7 LAYOUT PRINCIPLE FOR CWR TURNOUT ON BRIDGE

China covers a vast territory. Affected by environment protection or land saving policies or geological conditions, some stations may be set on bridges or viaducts during the construction of high-speed railways, passenger lines, mixed passenger and goods express railways, and urban mass transit systems. Trans-station CWR tracks may be laid on a bridge. CWR turnouts on a bridge involve the technologies of CWR turnouts, CWR track on bridge, and adaptability of bridge and rail foundation to turnouts. The complicated relation between rail stress and deformation of CWR turnouts and bridge−rail interaction of CWR turnouts on the bridge must be taken into account at the same time. In this case, the issues of CWR turnouts on bridges cannot be explained with the theories and practice of CWR track on bridges or CWR turnout solely. The technologies of CWR turnouts on bridges will be detailed in Chapter 7.

CHAPTER

DESIGN OF CWR TURNOUT ON BRIDGE

7

Two key technological obstacles must be overcome for continuously welded rail (CWR) turnout on bridge.

Longitudinal turnout−bridge interaction: CWR turnouts and CWR track on a bridge are two challenging technologies for high-speed railway (HSR) lines, since trans-section CWR track applies along the whole line. As for CWR turnout on bridge, a complicated longitudinal turnout−bridge interaction system takes shape with the mutual influence of expansion of turnout inner rails and expansion of the bridge.

Dynamic turnout−bridge interaction: The structural complexity and irregularities are correlated for a turnout, affecting traveling speed. For a CWR turnout on bridge, the greater impact in the turnout area will aggregate the dynamic response of bridge; moreover, the vibration of the bridge will reduce riding safety, quality, and comfort in a high-speed turnout. Therefore, ensuring riding safety and quality in a high-speed turnout on a bridge becomes another technological challenge for railway designers.

7.1 REGULARITY OF LONGITUDINAL INTERACTION OF CWR TURNOUT ON BRIDGE

CWR turnouts on bridges are quite different from CWR tracks on bridges. In terms of structure, CWR tracks are simple, with the same structure on all bridge spans, whereas turnout structure varies with bridge spans. Thus, the turnout−bridge relative position will be considered in calculation. In view of calculation theories, for CWR track on bridge in the fixed region of CWR line, the temperature force is induced by bridge expansion, but has nothing to do with temperature change range. As for CWR turnout on bridge, even if no bridge expansion exists, the inherent expansion of inner rails will cause rail temperature change, leading to interaction between turnout and bridge. Thus, taking into account the influences of track longitudinal resistance and longitudinal horizontal stiffness of bridge substructures, a complete analysis model of turnout−bridge systems must be developed to explore the distribution regularity of longitudinal force and displacement of CWR turnout on bridge.

7.1.1 TURNOUT−BRIDGE−(SLAB)-PIER INTEGRATED MODEL

For a CWR turnout on bridge, turnout−bridge interaction is not completely the same as rail−bridge interaction in a CWR line. Temperature change in the bridge beam, vehicle load, braking/acceleration

Design of High-Speed Railway Turnouts.

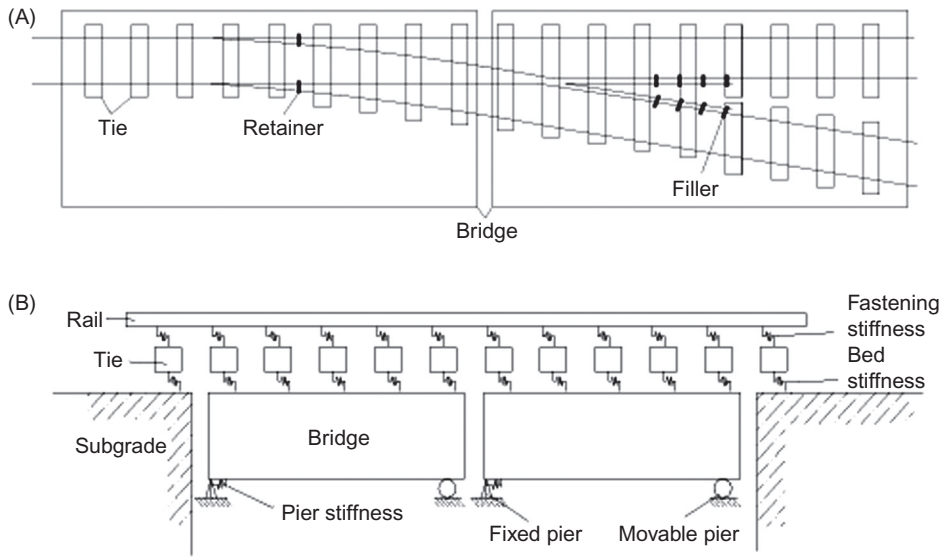

FIGURE 7.1

(A) Model of CWR turnout on bridge (plan). (B) Model of CWR turnout on bridge (elevation).

of vehicles, and thermal expansion of inner rails will cause relative displacement between bridge beam and track (including turnout) on a bridge. This displacement induces additional longitudinal force in the rail, but imposes a counterforce of the same amount in the opposite direction on the bridge deck. With the force transmission among beam, bearing, and pier, a mechanical equilibrium system is formed between bridge and track (including the turnout) on a bridge. Turnout–bridge interaction forces consist of temperature force, flexural force, rail breaking force, and braking force. Normally, these longitudinal forces are assumed not to interfere with each other for CWR turnout on bridge, and will be calculated separately. In practice, since CWR turnouts on bridges are generally near a station and exposed to frequent braking and starting of vehicles, flexural force and braking force may be superposed.

1. Integrated calculation model of track–bridge–pier for ballasted track [85]

   Refer to Figure 7.1 for modeling details. In the model of a ballast CWR turnout on bridge, as the inner rails expand, the tie will move and deflect longitudinally. In this process, the force will be partially transmitted to stock rail via fastenings, and partially to the bed and the bridge through ties. Longitudinal displacement will occur on the bridge deck due to expansion or flexion. The force transmitted to the pier from a turnout causes longitudinal displacement on the pier top and induces the longitudinal displacement of the bridge. Meanwhile, bridge displacement will be transferred to turnout through the bed, leading to redistribution of longitudinal force of the rail, affecting the deformation and stress of the bridge.

   Thus, rails, ties, bridge, and piers constitute a mutually interacting and interfering coupled system. An integrated model is helpful to better explore the deformation and stress regularities of turnout and bridge. In the coupled system, all resistances are nonlinear; however, normal resistances or linear resistances may also be taken into account. Single turnouts or turnout

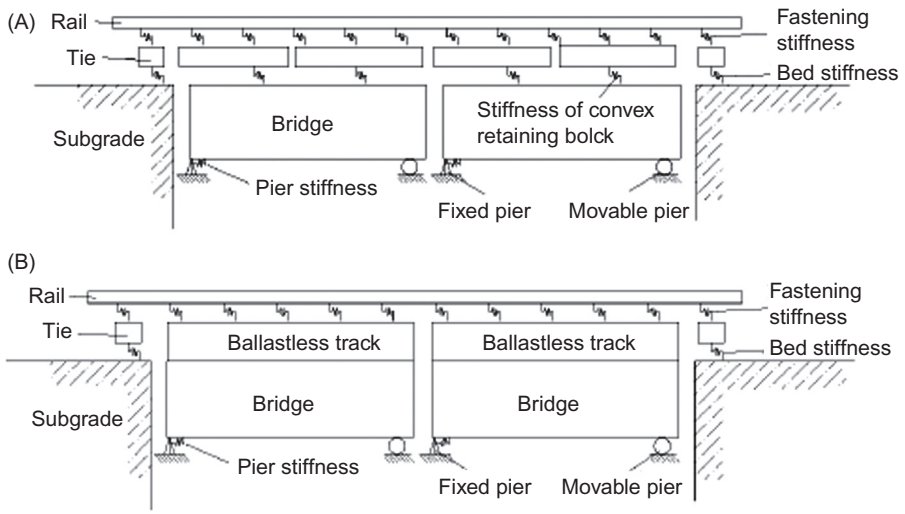

FIGURE 7.2

(A) Model of ballastless CWR turnout on bridge with longitudinal convex retaining blocks (elevation). (B) Model of ballastless CWR turnout on bridge with Π-shaped reinforcements.

groups are available. The bridge beam may be of a simply supported type, continuous type, or other type. To avoid boundary effects, a certain length of track on common subgrade will be considered adjacent to two ends of the bridge.

2. Integrated calculation model of track−bridge−pier for ballastless track [86]

   See Figures 7.1A and 7.2 for plan and elevation of the model, respectively. For a ballastless CWR turnout on bridge, the turnout is laid on reinforced concrete slabs. If an intermediate course is constructed in between, relative sliding is allowed between the turnout and the slab. The force is transmitted via longitudinal or lateral convex retaining blocks, and the interaction between turnout and bridge differs from that in a ballast track. In this case, the CWR turnout on bridge can be viewed as a three-tier system composed of turnout, slabs, and beams. The fasteners between the turnout and slab are modeled with springs, and the slabs and beams are coupled by springs, as shown in Figure 7.2A. If the slabs and bridge are connected by Π-shaped reinforcement, no relative sliding is allowed between the turnout and slab. In this case, the CWR turnout on bridge can be regarded as a two-tier structure composed of turnout and beams, as shown in Figure 7.2B.

3. Integrated calculation model of turnout−slab−bridge−pier for ballastless track with longitudinally coupled base slabs.

   For a ballastless CWR turnout on bridge with base slabs longitudinally coupled, the turnout, turnout slabs, base slabs, bridge beams, and piers will be integrated and an integrated model of the turnout−slab−bridge−pier will be established to analyze deformation and stress. In the model, the influences of longitudinal resistance of fastening, longitudinal resistance between turnout slabs and base slabs, frictional resistance of sliding course between base slab and bridge, expansion stiffness of base slab, longitudinal horizontal stiffness of pier top, and other critical parameters will all be analyzed. The model is shown in Figure 7.3.

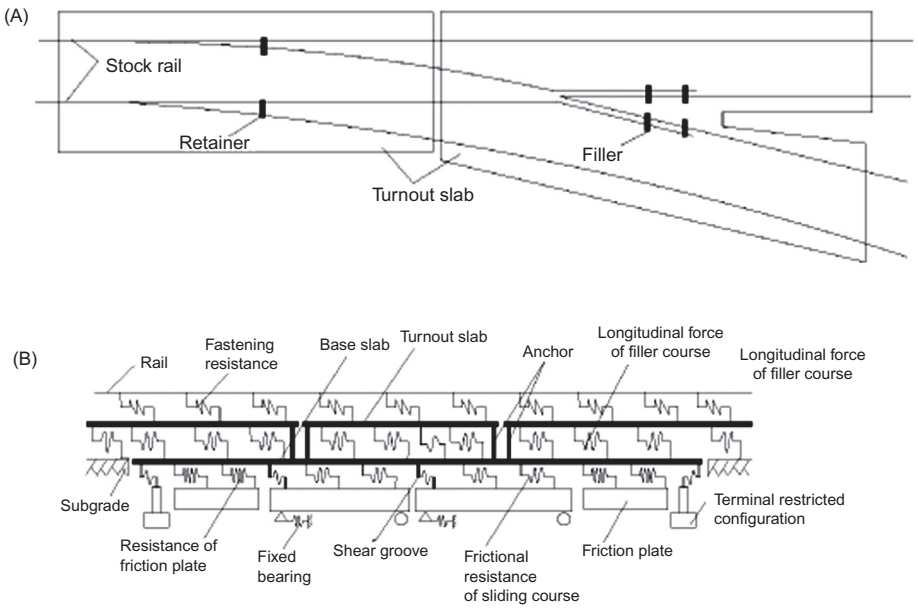

FIGURE 7.3

(A) Model of ballastless CWR turnout on bridge with longitudinally coupled base slabs (plan). (B) Model of ballastless CWR turnout on bridge with longitudinally coupled base slabs (elevation).

In the model, the interactions among rails, fillers, retainers, turnout slabs, base slabs, bridge, piers, friction plate, terminal restricted configuration, longitudinal and lateral convex retaining blocks on base slabs, and shear grooves between base slabs and bridge are analyzed. The longitudinal resistances of the rail−turnout slab, turnout slab−base slab, base slab−bridge, and base slab−friction plate are assumed to be nonlinear to make the calculation model more accurate. BTWRC, a generalized calculation program for longitudinal interaction between a bridge and welded turnout on the bridge, is developed based on the above model.

7.1.2 REGULARITY OF LONGITUDINAL INTERACTION BETWEEN SIMPLY SUPPORTED BEAM BRIDGE WITH BALLAST TRACK AND TURNOUT [87]

In many countries, CWR turnouts are not laid on simply support beams for HSRs. It is believed that significant additional temperature force and displacement will occur at the seam of beams, which will affect the stability and geometry of a turnout. Great dynamic impact will occur when a high-speed train passes through the seams. Therefore, the weak parts of a turnout, such as the switch and crossing, are not allowed to be laid on seams of beams. For a 200 km/h speed-up railway in China, certain CWR turnouts are laid on simply supported beams due to the restriction of the bridge structure; however, the switch rails and point rails are not laid on seams. Studies are focused mainly on regularities of stress and deformation of CWR turnouts on a

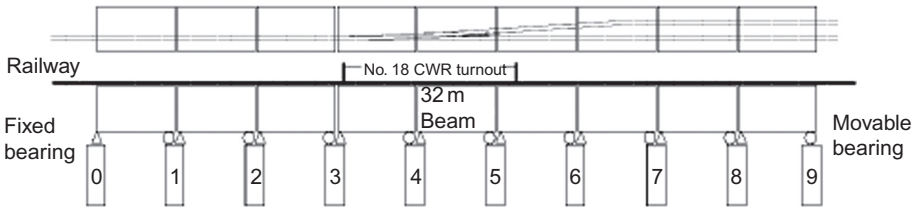

FIGURE 7.4

Layout of turnout and bridge beams.

simply supported beam bridge with ballast track, hopefully avoiding peak additional force in the turnout and minimizing integral creeping of the turnout.

1. Calculation parameters

   Take a Chinese No. 18 CWR turnout for 250 km/h on a 9×32 m simply supported beam bridge, for example; the turnout is laid on three spans in the middle. See Figure 7.4 for turnout–bridge layout.

   The longitudinal resistance is taken as 12 kN per tie in the ballast section. In the turnout, the unit longitudinal resistance per tie is 4.6 kN/m, and the tie spacing is 0.6 m. Fastening resistance is taken as the normal resistance of type-II fasteners, that is, 12.5 kN per set. The temperature change range of bridge is 15°C. The longitudinal stiffness of abutments at two ends is 1×10^7 kN/m, and the stiffness of intermediate piers is 1×10^5 kN/m. The beam is a monolithic box beam type. The distances between the centroid of the section and top flange and lower flange are, respectively, 1.6266 and 1.5774 m. The moment of inertia of cross section is 3.7044 m^4/line.

   For comparison, the bridge span, bearing layout, bridge beam structure, pier/abutment stiffness, etc. of ordinary CWR track on bridge are the same as CWR turnout on bridge, except that two tracks are laid on the bridge. The structure, bed, and fastening stiffness, etc. of a CWR turnout on subgrade are the same as CWR turnout on bridge.

2. Temperature force

   For temperature change range of 50°, the comparative results of temperature forces and longitudinal displacement of a ballast CWR turnout on bridge, CWR track on bridge, and CWR turnout on subgrade are given in Figures 7.5 and 7.6, respectively. In the figures, the x-axes represent distance to the left abutment, positive on the right; the y-axes represent temperature force (compressive force = positive) and displacement (right = positive), respectively.

   From the calculation results, the maximum additional temperature force of rails in CWR turnout on bridge is far greater than that in ordinary CWR track on bridge, and above that in a turnout on subgrade. Additionally, the longitudinal force of the pier/abutment is much greater than ordinary CWR track on bridge, which will rise with the change amplitude of rail temperature. However, for ordinary CWR track on bridge at a fixed area, the longitudinal force of the pier will only change with the temperature of the bridge, not the rail.

3. Flexural force

   The flexural force of CWR turnout on bridge is calculated with Chinese standard railway live load in the following four cases.

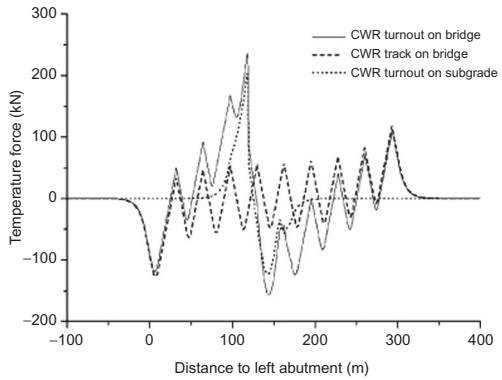

FIGURE 7.5

Additional temperature force of straight stock rail.

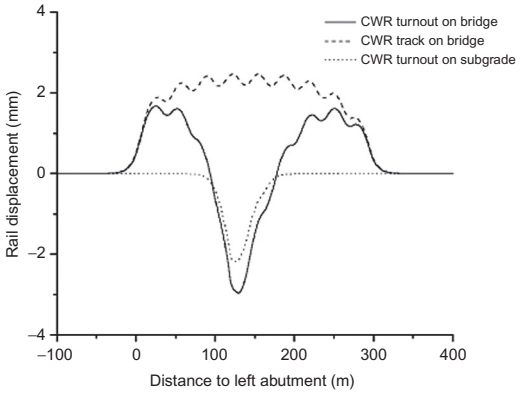

FIGURE 7.6

Longitudinal displacement of straight stock rail.

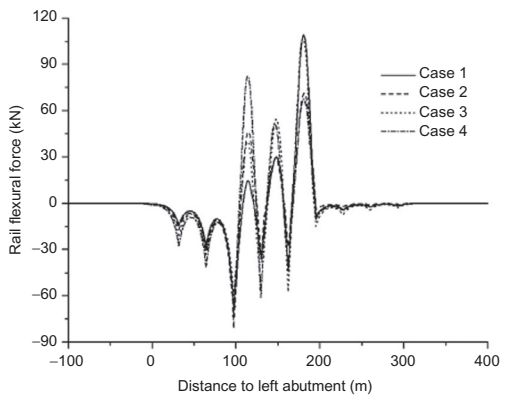

FIGURE 7.7

Additional flexural force of stock rail.

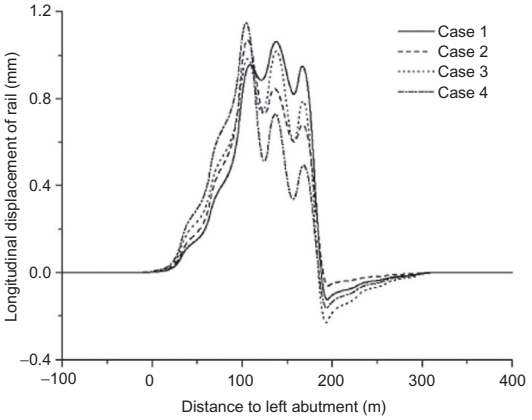

FIGURE 7.8

Flexural displacement of stock rail.

Case 1: from left to right, full-span load on all beam spans in the main line in the turnout area, no load in the diverging line

Case 2: from right to left, full-span load on all beam spans in the main line in the turnout area, no load in the diverging line.

For comparison, two load cases for flexural force of ordinary CWR track on bridge are considered simultaneously:

Case 3: from left to right, full-span load on all beam spans in the main line, no load in the diverging line; and

Case 4: from right to left, full-span load on all beam spans in the main line, no load in the diverging line.

The comparative results of flexural force and displacement of straight stock rails of the turnout with ordinary CWR track on bridge are depicted in Figures 7.7 and 7.8, where the *x*-axes

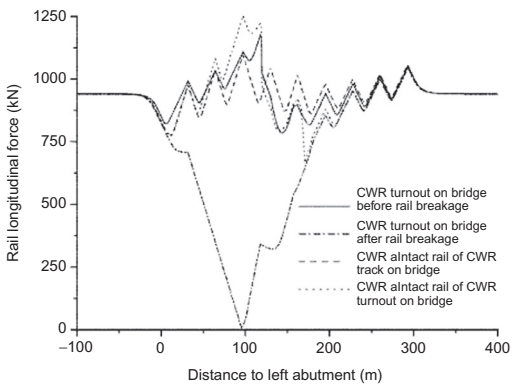

FIGURE 7.9

Distribution of rail breaking force in case 1.

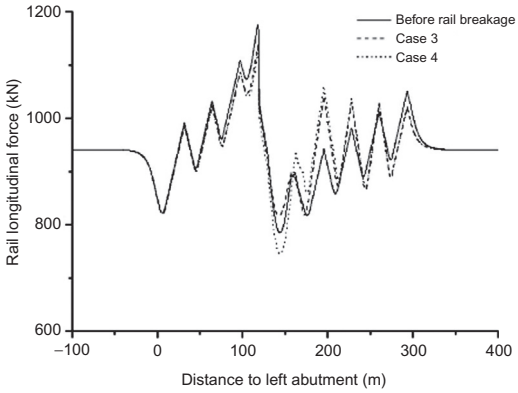

FIGURE 7.10

Comparison of longitudinal force of intact stock rail.

represent distance to left abutment, and *y*-axes represent additional flexural force of rail (compressive force = positive).

From the calculation results, the distribution regularity of additional flexural force of CWR turnout on bridge differs from that of ordinary CWR track on bridge. This is determined not only by riding direction and bearing layout, but also by turnout−bridge relative location, relative direction of turnout, fixed bearing of bridge, etc. Calculation is performed according to actual conditions.

4. Rail breaking force

Rail breakage may occur at places with the maximum longitudinal force of rail, normally at bridge ends, where greater additional temperature force may appear. The breakage of one rail is considered in calculation.

The calculation is deduced from the regularity of additional temperature force of CWR turnout on bridge, as shown in Figure 7.5, in combination with six cases given below:

Case 1: breakage of straight stock rail at beam end in turnout front

Case 2: breakage of curved stock rail at beam end in turnout front

Case 3: breakage of straight stock rail at pier/abutment in turnout rear

Case 4: breakage of long point rail at pier/abutment in turnout rear

Case 5: breakage of short point rail at pier/abutment in turnout rear; and

Case 6: breakage of curved stock rail at pier/abutment in turnout rear.

In calculating rail breaking force, temperature rise of rail and bridge, as well as the turnout−bridge system are taken into consideration. Moreover, only one rail is broken; other rails are in normal condition. As far as case 1 is concerned, the distribution of longitudinal force after rail breakage is depicted in Figure 7.9 (tensile force = positive).

If the straight stock rail is broken, the longitudinal force at the broken gap is zero, and that in the CWR turnout is small. However, the increase in longitudinal displacement of turnout ties and bridge leads to increasing longitudinal force of curved stock rail at the position corresponding to the broken gap, from 1108.1 to 1254.8 kN (Figure 7.10).

For a temperature drop of 50°C for turnout rails, the calculation results for six cases are given in Table 7.1, where the right displacement and right longitudinal force of pier/abutment are positive.

Table 7.1 Comparison of Calculation Results

Calculation Results	Case 1	Case 2	Case 3	Case 4	Case 5	Case 6
Maximum longitudinal force of intact stock rail (kN)	1252.2	1254.5	1141.1	1137.4	1130.8	1139.3
Rail broken gap (mm)	59.8	60.7	46.3	43.6	43.8	45.8
Maximum stress of retainer at heel of switch rail (kN)	218.2	221.7	116.2	106.5	107.1	116.1
Maximum stress of filler at end of wing rail (kN)	135.9	133.6	166.8	159.5	159.3	167.8
Displacement of point of straight switch rail with respect to tie (mm)	21.4	1.8	18.8	18.8	18.7	18.5
Displacement of point of curved switch rail with respect to tie (mm)	1.8	21.4	18.5	18.7	18.8	18.8
Displacement of point of point rail with respect to tie (mm)	6.1	5.7	7.7	4.8	7.5	8.0
Longitudinal force of pier 3 (kN)	616.1	618.3	343.3	361.4	362.3	343.5
Longitudinal force of pier 4 (kN)	897.4	897.6	357.3	454.0	457.7	358.2
Longitudinal force of pier 5 (kN)	742.8	712.0	203.3	118.0	107.5	197.2

As can be seen from Table 7.1, rail breakage in the turnout front (either in the main or diverging line) causes an increase in the maximum longitudinal force of intact stock rail. The broken gap, longitudinal displacements of switch rail/point rail with respect to tie, and longitudinal force of pier/abutment are greater than for the case in which the rail breakage occurs on the right of a continuous beam in turnout rear. In case of rail (straight or curved stock rail, or long or short point rail) breakage on the right of a simply supported beam in turnout rear, the longitudinal force of intact stock rail, broken gap, longitudinal displacement of switch rail/point rail with respect to ties, and longitudinal force of pier/abutment of a continuous beam are similar, but smaller than rail breakage in the turnout front. This is because the expansion displacements of inner rails and broken rail are opposite. To control the broken gap, maximum longitudinal force of rail should not occur in the turnout front for CWR turnout on bridge; in other words, rail breakage should not occur in front of inner rail expansion.

5. Braking force

The braking force is calculated with the Chinese standard railway live load, based on the wheel−rail friction coefficient 0.164 and an action length of three beam spans in the turnout. The expansions of bridge and inner rails are not considered. The following four cases apply:

Case 1: passage in the main line, braking force from right to left

Case 2: passage in the main line, braking force from left to right; and

Case 3: passage in the diverging line, braking force from right to left.

For comparison, the cases for calculating braking force on ordinary CWR track on bridge will be considered, where the loads are applied on the corresponding three spans and the braking force is applied from right to left.

In case 1, the comparative results of additional braking force of straight/curved stock rail and ordinary CWR track on bridge are depicted in Figure 7.11 (compressive force = positive); beam−rail relative displacement is given in Figure 7.12 (right = positive).

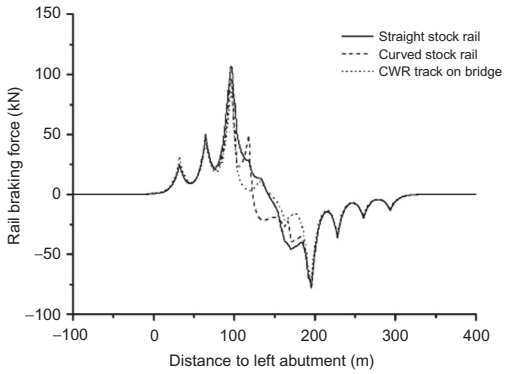

FIGURE 7.11

Braking force in case 1.

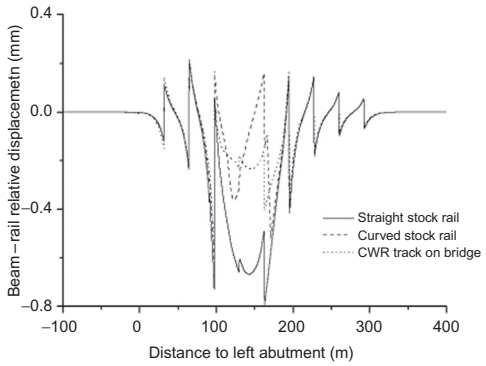

FIGURE 7.12

Beam−rail relative displacement in case 1.

From the calculation results, the braking force of CWR turnout on bridge is much greater than for CWR track on bridge. This is mainly because the inner rails are regarded as a breathing zone, which will expand to the left under braking force. Meanwhile, partial longitudinal force will be transmitted to the straight stock rail through fastenings and bed resistance. The additional braking force and relative displacement of turnout are greater for stock rail as compared with curved stock rail, as the braking force is distributed on the latter locally, with the rest being shared by the straight switch rail and long point rail.

When the braking force is applied from left to right, the maximum compressive forces of CWR turnout on bridge and CWR track on bridge are slightly smaller than those under the braking force in the opposite direction. This is dependent on the layout of bridge bracings. The regularities of additional braking forces, for straight stock rail for passage in the main line as compared with curved stock rail for passage in the diverging line, are alike.

7.1.3 REGULARITY OF LONGITUDINAL INTERACTION BETWEEN TURNOUT AND CONTINUOUS BEAM BRIDGE FOR BALLAST TRACK

CWR turnouts are generally laid on a continuous beam bridge in HSR due to favorable integrity of this bridge. A laterally integral continuous beam bridge means an integrally continuous and stable foundation for CWR turnouts. The impact of bridge expansion on a CWR turnout can be minimized by optimizing turnout−bridge relative location, so as to maintain turnout stability and geometry.

1. Calculation parameters

   For example, for a Chinese No. 18 CWR swing nose turnout of 60 kg/m rail laid on (32 m + 48 m + 32 m) continuous beams, the layout is shown in Figure 7.13. The turnout is 69 m in length, located in the middle of continuous beams. The distance from turnout beginning/end to the corresponding beam end is 21.5 m. The fixed bearing of the beam lies in the

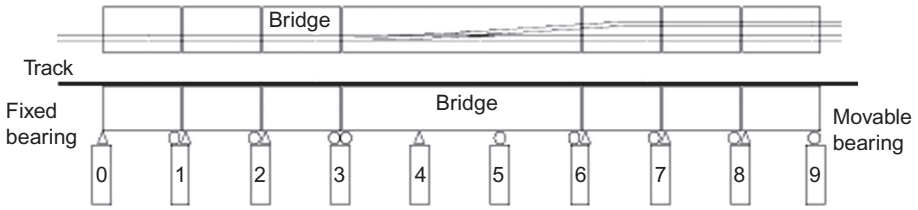

FIGURE 7.13

Arrangement of turnout and continuous beams.

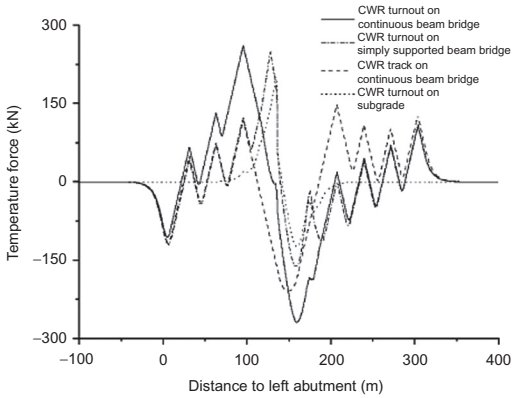

FIGURE 7.14

Additional temperature force of straight stock rail.

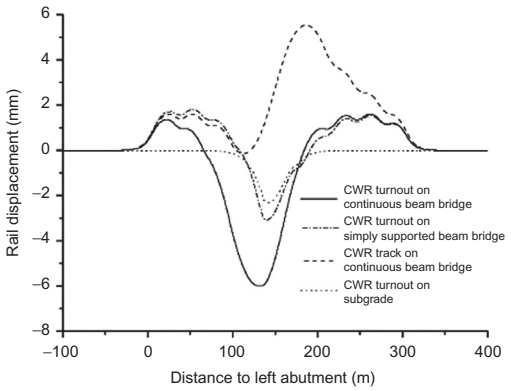

FIGURE 7.15

Displacement of straight stock rail.

turnout front. Three-span (3×32 m) simply supported beams are arranged beside the turnout. The same calculation parameters apply.

2. Temperature force

For a rail temperature rise of 50°C, the comparative results of temperature forces for CWR turnout on bridge with ballast track, CWR track on bridge, and CWR turnout on subgrade are described in Figure 7.14, and the comparative results of expansion displacement of straight stock rail are given in Figure 7.15.

According to calculation results, the temperature force of stock rail in a CWR turnout on a continuous beam bridge differs from that in CWR turnout on subgrade, ordinary CWR track on bridge, and a CWR turnout on a simply supported beam bridge. The maximum temperature force of stock rail on a continuous beam occurs at two ends of the beam, and additional tensile force occurs in the middle of the beam. No peak value occurs at retainers as in a CWR turnout on subgrade. This feature benefits the consistency of turnout geometry.

In ordinary CWR track on bridge away from the turnout area, the regularity of additional temperature force of the rail and magnitude resemble those in CWR track on bridge. On the 3×32 m simply supported beams beside the turnout area, the impact of temperature force is

minor. This means that the CWR turnout on bridge will impact the adjacent sections within a range of 100 m.

For a CWR turnout on a continuous beam bridge, pier longitudinal force in the turnout area is much greater than in a CWR turnout on a simply supported beam bridge with the same span layout, and in ordinary CWR track on bridge. This is due mainly to the fact that a great portion of longitudinal force is transmitted to the piers of a continuous beam bridge via the bed when the inner rails expand to the left, and the rest is transmitted to stock rail through ties and fasteners. So the longitudinal forces transmitted to piers at two ends of a fixed bearing of a continuous beam are not equivalent, increasing the stress of the pier. In this case, the layout of fixed bearings of continuous beam and turnout−bridge relative position will be optimized to ease pier longitudinal force.

3. Other beam−rail interactions

By calculating flexural force, it turns out that the impact of flexural force on the stress and displacement of rails and force transmission parts, and pier longitudinal force in CWR turnout on bridge is less prominent than the impact of temperature force. Therefore, flexural force is not a verification focus.

By calculating rail breaking force, it turns out that if a rail in the turnout front is broken in a CWR turnout on a continuous beam bridge, the other rail is exposed to higher breakage risk as compared to CWR track on bridge. The tie at the broken gap deflects severely, which may lead to serious deformation of turnout fastenings and even turnout geometry change. So the turnout with a broken rail must be elaborately renovated. Owing to the significant impact of inner rail expansion on pier stress, the pier longitudinal force under rail breakage on the left of a continuous beam is greater than that under rail breakage on the right of the beam in CWR turnout on bridge.

By calculating braking force, it turns out that peak rail braking force occurs at continuous beam ends. For left-to-right braking force, maximum additional compressive force occurs at the right beam end, and maximum additional tensile force at the left beam end and vice versa. The braking compressive force and tensile force of stock rail in CWR turnout on bridge are greater than those in CWR track on bridge. The maximum beam−rail displacements at left and right beam ends are about 1.6 and 1.3 mm, greater than those in CWR track on bridge (1.1 and 1.0 mm). So the longitudinal stability of CWR turnout on bridge is poorer than CWR track on bridge under braking force. Even so, the turnout is frequently exposed to braking or starting load, and thus it may be less stable than a turnout in a crossover or connecting line. This factor, together with temperature force and rail breaking force, leads to longitudinal instability of CWR turnout on bridge.

4. Impact of span length of continuous beam [88]

Take the three-span continuous beam in Figure 7.13, for example; four span layouts, (32 m + 32 m + 32 m), (32 m + 48 m + 32 m), (48 m + 48 m + 48 m), and (48 m + 60 m + 48 m), corresponding to four cases, are considered. A No. 18 CWR turnout lies in the middle of the beam, where the distances between turnout beginning/end and left/right beam ends are the same (13.5, 21.5, 37.5, and 43.5 m for four cases, respectively). The fixed bearing of a continuous beam is arranged in the turnout front; 3×32 m simply supported beams are provided beside the continuous beam.

Table 7.2 gives the stress and deformation of a pier and CWR turnout on a continuous beam bridge with different span lengths under temperature force. It can be seen that the additional

Table 7.2 Comparison of Calculation Results

Calculation Cases	Case 1	Case 2	Case 3	Case 4
Maximum additional temperature compressive force of straight stock rail (kN)	266.7	261.9	285.2	286.2
Maximum expansion displacement of straight stock rail (mm)	−6.1	−6.0	−7.4	−7.4
Maximum stress of force transmission components at heel of switch rail (kN)	39.1	27.2	8.7	8.4
Maximum stress of filler at end of wing rail (kN)	144.1	141.6	132.3	129.9
Displacement of point of straight switch rail with respect to tie (mm)	−17.7	−17.1	−16.3	−16.1
Displacement of point of point rail with respect to tie (mm)	−6.7	−6.5	−6.0	−5.9
Longitudinal force of left abutment (kN)	−294.6	−293.2	−298.7	−299.0
Longitudinal force of pier 1 (kN)	−134.7	−132.1	−144.4	−145.1
Longitudinal force of pier 2 (kN)	−262.8	−257.0	−282.9	−284.2
Longitudinal force of pier 4 (kN)	−1186.2	−1350.3	−1500.7	−1609.4
Longitudinal force of pier 6 (kN)	−259.9	−170.6	−59.3	1.6
Longitudinal force of pier 7 (kN)	−150.2	−115.7	−70.1	−44.0
Longitudinal force of pier 8 (kN)	−170.2	−157.4	−140.0	−130.2
Broken gap of straight stock rail at beam end at turnout front (mm)	63.4	64.7	65.2	65.2
Maximum additional tension of intact rail (kN)	438.0	437.5	469.4	478.4

temperature force of rail at the beam end and longitudinal force of pier increases with lengthening of the span, in that the temperature span of the bridge increases, the same as CWR track on bridge. On the other hand, the longitudinal force of force transmission components and displacements of switch rail/point rail with respect to ties decreases with span length. This is because the distances between turnout beginning/end and beam ends are widened with lengthening of the span, and the turnout center moves farther to the right of the fixed bearing of the continuous beam. In this case, the right displacement of a continuous beam on a turnout is intensified, effectively compensating for the left displacement of inner rails. In short, lengthening the bridge span is conductive to stress in a CWR turnout. However, it may increase the stress of section and pier, so a reasonable span length is required.

5. Impact of distance between turnout beginning/end and beam ends

For the three-span continuous beam depicted in Figure 7.13, the analysis is based on the distances between turnout beginning and left expansion gap of the continuous beam of 0, 10, 21.5, 30, and 43 m (corresponding to five cases), and the distances between turnout end and right expansion gaps of the continuous beam of 43, 33, 21.5, 13, and 0 m. Other parameters are the same as above.

Given the different distances between turnout beginning/end and beam ends for a CWR turnout on a continuous beam bridge, the additional temperature forces of stock rail are shown in Figure 7.16. In the figure, the nearer the distance between turnout beginning and left expansion gap of the continuous beam, the greater the distance between turnout end and right beam end, and the greater the additional temperature force of stock rail at the expansion gap of the

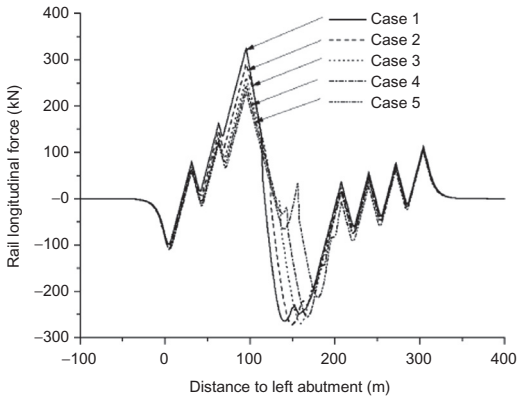

FIGURE 7.16

Additional temperature force of stock rail.

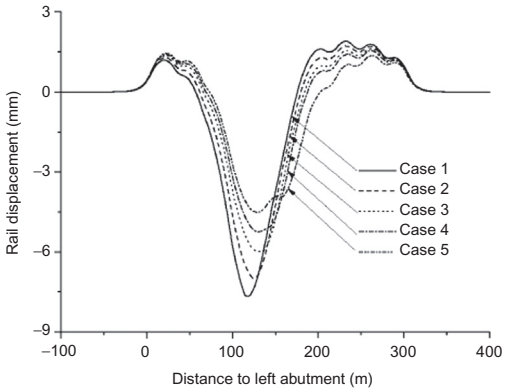

FIGURE 7.17

Expansion displacement of stock rail.

continuous beam in the turnout front. This is because the shorter distance between turnout beginning and left expansion gap of the continuous beam expands the expansion scope of the bridge beam and inner rail in the same direction, while it reduces the expansion scope in the opposite direction. Therefore, more longitudinal force of the inner rail will be transmitted to the left end of the continuous beam. When the distance between turnout beginning and the left beam end is 0 m, the maximum additional temperature force of stock rail is about 324.0 kN, 40.7% greater compared to the additional temperature force (230.3 kN) at a distance of 43 m. Thus, farther distance between turnout beginning and left end of continuous beam is preferable.

When the distance between the turnout end and the right end of the continuous beam is small, the additional temperature force of stock rail is small, while peak value occurs at heel of switch rail, leading to lateral instability of the turnout. Therefore, a reasonable distance between turnout end and the right end of the beam is required. By comparison, given a limit length for a continuous beam, the distance between turnout beginning and left beam end should be greater than the distance between turnout end and right beam end.

Figure 7.17 presents the expansion displacement of stock rail in a CWR turnout on a continuous beam bridge with different distances between turnout beginning/end and beam ends (right = positive). As shown in the figure, a shorter distance between turnout beginning and left beam end corresponds to greater expansion displacement of stock rail and longitudinal instability of turnout. Hence, greater distance is favored.

Meanwhile, as revealed by calculation results, the longitudinal force of a retainer at the heel of switch rail, longitudinal displacement of stock rail/point rail with respect to ties, and a broken gap of stock rail at the beam end in a turnout front will not change with the distance between turnout beginning and beam end unidirectionally. The minimum stress of the retainer and longitudinal displacement of switch rail/point rail with respect to ties occurs only at proper distances between turnout beginning/end and beam ends, where the minimum effect is produced due to the superposition of expansions of the inner rail and bridge in the same direction and in opposite directions. The broken gap of a rail is significantly affected by the temperature span of the

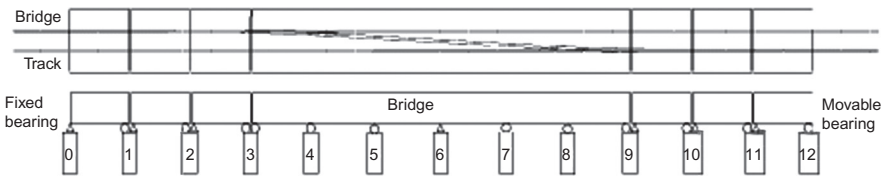

FIGURE 7.18

Layout of turnouts in a single crossover.

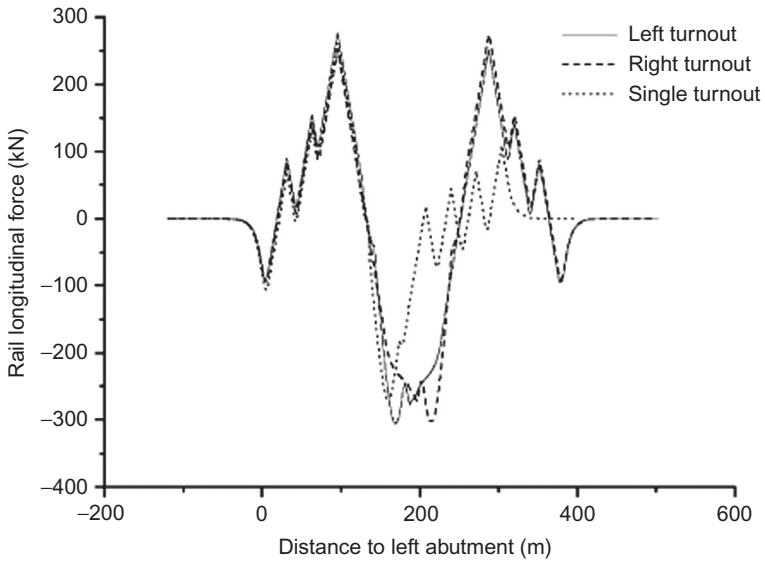

FIGURE 7.19

Additional temperature force of single crossover turnouts.

continuous beam, but slightly affected by turnout−bridge relative position. In comparison with common bridge beams (3×32 m) and turnout length (69 m for No. 18 turnout), the distance between turnout beginning and left beam end should be greater than 18 m, and the distance between turnout end and right beam end should be greater than 9 m. So the minimum bridge beam length required for a No. 18 CWR turnout is 96 m.

6. Regularity of stress and deformation of crossover turnout on continuous beam bridge [89]

Figure 7.18 presents the layout of a crossover turnout on a continuous beam bridge (beam span: $3-32$ m $+ 6 \times 32$ m $+ 3-32$ m, track distance: 5.0 m). The fixed bearing of the beam is in the middle. The turnouts (Chinese No. 18 turnout for 250 km/h) in a single crossover are antisymmetrically laid in the middle of the continuous beam. The CWR turnout on bridge as shown in Figure 7.13 is regarded as a reference case.

The distribution of the additional temperature force of stock rail in left and right turnouts in the crossover and the comparative results with a single turnout are given in Figure 7.19. From

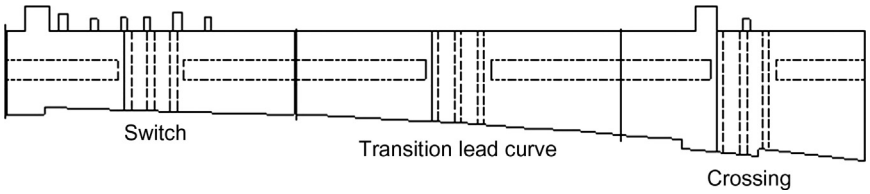

FIGURE 7.20

Layout of slabs in ballastless turnout.

the figure, the additional temperature force of stock rail in left and right turnouts follows an antisymmetrical distribution. Although the maximum temperature span of a continuous beam for single crossover turnouts is 128 m, with symmetric layout, the longitudinal force of the left turnout on the bridge offsets that of right turnout on the bridge. Consequently, the maximum additional temperature force at the end of a continuous beam is slightly higher than that of single turnout at the temperature span of 72 m. This means that this single crossover turnout layout is fine.

According to calculation results, the stress of force transmission components and expansion displacement of switch rail/point rail are smaller than those in the single turnout. The stress on a fixed pier of a continuous beam approximates 0. This means that the turnout−bridge arrangement is conducive to bridge stress.

7.1.4 REGULARITY OF LONGITUDINAL INTERACTION BETWEEN CONTINUOUS BEAM BRIDGE WITH BALLASTLESS TRACK AND TURNOUT

Most HSRs involve ballastless track. The rail foundation for CWR turnout on bridge consists mainly of three types: concrete bed with Π-shaped reinforcement, bed slab with convex retaining block, and turnout slab with longitudinally coupled base slabs. The first two types are of blocky structure.

1. Blocky slabs

   For a Chinese No. 18 CWR swing nose turnout of 60 kg/m rail laid on (32 m + 48 m + 32 m) continuous beam, the layout of beams and turnout is plotted in Figure 7.13. The types of Π-shaped reinforcement and convex retaining block are considered, where the longitudinal stiffness of convex retaining block bearing is taken as 250 kN/mm. Three bed slabs are arranged in the turnout area, with lengths of 20, 29, and 20 m (see Figure 7.20). The temperature change of the bed slab is 24°C, the daily temperature difference of bridge with ballastless track is 20°C, and other parameters are similar.

   The additional temperature force of stock rail for ballastless CWR turnouts on bridge with the two given foundation types, and that of ballast CWR turnout on bridge, ballastless CWR track on bridge, and ballast CWR turnout on subgrade are given in Figure 7.21. The expansion displacement of straight stock rail is given in Figure 7.22. In the figures, the additional temperature force of a ballastless CWR turnout on bridge follows the same rule as ballast CWR turnout on bridge. However, with the great daily temperature differential of the bridge, the additional

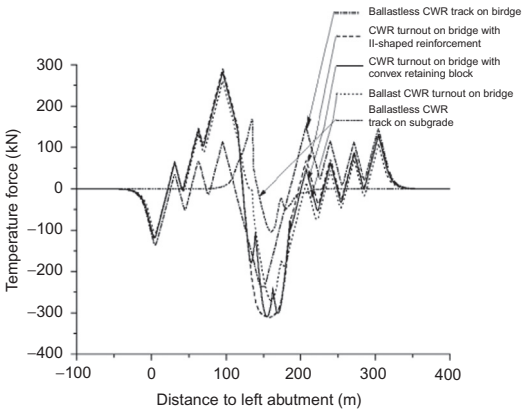

FIGURE 7.21

Temperature force of stock rail.

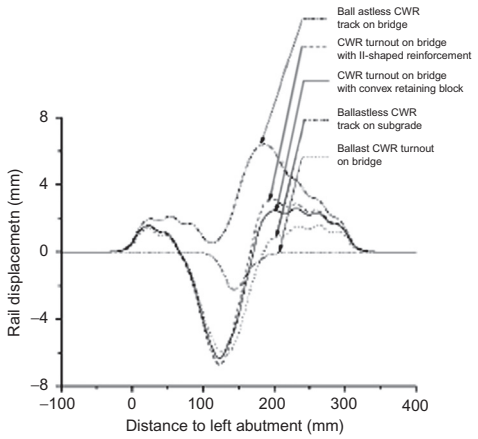

FIGURE 7.22

Expansion displacement of stock rail.

temperature forces of the two given track types are greater than in ballast CWR turnout. For the additional temperature forces of the two types, convex retaining block type is smaller than the Π-shaped reinforcement type. This is because the bed slabs are connected to the bridge through the longitudinal springs of convex retaining block bearings, which eases the longitudinal force transmitted from bridge to turnout [90].

According to the calculation results, as compared with ballast CWR turnout on bridge, the switch rail and point rail exhibit smaller displacement with respect to the turnout slab due to the greater bed resistance of the two types of turnouts. However, the additional temperature force of stock rail and stress of piers of continuous beam and simply supported beam in the turnout front increase. As for the stresses of stock rail and bridge piers of the two turnout types, the convex retaining block type is smaller than the Π-shaped reinforcement type. Thus, ballast track with convex retaining block is preferred in HSRs in China.

2. Bed slab with longitudinally coupled base slabs

This track type differs greatly from other common ballastless tracks. For Chinese CRTS II slab-type ballastless track with longitudinally coupled base slabs on the bridge, the track is composed of elastic fastenings, track slab, mortar adjustment course, continuous base slab, sliding course, and lateral blocks. Friction plates, terminal restricted configuration, and transition plates are arranged on subgrade near the abutments at two ends. High-strength extruded plates are installed at the expansion gap of the beam. In laying the CWR turnout, the base slabs of the up and down lines at the crossing may be coupled.

a. Calculation parameters

The turnout−bridge layout is shown in Figure 7.13, and the calculation model is given in Figure 7.3. In the calculation, the base slabs on the bridge are longitudinally coupled; the friction plates on the subgrade at two ends are 50 m long, respectively. The base slab and friction plate are 0.3 m in thickness. The sliding course is composed of two layers of geotextile and one layer of geomembrane; the friction coefficient is taken as 0.35.

In calculating the temperature force, only the gravitational distribution of turnout slab and base slab is considered, and thus the maximum frictional resistance between base slab and bridge is approximately 9.8 kN/m (maximum displacement 0.5 mm). In calculating the braking force, the weight of the carbody will be considered; the maximum frictional resistance under the node between base slab and bridge is about 19.6 kN/m. At temperature drop, the reduction in longitudinal expansion stiffness after base slab fracture will be considered; the reduction factor is taken as 0.1. At temperature rise, the fractured base slab is under stress, no reduction in longitudinal expansion stiffness exists, and the reduction factor is taken as 1.0. By conversion, the shrinkage and creep of base slab equal a temperature drop of 30°C. Superposing the similar temperature drop in track slab gives 54°C. The effect of shrinkage and creep at temperature rise is not considered; the temperature rise is taken as 24°C. The sliding course on the friction plate is made up of two layers of geotextile; the friction coefficient is taken as 0.5. The longitudinal resistances between base slab and friction plate under no load and under load are 14.0 and 28.0 kN/m, respectively.

Track slabs (0.2 m thick) are coupled by longitudinal connectors, while the slab and base slab are closely bonded by emulsified asphalt mortar or self-leveling concrete, with a bonding resistance of 63.8 kN/m. On the fixed bearing of the bridge, the base slab and bridge deck are coupled by pins (lateral stiffness of single pin is 6.25×10^4 kN/m). Two rows (eight each) of φ28 shear reinforcements are arranged. In case of track slab fracture, longitudinal stiffness reduction will be considered at temperature drop, and the reduction factor is taken as 0.7. The reduction is neglected at temperature rise. Track slabs are prefabricated. The impact of shrinkage and creep is disregarded. The value for temperature rise/drop is greater than the daily temperature difference of the bridge, taken as 24°C.

The base slab is connected with the terminal restricted configuration at two ends. The longitudinal horizontal stiffness of the terminal restricted configuration is 1.0×10^8 kN/m. The base slabs are longitudinally coupled in the main line of the turnout. In the diverging direction in turnout rear and on subgrade, concrete bed with Π-shaped reinforcements are used. The coupling force between track slab and foundation equals the longitudinal resistance of a single fastener, that is, 5.0×10^4 kN/mm. The temperature variation of rail is 50°C. The braking load is 16 kN/m, with a loading length of up to 300 m. Type-II fasteners are used in the turnout area, where the resistance under load is 12.5 kN/mm (maximum displacement 0.5 mm) and the resistance under no load is 25 kN/mm. WJ-8 fasteners are used in the section, with the resistances under load and under no load being 15 kN/mm (maximum displacement 0.5 mm) and 30 kN/mm, respectively. Other parameters are the same.

b. Temperature force

In case of temperature drop, the additional temperature forces of stock rails in CWR turnout on bridge, ballastless CWR turnout on bridge with convex retaining block, CWR track on bridge with longitudinally coupled base slabs, and ballastless CWR turnout on subgrade are depicted in Figure 7.23. As far as additional temperature force is concerned, the turnout with longitudinally coupled base slab is much smaller than a ballast CWR turnout on bridge with convex retaining block, and even smaller than CWR turnout on subgrade. The CWR track on bridge also has a small additional temperature force, as a sliding course is provided between the longitudinally coupled base slabs and the bridge, which isolates the

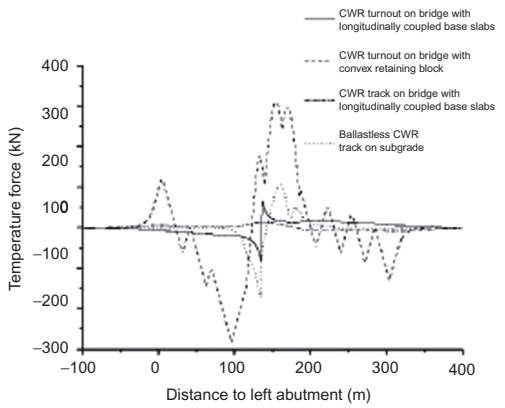

FIGURE 7.23

Additional temperature force of stock rail.

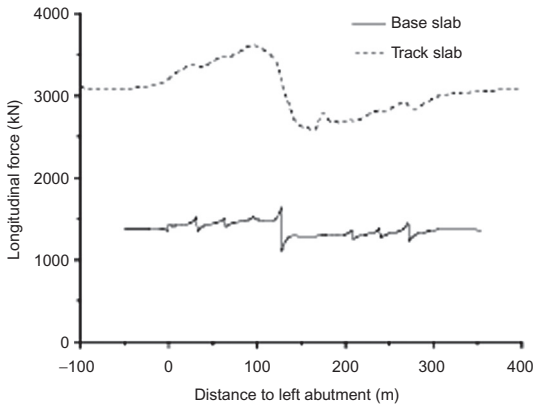

FIGURE 7.24

Longitudinal force of base slab and track slab.

impact of bridge expansion on the expansion of track and CWR turnout on bridge. In this case, the longitudinal temperature force of the bridge is distributed to the terminal restricted configuration at two ends and the friction plates. Meanwhile, the temperature force of the inner rail of the turnout is transmitted to the base slab via the track slab. So the longitudinal force of pier is small.

In the ballastless track system, with the longitudinally coupled base slabs and sliding course between base slab and bridge deck, the great bridge expansion displacement induces a small longitudinal displacement of the base slab through friction force of the sliding course, forming a frame structure composed of pier and base slab. The impact on stress and deformation of CWR turnout on bridge is small. Therefore, this foundation type is ideal for CWR turnout on bridge.

The distribution of stress on the base slab and track slab is plotted in Figure 7.24. In the drawing, the abrupt change of longitudinal force is induced by the concentrated force of pins. The maximum longitudinal force of a row of pins equals 145.3 kN. The longitudinal force at the end of the base slab is the resistance of the terminal restricted configuration, taken as 1377.7 kN maximally. As far as longitudinal force is concerned, track slab is greater than base slab. This is due to the severe stiffness reduction of the base slab and the decrease in bearing cross section. The maximum tensile forces of track slab and base slab are 3629.1 and 1649.7 kN, respectively.

The distribution of longitudinal displacement of the base slab, track slab, and bridge is depicted in Figure 7.25 (right = positive). The maximum displacements of base slab and track slab are 4.5 and 4.0 mm, respectively. The slippage between the two is minor. The displacement of the terminal restricted configuration is about 0.014 mm. As can be seen from the figure, the displacements of base slab and bridge at the fixed bearing of bridge are similar due to the force transmission effect of pins, with displacement difference of 0.2 mm. Other places have remarkable displacement differences. This indicates that the antifriction effect of the sliding course is prominent.

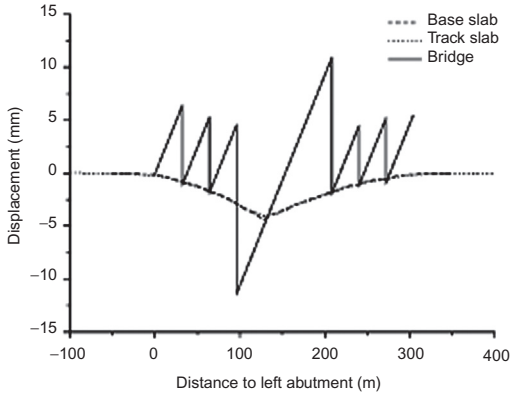

FIGURE 7.25

Displacements of base slab, track slab, and bridge beam.

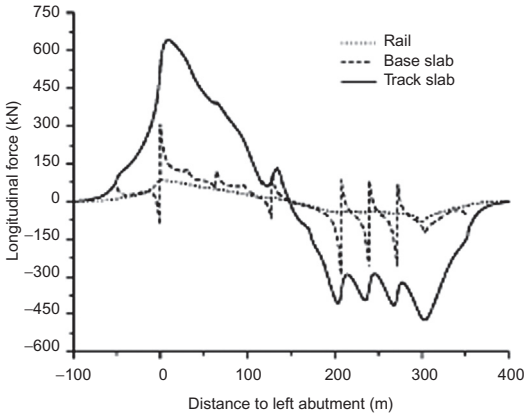

FIGURE 7.26

Distribution of braking force.

The calculation parameters at temperature rise differ greatly from those at temperature drop; therefore, calculated results vary significantly between the two cases, as shown in Table 7.3. By comparison, the difference in stress of track slab, base slab, and terminal restricted configuration is the most prominent; this is due to different longitudinal stiffnesses in two temperature change cases. At temperature rise, the track slab and base slab are mainly under compressive force, as compared with CWR track on bridge; the compressive force of the track slab increases from 8.7 to 9.3 MPa, and the base slab from 8.2 to 8.7 MPa, well below the allowable value. Therefore, the structural design will not be based on the case of temperature rise, except for the design of the terminal restricted configuration and pins. For CWR turnout on bridge, pier stress may be greater than that of CWR track on bridge, but it is smaller than that at temperature drop. Therefore, the case of temperature rise is not considered in verifying pier stress. The stress and deformation of CWR turnout are equivalent to those in CWR turnout on subgrade and CWR turnout on bridge at temperature drop. As compared with CWR track on bridge, at temperature drop, the tensile force of the base slab increases from 2.0 to 2.2 MPa, and that of the track slab from 5.4 to 7.1 MPa. This may lead to cracks in the track slab. Therefore, tensile force is regarded as a control factor in structural design. The case of temperature drop will be included in studying the regularity of turnout−bridge interaction.

c. Braking force

Braking force is applied from right to left on the rail surface in the main direction of the turnout. Figure 7.26 presents the distribution of longitudinal force of the rail, track slab, and base slab. As can be seen from the drawing, the maximum additional compressive forces of rail, track slab, and base slab occur at the left abutment (locomotive head), respectively 86.4, 286.4, and 639.8 kN. The stresses of terminal restricted configuration and each row of pins are 90.2 and 211.0 kN, smaller than those under temperature force.

d. Impact of friction coefficient of sliding course between base slab and bridge deck

The sliding course between the base slab and bridge deck consists of two layers of geotextile and one layer of geomembrane. The friction coefficients of 0.05, 0.15, 0.25, 0.35,

Table 7.3 Comparison of Calculated Temperature Forces at Temperature Rise or Drop

Temperature Change	Temperature Drop		Temperature Rise	
Ballastless Track	**Turnout on Bridge with Longitudinally Coupled Base Slabs**	**Track on Bridge with Longitudinally Coupled Base Slabs**	**Turnout on Bridge with Longitudinally Coupled Base Slabs**	**Track on Bridge with Longitudinally Coupled Base Slabs**
Maximum additional temperature force of straight stock rail (kN)	88.0	10.7	−107.2	−10.1
Maximum expansion displacement of straight stock rail (mm)	−4.4	0.4	2.8	−0.4
Maximum stress of force transmission components at heel of switch rail (kN)	212.2	–	225.5	–
Maximum stress of filler at end of wing rail (kN)	142.7	–	146.7	–
Displacement of point of straight switch rail with respect to stock rail (mm)	−19.2	–	19.4	–
Displacement of point of point rail with respect to wing rail (mm)	−9.1	–	9.4	–
Longitudinal force of abutment 1 (kN)	−390.1	−417.7	481.8	456.2
Longitudinal force of pier 2 (kN)	−114.8	−51.2	88.4	44.2
Longitudinal force of pier 3 (kN)	−186.4	−50.7	131.1	43.2
Longitudinal force of pier of fixed bearing of continuous beam (kN)	−508.1	−124.6	310.7	82.1
Longitudinal force of pier 6 (kN)	−397.5	45.0	298.3	−6.2
Longitudinal force of pier 7 (kN)	−247.0	21.7	205.3	1.7
Longitudinal force of pier 8 (kN)	−191.7	−1.4	166.7	11.1
Longitudinal force of base slab (kN)	1649.7	1532.9	−6676.3	−6278.7
Longitudinal force of track slab (kN)	3629.1	2756.5	−4730.6	−4446.3
Longitudinal force of terminal restricted configuration (kN)	1367.7	1384.0	−6125.7	−6101.0
Longitudinal force of a row of pins (kN)	290.6	180.2	−392.0	−202.0
Displacement of base slab (mm)	4.5	0.9	−2.3	−0.4
Displacement of track slab (mm)	4.0	0.8	−2.3	−0.4
Displacement of terminal restricted configuration (mm)	0.01	1.06	−0.06	−0.06

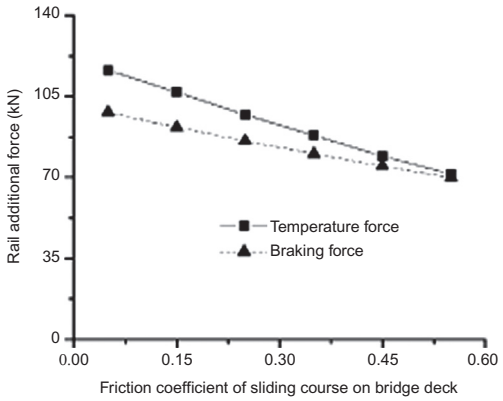

FIGURE 7.27

Change of additional temperature force of stock rail with frictional resistance of bridge deck.

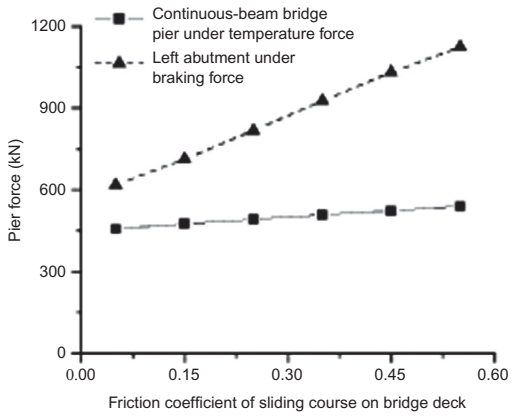

FIGURE 7.28

Change of longitudinal force of pier with frictional resistance of bridge deck.

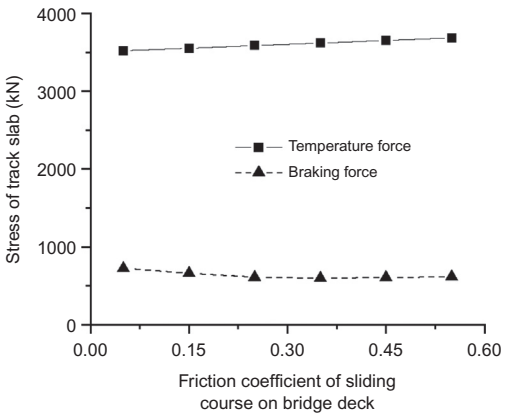

FIGURE 7.29

Change of longitudinal force of track slab with frictional resistance of bridge deck.

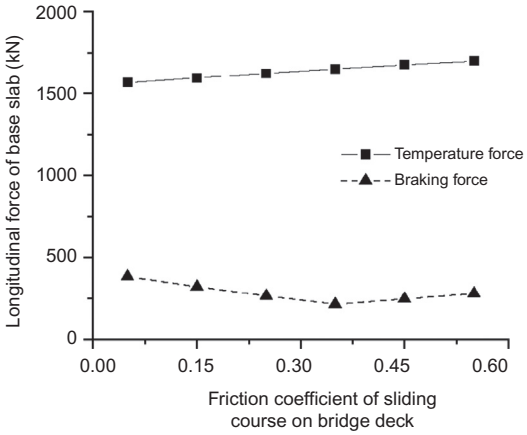

FIGURE 7.30

Change of longitudinal force of base slab with frictional resistance of bridge deck.

0.45, and 0.55 are included. Only the gravitational distribution of the turnout slab and base slab is considered in calculating temperature force; therefore, maximum frictional resistances between base slab and bridge of 1.4, 4.2, 7.0, 9.8, 12.6, and 15.4 kN/m are considered, while the frictional resistances under load are taken as 2.8, 8.4, 14.0, 19.6, 25.2, and 30.8 kN/m. Other parameters are the same. The impact regularity of the friction coefficient of the sliding course on the turnout–bridge system is analyzed in the cases of temperature drop and braking, as shown in Figures 7.27–7.30.

According to the calculated results, under temperature force, the greater the friction coefficient of the sliding course, the greater the longitudinal force transmitted to the base slab and track slab from the bridge, and in turn, the greater the longitudinal force of the pier. Moreover, the expansion distance of the base slab increases with longitudinal force, leading to stress increase in the pins. The expansion distance of the track slab is reduced slightly. To sum up, the greater coefficient of the sliding course has little effect on the turnout (the stock rail has little additional temperature force, and the displacement of switch rail/point rail varies slightly), but has greater impact on the base slab, track slab, pier, and pin stress. Therefore, a smaller coefficient is preferred.

Where braking force is applied, the longitudinal force of the rail will be transmitted to the track slab, base slab, and pier/abutment in turn via fasteners. The pier/abutment longitudinal force increases with the friction coefficient of the sliding course, while the longitudinal displacement and force of the track slab and base slab decrease. The stress of pins is smaller.

If the sliding course is damaged during operation, the friction coefficient will increase. For safety, the design of a turnout–bridge system must be verified with the maximum friction coefficient within safe limits. Meanwhile, the maximum friction coefficient of the sliding course must be within a certain range during its useful life. It is specified that the comprehensive friction coefficient should not exceed 0.35 after 3 million episodes of abrasion.

7.2 DYNAMIC CHARACTERISTICS OF VEHICLE–TURNOUT–BRIDGE COUPLED SYSTEM [91]

HSRs are quite demanding in terms of plane and vertical section design and track smoothness, and are in closed operation. Lots of HSRs are built on viaducts or large bridges, so many station throats are located on bridges, much more than those for common railway lines [92,93]. As wheel load transition occurs on two rails at the switch and crossing, the switch rail and point rail must be thickened and heightened gradually, which inevitably induces certain structural irregularities in the turnout, impacting riding speed. The line on a bridge is designed based on the results of numerous dynamic simulation analyses and dynamic tests on irregularities of a section; however, the impacts of structural irregularities of a turnout are not considered. High-speed turnouts are designed for subgrade and uniformly settled foundations. Affected by turnout structure, manufacture, assembly, laying, maintenance, and repair, a turnout cannot achieve the same riding safety and comfort as a section, despite great efforts on the design of wheel–rail relation, track stiffness, etc. High-speed turnouts on subgrade are the main source of vibration that induces shaking of vehicles. When a high-speed turnout is laid on a bridge, the superposition of structural deformation and deflection of the bridge and structural irregularities of the turnout will make riding safety and comfort even worse; in severe cases, speed restrictions may apply [94,95]. So it is necessary to carry out in-depth dynamic simulation analysis on train–bridge–turnout systems.

The vehicle–bridge–turnout coupled dynamic response model should be constructed based on vehicle–track–bridge dynamics and theories of turnout dynamics for dynamic simulation. In the simulation, the study of vehicle–turnout–bridge dynamic performance, assessment of structural design schemes, and optimization of system parameters will be performed with numerical simulation methods, based on the integrated system of EMU train, turnout, and bridge, finite element

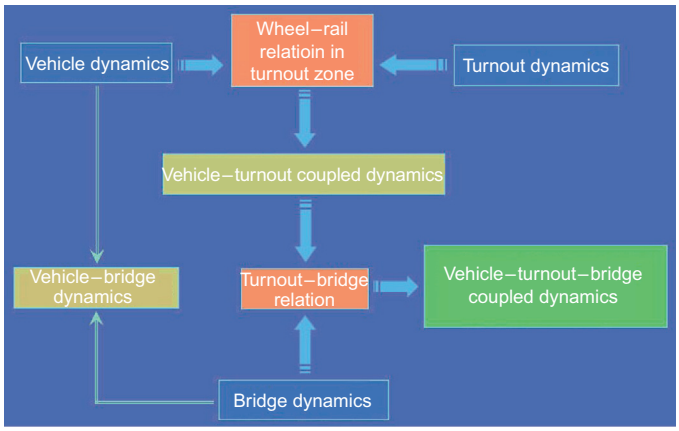

FIGURE 7.31

Dynamic coupled system of CWR turnout on bridge.

method for vehicle dynamics, turnout dynamics, and bridge dynamics, as well as the wheel–rail relation and turnout–bridge relation in the turnout area [96,97,100]. Please see Figure 7.31 for a vehicle–turnout–bridge coupled system.

The vehicle model is given in Figure 2.20, and the full model of a swing nose turnout is given in Figure 4.29. Railway bridges have diversified structures and complicated compositions. With the development of finite element theory and computational technologies, the finite element method and mode coordinate method are widely used to build bridge dynamics equations in analyzing vehicle–bridge coupled vibration. In the finite element method, the kinematic equation of the system is established directly from the geometrical model of bridge structure, and the vibration of the integral bridge can be analyzed. This method is available for details of bridge structure, but has greater degrees of freedom [98,99]. Figure 7.32 is an end view of vibration of the vehicle–turnout–bridge system.

Based on the dynamic analysis model of the vehicle–turnout–bridge system, a generalized dynamic simulation analysis software for vehicle–turnout–bridge systems (DATBS, i.e., Dynamic Analysis of the Turnout and Bridge System) has been developed by the author for dynamic simulation and evaluation of high-speed trains in CWR turnout on bridge.

7.2.1 REGULARITY OF DYNAMIC INTERACTION OF CROSSOVER TURNOUT ON UNIFORM CONTINUOUS BEAM BRIDGE [91]

1. Calculation parameters

   The turnout layout is given in Figure 7.33 with the example of a No. 18 ballastless crossover turnout laid on a 6×32 m continuous beam bridge on the Beijing–Shanghai line. The track distance of 5.0 m and CRH380 EMU train are taken into account in the example.

   The prestressed concrete continuous beam bridge is of integrated double-track type. The beam is made of C50 concrete with a single cell and single box section, height of 3.05 m, and elastic modulus of 35.5 GPa. The intermediate cross section area of the beam (middle part) is

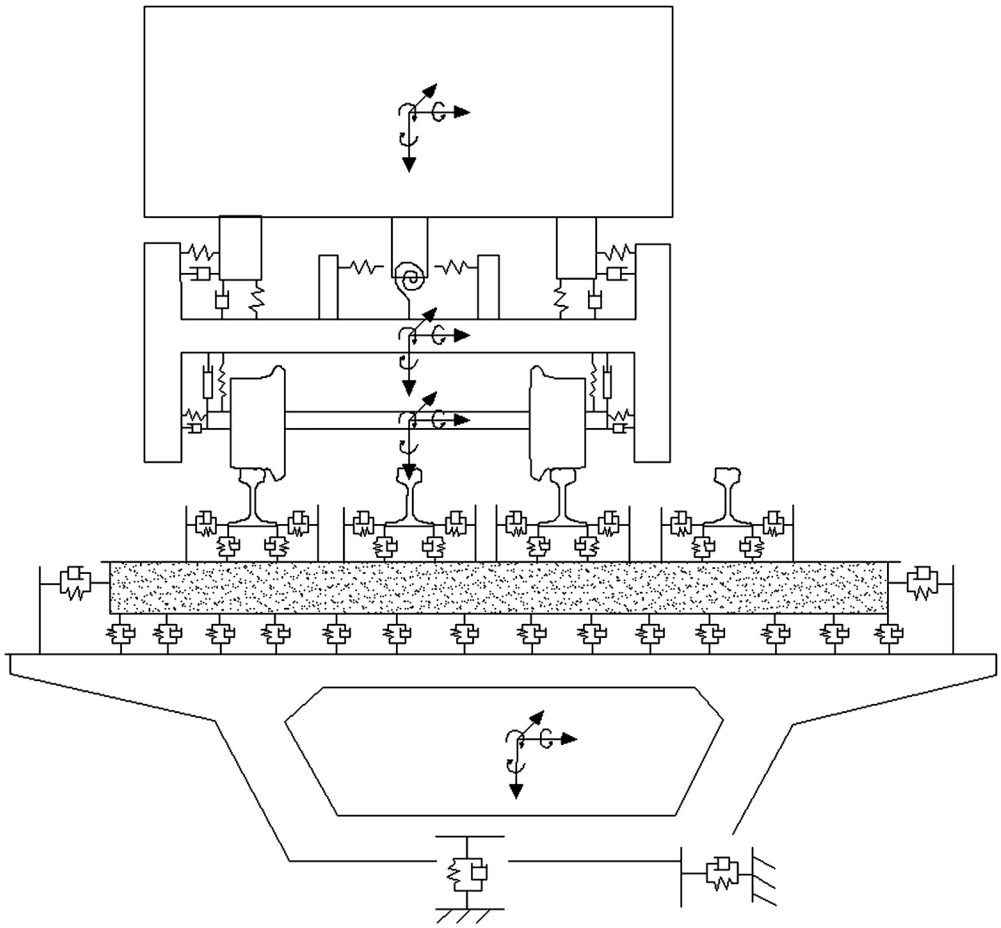

FIGURE 7.32

End view of vehicle–turnout–bridge dynamic model.

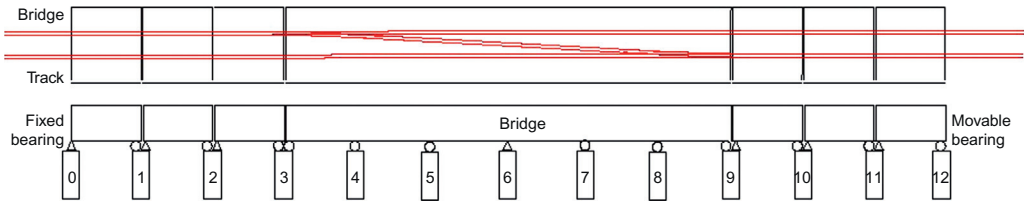

FIGURE 7.33

Turnouts in single crossover.

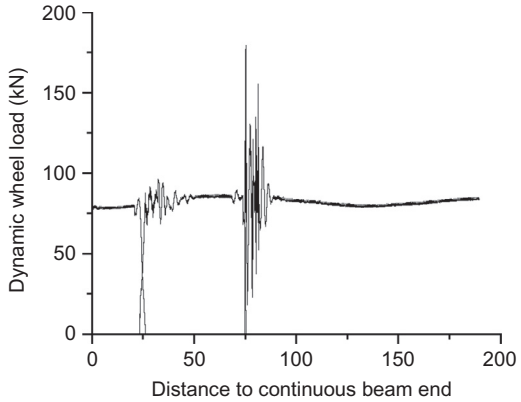

FIGURE 7.34

Distribution of dynamic wheel load.

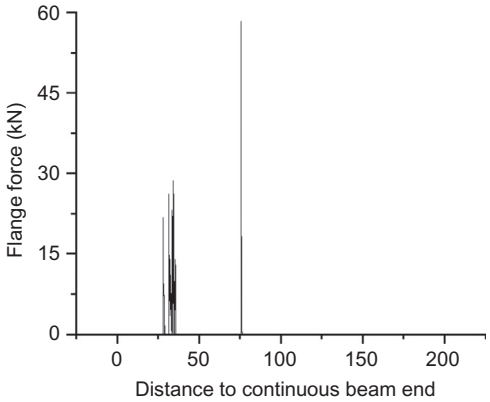

FIGURE 7.35

Distribution of flange force.

12.706 m^2. The vertical and lateral moments of inertia of the beam are 15.908 and 300.26 m^4, respectively. The bearing has a cross section area of 22.73 m^2, with vertical and lateral moments of inertia, respectively, of 21.196 and 400.07 m^4.

The substructure of the turnout is composed of 240-mm-thick turnout slabs bonded with the base through pins and mortar adjustment course. C50 concrete and HRB335 rebars are used. The mortar adjustment course is 3 cm thick, composed of asphalt and cement, with the elastic modulus of 700−10,000 MPa and bearing stiffness of 21 GPa/m. The base slabs are longitudinally connected in the whole bridge, and are made of C30 concrete, generally 180 mm in thickness. Shear groove consolidation devices are provided above the fixed bearing per span of beams. Common or clamping type lateral blocks are arranged longitudinally along the line. Rigid foamed plastic plates are provided at bridge beam gaps. Friction plates, terminal restricted configuration, and transition plates are installed on the subgrade adjacent to abutments at the bridge ends.

In the calculation, two trains traveling in up and down lines at the same time may be taken into account.

2. Dynamic responses of ballastless turnout on bridge

Figure 7.34 gives the distribution of dynamic load of the inner wheel at the front axle of an EMU train bogie, where the origin of the x-axis represents the left of a continuous beam. Calculation results will be compared with those for a high-speed turnout on subgrade, as shown in Figure 4.34 [101,102]. From the figure, the cooperation of structural irregularities of turnout and bridge vibration intensifies the fluctuation of dynamic wheel load as compared with a CWR turnout on subgrade. The maximum dynamic wheel load can be up to 178.4 kN. The fluctuation of wheel load of the rear axle of a bogie follows the same rule.

The distribution of flange force of the inner wheel at the front axle of an EMU train is shown in Figure 7.35, the same as in a CWR turnout on subgrade; that is, the wheel and rail will come into contact locally at the switch and crossing. The maximum flange forces at the switch and crossing are, respectively, 29.1 and 58.8 kN.

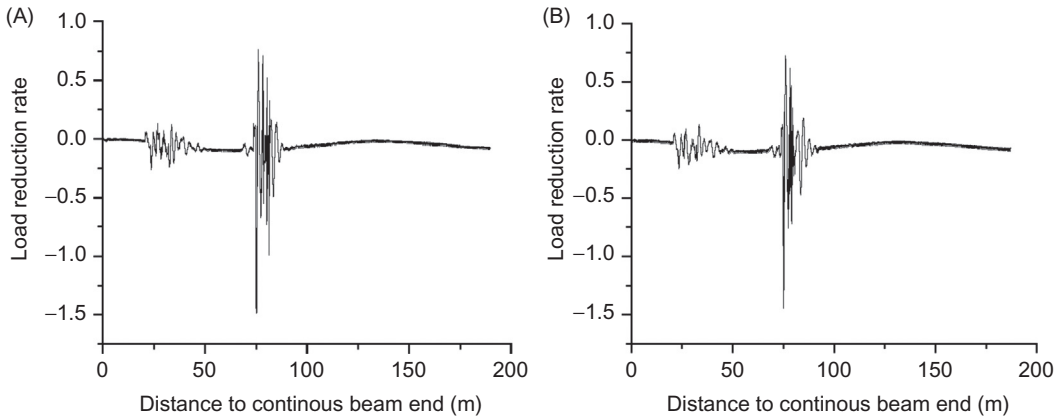

FIGURE 7.36

(A) Load reduction rate of inner wheel at front axle. (B) Load reduction rate of inner wheel at rear axle.

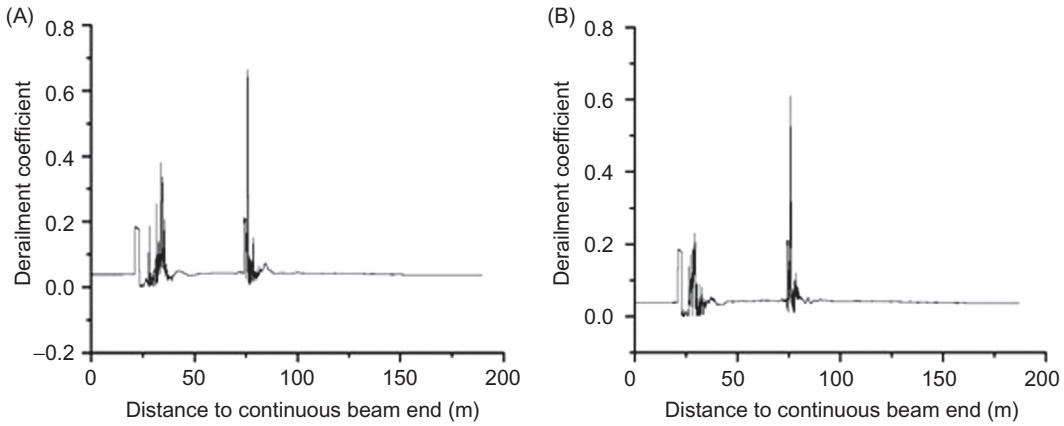

FIGURE 7.37

(A) Derailment coefficient of front axle. (B) Derailment coefficient of rear axle.

The distribution of load reduction rate induced by dynamic load fluctuation of the inner wheels at front/rear axle is shown in Figure 7.36. The maximum load reduction rates of the inner wheel at the front axle at the switch and crossing are, respectively, 0.15 and 0.78; those of the inner wheel at rear axle are, respectively, 0.15 and 0.74. The load reduction rates of the outer wheels (front/rear axle) fluctuate slightly, with a maximum value of 0.32, which is below the allowable limit (0.8).

The distribution of the derailment coefficient of front/rear axle is given in Figure 7.37. The maximum derailment coefficients of the front axle at the switch and crossing are, respectively, 0.38 and 0.67, and those of the rear axle are, respectively, 0.21 and 0.61. The derailment coefficient at the switch equals that in CWR turnout on subgrade, and is greater at the crossing. However, both are below the allowable limit of 0.8.

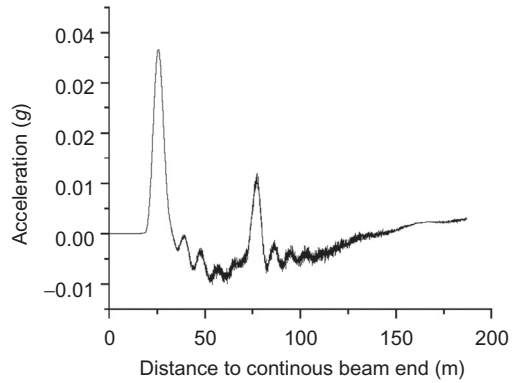

FIGURE 7.38

Lateral acceleration of carbody.

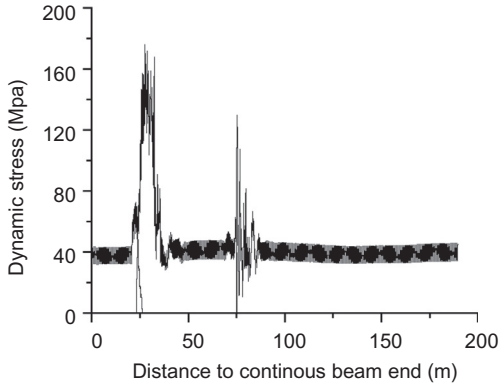

FIGURE 7.39

Distribution of dynamic stress of rail.

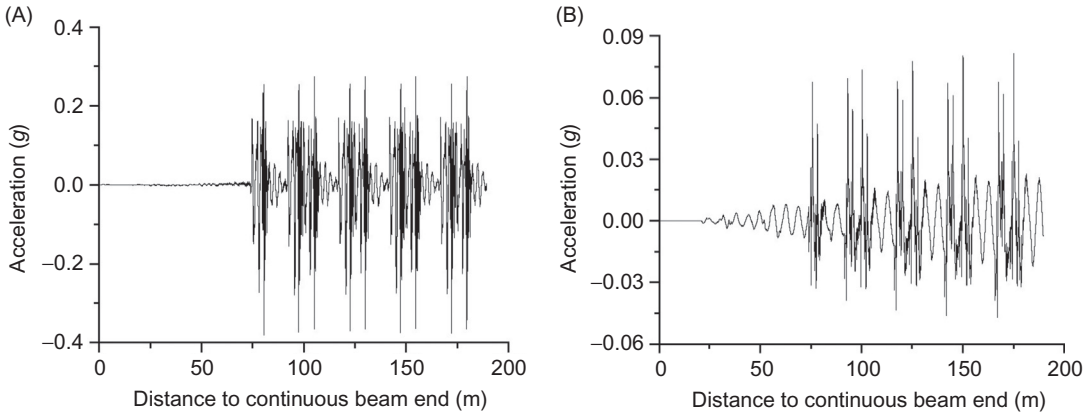

FIGURE 7.40

(A) Vertical vibration acceleration of bridge. (B) Lateral vibration acceleration of bridge.

The distribution of lateral vibration acceleration of a carbody is shown in Figure 7.38. The maximum values at switch and crossing are, respectively, 0.037 *g* and 0.012 *g*; both are acceptable.

The distribution of dynamic stress of rails under the inner wheels is shown in Figure 7.39. In the figure, the dynamic stress of rails at the switch and crossing will increase slightly under the combined action of dynamic wheel load, flange force, and vertical and lateral deformation of the bridge. The maximum dynamic stresses of switch rail and point rail are, respectively, 177.2 and 130.7 MPa. The dynamic stress of rails in the transition lead curve is the smallest.

The distribution of vertical and lateral vibration acceleration of the bridge under the front axle is given in Figure 7.40. The vibration acceleration is small for smooth track. The vertical and lateral vibration acceleration can achieve 0.375 *g* and 0.078 *g* maximally, induced by track irregularities; however, both are acceptable.

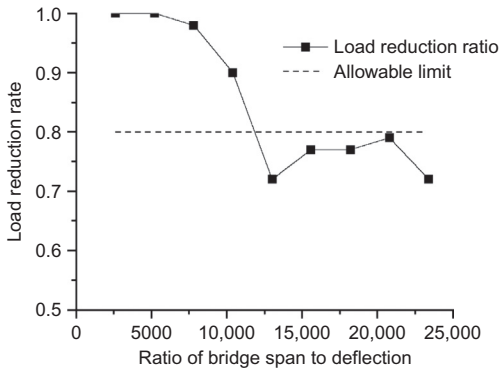

FIGURE 7.41

Change of load reduction rate with deflection/span ratio.

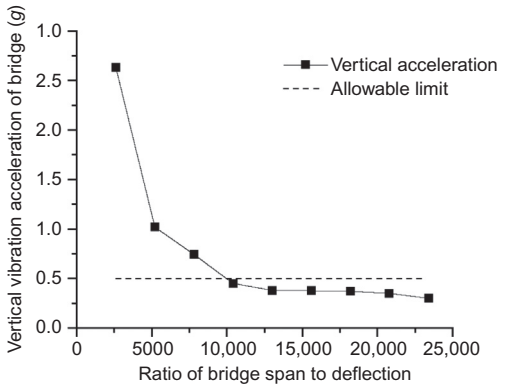

FIGURE 7.42

Vertical vibration acceleration of bridge with deflection/span ratio.

3. Impact of vertical stiffness of bridge on dynamic responses of CWR turnout on bridge

The vertical stiffness of a bridge can be expressed by the deflection/span ratio. Greater vertical bending stiffness means smaller deflection and smaller deflection/span ratio. In addition, lateral stiffness increases with vertical stiffness. The changes of load reduction rate and vertical vibration acceleration of the bridge with deflection/span ratio are given in Figures 7.41 and 7.42.

According to the calculation results, as the vertical stiffness of the bridge increases, the wheel—rail interaction indicators, such as dynamic wheel load, flange force, load reduction rate, derailment coefficient, lateral vibration acceleration of carbody, and vertical and lateral vibration acceleration of bridge, decrease. This is due mainly to the fact that the bridge with greater vertical stiffness can provide a more stable and reliable foundation for the turnout, thus easing the coupled vibration of the vehicle—turnout—bridge system. However, this impact may be less prominent when the vertical stiffness of bridge reaches a certain value. Considering the minimum vertical stiffness of bridge required by dynamic responses, the deflection/span ratio (load on the span of beams at the crossing) of the continuous beam under ZK load in China should not be below 1/12,000.

7.2.2 REGULARITY OF DYNAMIC INTERACTION OF SINGLE TURNOUT ON NONUNIFORM CONTINUOUS BEAM

1. Dynamic response of No. 18 turnout in main line on nonuniform continuous beam

Two No. 18 turnouts (see #5 and #7 in Figure 7.43) are symmetrically laid on a 4×32 m continuous beam in a station throat on the Beijing—Shanghai line, where the sub-rail foundation is composed of ballastless track with longitudinally connected base slabs.

When an EMU train travels in a No. 18 high-speed turnout on 4×32 m nonuniform beams in main/diverging directions, the distribution of dynamic responses of the vehicle—turnout—bridge system follows the same rule as on a 6×32 m uniform beam. The two

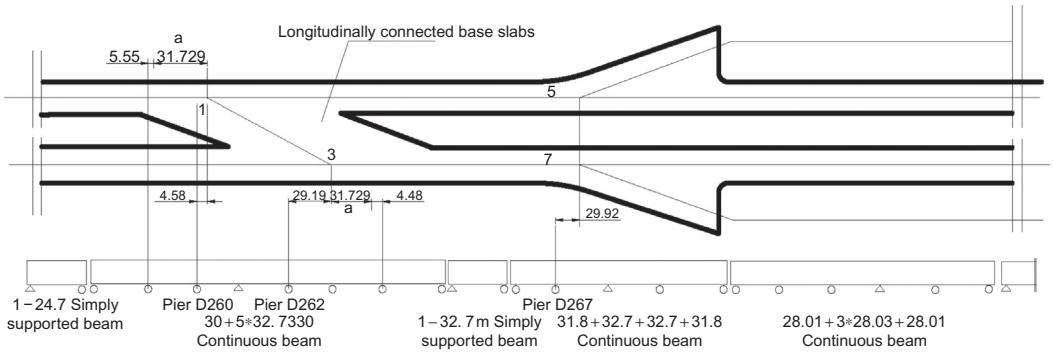

FIGURE 7.43

Relative position of turnout base slab and bridge in a station throat on Beijing−Shanghai line.

types of beams have the same cross section for the first span at turnout front, but differ in the number of spans and bridge cross section under the turnout. So the cross section of the span on the right of the 4×32 m uniform continuous beam will have greater flexural stiffness, whereas the vertical deflection deformation of the beam is small under train load. For nonintegrated bridge deck, different beam types will be adopted in the main and diverging lines: 4×32 m uniform continuous beam in the main line and 32 m simply supported beam in the diverging line. Table 7.4 presents the dynamic responses of a high-speed train traveling in high-speed turnouts on three types of continuous beams in main/diverging lines.

According to the calculation results, for a 4×32 m nonuniform continuous beam, the cross section and flexural stiffness are greater at the crossing, but the vertical deformation of the bridge is smaller than that of a 6×32 m uniform continuous beam; therefore, the dynamic wheel load, flange force, derailment coefficient, and vertical and lateral vibration acceleration of the bridge decrease when an EMU train travels in the main or diverging direction; in particular, the vertical vibration acceleration of the bridge drops significantly.

For a 4×32 m uniform continuous beam, the cross section and flexural stiffness of the bridge at the crossing are less than those of a nonuniform continuous beam, the dynamic responses (load reduction rate, derailment coefficient, etc.) are significant, and the load reduction rate can even achieve the allowable limit. Thus, where design difficulty occurs due to a wide bridge deck and an integrated deck is available in the main line only, the vertical stiffness of the bridge may be increased depending on the actual number of bridge spans.

2. Dynamic responses of No. 42 turnout in connecting line on nonuniform continuous beam

Figure 7.44 shows a Chinese No. 42 turnout laid on a 7×32 m continuous beam in a connecting line on the Beijing−Shanghai line. The distribution of dynamic wheel load and lateral vibration acceleration of the carbody when an EMU train travels in the main line are shown in Figures 7.45 and 7.46.

For a No. 42 turnout on a 7×32 m nonuniform continuous beam, the dynamic responses are well below those for a No. 18 turnout owing to small structural irregularities of the turnout. This indicates that the turnout−train−bridge coupled vibration is small due to the mild vibration impact

Table 7.4 Comparison of Dynamic Responses of Vehicle–Turnout–Bridge System for Three Types of Continuous Beam

Type of Continuous Beam	6 × 32 m Uniform Beam		4 × 32 m Nonuniform Beam		4 × 32 m Uniform Beam	
Turnout Direction	**Straight Direction**	**Diverging Direction**	**Straight Direction**	**Diverging Direction**	**Straight Direction**	**Diverging Direction**
Vertical deflection/span ratio of span at the crossing under ZK load	16,135		21,239		16,108	
Dynamic wheel load (KN)	179.4	118.1	178.8	112.9	178.3	119.2
Flange force (KN)	58.7	58.4	58.0	58.3	58.3	59.3
Load reduction rate	0.77	0.42	0.78	0.48	0.81	0.52
Derailment coefficient	0.66	0.57	0.56	0.56	0.60	0.58
Dynamic stress of rail (MPa)	177.4	178.4	187.0	186.6	189.1	187.2
Spread of switch rail (mm)	0.41	0.63	0.42	0.63	0.42	0.63
Spread of point rail (mm)	0.44	0.18	0.39	0.23	0.25	0.17
Lateral vibration acceleration of carbody (*g*)	0.037	0.078	0.037	0.078	0.037	0.079
Vertical vibration acceleration of bridge (*g*)	0.375	0.046	0.064	0.027	0.065	0.028
Lateral vibration acceleration of bridge (*g*)	0.078	0.120	0.041	0.104	0.044	0.115
Vertical deflection of bridge at maximum load reduction rate (mm)	0.094	0.133	0.227	0.210	0.322	0.291
Vertical deflection angle of bridge at maximum load reduction rate (0.001 rad)	0.032	0.029	−0.025	−0.021	−0.027	−0.023

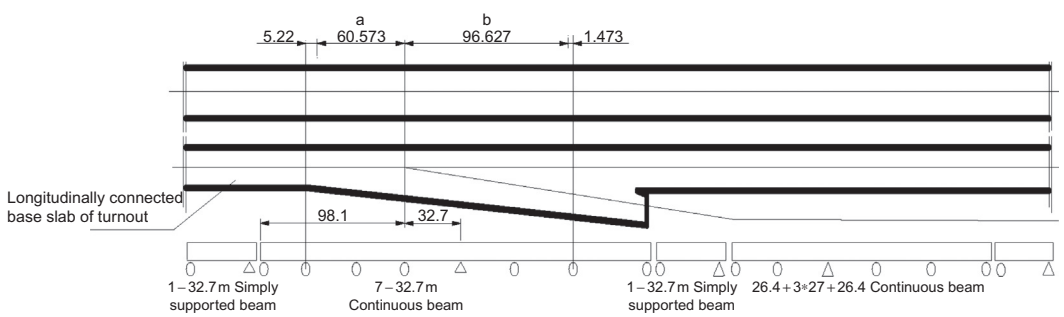

FIGURE 7.44

Relative position of bridge and base slab of No. 42 turnout in connecting line on Beijing–Shanghai line.

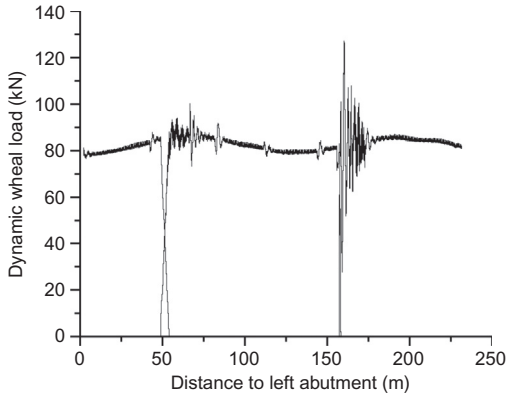

FIGURE 7.45

Distribution of dynamic wheel load when traveling in main line.

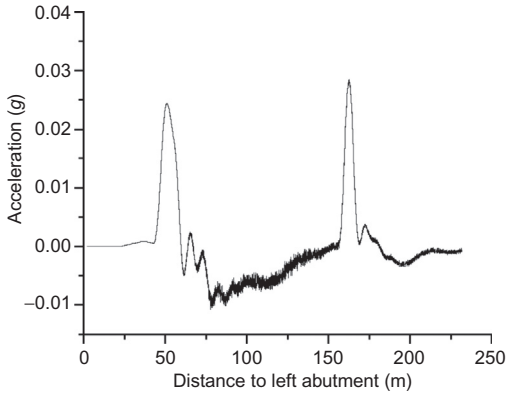

FIGURE 7.46

Lateral vibration acceleration of carbody when traveling in main line.

at the crossing. For a No. 42 turnout, the wheel load will be transited in a longer range on wing rail/point rail; therefore, the lateral vibration acceleration of the carbody at this part exceeds that at the switch when an EMU train travels in the main line.

In conclusion, owing to smaller structural irregularities at the switch and crossing, a No. 42 turnout on a 7×32 m nonuniform continuous beam will have smaller coupled vibration in the vehicle−turnout−bridge system, superior to a No. 18 turnout on bridge.

7.3 DESIGN REQUIREMENTS OF CWR TURNOUT ON BRIDGE

For riding safety and comfort, turnouts on bridges and subgrades may not have significant differences in geometry, line types, technical parameters, and manufacturing processes. To maintain the normal geometry and operational condition of turnouts on bridges against temperature change, vertical load of train, braking, or acceleration, the layout and design of bridges in a turnout area must be adjusted or altered properly. The layout of a turnout and bridge shall be fully studied prior to railway construction. This will not increase the investment greatly; instead, it can facilitate construction and operation in the future.

7.3.1 LAYOUT OF TURNOUT AND BRIDGE

Typical layouts of bridges and turnouts given below are proposed for No. 18 high-speed turnouts.

1. Single turnout on bridge

   The 4×32 m continuous beam may be adopted. The distances between the point of switch rail and the expansion gap at beam end and between heel of point rail and expansion gap at beam end are equal. The arrangement of turnout and bridge is given in Figure 7.47.

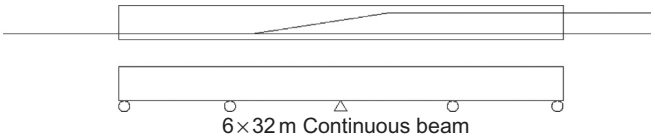

FIGURE 7.47

Layout of turnout and bridge for single turnout.

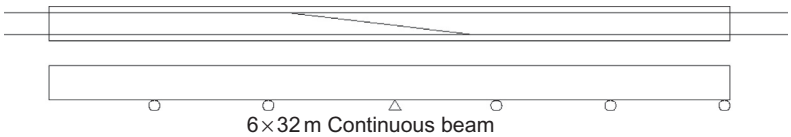

FIGURE 7.48

Layout of turnout and bridge beam for single crossover.

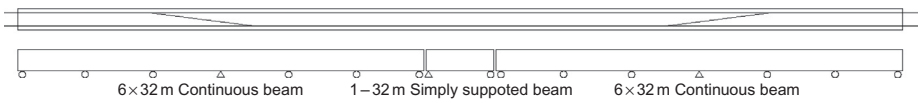

FIGURE 7.49

Layout of turnout and bridge beam for double crossover.

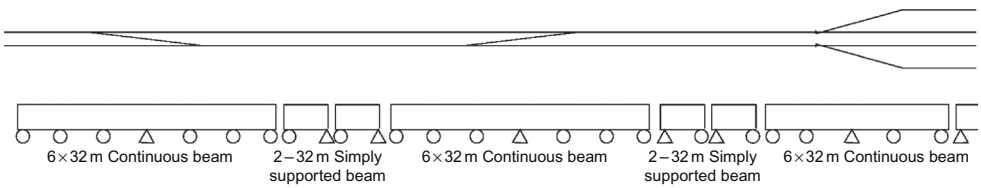

FIGURE 7.50

Layout of turnout and bridge beam for overtaking station.

2. Single crossover on bridge

   The 6×32 m continuous beam may be adopted. The centers of the crossover and continuous beam correspond. See Figure 7.48 for layout of the turnout and bridge beam.

3. Double crossover on bridge

   The combination of 6×32 m continuous beam, 32 m simply supported beam, and 6×32 m continuous beam may be adopted. The layout of the turnout and bridge beam is shown in Figure 7.49, or may be two-span or multi-span simply supported beam type in the middle.

4. Typical throat in elevated station

   The combination of 6×32 m continuous beam, $2-32$ m simply supported beam, 6×32 m continuous beam, $2-32$ m simply supported beam, and 4×32 m continuous beam may be adopted for bridge spans in overtaking stations. See Figure 7.50 for details.

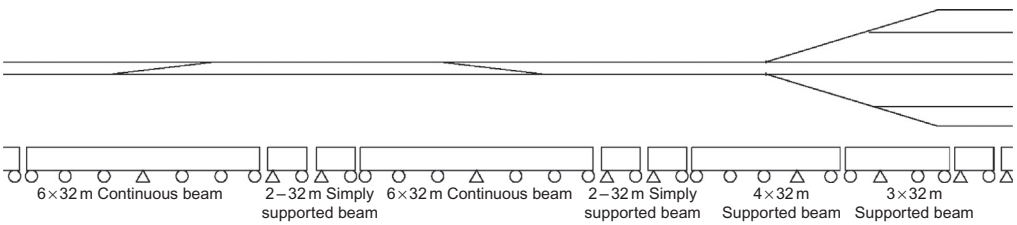

FIGURE 7.51

Layout of bridge beam and turnout for intermediate station.

The combination of 6×32 m continuous beam, 2−32 m simply supported beam, 6×32 m continuous beam, 2−32 m simply supported beam, 4×32 m continuous beam and 3×32 m continuous beam may be adopted for bridge spans in intermediate stations. See Figure 7.51 for details.

7.3.2 DESIGN REQUIREMENTS FOR CWR TURNOUT ON BRIDGE

Based on previous studies, recommendations on technical requirements for CWR turnout on bridge are given below, for the reference of designers.

1. General technical requirements
   - **a.** The geometric dimensions and structures shall be consistent with turnout on subgrade, and the speed shall not be inferior to that of the subgrade counterpart. If necessary, structure strengthening and optimization of wheel−rail relation and track stiffness design may be performed, or a turnout with greater number may be used
   - **b.** The rail joints in main/diverging directions and the joints between turnout and section shall be welded or glued insulted joints
   - **c.** One series of beams in a CWR turnout shall have the same sub-rail foundation. The transition between ballast and ballastless track foundation and between different ballastless track structures shall take place in a non turnout area or on subgrade. The length of interposed rail shall be compatible with bridge length
   - **d.** Base slabs shall be used for ballastless track, which shall be longitudinally connected. Otherwise, the base slab shall be connected with the bridge deck with Π-shaped reinforcements or longitudinal/lateral convex retaining blocks
   - **e.** The rail laying temperature shall be the same in one series of beams in the turnout, and shall also be consistent with nearby section line. As a rail link, the rail laying temperature difference between a CWR turnout and nearby section shall not exceed 3°C
   - **f.** Rail expansion joints may not be installed on bridges with CWR turnouts. If it is required, the distance between the expansion joint and turnout ends shall meet relevant requirements; and
   - **g.** For common track and turnout zones on bridges, different fastenings may be used; however, the same fastenings are preferred to facilitate later maintenance. The fastenings per span of beams shall be the same. On the stock rail with expansion joint or in areas with greater

temperature force, to ease the pier stress, a certain number of small-resistance fasteners shall be arranged, which shall be at least 25 m away from turnout beginning and end.

2. Requirements for bridge structure
   - **a.** For main line or connecting line turnouts on bridges, the bridge beam in the turnout area shall be of continuous structure. A frame bridge with a span length of 6−12 m and concrete continuous beam or concrete continuous rigid frame is preferred. In unfavorable conditions, ballast turnout for 160 km/h and above may be laid on concrete simply supported beams. In addition, the superstructure and substructure of the bridge shall be in harmony with the landscape
   - **b.** Turnout groups in the throat area and single crossover turnouts shall be laid on one series of beams. Two turnouts with intermediate straight lines longer than 600 m shall be laid on two series of beams. One span or multiple-span simply supported beams shall be provided between two adjacent beam series
   - **c.** The bridge deck in the turnout area on one series of beams shall be of integrated structure. In unfavorable conditions, such as in complicated throat areas with more than four tracks, the turnout in the main line or station line may be laid on different integrated decks. However, the relative displacement of two pieces of beam shall be technically acceptable
   - **d.** For single crossover turnouts on bridges, the bridge deck in the turnout area shall be of uniform width. For turnouts in throats or connecting lines, the bridge in the turnout area may be of nonuniform beam structure
   - **e.** Piers, at least the pier under a piece of beam, shall be of integrated structure
   - **f.** Bridge beam bearings may be of longitudinally and laterally fixed or movable type, longitudinally fixed and laterally movable type, or longitudinally fixed and laterally fixed type, depending on design control requirements for longitudinal or lateral horizontal displacement
   - **g.** The bridge deck shall be wide enough to install switch machines. The distance from the centerline of the main or diverging track to the edge of the switch machine installed on corresponding track shall be at least 3.0 m (within 5 m in front or in the rear of a switch machine). In addition, the installation of signaling devices (e.g., fouling post) should also be feasible; and
   - **h.** The vertical flexural limit of a continuous beam in the turnout area shall meet the requirements of riding safety and quality.
3. Requirements for turnout−bridge relative position
   - **a.** The CWR turnout shall be laid in the middle of a series of continuous beam whenever possible. The distance between turnout beginning and corresponding beam end shall be at least 18 m. As for the distance between turnout end and corresponding beam end, 9 m is preferred for ballast turnout, and 18 m or above is preferred for ballastless ones
   - **b.** If rail expansion joints are required at the end of a long and large continuous beam, the joints shall be installed at turnout rear, with the distance from turnout rear of at least 45 m. When being installed at turnout front, the distance from turnout front shall be at least 60 m. Where the expansion joints are arranged at both turnout front and rear, the distance between the expansion joint and turnout beginning/end shall be 10 m at minimum
   - **c.** For a CWR turnout on bridge, the crossing (normally the actual point of a point rail) shall be laid in the vicinity of the 1/8−1/4 span. The two turnouts in a single crossover may be

laid asymmetrically on continuous beams, so that the crossing may not be laid in the middle of the span or on the pier; and

d. If the two turnouts in a single crossover are laid symmetrically on continuous beams, the fixed bearings shall be arranged in the middle of the beam. If the two turnouts in a single crossover are laid asymmetrically on continuous beams, or a single turnout is laid on nonuniform continuous beams, the fixed bearings shall be laid on the side of the crossing that is close to the beam end.

CHAPTER

CONVERSION DESIGN OF HIGH-SPEED TURNOUTS

8

Conversion equipment is an important part of a turnout, which should have conversion, locking, and indication functions. For the conversion function, the operational direction of a turnout is shifted by lining the switch rail or swing nose rail with the conversion equipment, thus guiding the rolling stock to change lines. Locking function relates to the fact that the conversion equipment, after turnout conversion, must lock the turnout to bring the switch rail (point rail) and stock rail into contact. Indication function refers to the fact that after turnout conversion, the conversion equipment must display the normal position (closed straight switch rail and curved stock rail) and reverse position (closed curved switch rail and straight stock rail) of the turnout [103,104].

The design of turnout conversion involves structural design of conversion machines, locking machines, installation devices and closure detectors, computational check and relevant tests on design of traction points, switching throw, switching force, scant displacement, minimum flangeway, expansion displacement, and synchronous conversion and inclusion.

8.1 CONVERSION STRUCTURE AND PRINCIPLE

8.1.1 CONVERSION STRUCTURE [105]

1. Switch machine and installation devices

   The switch machine is the actuator of the conversion system. It has the conversion, locking, and indication functions, and is capable of converting and locking the switch rail or point rail and indicating its position and status in the locking zone. For the conversion function, it must have adequate tractive force for converting the switch rail (point rail), and enabling the rail to return to normal position in case of conversion failure. For the locking function, it must securely lock the switch rail (point rail) switched to a certain limiting position without releasing under external force; however, no locking occurs in case of conversion failure. For the indication function, it should indicate normal or reverse position, and turnout trailing. The switch machine may be an AC or DC motor, or be driven mechanically, hydraulically, or pneumatically. There are concentrated types and nonconcentrated types. At present, three types of switch machines are applied to speed-up turnouts and high-speed turnouts in China: S700K electric switch machines, ZDJ9 electric switch machines, and ZYJ7 electrohydraulic switch machines.

Design of High-Speed Railway Turnouts.

For speed-up lines and high-speed lines above 200 km/h, the switch machines should have double-locking function, that is, both operating rod and detecting rod (for closure detection) are provided with the locking function. The operation of a switch machine has to undergo the process of shutting off the original indication contact, unlocking, converting, locking, and connecting to a new indication contact. For an externally locked turnout, the switch machine should be capable of determining the applicable scope of the throw and indication rod of the switch machine as per the spread of the turnout. At different traction points, the turnout spread differs, and so do the applicable parameters of the switch machine. If conversion requirements are met, the parameters of the switch machine are simplified for versatility and standardization.

Installation devices connect the conversion equipment and engineering equipment. The devices are of three types: angle steel foundation, steel tie foundation, and angle block foundation. Angle steel foundations were used in early low-speed turnouts in China; however, they are not applicable to high-speed turnouts as they involve great free position of ties, which causes inconvenience to bed tamping, and strong vibration and shock of conversion equipment. For the steel tie foundation, the supporting plate of the conversion equipment is connected to steel ties, facilitating the operation of large maintenance machines. As for the angle block foundation, the vibration and impact of conversion equipment induced by a traveling train are much smaller than with angle steel foundations; the installation position of the switch machine is lowered, minimizing the risk of being damaged by suspended object under the train. Moreover, the operating and indication rods may be straight, which increases rod strength but occupies a certain free position of the tie, affecting the tamping work.

Selection of switch machines and structural design of angle block foundation are the main contents of the design of high-speed turnout in China. Figure 8.1 shows the installation devices for switch machines in ballast and ballastless turnouts.

2. Arrangement and distribution of traction points

The arrangement and distribution of traction points may be affected by switching resistance, turnout spread, scant displacement of switch rail, type of heel structure of switch rail, etc. As global railway construction forges ahead, single-point traction mode has been replaced by

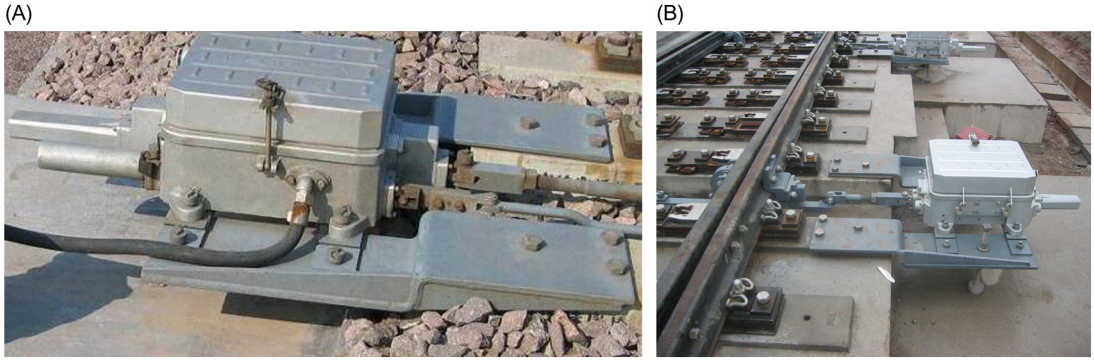

FIGURE 8.1

(A) Switch machine in ballast turnout. (B) Switch machine in ballastless turnout.

multi-point traction mode (for both switch rail and point rail) for turnouts. Multi-point traction mode is of two types: multi-machine multi-point traction point and one-machine multi-point traction mode.

For multi-point multi-machine traction mode, each traction point is an independent element of conversion, locking, and control, and provided with one switch machine for independent traction. The switch machines are connected by control circuit. The synchronous movement of switch rail and point rail is actuated mechanically or electrically. As every traction point is a relatively independent module, it may be synchronized with other traction points in addition to normal performance of conversion, locking, and indication functions. In case conversion, locking, or indication failure occurs at a traction point, the conversion system will produce no indication. Therefore, this traction mode is safer, more reliable, and more convenient for management. However, it involves many devices, and each module is provided with one machine and connected to the control room by separate cable line, which will be rather costly.

For one-machine multi-point traction mode, only the first traction points at the switch rail and point rail are provided with a switch machine for traction. The tractive force at the first traction point will be transmitted to other traction points through conduits to enable conversion, locking, and indication functions at other traction points. In case of operating failure (conversion failure, blockage, or no indication) at any traction point, the conversion system will produce no indication; instead, it will prompt the user that the turnout has not been converted as specified. This mode involves fewer switch machines, and other traction points can be operated by the connection of conduits, so it is cheaper.

Multi-machine multi-point traction mode has been adopted to suit the requirements of previous operational practice for high-speed turnouts in China.

3. Locking modes

Secure locking is critical for turnout conversion systems. There are two locking modes: external and internal locking. External locking refers to the fact that the properly converted switch rail or point rail is locked on the corresponding closed stock rail or wing rail. This mode is effective and has little impact on the switch machine, but has a complex structure. As for internal locking, the working switch rail or point rail will be locked on the device inside the switch machine via a switch rod. This mode is less effective and has greater impact on the switch machine. In terms of safety, external locking outperforms the internal type for high-speed turnouts, so it is required.

For high-speed turnouts in China, the external locking device of a switch rail is composed mainly of connecting iron, clevis pins with head, locking hook, retaining clamping plate, locking frame, locking block, and locking rod, as shown in Figure 8.2. The external locking device of a point rail is composed mainly of a locking rod, locking hook, and locking frame, as shown in Figure 8.3. For external locking, the locking frame is mounted on the wing rail directly. The flange of the point rail is inserted in the wedge slot of the locking hook, where the point rail can expand forward and backward in the slot. The conversion and locking of the point rail are enabled by the traction produced by lateral movement of the locking rod. The closure status of the point rail may be regulated by adding or removing adjusting spacers between the locking block and locking frame. The locking devices at the first traction point and other traction points are shown in upper and lower diagrams, respectively.

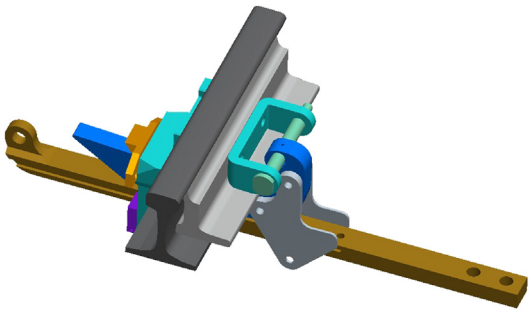

FIGURE 8.2

External locking device for switch rail.

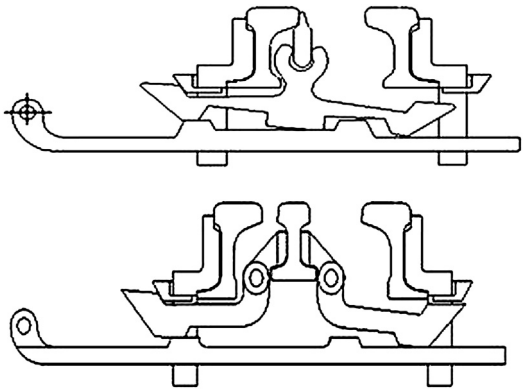

FIGURE 8.3

External locking device for point rail.

4. Operating modes of switch rail

   The switch rail may act simultaneously and separately. For simultaneous movement, two switch rails are connected by links, forming a frame structure; this features easier conversion of integral switch rails, simultaneous movement and locking of two switch rails, as well as great switching resistance. For separate movement, the two switch rails are not connected by link, but will perform unlocking, conversion, and locking functions separately, with the aid of an external locking device. As two switch rails move separately, the switching resistance of the system is reduced, which makes the conversion operation easier. The separate movement type has been adopted for high-speed turnouts in China.

5. Synchronous conversion of switch rails

   Synchronous conversion refers to the fact that the switch rails move to position simultaneously at each traction point. If the closed or separated switch rails fail to move to position at the same time, obviously it can be found that the switch rails move out of step, that is the conversion is asynchronous. As the traction of conversion and locking of switch rails by conversion equipment occurs at traction points only, simultaneous movement of the traction points is a prerequisite to synchronous conversion. This may be affected by the throw of the switch machine, locking throw and clearance of locking, movement sequence of traction points, turnout spread, switching resistance of the switch rail, line type of switch rail, etc. Therefore, those influencing factors must be compatible for synchronous conversion of switch rails.

   For high-speed turnouts in China, this is enabled by using switch machines with different rated throws and different starting sequences so as to avoid peak current of the motor.

6. Closure detection

   In addition to converting and locking switch rails and point rails, the conversion system must be capable of detecting and monitoring the closure of switch rails and point rails, and giving alarms and prompts in case of unsatisfactory closure status. Detection applies to traction points and the position between two adjacent points.

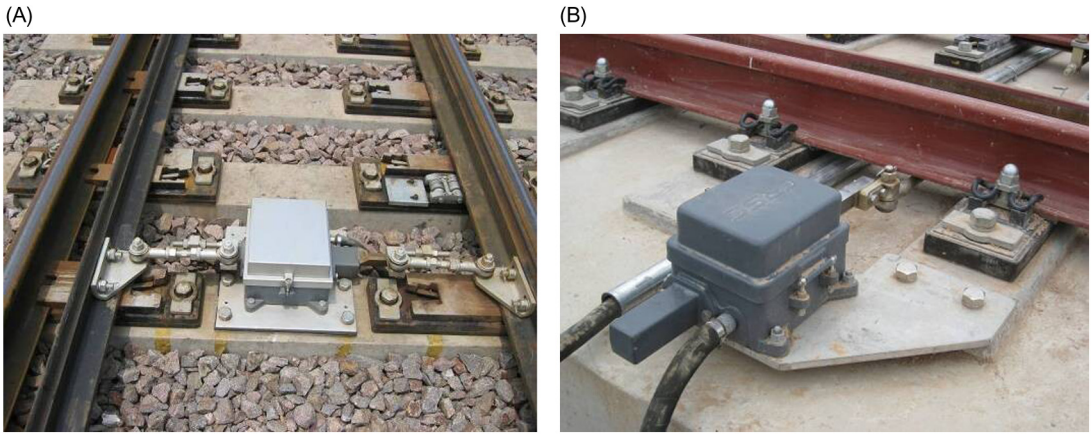

FIGURE 8.4

(A) JM-A1 closure detector. (B) JM-A closure detector.

For Chinese turnouts with the multi-point multi-machine traction mode, the closure detection at a traction point is done by the switch machine at this point, whereas closure between two traction points is made by a closure detector mounted in between. The detection contacts of closure detectors are serially connected in the indication circuit of the conversion system. In case of any abnormal indication from the switch machine at a traction point or abnormal indication of closure detection between two traction points, the conversion system will prompt the user that the turnout is in abnormal condition and will be maintained. This function is of great significance for normal operation of turnouts.

JM-A1 and JM-A closure detectors are used in China; they are installed in the center and two sides of the track, between two traction points, as shown in Figure 8.4. No indication is produced in case of 5 mm inclusion. No closure detector is provided between the traction points on point rails at present.

8.1.2 PRINCIPLE OF TURNOUT CONVERSION [106]

In practice, the switch rail and point rail will be converted as per the required route direction of trains with the aid of connections between operating rods and switch machines. During conversion, the operating rod of a switch machine will exert switching force on the switch rail and point rail at traction points to enable specified displacement at those traction points, that is traction throw. The switching force at a traction point equals the concentrated counterforce at this point. When being converted to position, the rails will be locked securely with external locking devices. Normally, in addition to the lining operation, a margin is reserved for the total capacity of the switch machine to ensure proper lining. For multi-machine multi-point traction, each machine is separately circuited with the control room and controlled through an AC control circuit. In this case, proper design of traction throw may be conducive to simultaneous, synchronous, and coordinated conversion of the switch rail and point rail.

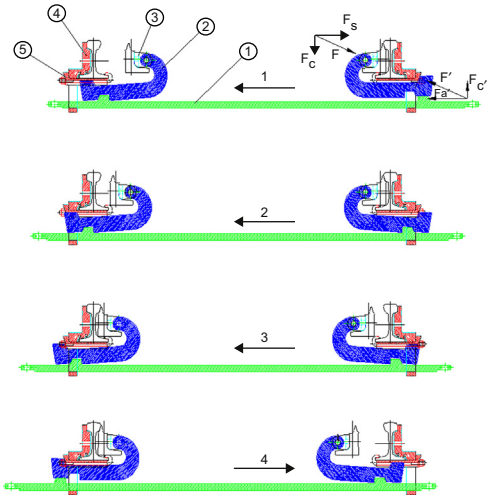

FIGURE 8.5

Conversion process of switch rail.

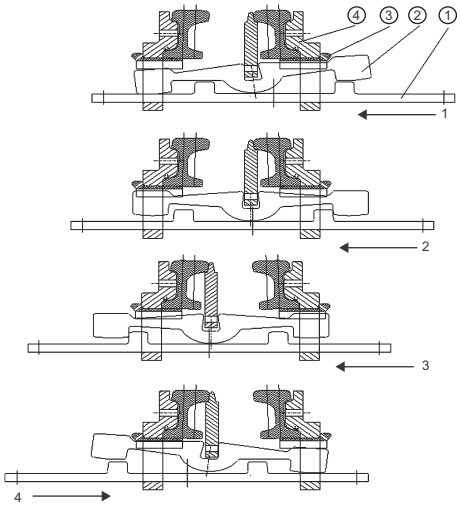

FIGURE 8.6

Conversion process of point rail.

1. Multi-machine multi-point traction mode

   The conversion process for switch rail with multi-machine multi-point separate movement mode is shown in Figure 8.5: releasing the locked switch rail at one side, converting, and relocking the switch rail converted in position. In this process, the resultant force of the hook will pass through the cross section center of the switch rail, and the switch rail and locking hook are in good stress state. The hook-type external locking of the switch rail is mainly composed of locking rod (①), hook (②), connecting iron (③), and locking frame (④, ⑤).

   The hook-type external locking of point rail consists of a locking rod ①, hook ②, connecting iron ③, and locking frame ④; see Figure 8.6 for the operating principle. The locking frame is directly mounted on the wing rail; the flange of the point rail is inserted in the wedge slot of the locking hook, where the point rail can expand freely in the slot. The point rail is converted and locked through the traction of lateral movement of the locking rod. The closure status of the point rail may be regulated by adding or removing adjusting spacers between the locking block and locking frame.

   The external locking process of the point rail: The locking rod (①) moves left from position 1 to position 2; the external locking hook (②) rotates for release; the locking rod moves further left to position 3, and drives the conversion of the switch rail to the other side through the hook; the locking rod moves further left to position 4, the hook rotates and locks the rail, and one operation process is complete. At position 4, the right movement of the locking rod follows the same sequence as above, so as to complete another operation process.

2. One-machine multi-point traction mode

   For high-speed turnouts in France, one-machine multi-point traction is used, and the switch rails move simultaneously and are locked with an external locking device. The locking is secured by employing external locking at traction point 1, and the traction force is transmitted

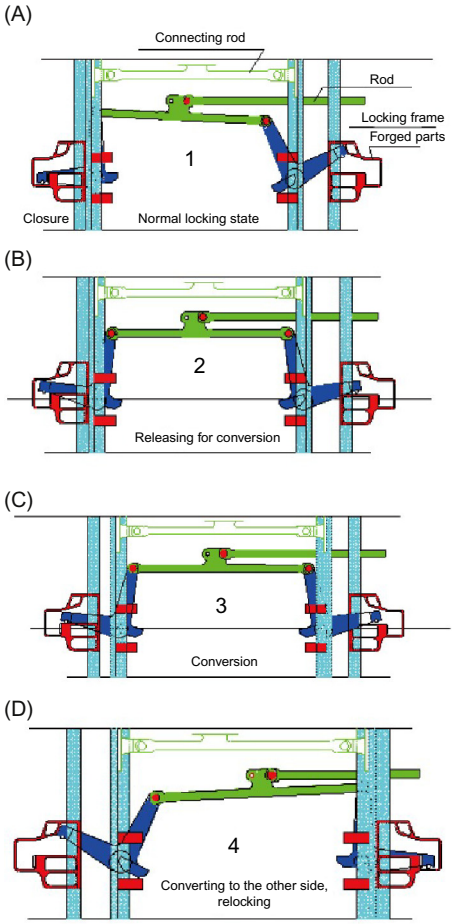

FIGURE 8.7

Conversion principle for one-machine multi-point traction mode: (A) Step 1; (B) Step 2; (C) Step 3; (D) Step 4.

to other traction points via conduits to realize synchronized movement of all traction points. The throws of traction points are distributed via a crank, which can amplify the electrical power. The principle of conversion and locking of the switch rail is shown in Figure 8.7. The main process includes locking, releasing, converting, and relocking.

8.2 CALCULATION THEORY OF TURNOUT CONVERSION [106]

The arrangement of traction points and throw design are based on the calculation results for switching force. Normally, the minimum number of traction points is preferred. The switching force at

each traction point should not exceed the rated power of the switch machine, but the minimum flangeway should be maintained after conversion of the switch rail. For smoothness, the scant displacement of conversion of switch rail and point rail must be within the allowable range of gauge deviation. In case of inclusion at any traction point or between traction points, no or fewer closure detectors are to be installed, provided that the closure status can be judged from the inordinate abnormality of switching force.

8.2.1 CALCULATION MODEL [107,108]

An analysis model of high-speed turnout conversion is established as per finite element theory, as shown in Figure 8.8. In the model, special configuration and critical details (e.g., characteristics of sections of switch rail/point rail, location of traction point and throw) and linear and nonlinear factors during conversion (e.g., friction force, counterforce of closure, and jacking block and fastening resistance) are taken into account. The effect of the counterforce of closure and jacking block and the fastening support are modeled with nonlinear springs. The switch rail and point rail are modeled with nonlinear, nonuniform beams; fasteners are modeled with nonlinear springs. The fillers between long and short point rails ahead of the heel are modeled with springs, and fillers at heel are modeled with uniform beams.

1. Calculation model for conversion of switch rail

   For separate movement conversion, the straight and curved switch rails are converted at the same time. The separated switch rail will move first, followed by the closed rail. For simultaneous movement conversion, two switch rails will move to position simultaneously. In terms of the traction and conversion modes for turnouts in China, separate movement external locking is to be analyzed in detail. Where the straight and curved switch rails have the same traction throw, given the number of traction points of n, the conversion distance of traction points at a given time consists of conversion distance of the closed switch rail (D) and that of the separated switch rail (D'):

$$\begin{cases} D = [D_1 \quad \dots \quad \dots \quad D_n] \\ D' = [D'_1 \quad \dots \quad \dots \quad D'_n] \end{cases} \tag{8.1}$$

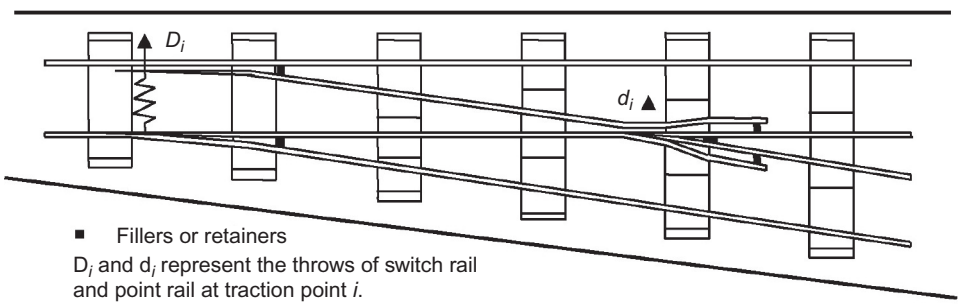

FIGURE 8.8

Analysis model of turnout conversion.

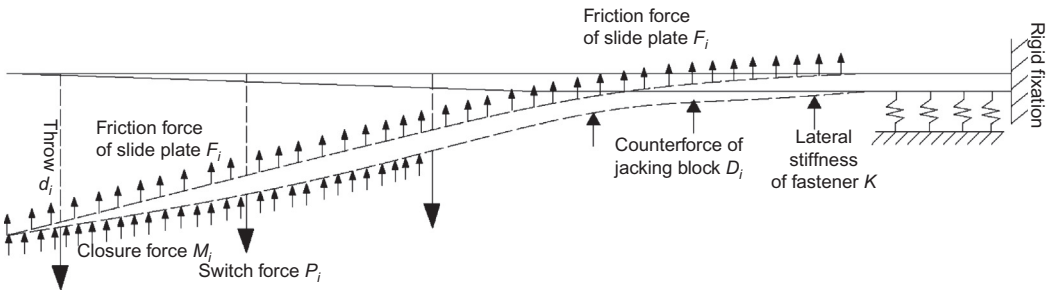

FIGURE 8.9

Calculation model for conversion of switch rail.

Total switching force at traction points on corresponding switch rail:

$$P_J = \lfloor P_{J_1} \quad \dots \quad \dots \quad P_{Jn} \rfloor \tag{8.2}$$

The calculation model is elaborated in Figure 8.8, and the model for conversion of the switch rail is plotted in Figure 8.9. The corresponding positions of the actual point of the switch rail, tie, and tie center are taken as nodes of the switch rail. The traction points are linked by nonlinear springs. The conversion time difference between straight and curved switch rails can be ensured by modifying the spring parameters. In calculating simultaneously moving switch rails, the straight and curved switch rails are linked by uniform beams; the initial conversion of the switch rail can be ensured by modifying initial parameters of the switch rail.

The straight and curved switch rails cling to the stock rails at design initial position. All rail parts are manufactured and laid in strict accordance with design dimensions. During traction and conversion, the closed switch rail will be separated and reclosed through lining. The converted position and design initial position will not coincide exactly. The gap between the two positions is the scant displacement of conversion of switch rail.

2. Calculation model for conversion of point rail [109]

After refining the calculation model shown in Figure 8.8, the calculation models of the point rail with a single flexible rail and double flexible rails are given in Figure 8.10. The actual point of the point rail is movable. The retractility of fillers between point rails and between point rail and wing rail will be considered. The state of the point rail in the curve can be realized by controlling the coordinates of the node of the short point rail. During calculation, the coordinate of each node at the crossing coincides with the design. The dimensions and spacing of ties are also consistent with the design.

For a point rail with a single flexible rail, the short point rail is provided with a diagonal joint at the heel, which is unfavorable for high-speed traveling in the diverging line. The point rail with double flexible rails is used in high-speed turnouts in the diverging direction. This point rail is of integral framework structure, characterized by great lateral stiffness and difficult control of conversion line type.

When a train travels in a straight direction, the point rail is in normal position, and the long point rail will operate. When traveling in the diverging line, the point rail in normal position will be converted to reverse position with the aid of conversion equipment, and the conversion

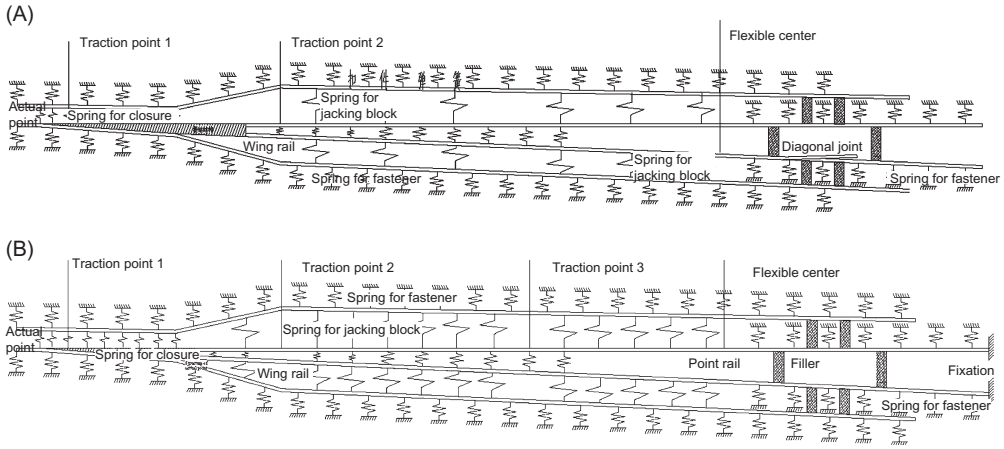

FIGURE 8.10

(A) Calculation model for conversion of point rail with single flexible rail. (B) Calculation model for conversion of point rail with double flexible rails.

is realized by the switch machine through the rod. The switching force on the traction point is the counterforce of the point rail on the switching rod. In terms of traction and conversion, the throws at all traction points on long and short point rails are the same. Assuming that n traction points are arranged, the throw is:

$$d = \begin{bmatrix} d_1 & \dots & \dots & d_n \end{bmatrix} \tag{8.3}$$

Total switching force at traction point on corresponding point rail:

$$P_X = \begin{bmatrix} P_{X1} & \dots & \dots & P_{Xn} \end{bmatrix} \tag{8.4}$$

The point rail will remain in the initial position during passage in the main line. In calculating the scant displacement between normal and reverse positions, it is assumed that there is no friction force, closure force, or lateral flexural stiffness at the heel during conversion, and the working surface of the switched point rail can reach the ideal state $Y(i)$. However, when linear or nonlinear factors, for example friction force, closure force, jacking block force, and fastening resistance, are considered, the line type $y(i)$ can be obtained after converting from normal position to reverse position. The scant displacement of conversion can be obtained by $\Delta(i) = Y(i) - y(i)$. Another line type can be obtained when the point rail is converted in the opposite direction, and relevant scant displacement can be calculated accordingly.

3. Mechanical equation and solution for conversion calculation

The equation of mechanical equilibrium for turnout traction and conversion can be solved by the principle of minimum potential energy of variation. Of the coordinating displacements that satisfy boundary requirements, the total potential energy of the system will reach the limit value due to displacement under equilibrium condition

$$\delta U + \delta V = 0 \tag{8.5}$$

where U and V are the first-order variation of total strain energy and total potential energy of the system, respectively. With the variational expressions of all energies, the stiffness matrix and load matrix of the system can be formed.

For general structure, it is difficult to obtain an algebraic solution of nonlinear equation directly; however, it may be obtained by numerical solutions. During the conversion, a number of nonlinear factors exist that may induce load/displacement change, so the combination of incremental method and modified Newton−Raphson method may be applied to solving the nonlinear equations. On the one hand, the load can be divided into increments and imposed by steps as per incremental methods; so, on the other, iteration is performed in one increment, so as to obtain adequately accurate solution.

8.2.2 ONE-MACHINE MULTI-POINT TRACTION MODE [11O]

For one-machine multi-point traction, the switch machine is provided at the first traction point, and the switching force will be transmitted to other traction points via double conduits. The switching throws of traction points are distributed by a crank, and the electrical power may be amplified. See Figure 8.11 for a schematic diagram of calculation.

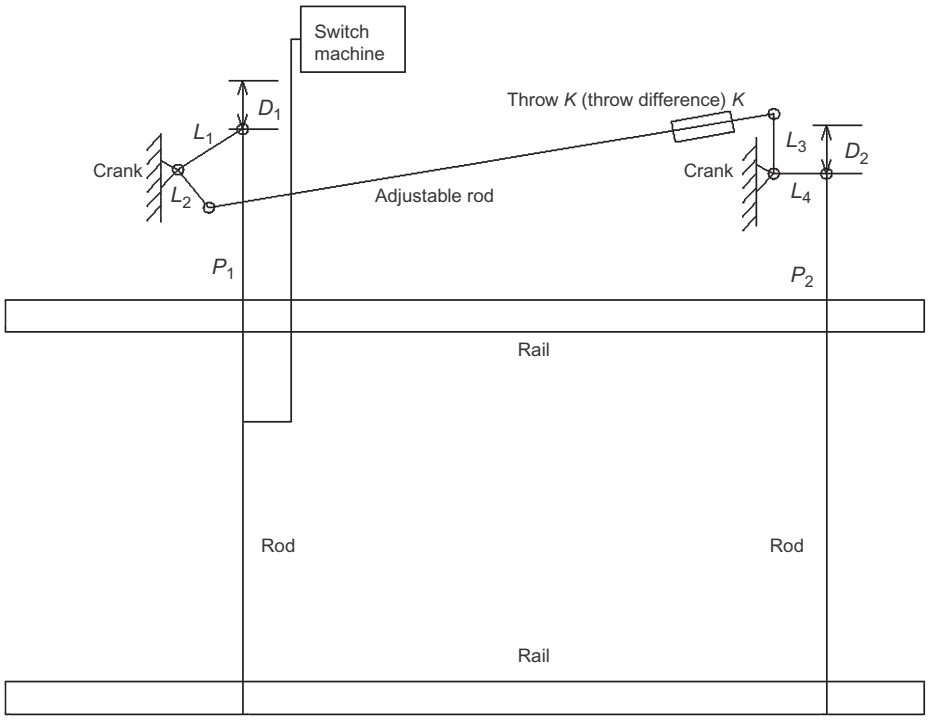

FIGURE 8.11

Schematic diagram of conversion calculation for one-machine multi-point traction mode.

The dimension of the crank can enable the synchronous movement of traction points. During conversion, the throws of traction points are distributed by the crank. However, considering certain idle throws for the adjustable rod, the throw of the traction point will not be designed exactly as per crank size. Given the throw of traction point:

$$D = \begin{bmatrix} D_1 & \dots & \dots & D_N \end{bmatrix} \tag{8.6}$$

Switching force at corresponding traction point during conversion will be:

$$P = \begin{bmatrix} P_1 & \dots & \dots & P_N \end{bmatrix} \tag{8.7}$$

Then, the electric power of switch machine can be obtained as per force transmission features of the crank:

$$\sum P = P_1 + \frac{L_4}{L_3} \cdot \frac{L_2}{L_1} \cdot P_2 \tag{8.8}$$

During conversion, the rod will exert switching force on the switch rail and point rail at traction points, enabling the given displacement and traction throw of each traction point. The switching force at a traction point is the concentrated counterforce at the point. The electric power and switching force at a traction point will change constantly during conversion. The peak values of electric power and switching force may not coincide exactly.

8.2.3 TEST OF FRICTION COEFFICIENT OF SLIDE PLATE

As per laboratory tests, for a common slide plate with a smooth surface, the friction coefficient is 0.153−0.191 if not greased, or 0.107−0.148 if greased. This indicates that greasing can reduce the friction effectively. In case one end of the side plate is lifted by 10 mm and inclined, the coefficient will be 0.196−0.210 if not greased, or 0.128−0.155 if greased. As the inclination and surface unevenness may increase, this coefficient is taken as 0.25 in calculation.

For a rollered slide bedplate, if the lifting amounts of two rollers are equal, the coefficient will be 0.044−0.069; the value will be 0.054−0.094 for rollers with different lifting amounts. This coefficient is taken as 0.10 in calculation [112].

8.3 STUDY AND DESIGN OF HIGH-SPEED TURNOUT CONVERSION

In studying and designing high-speed turnout conversion with related calculation theory, the switching force (lining force) will not exceed 6 kN, the minimum flangeway shall be at least 65 mm, the maximum scant displacement shall not exceed 2 mm, and the gaps between closed rails shall not exceed 0.5 mm.

8.3.1 SWITCH RAIL OF HIGH-SPEED TURNOUT

1. Movable length [111]

   The movable length will be minimized during traction and conversion, as the switch rail is relatively long; the movable length will be strictly constrained, which may be shortened by

moving the fixed end forward, if possible. The forward-shifting of the fixed end of the switch rail can reduce the expansion amount of the rail under temperature load, thus diminishing the risk of blockage. In addition, this measure can increase the lateral flexural stiffness of the switch rail, and decrease scant displacement, maintaining the line type of the switch rail during operation. However, shortening of the movable length is accompanied by a shorter distance between the last traction point and heel, which may increase the switching force at the traction point, or even lead to nonconforming flangeway. The movable length of curved switch rail of a No. 18 turnout in China is obtained with Eq. 2.17, that is 18,745 mm. To ensure proper minimum flangeway width in the case of shorter switch rail, nonlinear traction throw may be used, but this may increase the switching force.

2. Impact of arrangement of traction points

For high-speed turnouts in China, the throw of the first traction point on the switch rail is 160 mm. The throws of other traction points will change linearly as per the distance to heel. As the arrangement of traction point differs, the switching force and scant displacement may vary accordingly.

An illustration is given with the example of Chinese No. 18 turnouts, where three traction points are arranged on the switch rail. Table 8.1 presents the calculated switching forces and scant displacements of switch rails with common slide plates for different arrangements of traction points. The distribution of scant displacement is plotted in Figure 8.12. It can be seen that the switching forces at the three traction points are all acceptable. The spacing of traction points increases; the total friction force of slide plate and gap between switch rail and stock rail increase accordingly. However, as the distance between the last traction point and heel decreases, the scant displacement drops significantly.

If four traction points are provided, with spacings of 3.6, 4.2, and 4.2 m, the maximum scant displacement will be 2.0 mm, and the maximum gap between closed rails is about 0.22 mm. The distribution of switching force is plotted in Figure 8.13. In the figure, as the throw of the switch rail increases, the switching force increases accordingly. At the moment when the switch rail clings to the stock rail or jacking block, the change of line type will lead to a sharp change of switching force at the last traction point.

In the design of Chinese speed-up turnouts, the last traction point is generally arranged at the end of the closed zone (spacing of traction points: 4.2 m). In this way, the closure status at

Table. 8.1 Switching Force and Scant Displacement of Switch Rail of Chinese No. 18 Turnouts

Spacing of Traction Points (m)	Switching Force at Traction Point 1 (N)	Switching Force at Traction Point 2 (N)	Switching Force at Traction Point 3 (N)	Gap at Closed Zone (mm)	Scant Displacement of Conversion (mm)
4.2, 4.2	881.7	828.4	5456.4	0.22	6.71
4.2, 4.8	909.5	1124.7	5696.6	0.22	5.58
4.8, 4.8	1049.1	1254.9	5420.2	0.36	4.63
4.8, 5.4	1010.3	1395.4	5047.2	0.32	3.84
5.4, 5.4	1208.2	1568.2	4878.6	0.53	3.18
5.4, 6.0	1168.4	1787.8	4738.4	0.49	2.64

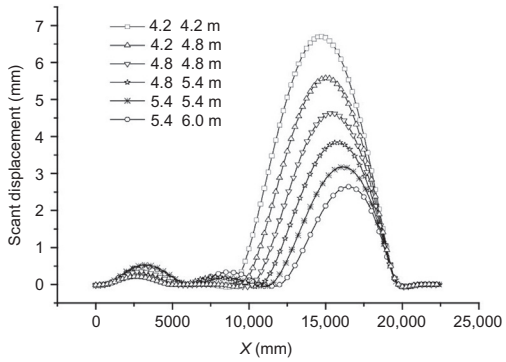

FIGURE 8.12

Impact of arrangement of traction points on scant displacement.

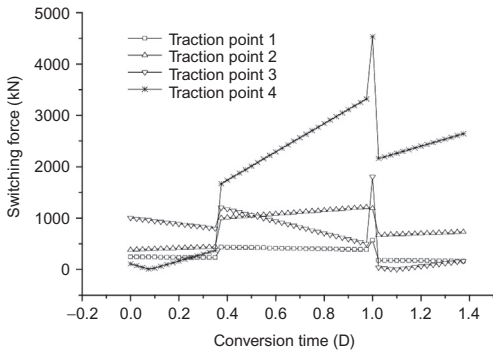

FIGURE 8.13

Distribution of switching force for four-point traction mode.

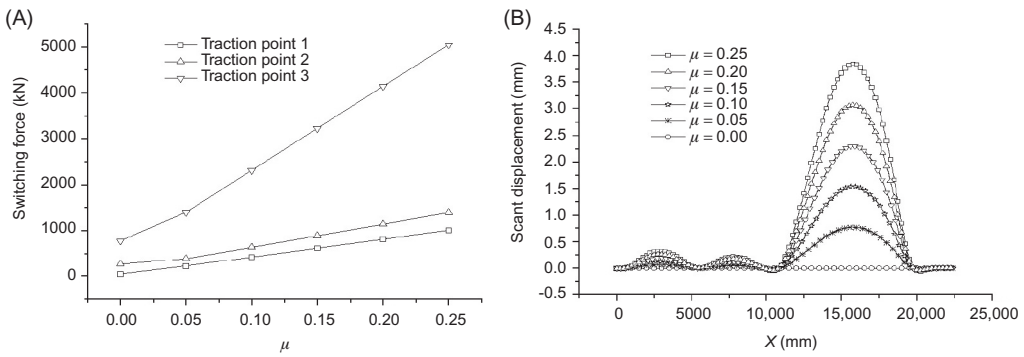

FIGURE 8.14

(A) Change of switching force with friction coefficient of slide plate. (B) Change of scant displacement with friction coefficient of slide plate.

this zone can be monitored with the indication rod. As in large number turnouts for high speed, the greater distance between the last traction point and heel may cause inordinate scant displacement. By comparison, for No. 18 turnouts in China, if three traction points are arranged on the switch rail, the spacings of traction points will be 4.8 and 5.4 m, and the distance between the last traction point and fixed position is 8.04 m. Additionally, rollered slide plate may be used to reduce switching force and scant displacement.

3. Impact of friction coefficient of slide plate [113]

The change of switching force at various traction points and scant displacement of switch rail of No. 18 turnouts with friction coefficient of the slide bedplate are depicted in Figure 8.14. As per the calculation results, the switching force at various traction points increases with the friction coefficient; in particular, the last traction point witnesses a significant increase.

Similarly, the scant displacement and gap between switch rail and stock rail increase with the coefficient. At a friction coefficient of 0.1, the maximum scant displacement is about 2.0 mm, meeting the design requirement. Therefore, rollered slide plate is required to reduce the friction coefficient reasonably.

4. Impact of roller arrangement

   The first rollered slide plate is arranged at the tie right before the first traction point on the switch rail (for No. 18 high-speed turnouts in China), and the rest slide plates are arranged as per tie spacing. The calculated switching force and scant displacement of switch rail under different arrangements of rollered slide plate are listed in Table 8.2. The rollers mitigate the switching force prominently, ensuring the switching forces at all traction points are acceptable and easing the scant displacement effectively. Six rollers enable good contact status between switch rail and stock rail, effectively easing the scant displacement between traction point 3 and heel, as well as resulting in a smaller switching force. Hence, this design is employed in No. 18 high-speed turnouts in China.

5. Easement of scant displacement with reverse deformation [114]

   For smaller scant displacement, reverse deformation, as shown in Figure 8.15, may be preset between the last traction point and heel, where the rise equals the scant displacement. The scant displacements of the switch rail of No. 18 and 42 turnouts with reverse deformation of different wavelengths and shapes are plotted in Figure 8.16.

   According to the calculation, circular reverse deformation on the switch rail may lead to negative scant displacement, which may further cause greater counterforce of the jacking block and a substantial rise in switching force. On the contrary, cosinusoidal reverse deformation enables good line type of switch rail. For a No. 18 turnout, 9.0-m-long cosinusoidal reverse deformation is preferable, accompanied by a maximum switching force of 3653.6 N and

Table 8.2 Switching Force and Scant Displacement of Rollered Switch Rail

Number of Rollers/Tie Spans	Switching Force at Traction Point 1 (N)	Switching Force at Traction Point 2 (N)	Switching Force at Traction Point 3 (N)	Gap at Closed Zone (mm)	Scant Displacement of Conversion (mm)
0/0	1010.3	1395.4	5047.2	0.32	3.84
5/6	654.9	888.3	3600.6	0.26	2.54
6/5	548.4	893.0	3253.6	0.23	1.98
7/4	436.2	888.8	3371.1	0.17	2.11

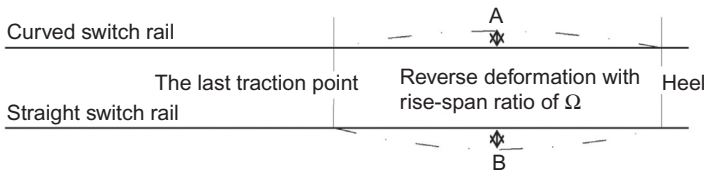

FIGURE 8.15

Arrangement of reverse deformation for switch rail.

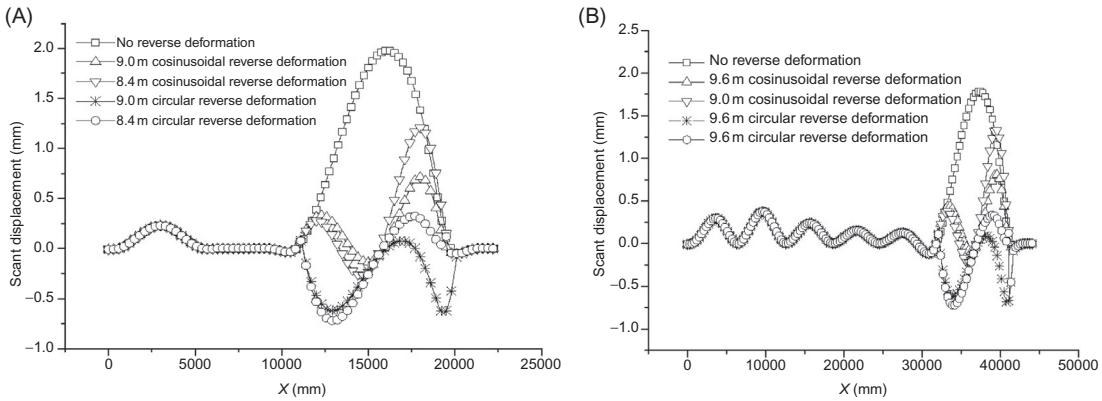

FIGURE 8.16

(A) Scant displacement of switch rail of No. 18 turnout. (B) Scant displacement of switch rail of No. 42 turnout.

Table 8.3 Impact of Inclusion on Switching Force at Various Traction Points of Switch Rail

Location of Inclusion	Size of Inclusion (mm)	Switching Force at Traction Point 1 (N)	Switching Force at Traction Point 2 (N)	Switching Force at Traction Point 3 (N)
Traction point 1	4	>6000	1169.2	3253.7
	6	>6000	1505.5	3253.7
	8	>6000	1841.9	3253.7
Between traction points 1 and 2	4	5869.1	5813.7	3254.0
	6	>6000	>6000	3254.3
	8	>6000	>6000	3254.5
Traction point 2	4	2067.7	>6000	2093.8
	6	2793.9	>6000	2791.9
	8	3543.6	>6000	3687.3
Between traction points 2 and 3	4	383.0	>6000	>6000
	6	383.0	>6000	>6000
	8	383.0	>6000	>6000

maximum scant displacement of 0.48 mm. For a No. 42 turnout, 9.6-m-long cosinusoidal reverse deformation is the optimum, associated with a maximum switching force of 3759.4 N and maximum scant displacement of 0.83 mm.

6. Impact of inclusion

Should any abnormal rigid body (a so-called inclusion) exist between two traction points of switch rail, for No. 18 turnouts in China, the switching forces at all traction points will be as listed in Table 8.3.

From Table 8.3, inclusion will greatly impact the switching force, particularly at traction points. An inclusion between two traction points may exert greater influence on nearby traction

Table 8.4 Results of Dynamic Simulation in Case of Inclusion

Safety Factor		Derailment Coefficient			Load Reduction Rate			Spread of Actual Point of Switch Rail or Point Rail (mm)		
Size	**Inclusion (mm)**	**3**	**4**	**5**	**3**	**4**	**5**	**3**	**4**	**5**
Location	Traction point 1 on switch rail	0.33	0.46	0.69	0.18	0.26	0.40	3.34	**4.57**	**5.90**
	Between traction points 1 and 2 on switch rail	0.42	0.66	0.85	0.21	0.30	0.47	2.11	2.74	3.58
	Traction point 2 on switch rail	0.55	0.76	1.02	0.24	0.35	0.58	1.46	1.98	2.57
	Between traction points 2 and 3 on switch rail	0.40	0.59	0.76	0.19	0.32	0.44	0.84	0.91	0.95
	Traction point 3 of switch rail	0.34	0.51	0.62	0.17	0.23	0.30	0.77	0.79	0.78
	Traction point 1 on point rail	0.74	0.92	1.12	0.45	0.62	0.78	3.88	**4.97**	**6.21**
	Between traction points 1 and 2 on point rail	0.94	1.17	**1.38**	0.50	0.68	**0.85**	3.30	**4.33**	**5.54**
	Traction point 2 on point rail	0.91	1.04	**1.22**	0.46	0.66	0.79	2.86	3.80	4.91

points, and smaller influence on the rest. The switching force is below 6000 N only when a 4-mm inclusion exists between traction points 1 and 2. In other cases, scant displacement and locking failure may occur. To detect an inclusion greater than 4 mm between traction points 1 and 2, a switch machine with rated capacity of 2500 N may be adopted, so as to prevent inordinate switching force under normal conditions, or locking failure in case of abnormality.

According to the theory of turnout dynamics, supposing an EMU train travels in a No. 18 high-speed turnout in China in the main direction at 350 km/h; in case of inclusions (rigid) of different sizes between traction points, the analysis results of dynamic simulation will be as given in Table 8.4.

The derailment coefficient, load reduction rate, and spread of switch rail (point rail) will increase with greater size of inclusion. The maximum values of derailment coefficient and load reduction rate occur when inclusions exist at traction point 2 and between traction points 1 and 2. For this reason, in case of gaps of 4 mm and above between switch rail and stock rail or between point rail and wing rail at the centerline of external locking at the traction point for high-speed turnouts in China, no indication of locking or indication will be enabled. At the closed zone of the switch rail or point rail, no indication will be enabled in case of an inclusion of 5 mm or greater between traction points. Therefore, to ensure safe transport, high-speed turnouts must go through laboratory and field tests following the principle of "no locking in case of 4 mm inclusion at any traction point" and "indicating in case of 4 mm inclusion, and no indication in case of 5 mm inclusion between traction points."

7. Impact of conversion time difference

Conversion time difference involves the conversion time difference between two switch rails and that at different traction points. For separate movement switching, the straight and curved

Table 8.5 Impact of Conversion Time Difference on Switching Force of Switch Rail

Conversion Time Difference (mm)	Switching Force at Traction Point 1 (N)	Switching Force at Traction Point 2 (N)	Switching Force at Traction Point 3 (N)
All traction points move to position simultaneously	548.4	893.0	3253.6
Traction point 1 moves to position 0.1 D in advance	4111.9	893.7	3479.4
Traction point 1 moves to position 0.1 D late	405.5	3417.8	3107.9
Traction point 2 moves to position 0.1 D in advance	510.7	2185.2	2647.0
Traction point 2 moves to position 0.1 D late	5082.2	1856.0	5939.8
Traction point 3 moves to position 0.1 D in advance	648.6	719.3	4055.1
Traction point 3 moves to position 0.1 D late	452.5	2625.1	2872.9

switch rails may act successively. As per the calculation, the greater the time interval, the better the conversion independence of two rails, and the greater the maximum value of superposed switching force. In terms of conversion control, extremely long intervals may cause design difficulty to the conversion equipment. Therefore, a value of 0.375 time of throw difference is recommended.

Conversion time difference may also occur between different traction points. Taking 0.1 D (0.1 time of throw difference) as the basic time difference, the impacts of time difference at various traction points on the switching force of switch rails are demonstrated in Table 8.5. In the table, the traction points may witness great change of switching force if the traction points move to position asynchronously. In particular, the greatest impact appears in the case of late movement of traction point 2. Therefore, it is suggested to control the conversion time difference of traction points within 0.1 D for high-speed turnouts.

8.3.2 POINT RAIL OF HIGH-SPEED TURNOUT

The swing nose crossing is far more complex than the switch in structure, as it may involve a single flexible rail type with a diagonal joint (pointed rail/stock rail at crossing heel) or double flexible rail type without diagonal joint in the diverging line, frog assembled by long and short point rails or solid frog. Moreover, stress conditions differ when converting from normal position (main line in operation) to reverse position (diverging line in operation) or the opposite, given that the switching forces in the two directions are the same. Therefore, the conversion design should be based on the structure.

1. Point rail with single flexible rail
   a. Impact of interval of traction points

Table 8.6 Impact of Interval of Traction Points on Switching Force of Point Rail

Movable Length (mm)	Interval (m)	Throw (mm)	Conversion Direction	Switching Force at Traction Point 1 (N)	Switching Force at Traction Point 2 (N)	Scant Displacement (mm)
6905	3000	119, 65	To reverse position	1886.6	5827.7	1.54
			To normal position	472.2	1094.3	1.52
7505	3600	119, 59	To reverse position	2132.3	4859.1	1.44
			To normal position	1576.8	3194.6	1.41
8105	3600	119, 64	To reverse position	1741.8	4032.3	2.53
			To normal position	1720.2	2765.0	2.50

Take a Chinese No. 18 turnout, for example; if two traction points are arranged on a point rail, the impacts of interval of traction points and movable length on switching force are as given in Table 8.6.

It can be seen from Table 8.6 that the switching force for conversion from normal to reverse position is greater than that in the opposite direction, which results mainly from the great bending deformation energy during the conversion from normal to reverse position. When converting in reverse, the bending deformation energy is released gradually. Shorter movable length is associated with greater bending deformation energy and greater switching force from normal to reverse position. The scant displacement can be obtained by measuring the long point rail in normal position, or the short point rail in reverse position. The scant displacements of the point rail with a single flexible rail in normal and reverse positions follow the same distribution rule. Greater distance between the last traction point and the heel of the point rail leads to greater scant displacement and smaller switching force. Therefore, the movable length of the point rail shall be determined based on both the scant displacement and switching force.

The conversion of a point rail must overcome its own stiffness and the resistance of relevant components (e.g., slide plate). Greater flexural stiffness of the point rail produces a better constraining effect of the heel, greater switching force, better control of line type of point rail, and smaller scant displacement. Comparatively, the following parameters are a reasonable design for the point rail of Chinese No. 18 turnouts: distance between actual point and flexible section of 7.505 m, interval of traction points of 3.6 m, throws of 119 and 59 m.

b. Impact of friction coefficient of slide plate

Figure 8.17 demonstrates the impact of different friction coefficients of slide plate on switching force and scant displacement of the point rail of a No. 18 turnout. Switching force and scant displacement will increase with a rise in the coefficient. The friction coefficient

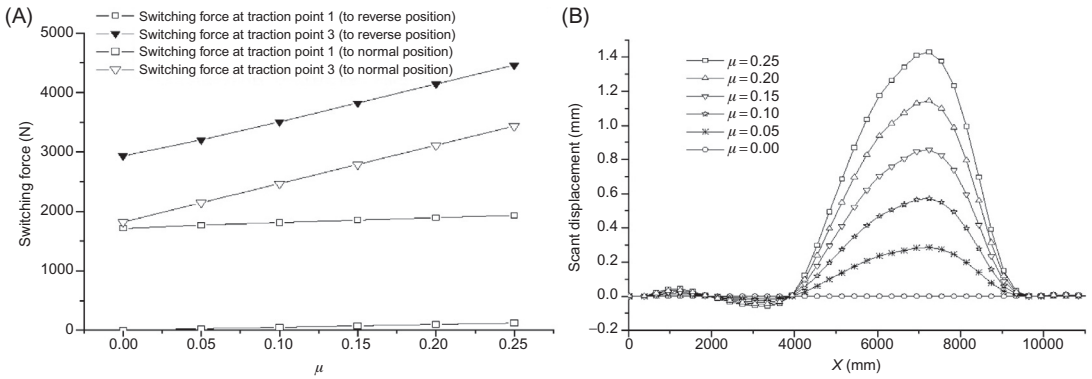

FIGURE 8.17

(A) Change of switching force with friction coefficient of slide plate. (B) Change of scant displacement with friction coefficient of slide plate.

Table 8.7 Maximum Switching Forces at Different Traction Points of Point Rail in Case of Inclusions of Different Sizes

Location of Inclusion	Size of Inclusion (mm)	From Normal to Reverse Position		From reverse to normal position	
		Switching Force at Traction Point 1 (N)	Switching Force at Traction Point 2 (N)	Switching Force at Traction Point 1 (N)	Switching Force at Traction Point 2 (N)
Traction point 1	4	>6000	12888.0	>6000	7296.6
	6	>6000	17178.0	>6000	10377.0
	8	>6000	21468.0	>6000	13457.0
Between two traction points	4	31721.0	46448.0	30279.0	41164.0
	6	46617.0	62620.0	45364.0	51395.0
	8	61499.0	88790.0	58449.0	71630.0
Traction point 2	4	18893.0	>6000	14720.0	>6000
	6	27374.0	>6000	22060.0	>6000
	8	35854.0	>6000	29399.0	>6000

may be eased by providing a flexible segment at the heel, greasing the slide plate, or employing a rollered slide bed, which can effectively reduce the switching force and scant displacement.

c. Impact of inclusion on switching

For the point rail of a No. 18 turnout, the calculated switching forces in case inclusions of different sizes appear at or between two traction points are listed in Table 8.7.

Table 8.8 Results of Throw Optimization of Traction Points for Point Rail with Double Flexible Rails

Scheme	Conversion Direction	Switching Force at Traction Point 1 (N)	Switching Force at Traction Point 2 (N)	Switching Force at Traction Point 3 (N)	Scant Displacement (mm)
1	To reverse position	2585.1	1872.3	5583.5	2.62
	To normal position	872.3	2355.3	2772.8	1.12
2	To reverse position	2769.6	1928.9	6313.3	1.64
	To normal position	879.2	2512.5	2234.7	0.66
3	To reverse position	2817.1	1928.9	6462.5	1.67
	To normal position	879.2	2551.3	2234.7	0.66
4	To reverse position	2531.6	1943.4	4240.2	2.12
	To normal position	872.2	1906.2	2745.6	1.10

From Table 8.7, if an inclusion of 4 mm and greater appears at or between traction points, the switching force exceeds the capacity (6000 N) of the switch machine by a large margin. In this case, two traction points cannot be converted to position. The inclusion may be detected simply by the switching force, not necessarily by the closure detector.

2. Point rail with double flexible rails

Chinese No. 42 high-speed turnouts adopt a point rail with assembled double flexible rails, where the movable length is 18.175 mm and the long and point rails are coupled with fillers and high-strength bolts. Three traction points are arranged on the point rail. To reduce the switching force, four design schemes are analyzed. Scheme 1 adopts intervals of 4.8 and 5.965 m, the distance between traction point 3 and fixed part of 6.9 m, and design throws of all traction points of 110, 79, and 41 mm as per the throw of traction point 1 and the linear change of distance to the flexible center. Scheme 2 shortens the distance between the last traction point to fixed end to 5.1 m and adopts throws of 110, 77, and 35 mm. Scheme 3 adopts the same distance between the last traction point and fixed end, but optimizes the throws as 113, 79, and 36 mm. Scheme 4 adopts the constant distance of 6.9 m between the last traction point and fixed end and optimized throws of 113, 79, and 36 mm. The switching force and scant displacement of these schemes are given in Table 8.8.

As is shown in Table 8.8, the assembled double flexible rails form a frame structure with fillers at the heel, characterized by high lateral flexural stiffness and integrity, ensuring homogenous distribution of switching force. The bending deformation energy may be released when conversion from reverse to normal position; therefore, the switching force and scant

displacement in this conversion direction are smaller than in the opposite conversion direction. Among three traction points, the greatest switching force occurs at the last one, which is thus taken as the control factor for the switching force. Scheme 4 produces the least switching force as compared with the other schemes, and was therefore adopted for No. 42 high-speed turnouts in China.

CHAPTER

DESIGN OF RAIL SUBSTRUCTURE AND COMPONENTS

9

The study and design of rail substructure and components, including fastenings and tie plates, comes after the layout design (plane line type, structural selection, traction, conversion, etc.) and design of critical technologies [wheel−rail relation, track stiffness, continuously welded rail (CWR), etc.]. The latest technologies of rails, fasteners, ties, ballastless track, and ballast bed will all be applied to high-speed turnouts and upgraded with structural characteristics of turnouts. High-speed turnouts integrate the technologies of track structure in high-speed railways.

9.1 RAIL SUBSTRUCTURE

The substructure for high-speed railway lines may be of ballast or ballastless type.

Ballast track mainly adopts concrete ties, either monoblock long ties or hinged short ties. Monoblock long ties have good integrity and are conducive to retaining track geometry, but disadvantageous in transport of assembled turnouts. Hinged short ties prevail in ballast high-speed turnout in Germany, which facilitate the split transport and effectively ease beating on the bed by ties. This type of tie had been used in the Xiamen−Shenzhen line in China; however, it was proven in practice to have poor retention of track geometry during tamping. At present, all Chinese high-speed turnouts use monoblock long ties. Prestressed concrete long ties are also used in China. German ballast turnouts also use steel ties to accommodate switch rods interiorly to ease the tamping operation. This tie had been used in speed-up turnouts in China, but were abandoned due to poor retention of stability on gravel ballast beds [115,116].

Ballastless turnouts may have a rail substructure of concrete bearing blocks, embedded concrete long ties, concrete turnout slabs, or polymer composite ties. Concrete bearing blocks are commonly seen in urban mass transit, coupled with bed slabs with Π-shaped reinforcements. This structure features simple manufacture and construction, but it cannot enable high precision of turnout laying due to the inclination and difficult positioning of the bearing blocks. Composite ties are mainly used in subways and urban mass transit, featuring easy production, laying and maintenance, and good insulation and flexibility, but less favorable installation accuracy. The technology of embedded concrete long ties is borrowed from the Radar railway station in Germany, featuring easy construction and stable structure. Concrete turnout slabs are German Bogl slabs, which have shorter construction duration and high precision of positioning. By comparison, embedded concrete long ties and turnout slabs have been adopted as the substructure of ballastless turnout for Chinese high-speed railways (HSRs) [117,118].

Design of High-Speed Railway Turnouts.

9.1.1 TIE OF BALLAST TURNOUT

1. Profile and size
   a. Length

      The length of ties varies as impacted by layout type and other factors of the turnout, but generally taken as 2.6−4.8 m (increment: 0.1 or 0.15 m). To make fabrication easier, an even number of ties of the same length will be manufactured. The ties at turnout front are 2.6 m long to facilitate connection with the railway section with type III concrete ties, as well as maintaining the stability of CWR track at turnout front. The distance between the center of outer rail in curved track and the end of tie is not constant; however, it must at least satisfy the requirement of anchorage length of prestressed reinforcement. To minimize the number of long ties at turnout rear and ease laying and maintenance, short ties may be used in the transition between turnout rear and adjacent section. For ties at traction points, which must accommodate conversion equipment, three installation holes will be arranged, and the tie will be lengthened by 120−280 mm as compared with nearby ties.

      The distance from tie end to the first sleeve (bolt hole) is essential for preventing longitudinal cracks on the concrete surface around the sleeve. In China, high-speed and speed-up turnouts adopt the same design value, 364 mm.

      The tie spacing is 600 mm for Chinese high-speed turnouts. To ensure construction accuracy and track geometry under high-speed traffic in the main line, all ties will be perpendicular to the main direction of the turnout. The tie is applicable to turnouts in crossover and receiving-departure lines with track distance of 4.6 m and above.

   b. Profile

      The tie may have a shoulder or not. Compared with shouldered concrete ties, the shoulderless type features less longitudinal cracking, greater carrying capacity, easy manufacture, simple profile, and good appearance; moreover, it enhances the carrying capacity of the intermediate section of ties without necessarily increasing the reinforcement quantity or impairing the carrying capacity of the rail substructure. Shoulderless ties of uniform height are used in high-speed turnouts in China. The rail-supporting surface is not canted at the base.

   c. Section

      The bottom width of a tie is designed as 300 mm to achieve the same effective bearing area as type III concrete ties in China. The design top width is 260 mm, wider than that of its type III concrete counterpart, so as to facilitate the installation of special tie plates and avoid demolding difficulty. The design height of tie section is 220 mm to meet the requirement of carrying capacity.

   d. Bolt hole for fastener

      Ties are coupled with tie plates by a row of bolts. As ties are perpendicular to the rails in the main line, pre-embedded plastic sleeves will be located on the longitudinal axis of symmetry of the tie. The bolt holes on the tie plates under rails in curved track will be provided with graded deflections, enabling the perpendicularity of the assembled tie plate and tie to the rail. In either left-handed or right-handed turnouts, the tie plates under rails in curved track are in symmetry.

2. Strength of concrete tie

a. Strength of concrete

The concrete tie of a high-speed turnout in China is designed as a C60 tie with design tensile and compressive strength of 2.45 and 29.5 MPa. The allowable stress varies with different load conditions.

- Allowable compressive prestress: To avoid minor cracks in concrete ties due to excessive compressive prestress, the design compressive prestress of concrete tie shall not exceed the strength of concrete cylinder by $0.15-0.30f'_c$. The maximum compressive prestress on a calculated section shall not be above 12 MPa after total prestress loss.
- Allowable stress for static load test: The grade of concrete shall not be below C45 in transmitting stress (or applying prestress). A static load crack resistance test is performed within 48 h after demolding of the tie, during which the C45 concrete is considered and the standard values of tensile and compressive strength are taken as 2.75 and 30 MPa, respectively.
- Allowable stress for fatigue test: The prevailing fatigue tests on ties in China are based on cracks but with restrictions on the width of residual cracks. C60 concrete with design compressive strength of 29.5 MPa is considered in the test.
- Allowable stress under design load: Under design load, no cracks are allowed on the concrete at the tensile edge of the tie section. The tensile stress shall not exceed 0.7 times design tensile strength of the tie, that is, 1.72 MPa. Meanwhile, the maximum compressive force on concrete in the compressive area shall not be greater than 0.7 times the design compressive force, that is, 20.65 MPa.

b. Prestressed reinforcement

As per the design, the concrete tie for high-speed turnout is provided with ϕ7 mm reinforcement. The ϕ7 mm prestressed spiral rib wire is provided with ultimate tensile strength of 1570 MPa, yield strength of 1330 MPa, and design strength of 1000 MPa. The wire has a relaxation rate of 2.5% (grade II). The tensile stress shall not exceed 70% of the yield strength, designed as $0.68\sigma_b$. The bonding strength is about 3.0−3.17 times the tensile strength. The transmission length of stress is approximately 45−60 times the wire diameter. The wire has a nominal section area of 38.5 mm^2 and nominal weight of 0.302 kg/m.

The total loss of prestress will exert a direct impact on effective compressive prestress. The raw materials and processes shall be qualified with the loss coefficient of prestress not greater than 20%. To ensure homogenous compressive prestress on concrete ties, an automated tension process is preferred, where the deviation of blanking length of wire shall not exceed 2 mm and the error of tensile stress of reinforcements shall not exceed 5%. Meanwhile, the precise positioning of reinforcements on cross section may be guaranteed by enhancing the stiffness of steel die. Defects of concrete ties, such as longitudinal cracks, may be eliminated by upgrading demolding strength of ties, ensuring curing of at least 2 h under ambient temperature, prolonging the storage in plant, and applying external load 28 days after production. The prestressed wire must be reasonably destressed. The transmission length of prestressed reinforcement may be ensured by releasing the stress slowly or keeping the tensioning force for destressing below 325 kN, so as to avoid horizontal or vertical cracks due to excessive concentrated stress on the tie end.

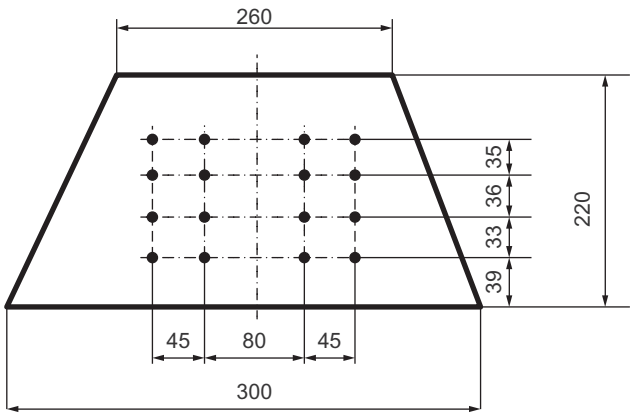

FIGURE 9.1

Diagram of tie reinforcement.

Table 9.1 Distribution Coefficients of Wheel Load in China

Type of Rail / a (cm) / D (kN/cm)	50		60		75		
	55	57.5	57.5	60	57.5	60	62.5
700	0.47	0.48	0.43	0.44	0.39	0.41	0.42
1000			0.47	0.48	0.43	0.44	0.45
1200					0.44	0.45	0.47

To prevent concrete tie upwarp due to creep affecting turnout smoothness, $16 \times \phi 7$ mm reinforcements are arranged in symmetry, as shown in Figure 9.1.

c. Construction of reinforcement

The concrete tie is manufactured by a pre-tensioning process. The prestress is variational in the anchorage zone of prestressed reinforcement at the tie end. For a better stress state at tie end during pre-tensioning and operation, a number of stirrups are provided. The stirrups are arranged at intervals of 200−300 mm along the length of turnout, forming a powerful reinforcement framework with prestressed reinforcement.

3. Calculation check of carrying capacity [119]

a. Dynamic pressure on tie

The maximum pressure on a tie is generally expressed by $R_d = \gamma * P$, where γ and P represent distribution coefficient of wheel load and design dynamic wheel load, respectively, obtained from Eq. (3.1). Table 9.1 lists the distribution coefficients of wheel load calculated as per the main rolling stock and track types in China. Required coefficients may be referred to by rail type, tie spacing a, and rail support stiffness D from the table. For the ties of high-speed turnouts in China, 0.48 is taken in the design.

b. Bending moment of design load

In the bed reaction force diagram for sub-rail section bending moment, the central part of the tie is partially supported, whereas in the bed reaction force diagram for intermediate section bending moment, even distribution applies along the full length of the tie. This design can meet the requirements of fully ballasted track during laying and maintenance. The calculated maximum negative bending moment is 11 kN m, and the maximum positive bending moment is 23 kN m.

c. Maximum compressive prestress

On concrete ties for high-speed turnout, 16 pieces of ϕ7 mm reinforcements are arranged symmetrically with design tensile stress of $0.68\sigma_b$. The maximum compressive prestress of calculated concrete section is 8.8 MPa, below the required limit (12 MPa).

d. Static load crack resistance test and test value

The design crack resistance bending moment of tie section is:

$$M_{cr} = \sigma_{pc} W_0 = 1.75 f_{tk} W_0 \tag{9.1}$$

where M_{cr} is the crack resistance bending moment of tie section, that is, the carrying capacity of the tie; σ_{pc} is the normal compressive prestress of tensile edge of concrete; W_0 is the bending elastic modulus of the tensile edge of calculated section; f_{tk} represents the standard tensile strength of concrete; and 1.75 is the plasticity coefficient of bending elastic modulus of the section.

According to the calculation, the carrying capacities of ties in the positive and negative direction are 24.5 and 22.7 kN m, respectively. For a given section area and number of prestressed reinforcements, the design crack resistance bending moment is a constant. Laboratory test is performed with the simple method of "two-point support, one-point loading." In the test, the offset distance is taken as 600 mm, and tie length as 2600 mm. The central part of the tie is tested. The test loads for crack resistance are taken as 240 and 190 kN in positive and negative directions, respectively.

e. Fatigue strength test and test value

The fatigue test of a tie is based on cracks and restricted width of residual cracks. As specified in the design method for prestressed concrete ties in China, the crack width must be within 0.2 mm under a given load to limit the width of residual cracks on ties within 0.05 mm. Therefore, the maximum nominal tensile stress of the tensile edge of the section is 7 MPa. Then, the test value for fatigue strength of tie is:

$$P_{max} = k_3 P \tag{9.2}$$

where P represents the test value under static load, k_3 is taken as 1.05−1.10, and nominal tensile stress of the section is 7 MPa. The calculated test loads are 255 and 200 kN in positive and negative directions. The design crack resistances are 34.1 and 32.1 kN m in the positive and negative directions, respectively.

f. Stress on bed top

According to the supporting diagram of sub-rail tie sections and dynamic pressure on ties, the calculated maximum stress on the bed top under the tie is about 0.41 MPa, under the allowable limit 0.5 MPa for gravel ballast bed. This means the supporting area is sufficient to support the tie bottom.

g. Lateral resistance of tie

Lateral resistance of ties is critical for turnout stability, which may be estimated with the Japanese equation:

$$F = 7.5W + 290rG_e = 18rG_s, \tag{9.3}$$

where

F = lateral resistance (N) of tie for ballast bed
W = weight (kg) of tie
G_s = bending moment (cm^3) of sleeper lateral area with respect to ballast top.
r = bed density (kg/cm^3), about 1.8×10^{-3} kg/cm^3 after stabilization.

The deviation between theoretical calculated value and measured value is generally within 10%. Therefore, the calculation is applicable to verifying the rationality of tie lateral resistance.

For the short tie at turnout rear, in case of lateral resistance deficiency for track stability, the tie may be embossed on the bottom. For ties for installing switch rods, where no ballast is arranged between the ties, ballast curb may be provided on the other end to intercept the ballasts, maintain the spacing between two ties at the switch machine, and increase lateral resistance.

9.1.2 EMBEDDED LONG TIE FOR BALLASTLESS TRACK [120]

1. Section and reinforcement

The upper and lower section widths and height of concrete ties for ballastless turnouts are 260, 290, and 130 mm, respectively. The main reinforcements are composed of four pieces of ϕ7.0 mm prestressed wire and eight pieces of ϕ14 mm common deformed bars. The section and reinforcement remain the same along the length in the direction of the turnout. A steel truss is formed by four pieces of ϕ14 mm deformed bars and four pieces of ϕ8 mm deformed bars. The bottom of the concrete section is exposed to allow better coupling between tie and ballast turnout. For the calculated section, the height of prestress center is 104 mm and the centroid height is 105 mm; the eccentricity is minor. The total prestress tension is 100 kN with tension coefficient of 0.414. Considering the low degree of prestressing, little creep upwarp may be produced. See Figure 9.2 for the tie section of a ballastless turnout.

The arc-shaped corner (arc radius = 15 mm) of the tie end in the vertical direction can eliminate cracks on the bed surface. The design distance from tie end to the first sleeve is 260 mm. However, for a short tie at turnout rear, this limit value cannot be guaranteed; therefore, the tie end may be enhanced with stirrups, as shown in Figure 9.3.

Tie spacing is generally 600 mm, except that the ties for a switch rod have a span of 650 mm, and the span between this tie and adjoining ties is 575 mm. The tie length has two increment types: 100 and 150 mm, perpendicular to the working surface in the main track. The short ties at turnout rear in the diverging direction are perpendicular to the track.

2. Ballastless track foundation in turnout zone

In a high-speed railway line, the ballastless turnout zone with embedded ties is composed of a high-speed turnout, type II positive elastic clips, embedded tie, bed slab, RC base slab, and subgrade, as shown in Figure 9.4. Cast-*in-situ* RC bed slabs are made of C40 concrete, with design thickness of 350 mm; its width depends on the layout dimensions of the turnout. The RC

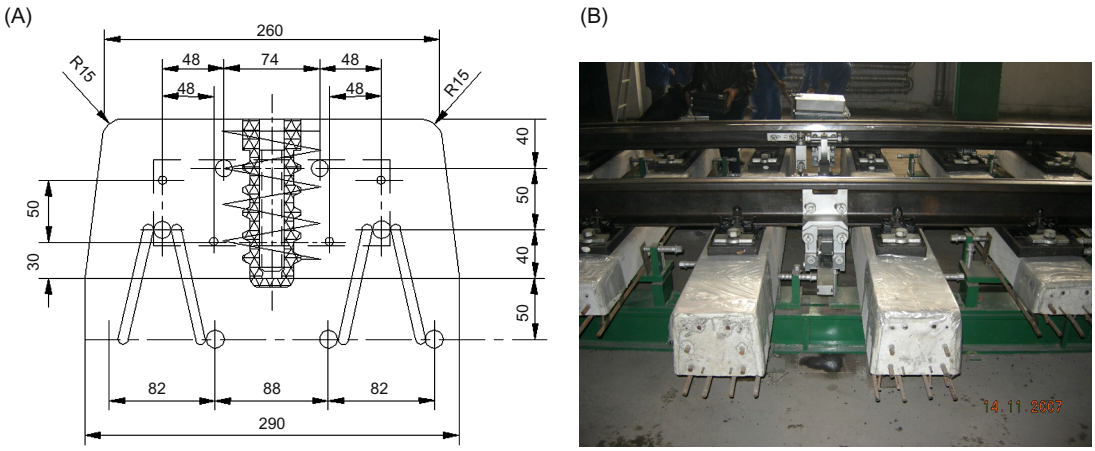

FIGURE 9.2

(A) Section of ballastless tie. (B) Shop assembly of ties.

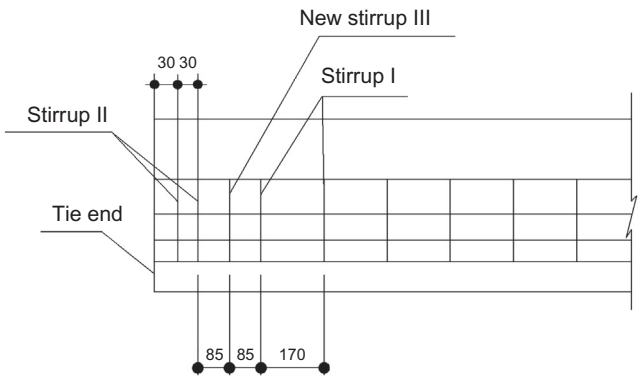

FIGURE 9.3

Arrangement of stirrups at the end of short tie at turnout rear.

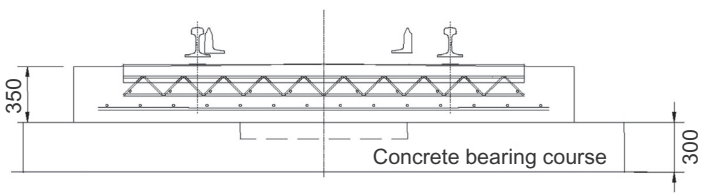

FIGURE 9.4

Bed structure in turnout zone.

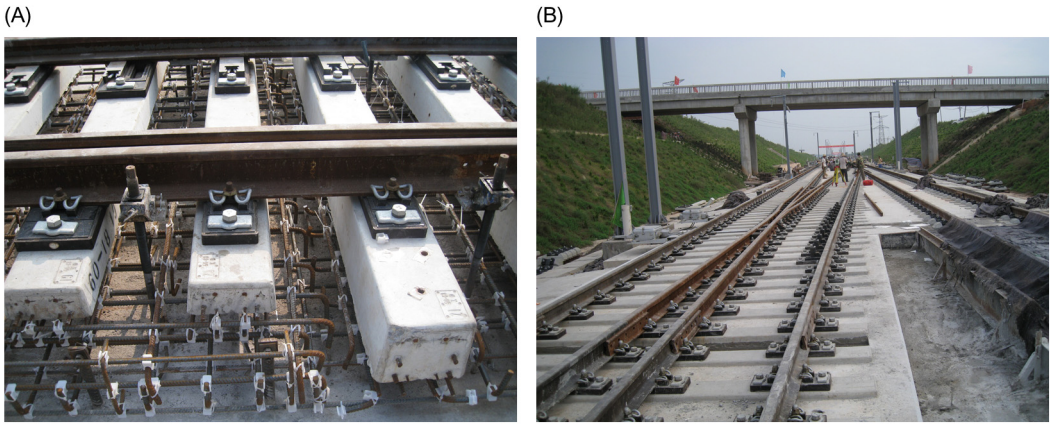

FIGURE 9.5

(A) Reinforcement in bed slab. (B) Cast concrete bed.

base slab is made of C20 concrete, 300 mm in depth. The foundation bed of the subgrade is composed of a surface course and a bottom course. The surface course is made of graded gravel or sandy gravel. The total depth of the surface course of the foundation bed and concrete bearing course is greater than 0.7 m. The 2.3-m-deep bottom course of the foundation bed is filled with group A or B fillings. The subgrade coefficient (K30) at the surface course of the foundation bed should be at least 190 MPa/m.

To minimize contractive cracks in the bed center in the longitudinal direction, expansion gaps are arranged at certain intervals along the longitudinal direction of the bed. The expansion gaps may be true or dummy type. The bed slab has a design unit length of 18 m, with dummy gaps provided every 6 m. True gaps are formed by 12-mm-thick bitumen-impregnated wood fillers that separate the bed slab, aligned with foundation gaps. Dummy gaps may be formed by sawing, with height 1/3 of the section height.

The lateral width of the bed slab is variational along the longitudinal direction of the turnout, which is based on rational bed strength and thickness of the concrete protection layer. Preferably, the bed width should vary continuously to ensure the smoothness and pleasant appearance of bed sides in the whole turnout zone. The edge of a bed with a certain width is reserved for switch machine installation. In straight track, the bed edge will be in a continuous straight line, and the switch machine will be installed on ties with the thinnest protection layer (50 mm deep). In diverging track, the bed edge is joined by several separated straight segments to ensure smoothness of line type.

The bed slab, based on the height of the edge, will be provided with an A-shaped slope of 1.5%. The bed height will be determined in combination with track elevation and construction height of the entire ballastless track. The bed is provided with upper and lower rows of ϕ18 mm deformed bars, with a horizontal grid interval of 190 mm. The foundation is provided with upper and lower rows of ϕ14 mm deformed bars with a horizontal grid interval of 200 mm. See Figure 9.5 for details.

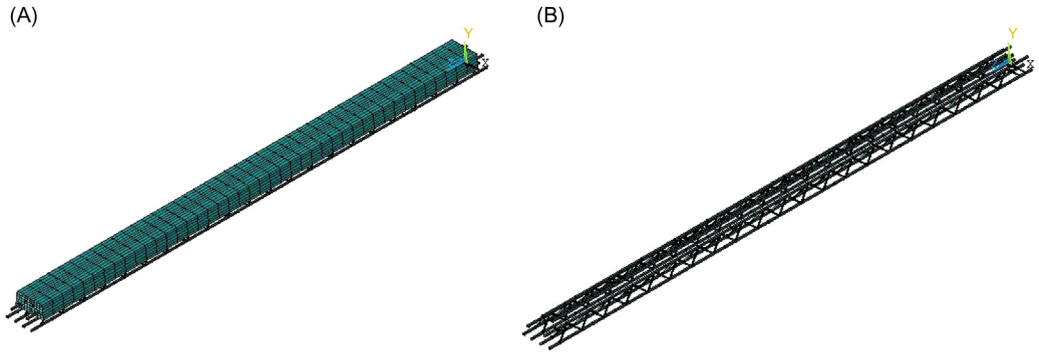

FIGURE 9.6

(A) Calculation model of concrete tie. (B) Model of reinforcement.

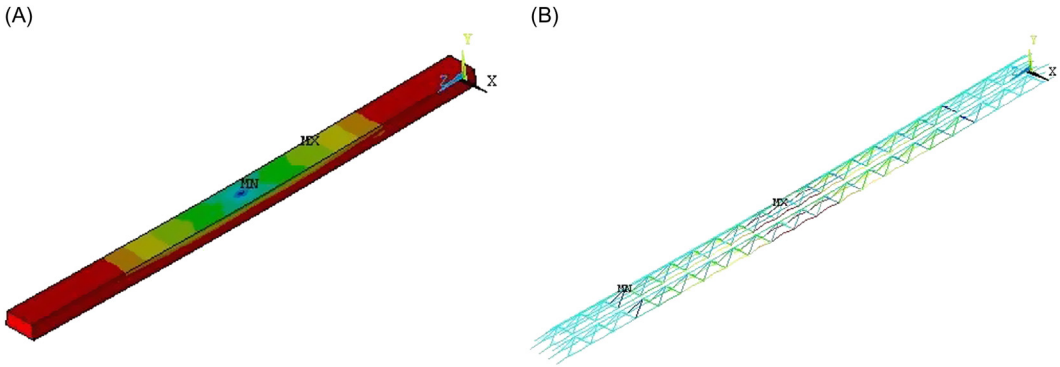

FIGURE 9.7

(A) Distribution of stress on concrete tie. (B) Distribution of stress on reinforcement.

3. Loads on tie

a. Construction loads

Ballastless turnout ties are characterized by fewer prestressed reinforcements, smaller prestress, and greater length; therefore, they are exposed to deformation and cracking under external load during transport and construction. A tie calculation model (Figure 9.6) is constructed with the ANSYS finite element software to determine the tolerable load on ties during construction and transport. As per the calculation, the tie concrete will crack under a concentrated load of 12 kN, with a vertical displacement of up to 9.7 mm. The stress distribution and displacement of a 3.2-m-long tie is plotted in Figures 9.7 and 9.8. To ensure the

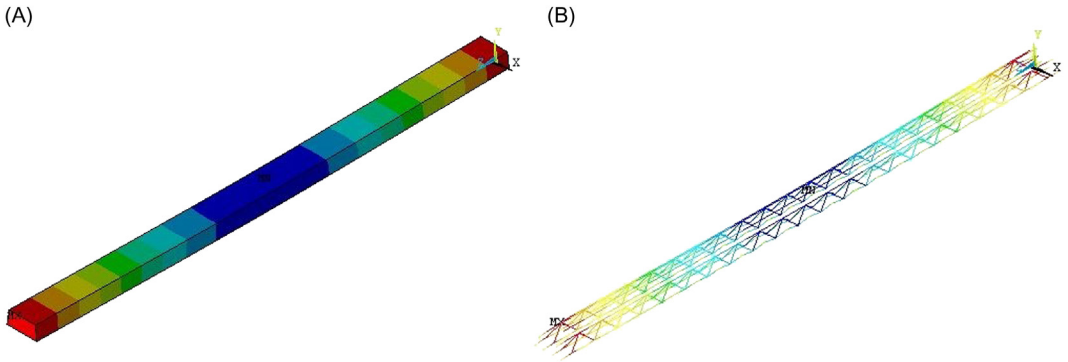

FIGURE 9.8

(A) Distribution of displacement of concrete tie. (B) Distribution of displacement of reinforcement.

proper strength and deformation of ties during construction, at most three workers can stand on one tie at the same time during casting. Moreover, the hoisted or stacked ties may not exceed four layers.

b. Operation loads

A calculation model of coupled tie and concrete bed will be developed. The stress and deformation under the combined impact of vertical and lateral loads (the same as for bedplate) of a train, longitudinal temperature force transmitted by fasteners, and braking force (maximum longitudinal force of fastener) of train will be analyzed. According to ANSYS finite element software, the calculated stresses of bed, tie, and reinforcement are acceptable to elasticity capacity. The distribution of stress is given in Figure 9.9. The reinforcement may bear no operation load when there are no cracks on bed concrete.

The interface of tie and bed slab is prone to cracks due to poor bonding strength. According to the calculation, if cracks are formed, they may develop toward the tie bottom as the restriction of bed slab on tie disappears on one side. In this case, a number of vertical reinforcements (either diagonal reinforcement or stirrup) will be provided in the tie to effectively limit the development of cracks. Ties with holes for a switch machine may have poorer stress status, particularly when cracks are formed on the interface; the risk of crack development on the tie bottom is great. Therefore, side reinforcement is necessary for such a tie.

4. Load on concrete foundation

Owing to the complicated structure of ballastless track and nonuniform dimensions of bed slabs in the turnout zone, the traditional model of elastic subgrade beam slabs is not suitable for calculating the vertical stress, or reflecting the slab bending under load at different positions. For this, a full model of turnout, fastener, bed slab, and base is established to obtain the specific stress and deformation of the bed slab and rails under load at different positions, so as to determine the design load for bed slabs. See Figure 9.10 for details.

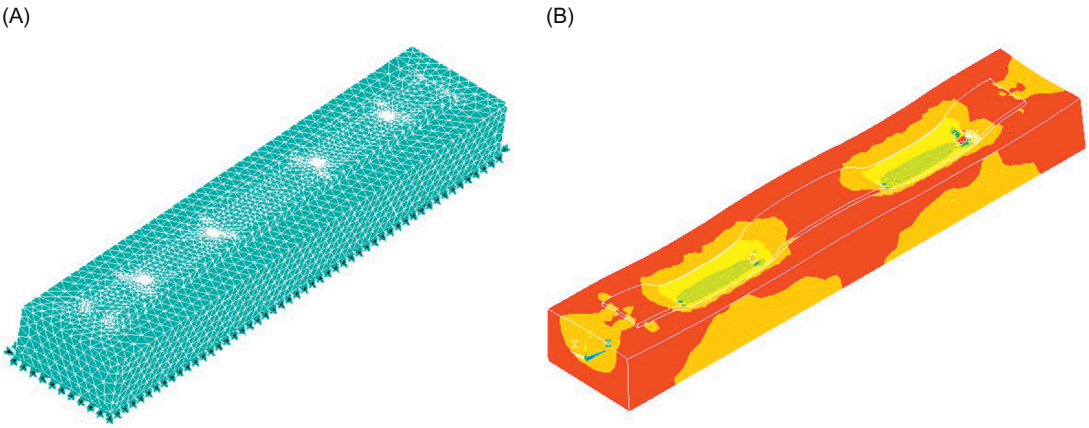

FIGURE 9.9

(A) Calculation model of coupled tie and bed. (B) Distribution of stress on tie and bed.

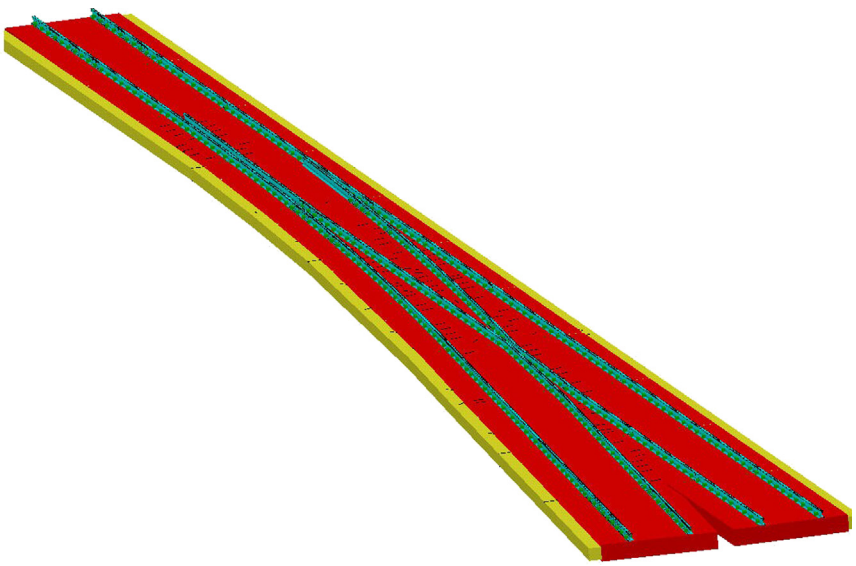

FIGURE 9.10

Analysis model of ballast turnout.

In the model, the rails are modeled with beams, fasteners with linear springs, and bed slab and base, with elastic foundation slab element. The bearing coefficient of the slab bottom is taken as the foundation coefficient K30. The double-layer slab is converted into a single-layer slab with equivalent stiffness depending on different coupling modes of bed slab and base. The stress under load is calculated based on the equivalent single-layer slab on elastic subgrade.

The bending moment and stress of each layer can be obtained as per the stiffness of the layer (upper or lower).

Double-layer slab falls into three types by interfacing conditions: separate type with fully smooth interface, bonded type with fully bonded interface, and a type with partially smooth and partially bonded interface. If the isolation layer or concave and convex retaining blocks are arranged between the bed slab and the base to transmit longitudinal force, a separate double-layer slab with fully smooth interface is considered in the calculation. For a bed slab connected with the base slab via Π-shaped reinforcement, the bonded type with fully bonded interface may be considered.

As a separate double-layer slab has no frictional resistance, the upper and lower layers will bend around the respective middle surface under load, as shown in Figure 9.11. Assuming that there is no vertical compressive deformation on each layer, and the deflection curves are of the same curvature, the total bending moment of the double-layer slab equals the sum of the bending torque of each layer. The bending stiffness of the slab is also composed of the bending stiffness of each layer:

$$M = M_1 + M_2 \tag{9.4}$$

$$D = D_1 + D_2 = \frac{E_1 h_1^3}{12(1-\mu_1^2)} + \frac{E_2 h_2^3}{12(1-\mu_2^2)} \tag{9.5}$$

$$M_1 = \frac{D_1}{D} M, \quad M_2 = \frac{D_2}{D} M \tag{9.6}$$

where

M, D = total bending moment and total bending stiffness of double-layer slab under load
M_1, M_2 = bending moment of upper and lower layer of slab
D_1, D_2 = bending stiffness of upper and lower layer of slab
h_1, h_2 = thickness of upper and lower layer of slab
E_1, E_2 = elastic modulus of upper and lower layer of slab; and
μ_1, μ_2 = Poisson's ratio of upper and lower layer of slab.

Given the same Poisson's ratio of two layers, the equivalent thickness h_e of a single-layer slab with the same total stiffness as the double-layer slab will be:

$$h_e = \sqrt[3]{\frac{12(1-\mu^2)D}{E}} \tag{9.7}$$

where E represents the elastic modulus of the single-layer slab, taken as that of a layer of the double-layer slab, that is, the elastic modulus of the upper layer in the text.

As calculated, the bending moment of a single-layer slab of equivalent stiffness under load equals the total bending moment M of a double-layer slab. Then, the bending moments M_1 and M_2 of upper and lower layers can be obtained, and then the bending tensile stresses σ_1 and σ_2 of upper and lower layer can be calculated by:

$$\sigma_1' = \frac{6M_1}{h_1^2}, \quad \sigma_2' = \frac{6M_2}{h_2^2} \tag{9.8}$$

As a bonded double-layer slab has no interlayer displacement, the double layers will bend around the middle surface under load, just as the single-layer slab, as shown in Figure 9.12. The position of the middle surface may vary with the thickness and elastic modulus of two

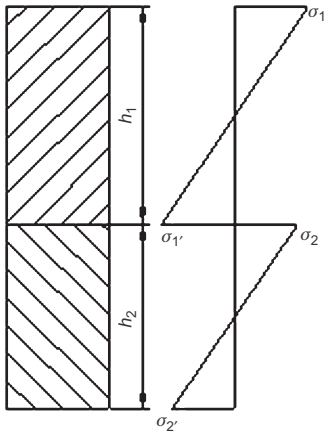

FIGURE 9.11

Distribution characteristics of stress of separate double-layer slab.

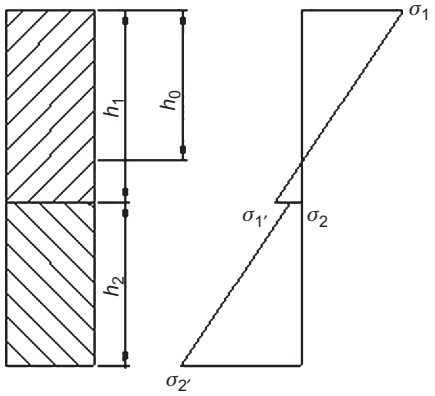

FIGURE 9.12

Distribution characteristics of stress of bonded double-slayer slab.

layers. The middle surface of an equivalent single-layer slab may be obtained with the resultant stress on the section.

$$h_0 = \frac{E_1 h_1^2 + 2E_2 h_1 h_2 + E_2 h_2^2}{2(E_1 h_1 + E_2 h_2)} \tag{9.9}$$

The bending stiffness of an equivalent single-layer slab can be calculated with the position of middle surface.

$$D = \frac{E_1}{3(1-\mu_1^2)}[h_0^3 - (h_0 - h_1)^3] + \frac{E_2}{3(1-\mu_2^2)}[(h_0 - h_1)^3 + (h_1 + h_2 - h_0)^3] \tag{9.10}$$

With elastic modulus E_1 and bending stiffness D, the equivalent thickness of the single-layer slab h_e is:

$$h_e = \sqrt[3]{\frac{12(1-\mu^2)D}{E_1}} \tag{9.11}$$

Further, with the bending stiffness and equivalent thickness, the bending moment and corresponding maximum stress σ_e at the slab bottom of a single-layer slab under load can be obtained. The stresses of the two layers of double-layer slab can be derived accordingly:

$$\begin{aligned}
\sigma_1 &= \frac{2h_0}{h_e}\sigma_e \\
\sigma_1' &= \frac{2(h_1 - h_0)}{h_e}\sigma_e \\
\sigma_2 &= \frac{2(h_1 - h_0)}{h_e}\frac{E_2}{E_1}\sigma_e \\
\sigma_2' &= \frac{2(h_1 + h_2 - h_0)}{h_e}\frac{E_2}{E_1}\sigma_e
\end{aligned} \tag{9.12}$$

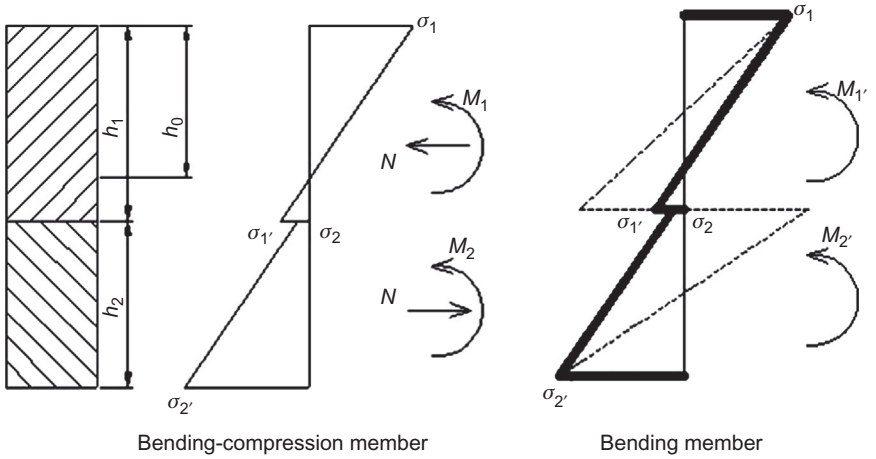

FIGURE 9.13

Characteristics of distribution of stress on bending-compression members and bending members.

As per Figure 9.12, the stress distribution of each layer of the slab follows the same rule as the bending-compression (tension) member; therefore, the design stress may follow the stress of either the bending-compression (tension) member or the bending member, as given in Figure 9.13.

$$M_1 = \frac{1}{6}(\sigma_1 + \sigma_1)h_1^2,\ \ N = (\sigma_1 - \sigma_1)h_1,\ \ M_2 = \frac{1}{6}(\sigma_2 + \sigma_2)h_2^2 \tag{9.13}$$

$$M_1' = \frac{1}{6}\sigma_1 h_1^2,\ \ M_2' = \frac{1}{6}\sigma_2' h_1^2 \tag{9.14}$$

For a multi-layer slab, the calculation may be performed by breaking down the slab into separate double-layer slab and bonded double-layer slab as per the actual interfacing status of two adjoining layers.

For a Chinese No. 18 turnout, the track response of the *i*th slab under vertical load is plotted in Figure 9.14. The calculation results may be used to design the reinforcement of this track slab.

9.1.3 SLABS FOR BALLASTLESS TURNOUT

Ballastless slab turnouts featured stable structure, smaller track height, less cast-*in-situ* concrete, convenience, and fast construction. The construction can be commenced before the mobilization of rails. They are widely used in Chinese HSRs (e.g., Wuhan−Guangzhou, Shanghai−Hangzhou, Beijing−Shanghai, Beijing−Shijiazhuang, and Shijiazhuang−Wuhan).

1. Structural design

   There are two types of slab track in the turnout zone: slab track with leveling course and that with filler course. The slab track with leveling course is composed of turnout parts, slabs, base, and leveling course. The turnout slab will be fine-tuned on the finished leveling course.

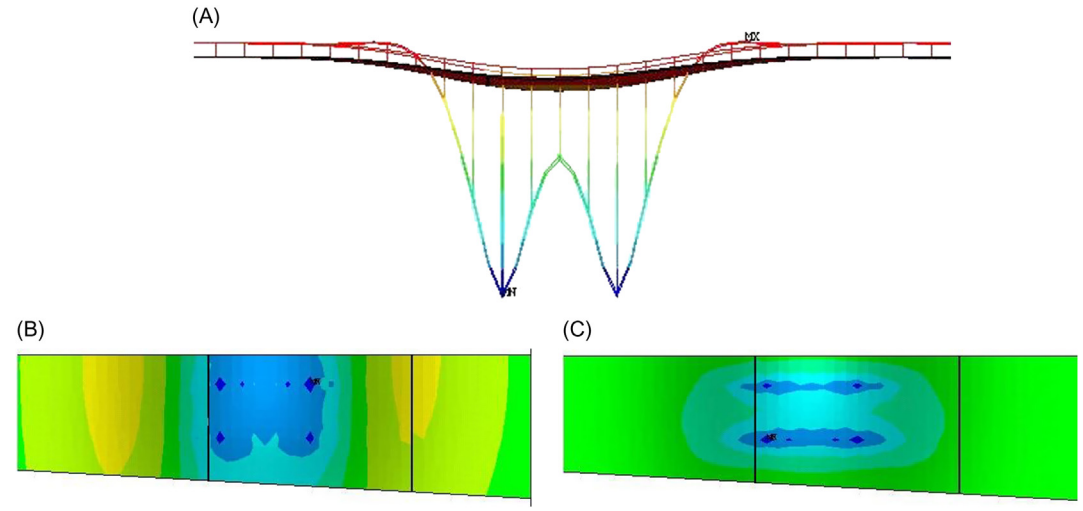

FIGURE 9.14

(A) Distribution of vertical displacement of rail and bed slab. (B) Distribution of longitudinal stress of bed slab. (C) Distribution of lateral stress of bed slab.

Self-compacting concrete will be placed between the slab and leveling course. The turnout slab is connected with the base through Π-shaped steel trusses reserved on the slab bottom. The track is limited longitudinally and laterally with the bonding force and friction force between turnout slab bottom and base and shearing force of Π-shaped steel truss. The turnout slab is made of C55 concrete, provided with a 0.5% lateral drainage slope on slab surface. The support rail bed has no slope. The base is made of 180-mm-deep C40 self-compacting concrete with good fluidity, about 400 mm wider than the slab in the lateral direction, provided with a 4% drainage slope on the projected edge. The leveling course is made of 130−200-mm-deep C25 concrete, about 300 mm wider than the base slab in the lateral direction. It may not be reinforced. On the slab bottom, Π-shaped steel trusses are reserved to be built in the base, so as to integrate the slab and the base. See Figure 9.15 for specific structure.

The slab track with filler course is composed of turnout parts, turnout slabs, filler course, and base. The turnout slab will be fine-tuned on the finished concrete base. The filler course will be placed between the turnout slab and base. Pins will be inserted into the holes on the turnout slabs and base. The track is limited longitudinally and laterally with the bonding force and friction force between turnout slab bottom and base and shearing force of Π-shaped steel truss. The turnout slab is made of C55 concrete, provided with a 0.5% lateral drainage slope on slab surface. The support rail bed has no slope. The fillers must have good construction performance (fluidity, expansivity, and degree of dissociation), mechanical property (compressive strength, shear strength), and durability. Emulsified asphalt mortar is generally used. The C40 concrete base may be continuous in the turnout zone, about 400 wider than turnout slab in the lateral direction and provided with a 4% drainage slope on the projected edge. The turnout slabs and base are securely connected by pins.

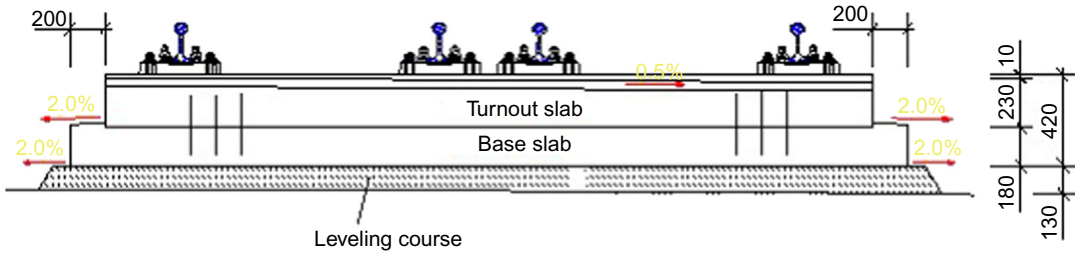

FIGURE 9.15

Track structure in turnout zone with leveling course.

Turnout slabs may be blocked to facilitate production and construction. The turnout slab extends from the center of the expansion gap in front of the switch rail to a position as determined by track structure at turnout rear. At the switch and crossing, the slabs are divided by the foundation pit for the switch rod. According to conversion requirements, the space for the switch machine should be reserved on the slab. For No. 18 turnouts in China, the maximum and minimum lengths of turnout slab are 5900 and 4560 mm, respectively.

Slab depth relates to operational conditions of the railway line (train load), track height, turnout slab structure (concrete performance, application of prestressing, or rate of common reinforcement), and height of the support rail bed. According to mechanical analysis and design of structural reinforcement, the slab depth is defined as 240 mm (including the height of support rail bed).

As the track geometry is variational in a turnout, the lateral width of the turnout slab may also vary in the longitudinal direction of the line. In the design, sufficient strength and stability of slab, depth of concrete protection layer, and a minimum distance of 300 mm from sleeve to slab side must be ensured. The slab width will be continuously variational. The slab edge is in a straight line in the main track, varying along the line type of the curve rail. Two neighboring slabs will have continuous widths to make the turnout edges smooth and aesthetically appealing. In terms of transport, at least one of the dimensions (length and width) should be greater than 3500 mm. In China, the maximum slab width for a No. 18 turnout is 5445 mm.

A lateral full-length support rail bed 260 mm wide is arranged on top of the turnout slab, which has a minimum height of 12 mm at the rail base. For Chinese fastenings, the total height of pads is 56 mm, and the minimum clearance between the rail base and slab surface is 68 mm, meeting the requirements for operating spaces for small track-lifting machines during maintenance.

The structural reinforcement of turnout slab is composed of an upper and a lower layer, with interlayer spacing of 100−120 mm. Each layer is in the form of a crisscrossed grid, with average grid spacing of 120 mm (longitudinally) × 125 mm (laterally). Both the longitudinal and lateral reinforcements are of Grade HRB335 ϕ12 and ϕ14 mm. The minimum depth of the concrete protection layer for the main reinforcement is 30 mm.

For a ballastless turnout on subgrade, the slabs are connected with the base with Π-shaped reinforcements (ϕ12 mm, Grade HRB335) reserved on the slab bottom. Meanwhile, the slab bottom is provided with a coarse surface (roughening) to enable secure connection with the

self-compacting concrete of the base. For a ballastless turnout on a bridge, the slabs are connected by means of filler course and pins, where holing will be performed as per detailed reinforcement layout so as to avoid interference with reinforcements during other holing operations. Each slab is to be anchored with at least eight pins.

Three insulation types are used for ballastless track slabs in China: heat-shrinkable sleeves, epoxy-coated reinforcement, and plastic insulating clamps for reinforcement. The ballast track slabs are insulated with lateral epoxy-coated reinforcement, with the electric resistance between reinforcements no less than 2 MΩ. The spiral reinforcement around the sleeve and embedded nuts for electrical equipment must not come into contact with reinforcements nearby during manufacturing; therefore, adjoining reinforcements will have insulation coat applied, and sleeve spiral reinforcement may be installed after the coat becomes dry to achieve required insulation performance of turnout.

2. Stress analysis

A calculation model of "beam-slab-slab" for turnout slab under vertical train load should be established. In the model, the turnout rails are modeled with beam elements, the turnout slab and base are deemed shell elements, and the leveling course is regarded as an elastic foundation plate.

The warping stress of a turnout slab can be obtained by the Westgaard theory in two cases: "cold at the top + hot at the bottom" and "hot at the top + cold at the bottom." The two cases employ the same temperature gradient. For a 220-mm-deep turnout slab or bed slab, the coefficient of warping stress is approximated as 1.0 with the equation below:

$$\sigma_{qx} = \sigma_{qy} = \frac{E\alpha_t\beta_h T_g h}{2} \tag{9.15}$$

$$M_q = \frac{q_q h^2}{6} \tag{9.16}$$

where

σ_{qx} = the maximum longitudinal warping stress
σ_{qy} = the maximum lateral warping stress
E = transformed elastic modulus of reinforced concrete
α_t = expansion coefficient of concrete
β_h = slab depth correction coefficient of temperature gradient
T_g = temperature gradient
h = depth of turnout slab; and
M_q = bending moment of turnout slab induced by temperature gradient.

The bending moment of turnout slab under lateral force:

$$M_q = \frac{1}{2} \times 0.3 \times Q \times H/a \tag{9.17}$$

where 1/2 indicates that the upper and lower bending moments of the slab are the same, equaling half of the total value under lateral load; 0.3 refers to the distribution coefficient of lateral force along longitudinal direction of track; Q is lateral force, taken as 70 kN; H represents the clearance between the action point of lateral force and slab top, equaling the slab depth, 0.22 m.

Affected by subgrade settlement and deflection deformation of the bridge, given that turnout slabs and base are consistent in deformation, the bending moment on corresponding turnout slab will be:

$$M_u = EI\rho_{max} \tag{9.18}$$

where EI is the bending elastic modulus of turnout slab and ρ_{max} is the deformation curvature of the foundation. To ensure the rationality and economic efficiency of design, the combined loads for additional bending moment of subgrade settlement may adopt a combination coefficient of 0.5.

In view of load combination, longitudinally, the combination of "vertical train load + temperature warping" (main forces) will be taken as the design load, and the combination of "vertical train check load + temperature warping + inhomogeneous settlement of foundation" (main forces + additional force) will be taken as the check load. Laterally, the combination of "vertical train load + lateral load + temperature warping" (main forces) will be taken as the design load.

The strength and cracks of turnout slabs can be verified with the design bending moment, check bending moment, structural dimensions, and reinforcement. Under design load, the compressive stress of slab concrete is 5.82 MPa, the tensile stress of reinforcement is 172.83 MPa, and the crack is 0.18 mm wide. Under check load, the compressive stress of slab concrete is 6.42 MPa, the tensile stress of reinforcement is 190.63 MPa, and the crack is 0.19 mm wide, within the allowable range.

3. Other verifications

Besides the above verification, the slab strengths during manufacturing, transport, and construction will also be verified, supplemented by verification of the strength of the Π-shaped reinforcement, shear stress of concrete at embedded sleeve and around lifting sleeve, etc.

The quality of steel die, formation of reinforcement framework, and positioning of embedded sleeve are critical processes in manufacturing turnout slabs. High precision and rapid fine-tuning are essential during laying.

9.2 PLATES OF TURNOUT

In a turnout, switch rails and point rails are made of AT rails with lower height; slide bedplate with a certain height will be arranged at the rail base to ensure normal rail height and conversion. Check rails and other parts are similar. In addition, to ensure consistent rail height, the fastenings in the transition lead curve must be provided with tie plates for indirect fixation and saving of the tie shoulder. There are several types of tie plates, including common level plates, check rail plates, slide bedplates, full-length plates, switch heel plates, and crossing plates.

Rails with canted tops are provided with level plates, while rails with canted bases are provided with canted plates. Practically, the pads shall have a certain depth and width to limit the compressive stress transmitted to the tie within an allowable range and prevent the plate from bending or fracturing with inherent stiffness. The plate depth is normally 20 or 25−30 mm in the case of smaller fastening stiffness or greater axle load. On a single tie, the plate is generally 180 mm wide.

Shouldered plates are preferred to minimize variation of track gauge and increase resistance against lateral displacement of rails.

9.2.1 FORCES ON PLATES [121]

1. Vertical force from rails

   Comparing a rail to an infinitely long beam on the subgrade, the pressure on each tie produced by wheel load P can be calculated from the Winkle assumption and continuous resiliently supported beam model:

$$R_{\max} = \frac{aPK}{2} \tag{9.19}$$

   where a and k denote tie spacing and stiffness ratio coefficient, respectively; $k = \sqrt[4]{D/4EIa}$, wherein D and EI represent respectively fastening support stiffness and rail flexural stiffness.

   For semi-infinitely long beams, finitely long beams, and nonuniform rails (e.g., switch rail, point rail, and check rail), the tie pressure induced by wheel load can be obtained with the finite element method.

2. Lateral force from rails

   The lateral force of tie from rails of infinitely long beams can also be obtained with Eq. (9.19). Normally, nylon gauge blocks, serving as cushion pads, are arranged between tie plates and rails. The blocks with greater stiffness can transmit all lateral force of rails to tie plates under the worst conditions.

3. Longitudinal force from rails

   Rail longitudinal force will be transmitted to the tie plate via frictional resistance of fastening only when the rail slides with regard to the tie plate. The longitudinal force may at most equal the longitudinal resistance of fastening. It is small and may be omitted in calculating tie plate strength.

4. Vertical force from fasteners

   Tie plates are provided with iron shoulders for elastic clips. The elastic clip front will clamp the base of stock rail; for bolted fasteners, the elastic clip rear will be supported on the iron shoulder. The pressure applied by an elastic clip on an iron shoulder is approximated as the fastening pressure. The T-shaped bolt on an elastic clip will be tightened to apply tension on the iron shoulder. This tension doubles the fastening pressure. For boltless fasteners, the vertical load applied by an elastic clip on an iron shoulder follows the same case.

9.2.2 CHECK RAIL PLATE [122,123]

1. Structure

   At a fixed crossing, as affected by track interruption, the passage of wheels at gaps is ensured by the restriction of the check rail on the opposite wheel. Meanwhile, the check rail mitigates rail wear. The check rail provided in diverging track of acute swing nose crossings can mitigate the lateral wear of the swing nose rail and ensure rail closure.

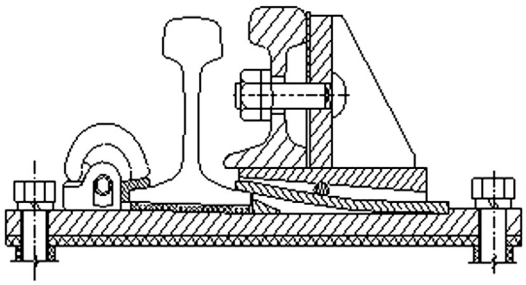

FIGURE 9.16

H-shaped check rail.

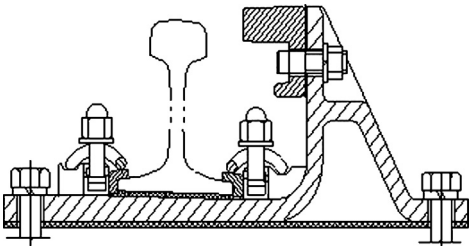

FIGURE 9.17

Rolled channel check rail with solid plate.

In the early speed-up turnouts in China, an H-shaped check rail (Figure 9.16) was used. Check rail is made of common rails, with a groove reserved beneath the bedplate of the rail plate. Spring sheet steel will be inserted from the inside. The inside of stock rail will be clamped by an elastic clip through pinning. The two sides of the stock rail are fastened by elastic fasteners of different types. The gauge at the inside of the stock rail cannot be adjusted easily because of the existence of the bedplate. Check rail plates are welded to the rail, featuring poor integrity and easy breakage and fracture.

For better integrity and channel quality of plate, rolled channel check rail with solid plate, as shown in Figure 9.17, was developed in China. The rolled check rail is of stable quality. The cast plate has improved integrity. Clamped by elastic clips, the two sides of stock rails are exposed to even elasticity. However, casting greatly affects the use life of plates and causes maintenance inconvenience to elastic fasteners under the check rail. Channel check rails, with the basic features of H-shaped check rail, lower height, and leave greater space beneath for elastic fasteners. Therefore, they are widely used in China.

The structure of check rails has been optimized in high-speed turnouts in China, as shown in Figure 9.18. Rolled channel check rails are used, wherein the rail plate is welded similarly to the slide bedplate. Holes are reserved interiorly to accommodate the approximately n-shaped elastic clips (the same as the switch). This structure is simple, stable, and easy to maintain.

2. Stress analysis

Figure 9.19 shows a calculation model of a check rail plate (material: QT400-15). The distribution of equivalent stress and lateral displacement is obtained with commercially available finite element software, as plotted in Figure 9.20.

According to the calculation, the stresses on the tie plate are mostly under 100 MPa, while the stresses around the bolt hole are under 200 MPa. High stress occurs at the junction of the bracing plate and base slab, about 250 MPa maximally. Within the allowable scope of material strength, the maximum lateral displacement is about 0.5 mm at the upper part of the bracing plate.

9.2.3 COMMON PLATES

Rail plates are an integral part of a turnout, transferring the rail load to the ties. A rubber pad is arranged under the plate to ensure fastening elasticity. An adequately rigid cushion pad is arranged

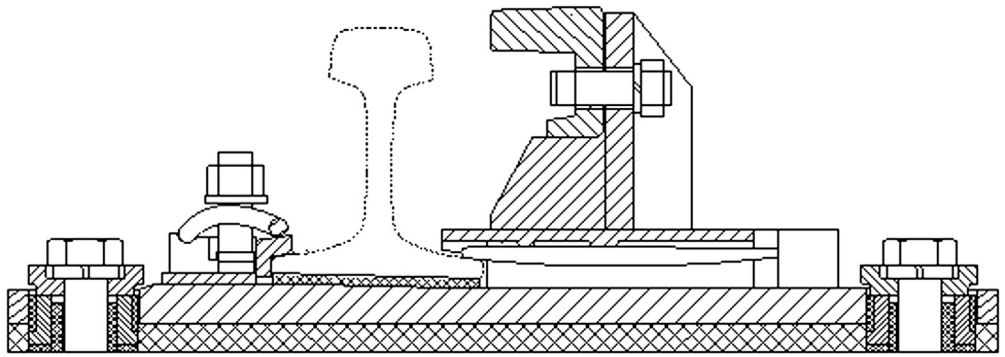

FIGURE 9.18

Check rail of high-speed turnout.

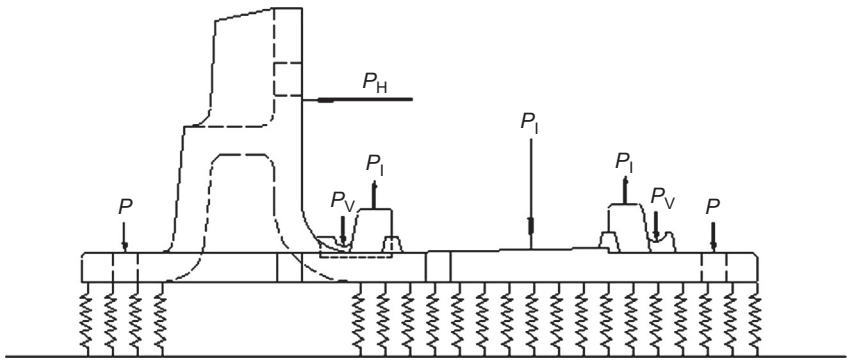

FIGURE 9.19

Mechanical analysis model of check rail plate.

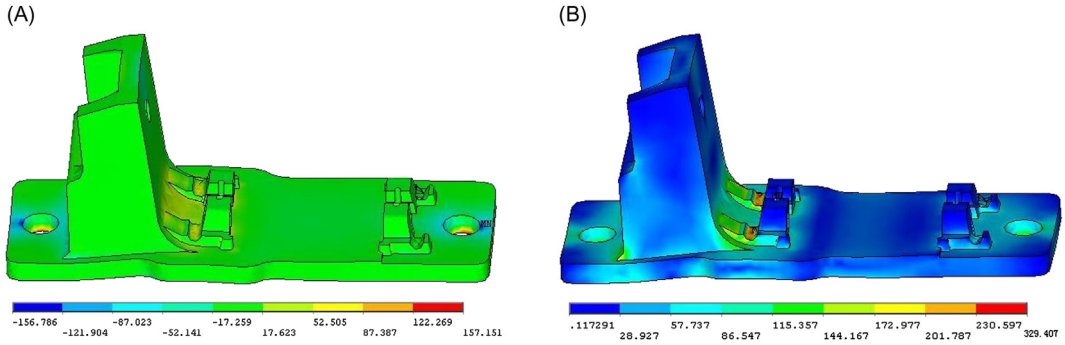

FIGURE 9.20

(A) Equivalent stress of check rail plate. (B) Lateral displacement of check rail plate.

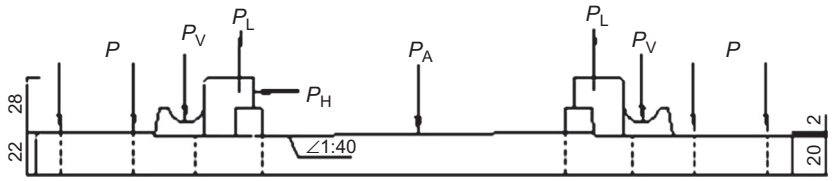

FIGURE 9.21

Arrangement of load on tie plate.

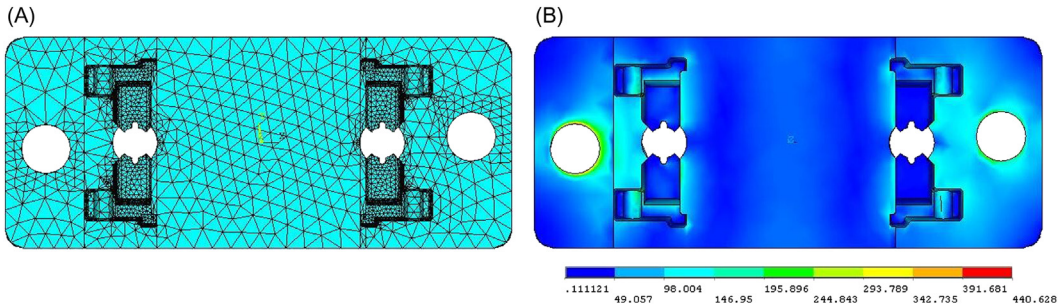

FIGURE 9.22

(A) Analysis model of plate. (B) Distribution of equivalent stress on plate.

under the rail, connecting the rail and tie via bolts and fasteners. Rail plates are forged from ZG200-400, with minimum yield strength of 200 MPa and minimum tensile strength of 400 MPa. The plate depth depends on operational conditions, generally taken as 20 mm. Figures 9.21 and 9.22 present the stress analysis model and distribution of calculated equivalent stress, respectively.

As per the calculation, the stresses are small in most areas, and relatively high around bolt hole and beneath the iron shoulder for elastic clips, but both are acceptable.

Fatigue strength of the plate may be checked with commercial finite element software. Defining the events and loads as per the possible positions of fatigue failure (often the positions with maximum stress), entering S-N curve and Sm-T curve of the material, and specifying the number of cycles can obtain the allowable fatigue cycles of 3,820,000 and fatigue coefficient of 0.524.

9.2.4 ELASTIC FASTENING AND ANTIFRICTION ELASTIC CLIPS OF SLIDE PLATE AT SWITCH

The slide plate is an important part of a turnout, supporting the switch rail and fastening the stock rail along the full length of the switch rail. It ensures the elastic fastening of stock rail and has a small friction coefficient.

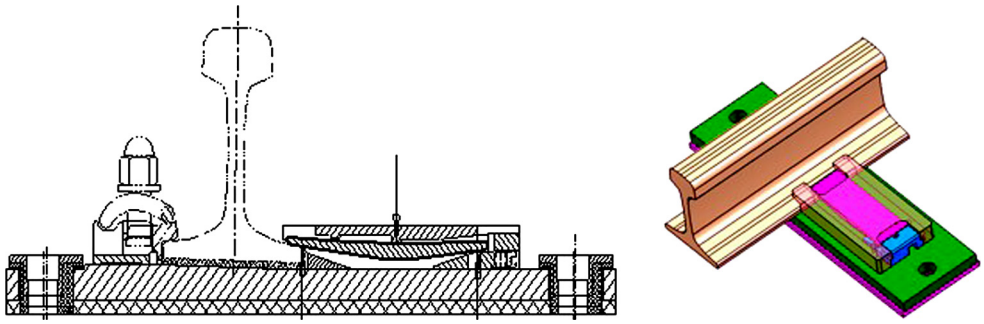

FIGURE 9.23

Clamping by wedge-shaped adjusting elastic clip.

(A) (B)

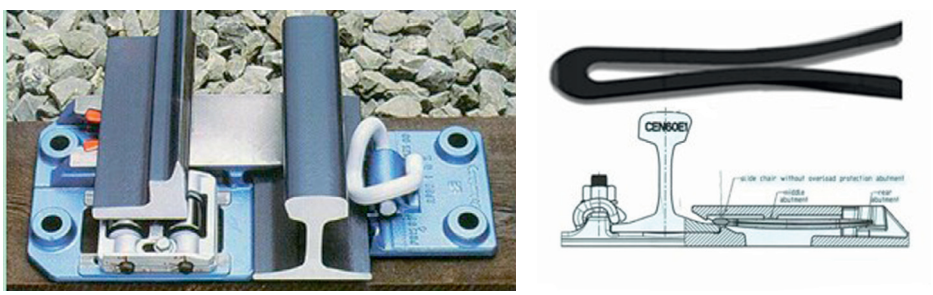

FIGURE 9.24

(A) Solid elastic clip. (B) Clamping-type elastic clip.

1. Design of elastic clips of slide plate

The slide plate of Chinese common turnouts is welded by upper and a lower steel plates, which clamp the inside of the stock rail rigidly, featuring poor elasticity. In speed-up turnouts, the slide plate clamps the stock rail by means of elastic clips and pins; however, partial elastic clips and pins are damaged in practice. Figure 9.23 presents a wedge-shaped adjusting elastic clip which is relative complex.

In other countries, in turnouts for the same speed, the elastic clips of the slide plate mainly include solid elastic clips from Schwihag (Switzerland) and indirect fixation elastic clips from BWG (Germany). Schwihag elastic clips are of $\propto$ shape (as shown in Figure 9.24), with fastening force of 12 kN, capable of clamping the stock rail effectively, providing sufficient fastening resistance and preventing rail tilting. The type of elastic clip is for curved nonuniform sections, characterized by complex line type, sophisticated technology, simple structure and installation, and stable performance. It is widely used globally in high-speeds turnout in France. It is also used in high-speed turnout in China.

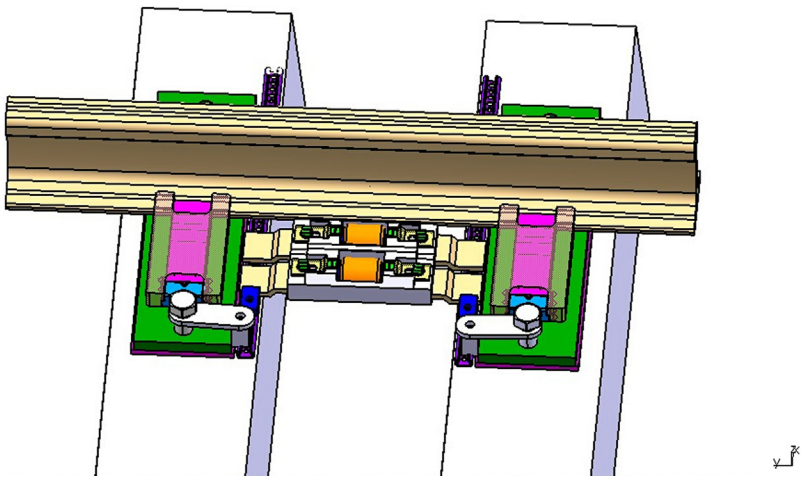

FIGURE 9.25

Rollers between turnout ties.

2. Antifriction

As per the design of turnout conversion, the friction force between the switch rail and slide plate is a main aspect of switching force. In high-speed turnouts, this friction force is reduced technologically. Moreover, the slide plate facilitates the gauge adjustment of stock rail.

There are two main antifriction modes for turnout slide bedplates. First is mechanical mode, in which the switching resistance is reduced by replacing the sliding friction with rolling friction by means of a rollered slide plate (Figure 1.45), rollers between ties (Figure 9.25), and a ball slide plate (Figure 1.61). Schmidt (Germany) has developed a roller device arranged between two turnout ties near the traction points, as shown in Figure 9.25. For this structure, a connecting brace is mounted on the tie edge, which connects with the tie blot via a limiting device and connects with the roller frame via a connecting plate. The vertical height of the roller at different positions is adjusted by a height-adjusting bolt. This roller structure may be applied to existing turnouts, and has been used in China. However, it is rather complex and hard to install.

The second mode involves modifying the surface material of slide plate. Thin plates made of self-lubricating material are attached to the slide plate in different ways to form a lubricating free slide plate, such as the solid bonded structure and partially embedded structure shown in Figure 9.26. Self-lubricating materials mainly include porous oil-soaked material, oil-bearing powdered metallurgy material, oil-bearing ceramics, graphite-dispersed alloy, plasma sprayed ceramic coating, polymer coating, and special plastics. The thin plates made of those materials are attached to the slide plate by means of welding, spraying, embedding, and bonding.

The Schwihag rollered slide plate, shown in Figure 9.24, is employed in high-speed turnouts in China. This slide plate is highly versatile, provided with tapping holes on the bottom, and capable of being used for different throws by moving the rollers horizontally. The desired vertical height of the roller at different locations can be realized by rotating the eccentric roll shaft. The

FIGURE 9.26

(A) Bonded antifriction course. (B) Embedded antifriction course.

rollers are mounted when the switch rails are open, with a 2-mm gap from the outer side of the base of the switch rail to avoid great initial lining resistance. The roller closer to the switch rail is 2.5−3 mm higher than the top of slide bed. Two or three rollers are arranged in the front of the switch rail with greater throw, and only one roller is mounted in the rear where the throw is smaller. The roller shaft is securely locked after proper vertical height and horizontal position of the rollers are defined. The rollers are mounted on one side of the slide bed.

Nickel is added as the main content of the antifriction coat of the slide bedplate in high-speed turnouts in China. The nickel coat is not less than 0.15 mm thick, applied by brushing electroplating. This coat has good corrosion and rust prevention performance and can be well bonded with the base material. The nickel-plated bedplate can achieve a surface hardness of HV550. Practice shows that nickel plating can reduce the friction coefficient of the slide plate and improve the wear and rust resistance of the slide bedplate.

9.3 COMPONENTS OF TURNOUT FASTENINGS

The structure of fastenings and design of rail pads and tie plate pads for high-speed turnouts in China have been discussed in the first five chapters. This chapter will introduce the structural design of tie plates, as well as the design of elastic clips and anchoring bolts of ties and other components.

1. Stress of elastic clips [124]

   Previously, special narrow fasteners were developed for turnouts in China, with the hope of providing elastic fastenings at various parts of the turnout, particularly at the narrow part at heel of the switch rail. This type of fastener has been on trial in Shanghaiguan Station. The structure is plotted in Figure 9.27.

   This elastic clip has a diameter of 13 mm and a design stroke of 10 mm. In normal operating conditions, the jaw in front of the middle part of the elastic clip will come into contact with

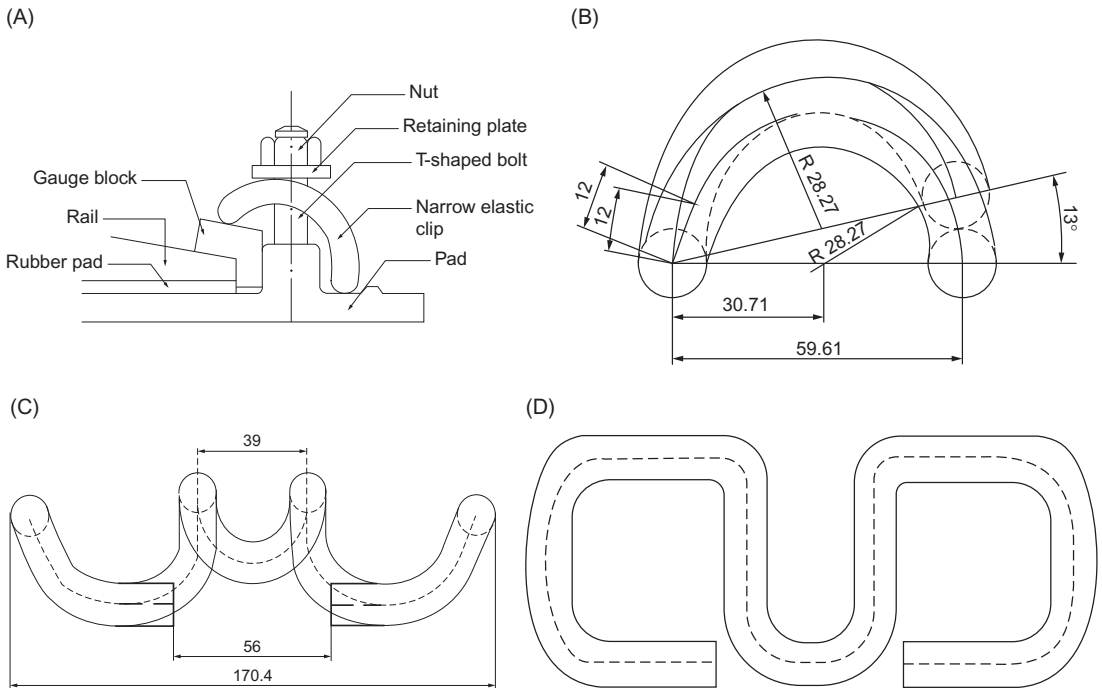

FIGURE 9.27

(A) Narrow elastic clip (assembly drawing). (B) Narrow elastic clip (side view). (C) Narrow elastic clip (front view). (D) Narrow elastic clip (top view).

gauge block (three-point contact). The entire elastic clip is 170.4 mm long, 59.61 mm wide, and 34 mm high, which is longer by 36.4 mm, narrower by 8.39 mm, and higher by 6.6 mm, as compared with Chinese type II elastic clip. The elastic clip is made of $60Si_2CrA$ spring steel. With the use of commercial finite element software, given a fastening force of 10 kN, the stroke of the narrow type elastic clip is 9.92 mm, and the maximum stress is about 1359 MPa (induced by torsional deformation and occurs in the rear of elastic clip in symmetry), as shown in Figure 9.28. This elastic clip has an performance equivalent to the Chinese type II elastic clip (Figure 9.29).

2. Stress analysis of locking fasteners for ties

The coupling of fastenings and ties is a critical part of the design. As demonstrated by operational practice in Chinese speed-up turnouts, an embedded composite structure of steel sleeve and nylon sleeve is used. The nylon sleeve in the steel sleeve is made of glass fiber-reinforced nylon 66, which can be replaced easily when damaged. The coupling bolt has a diameter of 30 mm, having good resistance against lateral force. The 8-mm pitch can enable the root

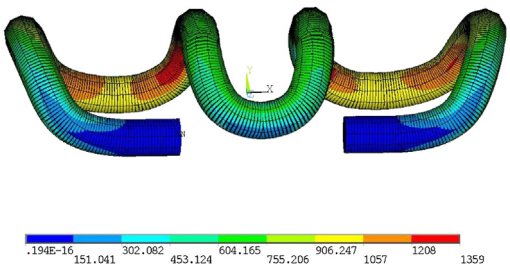

FIGURE 9.28

Stress distribution of narrow elastic clip.

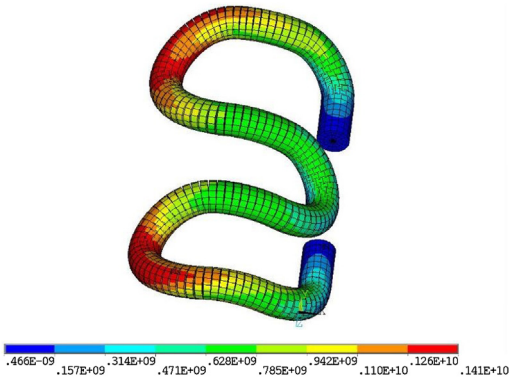

FIGURE 9.29

Stress distribution of type II elastic clip.

strength of the nylon sleeve. The 40-mm-long threadless part in the nylon sleeve enables the bolt to have maximum bending moment at the threadless part. With an outer diameter of 45 mm, the strength of nylon sleeve can be ensured and longitudinal cracks of the bolt holes in concrete ties can be minimized.

The anchorage system of the turnout tie may be exposed to vertical lifting force and lateral force from the train, transmitted by the tie plate generally. The vertical lifting force is loaded in tightening the bolt, which must be not lower than 100 kN from a technological perspective. The lateral force of the train is imposed on the bolt in the center of tie plate depth, taken as 50 kN. By use of commercial finite element software, the equivalent stresses of the components under the combined effect of lifting force and lateral force is as shown in Figure 9.30. The strengths of all parts are within allowable limits.

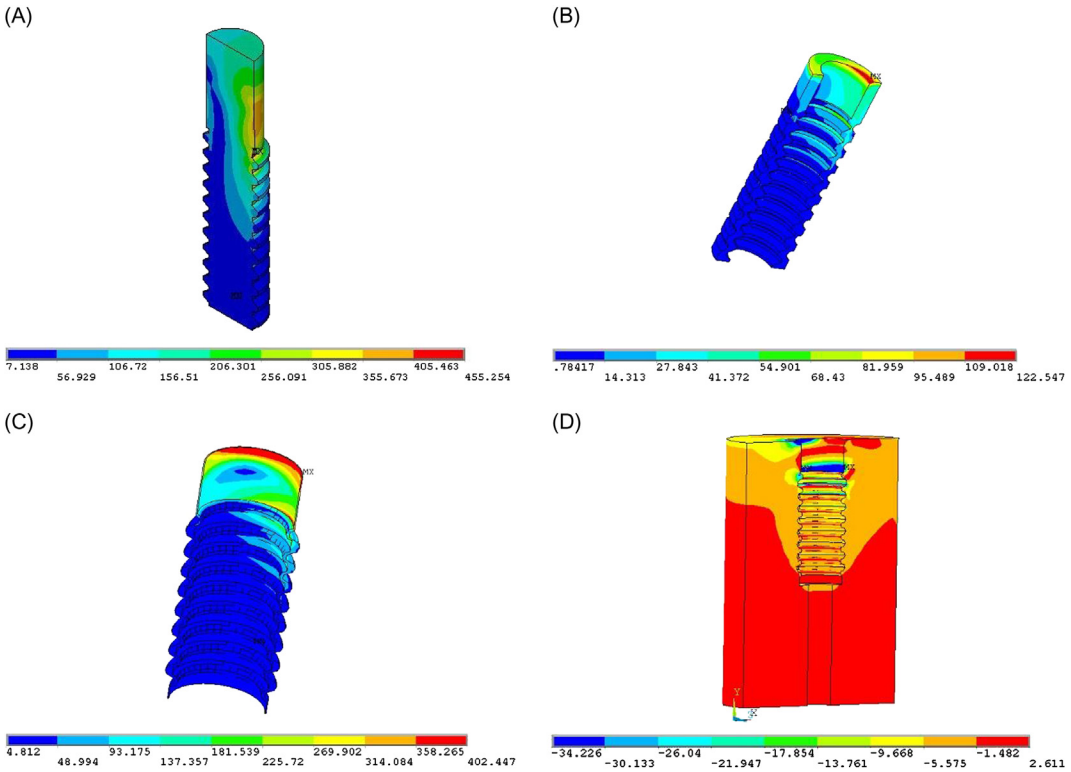

FIGURE 9.30

(A) Equivalent stress of bolt. (B) Equivalent stress of nylon sleeve. (C) Equivalent stress of steel jacket. (D) Tensile stress of tie concrete.

3. Tests on turnout fastenings [125]

Laboratory tests on fastening are important, coming after the structural design and calculation check, and aiming at exploring the structural rationality, verifying conformance to design requirements, and detecting assembly defects. The tests include an assembly fatigue test and tests of pad stiffness, fastening resistance, fastening force, and insulation performance.

The fatigue property of the fastening will be tested comprehensively to explore the long-term behavior of the fastening. For this, all fasteners will be assembled on the tie first, a 45° force application rack will be used, and a 20−100 kN load will be applied to the crack repeatedly for the fatigue test, as shown in Figure 9.31.

FIGURE 9.31

Fatigue test for fastener assembly.

Test results: No damage occurs to the fasteners after 3 million cycles of loading, and all parts meet the design strength. The static stiffness of the rubber pad increases by 3−8% after testing, meeting design requirements. Dynamic lateral movement of the rail head was 1.5 mm during the test, below the technical limit of 1.53 mm during passage of a train in the main line. The gauge variation is smaller than 1 mm after 3 million cycles of fatigue testing, below the required limit of 6 mm. As demonstrated by practical use in high-speed turnouts in China, this fastening can maintain the gauge excellently and ensure homogeneous elasticity. Moreover, it is easy to install and adjust.

CHAPTER

THEORETICAL VALIDATION OF HIGH-SPEED TURNOUT DESIGN 10

For the development of Chinese high-speed turnouts, the author proposes a dynamic analysis theory of turnouts to solve the technical problems of wheel−rail relations, track stiffness, and vehicle−turnout−bridge coupled vibration, as well as train shaking in a turnout during maintenance. In addition, a calculation theory of continuously welded rail (CWR) turnouts is developed to solve the problems of design and laying of trans-sectional CWR line and CWR turnout on bridge. The study is supplemented by improvement of the calculation theory of turnout conversion, optimization of the arrangement of traction points, and formulation of antifriction measures. However, these analysis theories must be verified with laboratory and field tests, and upgraded from time to time to provide guidance for structural design of high-speed turnouts.

10.1 VALIDATION OF TURNOUT DYNAMIC SIMULATION THEORY

The former MOR of China had organized a dozen dynamic tests on high-speed turnouts with real cars in a number of railway lines (Qingdao−Ji'nan, Suining−Chongqing, Wuhan−Guangzhou, Ningbo−Wenzhou, Wenzhou−Fuzhou, Shanghai−Nanjing, and Shanghai−Hangzhou lines) to test the structural safety, dynamic performance, and rationality of design theories of Chinese high-speed turnouts. It turned out that Chinese high-speed turnouts are theoretically correct and structurally feasible and reliable, meeting riding safety and quality requirements.

The high-speed turnout dynamics design theory is justified with the test results in four aspects.

10.1.1 COMPARISON OF DYNAMIC RESPONSES [126−128]

Table 10.1 presents the results of real car dynamic tests and numerical simulations. It can be seen from Table 10.1 that:

1. The calculated value and measured value are roughly the same for each dynamic response, varying similarly with traveling speed, passage direction, and type of turnout and sub-rail foundation. But the calculated value and measured value do not coincide perfectly due to fabrication or assembly error and laying conditions. This indicates that the turnout dynamic theory is dependable in assessing turnout safety and dynamic performance.
2. The calculated values of derailment coefficient, load reduction rate, lateral wheelset force, and dynamic stress of the point rail are defined as maximum values during the passage of a train in

Design of High-Speed Railway Turnouts.

Table 10.1 Comparison of Dynamic Responses

Test Site		Jiaozhou North Railway Station in Qingdao–Ji'nan Line		Caijia Railway Station in Suining–Chongqing Line		Wulongquan Railway Station in Wuhan–Guangzhou Line	
Turnout Type		No. 18 Ballast Turnout for 250 km/h		No. 18 Ballastless Turnout for 250 km/h		No. 18 Ballastless Turnout for 350 km/h	
Test Time		June and November 2006		January 2007		January 2009	
Passage Direction / Type of Train		Main Line EMU	Diverging Line Wagon	Main Line EMU	Diverging Line EMU	Main Line EMU	Diverging Line EMU
Maximum speed (km/h)		250	90	200	90	350	90
Derailment coefficient	Calculated value	0.38	0.47	0.53	0.49	0.58	0.36
	Measured value	0.21	0.43	0.46	0.35	0.54	0.43
Load reduction rate	Calculated value	0.48	0.49	0.36	0.47	0.28	0.47
	Measured value	0.26	0.40	0.55	0.30	0.50	0.26
Lateral wheelset force on switch rail (kN)	Calculated value	39.4	63.9	28.4	55.3	26.4	26.9
	Measured value	17.9	52.8	7.0	38.3	23.0	28.3
Stress of point rail (MPa)	Calculated value	79.3	121.1	87.5	80.7	81.1	90.4
	Measured value	46.0	123.0	–	53.3	76.1	–
Spread of switch rail (mm)	Calculated value	0.76	0.47	0.77	0.46	0.78	0.47
	Measured value	0.64	0.49	0.28	0.60	0.75	0.33
Spread of point rail (mm)	Calculated value	1.04	0.93	1.28	0.84	1.17	0.79
	Measured value	0.65	0.89	1.34	1.34	0.35	0.29
Acceleration of tie (g)	Calculated value	15.4	22.0	2.4	0.8	3.5	0.8
	Measured value	14.5	19.4	1.3	–	8.5	0.6

a turnout. Measured values are defined as the maximum value at a measuring point. Thus, calculated values are greater than measured values.

3. The spread of the actual point of the switch rail (point rail) varies greatly with the locking state. Despite minor changes of calculated values, test values may differ significantly for different passage directions and turnout types.
4. As demonstrated in the test in the Suining–Chongqing line, the measured load reduction rate is greater than the calculated value during the passage of an EMU train in the main line. This is because significant welding irregularity has not been considered in the calculation. The measured load reduction rate of another turnout is about 0.28.
5. In the test in the Wuhan–Guangzhou line, the measured vibration acceleration of ballastless turnout tie is larger than the calculated value. This may be induced by poor integral bearing state of the turnout slab (the tie and concrete bed are in good bonding status). The measured maximum value of another turnout is about 2.1g.

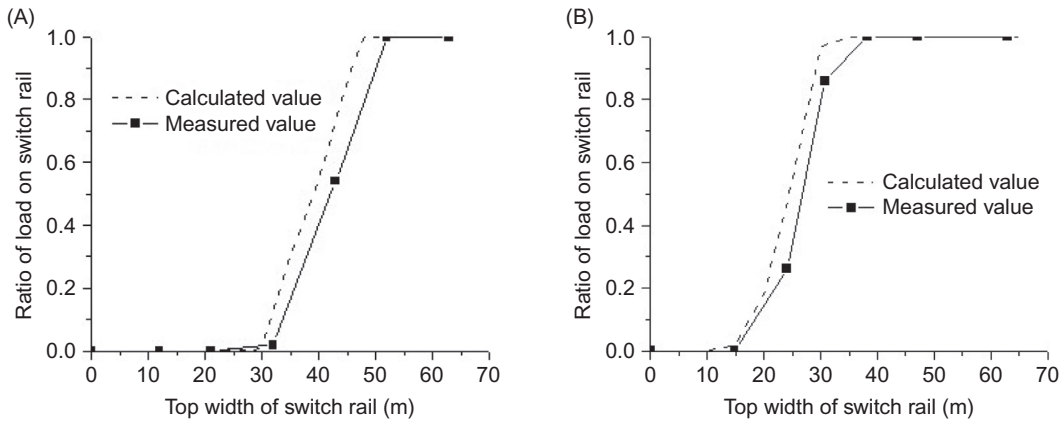

FIGURE 10.1

(A) Wheel-load transition scope in turnout in Qingdao−Ji'nan line. (B) Wheel-load transition scope in turnout in Wuhan−Guangzhou line.

10.1.2 COMPARISON OF WHEEL-LOAD TRANSITION

The turnout dynamic theory can also be justified with the test of the transition scope of wheel load. The transition scope of wheel load is defined by measuring the vertical load at various measuring points on the switch rail with different cross sectional widths by means of rail a web compression method. Tests were performed in No. 18 ballast turnouts for 250 km/h in the Qingdao−Ji'nan line and No. 18 ballastless turnouts for 350 km/h in the Wuhan−Guangzhou line on the distribution rules of wheel load on a switch rail when an EMU train travels in the main line. The comparison with calculated values is plotted in Figure 10.1.

This figure reflects the fact that the calculated and measured transition scopes of wheel load coincide very well, but differ slightly due to fabrication and assembly error and an insufficient number of measuring points. In the Qingdao−Ji'nan line, the measured wheel-load transition scope covers a range of 30−50 mm (top width of switch rail), and the calculated scope is 29−48 mm. In the Wuhan−Guangzhou line, the measured range is 15−37 mm and the calculated range is 15−34 mm. Both the calculated and measured values change similarly. Therefore, the results of turnout dynamic simulation are credible, and the calculation theory does work.

10.1.3 COMPARISON OF WHEELSET LATERAL DISPLACEMENT [129]

A measurement system for lateral wheelset displacement in the turnout zone has been developed by Southwest Jiaotong University to further explore the feasibility of turnout dynamic theory. Figure 10.2 is a schematic diagram of the measurement system. In the process, a laser transducer is arranged beside the line (see Figure 10.3) to measure the lateral displacement of the outside of the wheelset during passage of an EMU train in the turnout. The traveling path of the wheelset in the turnout can then be derived, as shown in Figure 10.4.

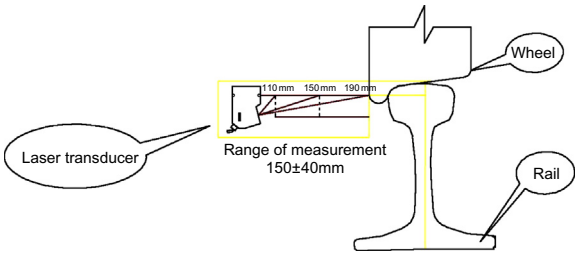

FIGURE 10.2

Schematic diagram of test on wheelset lateral displacement.

FIGURE 10.3

Arrangement of test device for wheelset lateral displacement on site.

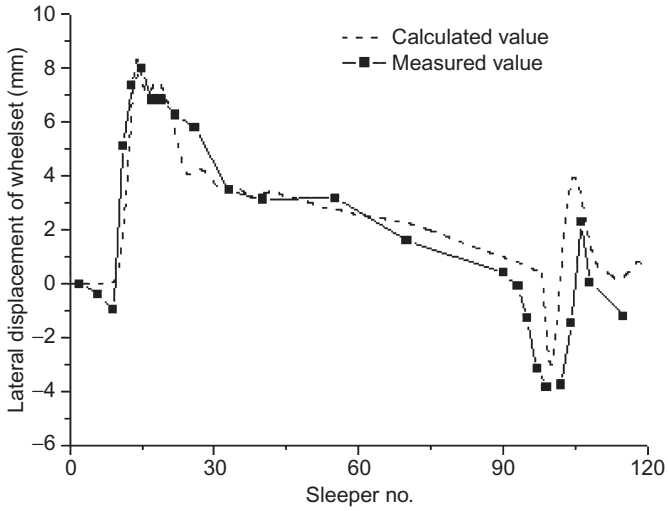

FIGURE 10.4

Distribution of wheelset lateral displacement of EMU train traveling in main line.

In 2007, Southwest Jiaotong University performed a test on lateral wheelset displacement in the turnout zone (No. 18 turnout for 250 km/h) in the Hefei−Nanjing line using French technology. The comparison of measured and calculated values is given in Figure 10.4. It was found that the calculated and measured lateral wheelset displacements coincide well when an EMU train travels in the main line, justifying the turnout dynamic theory and simulation results further.

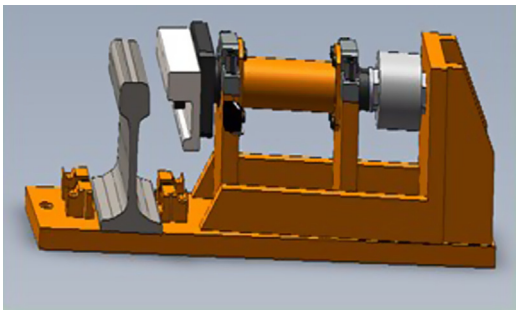

FIGURE 10.5

Test device for lateral force of check rail plate.

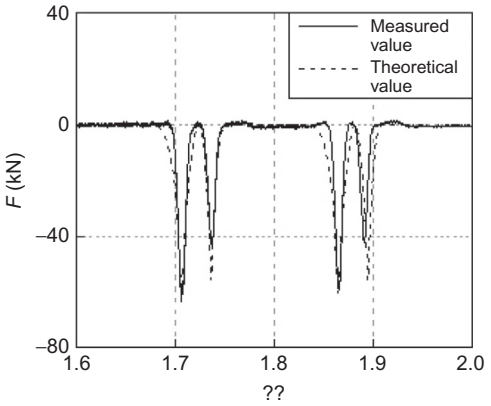

FIGURE 10.6

Comparison of lateral force of check rail.

10.1.4 TEST ON LATERAL FORCE OF CHECK RAIL

A test device (see Figure 10.5) was developed by Southwest Jiaotong University to measure the lateral impact force on a check rail plate. The test device is composed of a baseboard with mounting holes and installation components for stock rail, supports for rigid axle and transducer fixed on the baseboard, a rigid axle mounted on a rigid axle support, a force transducer mounted on a transducer support, and a displacement transducer mounted on a rigid axle support near the check rail of the turnout via linear sliding bearing. The rigid axle connects to the force transducer at one end, and fixed with a connecting block of check rail on the other end. During use, the test device is installed on the tie with the mounting holes on the baseboard, the stock rail in the installation components for stock rail on the board, and the check rail on a connecting block. The rigid axle is vertical to the installing surface of the check rail. When a train travels in the turnout, the lateral impact force on the check rail is transmitted to the rigid axle via the connecting block, and then to the force transducer, where it is measured. The displacement of the check rail can be detected by a displacement transducer. This is the process of field testing of lateral impact force and lateral displacement of the check rail in a turnout produced by wheel passage.

Tests on lateral impact force were performed on three selected plates in a turnout in the Chengdu railway administration in 2010. The calculation theory is justified further. See Figure 10.6 for the waveform of impact force and a comparison of calculated and measured values.

10.2 VALIDATION OF ANALYSIS THEORY OF LONGITUDINAL INTERACTION OF CWR TURNOUT ON BRIDGE

10.2.1 MODEL OF CWR TURNOUT ON BRIDGE [130,131]

Different from a CWR line on bridge or CWR track on subgrade, a CWR turnout on bridge features complex stress conditions. In this context, an indoor CWR turnout model (scale: 1:3, as shown in

FIGURE 10.7

Model of CWR turnout on bridge.

FIGURE 10.8

FBG strain sensor.

FIGURE 10.9

FBG temperature sensor.

Figure 10.7) was developed by Southwest Jiaotong University to explore the relation between the bridge and CWR turnout and to justify the calculation theory for turnout−bridge longitudinal interaction. In the model, a No. 18 swing nose turnout of 60 kg/m rail is modeled with 8 kg/m rail, a 3×32 m concrete bridge with a 3×10 m steel box beam, and fastening with clips. The model is 50 m in length, with counterforce piers arranged at both ends. The steel box beam is heated with fuel gas, and the steel with 36 V, 6000 A DC power.

The rail strain is measured by an FBG strain sensor (Figure 10.8) mounted in the middle of the rail web. The temperature of the bridge and rail is measured by an FBG temperature sensor (Figure 10.9). In the test, the temperature and strain are tested with an LG-FBG-YC interrogator. With the wavelength collected by the temperature sensor and strain gauge and other related parameters obtained, the temperature and temperature force of rail can be calculated.

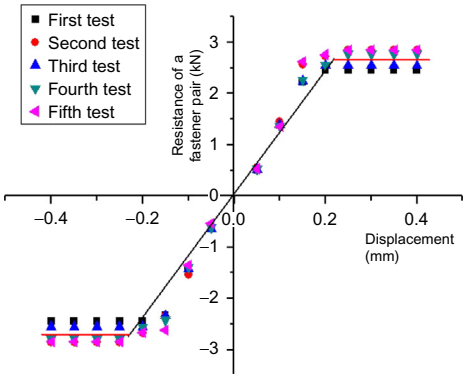

FIGURE 10.10

Curve of fastening resistance.

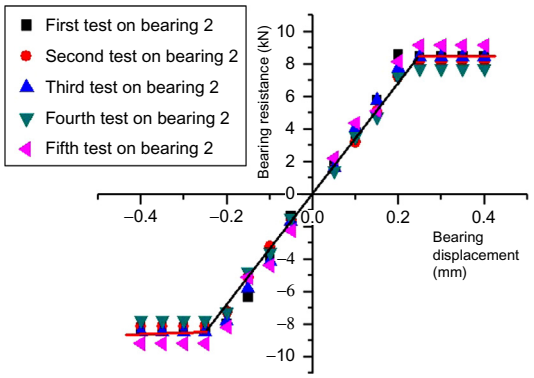

FIGURE 10.11

Curve of resistance of movable bearing.

According to the test results, the maximum longitudinal resistance of a single fastening is 2.7 kN (see Figure 10.10 for the load-resistance curve). The curve of longitudinal resistance for a movable bearing is given in Figure 10.11. The longitudinal horizontal stiffness of pier 1 is taken as 9.9 kN/mm, and that of pier 4 as 14.5 kN/mm.

A number of conditions can be modeled in the test, such as simply supported beam and continuous beam bridge, unit track bed slab, longitudinally connected base slabs, and fixed and movable bearing. Figure 10.12 presents a comparison of partial test results and calculated results of temperature force of the stock rail.

As can be seen from the above, the calculated theoretical value and test value of the temperature force of stock rail differ slightly but follow basically the same change rule. This proves that the turnout−slab−beam−pier integrated calculation model and theory are valid (Figure 10.13).

In addition, the flexural force of the model of CWR turnout on bridge can be tested with a loading test. The comparison of calculated value and test results under partial conditions is plotted in Figure 10.14. The calculated and measured values are basically identical, further justifying the calculation theory for CWR turnout on bridge.

10.2.2 FIELD TEST ON CWR TURNOUT ON BRIDGE [134]

On June 16 and August 16−22, 2006 and July 14−19, 2007, Southwest Jiaotong University performed tests on rail longitudinal force in CWR turnout #1 on No. 1 Meichi Bridge in Meichi Railway Station on the Zhejiang−Jiangxi line (Figure 10.15). The railway line has a design speed of 200 km/m in the main line. The ballast track and main track are trans-sectional CWR tracks laid at one time. No. 1 Meichi Bridge is a 2832-m-long bridge with multiple tracks. The turnout on the bridge is assembled with 32 m simply supported beams with small vertical stiffness. Seven No. 12 CWR turnouts are laid in the main line, all belonging to speed-up swing nose turnouts with concrete ties. They were the first CWR turnouts laid on a bridge in China.

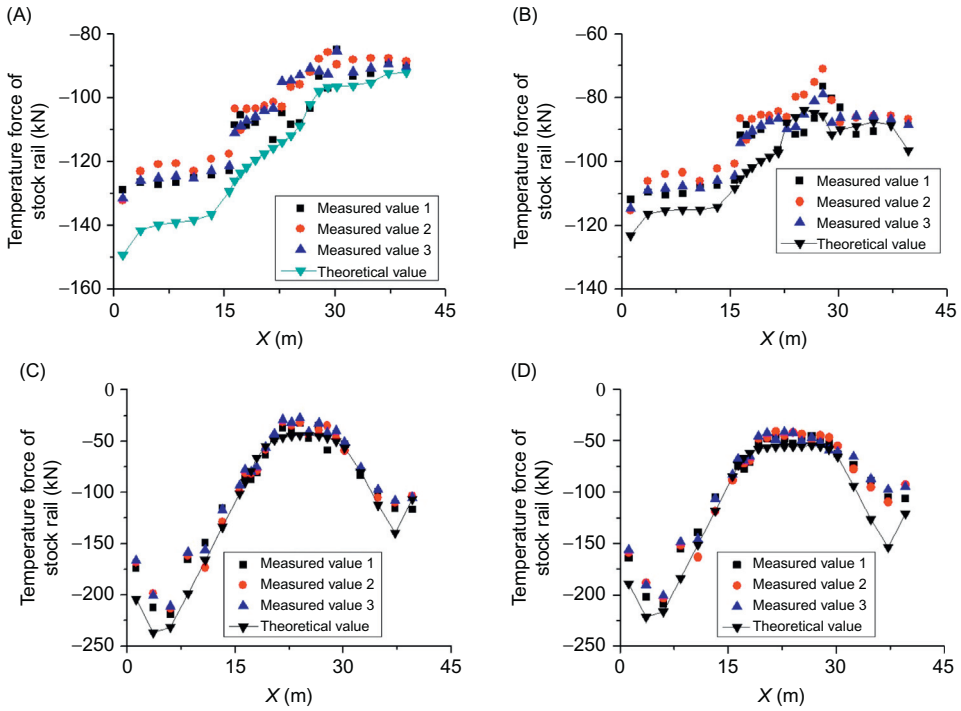

FIGURE 10.12

(A) Temperature force of continuous beam bridge with longitudinally connected slabs. (B) Temperature force of simply supported beam bridge with longitudinally connected slabs. (C) Temperature force of continuous beam bridge with unit slab. (D) Temperature force of simply supported beam bridge with unit slab.

FIGURE 10.13

Loading test on the model.

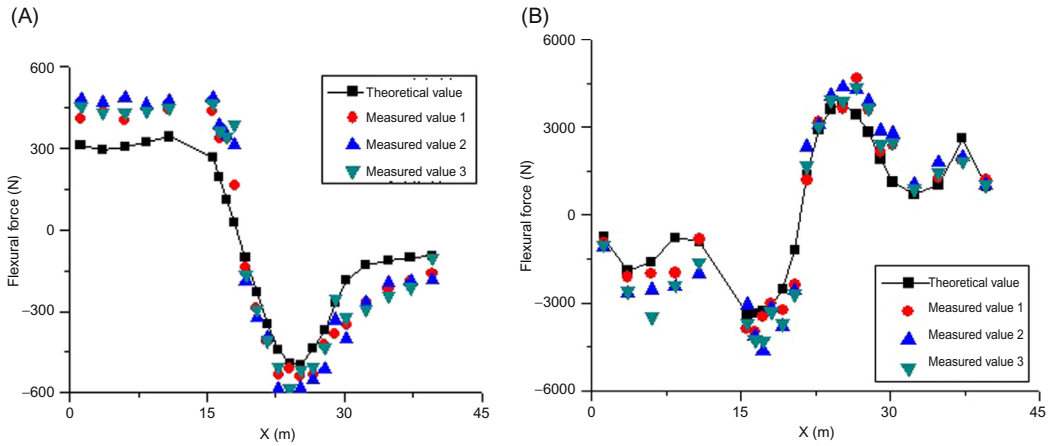

FIGURE 10.14

(A) Flexural force of simply supported beam bridge with longitudinally connected slabs. (B) Flexural force of simply supported beam bridge with unit slab.

FIGURE 10.15

CWR turnout on bridge in Zhejiang–Jiangxi line.

1. Longitudinal resistance of bed

   The longitudinal bed resistance on the bridge and subgrade was tested; it had been tested early in 2006 when the line was just open to traffic and 1 year after operation (traffic capacity: 100 million tons) for comparison. The test results are shown in Figure 10.16.

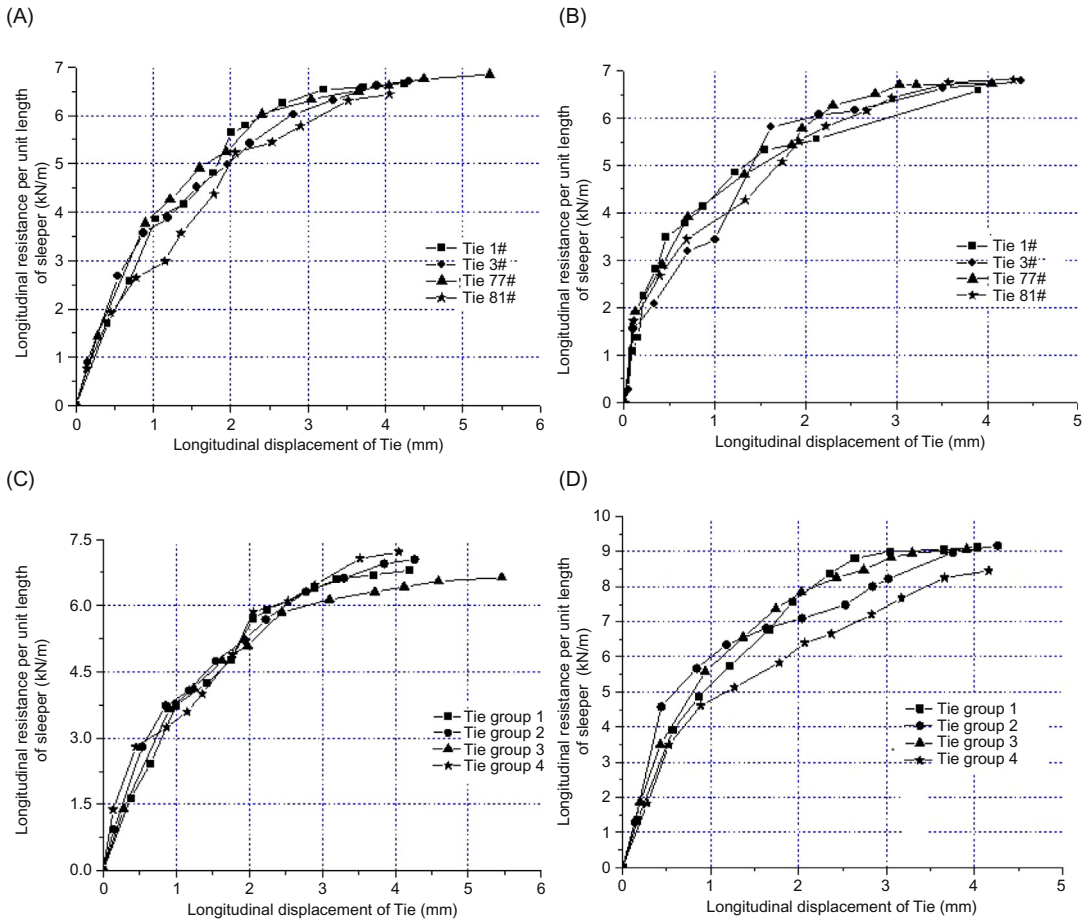

FIGURE 10.16

(A) Track resistance on bridge before being open to traffic. (B) Track resistance on bridge after 1 year's operation. (C) Track resistance on subgrade before being open to traffic. (D) Track resistance on subgrade after 1 year's operation.

As can be found from the test results, the bed resistance per unit length of tie on bridge is 5.0−5.7 kN/m and the bed resistance on subgrade is 5.0−5.9 kN/m at tie displacement of 2 mm in the initial operating stage of the line. One year later, the two values changed to 5.5−6.0 and 6.6−7.8 kN/m, respectively, at a tie displacement of 2 mm. The values of longitudinal bed resistance in the CWR turnout on bridge in the initial operating state and after a short period of operation differ slightly. This is because the ballasts vibrate with the bridge during passage of a train. Smaller vibration can enhance the compactness of the bed, while greater vibration amplitude and frequency weaken the stability of the bed. The same rule is displayed in indoor

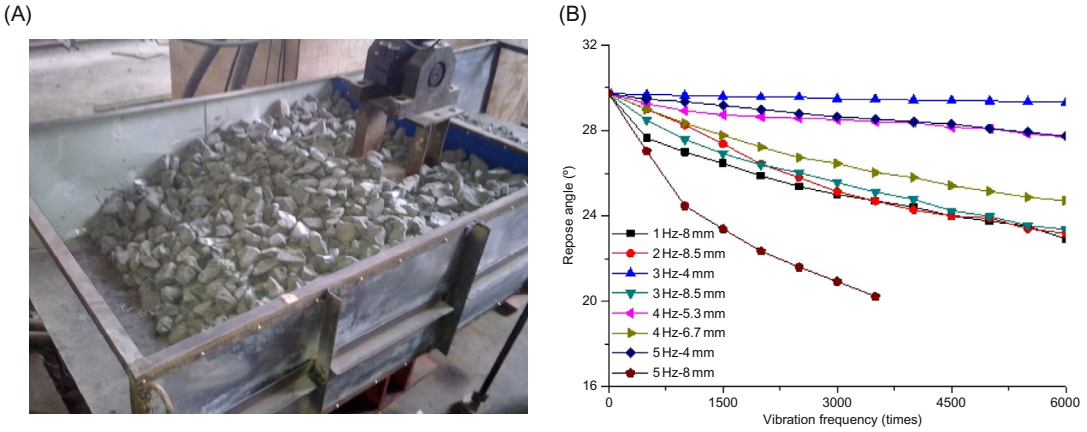

FIGURE 10.17

(A) Vibration test on ballast pile stability. (B) Change of repose angle of ballast pile.

vibration tests (Figure 10.17). On the other hand, a ballast bed will be compacted gradually with increasing gross load. This explains why the bed resistance on the subgrade is greater than that on the bridge.

Southwest Jiaotong University performed the vibration tests on the ballast pile to test its stability. In the test, the stability of the ballast bed can be expressed as the repose angle of the ballast pile. The greater the vibration frequency and amplitude, the smaller the repose angle and the poorer the stability of ballast pile.

For No. 1 Meichi Bridge, the measured first-order vertical natural vibration frequency of the simply supported beam is 3.6 Hz, owing to the small vertical stiffness of the bridge. This value meets the technical requirements for a 200 km/h mixed passenger and freight line (3.02 Hz), but it is below the first-order vertical natural vibration frequency of a 32 m simply supported T-shaped beam (5.0 Hz) and that of a simply supported box beam for high-speed railway lines (8.0 Hz). Therefore, the CWR turnouts on this bridge are of poor stability and retention of track geometry, leading to great maintenance load and inordinate lateral vibration acceleration during the passage of a train in the main line. This has aroused wide concern and attention among railway researchers.

2. Rail temperature force

Figure 10.18 presents a comparison of test and calculated values of temperature force of stock rail at turnout #1 on No. 1 Meichi Bridge. The measured values of longitudinal resistance of the turnout and temperature changes of the bridge and rail are adopted in the theoretical calculation. The test principle for additional temperature force of rail is as follows: binding two brackets (gauge length $L_0 = 210$ mm) on the rail web, measuring the variation of spacing between two brackets (ΔL) with a temperature-independent invar leveling staff, and then calculating the additional temperature force of rail based on measured data, with $\Delta LEF/L$ (E and F denote elastic modulus and section area of the rail, respectively). A TS-3 tester of additional temperature force of rail developed by Beijing Jiaotong University is used in the test, as shown in Figure 10.19. As can be seen from the calculated theoretical values and test values,

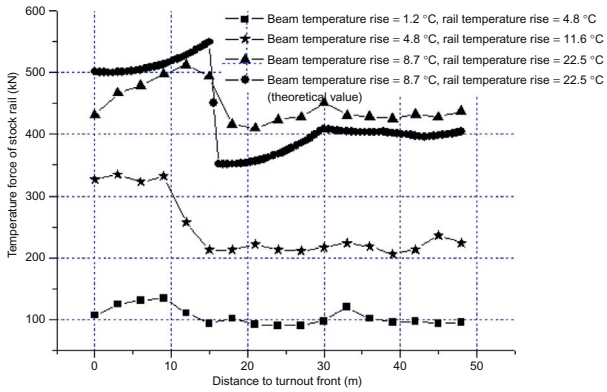

FIGURE 10.18

Longitudinal temperature force of straight stock rail.

FIGURE 10.19

TS-3 tester for additional temperature force of rail.

the temperature force of straight stock rail will change abruptly at the heel of the switch rail. At temperature rise of 8.7°C and 22.5°C, respectively, of the bridge and the rail, the calculated and measured values of temperature force of a straight stock rail follow the same change rule, but the calculated value is greater, and thus safer for design. This may be produced by the smaller value of fastening resistance or test error of temperature force during calculation.

10.3 VALIDATION OF ANALYSIS THEORY OF VEHICLE–TURNOUT–BRIDGE DYNAMIC INTERACTION

To verify the dynamic interaction of a vehicle–turnout–bridge system, real vehicle field dynamic tests were performed on a 350 km/h ballastless CWR turnout on bridge in the Zhengzhou–Xi'an line and a 200 km/h ballast CWR turnout on bridge in the Zhejiang–Jiangxi line.

1. CWR turnout on bridge in Zhengzhou–Xi'an line [135]

   In Weinan Railway Station in the Zhengzhou–Xi'an line, the throat areas at two ends of the station are built on a nonuniform continuous beam bridge. The No. 18 ballastless turnout for 350 km/h laid in the throat was developed by China Railway Baoji Bridge Group Co., Ltd with the technology of the French company Cogifer. From November 25 to December 5, 2009, Southwest Jiaotong University performed turnout–bridge integrated dynamic tests on ballastless CWR turnout #2 on the bridge in the left throat of Weinan Railway Station, as shown in Figure 10.20, where the bridge is of $32.7 + 3 \times 48 + 32.7$ m continuous beam type. The calculated theoretical values and field test values are given in Table 10.2. In the test, the maximum traveling speed in the turnout is 330 km/h.

   As shown in Table 10.2, the simulated and measured values of dynamic indicators, including wheel–rail vertical force, stress on the switch rail, deflection of the bridge, and vibration acceleration, are basically the same, except the derailment coefficients at the switch front, which differ significantly (in the simulation, only the structural irregularities of the turnout are

FIGURE 10.20

Tested CWR turnout on bridge in Zhengzhou−Xi'an line.

Table 10.2 Simulated and Measured Results for CWR Turnout on Bridge in Zhengzhou−Xi'an Line

Item	Passage of an EMU Train in Main Line of a Turnout on Bridge	
	Test Results at 330 km/h	Calculated Theoretical Results at 350 km/h
Derailment coefficient at switch front	0.67	0.35
Load reduction rate at switch front	0.26	0.27
Vertical wheel−rail force at switch (kN)	83.9	108.2
Vertical wheel−rail force at guiding rail	72.5	84.9
Vertical wheel−rail force at crossing (kN)	104.3	116.9
Stress on switch rail at top width 20 mm (MPa)	115.4	139.3
Spread of actual point of switch rail (mm)	0.28	0.43
Midspan deflection of calculated beam span (mm)	1.75	1.74
Midspan vertical vibration acceleration of calculated beam span (m/s^2)	1.65	1.29
Midspan lateral vibration acceleration of calculated beam span (m/s^2)	0.77	0.43

considered, not the actual track irregularities of the turnout at the switch). This indicates that the simulation can effectively reflect the dynamic characteristics of vehicle−turnout−bridge systems under the dynamic load of high-speed trains and is reliable.

2. CWR turnout on bridge in Zhejiang−Jiangxi line [136]

Two dynamic and static integrated tests were performed successively on the dynamic performance of CWR turnout on bridge and the bridge under the loads of 200 km/h EMU trains,

FIGURE 10.21

Tested turnout on bridge in Zhejiang–Jiangxi line.

160 km/h passenger trains, and 120 km/h freight trains, aiming at assessing the riding safety and quality of the turnout on a simply supported beam bridge in the Zhejiang–Jiangxi line in operation. The test site is shown in Figure 10.21. The calculated theoretical values and measured values are listed in Table 10.3.

From Table 10.3, the calculated and measured values of derailment coefficient, wheel–rail vertical force, stress on switch rail and point rail, deflection of bridge, vibration acceleration, etc. are similar, justifying the calculation theory of the dynamics of turnout on bridge. The calculation theory is dependable and feasible for dynamic simulation and assessment of a CWR turnout on bridge, and capable of providing guidance for the structural design.

10.4 VALIDATION OF HIGH-SPEED TURNOUT CONVERSION

Numerous conversion tests have been performed indoors and on site to verify the conversion theory and design schemes of high-speed turnouts.

10.4.1 FIELD TEST IN QINGDAO–JI'NAN LINE [137]

In 2006, conversion tests were performed on Chinese No. 18 turnouts for 250 km/h in Jiaozhou North Railway Station in the Jiaozhou–Ji'nan line. The measured and calculated values are listed in Tables 10.4 and 10.5.

As can be seen from above Tables 10.4 and 10.5, the switching forces of switch rails measured on site are dispersive and highly random, which may be induced by operational conditions of the turnout. However, the distribution rules of the calculated and measured values are identical. As for point rails, the calculated and measured switching forces basically coincide. This indicates that the above-mentioned conversion calculation theory may aid the research and design of turnout conversion. Notwithstanding, considering the calculation inaccuracy caused by many influencing factors, the study should be supplemented by laboratory tests.

Table 10.3 Simulated and Measured Results of the Turnout on Bridge in Zhejiang–Jiangxi Line

Item	Passage of an EMU Train in Main Line		Passage of a Wagon in Main Line	
	Test Value	Calculated Theoretical Value	Test Value	Calculated Theoretical Value
Derailment coefficient at switch front	0.23	0.29	0.29	0.24
Load reduction rate at switch front	0.33	0.19	0.38	0.19
Vertical wheel–rail force at switch (kN)	94.5	105.2	143.1	133.5
Vertical wheel–rail force at guiding rail (kN)	83.9	90.5	103.3	112.0
Vertical wheel–rail force at crossing (kN)	105.6	139.0	175.6	171.3
Lateral wheel–rail force at switch (kN)	30.5	28.9	27.4	36.4
Lateral wheel–rail force at guiding rail (kN)	19.7	4.9	14.7	8.9
Lateral wheel–rail force at crossing (kN)	34.6	40.9	32.6	32.1
Stress on switch rail at top width 20 mm (MPa)	48.9	46.8	63.4	63.0
Stress on switch rail at top width 50 mm (MPa)	46.1	56.5	69.9	69.0
Maximum stress on point rail at top width 20 mm (MPa)	39.5	38.3	50.6	54.0
Maximum stress on point rail at top width 50 mm (MPa)	42.0	44.7	83.7	77.9
Spread of actual point of switch rail (mm)	0.482	0.556	0.678	1.088
Midspan deflection of calculated beam span (mm)	2.560	2.204	5.764	5.166
Lateral vibration amplitude of calculated beam span (mm)	0.162	0.120	0.212	0.124
Midspan vertical vibration acceleration of calculated beam span (m/s^2)	0.432	0.490	0.981	1.346
Midspan lateral vibration acceleration of calculated beam span (m/s^2)	0.245	0.327	1.286	1.436

10.4.2 LABORATORY TEST OF CONVERSION OF SWITCH RAIL OF NO. 42 TURNOUT [138]

In a test, six traction points are arranged at the switch of a No. 42 turnout, with design throws of 160, 136, 112, 88, 63, and 35 mm. Three test cases are employed: case 1—rollered and ungreased slide plate; case 2—rollerless and ungreased slide plate; and case 3—rollerless and greased slide plate. The test curve of switching resistance of the switch rail in case 1 is plotted in Figure 10.22. The test results of switching force in all cases are listed in Table 10.6.

As can be seen in Figure 10.22, the switching forces at traction points are time dependent in converting the switch rails; the maximum switching force occurs at the moment when the curved and straight switch rails move simultaneously or the switch rails are closed. As can see in Table 10.6, in the case of rollerless and ungreased slide plates, the switching resistances at traction points in the

Table 10.4 Measured and Calculated Values of Switching Force of Switch Rail

Switching Force (N)	Measured Value (Normal Position)	Measured Value (Reverse Position)	Calculated Value (Rollerless)	Calculated Value (Rollered)
Traction point 1	1020−1520	700−2100	1010.3	548.4
Traction point 2	1300−3260	1280−2240	1395.4	893.0
Traction point 3	3480−5020	3220−3520	5047.2	3253.6

Table 10.5 Measured and Calculated Values of Switching Force of Point Rail

Switching Force (N)	Measured Value (Normal Position)	Measured Value (Reverse Position)	Calculated Value (Normal Position)	Calculated Value (Reverse Position)
Traction point 1	2000−3340	1000−3060	2132.3	1576.8
Traction point 2	4840−6500	2800−4080	4859.1	3194.6

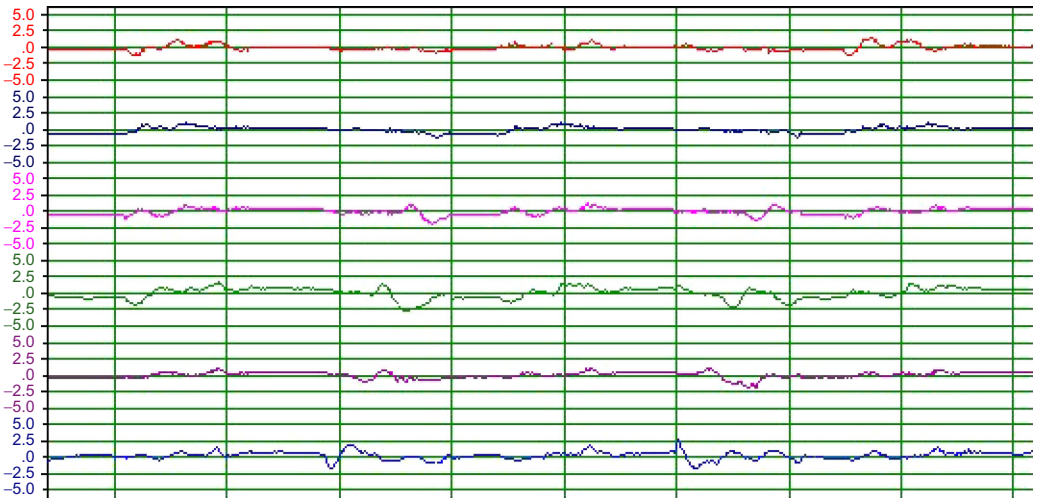

FIGURE 10.22

Test curve of switching force of switch rail of No. 42 turnout.

rear of switch rail are much greater compared with other cases; in particular, the switching forces at traction points 4 and 6 are beyond the output capacity of the switch machine. In the case of rollered slide plates, compared with case 2, the switching resistances at two traction points in the front of the switch rail are greater, but the absolute values are relatively small, and the switching resistances at the other traction points in the rear are comparatively smaller. In the case of rollerless and greased slide plates, the switching force resembles that in case 1; the switching resistances at two traction points in the front of the switch rail are greater than those in case 2, but the absolute values are small,

Table 10.6 Test Results of Switching Force of Switch Rail of No. 42 Turnout

	Case 1		Case 2		Case 3	
Switching Force (N)	**Normal Position**	**Reverse Position**	**Normal Position**	**Reverse Position**	**Normal Position**	**Reverse Position**
Traction point 1	2660	1640	1760	1640	2640	2220
Traction point 2	2000	2500	1940	1000	2300	2040
Traction point 3	2200	3800	3080	3160	1980	3560
Traction point 4	2260	5400	3640	6460	4440	4540
Traction point 5	2200	2220	3460	5040	2680	4520
Traction point 6	2540	3900	3880	7200	1780	3580

and the switching resistances at the other traction points in the rear are much smaller than those in case 2. This reflects the fact that rollers and greasing can effectively reduce the friction coefficient of the slide plate and switching force. This rule is consistent with calculation results.

10.4.3 CONVERSION TEST ON POINT RAIL WITH DOUBLE FLEXIBLE RAILS OF NO. 42 TURNOUT

A point rail with double flexible rails was first used in No. 42 turnouts in China, where the front end is assembled with long and short point rails and the heel is connected by long and large fillers. As this turnout type has much greater lateral stiffness compared with the single flexible rail structure, it is necessary to carry out tests on the switching forces at traction points, so as to provide information for theoretical calculation and conversion design.

Test cases:

Case 1: ungreased slide plate
Case 2: converting the greased slide plate five times before test
Case 3: greasing slide plate, decreasing the throws at traction points 2 and 3 by 2 and 4 mm, respectively
Case 4: greasing slide plate, decreasing the throws at traction points 2 and 3 by 4 mm and each; and
Case 5: decreasing the throw at traction point 2 by 4 mm, converting the greased slide plate repeatedly before test.

The test curves of switching force at traction points on the point rail in cases 1 and 2 are plotted in Figure 10.23, and the results of the conversion tests in all cases are listed in Table 10.7.

As can be seen Table 10.7, the maximum switching force occurs in case 1, reaching 4740 N at traction point 3 when converting from normal to reverse position.

In case 2, when converting from normal to reverse position, the switching forces decrease to 660, 780, and 820 N, respectively, after greasing; when converting in reverse, the switching force at traction point 1 increases by 1020 N after greasing, while the switching forces at other traction points remain roughly the same. This indicates that the switching force can be effectively mitigated by reducing the friction coefficient of the slide bedplate.

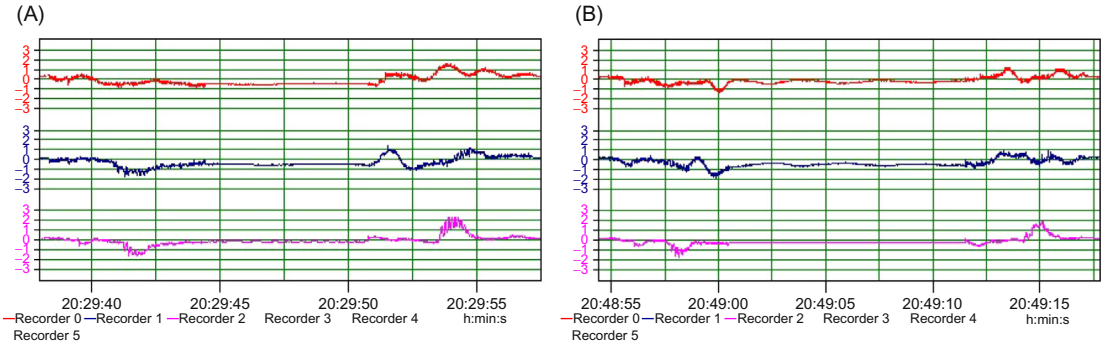

FIGURE 10.23

(A) Switching force in case 1. (B) Switching force in case 2.

Table 10.7 Test Results of Switching Force at Traction Points on Point Rail with Double Flexible Rails

Case	Switching Force (N)	Normal Position	Reverse Position
1	Traction point 1	3280	1720
	Traction point 2	2820	3380
	Traction point 3	4740	3180
2	Traction point 1	2620	2740
	Traction point 2	2040	3580
	Traction point 3	3920	3360
3	Traction point 1	2140	3040
	Traction point 2	1860	3260
	Traction point 3	3580	3600
4	Traction point 1	2500	2700
	Traction point 2	2200	2700
	Traction point 3	3320	3360
5	Traction point 1	2000	1960
	Traction point 2	2120	1940
	Traction point 3	3620	3340

In case 3, as compared with case 2, the switching forces drop by 480, 180, and 340 N, respectively, when converting from normal to reverse position, whereas the switching forces at traction points 1 and 3 increase by 300 and 240 N, respectively, and the switching force at traction point 2 drops by 320 N when converting in reverse.

In case 4, as compared with case 2, the switching forces at traction points 1 and 3 drop by 120 and 600 N, respectively, and the switching force at traction point 2 increases by 160 N when converting from normal to reverse position, whereas the switching forces at traction points 1 and 3 drop by 40 and 880 N, respectively, when converting in reverse.

In case 5, as compared with case 2, the switching forces at traction points 1 and 3 drop by 620 and 300 N, respectively, and the switching force at traction point 2 increases by 80 N when converting from normal to reverse position, whereas the switching forces drop by 780, 1640, and 20 N, respectively, when converting in reverse.

The above results indicate that the switching force of a point rail with double flexible rails can be reduced by optimizing throws of traction points, consistent with the calculation theory. Meanwhile, the switching force of the point rail will decrease with the adaptation of rail base and slide plate after repeated conversion tests. The test can help in obtaining the basic rule and numerical distribution of switching force and provide information for optimizing conversion design of point rails.

CHAPTER

11 MANUFACTURING TECHNOLOGIES OF HIGH-SPEED TURNOUTS

High technical performance of high-speed turnouts depends on manufacturing [139]. The processes of forging, heat treatment, finishing, etc. of slim bars in high-speed turnouts may sometimes reflect the state of the art of the manufacturing industry of a nation. For the construction of high-speed railways in China, about 8000 high-speed turnouts for 250 km/h and above are planned to be manufactured to meet the demanding requirements of short production periods, large quantities, and good quality. Based on experience with speed-up turnouts, and with the advanced manufacturing principles of other nations, the technology of step-by-step assembly and system integration has been developed in China, after settling several critical process difficulties. By the end of 2014, about 5000 sets of high-speed turnouts had been developed and produced solely by China with independent technology, which function normally, ensuring riding safety and quality.

11.1 MANUFACTURING EQUIPMENT AND PROCESSES

11.1.1 PROVIDERS OF HIGH-SPEED TURNOUTS IN CHINA

There are four high-speed turnout providers with annual capacity above 500 turnouts:

China Railway Shanhaiguan Bridge Group Co., Ltd (CRSBG), founded in 1894, is the first manufacturer of steel bridges and turnouts in China

China Railway Baoji Bridge Group Co., Ltd (CRBBG), founded in 1966, is a specialized manufacturer of steel bridges and turnouts in western China

China Railway Construction Heavy Industry Co., Ltd (CRCHI), founded in 2007, is a specialized manufacturer of turnouts and shields; and

Chinese New Turnout Technologies Co., Ltd (CNTT), is a joint venture co-established by CRSBG, BWG of Germany, and VAI of Austria in 2007, specializing in manufacturing high-speed turnouts developed by BWG.

11.1.2 MAJOR PROCESS EQUIPMENT

Large equipment with internationally leading technologies must be employed, as listed below, for high precision and smoothness in high-speed turnouts.

Design of High-Speed Railway Turnouts.

FIGURE 11.1

CNC planer-type milling machine.

FIGURE 11.2

CNC saw drill.

FIGURE 11.3

Welder for rails of dissimilar materials.

FIGURE 11.4

60 Mt press.

A CNC planer-type milling machine allows the operation of more than one cutter at the same time, while ensuring high precision and efficiency. This machine is applicable to the processing of planes and bevels of large parts in batch and mass production. CRCHI has introduced a 70-m-long CNC planer-type milling machine (Figure 11.1) for machining of large and long switch rails for high-speed turnouts, which have been confirmed to have satisfactory performance in machining efficiency and accuracy.

CRCHI and CRBBG have bought CNC saw drills with high precision, as shown in Figure 11.2. With this equipment, the precision of rail blanking and drilling can be increased by 0.1 mm. The welders for rails of dissimilar materials in CRBBG, shown in Figure 11.3, can bond high manganese steel and U75V (or other material) together at a shop. The 60 Mt frame-type oil presses (Figure 11.4)

are quite common in various manufacturers for forging the heels of switch rails and point rails. X-ray turnout detectors were also introduced by CRCHI and CRBBG to detect defects in large forged or heat-treated rails.

11.1.3 MANUFACTURING PROCESSES

Turnout providers play the principal roles in system integration, after-sales service, and product quality of high-speed turnouts. As a rule, they provide rails, tie plates, and other important rail members, as well as assembly, integration, transport, and handling. Parts, such as conversion equipment, turnout ties, and fastenings, are produced by other specialized manufacturers, which will be included in the purchase list of turnout ties.

Production processes: procurement of raw materials for rails and purchased parts, processing of rails and tie plates, assembly of finished parts, inspection and acceptance, packaging and warehousing, hoisting, transportation, and handling. In China, a mill supervision system is established to ensure satisfactory production quality, where the duly certified supervisor will be dispatched to monitor quality during the whole process of production.

11.2 KEY PROCESSES FOR RAILS

11.2.1 PROCESS FLOW AND MAIN CONTROL POINTS

1. Stock rail

   Key control parameters: straightness of aligned rail tops ($\leq$0.2 mm/m), straightness of a closed surface in the main direction (0.3 mm/m), smoothness of a closed surface in the diverging line without hard bending, and accuracy of spacing and height of holes. The specific flow: marking off → saw cutting → marking holes → holing → bending → milling the hidden tip point segment → fine tuning → full-length grinding and derusting of rail base, web, and top → assembly.
2. Switch rail

   Key control parameters: process quality of heels and dimensions, straightness, smoothness, and depressed amount of cross sections. Specific flow: marking off → saw cutting → press molding → aligning → laying out (redistribution of allowance) → milling a molded section rail base → grinding and detecting → marking off → saw cutting → marking holes → holing → aligning → milling a working surface of a rail base and rounding an R5 arc → milling a nonworking surface of a rail base and rounding an R5 arc → milling a flexible section → milling a working and a nonworking surface of a rail head → milling bolt grooves of the rail web → milling a rail top and derating → chamfering a 1:40 cant over the full length of the rail top → planing the surplus of the rail base and rail head → planing the molded rail head → detecting → quenching → fine tuning → full-length grinding and derusting of rail base, web, and top → assembly.

   The cap profile of a switch rail and point rail will be machined by 1 mm, and the machined external surface of rail base will be rounded with an R5 arc to eliminate soft structures

introduced by press forming of the heel and saddle-type wear. These measures can ease the sliding of switch rails and point rails, thus eliminating stress concentration.

3. Long point rail

   Key control parameters: process quality of heels, eccentricity and machining straightness, planeness and height difference of rail base. Specific flow: marking off → saw cutting → press molding → marking off → saw cutting → laying out and milling a molded section rail base → grinding and detecting → marking holes → holing → milling the longer side of a rail base and rounding an R5 arc → milling the shorter side of a rail base and rounding an R5 arc → milling a flexible section → milling the front rail base → milling and rounding the front rail base → - milling a working and a nonworking surface of the rail head → milling the rail top and derating → milling a 1:40 cant in the full length of the rail top → quenching → fine tuning → full-length grinding and derusting of rail base, web, and top → assembling with short point rail.

4. Short point rail

   Key control parameters: eccentricity and machining straightness, planeness and height difference of rail base. Specific flow: marking off → saw cutting → marking holes → holing → milling the longer side of a rail base and rounding an R5 arc → milling the shorter side of a rail base and rounding an R5 arc → milling the rail base in closure zone → milling a working and a nonworking surface of the rail head → milling the rail top and derating → milling a 1:40 cant in the full length of the rail top → milling rear rail top → bending → vertically cutting a nonworking surface of the rail base → planing an R25 arc → planing an R5 arc for the rail base → planing a working and a nonworking surface of the rail head → milling the rear closure zone → fine tuning → full-length grinding and derusting of rail base, web, and top → assembling.

5. Wing rail

   Key control parameters: machining accuracy of closure zone and torsional zone, eccentricity and machining straightness of rail base, top planeness and bending offset. Specific flow: marking off → saw cutting → aligning → marking holes → holing → milling a working surface of a rail base and rounding an R5 arc → milling a working surface of the rear rail head → twisting a 1:40 cant in the front → bending the front top → milling a 1:40 cant and profile of rail top on the front working surface → bending the rear top → milling a 1:8 cant in the hidden tip point segment and planing and grinding an R10 arc → fine tuning → full-length grinding and derusting of rail base, web, and top.

11.2.2 FORGING OF HEEL OF 60D40 RAIL AND QUALITY CONTROL [140,141]

1. Heel structure

   As depicted schematically in Figure 11.5, forging the heel of a 60D40 rail refers to converting a section of heel of a 60D40 rail to a 60 kg/m section by molding. After molding, the heel will fall into two zones: forged zone and transition zone. In the forged zone, the rail end is molded into different sectional forms. The transition zone, as the name implies, enables the transition between base material and the forged zone. The term “heel” is the general term for the rail ends to be hot forged, connecting with standard section rails.

2. Technical requirements

   In the forged zone, the test piece for macroscopic acid etching must be free of flakes, residual holes, cracks, folds, dissimilar metal inclusions, skull patches, laminations, macroscopic

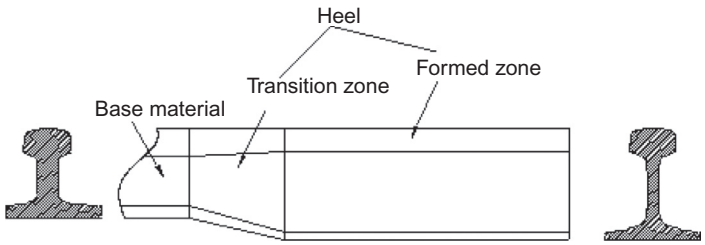

FIGURE 11.5

A 60D40 forged zone.

Table 11.1 Permissible Dimensional Errors for Forged and Transition Zones of Heel of Switch Rail (mm)

Location	Rail Height	Width of Rail Head	Width of Rail Base	Thickness of Rail Base	Height of Rail Head	Thickness of Rail Web	Symmetry of End Face at Rail Head	Symmetry of End Face at Rail Base	Verticality of End Face	Height of Fitting Surfaces of Clamping Plate
Allowance	±0.5	±0.5	+0.8 −1.0	±0.5	±0.5	+1.0 −0.5	0.5	1.0	1.0	±0.5

inclusions, and other harmful defects. Moreover, the metallurgical structure should be of pearlite with a few ferrolites and no martensite, bainite, or grain boundary cementite. In the forged zone and heat-affected zone, the decarburization depth at any part of the rail head should not be greater than 0.5 mm, and the mechanical performance should be equal or superior to the base material.

Table 11.1 lists permissible dimensional errors for the forged and transition zones of the heel of a switch rail and point rail. For a torsional angle of 1:40 at the heel end (toe end), the allowable deviation is 1:320. The forged zone of AT rail must not be processed at a temperature greater than 1160°C or heated repeatedly, or overburnt. No cracks, folds, lateral scratches, or vertical scratches greater than 0.5 mm are allowed on the surface of forged rail.

3. Structural variation and main defects of rails during forging

Forging is a major hot-forming process for metals, which, relying on the plasticity of metals, enables the metals to be deformed under force and generates desired parts or blooms with approximate size of parts through the transition and redistribution of the volume of metals. Moreover, forging produces desired shapes and dimensions, and improves the interior structure of metals significantly, thus improving the service performance. For this, parts or components exposed to greater or complex loads are all produced by this method.

Three bloom defects may occur in case of improper heating: first, defects induced by variation in the chemical state of the outer structure due to the impact of a medium (media); second, defects induced by abnormal variation in interior structure; and third, cracks induced by excessive stress due to inhomogeneous distribution of temperature in the bloom.

Decarburization relates to the reduction of carbon content in the steel surface during heating. During this process, the carbon in the steel reacts with hydrogen or oxygen under high temperature, producing methane or carbon monoxide. Decarburized layers may occur only when the rate of decarburization exceeds that of oxidation. Otherwise, decarburization will be insignificant, and the carbon and cementite content will be lower than that in the normal structure. Decarburization is affected mainly by the chemical composition of steel, heating temperature, holding time, and composition of furnace gas. The metallurgical structure of the rail will change greatly after decarburization. The decarbonized position may look like bright white spots under a microscope. Decarburization reduces rail strength greatly and impairs the mechanical properties of the rail. After decarburization of the rail, the surface plasticity decreases drastically, but the fragility increases, leading to minor cracks on the rail surface, or even cracking during molding. Decarburization will cause a difference in the structure and linear expansion coefficient of outer and inner layers; thus, the difference in structural transition and volume variation occurring subsequently during quenching may produce greater interior stress in the forging. Excessively low carbon content on the surface of decarburized rail will cause inadequate conversion of the structure into fine lamellar pearlite, seriously impairing the surface hardness of the rail. Additionally, rail strength may drop below the specified standard during use, accompanied by severe deterioration in surface abrasion resistance, which cuts down on the service life of the rail to a great degree.

When a rail is heated to a certain temperature, the grains will experience a change in lattice type and be recrystallized. This recrystallization will generally end with fine equiaxed grains. With the rise of temperature and prolonging of holding time, those fine grains may develop through merging with each other, wherein some diminish or even disappear, and others will develop further. The grains develop spontaneously under certain conditions. The development process is driven by the inhomogeneity of grain sizes and the interfacial energy difference before and after development. As smaller ones are absorbed, greater ones develop; this is the process of grain development. The development of rail grains is mainly affected by temperature. Higher temperature can accelerate the rate of development. In general, the grains can develop to a certain scale under certain temperatures; however, this process can proceed only upon temperature rise or prolonging of holding time. In forging the heel of the rail, when the rail is heated to the maximum temperature of 1150−1200°C, which is far above the required temperature for phase transformation of the rail, coarse grains will exist inside the rail, degrading the strength, plasticity, and ductility of the rail. In particular, where coarse grains with inhomogeneous sizes occur, rail performance will be seriously affected, leading to cracks at positions with coarse grains.

4. Control technologies for decarburized layer [142]

Decarburization occurs with the forging of the rail. The harmful effects of decarburization on the performance of switch rails may be mitigated by minimizing the decarburized depth of the rail during forging. This approach can be realized by the selection of forging temperature and heating modes, and control of forging time.

a. Selection of forging temperature

Normally, as the heating temperature rises, plasticity increases, deformation resistance decreases, and forgeability is improved. However, overheating may lead to overburning. In this regard, the blooms should be heated within a certain temperature range. The interval between the initial and final forging temperatures is defined as the range of forging temperature. Initial forging temperature is defined as the allowable maximum heating temperature of a metal for forging. The scope of forging temperature is specified as follows: A wider range is preferred to save consumption and improve productivity provided that good forgeability of the blooms can be ensured.

AT rails are made of high-carbon steel at about 1050°C. The initial forging temperature may be a bit higher, but below the overburning temperature. Overburning temperature refers to temperatures above the specified process temperature. Holding at the temperature for a long time, overheated steel will become needle-like pure ferrite. The initial forging temperature is determined as 1150−1200°C through repeated tests. For the process scheme of one-pass heating and multiple-pass forming, the forging temperature for rail blooms may drop to some extent as per the results of actual tests. If the final forging temperature is excessively high, coarse network carbide may be formed on the forged rail bloom after cooling, which may make the heated part of rail bloom brittle and thus affect rail quality. Therefore, final forging temperature is defined as 800−850°C.

b. Heating equipment and process

In heating the rails, different compositions of fuel gas may lead to different products of combustion, and different furnace atmospheres. Both coke and natural gas may generate furnace gas that induces decarburization of the rail after combustion. With the substitution of medium-frequency electric induction heating, the heating rate increases and the furnace atmosphere is ameliorated.

The principle of this heating mode lies in the concept that by providing an inductor with MF alternating current, an alternating magnetic field is formed inside and outside the coil, making the rail produce an induction current with the same frequency as, but opposite to, the current in the inducer. The circuit formed by the current is known as a "vortex," which converts the current into heat energy for heating the rail.

In China, an induction heater with a circular cross section (Figure 11.6) is used in producing high-speed turnouts, which ensures the homogenous and reasonable distribution of the full-section temperature field of the rail. After testing the temperatures of rail sections in various angles (Figure 11.7A) in the inducer, the heating angle represented by F is selected. In addition, the longer side of the rail base is placed upward and twisted by 30−60°; this measure enables the initial forging temperature, prevents overburning, and ensures a temperature difference less than 50°C between the rail core and surface and homogenous heat transfer.

Heating recipes (Table 11.2), such as rate of heating with furnace and holding time, are determined by testing the temperature difference between the rail core and surface.

c. Timing of forging

In forging the blooms, as the temperature drops with the loss of heat, plasticity becomes weaker and deformation resistance becomes greater. Deformation may cease when the temperature drops to some extent. In this case, as cracks may easily occur, forging should be

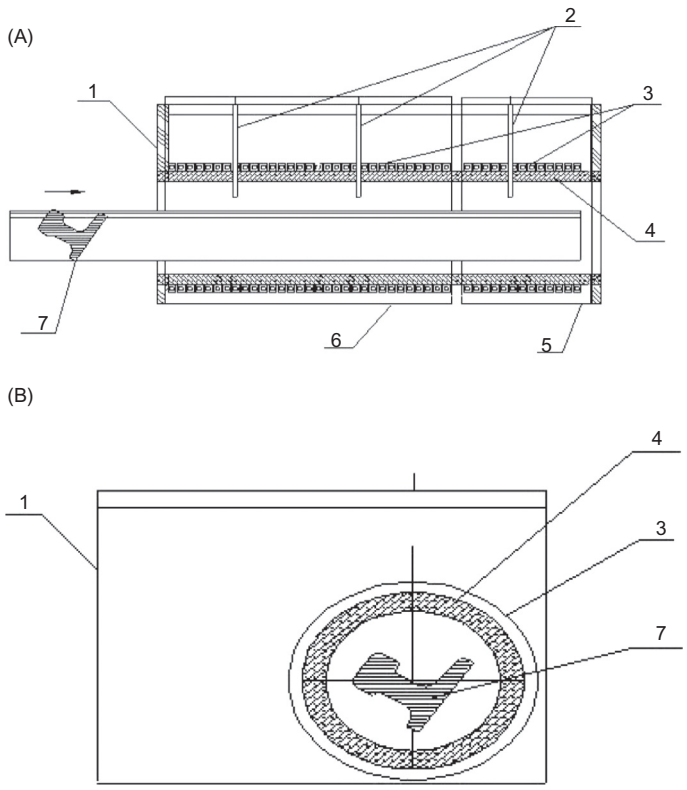

FIGURE 11.6

Cross section of induction furnace with circular cross section: (A) Cross section; (B) Vertical section. (1: Furnace stack; 2: IR temperature detector; 3: Induction heating coil; 4: Hearth; 5: Hearth front; 6: Hearth rear; 7: Heel of rail.)

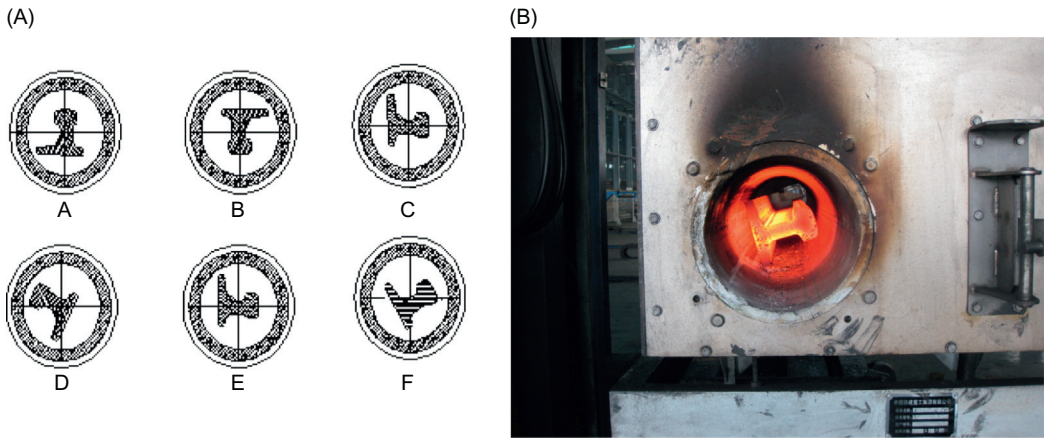

FIGURE 11.7

(A) Different heating angles. (B) Actual heating angle.

Table 11.2 Parameters of Induction Heating

Heating	Electric Power (%)	Heating Temperature (°C)	Duration
Rapid temperature rise	100	~900	Heating with furnace
Temperature control	40–60	900–1100	60–100 s
Holding	30–50	1160–1250	40–90 s

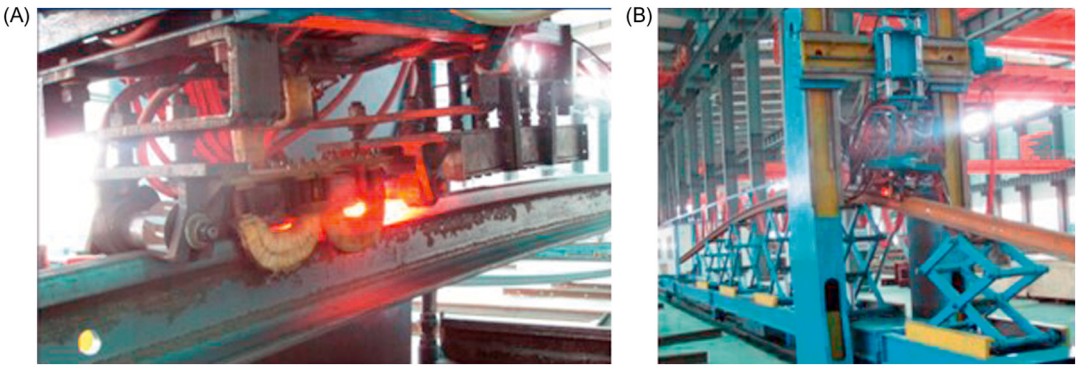

FIGURE 11.8

MF induction heat treatment of rails.

suspended temporarily, and reheating is required. Calculations show that, at room temperature, it takes only 3 min to cool down the initial temperature of 1160°C to 850°C. For a shorter auxiliary forging time, high-speed turnout manufacturers in China have introduced the French automatic transfer systems and German mold systems. The automatic feeder can enable the functions of lateral and longitudinal positioning, clamping, and 360° tilting of the rail under preset parameters. The integrated mold system combines the functions of automatic heating, preforming, reshaping, final forging, and trimming of mold cavity. With these facilities, the heel of 60D40 rail can be forged by one-pass heating and three-pass forging.

11.2.3 HEAT TREATMENT AND QUALITY CONTROL [143]

1. Improvement of slack quenching process for heat treatment of switch rail

   When the switch rail is heated by induction to complete austenitizing, the rail is heated continuously with soft coolant to obtain fine pearlites; this process is called the slack quenching process. In China, the processes of MF induction heating and quenching by cooling with compressed air and water spray employed in producing high-speed turnouts require continuous cooling mode, where the pearlite transition occurs from 700°C to 550°C, and the cooling rate is 2–5°C/s; moreover, fine pearlites can be obtained after heat treatment, and the hardness of the rail can reach 320–390HBW, as shown in Figure 11.8.

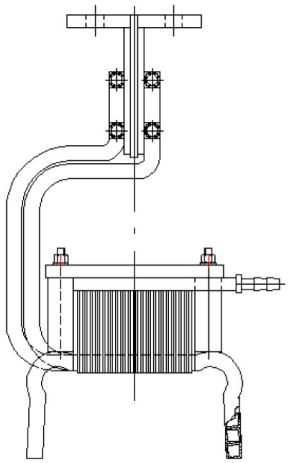

FIGURE 11.9

Modification of inducer.

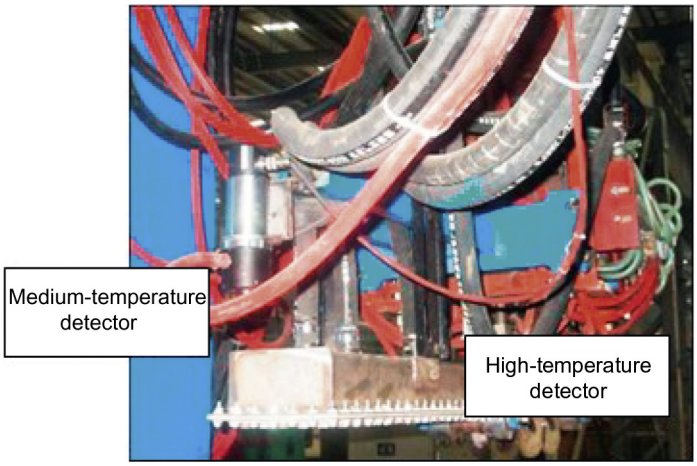

FIGURE 11.10

Online temperature detection.

The heat-treatment inducer is made of copper pipes, approximating the Π-shape of the rail. The coupling gaps between the inducer and rail head should be uniform, about 6−8 mm, so as to achieve the desired hardness and quenched depth of the rail section. However, affected by the "corner" effect of induction heat treatment, rail corners, where induction lines are concentrated, have greater current density; therefore, the heating temperature for rail corners will be higher than that for tread by about 100°C, and the hardness of two corners should also exceed tread hardness significantly. In view of this, China has modified the process by extending the transition arc of the inducer, decreasing the density of induction lines at the corners and reducing the vortex density (see Figure 11.9). After this modification, the temperature difference between the treat and corner drops from 100°C to 30−50°C, the temperature difference between heated layers of the rail is mitigated, the defects of overheating or overburning at the corners are prevented, and the homogeneous distribution of hardness in the rail head section is ensured.

Chinese high-speed turnout manufacturers employ online temperature detectors to monitor the heat treatment of rails, so as to achieve stable quality of heat treatment of rails. A high-temperature optical fiber temperature detector (Raytek of the United States) comes after the inducer, and a Raytek medium−temperature IR temperature detector is installed after the air-jet cooler, as shown in Figure 11.10. If the reading of the quenching temperature is too high, the cooling temperature will be too high; in this circumstance, the power shall be reduced and the air pressure increased. Otherwise, the power will be increased and the air pressure decreased. In addition, the quality of heat treatment of the rail is ensured by optimizing the structures of the air jet, the clamping device for introducing the rails, and guiding devices, as well as using of digital operating platforms.

2. Homogenization of surface hardness at heel of switch rail [144]

The AT switch rail and point rail are forged into standard rail through the processes of heating, hot molding, normalizing treatment, etc. In this process, the rails will experience a change

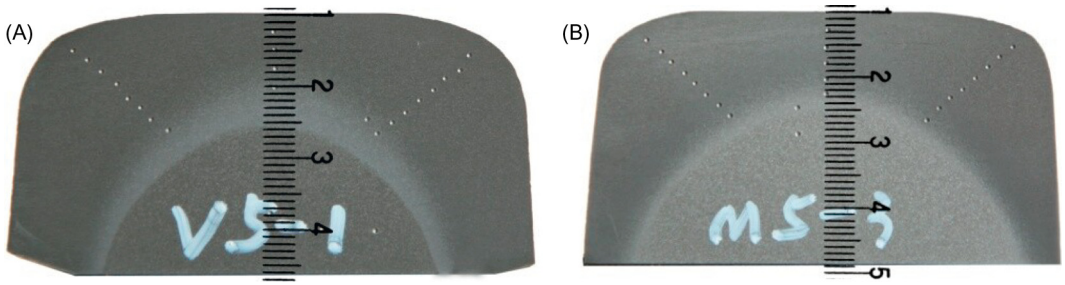

FIGURE 11.11

Profile of the heated layer at the heel of switch rail: (A) Forged zone; (B) Transition zone.

Table 11.3 Depth of Heated Layer of the Cross Section of Forged Zone at Heel of Switch Rail (mm)

	60D40-U75V	60D40-U75V	60D40-U71Mn	60D40-U71Mn
Test Site	**Forged Zone**	**Transition Zone**	**Forged Zone**	**Transition Zone**
a	11.5	9.0	13.0	12.0
b	15.0	9.5	15.0	12.0
c	13.0	8.5	12.0	11.0

in interior metallographic structure and mechanical performance, and become different from the unprocessed base material. According to the results of surface hardness tests on normalized and forged rail zones, the surface Brinell hardness (HB) is in discrete distribution. The HB value can be up to 72HBW, within 1 m range of the forged zone of the heel, increasing the risk of "saddle" wear at the heel of the switch rail. To improve the wear resistance of the top of the switch rail, the top of machined switch rail must be quenched in its full length; however, as compared with the base material, a great hardness difference occurs. To solve this problem, high-speed turnout manufacturers in China find another way: They process the cap profile of the rail head before heat treatment, cool the rail by continuous and slow air jetting or natural cooling, and provide MF induction heat treatment on the 1 m range of the forged zone of the heel of 60D40 rail. The forged zone of the heel of switch rail and the heated layer of the cross section of the transition zone are all cap shaped, as shown in Figure 11.11.

The test depths of forged zones and transition zones of the heel of U75V and U71Mn 60D40 switch rails are listed in Table 11.3. The depth of the heated layer and requirements for section hardness tests are given in Figure 11.12. As per the test results, the hardnesses at various points of the rail head section are all above 26.0HRC.

Before testing, the 1 m forged zone and heat-affected zone at the heel of 60D40 switch rail are taken as test pieces, and the rail tops are ground by about 1 mm to remove the oxide skin and decarburized layer. The test pieces, with the test points distributed as shown in Figure 11.13, are tested with an electronic HB tester (desktop) in the laboratory. Altogether, 24 points are tested, including 12 in the forged zone and 12 in the heat-affected zone. The statistics

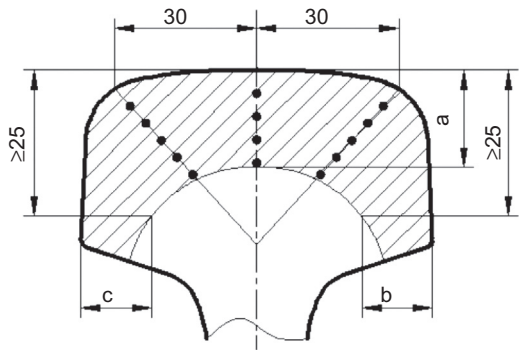

FIGURE 11.12

Depth of heated layer and HRC hardness test on the rail section.

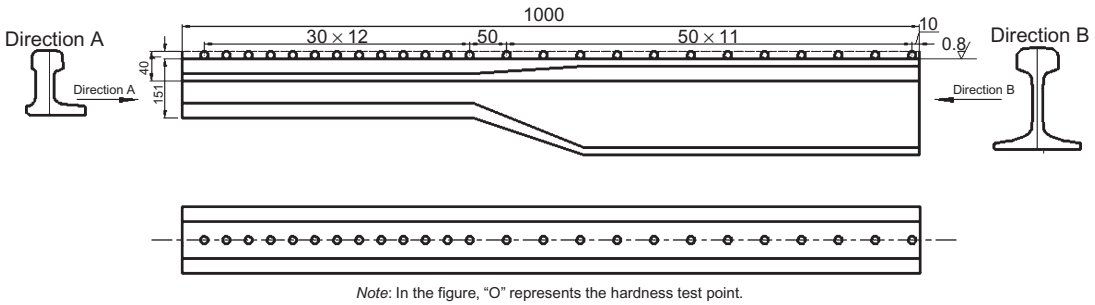

Note: In the figure, "O" represents the hardness test point.

FIGURE 11.13

Surface hardness test at heel of switch rail and point rail.

Table 11.4 Statistical Analysis of the Surface Hardness of Heel of 60D40 Rail (HBW)

Rail Type-Material	Sample Size	Max	Min	Average	Standard Deviation
60D40-U71Mn	24	295	288	292	1.5
60D40-U75V	24	329	311	320	4.8

of the HBW values of the heel of 60D40 switch rail are listed in Table 11.4. For 60D40-U71Mn forged and heat-affected zones, the difference between maximum and minimum hardness is 7HBW; for 60D40-U75V zones, this difference is 18HBW. The result implies that the hardness homogeneity of the heel of switch rail is greatly improved.

3. Flexural deformation of heat treatment of switch rail [145,146]

In the course of induction heating at the head of a switch rail, a temperature gradient exists when the temperature drops gradually from the surface to the inside, and the greater temperature gradient, the greater the deformation after quenching. During quenching, a powerful coolant

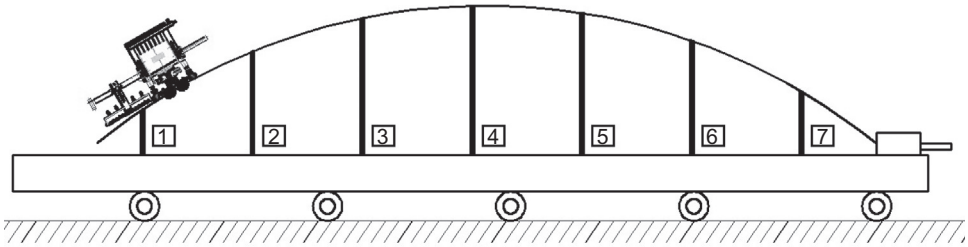

FIGURE 11.14

Schematic diagram of reverse pre-bending deformation of switch rail.

will cause a greater temperature difference between the exterior and interior and between different positions (with different section sizes) of the test pieces, and greater internal stress and heat-treatment deformation. The rail head shrinks after cooling, leading to upsweep of the rail. As for the stress condition, the rail head is under compressive stress and the rail base is under tensile stress. Finally, switch rail deformation is represented as shrinkage of the rail head, which shortens the rail and leads to upsweep at two ends visually.

In addition, the head of the switch rail is of various sections, the volume of heated layer differing among different sections. As the rolled coarse pearlites will be transformed into fine ones after air-jet cooling, the stress also differs among different volumes. For U75V rail, after heat treatment, the spacing of the resulting fine flake pearlites is about 0.07 μm, and that of the rolled coarse flake pearlites is about 0.16 μm [19], with a ratio of $0.07/0.16 = 0.44$. It can be seen that the rail head may shrink significantly after cooling, somewhat like the vertical positive bending deformation, exerting tensile stress on the rail base.

Switch rails are long and large in size, with a complex profile and uneven thickness. In hot-treating the head of the switch rail, great heat stress may occur due to the varying degrees of thermal expansion at various parts, leading to inhomogeneous plastic deformation of the work piece and distortion. The greater the length, the greater the shrinkage of the rail head and bending.

The actual shrinkage generated during production may affect the accuracy of the switch rail. The deformation of vertical warp impairs the smoothness of the rail. The residual tensile stress at the hot-treated rail base determines the service life of a switch rail.

In China, two technologies are generally used to control heat-treatment deformation of rails for high-speed turnouts. First, the deformation [22] is controlled by preheating the rail base and heating the rail head, minimizing the temperature difference between rail head and base, and reducing the upsweep scape during heating. Second, it is controlled by providing reverse deformation for switch rails through pre-bending with the use of clamping devices for introducing the rails for quenching.

Appropriate pre-bending reverse deformation may be defined by tests, which can be applied to the control of deformation of quenched switch rail. Figure 11.14 presents seven hydraulic shear supports used in quenching a 21,450-mm-long 60D40 switch rail, where the relevant shrinkage is 0.23 mm/m, and the length of curved line in the end is about 158 mm. Pre-bending reverse deformation can not only control rail warps effectively; it can also improve the efficiency of further alignment, contributing to the smoothness of rails. Meanwhile, as detected in the tests, the residual tensile stress at the base of the rails produced with this technology is well

Table 11.5 Residual Stress at the Base of Switch Rail

Material	Status of Heat Treatment	3 m in the Rear of the Point		50 mm Section		3 m in the Front of the Heel	
		Strain Difference (με)	Residual Stress (MPa)	Strain Difference (με)	Residual Stress (MPa)	Strain Difference (με)	Residual Stress (MPa)
U75V	Before	−465	96.3	−567	117.4	−898	185.9
	After	−523	108.3	−622	128.8	−536	111.0
	R_{after}/R_{before}	0.89		0.91		1.67	
U71Mn(k)	Before	−367	76.0	−386	80.0	−795	164.6
	After	−359	74.3	−312	64.6	−656	135.8
	R_{after}/R_{before}	1.02		1.24		1.21	

Note: R_{after} = *after treatment;* R_{before} = *before treatment.*

below 250 MPa, as shown in Table 11.5. In the test, the quenching shrinkage of the switch rail has been registered to provide reliable information for accurate baiting.

11.2.4 CONTROL OF LINE TYPE IN MILLING THE SWITCH RAIL [147,148]

China has adopted CNC planer-type milling machines for milling the switch rail. In the milling process, the rails are located by clamping using an electromagnetic chuck, and milled with indexable profile cutters.

1. Process of full-length machining

   Full-length machining of the top of a switch rail is employed for smooth connection of the profiles of the heads of the heels of switch rail and guiding rails and elimination of tool marks on the top surface of forged parts or any sudden change of light stripes on the rail top caused by unstable profile quality of the base material. The process is characterized by optimizing the profile of cutting tools for the rail top to make the processed profile approximate the design profile (deviation $\leq$0.05 mm); designing the cutters for special cap profiles of the working surface of 60D40 rail for profile modification of the rail top of the raw material; detecting the profile modification with special templates (Figure 11.15); and designing the special locating and clamping devices for the heels that have been provided with torsional inclination of 1:40.
2. Torsional angle and rail height difference

   Proper twisting is an important prerequisite to full-length milling of the top of the switch rail. Height differences among the rails determine the rail height after milling the heel of switch rail over the full length. Torsional inclination difference affects the symmetry of the milled profile of the rail head at the heel of switch rail, and thus impacts the smoothness of connections with guiding rails.

   The torsional angle can be measured with a high-precision goniometer (accuracy = 0.01°). The desired deviation of ±0.18° can be obtained by adjusting the torsion based on measurement results. In verifying the height difference, the rails will be placed on a special platform, where

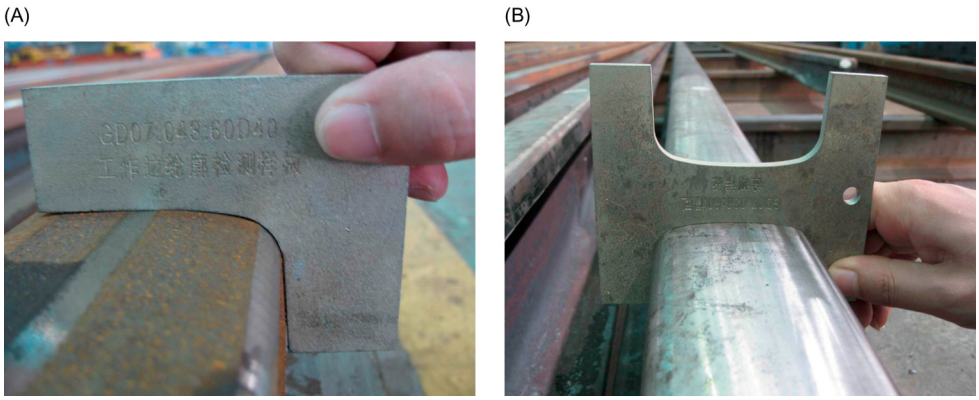

FIGURE 11.15

(A) Test template for profile modification of base material. (B) Test template for milling of cap profile of heel.

two special pads with a height difference of 34 mm are placed beneath the rail base of the base material and the forged rail base, respectively; the clearance measured between the rail base and pad should not exceed 0.5 mm.

3. Abrupt change of break point for the exit point of cutting tool

Generally, the cutter can exit naturally along the track of the line type of working surface in the process of milling. However, a break point may be formed at the exit point of the cutter due to the angle (Figure 11.16) between the processed and initial working surfaces. The break point is most remarkable in small number turnouts. This point cannot be removed by straightening, but becomes a small "bulge" (as shown in Figure 11.17) that may cause a sudden change in straightness and affect riding quality.

According to the process optimization scheme in Figure 11.18, the maximum heights of bended arcs are obtained by modeling with such parameters as bending degree, bending offset, rail type, and bending width for reference in CNC machining. The break point of milling can be eliminated by interpolating a reverse arc in the affected area of the bending arc. This process saves the planing process, simplifying work flow and shortening the process period [149].

11.3 KEY PROCESSES FOR HIGH-SPEED TURNOUT PLATES

The plates for high-speed turnouts must be very flat: The flatnesses of slide plate and other plates should be 0.2 and 0.5 mm, respectively, for smooth conversion of the switch rail and high geometric regularity of the track. The critical processes are described below.

1. Slide plate

Attention must be paid to the following key parameters in processing the slide plates:

Installation dimensions of elastic clips: The rear of slide bed is rather complex in structure, where the dimensions of all parts are closely related; therefore, the tolerance of dimensions shall

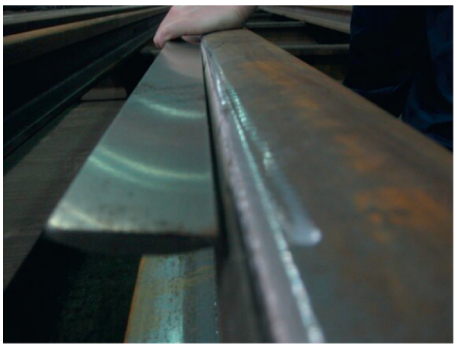

FIGURE 11.16

Measurement of straightness at the exit point of cutter.

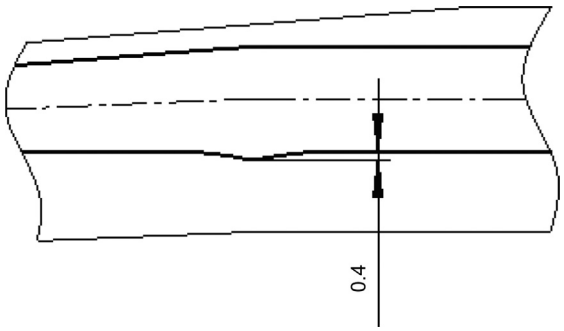

FIGURE 11.17

A "bulge" at the exit point after straightening.

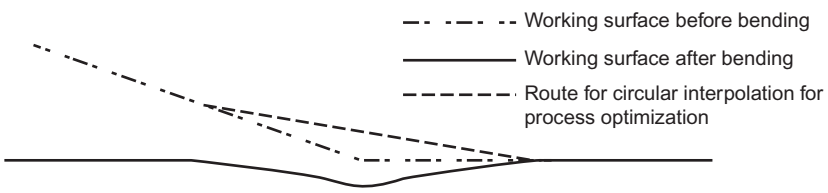

FIGURE 11.18

Optimized process for the break point of milling.

be strictly controlled. The height of the convex retaining block inside the slide bed will exert a direct impact on the clamping force of the elastic clip. In addition, improper height deviation of the slide bedplate may affect the post-welding allowance.

Surface quality of slide bedplate: Following inspection of the deviation of machining depth of the slide bedplate, a nickel-base alloy self-lubricating composite coating (MoS_2-bearing) will be applied to the slide bedplate by laser cladding, so as to solve the problems of inadequate depth of anti wear coating and insufficient binding force.

Machining accuracy of the base slab: The whole surface of the base slab will be machined. In machining the bolt holes, the deviation of pitch and aperture may be restricted through accurate laying out and CNC milling. Further, the precise location of bolt holes can benefit the accurate location of iron chair and slide bedplate in welding the plates. In addition, visual appearance can be effectively controlled by easing the surface roughness, hole edges, and all sharp corners through grinding.

Welding of plates: Special processing equipment will be designed to enable the proper welding dimensions of pads, mitigating the thermal deformation after welding. The location of slide plate and iron chairs may be controlled with integrally welded templates, which can reduce location deviation and control the scale of welding deformation. A weld jig is depicted in Figure 11.19.

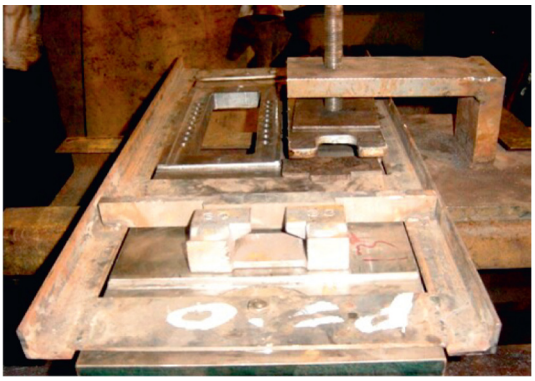

FIGURE 11.19
Weld jig for slide plate.

FIGURE 11.20
Dye penetration detection on the welds.

Quality control of welds: The process of welding the plates is verified with destructive tests, followed by dye penetration detection (Figure 11.20) on the welds.

2. Offset plate

   In drilling the holes on offset plates and crossing plates, the combined method of accurate laying out and CNC milling will be used. A template for the welded plate will be made. The template is provided with dual positioning (a master pin and a slave pin), where the master pin is for the positioning of longitudinal dimensions, the slave pin for rotational angle. During processing, dimensional and geometric tolerances shall be strictly controlled.

3. Check rail plate

   The bedplate and back plate of the check rail are complex in structure, produced by precise casting and subsequent machining, and welded with a ship position welding jig. The welding jig is provided to control welding precision.

4. Alignment and fixing of plate

   The plate quality can be effectively ensured by strictly controlling welding deformation and post-welding modification. Considering the impacts of finishing allowance, feed rate, thermal deformation during machining, and welding current on the flatness and parallelism of the plate, tests have been performed on the optimum control accuracy of cooling and control accuracy of heating for super-long plates. Through the tests, the process scheme of "machining by steps, controlling of alignment, and ensuring finishing" is established to enable desired plate quality.

11.4 ASSEMBLY AND ACCEPTANCE

11.4.1 ASSEMBLY PROCESS OF CRITICAL TURNOUT PARTS

Assembly is a critical step of trial production of turnouts, and also an important link for testing the design and machining of work pieces. This process mainly includes assembly of stock rail and switch rail, assembly of swing nose crossing, and laying of the whole turnout.

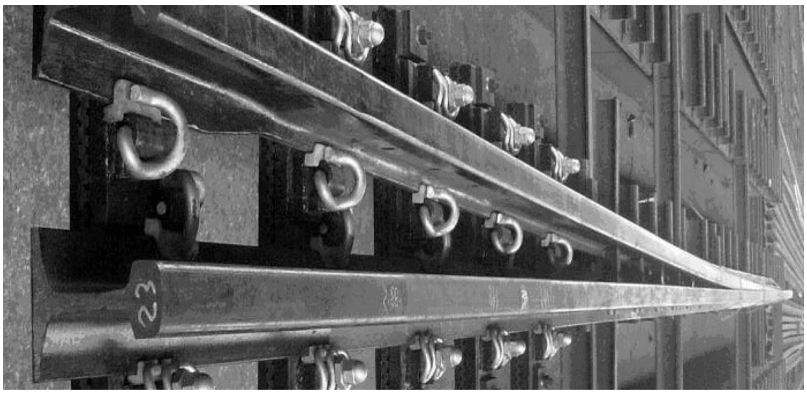

FIGURE 11.21

Components of stock rail and switch rail.

1. Stock rail and switch rail

   A high-precision testing platform and relevant devices for trial assembly will be provided. The platform will be the place for testing the line type and straightness of stock rail, switch rail, and fitting points, as well as for validating the design height difference of the rails after assembly, as shown in Figure 11.21. The specific flow of assembly is as follows:

   a. Placing the stock rail and switch rail on the testing platform equipped with rail ditch for stock rail and slide bedplate for switch rail (the same for the operating status of assembled stock rail and switch rail), measuring the straightness of the rails and closure status of switch rail (with slide bedplate and with stock rail), and adjusting or modifying the rail top immediately if necessary. Inspecting the height difference between the forged zone at the heel of switch rail and AT rail, as well as the inclination of the forged zone

   b. Checking the parts prior to assembly, particularly the grinding of sharp corners and other surface quality

   c. Coating the parts

   d. Assembling the plates (note the position and orientation)

   e. Assembling the jacking blocks

   f. Checking the closure status of switch rail, offset of jacking block, offset of fixed end, and spacing at the heel; and

   g. Commissioning and inspecting.

   Following a reasonable trial assembly, the rail members will be hoisted flexibly one by one (Figure 11.22), and placed in the special baskets for transferring. In this way, the transported rails should have good quality status.

2. Swing nose crossing

   The swing nose crossing will also be assembled on the testing platform. The flow is as follows:

   a. Testing the long and short point rails, performing trial assembly, verifying the installation of fillers, ensuring the line type, offset, and cross level of the base of short and long point rails, noting the influence of offset on the cross level of rail base when applying specified torsion on the bolts of fillers

FIGURE 11.22

Flexible hoisting of long and large components.

b. Stacking the plates on the platform designed for assembly of the crossing, verifying the position, and checking whether the bedplates, plates, and rail ditches are correct and in the same plane
c. Installing the wing rail and checking the bending angle of the rail
d. Coating the rail members; and
e. Assembling the long and short rails and verifying all parameters.

11.4.2 INTEGRAL ASSEMBLY

The manufacturers of turnouts have built special trial laying workshops for the assembly of whole turnouts in the factory. The workshops are designed with a multifunctional assembly platform (Figure 11.23), which can locate the turnout laterally and longitudinally to maintain the framework size. The devices for adjusting the height of ties are also installed to ensure tie cross level. The assembly of turnouts falls into two steps: initial assembly and fine tuning. The two steps must follow specific technical requirements.

1. Initial assembly

   Initial assembly includes the steps of commissioning of a trial assembly platform, placing of ties, placing of straight stock rail and switch rail, placing of swing nose crossing, and assembly of other rails and parts. The position, orientation, and correct connection of rails and plates are all the main concerns during this process.
2. Fine tuning

   Fine tuning is a crucial link to enable the laying quality of a turnout to meet the specified standard. It mainly includes: determining alignment, adjusting cross level, adjusting the plane line type of the turnout, assembling and adjusting the fillers, jacking blocks, and rail supports, adjusting the closed rails, and commissioning the conversion equipment. A properly assembled turnout is shown in Figure 11.24.

FIGURE 11.23

High-precision trial laying platform.

FIGURE 11.24

Assembled No. 18 high-speed turnout.

11.4.3 ACCEPTANCE AFTER ASSEMBLY

Five static geometrical deviations (gauge, cross level, longitudinal level, alignment, and twist) of the assembled turnouts have been stipulated in several Chinese standards (TB/T3301-2013, TB/T3302-2013, and TB/T3306-2013). The gaps between rails, between the rails and slide bedplates, and between the jacking block and rails are specified, and the limit deviation of height

Table 11.6 Requirements for Rail Closure

SN	Description	China	EN13232
1	Closure at switch rail and point rail, point of pointed rail at crossing heel and traction points	Gap < 0.5	Gap < 1.0
2	Other rail closure	Gap < 1.0	Gap < 1.0
3	Gaps between jacking block and rails	Gap < 1.0	Gap < 1.0
4	Gaps between switch rail/point rail and slide bedplate	Gap < 1.0	Gap < 1.0

difference at critical sections of switch rail and point rail are also introduced in these standards. In accepting the conversion equipment, the lock hook must operate smoothly and be effectively bonded with the lock block, without any locking failure or blockage. In the normal and reverse position, no locking may be performed when the gap between the switch rail (point rail) and stock rail (wing rail) is 4 mm or more at the traction points in the closure zone. No indication may be produced in case there is a 5 mm or more gap between the switch rail and stock rail at the closure detector. Further, the measured switching resistance must meet the output requirements of the switch machine.

The standard "railway applications−track−switches and crossings" [EN 13232-(1−10)] is formulated by UNIFE based on previous studies; it has been applied in most European nations and by many turnout companies for the design and manufacture of turnouts. At present, the China Academy of Railway Science (CARS) has been entrusted by UNIFE to prepare the technical code for high-speed turnouts.

China and UNIFE have different specifications on the limit of rail gaps. Table 11.6 shows the details.

11.4.4 SYSTEM INTEGRATION

Chinese high-speed turnouts are produced by way of system integration. In this process, the rails, connecting equipment, fastenings, ties, and conversion equipment will be considered as a whole.

The ERP (enterprise resource planning) system employed by Chinese high-speed turnout manufacturers is an IT-based management platform, which, with the ideal of systematic management, provides decision-making and operation modes for decision makers and employees, integrates all resources of the enterprise, and makes plans for procurement, production, cost, inventory, distribution, transport, finance, and human resources, so as to achieve optimum resource portfolios and obtain the most benefits. The system is a new integrated management information system evolved from MRP (material requirements planning) and has more functions. Management of the supply chain is the core idea.

CHAPTER

LAYING TECHNOLOGY 12

Laying is a key link for normal operation of a turnout. High precision in laying is a prerequisite to high riding quality and comfort in the turnout. At present, turnout laying is a concern for almost all nations with sophisticated technologies in high-speed turnouts, and has been regarded as an indispensable part of turnout technologies, of equal importance in design and manufacture.

Generally, the turnouts are laid mainly either by *in-situ* laying or *ex-situ* laying. For *in-situ* laying, the turnout parts are delivered to the laying site in bulk, as components or blocks; then the parts are assembled. For *ex-situ* laying, the turnout parts will be assembled at a shop and transported by segments, and then the parts will be assembled and laid on site with construction machinery; or the parts will be delivered in bulk and assembled on on-site an assembly platform before being transferred to the site for laying with special construction machinery. In new railway lines, traffic will not be affected due to track occupation; therefore, *in-situ* laying is preferred. *Ex-situ* laying is most common in turnouts in operating lines.

12.1 TRANSPORT [150]

12.1.1 MODES OF DELIVERY

There are three delivery modes for high-speed turnouts:

First, bulk transportation (Figure 12.1). For this delivery mode, the components of switch rails and stock rails (including rails and connectors); components of crossings (including wing rail, point rail, connectors, and tie plates); and other rail members, plates, and ties will be delivered to the site in bulk. This mode is advantageous in its simpler loading and hoisting, saving special transport vehicles and super-large lifting devices. However, greater dimensional deviation or poorer track geometry may occur during *in-situ* assembly, causing high workload during adjustment. This mode prevails in China.

Second, block transportation. For this mode, the rail members, fasteners, and ties will be assembled into track panels at the shop. A turnout may include several blocks (Figure 12.2). To solve the problems of long ties and overload transportation, ties longer than 3.2 m will be cut off in the diverging track and hinged. A rail flat car (Figure 12.3) will be used for transportation. Oversize lifting devices are required. This mode features high assembly precision and small adjustment amounts. But the hinged ties may affect the tamping of ballast track and cross level of the turnout. This is the dominant delivery type in Germany. This mode had been adopted earlier in China;

Design of High-Speed Railway Turnouts.

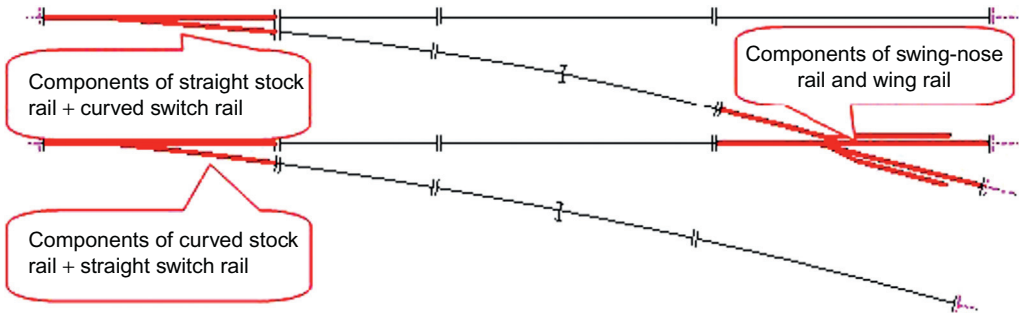

FIGURE 12.1

Bulk transport.

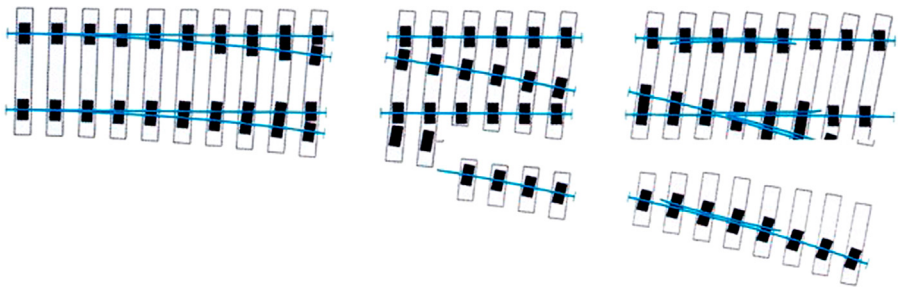

FIGURE 12.2

Blocking of a whole set of turnout.

FIGURE 12.3

(A) Block transport of turnout. (B) Block lifting of turnout.

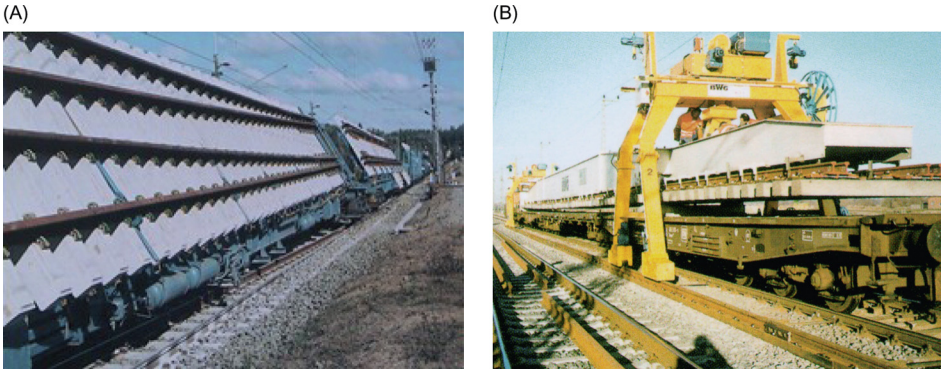

FIGURE 12.4

(A) Special transport vehicle for turnout. (B) Turnout hoister.

however, considering the poor retention of turnout cross level, the hinged ties in the ballast track have been replaced with monoblock long ties, and bulk delivery mode is now used.

Third, whole-set transportation. For this mode, all parts will be assembled and adjusted in the plant (except welded joints) and will then be delivered by special cars (Figure 12.4). This mode can maintain the turnout geometry and save the adjustment workload. However, it requires special transportation vehicles and is less efficient. In addition, oversize hoisting equipment will be involved. This delivery mode has been used in Europe.

12.1.2 HOISTING AND STORAGE

The elongated rails of the turnout are prone to irreversible plastic deformation during hoisting, transportation, and storage, which may affect the precision and laying effects of the turnout. China has formulated several technical standards for the hoisting and storage of turnouts. According to the standards, all turnout components and parts must not be damaged or contaminated during hoisting, transportation, and storage. The turnout components should be hoisted using qualified hoisting machinery as per marked positions. The components of switch rails and stock rails, components of swing nose crossings, auxiliary rails, and track panels are to be stacked on flat ground, stored by category, and temporarily fixed. The stacking of these rail members should not exceed four layers. Each layer shall be packed and leveled with timber plates arranged vertically in height direction. Ties will be stacked in length order, five layers at most. Two perpendicularly aligned timber plates will be arranged between every two layers. All turnout members will be protected from rain. The conversion equipment will be kept in special containers.

12.2 LAYING OF BALLAST TURNOUT

Ballast turnouts may be assembled and laid *in situ* or *ex situ*. Both laying methods are common in China [151,152].

12.2.1 *IN-SITU* ASSEMBLY AND LAYING

In-situ assembly and laying is typically employed in new ballast turnouts. Temporary track panels may be used (transitional measure) to facilitate laying in front of the turnout, avoiding construction disturbance, particularly local turnout deformation produced by construction vehicles during informal operations. So a temporary crossover may be laid at one end of the station for shunting and route changing. In this way, a turnout may be laid in another line without affecting the traffic smoothness of a line.

For *in-situ* assembly and laying, a temporary track will be constructed in the turnout area as a transitional measure, followed by initial ballasting and shaping, locking the turnout rails with connected long rails when the track bed is stabilized, erecting RTG cranes or track cranes in or near the turnout area, and mobilizing qualified turnout subassemblies. After that, the temporary track panels will be removed with cranes assisted by railway workers. Then, the ballast will be leveled and compacted by vibrators, on which the assembly platform will be constructed. RTG cranes or track cranes will be used in handling and assembling the turnout subassemblies. Following the *in-situ* assembly work, the turnout parts will be checked for geometry compliance, and welding will be performed in the turnout. Afterwards, the turnout subassemblies will be jacked with integral hydraulic lifting equipment for removing the platform, reballasting, and shaping. Then the turnout will be lowered, checked, and fine-tuned. When all turnout parts meet the geometry standard, the turnout rails will be welded with the long rails at two ends by locking. This is the whole process for laying a ballast turnout.

Figure 12.5 presents the specific construction process of the *in-situ* assembly and laying of a ballast turnout. It is divided into seven stages by the content and relevance between processes.

1. Construction preparatory stage

   In this stage, surveying and setting out will be performed to determine the positions of central stakes at turnout front, center, and rear. The turnout will be ballasted simultaneously with the main line. The pre-paved ballast will be compacted with a vibrating roller to achieve desired bed compactness. The compactness should be at least 1.7 g/cm^3, the reserved lifting amount should not be greater than 50 mm, and the allowable deviation of ballast levelness is 10 mm/3 m. Temporary track panels will be constructed in the turnout area, where the track will be reballasted, shaped, and tamped with large-size machinery to stabilize the bed. The ballasting and shaping of a temporary track panel will be performed simultaneously with the nearby section line. The tracks at two ends of the turnout will be properly maintained and provided with stress relief measures.

   The turnout parts will be preassembled and debugged in the plant. Then the parts will be properly marked and disassembled for delivery to the site by railway or road. The mobilized parts will then be hoisted and stored as required, and checked for straightness, intactness, and completeness. Gantry cranes will be erected beside the temporary track panel. The cranes will span two main tracks. The span is sufficient for hoisting the turnout parts and associated components without affecting the *in-situ* assembly of the turnout. After removing the short track panel and leveling the ballast bed, the assembly platform will be constructed *in situ*. The positions of ties will be properly marked.
2. *In-situ* assembly of the turnout

   After mobilization, the ties will be hoisted into position with gantry cranes. With the use of turnable RTG cranes with variable span or a 16T crane, the turnout parts will be unloaded and assembled on the platform. The parts will be assembled in the sequence of swing nose crossing,

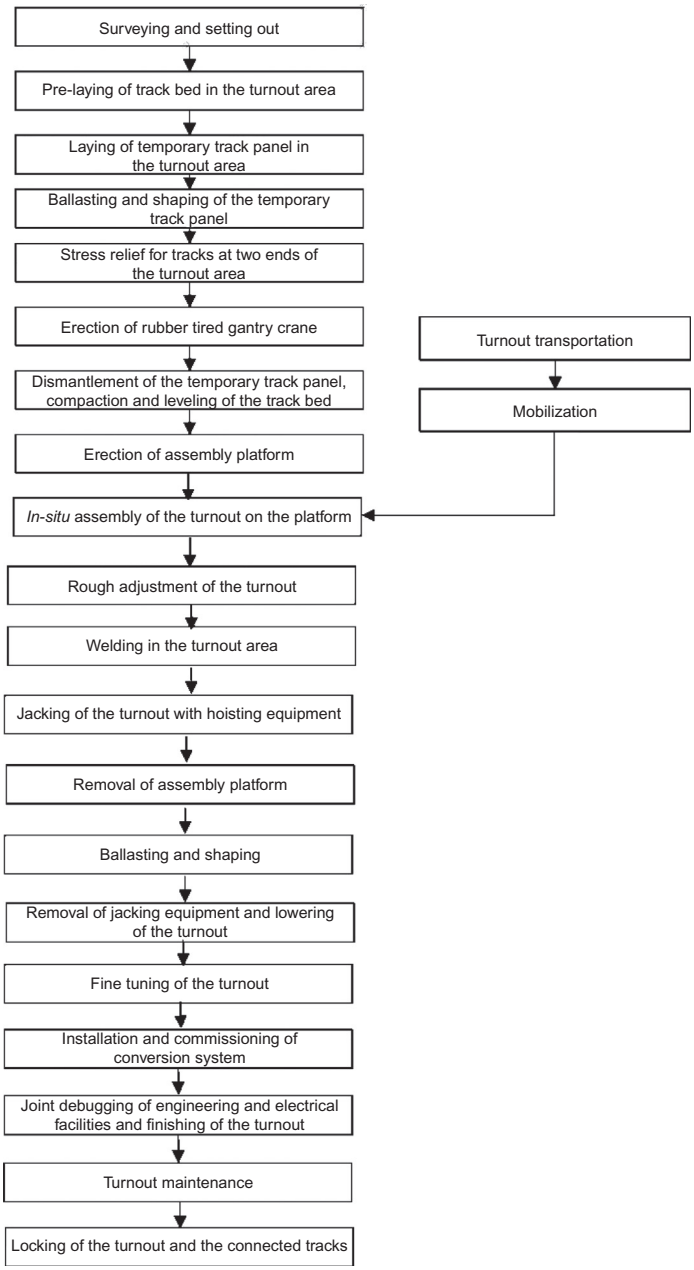

FIGURE 12.5

Process flow of *in-situ* laying of ballast turnout.

FIGURE 12.6

Thermite welding.

switch rail, stock rail, and rail of transition lead curve. The main processes and requirements in assembly are given below:

a. Laying the ties

Arranging the ties by number and as per turnout direction; regulating the longitudinal level of ties with leveler and maintaining the longitudinal level difference between two adjoining ties within 2 mm, and in the whole turnout within 5 mm; regulating tie spacing and longitudinal position as per drawings.

b. Laying the fastenings, tie plates, and other parts

c. Laying the swing nose crossing and guiding rail

Hoisting the members into position with cranes, tightening the bolts on the ties, and regulating the center of the actual point of the swing nose rail to the marked position.

d. Installing straight stock rail and curved switch rail

Hoisting the stock rail and switch rail into position, checking the gaps between the base of the switch rail and the surface of the slide bed, adjusting the longitudinal level of ties up to standard if necessary to eliminate inordinate gaps.

e. Fine tuning the position of tie plates and ties

Marking the position of ties on the rails in the straight direction, fine turning the position of tie plates and ties to keep the deviation within 3 mm.

f. Installing curved stock rail and straight switch rail

g. Properly orienting the turnout

Check the turnout orientation with square for correctness (allowable deviation of tie $\leq$5 mm); and

h. Coarse regulating of the turnout

Checking the position, geometry, closure status, height difference of turnout members with high-precision level gauge, and total station and track inspection device; regulating the longitudinal level or gauge of the track by adjusting the fasteners or tie height if required.

3. Welding in the turnout area

After assembly, the rails in the turnout area will be joined by thermite welding (Figure 12.6) as per the requirements for laying the continuously welded rail turnout. The welding temperature

FIGURE 12.7

Jacking the turnout with hydraulic jack.

FIGURE 12.8

Manual tamping of track bed.

must be within the range of allowable rail laying temperature, or it will not be lower than the design rail laying temperature by 20°C or below 0°C in unfavorable conditions. The welded joints will be detected on the whole section, any nonconforming joints will be disconnected and rewelded. The surface flatness of the rail will be measured with a flatness gauge. No vertical bulges greater than 0.2 mm or low joints are allowed. The lateral working surface at the rail head may be depressed by 0.2 mm at most; no bulges are allowed.

4. Lowering and placing of the turnout

   The whole turnout, after assembly and coarse adjustment, will be jacked with hydraulic jack as shown in Figure 12.7. Then the assembly platform will be dismantled, ballast refilled, and the turnout lowered. Minor lifting amounts will be reserved, generally 20−30 mm, to facilitate the maintenance of small diesel tamping machines for proper alignment, longitudinal and cross level, of the turnout, as shown in Figure 12.8.

5. Fine tuning

   Large maintenance machinery, such as a tamping wagon, will be used to adjust the longitudinal and cross level and alignment of the turnout, and to achieve desired compactness. Later, the longitudinal level and alignment of the rail will be fine tuned via the fastenings. The technology of fine tuning will be further introduced in Section 12.4.

6. Installation and debugging of the conversion equipment

   The geometry of turnout parts will be rechecked after fine tuning. If qualified, the conversion equipment will be installed, followed by detection and debugging of closure status, switching throws, switching force, and other relevant indicators. These indicators may be regulated by adjusting the fasteners, jacking block, fillers, locking block, etc.

   The main line of the turnout is opened with the control of station control center; the access route will be confirmed manually. A special maintenance team will be established to maintain or repair engineering and electrical facilities, and ensure that the turnout is in good condition under the operation of engineering cars before delivery and acceptance.

7. Welding of the turnout and connected tracks

   Contact welding is not feasible due to complex turnout structure. Thermite welding or small-sized gas pressure welding may be used. The turnout, once adjusted, will be jointed with rails at two ends within allowable rail laying temperature. The turnout cannot be stretched

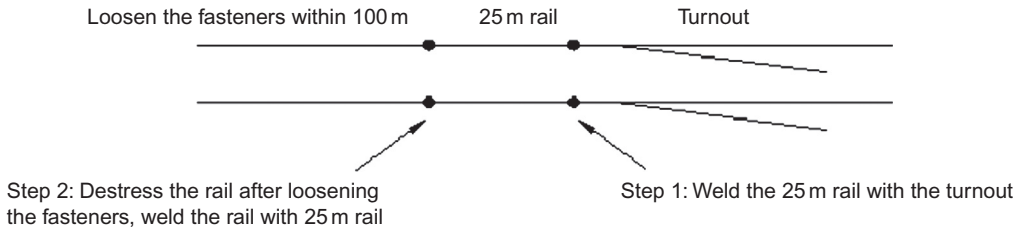

FIGURE 12.9

Locking of turnout at low temperature.

during welding; therefore, the rail fastenings within 100 m ahead of or behind the turnout will be loosened within the scope of allowable rail laying temperature. The rails can move easily with the support of rollers. Then the rails will be cut into long rail strings and jointed with turnout rails by thermite welding.

If the rail laying temperature is below the lower limit by less than 10°C, a 25-m rail section may be interpolated by thermite welding respectively at the turnout ends. Prior to stress relief, the fasteners on the 100-m-long rail segment ahead of the 25-m rail segment will be loosened first, and the rails will be supported with rotary drum for easy movement. The 100-m-long rail will be stretched with a rail pulling device as per the value obtained based on design rail laying temperature, until the design rail laying temperature is achieved. Then the rail pulling device will be maintained at a certain pressure, and thermite welding will be performed, as shown in Figure 12.9.

To retain the related position of turnout parts, the rails will be distressed in the turnout area; therefore, no welding can proceed when the rail laying temperature is lower than the allowable value by more than 10°C. The actual rail laying temperature will be recorded during welding. The welding head, being qualified in the detection, will be provided with creep observation stakes as per design requirements. The staggered amount of the points of two switch rails must not be greater than 5 mm after welding. For turnout with filler-type heel of crossing, the switch rail must be properly oriented and the blocks of retainer must be in the center with clearance at two ends not greater than ± 0.5 mm.

12.2.2 *EX-SITU* ASSEMBLY AND LAYING

For *ex-situ* assembly and laying mode, the turnout will be assembled on the platform erected on site, and fine tuned and adjusted with the lateral, longitudinal, and vertical adjustment devices on the platform. The entire assembled turnout will be loaded on the rail flat car and delivered to the site. After removing the temporary track panel, the assembled turnout will be laid with the hoisting equipment as shown in Figure 12.10.

As with *in-situ* assembly and laying mode, the turnout laid with *ex-situ* mode must also be maintained with care. The turnout will be provided with initial leveling by an inspection car, and ballasted and tamped manually. The initial maintenance is finished when the main line can be put into operation. Each station will have a special maintenance team for routine maintenance of the

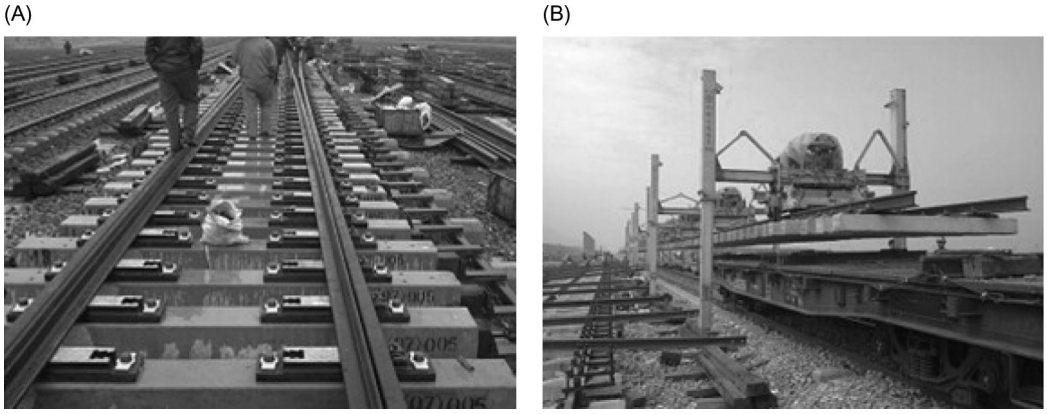

FIGURE 12.10

(A) Turnout on the assembly platform. (B) Translocation of turnout.

turnout. Fine tuning with the tamping machine comes last. Other processes are the same as in the *in-situ* mode. This mode is advantageous in its high efficiency and accuracy. However, subsequent maintenance is necessary after the turnout is laid in position, so as to maintain those advantages.

12.2.3 CONTROL MEASURES FOR LAYING QUALITY [153]

The following measures should be taken to ensure laying quality of the ballast turnout.

1. Professional team

   High-speed turnouts demand high accuracy in assembly and laying. As stated in Chinese code TB/T3306-2013, the deviation of track gauge and offset shall be within ±1 mm, and the deviation of cross and longitudinal level and alignment shall be within ±2 mm upon acceptance. Therefore, professional teams for handling, assembly, adjustment, and welding are essential for accurate laying of high-speed turnouts.
2. Mechanical equipment

   The handling of long and large rails and track panels must rely on special machinery (e.g., 20-m-long flat car, heavy cranes, tamping machines, and special hoisting tools). Otherwise, rail deformation resulting from poor laying quality may occur.
3. Precise engineering control survey

   The turnout is laid with the aid of precise engineering control survey technology. With this technology, the 3D coordinates of the turnout can be defined accurately. Additionally, a CPIII control network, inspection car, total station, and relevant adjustment software will be used to improve the precision of fine tuning.
4. Sophisticated maintenance

   Acceptance of delivery means that the high-speed turnout can allow normal passage of railway vehicles at design speed. In this regard, assembly and maintenance are critical to

laying a ballast turnout. Assembly can be ensured by skilled workers, special platforms, and mechanical equipment. Maintenance quality depends on the performance of large maintenance machines. Tamping is performed before the passage of railway vehicles (including engineering cars), so as to stabilize the foundation bed. The large maintenance machines work precisely at allowable traveling pace, without damaging the rail members or shifting the ties. For the point of point rail and heel of crossing featuring intensive rail members, a general tamping machine may not be available. In that case, a smaller tamping machine can be used instead.

5. Excellent welding quality

   A good deal of welding work will be done in laying high-speed turnouts. Welding is technologically challenging. Welding irregularity must be controlled within 0.2 mm/m by enhancing the welding quality or grinding. Therefore, a highly professional team is required.

12.3 LAYING OF BALLASTLESS TURNOUT

In China, a ballastless turnout may be laid in three modes. The first mode is *in-situ* laying of the ballastless turnout with embedded ties, advantageous in its easy construction. The second mode is *ex-situ* laying of the ballastless turnout with embedded ties, featuring high construction efficiency, but differing from the first mode in that the rail members, fasteners, and ties are assembled at the shop, compared to on site for the first mode. The third mode is *in-situ* laying of ballastless turnout with a slab track, advantageous in its fast and precise construction [154].

12.3.1 *IN-SITU* LAYING OF BALLASTLESS TURNOUT WITH EMBEDDED TIES: CONSTRUCTION PROCESS AND KEY TECHNOLOGIES

1. Construction process

   Construction processes: surveying and positioning; setting out central stakes at turnout rear and front and joints of track panel; laying assembly platform; assembling the turnout (the same procedures as with ballast turnout); installing tie supports, vertical support bolts, and adjusting the height; installing the anchor blocks or lateral supports and adjusting the lateral position of the turnout (first adjustment), as shown in Figure 12.11; removing the assembly platform, fixing the reinforcement and erecting formwork; calibrating and fine tuning the turnout (second adjustment); installing the switch equipment when the turnout is in good condition; jointly debugging the engineering and electrical facilities (third adjustment); removing the conversion equipment; checking, adjusting (fourth adjustment), and fixing; casting concrete, curing, removing the bracing system and formwork, as shown in Figure 12.12; checking and fine tuning (fifth adjustment); welding the turnout; installing conversion equipment, jointly debugging the engineering and electrical facilities (sixth adjustment); checking, adjusting (seventh adjustment), maintaining, and accepting.

   The bolts will be retightened following each fine tuning. Before acceptance of delivery, the service system and inspection system of the turnout will be established to ensure routine maintenance work.

FIGURE 12.11
Positioning and bracing system of the turnout.

FIGURE 12.12
Cast concrete track bed.

2. Key technologies

Before concrete is poured, the ballastless turnout is adjusted and positioned by vertical and lateral positioning and bracing systems. In addition, any rise of the track panel should be prevented during concreting. The stability, adjustment performance, and precision of the bracing systems will determine the geometric smoothness of a turnout. These are the technical concerns of this laying mode.

In laying a ballastless turnout, the laying condition and geometric smoothness of the turnout will be confirmed first. A great deal of adjustment work will be done; the turnout will be adjusted seven times in the whole laying process. Therefore, precise surveying and fine tuning of track geometry in the turnout area are also critical for laying the ballastless turnout.

12.3.2 *EX-SITU* LAYING OF BALLASTLESS TURNOUT WITH EMBEDDED TIES

For *ex-situ* laying mode, the track panel, after surveying, positioning, and erection of the assembly platform, will be hoisted and jointed into a whole turnout, as shown in Figure 12.13, saving the assembly process. That is the principal difference with *in-situ* mode. Subsequent procedures and processes are the same for the two modes.

12.3.3 LAYING OF BALLASTLESS SLAB TURNOUT: CONSTRUCTION PROCESS AND KEY TECHNOLOGIES

1. Sub-rail foundation

For ballastless slab turnout on subgrade, the turnout structure is composed of turnout parts, prefabricated slabs, self-compacting concrete base slab (filler course), and concrete cushion (base treatment) from top to bottom, as shown in Figure 12.14. Shear reinforcement is arranged between the slab and base slab.

For the turnout on bridge connected with a ballastless turnout with longitudinally coupled plates, the turnout structure is composed of turnout parts, prefabricated slabs, cement emulsified

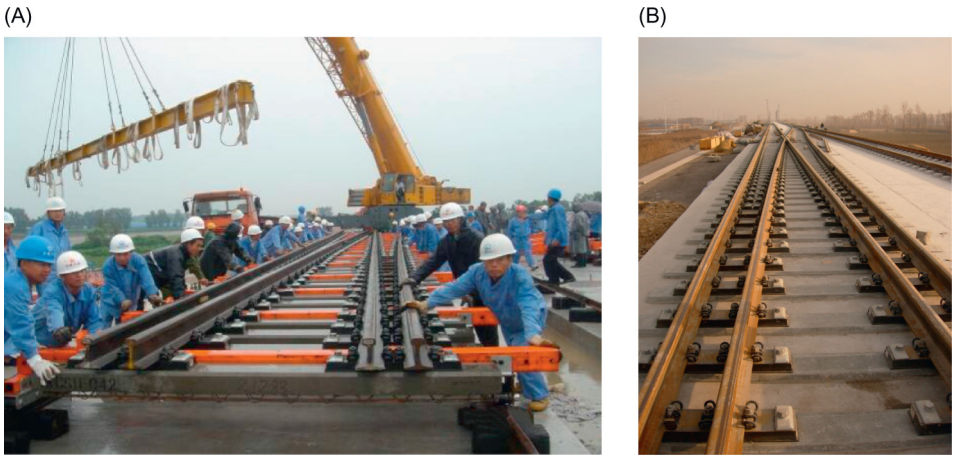

FIGURE 12.13

(A) Shifting of assembled turnout. (B) Cast concrete track bed.

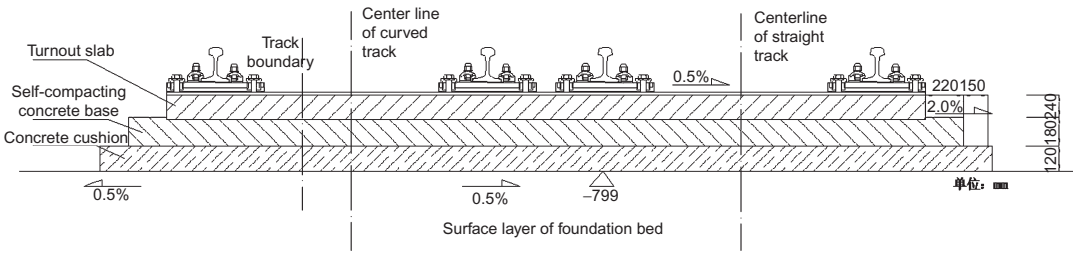

FIGURE 12.14

Turnout on subgrade.

asphalt mortar course (filler course), RC base slab, sliding course (two layers of geotextile and one layer of geomembrane), waterproof course (base treatment), and lateral blocks from top to bottom, as shown in Figure 12.15.

The prefabricated turnout slab is 240 mm thick, provided with 340-mm-wide lateral bearing platforms arranged at an interval of 600-mm longitudinally on the slab. The platforms have a flat surface. Among these platforms, 0.5% lateral drainage slope and lateral presplitting cracks (4 cm deep) are arranged on the slab surface. The slab is of RC structure (C55, HRB355 reinforcement) prefabricated in the factory.

The subgrade base is made of 180-mm-deep cast-*in-situ* C40 concrete with good fluidity (self-leveling concrete). The base slabs cover all the turnout area, about 200 mm wider than corresponding turnout slabs in the lateral direction, whose protruded edge is provided with a 2% drainage slope outside of the track system. The concrete cushion is 200 mm deep, about

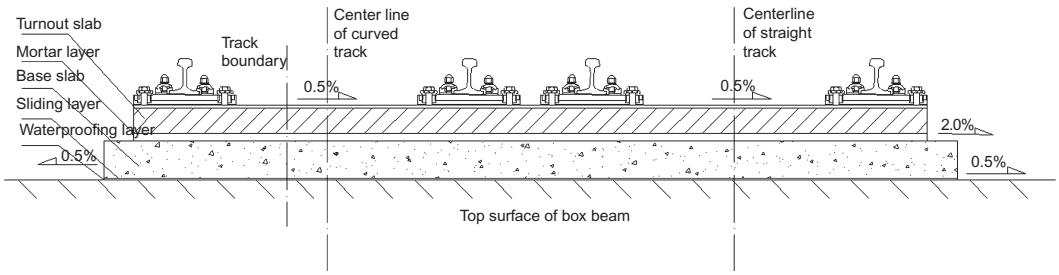

FIGURE 12.15

Turnout on bridge.

180 mm wider than the corresponding bottom laterally, whose protruded edge is provided with a 2% drainage slope outside of the track system. The structure is made of C25 plain concrete, without reinforcement.

The waterproofing course on the bridge beam is on top of the box beam, composed of a prime coat, a polyurea waterproofing coat, and an aliphatic polyurethane top coat. The slide course, composed of two layers of geotextile and one layer of Polyethylene (PE) film, is laid on the waterproofing course. The lower geotextile layer is bonded with the waterproofing course by three 20-cm-wide glue stripes. The PE film and upper geotextile layer are laid on the fixed lower geotextile layer. The friction coefficient between the PE film and geotextile layer is 0.35 at most. The base slab may slide against the bridge beam. The 200-mm-thick RC base slab (C40 concrete) is cast on the slide course in unit, which will be longitudinally tensioned and connected as per construction temperature. The cement emulsified asphalt mortar course is located between the turnout slab and bottom, which will be cast after fine tuning of slabs for fixing the slabs and providing elastic bearing for the ballastless track. The lateral blocks are arranged outside the slabs, with embedded reinforced connection with the sleeves for retaining block grooves reserved on the beam surface for lateral positioning of the turnout.

2. Construction process

The construction process for ballastless turnout on subgrade: setting out and positioning; construction of concrete cushion on subgrade; fixation of reinforcement at the bottom and installation of bearing blocks; laying, adjustment, and positioning of turnout slabs, as shown in Figure 12.16; formwork erection for base slab; casting of self-compacting concrete; assembly of the turnout; coarse adjustment of the turnout; installation of conversion equipment; fine tuning of the turnout; welding of the turnout, maintenance, and acceptance of delivery.

Construction process for ballastless turnout on bridge: setting out and positioning; deck treatment; construction of waterproofing course; paving of slide course, as shown in Figure 12.17; fixation of reinforcement at the base slab; installation of formwork, concreting, concreting of post-cast stripes on the plate positioning connectors; installation of bearing system for turnout slabs; laying, adjustment, and positioning of turnout slabs; casting of cement emulsified asphalt. The subsequent processes are the same as for ballastless slab turnout on subgrade.

(A)

(B)

FIGURE 12.16

(A) Installation of turnout slabs. (B) Adjustment of turnout slabs.

(A)

(B)

FIGURE 12.17

(A) Laying of slide course. (B) Positioning of turnout slabs.

3. Key technologies

Manufacturing accuracy of turnout slabs determines the installation accuracy of turnout rails; therefore, China has formulated strict technical standards for the manufacturing of turnout slabs (e.g., position deviation of bolt holes ≤0.5 mm, flatness deviation of rail support surface ≤1 mm). In addition, in China, embedded nylon sleeves, instead of drilling on site as in German turnouts, are used to further improve the accuracy of assembly of the turnout.

Fine tuning survey of turnout slabs is essential for accurate laying. In China, the 3D coordinates of the slab are obtained by measuring the four corners with the total station with a prism (Figure 12.18). The 3D adjustment can be determined as per the analysis results of the rapid fine-tuning system of the total station. Later, adjustment is made by the fine tuning claw

FIGURE 12.18

Prism.

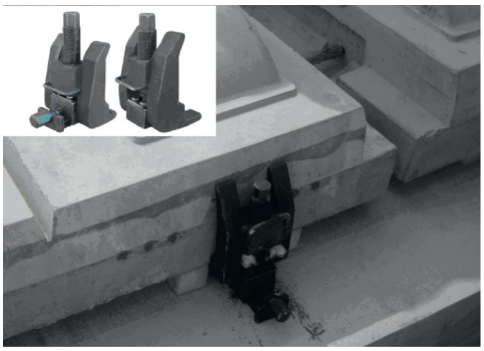

FIGURE 12.19

Fine-tuning claw.

(Figure 12.19), bit by bit until the design theoretical position and height are achieved. The allowable deviation is ±0.3 mm in all directions.

The base slabs on subgrade are made of self-leveling concrete to ensure fine tuning accuracy of turnout slabs and casting quality of base slabs. The construction quality is a main concern in realizing the desired quality of the solid slab bed. Self-leveling concrete is characterized by highly fluid, highly cohesive, tamping free, and anticontractible concrete featuring low water−cement ratio, more admixture, more fine aggregate, and smaller grading. For this, the mix ratio of the concrete must enable inner quality, such as concrete strength, compactness, and durability, as well as meet the requirements of construction process (e.g., high fluidity and fillability).

Cement emulsified asphalt mortar, filling in the course between the turnout slab and base slab, is an elastic material made by mixing asphalt with a couple of other polymers. This is a critical material and component of ballastless slab track. It is costly, but conducive to the stabilization and buffering of traveling vehicles. The material is made by blending a special asphalt emulsion, cement, admixture, fine aggregate, water, aluminum powder, defoaming agent, etc. at room temperature. As its performance relates to the durability and maintenance quantity of a ballastless slab track, the material must meet all required performance indicators (e.g., divergence, fluidity, resolution, gas content, expansivity, breaking strength, compressive strength, freezing resistance, and fatigue resistance).

12.3.4 CONTROL MEASURES FOR LAYING QUALITY OF BALLASTLESS TURNOUT

In addition to professional construction teams, mechanical equipment, and excellent welding performance as with ballast turnout, the following quality measures must be taken for ballastless turnout.

1. Prioritizing ballastless turnout construction

   The ballastless turnout must be constructed prior to other track structures to ensure the supply of high-performance concrete, provision of transportation access, adequate laying period, and operating conditions for thermite welding and track locking.

2. Stricter accuracy of positioning

   Unlike ballast tracks, a ballastless turnout is positioned upon concrete and cannot be rectified easily. In the construction of a Chinese station (North Jinshan Station, Shanghai−Hangzhou line), an inordinate geometric deviation (lateral deviation above 30 mm) occurred in a turnout and was rectified by adopting special lengthened plates, which impacted the homogenous distribution of track stiffness along the longitudinal direction of the turnout and the riding comfort, as well as the durability of turnout parts. Theoretically, this problem may be solved by demolishing the concrete track bed for recasting; however, this is costly and will cause great disturbance to operations. In view of the above, the setting out of turnouts and arrangement of control stakes must be performed accurately, and the turnout must be positioned and laid in strict accordance with the control stakes.

3. Stable and adjustable bracing system

   The fine tuning and fixing of a ballastless turnout are realized by the lateral/vertical bracing adjustment system. The system is composed of a lateral bracing adjustment device and vertical auxiliary bracing adjustment device on the tie, bracing pad, and fine tuning claw on the turnout slab, which may function in collaboration with a special measurement system for the turnout. The final laying accuracy of the ballastless turnout is determined by the adjustment performance and stability of the bracing device. Therefore, the manufacturing, installation quality, and structural stability of the bracing device must be fully guaranteed.

4. Scientific fine tuning technology

   Fine tuning comes after concreting, which offsets the geometric inaccuracy produced in construction by adjusting the height and gauge, thus ensuring the laying quality. However, in this stage, the turnout can only be adjusted by fastenings; any adjustment to a rail may affect the closure status and track geometry (any adjustment may affect the rest). Thus, unscientific adjustment measures may lead to possible negligence; if a geometric inaccuracy is rectified, other geometric defects may appear. So the turnout adjustment must be performed by special analysis software, so as to attain the optimum track line using minimal adjustments.

12.4 ACCURATE ADJUSTMENT TECHNOLOGY

Surveying and adjustment are key technologies of concern in ensuring high smoothness of a turnout laid on ballastless track. Much adjustment work is involved in a ballastless turnout, including rough adjustment, fine adjustment, adjustment before and after concreting, adjustment of laid rails, adjustment before and after welding, and adjustment before acceptance. Therefore, studies on accurate adjustment of turnouts are necessary to minimize the workload of adjustment and maximize adjustment accuracy [155,156].

12.4.1 DETECTION TECHNOLOGIES OF TURNOUT STATIC GEOMETRY

1. Engineering survey

   The construction of ballast track in a high-speed railway line boosts the renovation of measurement concept in railway engineering. Accurate geometric parameters are prerequisite to riding quality. Ballastless track involves a complex laying process, which cannot be rectified

easily after construction. Even a small inaccuracy may become a potential hazard to the whole project. Any later modification to track geometric parameters may be difficult and costly. Therefore, the construction quality of a ballast track is a key determining factor of successful construction of a high-speed railway. Construction parameters must be accurate to the millimeter. In conclusion, highly accurate measurement technology offers an important guarantee for the construction quality of ballast track.

However, high-precision measuring instruments and the measurement control network for a passenger-dedicated line established with high-level measurement approaches are insufficient in solving all possible problems in measuring ballastless track. In this context, a complete, effective, and accurate measurement system is required. A uniform spatial data reference must be established for the processes of surveying, construction, completion, and operational management of ballastless track. This can unify the data benchmarks for monitored track deformation throughout all stages, and can benefit the standardization of acceptance inspection and measured data by third parties. Therefore, a unified coordinate system and calculation datum should be established for control networks for survey, construction, and operational maintenance of high-speed railways. The three control networks will share the same coordinate system and calculation datum.

For ballastless track, the plane control network has three levels: CPI, CPII, and CPIII. CPI (basic plane control network), arranged along the track route and established as per GPS static relative positioning theory, is the datum for the plane control surveying at all levels of the whole line (section). CPII (track control network) is arranged near the track based on CPI, serving as the benchmark for track plane control during survey and construction phases and determining the starting and ending points of CPIII during the construction of ballastless track. CPIII (foundation pile control network) is a 3D control network arranged along the line, whose starting and ending points lie in CPI or CPII, which functions upon the completion of work under the track and serves as the benchmark for the laying and operational maintenance of ballastless track.

The Huanghai vertical datum (a unified Chinese vertical datum) is employed. The operation of the vertical control network may be hierarchical. The second-order leveling network is the first tier; it is the unified vertical control network of the whole line. The precise leveling network is the second tier, where the leveling points are arranged at an interval of 1 km.

Accurate adjustment or inspection of a ballastless turnout is performed by a track inspection device and high-precision total station based on the CPIII control network. During positioning, the track coordinates and alignment can be fixed reliably and accurately with the precise and dense control points of the CPIII network. High-precision free stationing of the total station, realized by the 3D linear-angular resection method based on trackside CPIII control points, is a prerequisite to precise measurement of a track's absolute position. Eight control points are provided in the turnout zone for free stationing (Figure 12.20). If unavailable, at least six backsight CPIII control points should be provided. During backsight positioning, the distance to the nearest control point should be at least 15 m, and the distance between two stations will be about 50 m. In addition, at least four backsight CPIII points will overlap for every two stations. TCA (Leica, German) or S-series (Trimble, USA) total stations with automatic sighting and target recognition functions are used to minimize sighting error. The total station will be erected on the centerline of the track and function by small-angle measurement to produce the minimum lateral error.

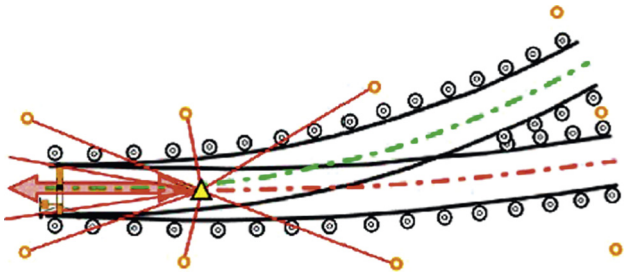

FIGURE 12.20

Layout of total station.

FIGURE 12.21

Track inspection device.

The measurement of absolute coordinates and relative position of the track geometry will proceed after free stationing. In this process, the total station will locate the prism of the track inspection device, as shown in Figure 12.21, and perform real-time observation with the movement of the track inspection device, so as to obtain the 3D coordinates of the prism. With the track inspection car provided with prism, the track gauge, cross and longitudinal level, and alignment of the track at each tie in either the main or diverging line can be measured accurately [157].

2. Inspection device of track geometry [158]

The inspection device for track geometry (track inspection device) is a special device for static detection of track smoothness. Internal monitoring geometric parameters include track gauge, cant, cross and longitudinal level, alignment, curve versine, torsion (twist), and gauge variation rate. External monitoring geometric parameters include centerline of track and plane (lateral) and height (vertical) deviation of left/right rail with respect to design alignment. There are two accuracy classes: class 0 and class 1. A class 0 track inspection device is mainly used on railways for 350 km/m at most. Class 1 track inspection devices can be applied to railway for 200 km/h at most.

The track inspection car is composed of a frame system, data acquisition and processing system, and analysis software, as shown in Figure 12.22. The frame is a T-shaped structure, compact and firm. The frame system integrates precise mechanical transmission and a high-precision sensor detection system, forming the measurement platform of the system. The data acquisition and processing system is a client server structure composed of a rugged notebook and multiple microcontroller units, capable of performing digital-to-analog conversion, data processing, and coordinate transformation of the monitored parameters, providing real-time display, alarm, and other operation tips, as well as interfaces for various types of total stations. The analysis software is characterized by friendly and intuitive MMI, diversified reports, and a powerful data management function. It is compatible with Office software.

Operating principle: The traveling wheels of the track inspection car roll on the rail surface under the action of gravity and thrust; three measuring wheels cling to the inner side of two rails under spring force, and the range is measured with the encoder connecting with the traveling wheels; the track gauge is measured with the linear displacement sensor connecting with the

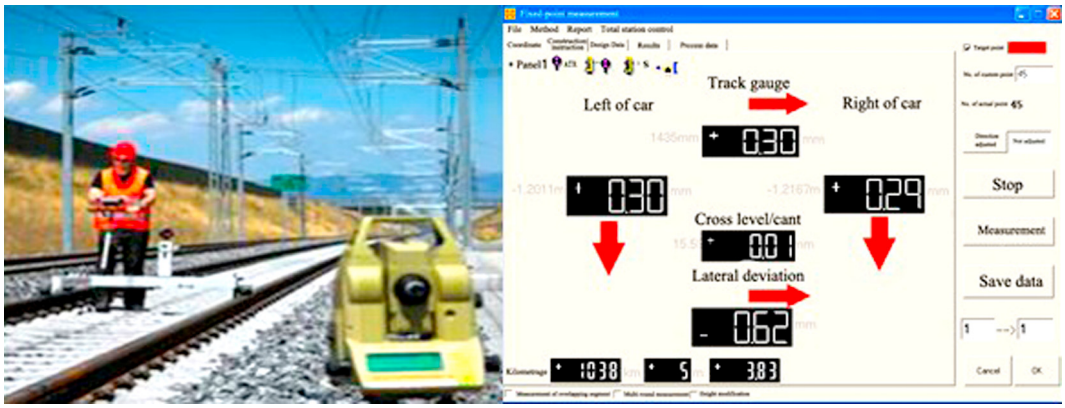

FIGURE 12.22

Composition of track inspection device.

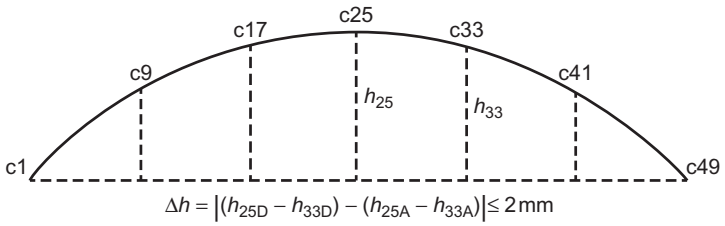

FIGURE 12.23

Medium-wavelength irregularity.

beam measuring wheel at the breathing end; the inclination of the left/right rail is measured with an inclinometer, and the cross level can be calculated correspondingly; the operating status and path of the track inspection device can be measured with an angular velocity sensor by means of strapdown, and the alignment and cross level can be calculated. For a class 0 track inspection device, the measured track gauge, cross and longitudinal level, and alignment can be accurate to ±0.3 mm, and linear distance (km) to ±1‰ [159].

12.4.2 ASSESSMENT STANDARD FOR TURNOUT STATIC GEOMETRY

Alignment and longitudinal level irregularities are two main indicators in accepting the static geometry of ballastless track in China, in particular, medium-wavelength irregularity and long-wavelength irregularity. Medium-wavelength irregularity: unit chord length = 30 m (or 48 tie spacings); measuring interval = 5 m (or 8 tie spacings); the difference between actual and design rise errors and offset deviation of a 10-m-long chord are not greater than 2 mm, as shown in Figure 12.23. Long-wavelength irregularity: unit chord length = 300 m (or 480 tie spacings);

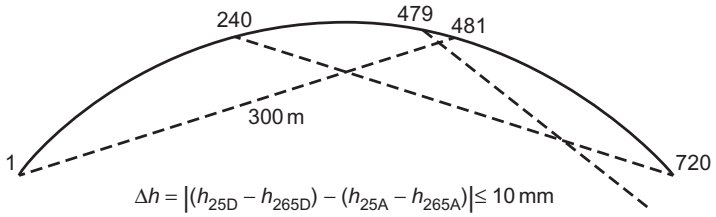

FIGURE 12.24

Long-wavelength irregularity.

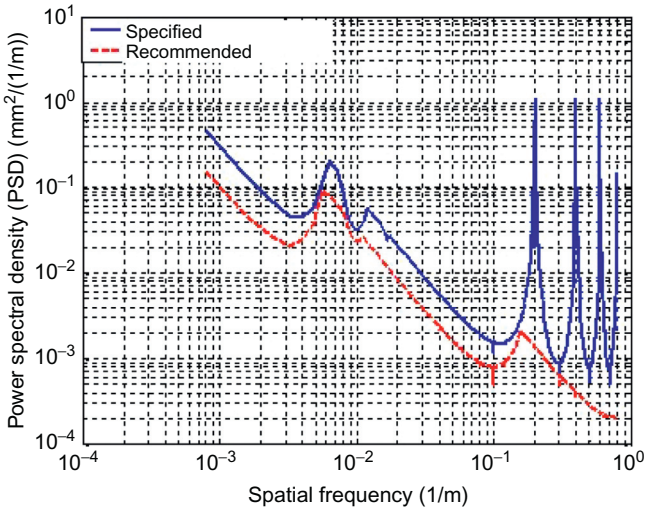

FIGURE 12.25

Maximum spectral density of track irregularity as per recommended and original standards.

measuring interval = 150 m (or 240 tie spacings); the difference between actual and design rise errors is not greater than 10 mm, as depicted in Figure 12.24.

Studies [1] show that the versine difference of a 10-m-long chord and the calibration value of a 30-m-long chord at a measuring interval of 5 m will exert a similar control effect on track irregularity. If the control effects are similar, the control indicators for track irregularities will be minimized to facilitate construction and maintenance work. Thus, one indicator is adopted. In addition, there is no effective control measure for track irregularity with wavelengths below 5 m. For the above reasons, in combination with field accessibility, it is recommended to control the longitudinal level and alignment irregularities of the track with the following methods: irregularity difference of two adjoining ties ≤1 mm, irregularity difference of two ties at an interval of 8 tie spacings ≤2 mm, irregularity difference of two ties at an interval of 240 tie spacings ≤10 mm. Figure 12.25 compares the maximum power spectral density of the track irregularity [161] as per the recommended and original standards. The figure shows that the recommended standard can enable the optimum track geometry.

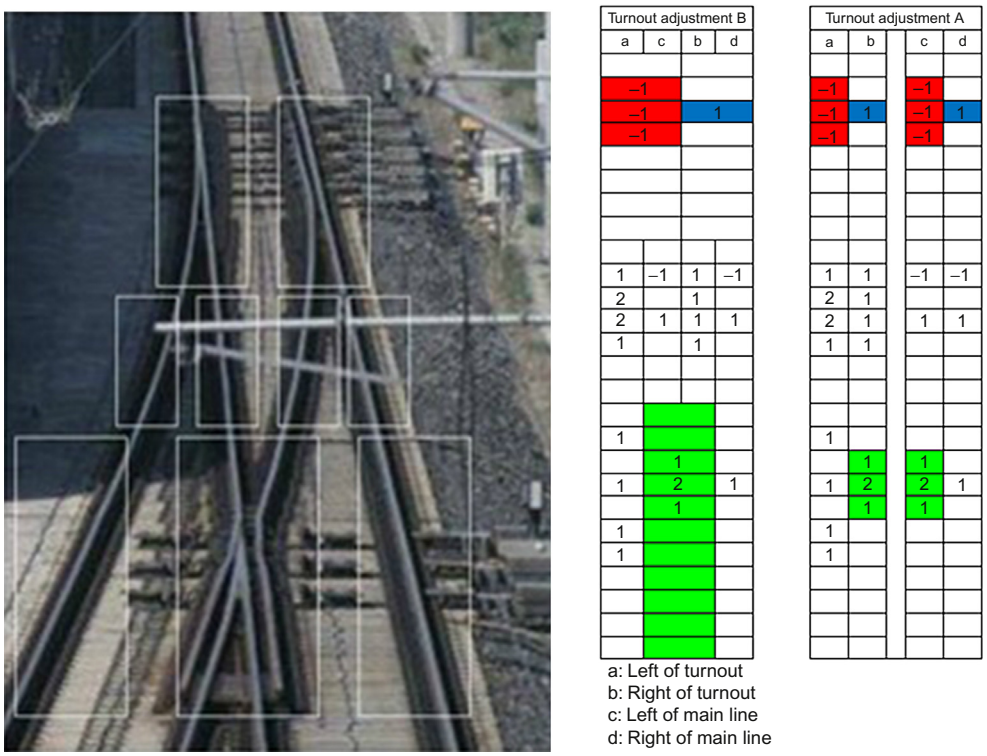

FIGURE 12.26

Interaction during joint debugging of main and diverging tracks.

12.4.3 BASIC REQUIREMENTS

1. Joint debugging of main and diverging tracks

   The structure of a turnout determines the interactive nature of rails in main and diverging lines at both switch and crossing, as the straight stock rail connects with the curved switch rail and the straight switch rail connects with the curved stock rail at the switch, while the curved and straight guiding rails are connected at the crossing, as shown in Figure 12.26. For joint debugging of main and diverging tracks, an adjustment value will be given for the key positions of the turnout, such as the connection parts of straight stock rail and curved switch rail, straight switch rail and curved stock rail at the switch, and that of curved and straight guiding rails at the crossing. Both tracks must be preferably acceptable, or, at a minimum, the main line must satisfy the acceptance standards for high speed, and the diverging line may satisfy standards for ordinary speeds. If the minimum requirements are not met, the turnout products will be inspected for qualification.
2. Reference versus nonreference rail

   To minimize adjustments and simplify the adjusting work, a rail will be defined as the reference rail to represent the longitudinal level and alignment of a turnout. If this rail is qualified

after adjustment, it means that the turnout integral geometry is acceptable. The other rail in the same track is the nonreference rail; if an adjustment is made, the cross level and track gauge of the turnout may change accordingly. If this rail is qualified after adjustment, it means that all geometric parameters in the turnout zone are acceptable. In China, the straight stock rail is defined as the reference rail for longitudinal level of the track, and the outer guiding rail is defined as the reference rail for track alignment.

3. Rational operation sequence

   The accurate adjustment of a turnout is performed as per the following operational sequence to reduce repeated work.

   a. From whole to part. This can be understood in two ways. First, the reference rail is adjusted before the nonreference one. Second, long-wavelength irregularity is controlled before its short-wavelength counterpart
   b. From main to diverging track. This measure aims to ensure riding quality in the main line; and
   c. From longitudinal level to alignment. During longitudinal level adjustment, the fastenings will be disassembled to aid the arrangement of the riser block beneath the tie plate. But an adjustment to alignment may be realized by regulating the gauge block, eccentric sleeve, or similar components, without the necessity of changing the height of the tie plate. This means that alignment adjustment is workable during longitudinal level adjustment; however, longitudinal level adjustment cannot be performed during alignment adjustment.

4. Minimum adjustment

   Certain principles shall be observed to minimize adjustment quantity, and to enable qualified turnout geometry with a minimum adjustment.

12.4.4 ANALYSIS SOFTWARE [162,163]

In China, certain adjustment software applications are employed for the adjustment (coarse and fine) work during the construction of ballastless turnout. In the Microsoft Excel-based software, the absolute spatial coordinates of the reference rail are controlled with the basic elements of longitudinal level and alignment (main direction), and the geometry of the nonreference rail is controlled with cross level and track gauge. When all indicators (e.g., longitudinal and cross level, alignment, gauge, plane twist, and variation rate of long- or short-wavelength longitudinal and cross level) are acceptable, the optimum adjustment quantity can be calculated as per integer linear programming, or possibly modified by manual adjustment. The adjustment software (Figure 12.27) includes two geometric conditions (height and plane) and irregularities in the main and diverging lines. The change of an irregularity may lead to changes in other irregularities. In the software, inordinate values are highlighted by a red background. The irregularity values before and after adjustment can be displayed graphically, as shown in Figure 12.28.

12.5 DYNAMIC DETECTION AND ACCEPTANCE OF HIGH-SPEED TURNOUT

1. Dynamic detection

   In the process of dynamic detection, inertial base platforms equipped with gyro, accelerometer, and laser measuring apparatus are used. In addition, the track inspection car

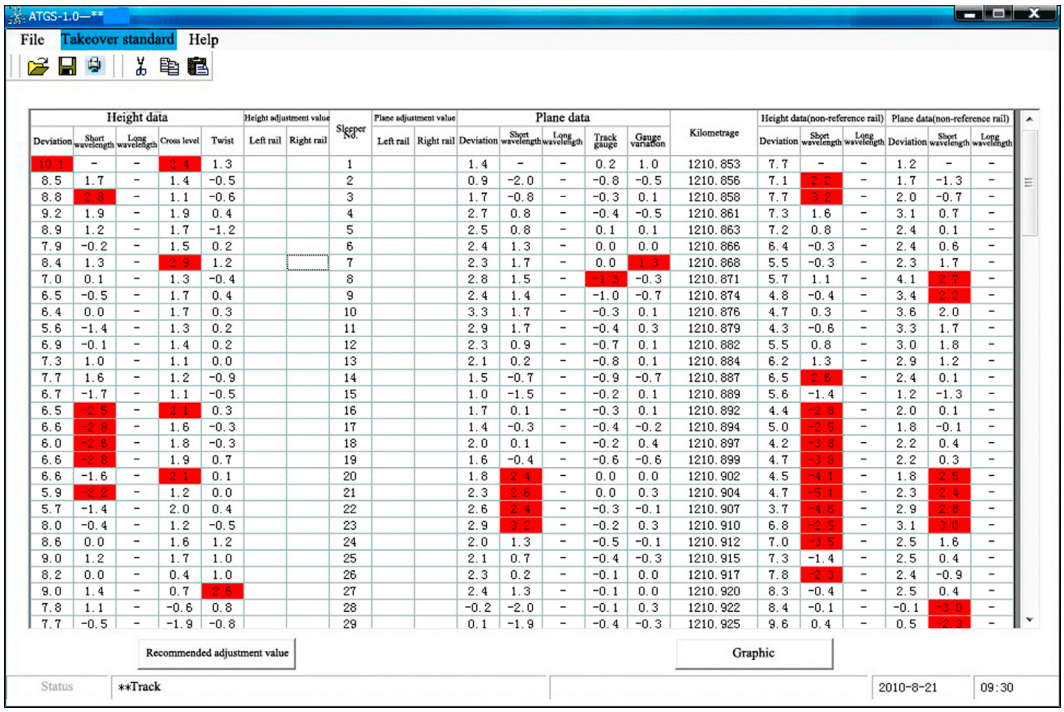

FIGURE 12.27

Interface of the adjustment software.

(precise positioning) and comprehensive inspection train are used to detect the geometry and acceleration of the dynamic response of vehicles. The comprehensive inspection train equipped with instrumented wheelset, acceleration sensor, and other measuring devices for dynamic responses is used to detect the dynamic responses of EMU trains. The main detection indicators include indicators of geometry irregularities (e.g., longitudinal and cross level, twist, track alignment, and gauge), riding indicators (e.g., vertical and lateral acceleration), and dynamic indicators (e.g., derailment coefficient and load reduction rate).

An inordinate load reduction rate is induced mainly by short-wavelength longitudinal level irregularities of the rail surface (wavelength 0.1−3.0 m, amplitude 0.5−1.0 mm), represented by inordinate flatness at the rail joint and surface, fastening defects, or abrupt change in sub-rail support stiffness. The flatness of welds and intactness of fastening and plates are the focus of field detection.

Continuous multiple-wavelength alignment irregularities, composite irregularities of alignment and cross level, and inordinate flatness on the working surface of the rail joint are the main causes of greater lateral force. Field detection focuses on alignment and cross level of the track. Detection may be aided by oscillograms. The closure status of fastenings and plates shall also be detected.

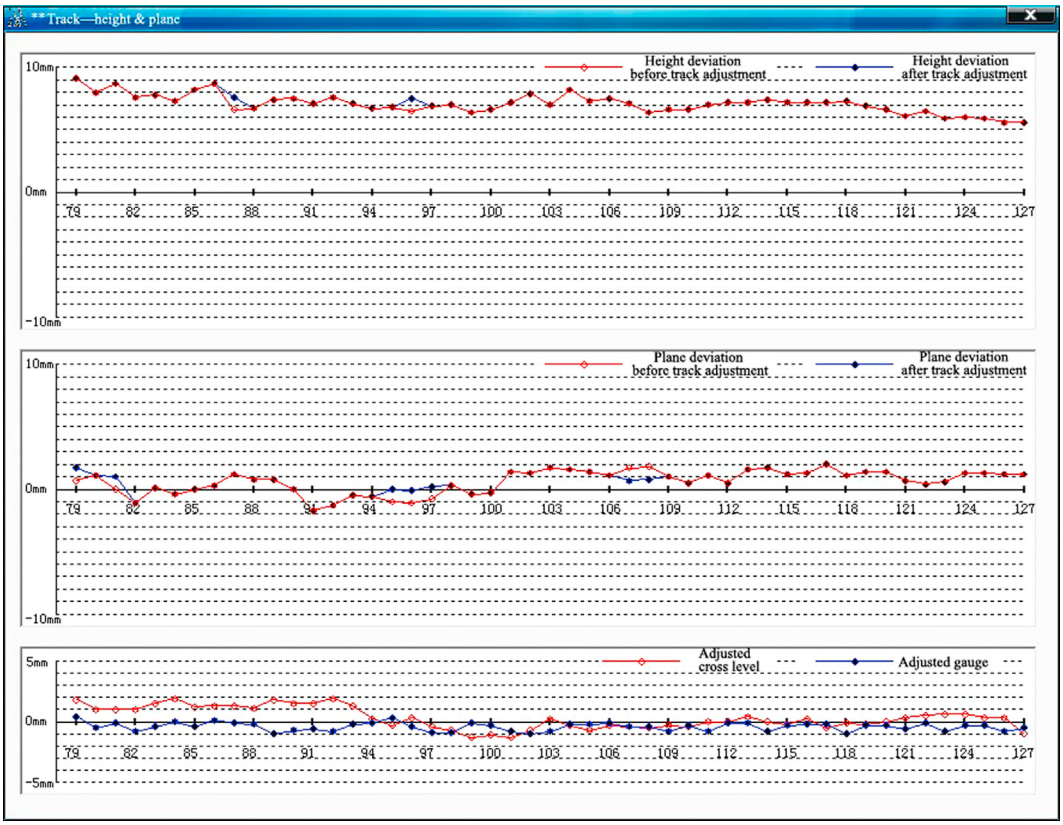

FIGURE 12.28

Graphic display of irregularity adjustment.

Greater wheel−rail lateral force or smaller wheel−rail vertical force may lead to an inordinate derailment coefficient. Welds, fastenings, deviation of track alignment and cross level, and composite irregularity of alignment and cross level of the track are the main objects of field detection.

Medium-wavelength alignment and longitudinal level irregularities of the track are the major causes of inordinate acceleration of the carbody. The light strips on the top of the switch rail and the connection quality between turnout and section are the focus of detection.

2. Dynamic acceptance standards

a. Acceptance standards for dynamic geometry irregularity

For high-speed railway lines for 250−350 km/h in China, acceptance of dynamic geometry irregularities is assessed by local amplitude and section quality, as given in Table 12.1. Local amplitude is assessed by kilometrage. In detection, it is specified that no Class II deviation is allowed, or the proportion of the railway section with Class I deviation for a single indicator shall not be greater than 5% per kilometer of line. In terms of track quality index

Table 12.1 Acceptance Standards for Dynamic Geometry Irregularities of High-Speed Railway

Classification		Acceptance Class I	Acceptance Class II	Safety Class III	Safety Class IV
Wavelength 42 m	Longitudinal level (mm)	3	5	8	10
	Alignment (mm)	3	4	6	7
Wavelength 120 m	Longitudinal level (mm)	5	7	12	15
	Alignment (mm)	5	6	10	12
Track gauge	Increase (mm)	+3	+4	+7	+8
	Decrease (mm)	−2	−3	−5	−6
Cross level (mm)		3	5	7	8
Twist (mm) (gauge length 2.5 m)		3	4	7	8
Gauge variation (‰) (gauge length 2.5 m)		0.8	1.0	–	–
Vertical acceleration of carbody (m/s^2)		/	1.0	2.0	2.5
Lateral acceleration of carbody (m/s^2)		/	0.6	1.5	2.0
Track quality index (mm)		4.0	5.0	–	–

Notes:

1. *The deviation of longitudinal level and alignment is the amplitude from the calculated zero line of the curve in the detected space to the wave crest.*
2. *Specified cant and cant runoff of the curve are not included in the cross level deviation.*
3. *The twist produced by cant runoff of the transition curve is included in the plane twist deviation.*
4. *The unbalanced centrifugal acceleration of the curved section is excluded from the deviation of lateral acceleration of the carbody.*
5. *In the table "/" represents "no requirements,"—means that the requirement is not available.*

(TQI, the sum of the standard deviation of seven irregularity indicators, i.e., longitudinal and cross level, gauge, alignment, and twist of left/right rail within a 200 m section), no Class II deviation shall occur in the whole line, and the cumulative length of the elements with Class I deviation shall not exceed 5%. Class III and IV deviations are defined as the basis for the process control and management of track geometry safety during joint debugging and commissioning. A railway section with a Class III deviation must be repaired immediately. In a railway section with a Class IV deviation, speed restrictions shall be implemented immediately, or the speed-up tests will be suspended, but may be resumed after track reconditioning.

During the acceptance tests on the dynamic geometry irregularities of the Hangzhou−Changsha line (opened in 2014) [2], no local deviations of Class II or above were detected in the whole line; railway sections with Class I deviations of gauge irregularity account for 0.18%; deviation of other indicators is 0. In addition, the average and peak TQIs are 2.2 and 3.8 mm, respectively. There is no section with a deviation of Class I or above. This implies that the construction quality of high-speed railways in China is excellent, and the technologies of laying, measurement, adjustment, and detection of ballastless track and turnout are mature in China.

Table 12.2 Assessment Criteria and Test Values for Dynamic Response Stability of EMU Trains

Item		Criteria	Test Value (Hangzhou−Changsha Line)
Derailment coefficient		≤0.80	0.38
Reduction rate of wheel load		≤0.80 Where two load reduction rate peaks occur successively at intermittent instrumented wheelset, it is determined to be inordinate.	0.59
Lateral wheelset force (kN)		$H \leq 10 + P_0/3$ (limit: 48 kN)	22.1
Lateral acceleration of frame (m/s^2)		≤8.0 (With the 0.5−1.0 Hz filtering processing, more than six vibration peaks occur consecutively.)	3.43
Excellent riding quality	Lateral	≤2.5	1.91
	Vertical	≤2.5	2.03

b. Assessment indicators for riding quality and safety of EMU train

The track must also be verified to ensure desired riding stability and quality of EMU trains at design speed. This can also offer a reference for dynamic acceptance. Table 12.2 presents the assessment indicators for riding stability. For riding quality indicators, the assessment criteria for passenger car as listed in Table 4.7 are available.

The maximum dynamic responses of an EMU train traveling at 350 km/h have been included in Table 12.2. It can be found in the table that the riding stability and quality in the section and turnout are acceptable during the passage of EMU trains, and the dynamic track geometry is favorable.

CHAPTER

13 IRREGULARITY CONTROL OF HIGH-SPEED TURNOUTS IN OPERATION

High smoothness is the most important technical requirement in high-speed turnouts, as it enables riding safety and stability. In previous chapters, the measures for ensuring high smoothness of turnouts in design, manufacturing, and laying have been highlighted. Such measures include controlling structural irregularity by optimizing wheel−rail contact, controlling dynamic irregularity during train passage by homogenizing fastening stiffness, controlling status irregularity (e.g., gaps of turnout parts) by improving accuracy in manufacturing, assembly, and laying, as well as controlling geometric regularity by accurate adjustment and strict standards of dynamic acceptance [164].

There are plenty of high-speed turnouts in use. Differences in manufacturing and laying technologies and the influence of various types of EMU trains and foundations will cause quality differences among turnouts in operation. In addition, turnout quality will degrade with increasing the traffic volume, which explains why the indicators of dynamic responses of the EMU trains exceed the limits listed in Tables 12.1 and 12.2 for certain turnouts during joint debugging, commissioning, and operation. The technologies of irregularity control for high-speed turnouts will be explored below, with cases in which the author has been involved.

13.1 STRUCTURAL IRREGULARITY INDUCED BY POOR WHEEL−RAIL RELATION

Case 1: inordinate lateral vibration acceleration of carbody induced by excessive height difference of the switch rail [165].

In China, comprehensive inspection trains, train-borne track inspection devices, etc. are used to inspect the track periodically during operation. Local irregularity (peak value) and sectional integral irregularity (mean value) are the two indicators for dynamic quality management.

1. Turnout #2 in Huangdu Station in the Beijing−Shanghai high-speed railway line

   Turnout #2 is a No. 42 ballastless turnout in the up line, made of 60 kg/m rails from CNTT Chinese New Turnout Technologies Co., Ltd. The turnout is of the plane line type of "easement + circular + easement" curve (radii of 10,119 m/4100 m/∞, respectively). It is 136.926 m long. The switch rail employs unique FAKOP technology from BWG. And the chainage of the point

Design of High-Speed Railway Turnouts.

of the switch rail is K1303 + 438 m. At the top width 15 mm of the switch rail, the stock rail will bend outward by 15 mm with a radius of 1600 m. Therefore, the actual top width of the switch rail at this part will be 30 mm.

The turnout is laid on Yunzaobin Bridge, on piers #4−10. The layout of the bridge span is 24.7 m + 4 × 32.7 m + 24.7 m. The bridge beams are single-box double-chamber continuous beams of cast-*in-situ* prestressed concrete, with the chainage of K1303 + 426 m−K1303 + 596 m. The plane and vertical section is of horizontal slope and straight line.

The train approaches the turnout from the turnout front for passage in the main line. For CRH380A and CRH2 EMU trains, traveling speeds of 295 and 245 km/h are considered, respectively. No passage in the diverging line is considered currently.

2. Results of dynamic inspection

The Beijing−Shanghai line was opened to traffic on June 30, 2011. Since then, dynamic inspection results of this turnout have been on the downgrade; in particular, the lateral vibration acceleration of carbodies keeps increasing. Three inspection devices have been adopted, with results as follows:

Portable train vibration analyzer: The lateral acceleration of carbodies of two types of vehicles (CRH380A and CRH2) exceeds the maintenance standard to varied degrees. For CRH380A, the mean amplitude of lateral acceleration of carbody is 0.08 *g*, and the maximum acceleration is 0.14, both below the level III standard (urgent repair) of 0.15 *g*. People may feel slight shaking in certain carbodies. For CRH2, the mean amplitude of lateral acceleration of a carbody is 0.13 *g*, and the maximum acceleration is 0.22 *g*, which exceeds the level IV standard (speed restriction) of 0.2 *g*. Therefore, people can feel obvious lateral shaking during passage in the turnout.

Train-borne track inspection device: The detection data of this device resemble those of the portable train vibration analyzer. Specifically, for CRH380A, the mean amplitude of lateral acceleration of a carbody is about 0.09 *g*, and the maximum acceleration is below level III standard. For CRH2, the mean amplitude of lateral acceleration of carbodies is about 0.11 *g*, and the maximum acceleration is about 0.16 *g*, beyond the level III standard.

Comprehensive inspection train: The detection results of this device also reflect the fact that the turnout is characterized by great lateral acceleration of carbodies, with a peak value of about 0.12 *g*, exceeding the level II standard (comfort) of 0.09 *g*. The turnout has been speed-limited (160 km/h) since October 5, 2011. However, significant lateral acceleration of carbodies exists when a comprehensive inspection train travels in the turnout at 160 km/h, with the peak value being about 0.06 *g*, equaling the level I standard (frequent maintenance) of 0.06. Detection details are given in Figure 13.1. In addition, greater gauge and alignment irregularities occur at the switch; the gauge irregularity is formed by the bending of stock rail, while the alignment irregularity is a structural irregularity produced by variation of wheel−rail contact points. As demonstrated by the analysis of design theory, the two types of irregularity are the major causes of inordinate lateral acceleration of carbodies.

Despite the different results, there is evidence of inordinate lateral acceleration of carbodies in the turnout for the three detection devices, but to varying degrees.

3. Improvement of track geometric irregularity before speed restriction

Regarding the inordinate lateral acceleration of EMU trains in turnout #2 in Huangdu Station, it was first assumed by the Shanghai railway bureau that the problem was due to lateral turnout

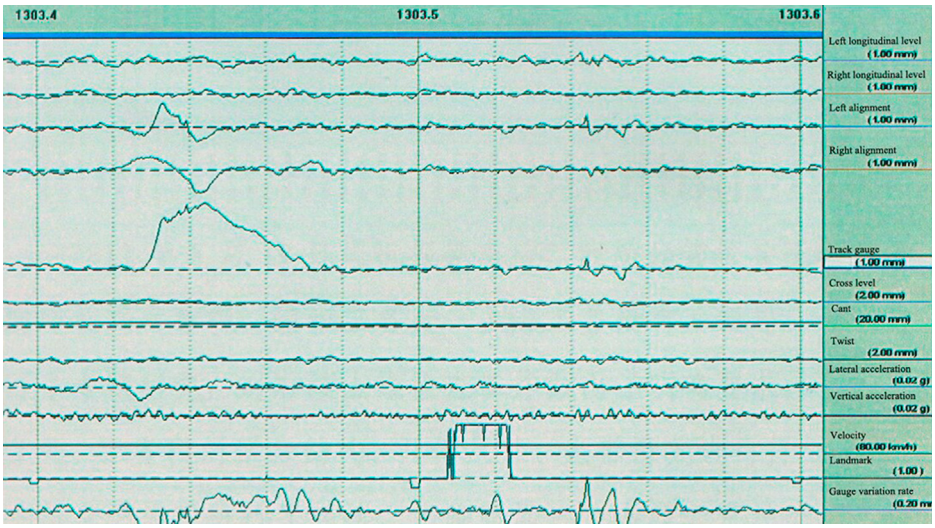

FIGURE 13.1

Detection results of dynamic inspection devices after speed restriction.

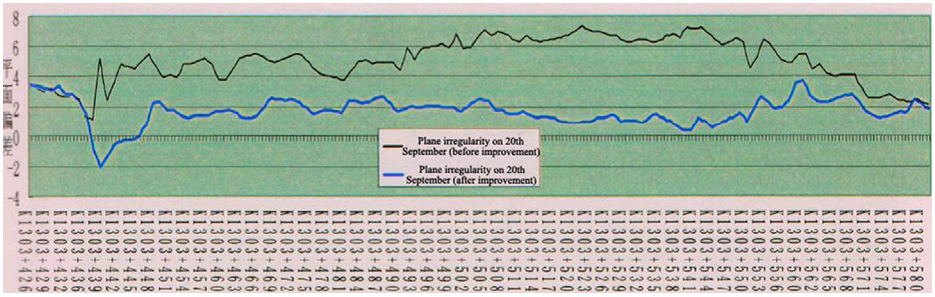

FIGURE 13.2

Plane deviation of turnout #2 in Huangdu Station.

geometric irregularity. For that, a track inspection car was used in CPIII to detect the plane deviation of the turnout. In Figure 13.2, the upper line represents the plane deviation with the straight switch rail as the reference rail, that is alignment irregularity [x-axis = kilometrage (m); y-axis = -plane deviation (mm)]. According to the measurement, the turnout is located in the scope of the long-wavelength alignment irregularity (wavelength: 150 m, amplitude: 7 mm) and meets the acceptance standard for track static geometry of high-speed railways in China (see Chapter 12 for details). However, the fastenings are adjusted by ties with accurate adjustment technology to maintain the peak alignment irregularity within −2 to +3 mm, as depicted by the lower line in Figure 13.2. Detection by train-borne track inspection device and portable train vibration analyzer

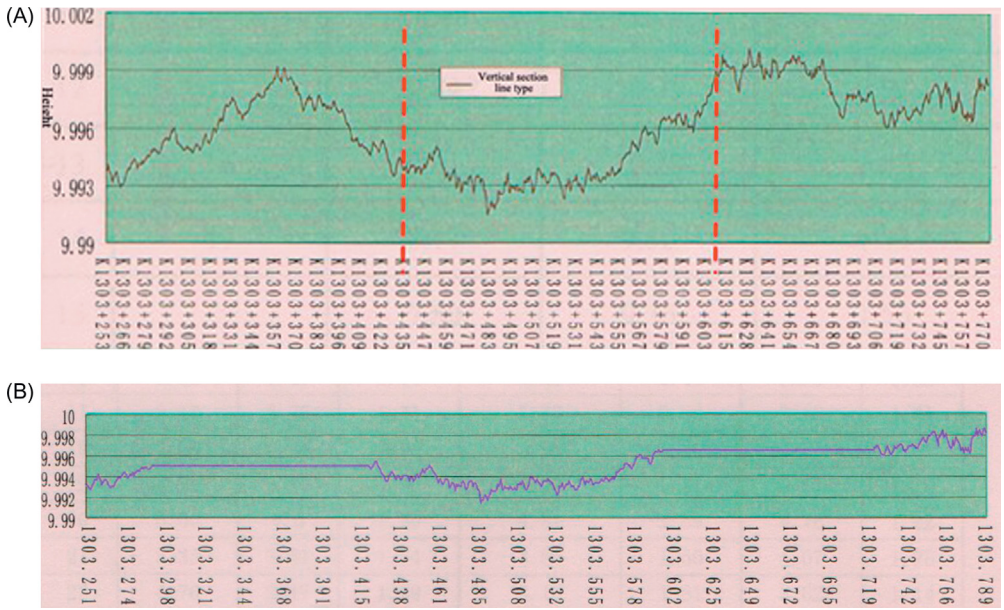

FIGURE 13.3

(A) Height difference of #2 turnout in Huangdu Station before improvement. (B) Height difference of turnout #2 in Huangdu Station after improvement.

demonstrates a smaller lateral acceleration of carbodies (reduced by approximately 0.01−0.03g), but the improvement is far from satisfactory.

Later, it was assumed that the track irregularity of the adjoining sections of the turnout led to the shaking of carbodies, and the vibration was intensified in the turnout, leading to inordinate acceleration. Therefore, an inspection car was used to detect horizontal and vertical plane deviation in the turnout and 160−180 m adjacent sections, as shown in Figure 13.3A [x-axis = kilometrage (m); y-axis = height (m)]. Results showed that longitudinal level irregularity (wavelength: 150 m, amplitude: 6 mm) exists in the sections adjacent to the turnout, and the height deviation is about 3 mm in the turnout area; however, both values are within the acceptance standard for track static geometry in high-speed railways in China. The longitudinal level irregularity in the sections adjacent to the turnout is regulated within 150 m to eliminate the effects. Figure 13.3B shows the detection results [x-axis = kilometrage (m); y-axis = height (m)]. The detection by train-borne track inspection device and portable train vibration analyzer demonstrates no significant change in the amplitude of lateral acceleration of carbodies.

The closure status of the turnout parts had also been detected by maintenance staff of the bureau as per Chinese code TB/T3302-2013, and was proved to be acceptable. This reveals that no status irregularity that can cause lateral movement of carbodies exists in the turnout. Moreover, the contact light stripe on the rail top of the turnout had been detected as per TG/GW 115-2012. Results showed that the light stripe is located in the middle of the rail top and is about 20−30 mm wide. This indicated that the wheel−rail contact relation is in a good state

FIGURE 13.4

Measuring the height difference of switch rail with a depth gauge.

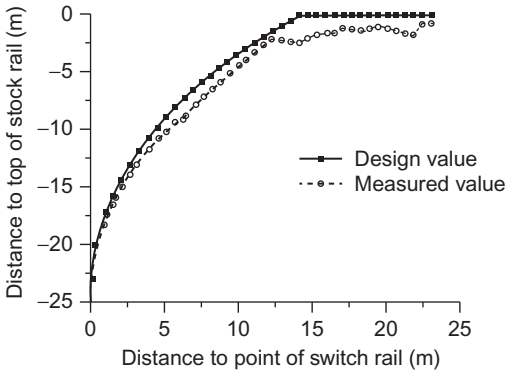

FIGURE 13.5

Measured height difference of the top of switch rail.

and will not affect riding quality in the turnout. Thus, speed restriction was applied to the turnout before learning the actual cause of the inordinate acceleration.

4. Inspection of height difference of top of switch rail

   Field detection was performed tie by tie on the height difference of rail tops between straight switch rail and curved stock rail. The detection method is shown in Figure 13.4. The comparative results of measured and design values are shown in Figure 13.5. According to the results, the actual height difference of the straight switch rail is typically greater than the design value. The deviation of height difference is particularly great within the transition scope of wheel load from stock rail to switch rail, with the peak value being about 2.3 mm, exceeding the limit value of 1 mm as specified in TB/T3302-2013.

   According to the turnout dynamics theory in Chapter 4, the dynamic responses during the passage of an EMU train at 295 km/h in the main line from turnout front can be analyzed, and the measured data and design values can be compared, as shown in Figure 13.6 (distance to turnout front is negative). The calculation shows that, during the passage, at design height difference of rail top, the amplitude of lateral acceleration of a carbody is about 0.016 g. However, at the actual height difference of the switch rail, the amplitude of lateral acceleration of carbodies is greater, about 0.037 g. The simulation results are smaller than the actual detection results by the comprehensive inspection train, as the horizontal and vertical plane height difference was not included in the simulation.

5. Improvement of height difference of switch rail

   A number of plates with sizes ranging from 1−2.5 mm were customized by the Shanghai railway bureau to justify the predication of turnout dynamics theory. In this process, plates of varied thicknesses are laid between the base of the switch rail and the slide bedplate to lift the switch rail as per the deviation of height difference of the top of the switch rail (see Figure 13.7). Figure 13.8 presents the comparative results of the height difference after improvement and the design value.

   When an EMU train travels at normal speed (not speed-restricted) in this turnout, such as a CRH380A train traveling at 295 km/h and a CRH2 train at 245 km/h, the detection results

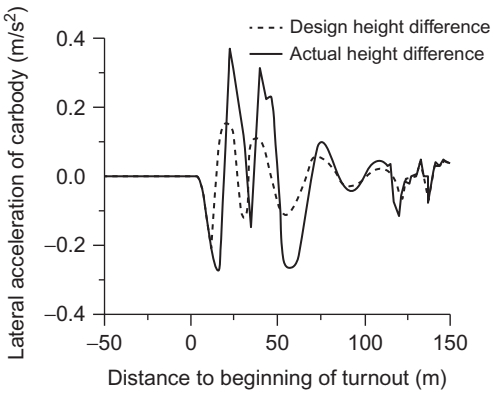

FIGURE 13.6

Simulation of lateral acceleration of carbody.

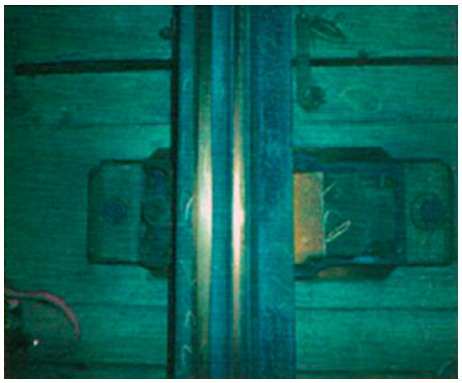

FIGURE 13.7

Plate under the switch rail.

(train-borne track inspection device and portable train vibration analyzer) showed that the amplitude of lateral acceleration of a carbody is below the level I standard (frequent maintenance). But this value is above the level II standard immediately after removing the tie plate from beneath the switch rail; in this circumstance the lateral acceleration of carbodies detected by the train-borne track inspection device during the first trial run of an EMU train is 0.11 *g*. This proves that the turnout dynamics theory is rational, that is, excess height difference of the switch rail leads to inordinate lateral acceleration of a carbody. Further, the deviation of this height difference may be rooted in manufacture, assembly, or laying error.

The tie plate beneath the switch rail is unsecured, applicable to tests only, instead of being regarded as a permanent improvement measure. After analysis of the structure of the slide plate (Figure 13.9), it was recommended to meet the design requirements for the switch rail by lifting the slide plate and applying slide plates of different depths to different ties. The turnout was checked by a comprehensive inspection train after 1 year of speed restriction release. The results are given in Figure 13.10. This demonstrates that no lateral acceleration of carbodies exceeds level I standard. This means that the problem of inordinate lateral acceleration of carbodies in turnout #2 in Huangdu Station in the Beijing−Shanghai line was eventually solved.

In the application of French technology to high-speed turnouts in the Hefei−Nanjing line, there were problems such as excessive height differences of switch rails, backward shift of wheel-load transition scope, and inordinate lateral acceleration of carbodies, which were solved by replacing the switch rail.

13.2 GEOMETRIC IRREGULARITY

Case 2: inordinate lateral vibration acceleration of carbody induced by long-wavelength irregularity

1. Inordinate lateral vibration acceleration during the passage of train in the turnout

   The Beijing−Tianjin intercity railway was the first high-speed railway line in China mainland. In this railway, No. 18 high-speed turnouts of CNTT are used, with allowable speed in the

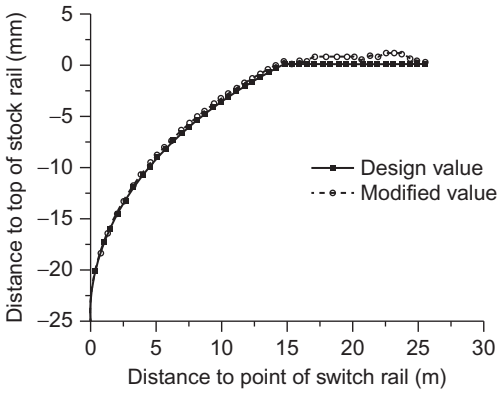

FIGURE 13.8

Height difference of top of switch rail after improvement.

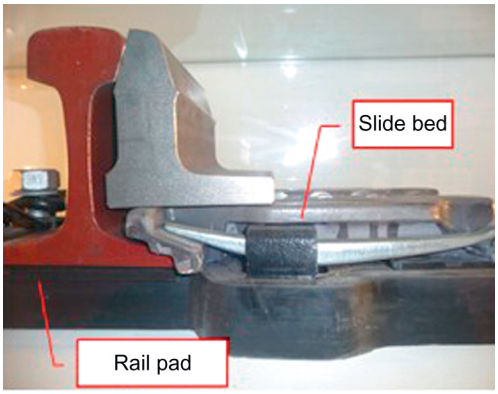

FIGURE 13.9

Structure of slide bed.

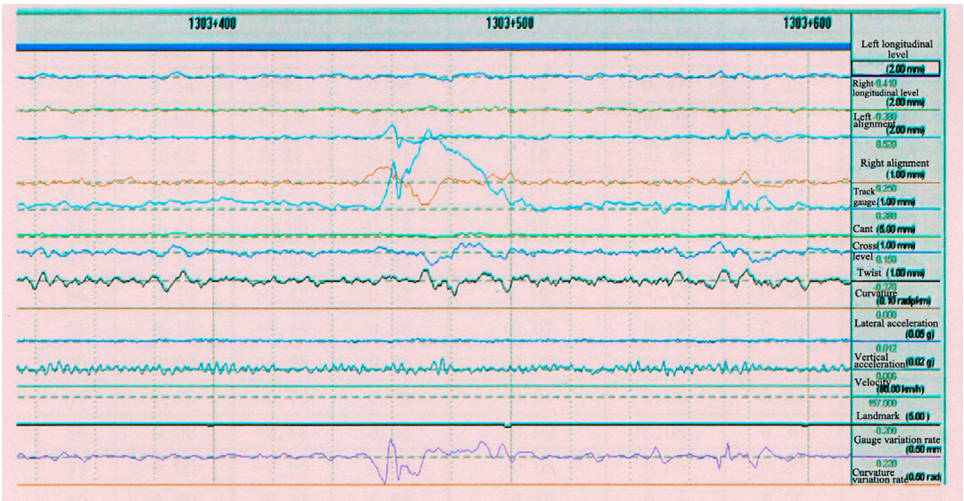

FIGURE 13.10

Detection results by dynamic inspection car after 1 year of improvement.

main line being 350 km/h. However, in the early days of operation, the Yizhuang Railway Station ran into a problem with the lateral acceleration of carbody exceeding level I standards when the train traveled in the turnout at high speed. A track inspection car was used to measure the height and plane deviation of the straight stock rail of the turnout (as indicated by the solid line in Figure 13.11). In the figure, the upward direction is positive for height deviation, and the direction to the outside of stock rail is positive for plane deviation. From the figure, it can be seen

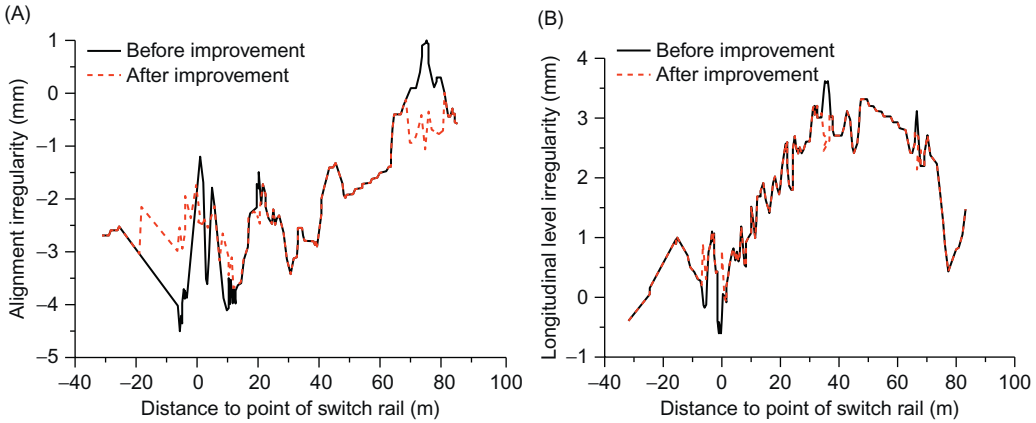

FIGURE 13.11

(A) Height deviation of turnout. (B) Plane deviation of turnout.

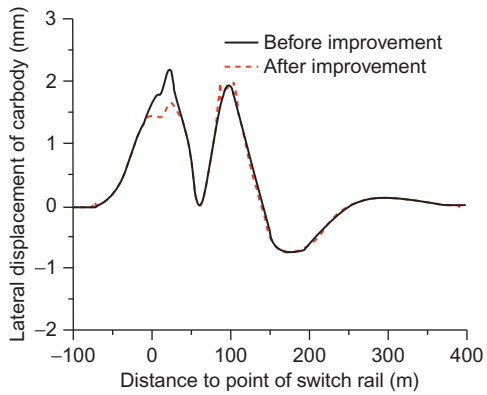

FIGURE 13.12

Lateral displacement of carbody.

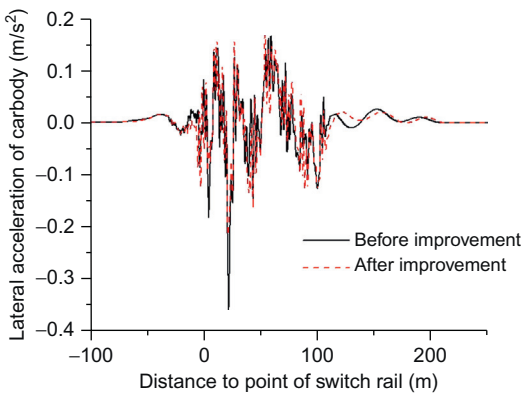

FIGURE 13.13

Lateral vibration acceleration of carbody.

that the turnout is located in the longitudinal level and alignment irregularity with regard to the full length of the turnout. This is obviously caused by construction error. The height and plane deviation of the other rail resembles the case of straight stock rail.

2. Improvement of turnout geometry irregularity

By adjusting the longitudinal and cross level of partial fastenings on site, the geometric deviation was eliminated by over 3 mm. The height and plane deviation of the turnout after improvement is demonstrated by the dotted line in Figure 13.11.

The fastenings were adjusted slightly, leaving a maximum height and plane deviation of 3 mm. Nevertheless, the effect is remarkable. The field operation revealed that the lateral acceleration of a carbody was below the level I limit during passage in the turnout at high speed. Meanwhile, according to the dynamic simulation (see Figures 13.12 and 13.13), when a

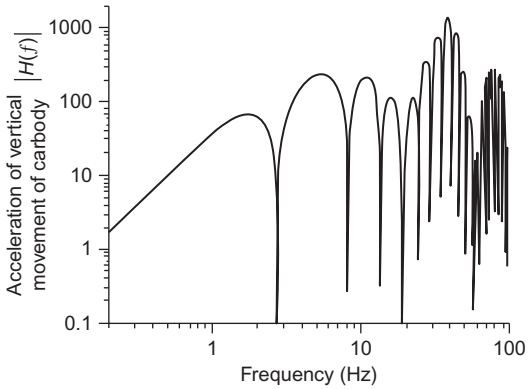

FIGURE 13.14

Acceleration spectrum of vertical movement of carbody.

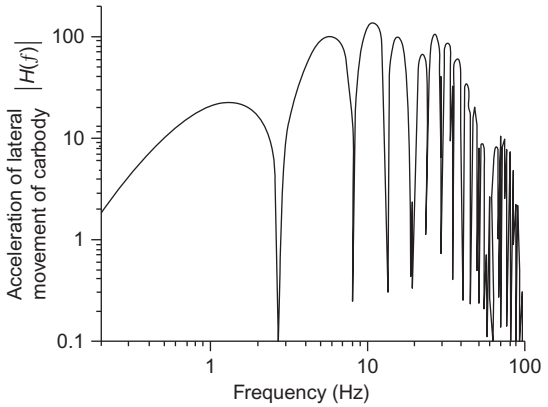

FIGURE 13.15

Acceleration spectrum of lateral movement of carbody.

high-speed train travels in the main line of the turnout at 350 km/h, the lateral displacement of carbodies is reduced insignificantly, from 2.2 to 1.7 mm at the switch. However, the lateral acceleration of a carbody at the switch is reduced significantly, from 0.036 to 0.022 *g*.

3. Analysis of train vibration induced by long-wavelength irregularity

A combination of pseudo-excitation method [166,167] and symplectic method [168,169] is employed to study the random 3D coupled vibration of the vehicle−track system. Figure 13.14 depicts the amplitude−frequency curve of the transfer function between the longitudinal level irregularity of the track and vertical movement vibration response of a carbody, while Figure 13.15 depicts the amplitude−frequency curve of the transfer function between track alignment irregularity and lateral movement vibration response of a carbody when a CRH2 train travels in the section at 350 km/h. The first-order basic frequency is about 1.8 Hz for vertical movement vibration and 1.4 Hz for lateral movement vibration. The sensitive wavelengths of longitudinal level and alignment irregularity of the track are 54.0 and 69.4 m, respectively. The turnout (No. 18), 69 m long, equals the sensitive wavelength of alignment irregularity, causing a "1 Hz vibration" in EMU trains. Therefore, even a slight improvement of the plane deviation of the turnout can enhance the lateral stability of the running train significantly and vice versa.

Case 3: inordinate load reduction rate induced by periodic irregularity during rail rolling

1. Inordinate load reduction rate during passage of the train in the turnout [169]

The Hangzhou−Ningbo line was opened to traffic on July 1, 2013. The railway adopted ballastless track in the full line, and No. 18 high-speed turnouts developed by China (main line speed: 350 km/h + 10%). The turnouts are provided by China Railway Construction Heavy Industry Co., Ltd. The turnout rails use U71Mnk rails produced by WISCO. In joint commissioning and debugging before operation, many station turnouts ran into a problem with the wheel-load reduction rate exceeding the limit given in TB10761-2013, that is 0.8. On March 29, 2013, when the CRH380A-001 comprehensive inspection train traveled in #1 No. 18 turnout

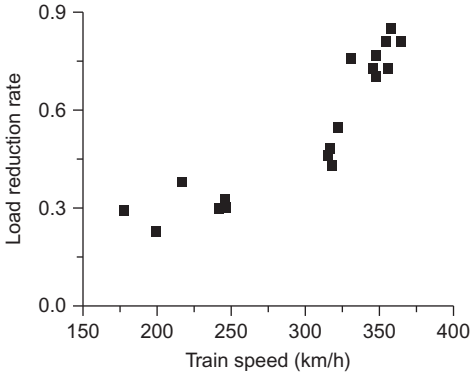

FIGURE 13.16

Load reduction rate.

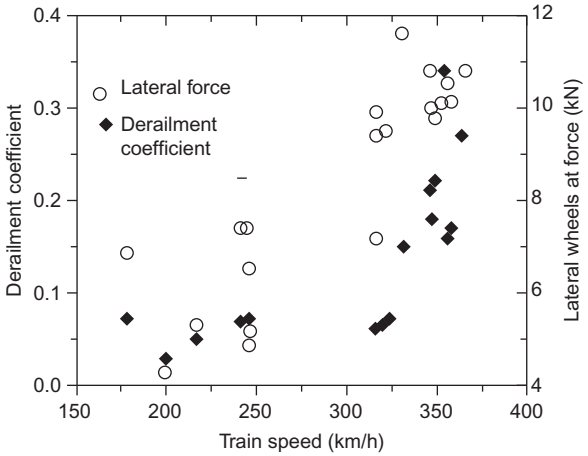

FIGURE 13.17

Derailment coefficient and lateral wheelset force.

in Shaoxing North Railway Station at 353.8 km/h, the peak wheel-load reduction rate was 0.81. As revealed by ground dynamic tests performed in parallel on the turnout, the load reduction rate exceeded 0.8 for more than one trip of an EMU train, and the peak value was 0.85. The test results are given in Figure 13.16. The derailment coefficient and wheelset lateral force obtained by ground test are shown in Figure 13.17, increasing with rising train speed, but within allowable limits (0.8 and 48 kN, respectively). The turnout geometry measured by the comprehensive inspection train was also acceptable. Ground inspection showed that the turnout geometry and wheel−rail relation were in good state; no damage or obvious rail corrugation existed on the rail surface, and the flatness of welded joints of the rail was within allowable limits (0.3 mm/m).

2. Detection results of rail corrugation gauge

An RMF 2.3 rail corrugation gauge of the German company Vogel & Plötscher was used to measure the surface flatness of turnout rails in the main line (see Figure 13.18 for measured results). In Figure 13.18, the red line represents straight stock rail, and the green line the inner rail. The irregularity of the rail in the turnout is greater than that in the section, and that at the crossing is greater than that at the switch, with the irregularity at the transition lead curve being the lowest. As specified in the technical conditions for delivery of 60 kg/m rail for 350 km/h high-speed railways in China, the vertical flatness of the rail must not exceed 0.3 mm/3 m and 0.2 mm/1 m. It can be seen that the turnout rail was beyond this limit, and the section rail was acceptable.

The RMF 2.3 rail corrugation gauge has a measurement span of 2.2 m and accuracy of 0.01, applicable to the wavelength of 0.01−3.0 m, as shown in Figure 13.19. The amplitude spectrum of rail irregularity can be obtained through spectrum analysis of the measured results, which is shown in Figure 13.20. In the figure, the first-order and second-order basic frequency wavelengths are 1.9 and 1.6 m, respectively. As for the amplitude spectrum of rail irregularity at the

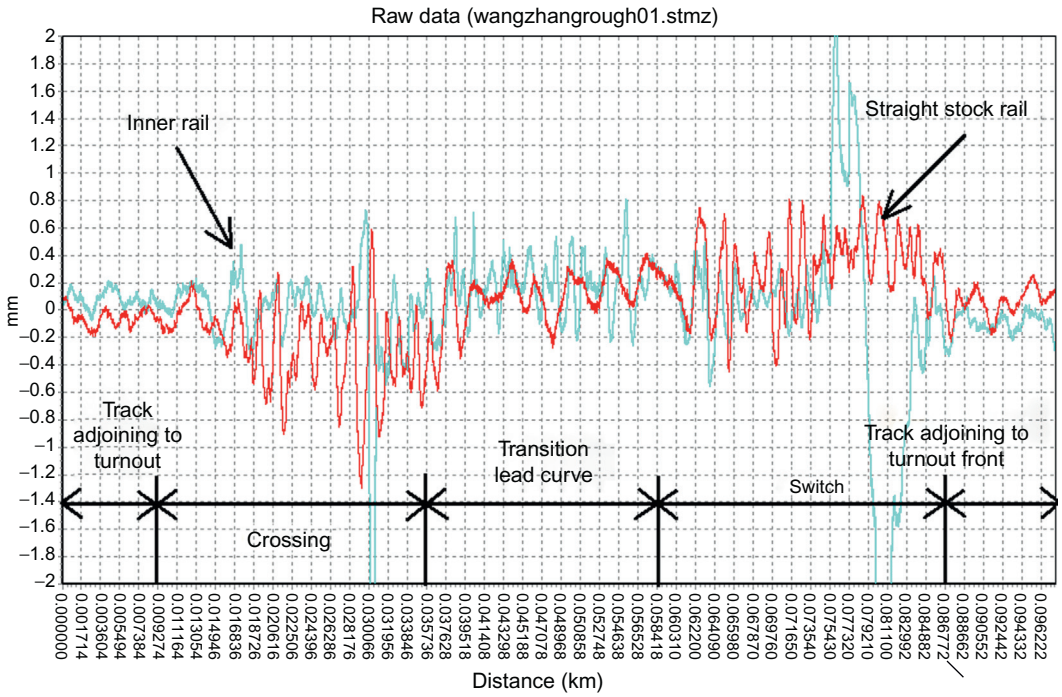

FIGURE 13.18

Flatness of rail surface in the turnout.

FIGURE 13.19

RMF 2.3 rail corrugation gauge.

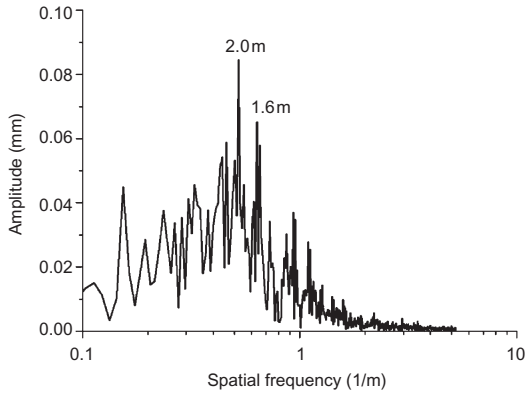

FIGURE 13.20

Amplitude spectrum of rail irregularity.

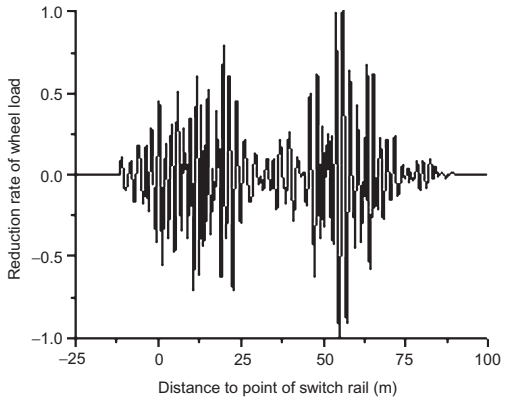

FIGURE 13.21

Distribution of load reduction rate when a train travels in the turnout.

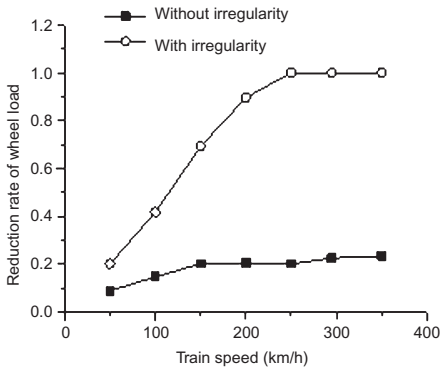

FIGURE 13.22

Variation of load reduction rate with train speed.

crossing, the first-order and second-order basic frequency wavelengths are 2.4 and 1.6 m, respectively. The frequency spectrum at the switch is the same as the basic frequency of the rail in the entire turnout. At the transition lead curve, the first-order and second-order basic frequency wavelengths are 4.1 and 3.1 m, respectively, which are approximated as the multiple of 0.4 and 0.8 m, respectively.

3. Results of turnout dynamic simulation

   A dynamic simulation was performed on the turnout, with an EMU train traveling in the main line at 350 km/h. The simulation results show that the maximum load reduction rate is about 0.81, 1.0, and 0.26, respectively, at the switch, crossing, and transition lead curve, as shown in Figure 13.21. The reduction rate of the wheel load increases significantly with added train speed. In order to maintain the load reduction rate below the limit (0.8), the train's speed in the turnout must not exceed 160 km/h. If the rail is absolutely smooth (without irregularity), as shown in Figure 13.22, the load reduction rate will increase at a smaller rate with added train speed. The simulation results are slightly larger than the results of the ground test. This is because the ground test has fewer measuring points, with no measuring points arranged at the most unfavorable positions. The simulation results also show that the vertical irregularity of turnout rails leads to inordinate wheel-load reduction rate when a train travels in the turnout at high speed.

4. Analysis of causes of periodic irregularity produced during rail rolling [170]

   High-speed railways require rails of high straightness. In China, major rail manufacturers (Ansteel, Baotou Steel, and WISCO) have all had their production lines reformed, and have replaced their former tension straightening process with compound ones. The vertical−horizontal combined straightener is a roll-straightening machine equipped with an upper row and a lower row of rollers, where the rails will be subjected to elastic-plastic bending forward and backward between the two rows, eventually being straightened. For instance, the vertical−horizontal combined straightener at WISCO, introduced by SMS of Germany, is

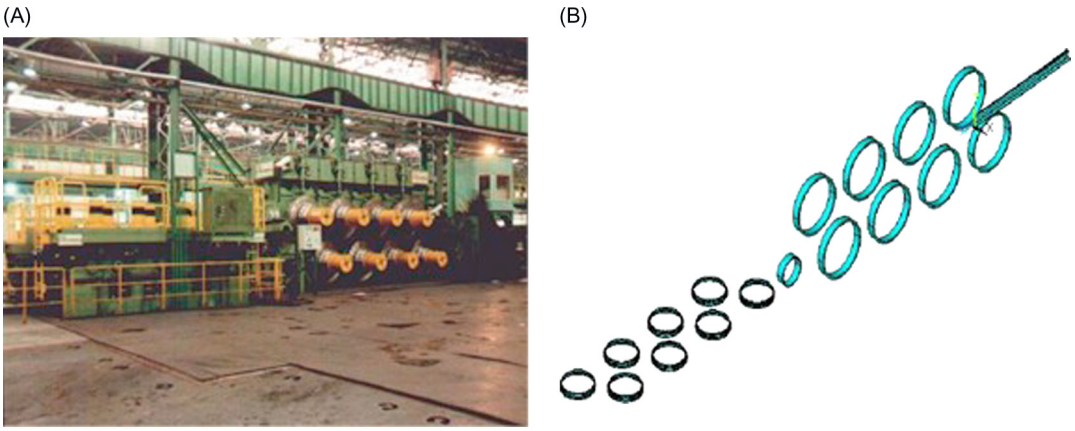

FIGURE 13.23

(A) Horizontal−vertical combined straightener. (B) Schematic diagram of rail straightening process.

composed of nine horizontal rollers and eight vertical rollers, as shown in Figure 13.23A. The horizontal rollers work at straightening the rails vertically, and the vertical rollers straighten the rails horizontally. No. 1−8 horizontal rollers have diameters of 110−1200 mm, and No. 9 roller has a diameter of 600 mm. These straightening rollers have a horizontal spacing of 1600 mm and vertical spacing of 900−1400 mm, with a maximum straightening force of 3600 kN. Figure 3.23 presents a schematic diagram of the rail straightening process.

The horizontal spacing of horizontal rollers is identical to the second-order basic frequency wavelength of vertical irregularity of the rail, as given in Figure 13.20. The horizontal spacing of the upper and lower rows of rollers is 0.8 m. Coincidentally, the first- and second-order basic frequency wavelengths of rail irregularity at the crossing and transition lead curve is approximated an integral multiple of 0.8 m. This indicates that the irregularity of the turnout rail is the periodic irregularity produced during the straightening process, which is caused by insufficient accuracy in the upward-and-downward process of the horizontal rollers. This irregularity may be eliminated by improvement of the process. The inordinate load reduction rate during the passage of high-speed trains in the turnout can be solved by replacing the existing rails with inadequate straightness.

Case 4: inordinate load reduction rate induced by welded joint irregularity

When a train travels at high speed, even a small-amplitude rail irregularity can lead to intense impact vibration to wheels and rail, producing great wheel−rail force. Short-wavelength irregularities on a rail surface can not only trigger intense wheel−rail impact, but can also cause a drop of wheel-load reduction rate, rail fracture, or even a derailment accident. In addition, it can produce significant wheel−rail noise during high-speed traffic [171,172].

Figure 13.24 presents the measured welded joint irregularity of thermite welding at the heel of switch rail of a No. 18 turnout. The peak irregularity within 1 m is 0.7 mm, exceeding the Chinese limit of 0.3 mm/1 m. Figure 13.25 gives the load reduction rate measured when a comprehensive

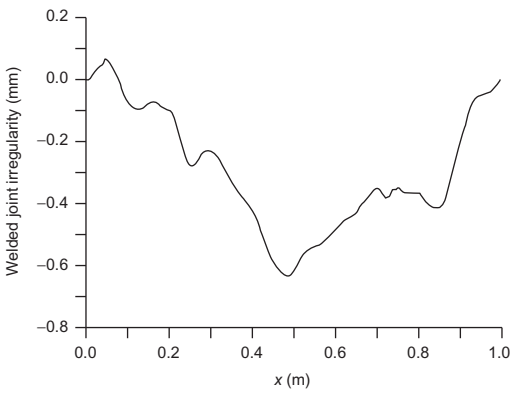

FIGURE 13.24

Welded joint irregularity.

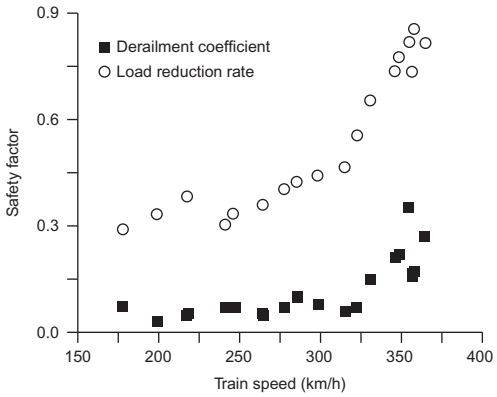

FIGURE 13.25

Change of load reduction rate with train speed.

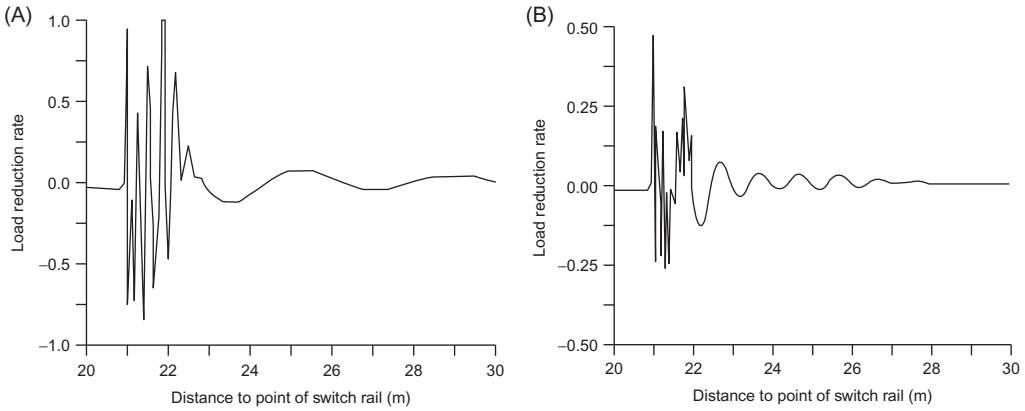

FIGURE 13.26

(A) Load reduction rate at an irregularity of 0.7 mm/1 m. (B) Load reduction rate at an irregularity of 0.3 mm/1 m.

inspection train travels at different speeds on the welded joints; the load reduction rate increases almost linearly with the train speed.

As shown by turnout dynamic simulation, the peak load reduction rate can be up to 1.0 when a train passes through the welded joint irregularity at 350 km/h, and the wheel load will fluctuate intensely, producing high-frequency vibration. For an irregularity of the same shape, if the irregularity is 0.3 mm, the calculated peak load reduction rate will be about 0.47, below the allowable limit 0.8. Figure 13.26 presents the distribution of load reduction rate under two different amplitudes of irregularity. If the welded joint irregularity of the rail exceeds 0.3 mm/1 m, the rail must be ground, or be disconnected and rewelded.

FIGURE 13.27

Scant displacement of switch rail of No. 38 turnout.

13.3 STATUS IRREGULARITY

13.3.1 FIELD SURVEY

Before the mass construction of high-speed railways, a pilot passenger-dedicated line was built between Qinhuangdao and Shenyang in China. It covers about 404 km and has a design speed of 250 km/h; it was opened to traffic on October 12, 2003. The passenger line (PDL) adopted No. 30 turnouts developed by China for the entire line. However, it suffered poor riding stability and comfort due to problematic and defective turnouts. Those turnout defects provided valuable experience for the development of high-speed turnouts in China. The following major turnout defects were detected in the field investigation.

1. Significant scant displacement of switch rail and swing nose rail

   As shown in Figure 13.27, the gauge in the rear of the switch rail and point rail (between the last traction point and the heel) was generally small. The gap between the jacking blocks was large. Many jacking blocks were disconnected. The maximum gauge decrease was 6 mm. According to the detection by rail inspection car, the geometric deviation is of level II inordinateness.

   The following causes are found by analysis:

   a. The switch rail and point rail suffered great switching resistance due to large friction force of the slide bed, leading to potential conversion failure
   b. The last traction point was so far from the heel of switch rail or point rail that the curvature and rise of the lateral bending in between increased, reducing the gauge as a consequence; and
   c. The gauge decrease at the traction point may have been induced by an incorrect starting position of slicing or slicing amount, and lack of shop assembly and trial laying of the stock rail, switch rail, and the switch for each turnout, resulting in intrinsic turnout defects when leaving the factory.

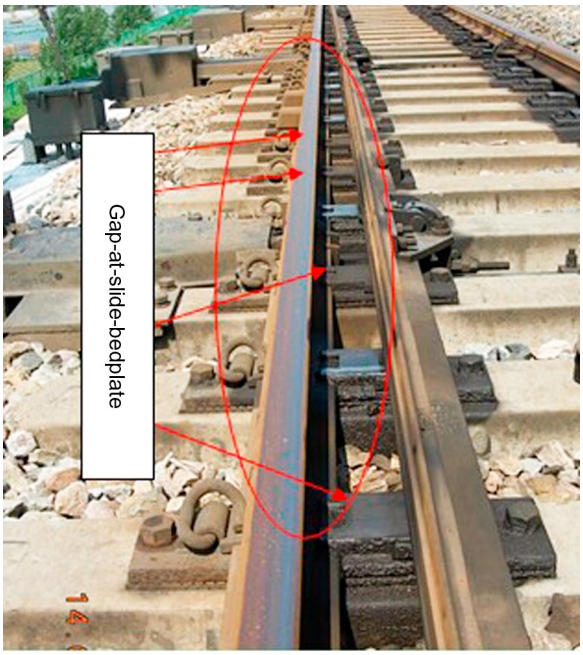

FIGURE 13.28

Gap at slide bed.

This problem may be solved by using a rollered slide bed to reduce switching resistance, optimizing the layout of traction points, improving the machining precision of rail members, and assembling the turnout at the shop.

2. Large gap at the slide bed

The switch rail and point rail are basically unsupported, as can be seen in Figure 13.28. The maximum gap is up to 2 mm, far above the maintenance standard 0.5 mm. In addition, this portion is hard to maintain. Lifting the turnout tie by track bed tamping may ensure the fit between the switch rail and slide plate, but may cause longitudinal level irregularity at the stock rail. Moreover, the lifted tie may soon sink under the dynamic impact of traveling vehicles, and the gap at the slide plate will reappear. In maintenance, a riser block was arranged beneath the slide plate, which also failed to eliminate this defect.

The gap at the slide plate may increase the impact force of the vehicle on the switch rail, intensify the jerking of the switch rail, or even in serious cases cause damage to the switch rail (by the rolling stock). It is also adverse to riding quality. The gap at the slide plate is generally caused by a cambered long switch rail or great height deviation of the slide plate, causing the tops of adjacent ties to not be on the same level. The slicing partially destresses the residue stress of the switch rail, and causes hogging of the switch rail. This phenomenon may be exacerbated in quenched switch rails.

Applicable remedies include improving the machining accuracy of the switch rail, point rail, and slide bedplate; destressing the residue stress of the switch rail/point rail using vibration stress relief (VSR); examining the fit tolerances of the switch rail, slide bedplate, and tie plate; and performing pre-assembly and adjustment at the shop to eliminate the gap before delivery of the turnout.

3. Poor fit of the switch rail and stock rail, and greater gauge at the switch

   The gauge at the switch is great (up to 4 mm), which is hard to adjust or maintain, and may cause poor fit between the switch rail and stock rail. This technical problem is common in speed-up turnouts. It can be attributed to a coupling of tie plate and turnout tie at the switch that makes the gauge adjustment infeasible. In this way, the gauge adjustment at this location may rely on the gauge blocks outside the stock rail with limited effect. This location is exposed to great wheel−rail lateral force, thereby making gauge hard to maintain, even with the aid of No. 5 or No. 15 gauge blocks customized on site. Applicable remedies include optimizing the coupling mode between the tie and tie plate, enabling the gauge adjusting function of the gauge block and tie plate at the same time, improving the machining accuracy of the switch rail and stock rail, and pre-assembling the turnout at the shop to eliminate the poor fit between the stock rail and switch rail.

4. Unsupported turnout tie at the traction point [173]

   It is difficult to perform tamping at traction points and installation positions for closure detectors in the turnout; therefore, unsupported ties occur frequently, affecting riding stability and rail stress. In the early days of speed-up turnouts, steel ties were adopted, which failed to achieve the desired effects due to a combination of factors, such as greater stiffness of fastenings, light-weight steel ties, and intense vibration at the steel tie. Applicable remedies include developing new steel ties, removing the switch rods for tamping, or installing the closure detector on the tie.

   In addition, such problems as welded joint irregularity, seriously worn top surface at the heat-treated heel of the switch rail and point rail, and flowed top of the switch rail and point rail exist in the turnout.

13.3.2 DYNAMIC SIMULATION ANALYSIS

Improper manufacturing and maintenance processes may also lead to status irregularities similar to those that occurred in the Qinhuangdao−Shenyang PDL. The effects of this typical status irregularity of the turnout on wheel−rail dynamic response in the turnout are studied using dynamic theory on the vehicle−turnout system. The study is based on a No. 18 turnout for 350 km/h, where the EMU train travels in the main line at 350 km/h. Details are given below:

1. Influence of gap at slide bed on wheel−rail dynamic interaction

   Assuming that there are gaps at the left slide bedplate at the second traction point on the switch rail and the first traction point on the point rail, by calculation, the changes of dynamic wheel load, dynamic stress of the switch rail and point rail, load reduction rate, and vertical vibration acceleration of the tie with the gap at the slide plate are as depicted in Figures 13.29−13.32.

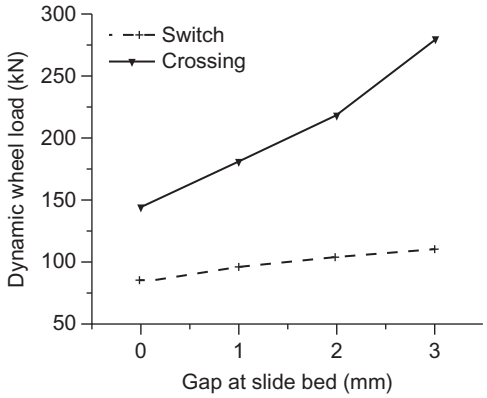

FIGURE 13.29

Change of dynamic wheel load with gap at slide bed.

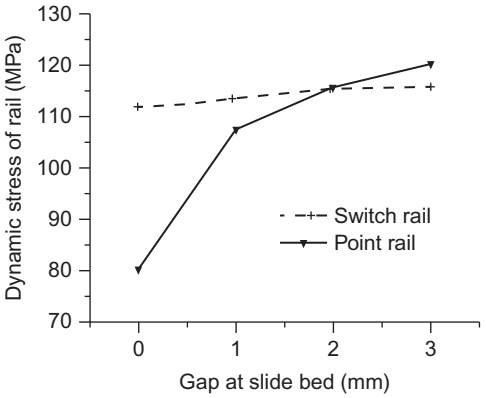

FIGURE 13.30

Change of dynamic stress of rail with gap at slide bed.

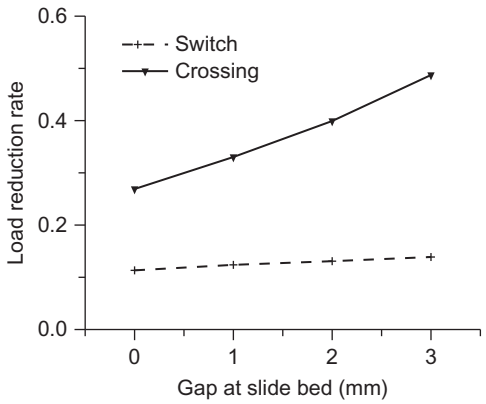

FIGURE 13.31

Change of load reduction rate with gap at slide bed.

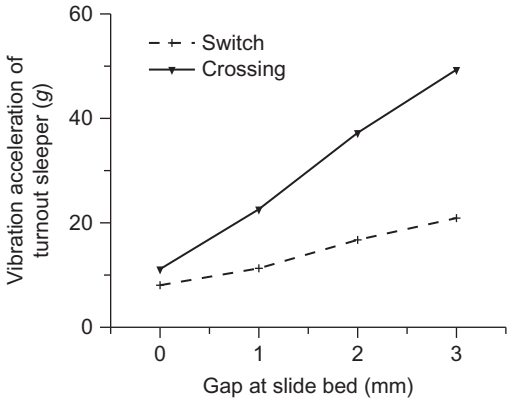

FIGURE 13.32

Change of vibration acceleration of turnout tie with gap at slide bed.

It can be seen from these figures that, at both the switch and crossing, the dynamic wheel load, rail dynamic stress, load reduction rate, and vibration acceleration of the tie will increase with the widening of the gap at the slide plate. Specifically, the growth in dynamic response at the crossing exceeds that at the switch by a large margin. Dynamic simulation shows that the gap at the slide plate will exert greater influence on the vertical dynamic response of the wheel−rail system than the lateral one. In addition, the gaps at different slide plates, multiple gaps, as well as the combination of several gaps may affect the wheel−rail dynamic interaction to varying degrees.

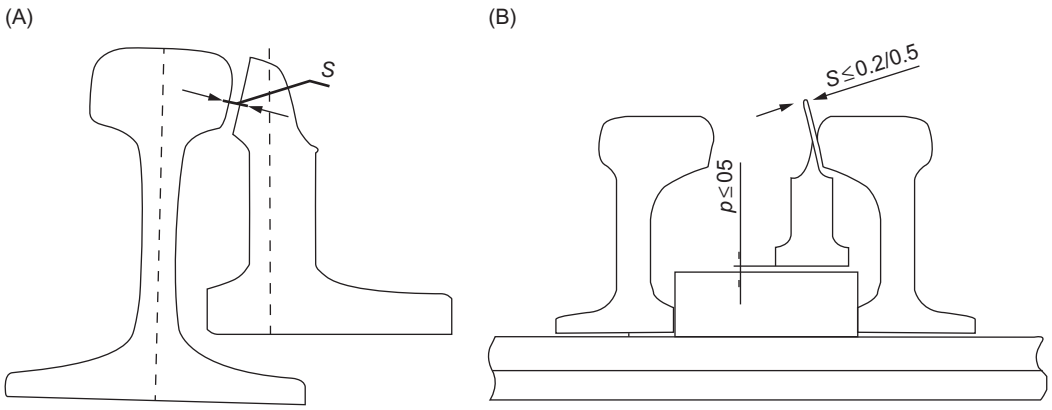

FIGURE 13.33

(A) Gap between switch rail and stock rail. (B) Gap between point rail and wing rail.

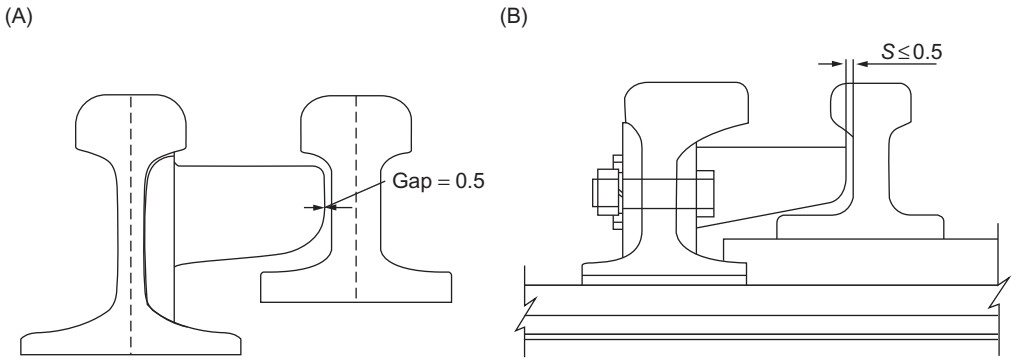

FIGURE 13.34

(A) Gap between switch rail and jacking block. (B) Gap between point rail and jacking block.

Therefore, in China, the gaps between the switch rail/point rail and slide plate cannot exceed 0.5 mm, and no continuous gaps of 0.5 mm are allowed, as specified in technical conditions for manufacturing of high-speed turnouts; the gaps between the switch rail/point rail and slide plate cannot exceed 1.0 mm; and no continuous gaps of 1.0 mm are allowed, as specified in technical conditions for laying of high-speed turnouts.

2. Influence of poor fit of switch rail and point rail on wheel−rail dynamic interaction

A poor fit of the switch rail and point rail includes poor fit of the stock rail/wing rail in the closure zone, as shown in Figure 13.33, and poor fit of the jacking block in the nonclosure zone, as shown in Figure 13.34.

Assuming that there are gaps in the stock rail/wing rail at the second traction point on the switch rail and between the first and second traction points on the point rail, by calculation, the

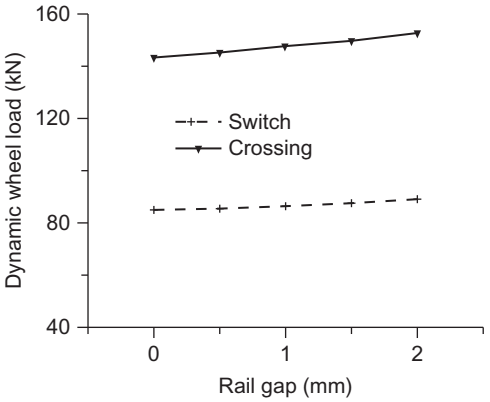

FIGURE 13.35

Change of dynamic wheel load with rail gap.

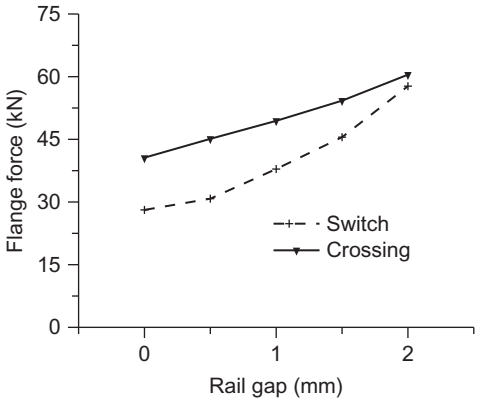

FIGURE 13.36

Change of flange force with rail gap.

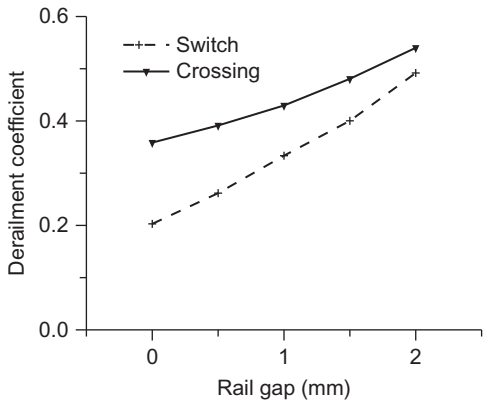

FIGURE 13.37

Change of derailment coefficient with rail gap.

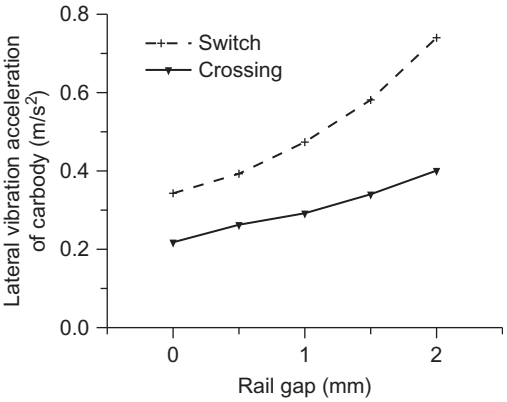

FIGURE 13.38

Change of lateral vibration acceleration of carbody with rail gap.

changes of dynamic wheel load, lateral wheel−rail force, derailment coefficient, and lateral vibration acceleration of carbodies with the rail gap are as depicted in Figures 13.35−13.38.

It can be seen from these figures that, as the gaps between the switch rail and stock rail, and between the point rail and wing rail increase, the dynamic wheel load, flange force, derailment coefficient, and lateral vibration acceleration of carbodies increase accordingly. Specifically, the growth in dynamic response at the crossing surmounts that at the switch by a large margin. Dynamic simulation shows that the rail gap exerts a greater effect on lateral dynamic interaction of the wheel−rail system than the vertical one.

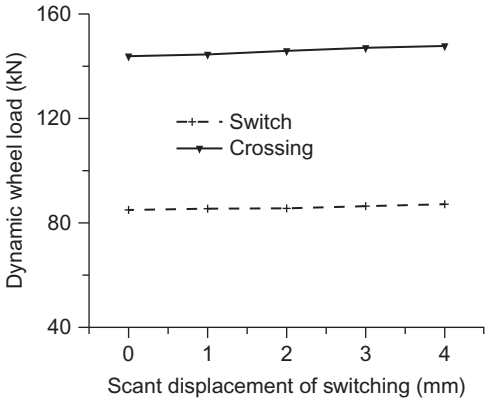

FIGURE 13.39

Change of dynamic wheel load with scant displacement.

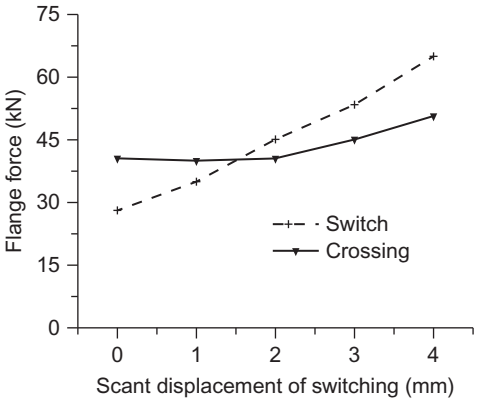

FIGURE 13.40

Change of flange force with scant displacement.

To prevent excessive rail gaps affecting riding safety and quality, in China, as specified in the technical conditions for manufacturing of high-speed turnouts, rail gaps must not exceed 0.2 mm from the point of the switch rail/point rail to the first traction point, and must not exceed 0.5 mm in other parts. In addition, as specified in the technical conditions for laying, rail gaps must not exceed 0.5 mm from the point of the switch rail/point rail to the first traction point, and must not exceed 1.0 mm in other parts. Smaller rail gaps at the point can prevent the occurrence of collisions between high-speed wheels and the rail point due to oversize spread.

3. Influence of scant displacement of switching on wheel−rail dynamic interaction

Assuming that gauge decrease occurs due to scant displacement of switching between the last traction point and the heel of the switch rail, and between the last traction point and the heel of the point rail, by calculation, the changes of dynamic wheel load, lateral wheel−rail force, derailment coefficient, and lateral vibration acceleration of carbodies with the scant displacement of switching are as depicted in Figures 13.39−13.42.

It can be seen from these figures that, at the switch, the dynamic wheel load, flange force, derailment coefficient, and lateral vibration acceleration of carbodies increase with increases in scant displacement of the switch rail. Normally, at the crossing, as the instant lateral impact between the flange and the point rail takes place between the first and second traction points on the point rail, in the case of smaller scant displacement of switching, the flange will not cling to the point rail in the rear of the traction point, and the change of maximum values of dynamic response is independent of the scant displacement of switching. Otherwise, in the case of greater scant displacement of switching, the flange will cling to the point rail with scant displacement, and the dynamic interaction of the wheel−rail system will increase with increasing scant displacement of switching of the point rail. Dynamic simulation shows that scant displacement of switching will exert a great effect on the lateral wheel−rail dynamic interaction. In China, the gauge decrease must not exceed 1 mm, as specified in the technical conditions for laying of

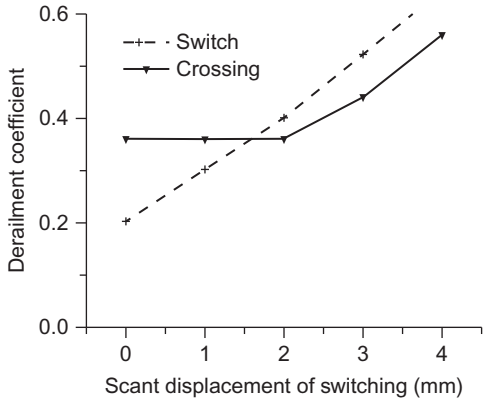

FIGURE 13.41

Change of derailment coefficient with scant displacement.

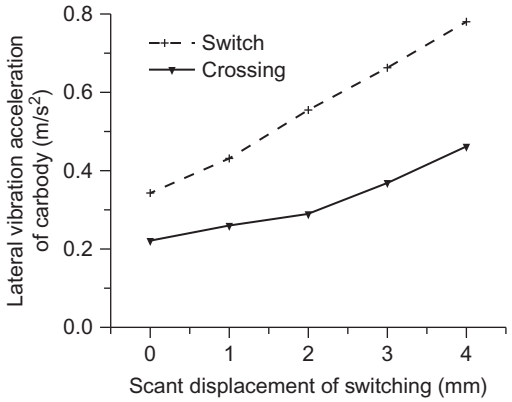

FIGURE 13.42

Change of lateral vibration acceleration of carbody with scant displacement.

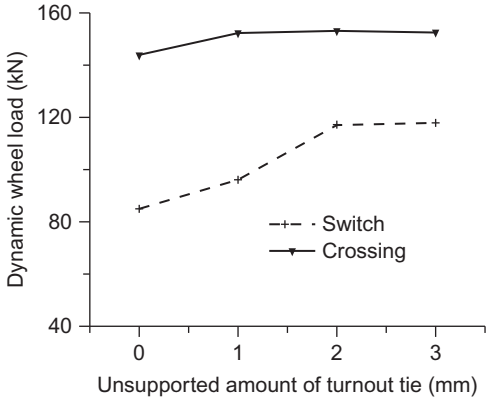

FIGURE 13.43

Change of dynamic wheel load with unsupported amount of tie.

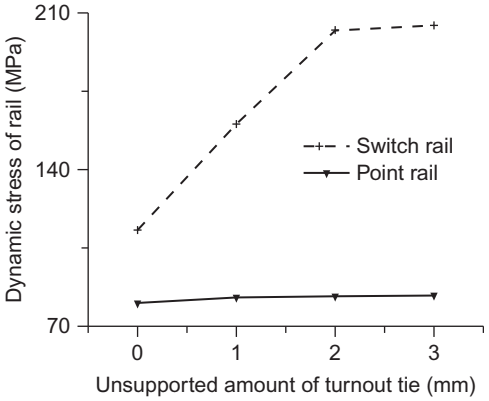

FIGURE 13.44

Change of rail dynamic stress with unsupported amount of tie.

high-speed turnouts, and must not exceed 2 mm as specified in the technical conditions for maintenance.

4. Influence of unsupported tie on wheel−rail dynamic interaction [174,175]

Assuming that the tie on the right of the second traction point on the switch rail and the first traction point on the point rail is unsupported, by calculation, the changes of dynamic wheel load, dynamic stresses of point rail and switch rail, load reduction rate, and vertical vibration acceleration of the tie with the unsupported amount of the tie are as depicted in Figures 13.43−13.46.

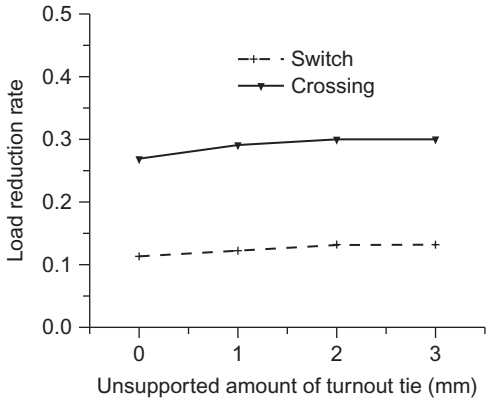

FIGURE 13.45

Change of load reduction rate with unsupported amount of tie.

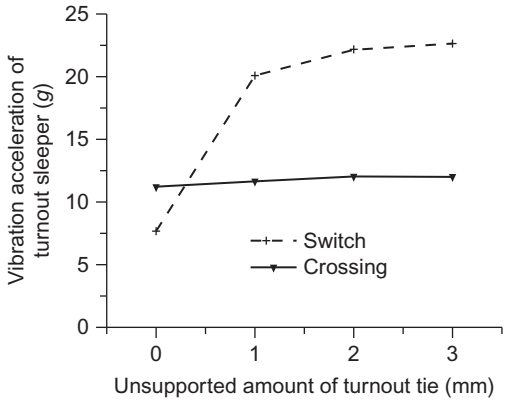

FIGURE 13.46

Change of vibration acceleration of tie with unsupported amount of tie.

It can be seen from these figures that, in cases where an individual turnout tie is unsupported, the dynamic wheel load, rail dynamic stress, load reduction rate, and vibration acceleration of the tie will increase with increased unsupported amounts of tie. However, this change rule does not prevail when more than 2 mm of the tie is unsupported, which means this tie is exposed to support failure, and the vehicle load is distributed onto the neighboring ties under the action of rail flexion. At the switch, owing to smaller stiffness of the track frame as compared with the crossing, the effects of unsupported ties on wheel−rail dynamic interaction become more remarkable. The change of unsupported individual tie is small, though; in most cases, several ties may be unsupported to varying degrees, which will exert a greater influence on wheel−rail dynamic interaction. Therefore, for ballasted turnouts in particular, tamping operation must be enhanced to avoid unsupported ties.

The type, location, amount, and degree of status irregularity in a turnout are random in nature in practical application. Additionally, several status irregularities may coexist that will collectively increase the wheel−rail dynamic interaction and degrade riding quality and safety in the turnout area. Therefore, any inordinate riding quality or rail damage detected in maintaining the turnout, even if status irregularities are within allowable limits, must be improved promptly.

CHAPTER

MAINTENANCE AND MANAGEMENT

14

Track maintenance technologies are an integral part of a high-speed railway technology system. A set of scientific management system must be established, and the track equipment must be inspected, maintained, and repaired regularly and periodically for high performance in riding safety, quality, and comfort and for the serviceability of track equipment. In this regard, the principal role of track maintenance is to keep the track equipment in good status, allowing high-speed trains to travel safely, stably, comfortably, and uninterruptedly at specified speeds, as well as to prolong the service life of the equipment.

In China, prevention is the first concern in maintaining high-speed railways (HSRs), supplemented by control measures, strict inspection, and cautious maintenance processes. Specifically, maintenance work should be performed in an organized way, including accurate inspection, comprehensive analysis, and precise maintenance, as per the regularity of track status, to prevent and control possible track problems effectively. As a supplement, other maintenance management systems, such as inspection−overhaul separation, specialized and district management of track equipment, maintenance skylight, informatized management of maintenance, and track maintenance based on a precise survey control network, are also applied.

The above maintenance principles and management systems are also applicable to high-speed turnouts. However, owing to the special features and important role in the safety of railway traffic as compared with common railway sections, the maintenance technologies for high-speed turnouts are somewhat different. This chapter will give a brief account of some up-to-date technologies in the maintenance and management of Chinese HSRs and any ongoing efforts.

14.1 MANAGEMENT POLICIES AND MAINTENANCE STANDARDS

14.1.1 TYPE OF MAINTENANCE WORK

Track maintenance work falls into three types: cyclical maintenance, frequent maintenance, and urgent repair. For cyclical maintenance, track equipment will be inspected and overhauled comprehensively based on a specified cycle to restore the normal technical status of the track as per the change rules and features of track components. For frequent maintenance, track equipment will be maintained frequently as per dynamic and static inspection results and changes in track status, so as to keep the track quality in balance. For urgent repair, urgent repair measures will be taken to ensure riding quality at the places with geometric dimensions exceeding tolerance control values or in cases of damaged track equipment affecting normal operations.

Design of High-Speed Railway Turnouts.

14.1.2 MANAGEMENT ORGANIZATION

The management organizations of Chinese HSRs are set up as per the principles of resource integration, professional enhancement, and centralized management, as well as high capability and high efficiency.

Track equipment of HSRs is divided by district and managed by relevant railway administrations. The railway administration is directly responsible for the safety, maintenance, and management of track equipment of HSRs under its authority, with subdivisions of engineering district, track workshop, and track section. The kilometrage of railways in operation managed by a track workshop is about 200−300 km, generally.

The infrastructure inspection center of the China Railway Corporation, inspection institute for engineering equipment of railway administration, and inspection sections involving heavy railway maintenance machinery are responsible for carrying out track inspection and rail detection periodically with comprehensive inspection trains, rail detection cars, etc.

The inspection sections involving heavy railway maintenance machinery and engineering mechanical sections are responsible for track overhaul with heavy railway maintenance machinery.

14.1.3 MODE OF MAINTENANCE

The track equipment follows the system of "maintenance skylight" and prefers a comprehensive maintenance mode that combines reliability-centered maintenance and planned preventive maintenance.

"Skylight" refers to the traffic interval for maintenance reserved on the train diagram. It is a technical measure for settling conflict between railway traffic and maintenance of equipment. All inspection and maintenance work is performed during the skylight period. The principle of "no train operation during construction and no construction during train operation" is to be strictly followed. There are two modes of skylight for HSRs: the skylight for comprehensive maintenance and the skylight for track inspection. Following each skylight, an inspection car will travel in the track to verify the availability for operation of EMU trains. The skylight for comprehensive maintenance is set at nighttime, lasting for at least 240 min, providing inspection and maintenance for infrastructure. The skylight for track inspection is set in the daytime, lasting for at least 60 min, devoted to track equipment inspection, investigation of workload, and inspection and collection of basic data.

Economy of scale is a must for improving the maintenance efficiency and quality of infrastructure and reducing relevant costs. To be specific, this includes building a comprehensive maintenance model featuring high efficiency and quality, low cost, integration, modernization, and informatization; integrating the management of engineering, electrical, and power supply services; and forming an objective integration-focused, informational, integration-based, and business operation−oriented organic complex through the integration of participants. Inspection, servicing, and repair are three separate parts of the maintenance work for the infrastructure of HSRs. The three parts cooperate with and supervise each other, integrating the engineering, electrical, and power supply service and improving maintenance efficiency through economies of scale.

Reliability-centered maintenance refers to the servicing and maintenance provided as per the actual technical needs of track devices. This type of maintenance does not discard, but instead combines the concept of planned preventive maintenance based simply on the status of devices. If the track equipment, as the scheduled period for planned preventive maintenance approaches, remains

intact, it may not necessarily be maintained. Conversely, if the devices are in a poor state even outside the maintenance period, maintenance work is required. The combination of reliability-centered maintenance and planned maintenance is an effective means of both saving maintenance costs and improving the economic efficiency during the overhaul life (service life of the track).

14.1.4 MAINTENANCE STANDARD

1. Control values of static geometry tolerance [176]

   The control values of static geometric tolerance of high-speed turnouts in China are listed in Table 14.1. In the table, the control values for construction acceptance are used for quality inspection after cycle maintenance, frequent maintenance, and urgent repair; the control values for frequent maintenance are for quality control that is frequently required for the track; the control values for urgent repair are for track renovation to be carried out in due time; and the control values for speed restriction are for speed control to ensure riding quality and comfort.

2. Control values of dynamic geometry tolerance

   Track dynamic irregularity is the dynamic response of track irregularity, which may be inspected with a comprehensive inspection train. The control of dynamic irregularity includes control of peak value and mean value.

   The inspection components of track dynamic irregularity include track gauge, longitudinal and cross level, alignment, twist, composite irregularity, vertical and lateral vibration acceleration of the carbody, and gauge variation rate.

Table 14.1 Control Values of Track Static Geometry Tolerance

Item		Construction Acceptance	Frequent Maintenance	Urgent Repair	Speed Restriction (200 km/h)
Gauge (mm)	Turnout area	+1 −1	+4 −2	+5 −2	+6
	Point of switch rail	+1 −1	+2 −2	+3 −2	−4
Cross level (mm)		2	4	6	7
Longitudinal level (mm)		2	4	7	8
Track alignment (mm)	Main line	2	4	5	6
	Offset	2	3	4	–
Twist (mm/3 m)		2	3	5	6
Gauge variation rate		1/1500	1/1000	–	–

Notes:

1. *Offset tolerance is the difference between the measured and calculated offset.*
2. *The limit for the height difference between the upper rail and the lower rail of the transition lead curve: for No. 18 or above turnout, 0 mm for construction acceptance, 2 mm for frequent maintenance, and 3 mm for urgent repair.*

Table 14.2 Tolerance Control Values of Track Dynamic Quality

Item		Frequent Maintenance	Comfort	Urgent Repair	Speed Restriction (200 km/h)
Level of Tolerance		**I**	**II**	**III**	**IV**
Gauge (mm)		+4 −3	+6 −4	+7 −5	+8 −6
Cross level (mm)		5	6	7	8
Twist (gauge length 3 m) (mm)		4	6	7	8
Longitudinal level (mm)	Wavelength 1.5−42 m	4	6	8	10
Track alignment (mm)		4	5	6	7
Longitudinal level (mm)	Wavelength 1.5−120 m	7	9	12	15
Track alignment (mm)		6	8	10	12
Composite irregularity (mm)		6	8	–	–
Vertical acceleration of the carbody (m/s^2)		1.0	1.5	2.0	2.5
Lateral acceleration of the carbody (m/s^2)		0.6	0.9	1.5	2.0
Gauge variation rate (‰) (gauge length 3 m)		1.0	1.2	–	–

Notes:
1. *The control values in the table are the half-peak values of the actual amplitude of track irregularity.*
2. *The limit for cross level excludes specified cant and cant runoff of the curve.*
3. *The limit for twist includes the twist induced by cant runoff of the easement curve.*
4. *The vertical acceleration of the carbody is assessed by 20 Hz lowpass filtering value, Level I and Level II lateral acceleration of the carbody by 0.5−10 Hz band-pass filtering value, and Level III and Level IV lateral acceleration of the carbody by 10 Hz lowpass filtering value.*
5. *Composite irregularity refers to the composite antiphase irregularity combining cross level and track alignment irregularity, defined by the algebraic difference between cross level and 1.5−4.2 m track alignment.*

In China, the deviation of high-speed track (including turnouts and rail expansion joints) has four levels (I = frequent maintenance, II = comfort, III = urgent repair, and IV = speed restriction). Table 14.2 presents standard limits for the amplitude of dynamic irregularity.

Control of the mean value of dynamic irregularity is expressed by track quality index (TQI). Table 14.3 presents the TQIs and the control values for each individual standard deviation for HSR tracks in China.

3. Control values of dynamic response of vehicles

Dynamic indicators of vehicles include derailment coefficient, load reduction rate, and wheelset lateral force. The lateral force and vertical force are measured with the passage of the

Table 14.3 Standard Value of Track Quality Indexes (TQI)

Item		Longitudinal Level	Track Alignment	Track Gauge	Cross Level	Twist	TQI
Wavelength	1.5–42 m	0.8 × 2	0.7 × 2	0.6	0.7	0.7	5.0

Note:
1. *The calculated length is taken as 200 m for individual standard deviation with wavelength of 1.5–42 m.*

instrumented wheelset of the comprehensive inspection train. The control values adopt the standards for dynamic acceptance as shown in Table 12.2.

4. Determination standard for rail defects

Rail (including the rails of turnouts, rail expansion joints, and glued insulated joints) defects mainly consist of wear, peeling, crack and spalling of rail head, scratch of rail top, rail corrugation, surface crack, internal crack, and corrosion.

Rail defects are classified by severity into minor defects, major defects, and rail fracture. Tables 14.4–14.6 show the criteria for minor and major rail defects.

14.1.5 EVALUATION OF TURNOUT QUALITY

Evaluation of the conditions of track equipment is to inspect and determine the basic quality of the track equipment in the main line. It is a basic index for assessing the management performance of track equipment and improvement of the conditions of track equipment, as well as the main basis for arrangement of a track maintenance plan. Evaluation of turnout quality is performed by group and follows a 100-mark system: 100–85: excellent; 80 (excl.) ~60: qualified; below 60 (excl.): unqualified. The evaluation covers track geometry, rail defects, etc. The evaluation of track irregularity mainly follows the method below:

1. Management method for local peak

The amplitude of local irregularity is evaluated by inordinateness penalty as per the four-level management criteria given in Table 14.2. In the table, any inordinateness of Level I criteria will be penalized 1 point; any inordinateness of Level II criteria will be penalized 5 points; any inordinateness of Level III criteria will be penalized 41 points; and any inordinateness of Level IV criteria will be penalized 101 points. The evaluation can be expressed by:

$$S = \sum_{i=1}^{4} \sum_{j=1}^{M} K_i T_j C_{ij} \tag{14.1}$$

where

S = total penalties per kilometer of track or set of turnout
K_i = penalty for deviations
T_j = weighting coefficient of irregularities, taken as 1 at present
M = the number of evaluated irregularities; and
C_{ij} = the number of deviations for inspected items.

Table 14.4 Criteria for Minor and Major Rail Defects

Type of Defects		Severity: Minor	Severity: Major	Remarks
Wear of rail head		The wear exceeds any of the limits listed in Table 14.6	The wear exceeds any of the limits listed in Table 14.6	
Scratch of rail top		Depth > 0.35 mm	Depth > 0.5 mm	
Rail spalling		–	Yes	
Rail corrugation		–	Valley depth ≥ 0.2 mm	
Weld concaveness		0.2 mm < concaveness < 0.4 mm	Concaveness ≥ 0.4 mm	Measured with 1 m ruler
Surface crack		–	Horizontal crack (thorough corrosion) at the lower jaw of rail head, horizontal crack at rail web, longitudinal crack at rail head, and cracks at rail base, etc. occur	The fish scale crack on the surface and near-surface of rail top induced by wheel–rail contact fatigue is excluded
Defects identified by ultrasonic testing	Welding and material defects	Welding defects or defects of internal rail material fail to meet the discarding criteria, but deviate from the discarding criteria by less than 6 dB	Welding defects or defects of internal rail material meet the discarding criteria	
	Internal crack	–	Tread concaveness (invisible defect) caused by lateral, longitudinal, oblique, and other cracks, and internal cracks	
Rail corrosion		–	After derusting, the depth of rail base is less than 8 mm or that of rail web is less than 12 mm	

Notes:

1. *Total wear = vertical wear + 1/2 side wear.*
2. *For full cross section regions of guide rails, wing rails, switch rails, point rails, and pointed rails at crossing heel, the vertical wear is measured at 1/3 top width (from standard working surface) of the rail; as for the machined zones of switch rails, point rails, and pointed rails at crossing heel, vertical wear is measured at the peak of the rail head.*
3. *Side wear is measured at 16 mm below rail tread (as per standard cross section).*
4. *Wear affecting the installation of conversion equipment is regarded as a major defect.*
5. *Valley depth is the vertical distance from adjacent crest to the valley.*

Simple and instructive to field remediation of inordinate irregularities though it is, the evaluation method cannot reflect the quality of the balance state of the track yet.

2. Management method for main value in a section

The TQI is a composite statistical outcome of the dynamic inspection data of track longitudinal and cross level, alignment, gauge, and twist irregularities. The value of TQI closely

Table 14.5 Criteria for Minor Wear of Rail Head

Description	Total Wear (mm)	Vertical Wear (mm)	Side Wear (mm)
Section rails and guiding rails	9	8	10
Stock rails and wing rails	7	6	8
Switch rails, point rails, and pointed rails at crossing heel	6	4	6

Note: Wear of stock rails, wing rails, switch rails, and point rails will affect closure and rail height difference. Therefore, the criteria for major and minor wear of turnout rails are stricter than those for section rails.

Table 14.6 Criteria for Major Wear of Rail Head

Description	Vertical Wear (mm)	Side Wear (mm)
Section rails and guide rails	10	12
Stock rails and wing rails	8	10
Switch rails, point rails, and pointed rails at crossing heel	6	8

correlates with track quality. Greater value relates to poor track quality and intense fluctuation. The statistical value of any individual irregularity also reflects the quality of the individual geometric irregularity. TQI is expressed by:

$$\mathrm{TQI} = \sum_{i=1}^{7} \sigma_i = \sum_{i=1}^{7} \sqrt{\frac{1}{n}\sum (x_{ij} - \bar{x}_i)^2} \tag{14.2}$$

where σ_i is the standard value of a geometric deviation, x_{ij} is the amplitude of a geometric deviation at a successive sampling points per unit section, $\bar{x}_i$ is the arithmetic mean of a geometry deviation, and n is the number of sampling points (there are generally 800 points in a 200 m unit section). This method can reflect track equilibrium quality, but it falls into the amplitude management group as with the management method for local peak. Yet it cannot demonstrate the wavelength and frequency domain characteristics of track irregularity.

3. Evaluation method for power spectrum of track irregularity [177,178]

The track irregularity spectrum is an effective means of describing the track irregularity of the whole line. In addition, it can reflect the amplitude−frequency characteristics of track irregularity.

Figures 14.1−14.4 present the power spectrums of longitudinal and cross level, alignment, and gauge irregularities of a ballastless track of Chinese HSR. Longitudinal level and alignment irregularities refer to vertical and lateral deviation of the track center from the design position. The track inspection system can provide measurements of left and right longitudinal level, as well as left and right track alignments; therefore, the actual longitudinal level and track alignment will be the mean values. The track irregularity spectrum ($\mathrm{mm}^{-2}/(1/\mathrm{m})$) is represented by a one-sided power spectrum under spatial frequency (1/m). The wavelength for HSR track irregularity management is 1.5−120 m. The track irregularity spectrum for wavelengths longer than

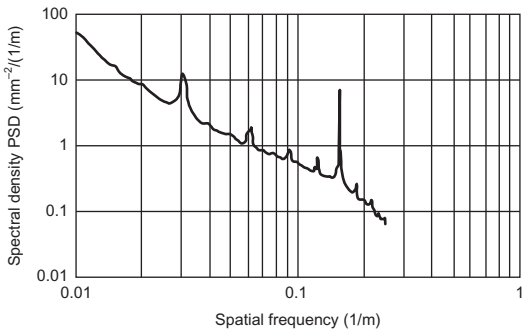

FIGURE 14.1

Spectrum of longitudinal level.

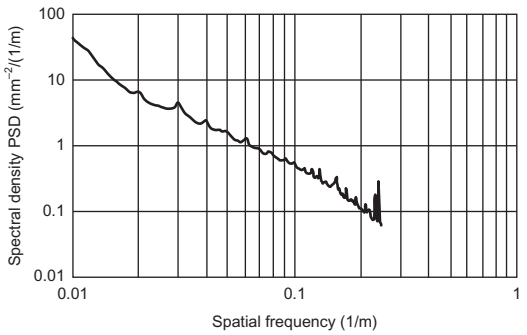

FIGURE 14.2

Spectrum of track alignment.

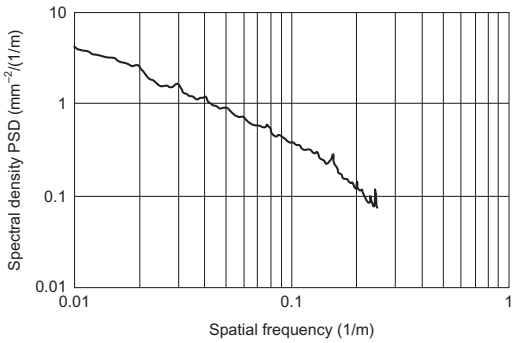

FIGURE 14.3

Spectrum of track gauge.

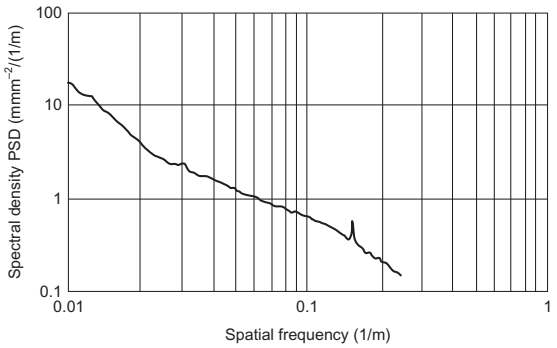

FIGURE 14.4

Spectrum of cross level.

120 m may be extended by a relevant fitting equation, while that for wavelength shorter than 1.5 m may be tested by special inspection equipment.

These four irregularity spectrums can be fit by the piecewise equation:

$$S(n) = \frac{A}{n^k} \tag{14.3}$$

where n denotes spatial frequency, and A and k are the coefficients of the equation.

4. Evaluation of track quality with the aid of vehicle dynamic response [2]

a. Evaluation of riding quality in a turnout using the lateral acceleration of the carbody

The lateral acceleration of the carbody may be used to evaluate riding quality in a turnout as put forth by CARS. Specifically, the composite weighted index (CWI) for evaluating the influence of turnout status on riding quality by weighting the peak and mean on the accelerometer is given by:

$$\text{CWI} = \frac{1}{2}\text{PV} + \frac{1}{4}\text{PPV} \tag{14.4}$$

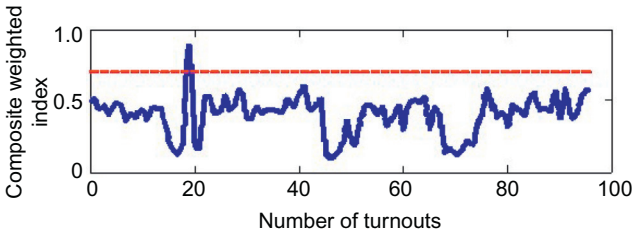

FIGURE 14.5

Distribution of CWIs of the turnout.

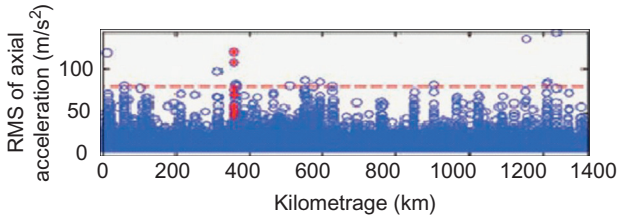

FIGURE 14.6

Distribution of RMS of axial acceleration for Beijing−Shanghai line.

where CWI refers to the composite weighted index for evaluation of riding quality in a turnout, PV is the absolute peak of the lateral acceleration of the carbody, and PPV is the distance between the adjacent peak and the valley.

Figure 14.5 depicts the CWI's distribution for a group of turnouts in the Beijing−Shanghai line. It can be seen in the figure that the CWIs of most turnouts are lower than 0.72 m/s^2, indicating that the turnouts are in good condition. Among these turnouts, only the CWI of the 19th turnout is up to 0.88 m/s^2, reflecting poor riding quality in this turnout. This result coincides with the manual measurement by train vibration analyzer.

b. Evaluation of the impact characteristics in a turnout using axlebox acceleration [178]

Axlebox acceleration is the most direct dynamic response when a train travels in the turnout, reflecting any track irregularities in the turnout area directly at the same time. CARS believes that the peak factors of the root mean square (RMS) of axlebox acceleration can be applied to evaluating the influence of the turnout on the impact property of the vehicle. Figure 14.6 presents the distribution of RMS of axlebox acceleration in the Beijing−Shanghai line. In the figure, red circles symbolize the position of fastening fractures, the red dotted line denotes the evaluation criteria.

c. Evaluation of dynamic characteristics of vehicle−track system using general energy index

Based on the concept of energy compaction efficiency, CARS put forward the general energy index (GEI; see equation below) to comprehensively evaluate the dynamic characteristics of a track−vehicle system, so as to distinguish the contribution of the irregularities of different wavelength components to input energy.

$$\mathrm{GEI} = \sum_{i=1}^{7} \alpha_i \sqrt{\frac{1}{n-1} \sum_{j=0}^{n-1} w_i(f_j) E_i(f_j)} \tag{14.5}$$

where $E_i(f_j)$ is the energy of the ith irregularity of wavelength f_j; $w_i(f_j)$ is the energy weighting coefficient of corresponding wavelength, which satisfies the normalization condition and can be obtained with the frequency response function between the vibration acceleration of the carbody and track irregularity; and α_i is the weighting coefficient of each irregularity, identical to the value of T_j in Eq. 14.1.

14.2 INSPECTION AND MONITORING TECHNOLOGIES FOR HIGH-SPEED TURNOUTS

14.2.1 INSPECTION OF TURNOUT STATUS AND GEOMETRY

For the inspection of track and turnouts, dynamic inspection is the dominant mode, supplemented by static mode; and static inspection and geometric inspection are equally applicable. Dynamic inspection relies mainly on the inspection results of the comprehensive inspection train. The tools involved in dynamic inspection are track inspection equipment, a train-borne track inspection device, and a portable train vibration analyzer.

1. Inspection period

   Period of dynamic inspection: once every 10−15 days for comprehensive inspection train; at least once daily for track inspection device on EMU train; at least half-monthly for portable track inspection device used in crew testing in the engineering section; and at least semi-annually for the inspection of track equipment with inspection devices.

   Period of static inspection: once monthly for turnout geometry inspection; for turnouts with major defects or track irregularity, track measurement instrument and inspection instrument will be used. The rails of the continuously welded rail (CWR) turnout are to be overhauled once quarterly for longitudinal displacement.

   Period of the turnout status inspection: once weekly for status inspection, and once annually for daytime inspection.
2. Dynamic inspection equipment
   a. Development of track dynamic inspection technologies in China

      GJ-1 track inspection system: developed in the 1950s, adopting chord-based method, mechanical transmission type.

      GJ-2 track inspection system: developed in the 1960s, adopting chord-based method, electric transmission type, read manually.

      GJ-3 track inspection system: developed in the 1980s, adopting inertia reference method, composite structure, not applicable to track gauge and alignment inspection, computer-based rating.

      GJ-4 track inspection system: developed in the mid-1990s, adopting inertia reference method, strapdown structure, applicable to a wide range of inspection items and computer-based processing. The servo track gauge lifting beam is of great vibration impact and potential safety hazard.

GJ-5 track inspection system: imported from IMAGEMAP of the United States in 2000, adopting laser-photogrammetric mode and inertia reference method, with the measuring beam mounted on the bogie, featuring high maintenance cost.

GJ-6 track inspection system: developed by China in 2013, adopting photogrammetric mode, inertia reference method, and high-speed digital camera, maximum speed 400 km/h, light measuring beam components, capable of long-wavelength inspection.

Comprehensive inspection train: The new type of comprehensive inspection trains (#0 for 200 km/h and #10) were developed with the launching of 200−250 km/h EMU trains during the sixth speed-up for railways in China in 2007. These inspection trains are capable of inspecting track geometry, traction power supply, communicating and signaling equipment, wheel−rail relation, pantograph-catenary contact state, riding comfort, etc. A couple of advanced technologies, such as modern measurement, time/space simultaneous localization, real-time transmission of high-capacity data, and real-time image processing, are employed for high-speed, dynamic, and multi-parameter simultaneous inspection.

High-speed comprehensive inspection train: developed by China based on the technical platform of CRH380B in 2011, with design speed of 400 km/h. With advanced inspection technologies and approaches, the inspection train is capable of performing accurate inspection and sampling in real time on the track, catenary, wheel−rail force, communication, signal, vehicle dynamic response, and bogie load, etc. when traveling at 350 km/h or above.

There are 45 track inspection trains in service as of 2014, including nine GJ-4 trains, 21 GJ-5 trains, and 15 GJ-6 trains. About nine comprehensive inspection trains are in service. Figure 14.7 is a picture of a CRH380B high-speed comprehensive inspection train.

b. Technical features of GJ-6 track inspection system

The GJ-6 train inspection system, relying on cross section measurement utilizing laser-photogrammetric technology and employing inertia gyro platform, combines the technical

FIGURE 14.7

Comprehensive inspection train for high-speed railways in China.

merits of the GJ-4 and GJ-5 models. With the leading technologies of inertia principle, image processing, digital filtering, and train-borne LAN, the system is capable of inspecting all track geometry status in real time when traveling at high speed. The system is composed of laser-photogrammetric components, inertial measurement components, signal processing components, data processing components, kilometrage calibration and simultaneous localization components, and mechanical suspension devices, as shown in Figure 14.8.

Main technical features:

Improving the image processing speed to 450 fps by adopting multiple-image parallel image processing technologies.

Realizing simultaneous sampling of the sensor and cooperation of multiple modules under high-speed traffic with the provision of advanced multifunctional control cards devoting to precise control of spatial sampling and synchronizing of the functions of the modules.

Developing multi-processor technology based on real-time operating system to maximally explore the potential of the equipment.

Optimizing the network structure and communication mode to overcome problems of data blockage and loss, etc.

Realizing real-time inspection on track geometry when a train travels at 400 km/h.

Developing new laser-photogrammetric measurement devices, optimizing system design with high-performance digital camera, which saves 75% of sensor components and improves system reliability. Figure 14.9 is a picture of a rail profile inspection system.

Establishing the antisunlight interference algorithm, which effectively improves the antisunlight interference capability of the equipment and prevents sunlight interference from affecting the inspection. Putting forward inspection methods for track long-wavelength irregularity, capable of inspecting track irregularity with wavelength of 120 m.

Developing a measuring beam (Figure 14.10) adapting to complex structure and severe operation environment at train speeds of 400 km/h.

Employing multidimensional inertial reference technology for multi-reference calibration; establishing a filtering method with multiple measurement references and real-time calibration; providing a detection algorithm for large radius curve based on phase difference Global Positioning System (GPS) and multiple inertial reference, capable of measuring large radius curve accurately.

3. Static inspection equipment

Track static inspection equipment includes track gauge, relative geometry car, absolute geometry car (e.g., #0 track inspection device), laser long-chord track inspection car, GPS inertial integrated navigation measurement car, measurement device for rail profile, straightness of rail welding head, and rail corrugation.

Figure 14.11 is a picture of a #0 track inspection device developed by Jiangxi Everbright Railway Equipment Development Co., Ltd. The device centers around the total station, and implements free stationing based on CPIII. It calculates the coordinates of track height/plane comprehensively by measuring the coordinates of prism point and position of the car, so as to obtain the deviation of track geometry with measurement accuracy of 1 mm. However, the measurement accuracy is ± 2 mm when calibrating the long wavelength with the midpoint of a 70 m chord, and ± 3 mm when calibrating with the midpoint of a 120 m chord.

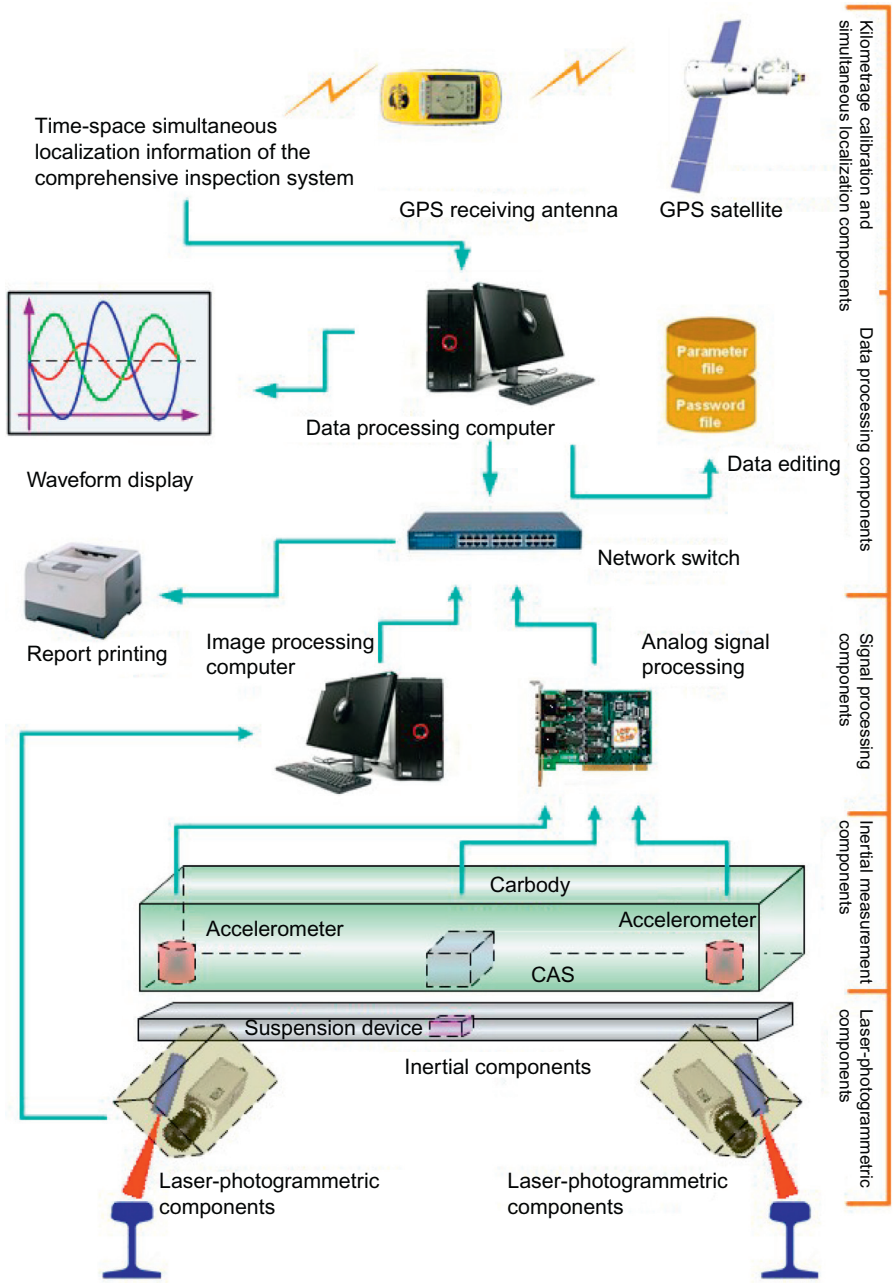

FIGURE 14.8

Composition of GJ-6 track inspection system.

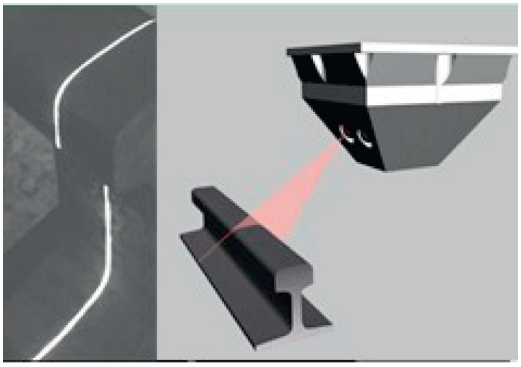

FIGURE 14.9

Digital camera.

FIGURE 14.10

Measuring beam.

FIGURE 14.11

#0 track inspection device in China.

4. Track inspection equipment

CARS developed a track inspection car (Figure 14.12) with the technologies of a multi-camera array and integrated light source. The track inspection car can recognize an abnormal position, missing fastenings, fracture, displacement, and reverse installation of elastic clips, as shown in Figure 14.13. It can identify a scratch in the rail surface (resolution: 1 mm laterally and 1.6 mm longitudinally) and rail corrugation, as shown in Figure 14.14. Also, it can identify cracks on a ballastless track slab and spalling of a retaining shoulder, as shown in Figure 14.15. In addition, it realizes simultaneous sampling, transmission, and control of speed and kilometrage information by integrating RFID, high-precision photoelectric encoder, GPS, and other positioning information sources and using data-fusing technology.

FIGURE 14.12

Comprehensive inspection train.

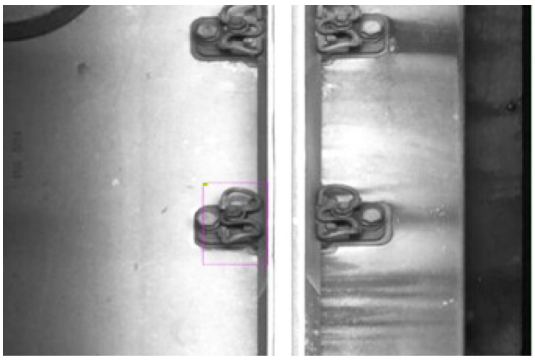

FIGURE 14.13

Identifying reverse installation of fastenings.

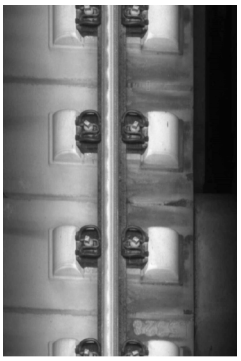

FIGURE 14.14

Identifying rail corrugation.

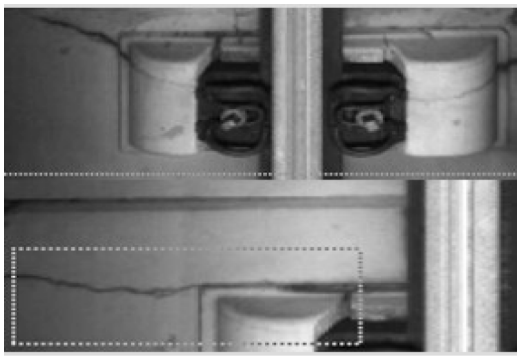

FIGURE 14.15

Identifying defects and damage to ballastless track.

By providing a rail corrugation inspection system on the track inspection car, and acceleration sensors on the left and right sides of the axle head of the car as per inertial reference principle, the amplitude and RMS value of rail corrugation can be obtained by anti-aliasing filtering of the acceleration signals and quadratic integral method. It is applicable to wavelengths of 0.1−1.5 m, amplitude of 0.2−3 mm, with measurement accuracy of 0.1 mm and measuring speed of 30−200 km/h.

5. Dynamic loading device of the turnout

China has developed a movable track dynamic loading test car successfully after the United States, Japan, and Sweden. The loading test car of China is composed of a dynamic loading car, instrumented testing car, train-borne loading system, and inspection system. The running gear of the dynamic loading car adopts the three-axle bogie of the locomotive, with loading wheels in the middle of the carbody for track loading (hydraulic loading), as shown in Figure 14.16.

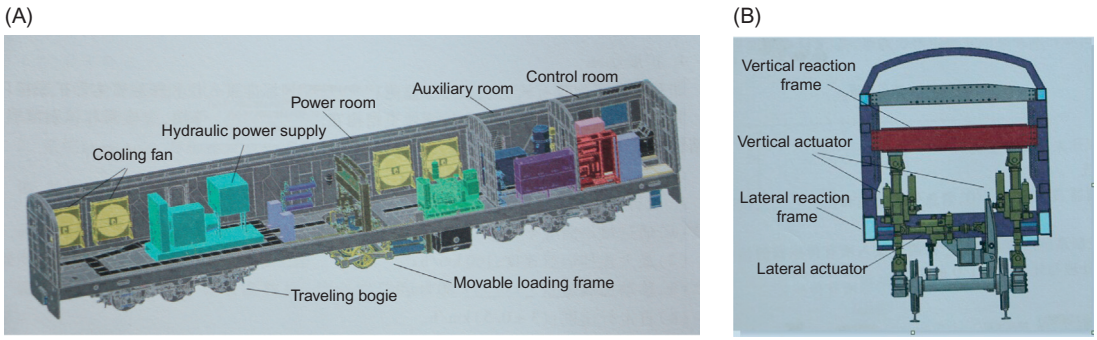

FIGURE 14.16

(A) Dynamic loading vehicle. (B) Hydraulic loading system.

The instrumented testing car adopts the carbody and running gear of the 25T passenger car, and is provided with devices such as a rigid inspection system.

The loading test car may be placed at a given point to apply static load, or dynamic loads of different frequency or waveform, random load or dynamic cyclic load at any given point of the track, to determine the static and dynamic mechanical properties of the track. Stationary loading capacity: maximum vertical loading force (single wheel), 200 kN; maximum vertical loading frequency, 50 Hz; maximum lateral loading force (single wheel), 150 kN, and maximum lateral loading frequency, 15 Hz.

The loading test car can apply constant load on the track laterally and/or vertically while moving, so as to measure the dynamic stress characteristics of the track without interruption. Dynamic loading capacity: maximum vertical loading force (single wheel), 150 kN; and maximum lateral loading force (single wheel), 100 kN.

With the wheel−rail force measurement system and rail displacement measurement system on the loading test car, the track deformation under loading force can be measured, and the track integral stiffness can be obtained. The elastic deformation of the track is measured as per the three-point chord reference method using a laser triangulation measurement sensor. The loading test car is also capable of inspecting the homogeneity of bridge−embankment transition, as well as track stiffness in the turnout area.

14.2.2 INSPECTION OF TURNOUT RAILS

1. Inspection period

Rail inspection includes flaw detection and inspection of appearance and surface damage.

For flaw detection, the rails of the main line and the turnout will be inspected periodically, mainly by the flaw detection car, or flaw detectors if necessary. The flaw detectors are to check any damage or defects identified by flaw detection car. Inspection by the flaw detection car will be performed at least seven times a year, with smaller detection intervals in winter. Inspection by the rail flaw detector will be performed on a yearly basis for rails in the main line and on a monthly basis for turnout rails. A weld flaw detector may be used to perform full-section flaw

detection on the welds in CWR track in the main line and in turnouts. As for the detection period, shop welds will be inspected once every 5 years, the welds of onsite flash welding once a year, and the welds of thermite welding once every 6 months.

The appearance of the rail will be inspected with a combination of inspection equipment and manual inspection. Manual inspection will be performed at least once a year. For rails, turnouts, and rail expansion joints with minor wear, inspection with a rail profilometer (abrasion tester) will be performed at least on a quarterly basis.

Spall cracks, surface cracks, and scratches will be inspected once quarterly, or provided with eddy detection and magnetic particle detection if necessary. Eddy detection is to inspect defects on the surface and near-surface of the rails in curved sections, particularly oblique cracks on the surface. Magnetic particle detection is to inspect the defects on post-welding joints, and the surface and near-surface of turnout rails. Magnetic particle detection in the turnout area is mainly performed at the rail top, lateral surface of the rail web, and top surface of the rail base along the full length of the switch rail, top surface of the point rail, as well as the top surface and lateral surface of the rail web of high manganese steel cast wing rails.

A flatness gauge is used at least once a year to inspect the flatness of field welds. Welds with minor concavity should be inspected at least once quarterly.

Any rail fracture or major defects identified in an inspection will be posted immediately to the relevant workshop and engineering district. In case of rail fracture, the railway line will be blocked immediately for repair. For major defects of rails, a speed restriction of 160 km/h will be implemented in promptly, and any urgent, temporary, or permanent measures will be taken accordingly.

2. Flaw detectors for high-speed railway rails

Flaw detection for railway rails in China is mainly performed by a large-size rail flaw detection car and smaller multi-channel flaw detector. The large rail flaw detection car is technologically sophisticated, efficient, and highly adaptable, but inflexible, which will be supported by manual inspection. The smaller multi-channel flaw detector is highly sensitive and adaptable, but unstable, as it may be affected by human factors (e.g., operator). The ultrasonic wave is highly sensible, effective, and accurate in detecting rail fatigue cracks and other internal defects due to the spreading nature in the rails. Therefore, ultrasonic flaw detection technology is widely employed by the rail flaw detection car worldwide.

China began to introduce the large-size rail flaw detection car since 1989. The first car was from GEMCO of Australia. In 1993, the SYS-1000 flaw detection car was bought from Pandrol Jackson Company of the United States, with operating speeds of 40 km/h. Based on the SYS-1000 inspection system, the Frontier inspection system was developed by SPERRY after 2000, with an operating speed of 60 km/h. In recent years, SPERRY developed a 1900-type inspection system for Chinese railways, which has learned from the technical features of rail flaw detectors for Chinese railways, provided with ultrasonic probes with a deflection angle of 70° to improve the detectability of compound fissures of the rail head. In addition, the diameter of the wheel probe was altered from 6.5″ to 9″ to reduce the path of ultrasonic waves in the wheel. At present, there are 26 rail flaw detection cars in China, of which 4 are for 40 km/h and 22 for 60 km/h; 4 are provided with the SYS-1000 system, 17 with the Frontier system, and 5 with the 1900 system, as shown in Figure 14.17.

China has developed a series of hand-propelled ultrasonic flaw detectors, including models JGT-5, DGT-90, SB-1, HT-1, and CGT-3, as shown in Figure 14.18.

FIGURE 14.17
Rail flaw detection car.

FIGURE 14.18
Rail flaw detector.

14.2.3 TURNOUT MONITORING SYSTEM

Turnouts are the weak point of track structure. As the switch rails and point rails are not provided with fastenings, if not detected, any rail fracture may lead to derailment. Worsened by the interference of all types of components and coverings of the rail base, cracks on switch rails and point rails may not be detected easily, even with the above flaw detection measures; the track circuit cannot be identified in time in case of these rail fractures due to the conductivity of tie plate. Therefore, rail fracture in high-speed turnouts is regarded as a safety risk source. During the practical operation of high-speed turnouts in China, several rail cracks have been detected, such as in the No. 18 turnouts in Leiyang Station in the Wuhan–Guangzhou line and the Danyang North Railway Station in the Beijing–Shanghai line. For this, China is devoted to seeking a monitoring system for turnout rail cracks. German and French turnout monitoring systems apply mainly to monitoring the operation of the switch machines to avoid conversion failure. In China, more attention is paid to safety monitoring than state monitoring. At present, monitoring is performed mainly on turnout rail cracks, switching force, turnout split during shunting, closure between the switch rail and the point rail, indication of the gap of switch machine, switching current, and voltage. This monitoring system has been applied to #8 turnout in the Changzhou North Railway Station in the Shanghai–Nanjing line [179].

Acoustic emission (AE) technology is applied to the monitoring of turnout rail cracks. AE, or stress wave emission, developed in the 1960s, is different from general ultrasonic detection. For this technology, external loading is used to instantly release the local source energy in solid material and produce a transient elastic wave; with the sound signal received, the internal defects of the material can be analyzed, and the integrity and features of the material can be assessed. PZT (lead zirconate titanate) piezoelectric ceramics are used to monitor the surface wave when a rail crack occurs; this system can detect any rail cracks by analyzing the vibration energy spectrum. In the meantime, the Kaiser effect may be used to avoid detection error. The Kaiser effect refers to the irreversibility of AE, that is, no significant AE takes place when repeatedly applying

FIGURE 14.19

Installation of piezoelectric sensor.

FIGURE 14.20

Spall at the top of the switch rail.

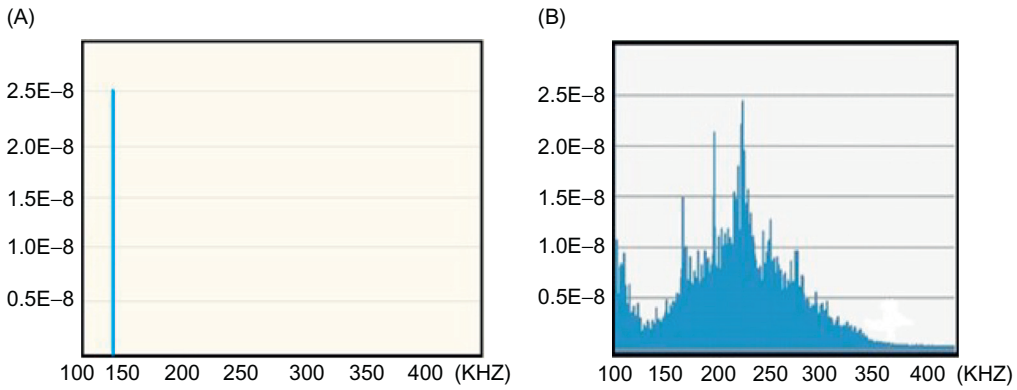

FIGURE 14.21

(A) Energy spectrum of a normal rail. (B) Energy spectrum of a defective rail.

a load smaller than the maximum load imposed previously. Figure 14.19 is a picture of a field piezoelectric sensor; Figure 14.20 shows a spall at the top of the switch rail detected in the North Marshaling Yard in Chengdu; and Figure 14.21 shows the energy spectra of normal and defective switch rail.

In the monitoring of switching force, the pin shafts for switch rod traction are substituted by force measuring pins. Rail closure is measured with an eddy current sensor. A wheelset sensor (Figure 14.22) is provided to monitor the running direction of the vehicle during shunting operations in the turnout area, and to identify any turnout spit by comparing with the normal and reverse positions of the turnout. Cameras can acquire the dynamic offset of the gap of a switching rod, measure spacing or displacement, monitor whether the inspection rod is placed in the gap as shown in Figure 14.23, and determine the closure status between the switch rail and point rail accordingly.

FIGURE 14.22

Wheelset sensor.

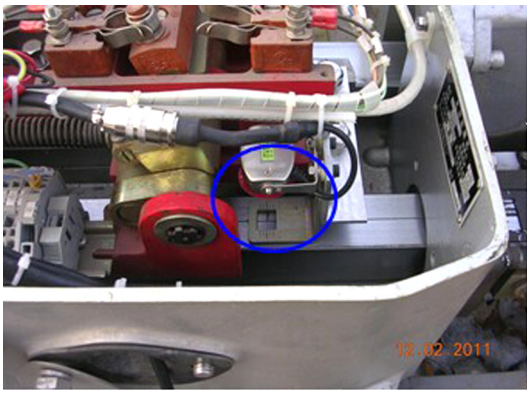

FIGURE 14.23

Gap monitoring of indication rod.

14.3 MAINTENANCE TECHNOLOGIES

14.3.1 RAIL GRINDING [180,181]

1. General requirements

Rail (main lines, turnouts, and rail expansion joints) grinding includes pre-grinding, preventive grinding, and maintenance grinding.

Pre-grinding is done after accurate track adjustment, aiming at decarbonizing the rail surface, adjusting the cross section of the rail, and eliminating rail damage by construction vehicles. The frequency of preventive grinding is determined by total passing tonnage and rail condition, once per passing tonnage of 30–50 Mt in principle, but no longer than 2 years. The grinding cycle for turnout rails is identical to that for rails in the main line. Maintenance grinding takes place when the rails are exposed to corrugation, fish scale crack, or other defects. The preventive grinding profile is determined by the combination of rail surface state and wheel—rail contact. In the absence of a grinding profile, rail grinding may be performed as per the type of EMU trains traveling in the line and referring to a preventive grinding profile. The maintenance grinding plan is determined by the severity of surface defects (rail corrugation, fish scale cracks), and must be capable of removing those defects effectively.

Rails may be ground or milled by a rail grinding train, turnout grinding train, or milling train. Rail welds may be ground with small rail grinders.

The maximum width of a grinding surface (see Figure 14.24): 5 mm in R13 zone; 7 mm in R80 zone; and 10 mm in R300 zone. The maximum change in the width of a grinding surface must not exceed the maximum width of the grinding surface by 25% or above within a length of 100 mm. The contact light band should be in the middle after grinding, about 20–30 mm wide. No continuous blue zone should appear on the grinding surface of the rail.

Surface roughness is measured with a portable roughometer perpendicular to the grinding path on one grinding surface within 10 mm. Six consecutive points will be measured, with roughness no greater than 10 μm.

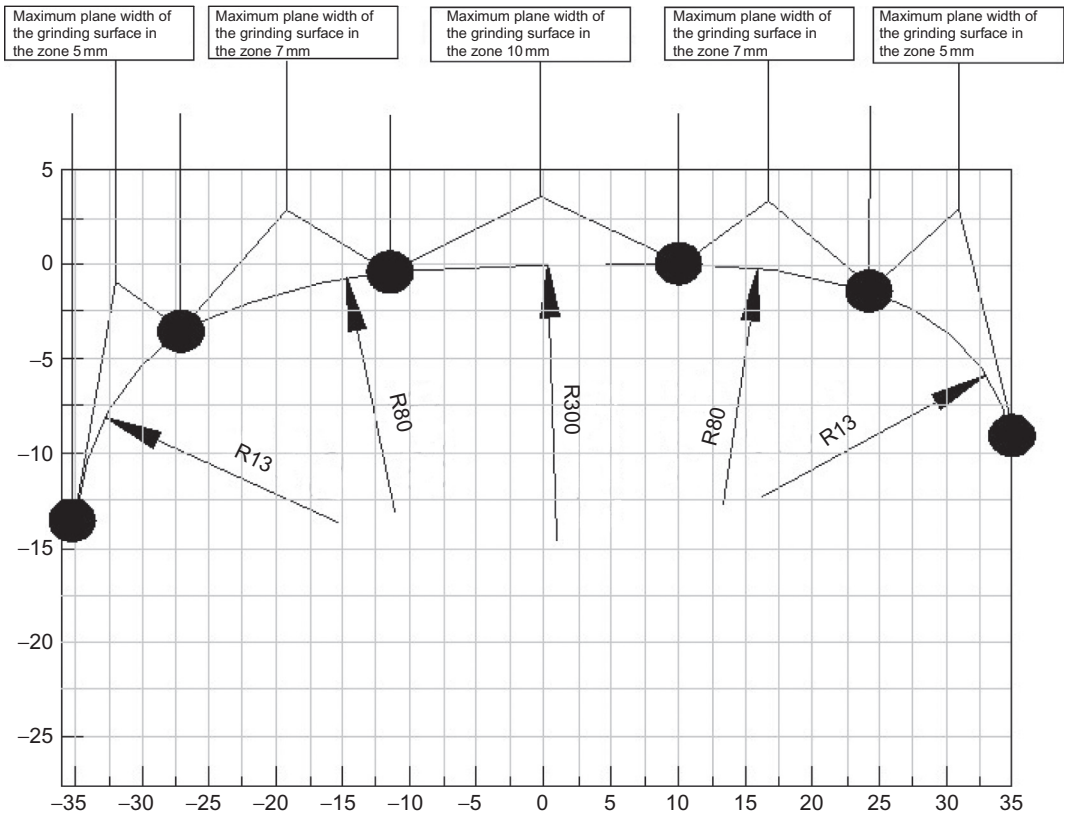

FIGURE 14.24

Diagram of the maximum width of rail grinding surface.

The grinding profile must meet design requirements and will be inspected and accepted with a template or rail profilometer (abrasion tester). Rail grinding work must meet the requirements in Tables 14.7 and 14.8.

2. Grinding of high-speed turnout

China has introduced two types of turnout grinding trains: CMG16 (or RR16MS) from SPENO of Switzerland, and RCH20C of HARSO company of the United States, as shown in Figure 14.25. Of the components of the turnout grinding train, the hydraulic driving grinding head makes it easier to control the deflection angle; a smaller grinding wheel improves adaptability in the narrow zone of the turnout; the vacuum dust collector mitigates operational pollution of the turnout and the environment. The basic principle of high-speed turnout grinding is to ease structural irregularity, improve riding quality, reduce wheel−rail contact stress, and prolong the service life of the rails. Take the cross section at top width 35 mm of the switch rail, for example: The recommended grinding profile of the top of the switch rail and stock rail is shown in Figure 14.26. Comparing the change of lateral structural irregularity of the switch

Table 14.7 Acceptance Standard for Rail Grinding

Item	Acceptance Standard (mm)	Measurement Method	Remarks
Inner working surface of rail head of rail base material	+0.2/0	Measure the rise with 1 m ruler	"+" represents recess
Wear at rail top or saddle wear of rail base material	+0.2/0		"+" represents bulging
Top surface of the weld	+0.2/0		"+" represents bulging
Inner working surface of the weld	+0.2/0		"+" represents recess

Table 14.8 Acceptance Standard for Grinding of Rail Corrugation

Item	Acceptance Standard				Measurement Method	Remarks
Wavelength (mm)	10–30	30–100	100–300	300–1000		
Length of sampling window	600	600	1000	5000		
Mean valley depth (mm)	0.02	0.02	0.03	0.15	Accurate to 0.01 mm and above, with measurement depth not smaller than the width of sampling window	Measured within 8 days after grinding or before total passing tonnage of 300,000 t after grinding
Permissible percentage of inordinateness	5%	5%	5%	5%	Within 100 m (train-borne inspection) or 30 m (manual inspection) for continuous measurement	

with lateral wheelset displacement before and after grinding, it can be concluded that lateral structural irregularity is reduced significantly after grinding, as shown in Figure 14.27. So grinding can greatly benefit the riding quality of EMU trains in turnouts.

For the operation of an RCH20C turnout grinding train, the grinding areas should be divided first as per Figure 14.28. In the figure, the work extends from point A to point H. At point B, the clearance between two adjacent rails in the main and diverging lines after the frog is 100 mm. Point C is at top width 20 mm of the frog. Point D is 100 mm in front of the throat. At point E, the clearance between the switch rail and the stock rail is 100 mm. Point F is at top width 20 mm of the switch rail. Point G is at top width 20 mm of the stock rail.

The RCH20C turnout grinding car employs grinding wheels. It consists of two identical grinding systems (each system has 10 grinding units), with the applicable grinding angle

FIGURE 14.25

Turnout grinding train.

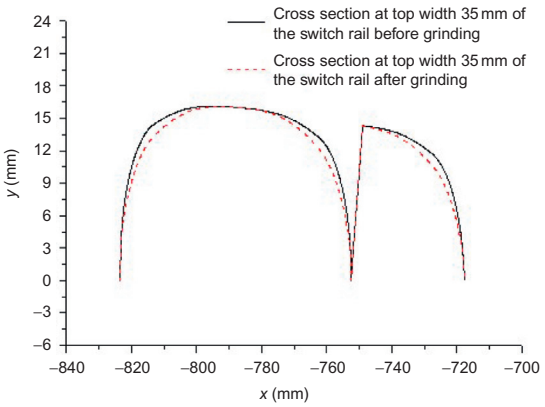

FIGURE 14.26

Recommended rail top profile.

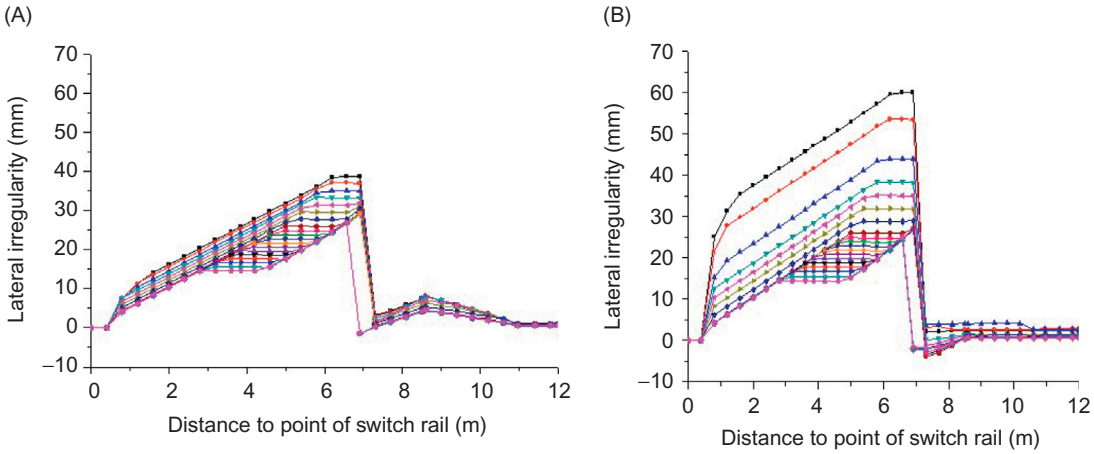

FIGURE 14.27

(A) Change of irregularity with wheelset lateral displacement before grinding. (B) Change of irregularity with wheelset lateral displacement after grinding.

ranging from 75° inside the rail to 45° outside the rail. The rail profile may be adjusted by grinding angles, as shown in Figure 14.29. The rail profile may be modeled as a tetradecagon. During the operation, the grinding angles, lateral position, and installation position will be programmed as per the grinding sequence set out in Table 14.9. The grinding speed is 7 km/h, and the rails will be ground 12 times. All rail top zones depicted in Figure 14.30 will be ground three times. Limited by capacity, partial segments of the turnout area cannot be ground without interruption, such as the segments B−D and E−G. In this case, those segments may be preground with a profile grinder by the engineering district, so as to achieve better grinding effect.

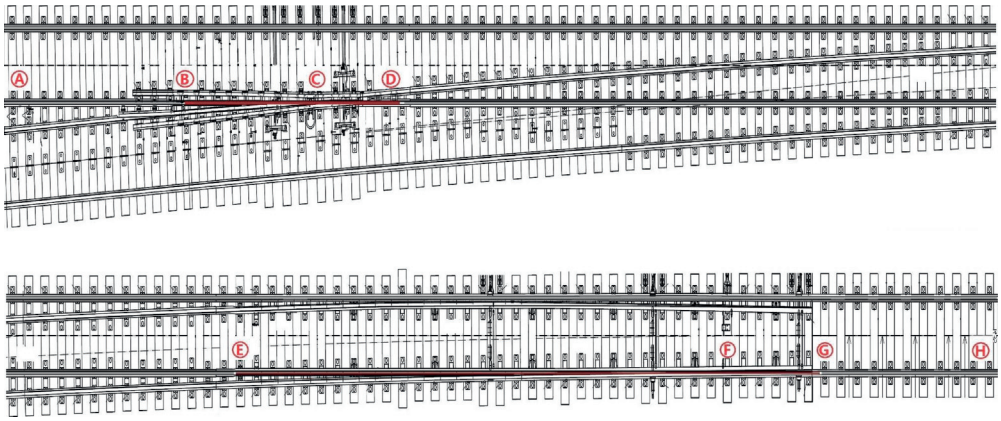

Notes:
Point A: Origin of operation
Point B: The place where the clearance between straight and curved rails is 100mm in rear of the frog
Point C: Frog (top width = 20mm)
Point D: 100mm in front of the throat
Point E: The place where the clearance between switch rail and stock rail is 100mm
Point F: Switch rail (top width = 20mm)
Point G: Point of switch rail
Point H: End of operation
Gray: Normal grinding zone
Red: Restricted grinding zone
White: Zone not to be ground

FIGURE 14.28

Division of grinding area in the turnout.

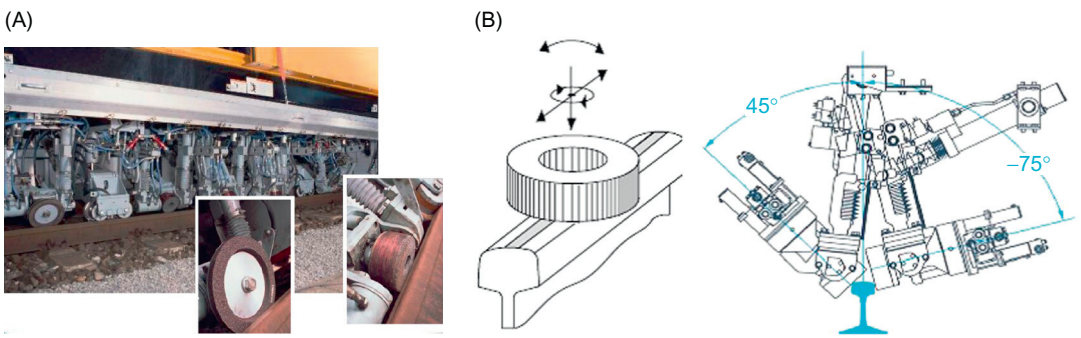

FIGURE 14.29

(A) Grinding unit. (B) Angle range of grinding.

The high-speed turnouts in the Hainan East Ring Intercity Railway are taken as an example. Before grinding, the rail top profile is unsatisfactory; the light bands on the tread caused by wheel−rail contact are 30−40 mm wide and distributed unevenly, instead of concentrating in the middle of the rail top. Certain light bands appear at the rail top or inside the rail.

Table 14.9 Turnout Grinding Mode and Sequence

Times	Mode	Angle	Grinding Area						
			A–B	B–C	C–D	D–E	E–F	F–G	G–H
1	1	45° −31°	Normal	Normal	Restricted	Normal	Normal	Restricted	Normal
2	13	22° −29°	Normal	Normal	Restricted	Normal	Normal	Restricted	Normal
3	3	29° −22°	Normal	Normal	Restricted	Normal	Normal	Restricted	Normal
4	15	14° −21°	Normal	Normal	Normal	Normal	Normal	Normal	Normal
5	5	21° −14°	Normal	Normal	Normal	Normal	Normal	Normal	Normal
6	17	6° −13°	Normal	Normal	Normal	Normal	Normal	Normal	Normal
7	7	13° −6°	Normal	Normal	Normal	Normal	Normal	Normal	Normal
8	19	2° −5°	Normal	Normal	Normal	Normal	Normal	Normal	Normal
9	6	−2° to 1°	Normal	Restricted	Restricted	Normal	Restricted	Restricted	Normal
10	14	1° to −2°	Normal	Restricted	Restricted	Normal	Restricted	Restricted	Normal
11	10	−9° to −2°	Normal	Restricted	Restricted	Normal	Restricted	Restricted	Normal
12	20	−2° to −9°	Normal	Restricted	Restricted	Normal	Restricted	Restricted	Normal

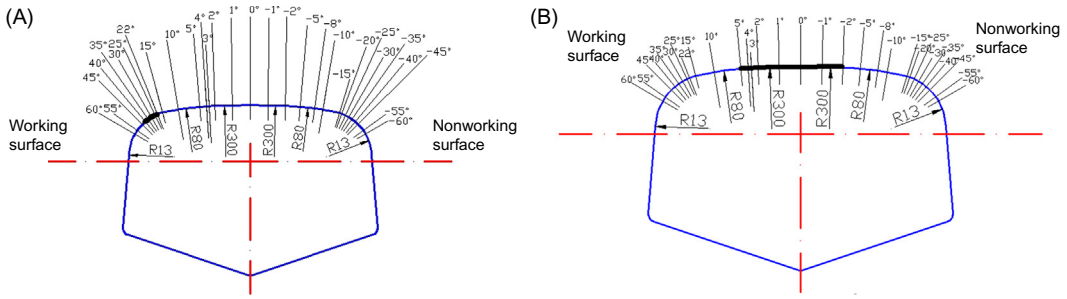

FIGURE 14.30

(A) Large-angle area at gauge corner. (B) Small-angle area at rail top.

FIGURE 14.31

Double light stripes.

FIGURE 14.32

Light stripe after grinding.

This causes two contact points between the wheel and the rail, leading to double light bands, as shown in Figure 14.31. After grinding, the light bands concentrate in the middle of the rail top, about 20−30 mm wide, without any double light bands, as shown in Figure 14.32. In addition, riding quality is greatly improved in the turnout, achieving the estimated grinding target.

3. High-speed grinding train

The Vossloh company of Germany has developed a high-speed grinding train with an operating speed of up to 80 km/h, as shown in Figure 14.33. The unit grinding amount is 0.05 mm. This grinding train is used mainly in preventive grinding to avoid rail fatigue and folds induced by rolling contact. Sets of rotatable grinding wheels at varied angles are used to grind the rail top profile completely, as shown in Figure 14.34. This grinding train has been borrowed by China to grind the rails in the Beijing−Shanghai line Figure 14.35. After grinding, roughness is not greater than 0.008 mm, making the rail surface smoother, without changing the tread profile. Figure 14.36 shows the grinding effect of this grinding train.

FIGURE 14.33

High-speed grinding train from Germany.

FIGURE 14.34

Sets of grinding wheels at different angles.

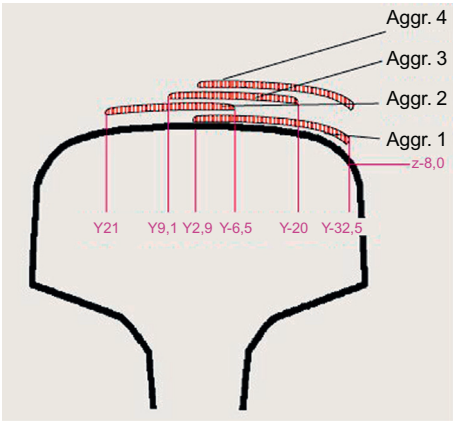

FIGURE 14.35

Grinding zones at rail top.

FIGURE 14.36

Ground rail top profile.

14.3.2 MAINTENANCE OF BALLASTED TURNOUT

1. Large track maintenance machines in China

Large track maintenance machines are favored by more and more nations under the development trend of high-speed, heavy-haul traffic and heavy track structure of railways. The rapid development of HSRs has accelerated technical progress in track maintenance machineries. Large track maintenance machines have long prevailed in Western developed countries. In addition, in those nations, the maintenance mode for HSRs is characterized by sophisticated machinery, excellent operation quality, and automatic intelligent control.

With the construction and operation of HSRs in China, large track maintenance machines have become inseparable from the formal operation of new railways and track maintenance. Large track maintenance machines are the dominant means of grinding, tamping, and maintenance operations on ballasted tracks. They are also used for track lining, tamping, and

FIGURE 14.37

CDC-16 turnout tamping machine.

FIGURE 14.38

CQS-550 turnout full-section ballast undercutting cleaner.

stabilizing during track cyclic maintenance and maintenance of sections. Before the tamping and maintenance work with these machines, effort is required to comprehensively survey and optimize the track plane and vertical section in the operation zone, analyze static and dynamic inspection data, develop maintenance designs, calculate and determine the work quantity, and formulate rational operation plans based on CPIII.

The development of large track maintenance machines in China is marked by a late start and rapid growth. Only a small number of machines were imported for testing in the early 1980s. However, in the late 1980s, Kunming (China) Railway Large Maintenance Machinery Co., Ltd introduced the production technology for the 08-30 tamping machine from Plasser & Theurer (Austria), and developed its own QQS-300 ballast cleaning machine (1987), SPZ200 ballast distributing and trimming machine (1988), and WD320 dynamic track stabilizer (1993). Thus, a complete set of large maintenance machines was established. In the 1990s, the manufacturing technologies for the DCL-32 continuous tamping machine and CDC-16 turnout tamping machine (Figure 14.37) were introduced from Plasser & Theurer, and the full-section ballast bed redistributing machine, turnout redistributing units, and plateau-type large maintenance machine were developed. At the beginning of the twenty-first century, Xiangfan Rail Vehicle Factory (former name of Gemac Engineering Machinery Co., Ltd), Beijing Feb. 7th Railway Transportation Equipment Co., Ltd, and Baoji CSR Times Engineering Machinery Co., Ltd have launched a series of new products independently, including the SPZ-350 four-axis ballast distributing and trimming machine, WY-100 material transport vehicle, QQS-450II ballast cleaning machine, YHG-1200 rail welding vehicle, CQS-550 track full-section ballast cleaning machine (Figure 14.38), YHGQ-720 digitally controlled pneumatic rail welding vehicle, and QJC-190 bridge−tunnel inspection vehicle. These maintenance machines fall into six categories, involving ballast cleaning, tamping, ballast distributing, stabilizing, material transport, and rail welding. The development of these machines has greatly promoted operational quality and efficiency, and accelerated the six speed-ups and construction of HSRs in China.

FIGURE 14.39

EM-SAT 120 high-precision automatic measurement vehicle.

FIGURE 14.40

Laser alignment vehicle.

2. Improvement technologies for long-wavelength irregularity

Long-wavelength track irregularity is a major factor impacting riding safety and passenger comfort during high-speed traffic. Long-wavelength defects of the track may lead to inaccurate geometric parameters in HSRs. However, these defects can hardly be removed by conventional chord inspection technology and track leveling modes. In recent years, the maintenance strategy for HSR track has shifted from conventional leveling to absolute geometric parameters of the track.

The EM-SAT 120 high-precision automatic measurement vehicle system (Figure 14.39) was imported by China from Plasser & Theurer. This system, integrating a 3D measuring system and high-precision tamping machine, is applicable to maintenance of the track with an anchor stake system, capable of restoring the design standard of the track after tamping, lifting, and lining, as well as eliminating long-wavelength irregularity. For this system, fixed reference points are arranged on marking stakes or catenary poles, laser long-chords are arranged between the measurement vehicle (EM) and satellite leading vehicle (SAT) to measure offset distance, and the absolute coordinate datum will be established with GPS. However, measurement accuracy is unsatisfactory.

In speed-up railways in China, large tamping machines are all equipped with a laser alignment system. Among these machines, the 08-32 and 09-32 tamping machines are provided with a one-dimensional laser alignment system (Figure 14.40), and can line the track automatically and effectively, with accuracy of track alignment after operation being up to ± 2 mm. The 08-475 heavy turnout tamping machine and 09-X combined-type tamping machine are provided with a 2D laser alignment system, which can line and lift the track automatically and effectively, with a maximum alignment distance of 150 m, satisfying the accuracy requirement of track alignment and eliminating the defect of long-wavelength longitudinal level irregularity. The laser alignment system for guiding the track lifting or lifting and lining operations of the tamping machine is marked by long-chord measurement; however, it does not reflect the merits of CPIII sufficiently, and the operation effect is still unsatisfactory.

Recently, China has developed a CPIII-based tamping technology that integrates operator, machine, and network and features a large scale-machine, accurate measurement, and accurate

tamping. During operation, the operators will convert the CPIII data into tamping parameters identifiable by the tamping machine or tamping−stabilizing machine and compare them with design values; they will then input the resulting amount of track lifting and lining for the tamping machine into the tamping machine's computer (ALC), so as to ensure accurate tamping and eliminate track geometry deviation. Practice shows that the application of the tamping−stabilizing machine can improve efficiency from 1.1 to 1.8 km/h, and is capable of effectively eliminating 70−120 m longitudinal level irregularity.

14.3.3 IMPROVEMENT OF THE SETTLEMENT OF BALLASTLESS TRACK FOUNDATION IN THE TURNOUT AREA

Ballastless track is characterized by a stable foundation and less maintenance work. It is the major track structure type of Chinese HSRs for 250 km/h and above. This track type includes CRTS I and II double-block type; CRTS I, II, and II slab type; embedded long tie type; and turnout slab type. However, ballastless track can be hard to maintain in case of any damage by settlement. Therefore, stricter quality requirements have been formulated during the construction of Chinese HSRs, covering ground treatment, embankment fill, bridge design, tunneling, concreting, placing of filler course, and laying of isolation course. China has a vast territory with complex geological and climatic conditions. Severe geological conditions (e.g., mollisol, deep soft soil, collapsed loess, and regional settlement) are a major challenge in the construction of ballastless tracks. Much settling has appeared in certain sections of the existing HSRs. For instance, in Jinshan North Railway Station in the Shanghai−Hangzhou line, foundation settlement led to a track settlement of 90 mm in the turnout area, and offset the distance from track centerline by 70 mm. After analysis and discussion, CARS and the Shanghai railway bureau put forward the following remedies which may be reserved for later use.

1. Fastener with large adjusting capacity

   The WJ-7 fastening is a bolted, shoulder-free fastener system developed by China. The design vertical adjustment capacity is −4 to +26 mm, realized by arranging riser blocks under the rail or the tie plate. The design lateral capacity is ±6 mm, realized steplessly by arranging slotted holes on the tie plate and moving the tie plate laterally. Regarding the requirement for large adjustment capacity, a series of technical measures, such as arranging steel riser blocks or cushion pads under steel riser blocks, or lengthening the anchor bolts, may be applied, with a vertical adjusting capacity of −4 to +70 mm, as shown in Figure 14.41. By lengthening the sizes of slotted holes on the tie plate, the lateral adjustment capacity of ±6 mm can be realized for a single rail.

   The WJ-8 fastening is a bolted and shouldered fastener system developed by China. The design vertical adjustment capacity is −4 to +26 mm, realized by arranging riser blocks under the rail or the tie plate. The design lateral adjustment capacity is ±7 mm, realized by replacing with insulated gauge blocks of gauge aprons with different numbers. Regarding the requirement for large adjustment capacity, technical measures, such as arranging steel riser blocks or plastic riser blocks under the tie plate or lengthening the screw spikes, may be applied, with a vertical adjusting capacity of −4 to +60 mm, as shown in Figure 14.42. With the arrangement of gauge blocks or aprons, the lateral adjustment capacity of 8 mm can be realized.

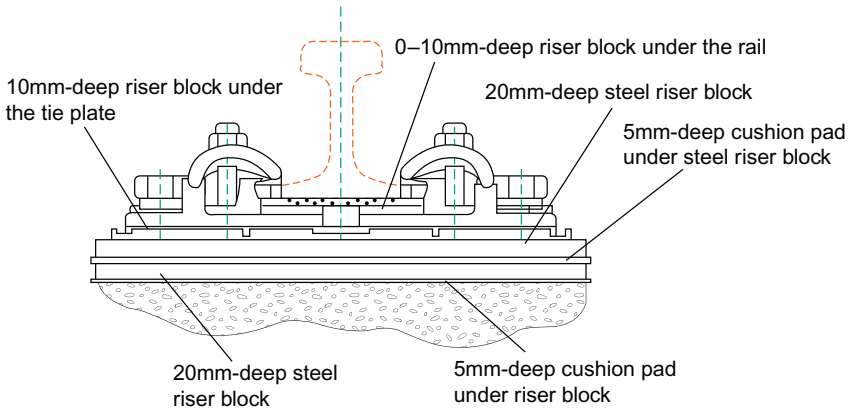

FIGURE 14.41

WJ-7 fastener with large adjusting capacity.

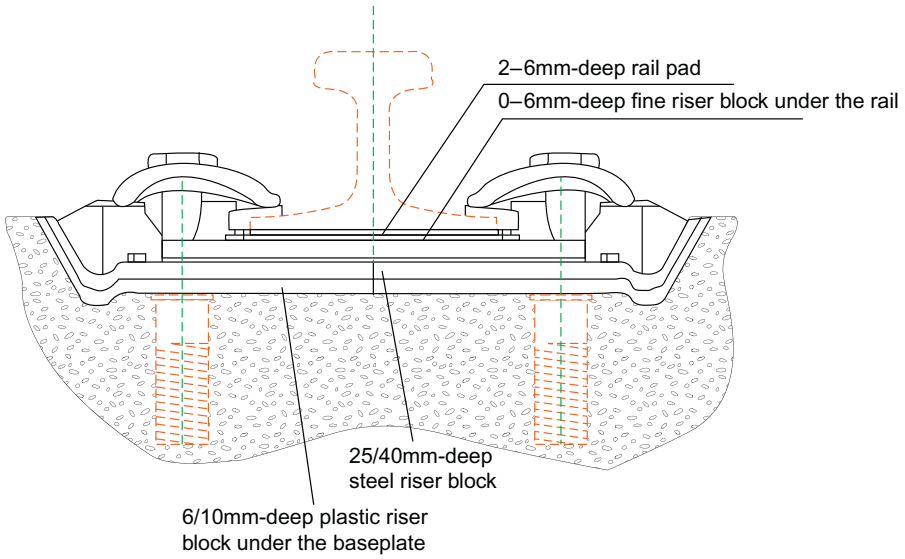

FIGURE 14.42

WJ-8 fastener with large adjusting capacity.

The turnout fasteners may also be adjusted vertically by using deeper tie plates or arranging steel riser blocks, with the vertical adjustment capacity of −4 to +60 mm. In the early period of the subgrade settlement in the turnout area in Jinshan North Railway Station, the longitudinal level irregularity of the area was improved by replacing with fasteners with large adjustment capacity, as shown in Figure 14.43.

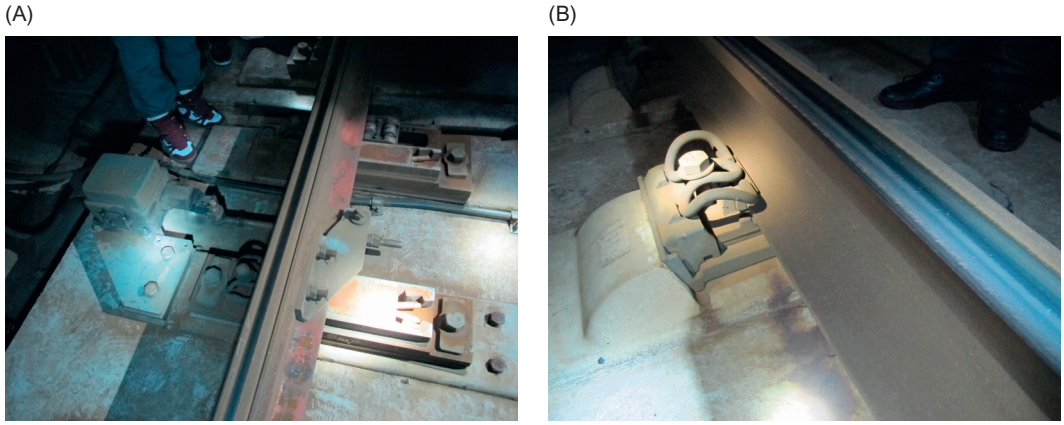

FIGURE 14.43

(A) Fastener with large adjusting capacity in a turnout. (B) Fastener with large adjusting capacity in a section.

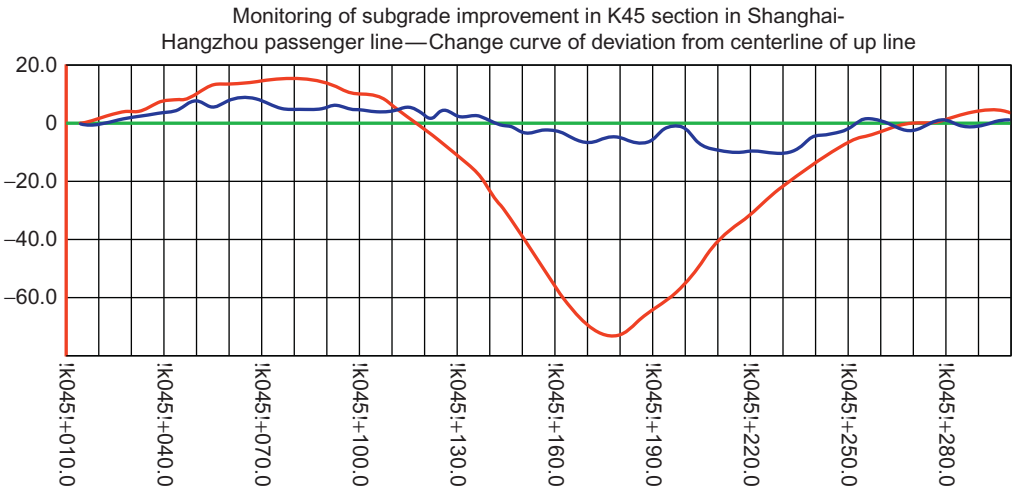

FIGURE 14.44

Comparison of deviation from track centerline before and after adjusting jet grouting pile.

2. Adjustment of HP jet grouting pile on subgrade

The K45 section in Jinshan North Railway Station in the Shanghai−Hangzhou line is the turnout area. The area deviates from track centerline by more than 70 mm due to subgrade settlement, as depicted by the red line in Figure 14.44. The Shanghai railway bureau attempted to remove this defect by driving HP jet grouting piles at the shoulders and grouting below the embankment, as shown in Figure 14.45. During the treatment process, the change of the subgrade soil mass was monitored and analyzed to determine the relation between the soil mass

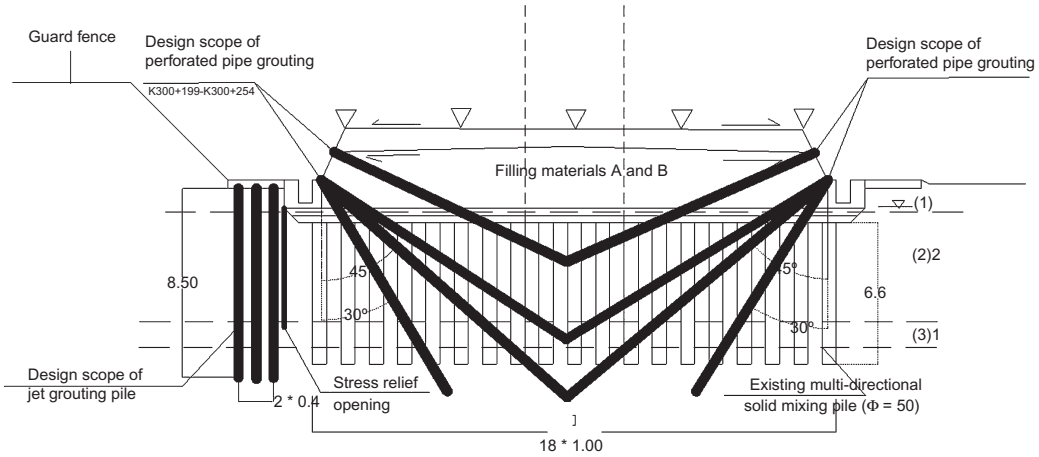

FIGURE 14.45

HP jet grouting pile and grouting scheme.

and various parameters, including the driving of jet grouting piles, grooving of stress relief grooves, stress relief openings, deviational survey openings, and pore-water pressure. A comparison with theoretical and laboratory models was performed to provide guidance for field operation. After this treatment, the track deviation was rectified by 67.4 mm, as depicted by the blue line in Figure 14.44.

3. Repairing and raising of filler course of track slab

   The filler course between the track slab and base slab is generally made of cement emulsified asphalt or self-compacting concrete, serving as a bearing and adjustment measure and a proper elasticity source. This course is relatively thin and is prone to cracks, spalling, and chipping under the action of train load, temperature, water, and foundation settlement. Present maintenance technologies for the filler course mainly involve repairing damaged corners and local gaps by filling polymers or chemical grouting. However, if the foundation settlement is beyond the adjustment capacity of the fastener, track slab raising technology may apply.

   China has developed a polymer cement mortar and vinyl-acrylic resin mortar for rapid repairs and has proposed the raising method for unit track slab by prefabricating the organic–inorganic composite mortar slab and filling the free space with resin mortar, as shown in Figure 14.46. A slab raising simulation test was performed at the maintenance base in Changzhou in the Shanghai railway bureau, providing technical reference for future improvement of large settlements of ballastless track.

4. Base raising by polymer grouting

   Polymer grouting is widely used in highway subgrade reinforcement and lifting of concrete pavement due to the simple nature of the technology, high efficiency, and good durability. It is an effective remedy for dealing with such defects as pavement settlement and suspending of concrete pavement induced by subgrade settlement.

   The polymer for ballastless track grouting is a two-component rigid polyurethane foam, nonreactive with water, in which the carbamate component is a product of isocyanate and hydroxy

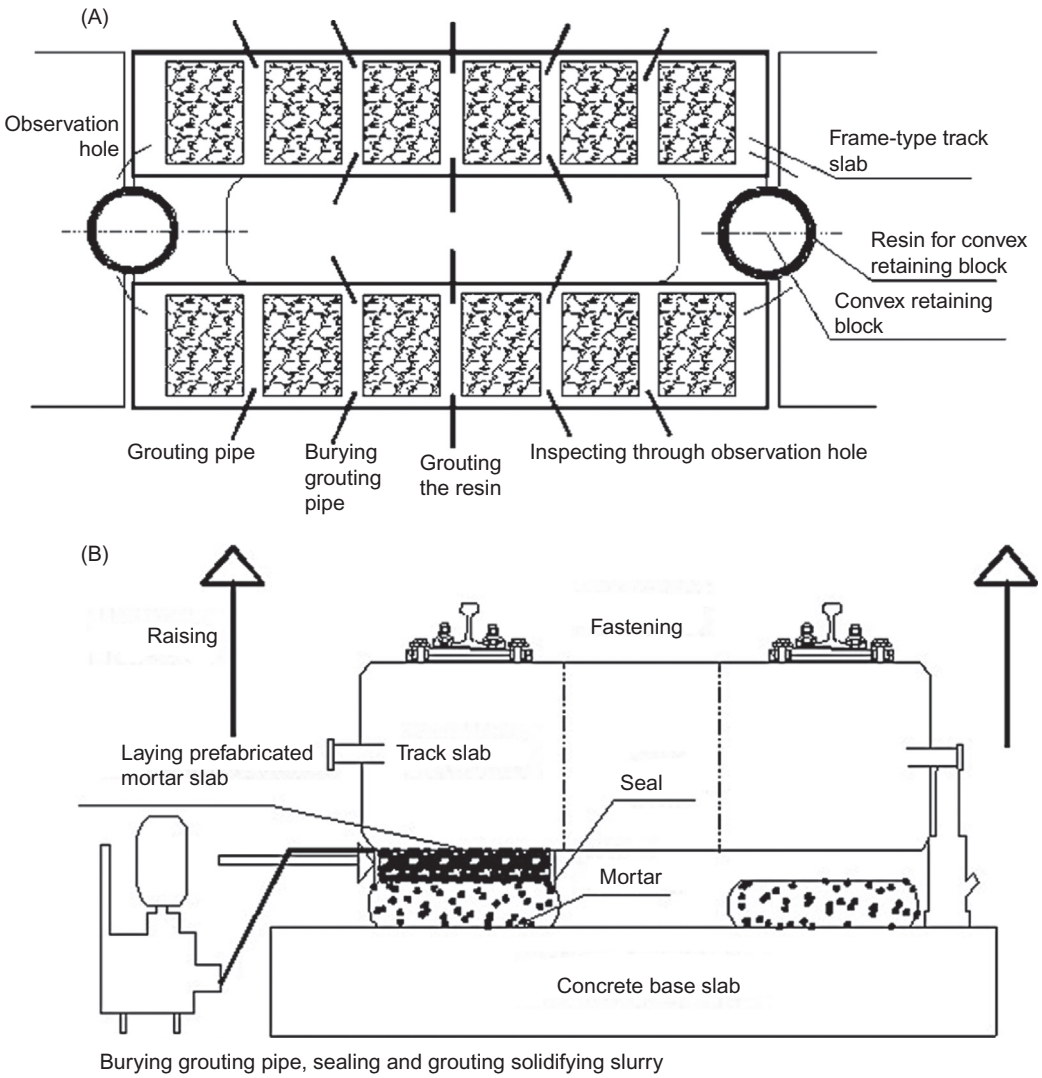

FIGURE 14.46

(A) Laying of composite mortar slab. (B) Filling by grouting resin.

compounds. The polymer has a density of 1/20 of cement density and the free swell ratio is 20:1. It can attain 90% of final intensity in 15 min. In addition, it is advantageous in its good fluidity, water impermeability, and environmental friendliness. After grouting into the subgrade, the product will expand rapidly and form a foamed solid due to reactions. The ballastless track is then lifted by the grouting pressure and expansion force of the grout. In addition, as the grout solidifies rapidly and forms a compacted mixture with graded crushed stones, it can support the ballastless track effectively, as shown in Figure 14.47.

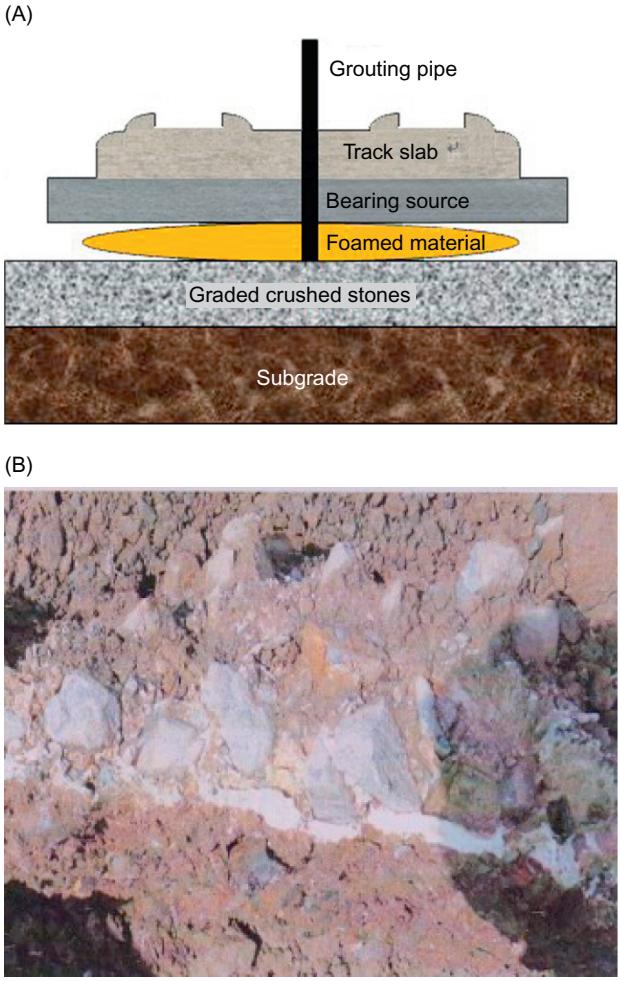

FIGURE 14.47

(A) Diagram of polymer grouting. (B) Mixture of polymers and graded crushed stones.

In 2012, CARS and the Beijing railway bureau performed ballastless track lifting tests by grouting imported polymer in Langfang Railway Station in the Beijing−Shanghai line, Wuqing Railway Station in the Beijing−Tianjin intercity railway, and Binhai Railway Station in the Tianjin−Qinhuangdao line. In 2013, CARS and the Shanghai railway bureau performed lifting tests on CRTSII slab tracks in straight and curved sections of the Hangzhou−Changsha line under construction. Results show that the track can be effectively lifted and the free space can be eliminated satisfactorily by optimizing the process and material properties. Therefore, this technology may be used for future mitigation of large settlements of ballastless track.

14.4 MANAGEMENT OF HIGH-SPEED TURNOUTS

14.4.1 PERMANENT WAY MANAGEMENT INFORMATION SYSTEM

Since 1999, the Permanent Way Management Information System (PWMIS) has been developed as instructed by the former MOR of China. This computer network information management system covers the three-level engineering management departments, namely China Railway Cooperation, railway bureau, and engineering district. In addition, it forms a permanent management information application system and network platform focusing on stationary equipment and graphical information management.

1. Composition and function of the system

   PWMIS is a database with shared information from all engineering disciplines, focusing on the management of stationary equipment and graphical information. It covers 13 business subsystems, including track equipment, bridge and tunnel equipment, subgrade equipment, track inspection in autumn, bridge and tunnel inspection in autumn, engineering dispatch, flood control, preparation of general diagrams, velocity diagrams, wiring diagrams and bridge sketch maps, and rail detection. It also consists of two maintenance subsystems: data synchronizing and system management. In 2008, the function of HSR equipment management was included, and subsystems such as track equipment, bridge/tunnel equipment, general diagrams, and velocity diagrams were improved. In 2011, a large track maintenance machine management information system was developed, consisting of the function modules of equipment management, construction, maintenance, and application of large machines.

   PWMIS is charged with data management functions such as data acquisition, transmission, database creation, inquiring, searching and reporting, and is capable of satisfying the requirements for business management of engineering departments in terms of track, bridges and tunnels, subgrade, and dispatch. Moreover, with the functions of information integration, reporting, statistics, inquiry, printing, graphic display, and data transmission and maintenance, it can provide prompt and accurate information for the construction, renovation, and maintenance of engineering equipment.
2. Management of accessed inspection and monitoring information

   Engineering inspection and monitoring data, such as track inspection cars, comprehensive inspection trains, train-borne track inspection devices, rain gauges, gale monitoring, and rail temperature monitoring of CWR track, can be accessed in the railway network through a railway security platform. In this way, all inspection and monitoring data are managed in a centralized way in PWMIS database of the railway network. This facilitates the management of equipment condition and timely handling of track defects.
3. Inquiry system of track video information

   In China, a railway engineering video information inquiry system has been developed to enhance the command capability of emergency repair in case of engineering equipment accident and disaster, and can get the actual geological and geomorphic information at the site of an accident in real time. The system integrates a railway electronic map, a general diagram of track equipment, and a wiring diagram of the station with track videos. In this way, information on the track engineering equipment along the line can be displayed intuitively and comprehensively, providing data support for the decision making and command of relative administrators.

4. Safety and production management information system for engineering equipment

   China has also developed an engineering safety production management information system to extend the capacity of PWMIS to safe production at the levels of district, workshop, and section. The system, consisting of the management modules of geographic information system (GIS), equipment, production, safety command, integrated management, and system management, provides integrated data platforms for inspection, operation, maintenance, equipment, and spatial geographic information. The management modules of equipment, production, and safety provide closed-loop management through the life cycle. Equipment management follows the process flow of "equipment application → defects (faults) → repairing → replacing → discarding." Production management follows the process flow of "inspection and monitoring → status analysis and predicating → maintenance planning → repairing → quality assessment → inspection and monitoring." Safety management follows the process flow of "equipment defects (faults) → improving → tracking → security assessment → equipment defects (faults)."

14.4.2 DIGITAL MANAGEMENT OF ENGINEERING EQUIPMENT

The concept of a "digital railway" is being developed gradually. Informatization based on digitalization of spatial information can reconstruct the railway in a digital network. "Digital engineering" is the core of the digital railway. At present, China is devoting much effort to the development and construction of a digitalized management system for HSR engineering equipment.

A digitalized management platform for engineering equipment is to be developed on the basis of railway electronic geo-maps, aerial surveys, remote sensing railway maps, geomorphological maps along the railway, integrated engineering thematic maps, railway live video, photos, survey and design data during the construction period, completion data, basic data on the equipment, dynamic inspection and monitoring data on the equipment, maintenance quantity for the equipment, traffic volume, velocity, and safety issues by using the technologies of GIS, GPS, or Compass Navigation Satellite System (CNSS), remote sensing (RS), Internet of things (IOT), and 3D visualization. This platform enables the integrated, centralized, and efficient management of engineering data and information sharing, providing technical support for safe production of engineering equipment.

The digitalized management system for HSR engineering equipment is a multidisciplinary and multi-field system. A great deal of data exchange and sharing is involved between the system and the disaster prevention and safety monitoring system, operation and dispatching system, and project management. Other interface systems of interest include the disaster prevention and safety monitoring system (natural disaster), EMU monitoring system (vehicle operation), EMU maintenance system (equipment status), power sources management system (equipment utilization), operation and dispatching system (defects), and emergency platform (defects).

The digitalized management system for HSR engineering equipment is conducive to the IT-based management of HSR engineering equipment over the entire life cycle in terms of survey, design, construction, management, inspection, monitoring, analysis, and maintenance. The digitalized engineering equipment platform enables integrated and intelligent analysis of information, provides scientific maintenance suggestions for equipment, and offers a comprehensive information service for decision making on the maintenance of engineering equipment in all directions.

14.4.3 RAMS MANAGEMENT OF HIGH-SPEED TURNOUTS

RAMS is an acronym for "reliability, availability, maintainability, and safety." In Europe, EN 50126 has long prevailed in the railway industry; this code was defined as IEC 62278: 2002 and later. In 2008, the code was adopted by China, renumbered as GB/T21562-2008, and renamed "Railway Applications: The Specification and Demonstration of Reliability, Availability, Maintainability and Safety (RAMS)." The application of RAMS is being improved gradually in the design, manufacturing, operation, and maintenance of high-speed turnout products for Chinese HSRs [182].

1. Definition and parameters of RAMS

   Reliability refers to the capability of a product, equipment, or system to perform relevant functions under given conditions and in a given time. Reliability falls into two categories: intrinsic reliability and operational reliability. Intrinsic reliability is reliability resulting from design and manufacturing. Operational reliability defines the performance level of intrinsic reliability of a product in actual use.

   Maintainability refers to the capability of the equipment of product to retain or restore relevant functions after being maintained as per specified processes or methods under given conditions and in a given time. This feature implies a degree of difficulty of the maintenance provided to the device or product. It is an intrinsic property specified by design.

   Availability is the possibility of access to a system for normal operation at a given moment when available. This feature implies the reliability and maintainability of a system. It is one of the three main features for system efficiency (with performance and dependability).

   Safety refers to the capacity of a system or product to prevent personal injury, system destruction, or major property loss, and to avoid hazard to people and the environment. The feature is based on reliability, availability, and maintainability.

   Take the life cycle of turnout products, for instance; the relationships among RAMS parameters are shown in Table 14.10.

2. Technical requirements of RAMS

   a. Quantitative requirements

      Turnouts are a product of railway transport. The quantitative requirements of RAMS of the turnouts are represented by RAMS parameters and relevant requirements thereof. As per EN50126-1 and EN50126-3, RAM parameters may be separated from safety parameters in the railway transport industry. Table 14.11 presents the basic RAM parameters of high-speed turnouts.

      For quantitative requirements of safety, two concepts are mentioned in EN50126-2: tolerable hazard rate (THR) and safety integrity level (SIL). The two parameters are used in safety-related systems such as automatic train protection. THR defines the requirements in terms of the fault rate of safety-related systems. SIL defines the requirements for the safety level of safety-related systems, classified into four levels (SIL4 is the highest requirement). The two parameters are somewhat correlated, as shown in Table 14.12. The railway transport authority will specify related SIL as per the significance of the safety-related system. Different SILs correspond to different RAMS management methods, design and analysis methods, and verification methods to be employed in the design. The reliability objective of the system at various levels, as shown in Table 14.13, must be satisfied.

Table 14.10 RAMS Parameters of Turnouts

Item	Parameter	Description	Equation	Remarks
Reliability	Mean time between failures (MTBF)	Reliability parameter of a maintainable product, equaling the ratio of total life of the product to total number of faults in given conditions and time	$\mathrm{MTBF} = \frac{\sum_{i=1}^{n} T_i}{r_a}$	T_i is the total startup time; r_a is the total number of failures of the product in a given period; n is the total number of products during that time
Maintainability	Mean time to repair (MTTR)	At a given maintenance level, the ratio of total time for repair maintenance to total number of faults of the repaired product in given conditions and time	$\mathrm{MTTR} = \frac{\sum_{i=1}^{r_a} T_{ri}}{r_a}$	T_{ri} is the maintenance time of the defective product (excl. management and logistics delay time); r_a is the total number of faults of the product in that time
	Mean time between maintenance episodes (MTBM)	Mean interval between maintenance episodes (preventive and repairing maintenance)	$\mathrm{MTBM} = \frac{\sum_{i=1}^{n} T_i}{r_a}$	T_i is the total startup time; r_a is the total number of maintenance; n is the total number of products in that time
	Mean time to maintain (MTTM)	Mean time for preventive and repair maintenance	$\mathrm{MTTM} = \frac{\sum_{i=1}^{r_a} T_{ri}}{r_a}$	T_r is the maintenance and repair time; r_a is the total number of maintenance episodes (incl. preventive and repair maintenance) in that time
Availability	Intrinsic availability (A_i)	The availability of a product when only repair maintenance is involved	$A_i = \frac{\mathrm{MTBF}}{\mathrm{MTBF} + \mathrm{MTTR}}$	
	Accessible availability (A_a)	The availability of a product when both repair and preventive maintenance are involved	$A_a = \frac{\mathrm{MTBM}}{\mathrm{MTBM} + \mathrm{MTTM}}$	
	Operational availability (A_o)	The availability of a product when preventive and repair maintenance, and repair and management delay are concerned	$A_o = \frac{\mathrm{MUT}}{\mathrm{MUT} + \mathrm{MDT}}$	MUT is mean up time, MDT is mean down time
Safety	Mean time between critical failures (MTBCF)	The ratio of total life of the product to total number of critical failures in a given conditions and time	$\mathrm{MTBCF} = \frac{\sum_{i=1}^{n} T_i}{r_a}$	T_i is total startup time, r_a is the total number of critical failures of the product, n is the total number of products in used in that time

Table 14.11 Basic Parameters of RAM of High-Speed Turnout

Type of Parameter		Description	Applicable Scope			Time for Verification	Mode of Verification
			Complete Set	System	Equipment		
Reliability	Main reliability	Mean time between failures (MTBF)	√	√	√	Finalization of design	Field test
		Mean time to failure (MTTF)			√	Finalization of design	Field test
		Main reliability $R(t)$	√	√		Finalization of design	Engineering calculation
		Failure rate λ			√	Finalization of design	Laboratory or field test
	Mission reliability	Mean time between critical failures (MTBCF)	√	√		Initial use	Field test
		Mission reliability $Rm(tm)$	√	√		Initial use	Field test
Maintainability	Parameters of maintenance time	Mean time to repair (MTTR)	√	√	√	Finalization of design	Field test or demonstration
		Maximum repair time	√	√		Finalization of design	Field test
	Parameters of maintenance manhours	Maintenance-life ratio	√	√	√	Initial use	Field test
Availability	Availability	Intrinsic availability (A_i)	√			Finalization of design	Engineering calculation
		Accessible availability (A_a)	√			Initial use	Field test
		Operational availability (A_o)	√			Initial use	Simulation verification
	Logistics support	Mean logistics delay time (MLDT)	√			Initial use	Field test
		Spares fill rate	√			Initial use	Field test

Table 14.12 Relationship between THR and SIL

Hourly THR per Function	SIL
$10^{-9} \leq \text{THR} < 10^{-8}$	4
$10^{-8} \leq \text{THR} < 10^{-7}$	3
$10^{-7} \leq \text{THR} < 10^{-6}$	2
$10^{-6} \leq \text{THR} < 10^{-5}$	1

Table 14.13 Target Reliability of System Levels

Type of Failure	Target Reliability Defined by Influence on Operation	Mean Time between Failures (MTBF)/h	Verification Method of Reliability
Significant	Significant failure during operation, causing an operation interruption of over 2 h	>3,750,000	Analysis
Major	Interruption at fault region, causing an operation interruption of 15 min−2 h	>750,000	Analysis
Minor	Operation interruption of 2−15 min	>54,000	Analysis
Insignificant	Failure causing an operation delay of less than 2 min or other failures not affecting train operation	>9000	Analysis

b. Qualitative requirements

The qualitative requirements of RAMS define the RAMS requirements of a product in nonquantitative ways. They are an integral part of RAMS technical requirements.

Qualitative requirements for reliability: reliability requirements that cannot be described by quantifiable indexes; requirements for operational reliability; design requirements for reliability of specific products, such as simplified design, redundancy design, derating design and allowance design, environmental protection design, thermal design, electromagnetic compatibility design, ergonomics design, and application of mature technology and selection and control of components/parts; and protective or preventive measures and requirements around failures that will or may jeopardize the system.

Qualitative requirements for maintainability: maintainability requirements that cannot be described by quantifiable indexes—for instance, parts requiring frequent adjustment, cleaning, and replacement must be easy to assemble and disassemble or available for *in-situ* maintenance; maintenance requirements for specific products, such as requirements for accessibility, dismantlement, modularization, handling, easy cleaning, normalization, interchangeability, and testability.

Qualitative requirements for safety: capability of preventing disastrous accidents in case of system failure by fault safety design, interlocking design, error prevention design, etc., while improving relevant reliability.

c. Requirements for work contents

Requirements for RAMS work contents are to enable products to meet relevant quantitative and qualitative requirements for RAMS. The user may supervise and manage the supplier by specifying compulsory RAMS work content in the procurement agreement for turnouts, so as to ensure the implementation of relevant quantitative and qualitative requirements for RAMS during the process of R&D and production of the products.

The turnout supplier must include those RAMS work contents into a relevant RAMS working plan, making arrangements reasonably and defining the type, implementation period, and connection between processes, so as to monitor the process. Table 14.14 shows a list of common RAMS work contents for turnout, which may be seen as a reference for engineering applications.

3. LCC analysis of high-speed turnouts [183]

In the past, planned preventive maintenance, an empirical maintenance mode instead of relying on scientific analysis of reliability and risks, was used in maintaining Chinese railway track structures. This mode places more importance on operational safety of the track components than economical efficiency. However, in the face of marketization reform of the Chinese railway management system and huge debts from HSR construction, the managers of the railway infrastructure had to find a way out, and attempted to reduce the cost of rail components, optimizing railway engineering maintenance technology based on reliability and guided by risk-informative safety management, so as to minimize the costs of engineering operation and maintenance while maintaining a certain safety level.

Life cycle cost (LCC) is the total cost of a product during its effective use. It includes the costs for product design, manufacturing, procurement, use, maintenance, and disposal. The comprehensive assessment of the costs for product procurement and use, etc. may be conducive to upgrading the performance and RAMS requirements of the product, and to reducing later use cost.

LCC is greatly affected by RAMS. High reliability and maintainability may relate to high purchase cost, but reduced maintenance cost from a relatively lower failure rate of the equipment in use. Rather, low reliability and maintainability may relate to low purchase cost but high maintenance cost of the equipment in use. Therefore, the selection of reliability and maintainability of the equipment should try to minimize the total cost of procurement and maintenance, that is, LCC, if other conditions are the same. The RAMS/LCC assessment model is to assess the equipment systems by efficiency and LCC.

The LCC of high-speed turnouts during the operation and maintenance may be analyzed as per the procedures given in Figure 14.48.

The concept of LCC originated from the Swedish railway system; operational and maintenance cost of turnouts is assessed with LCC technology by taking Swedish railway turnouts as an example. Results show that periodic preventive maintenance cost (including costs for equipment, labor, and spares) has greater weight, much more than corrective maintenance. In the breakdown of periodic maintenance, as shown in Figure 14.49, it can be seen that most costs are incurred on periodic replacement, inspection, and adjustment, while the rest is for tamping, grinding, and reconditioning of welding heads.

Table 14.14 RAMS Task List for High-Speed Turnouts

SN	Contents	Type	Features	Responsibility	
				User	Supplier
1	Defining technical requirements for RAMS	Management	RAMS	√	
2	System assurance plan	Management	RAMS	√	√
3	RAMS working plan	Management	RAMS		√
4	RAMS requirements on sub-suppliers	Management	RAMS		√
5	Failure report analysis and corrective action system (FRACAS)	Management	RAM		√
6	Hazard log	Management	Safety		√
7	Formulating design criteria of RAMS	Design and analysis	RAMS		√
8	Assigning reliability	Design and analysis	RAM		√
9	Modeling and prediction of reliability	Design and analysis	RAM		√
10	Failure mode, effects, and criticality analysis (FMECA)	Design and analysis	RAM		√
11	Fault tree analysis (FTA)	Design and analysis	RAM		√
12	Assigning maintenance	Design and analysis	RAM		√
13	Prediction of maintenance	Design and analysis	RAM		√
14	Reliability-centered maintenance analysis (RCMA)	Design and analysis	RAM		√
15	Preliminary hazard list (PHL)	Design and analysis	Safety		√
16	Preliminary hazard analysis (PHA)	Design and analysis	Safety		√
17	Subsystem hazard analysis (SSHA)	Design and analysis	Safety		√
18	System hazard analysis (SHA)	Design and analysis	Safety		√
19	Operational and support hazard analysis (O&SHA)	Design and analysis	Safety		√
20	Environmental stress screening test	Test and analysis	RAM		√
21	Reliability growth test	Test and analysis	RAM		√
22	Reliability qualification test	Test and analysis	RAM	√	√
23	Life test	Test and analysis	RAM	√	
24	RAM assessment	Test and analysis	RAM	√	√
25	Safety assessment	Test and analysis	Safety	√	√
26	RAMS review and verification	Test and analysis	RAMS	√	

In the thesis, the annuity costs of three types of No. 15 turnouts in the main line are studied with LCC technology, as shown in Figure 14.50. Specifically:

EV-UIC60-760-1:15: No. 15 turnout, UIC60 rails, fixed crossing, radius of transition lead curve = 760 m

EV-BV50-600-1:15: No. 15 turnout developed by Sweden, UIC60 rails, fixed crossing, radius of transition lead curve = 600 m; and

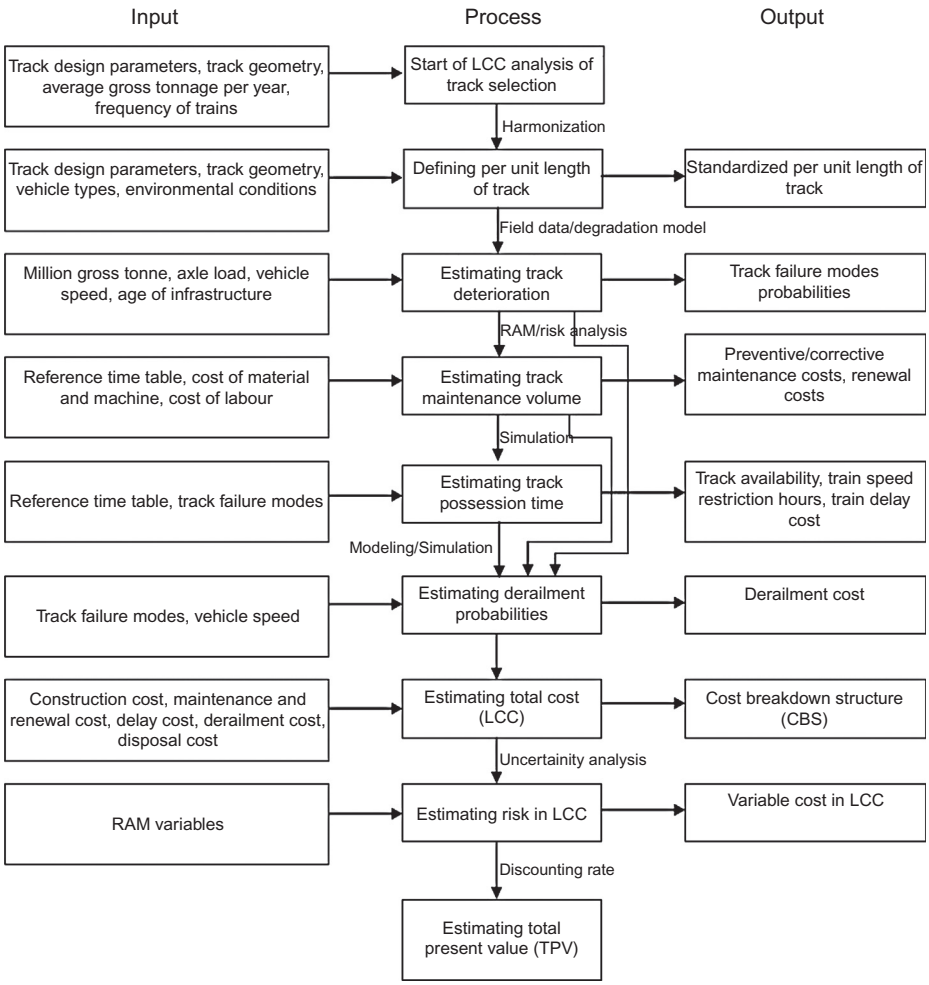

FIGURE 14.48

Lift cost analysis process during operation and maintenance period.

EVR-UIC60-760-1:15: No. 15 turnout, UIC60 rails, swing nose crossing, radius of transition lead curve = 760 m.

The analysis shows that the EV-BV50-600-1:15 turnout has a lower purchase cost than EV-UIC60-760-1:15 (lower by 8%), but it has relatively higher maintenance cost and a shorter life; therefore, its annuity cost is higher by 11% than the latter. EVR-UIC60-760-1:15 turnout has a higher purchase cost by about 43% (the highest of the three); notwithstanding the greatly reduced maintenance cost and prolonged life, it has the highest annuity cost.

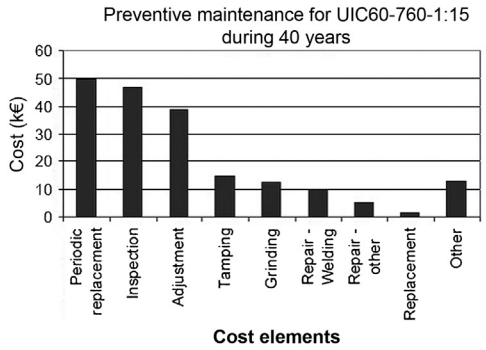

FIGURE 14.49

Composition of turnout cycle maintenance cost.

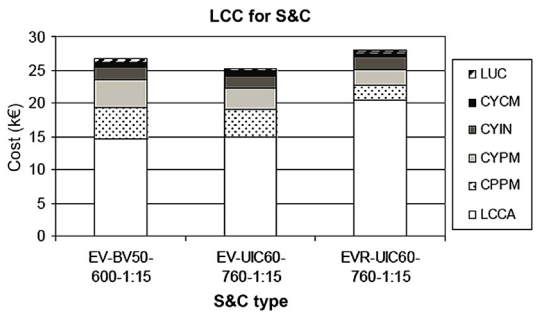

FIGURE 14.50

Comparison of LCC (annuity cost) for three types of turnouts.

LCC theory has been rooted in China for over 30 years. Initially, this theory was mainly used in formulating assessment and inspection policies around equipment status. At present, its application has been extended to various industries (e.g., power industry); however, application to the management of track equipment, such as turnouts, is rare. With the improvement of closed-loop management systems for HSR engineering equipment, collection and accumulation of basic data for asset management and the establishment of digitalized engineering equipment management platforms, the application of RMAS and LCC in Chinese HSR turnouts will expand gradually.

References

[1] W. Ping, Design Theory and Practice of High-Speed Railway Turnouts, Southwest Jiaotong University Press, Chengdu, 2011.
[2] C. Esveld, Modern Railway Track, second ed., MRT-Productions, Zaltbommel, 2001.
[3] Y. Sirong, Railway Engineering, second ed., China Railway Publishing House, Beijing, 2009.
[4] L. Chenghui, Railway Track, China Railway Publishing House, Beijing, 2010.
[5] W. Ping, L. Xueyi, C. Rong, Progress of turnout technology for Chinese high speed railway, High Speed Railway Technol. 1 (2) (2010) 6–13.
[6] W. Ping, C. Rong, C. Xiaoping, Key technologies in high-speed railway turnout design, J. Southwest Jiaotong Univ. 45 (1) (2010) 28–33.
[7] Y. Weiping, Technical characteristics of French high-speed railway turnouts, Chin. Railways 8 (2006) 40–41.
[8] F. Weizhou, Major technical characteristics of high-speed turnout in France, J. Railway Eng. Soc. 9 (2009) 18–35.
[9] H. Qimeng, Introduction of railway turnouts in France, Railway Stand. Des. 11 (1995) 1–4.
[10] L. Bernhard, Track Compendium, Eurail Press, Germany, 2005.
[11] L. Zuwen, Status and development of Chinese railway turnout, Chin. Railways 4 (2005) 11–14.
[12] Z. Zhifang, Analysis on the status quo of existing railway turnouts and the strategy of simplifying universal models, Railway Eng. 6 (2014) 1–3.
[13] S. Yujie, New research development of railway turnout, Chin. Railways 11 (2003) 24–28.
[14] W. Shuguo, G. Peixiong, A study on technologies of turnout in PDL, Chin. Railways 8 (2007) 21–28.
[15] G. Fu'an, Turnout design of foreign high-speed railway, Chin. Railways 2 (2006) 48–50.
[16] H. Huawu, Studies on technologies of high-speed railway turnouts in China, Eng. Sci. 11 (5) (2009) 23–30.
[17] S. Changyao, New stage of overall technology development of Chinese railway turnouts, J. Railway Eng. Soc. 85 (1) (2005) 51–60.
[18] G. Fu'an, Technological system for China's high-speed railways turnout, Chin. Railways 4 (2011) 1–5.
[19] L. Yubing, Discussion on standard technology of China's high-speed railway turnouts, Railway Stand. Des. 2 (2000) 7–10.
[20] S. Yujie, Study on plane design parameters of turnouts for Qinhuangdao-Shenyang PDL, J. China Railway Soc. 23 (4) (2001) 94–97.
[21] L. Jianxin, C. Chengbiao, Dynamic study on parameters of turnout plane design in passenger-dedicated railway, Railway Eng. 5 (2007) 86–89.
[22] The Third Railway Survey and Design Institute Group Corporation, Turnout Design Manual [M], People's Railway Publishing House, Beijing, 1975.
[23] X. Guoping, L. Qiuyi, Comparison and analysis on the types of the high-speed railway transition curves and their operative performance, Railway Invest. Surv. 5 (2005) 58–62.
[24] F. Xiao, L. Min, Y. Jia, Z. Ming, A general method of direct and inverse coordinate computation for different types of transition curves, Bull. Surv. Mapp. 6 (2008) 10–13.
[25] M.R. Bugarin, J.-M.G. Diaz-de-Villegas, Improvements in railway switches, Proc. Inst. Mech. Eng. Part F-J. Rail Rapid Transit 216 (4) (2002) 275–286.
[26] S. JiaLin, X. Yan, W. Shuguo, Simulation study on setting of rational line type for railway large number turnout, Railway Eng. 8 (2010) 125–127.
[27] China Railway Baoji Bridge Group Co. Ltd., Railway Turnout Parameter Manual, China Railway Publishing House, Beijing, 2009.

[28] Shenyang Railway Bureau Maintenance Department, Turnouts, China Railway Publishing House, Beijing, 1987.
[29] X. Shiru, Railway Track Theory, China Railway Publishing House, Beijing, 1997.
[30] C. Yang, Study on dynamic analysis and design methods of turnout layout geometry (Doctor Degree dissertation), Southwest Jiaotong University, Chengdu, 2013.
[31] H. Sugiyama, Y. Tanii, R. Matsumura, Analysis of wheel/rail contact geometry on railroad turnout using longitudinal interpolation of rail profiles, J. Comput. Nonlin. Dyn. 6 (2) (2011) 024501-1-024501-5.
[32] T. Rongchang, Structure and material of high-speed railway turnout, China Acad. Railway Sci. 19 (1) (1999) 95–108.
[33] W. Shuguo, Research on 60 kg/m rail No. 18 turnouts in passenger dedicated line, Railway Eng. 1 (2008) 81–83.
[34] Y. Xi, Development of railway turnouts in passenger dedicated lines, Railway Stand. Des. S1 (2006) 173–176.
[35] W. Shuguo, G. Jing, Study on the selection of AT rails for turnouts in passenger dedicated line, China Railway Sci. 29 (3) (2008) 63–67.
[36] Z. Qingyue, Z. Yinhua, C. Zhaoyang, Issues on rails for high speed railway, Railway Constr. Technol. 2 (2004) 54–57 62.
[37] J. Zhiwu, Recommendations on design and laying of turnouts in high speed railway, Railway Constr. Technol. 1 (2005) 12–13.
[38] Z. Qingyue, Z. Yinhua, C. Zhaoyang, Research and application of high speed rail, Chin. Railways 7 (2010) 16–19.
[39] W. Kaiwen, The track of wheel contact points and the calculation of wheel/rail gemetric contact parameters, J. Southwest Jiaotong Univ. 2 (1984) 9–99.
[40] Y. Juanmao, W. Kaiwen, Calculation of wheel rail contact geometry relationship of arbitrary shape, Roll. Stock 2 (1984) 24–28.
[41] Y. Guozhen, Geometrical parameters of wheel/rail contact with worn profile wheel tread, China Railway Sci. 2 (1982) 83–95.
[42] X. Jingmang, Study on rail wear damage mechanism and its simulation analysis of high-speed turnout (Doctor Degree dissertation), Southwest Jiaotong University, Chengdu (2015).
[43] H. Hertz, On the contact of elastic solids, Reine J. Angew. Math. (1882) 156–171.
[44] F.W. Carter, On the action of locomotive driving wheel, Proc. R. Soc. Lond. (1926) 151–157.
[45] K.L. Johnson, The effect of a tangential contact force upon the rolling motion of an elastic sphere on a plane, J. Appl. Mech. 25 (1958) 339–346.
[46] J.J. Kalker, On the rolling contact of two elastic bodies in the presence of dry friction (Doctoral thesis), TU Delft, 1967.
[47] Z.Y. Shen, J.K. Herdrick, J.A. Elkins, A comparison of alternative creep-force models for rail vehicles dynamic analysis, in: Proceeding of 8th IAVSD Symposium, 1984, pp. 591–605.
[48] J.J. Kalker, A fast algorithm for the simplified theory of rolling contact, Vehicle Syst. Dyn. 11 (1) (1982) 1–13.
[49] J.J. Kalker, Three Dimensional Elastic Bodies in Rolling Contact, Kluwer Academic Publisher, Dordrecht, 1990.
[50] X. Zhao, Z. Li, The solution of frictional wheel-rail rolling contact with a 3D transient finite element model-validation and error analysis, Wear 271 (1–2) (2011) 444–452.
[51] Z. Wen, L. Wu, W. Li, Three-dimensional elastic-plastic stress analysis of wheel-rail rolling contact, Wear 271 (1–2) (2011) 426–436.
[52] J.B. Ayasse, H. Chollet, Determination of the wheel rail contact patch in semi-hertzian conditions, Vehicle Syst. Dyn. 43 (3) (2005) 161–172.

[53] X. Quost, M. Sebes, A. Eddhahak, J.B. Ayasse, H. Chollet, P.E. Gautier, et al., Assessment of a semi-Hertzian method for determination of wheel-rail contact patch, Vehicle Syst. Dyn. 44 (10) (2006) 789–814.
[54] M. Sebes, J.B. Ayasse, H. Chollet, P. Pouligny, B. Pirat, Application of a semi-Hertzian method to the simulation of vehicles in high-speed switches, Vehicle Syst. Dyn. 44 (Suppl.) (2006) 341–348.
[55] X. Jingmang, W. Ping, Optimisation design method for rigid frog based on wheel/rail profile type, China Railway Sci. 2 (2014) 1–6.
[56] W. Ping, Study on the dynamics of railway turnouts (Doctor Degree dissertation), Southwest Jiaotong University, Chengdu, 1998.
[57] W. Ping, A study on variation regularity of load on switch of turnout, J. Southwest Jiaotong Univ. 34 (5) (1999) 550–553.
[58] W. Ping, Analysis of mechanical characteristic of switch of turnout, J. China Railway Soc. 22 (1) (2000) 79–82.
[59] W. Ping, W. Fuguang, Study on the coupling vibration between train and swing-nose turnout and simulation analysis, China Railway Sci. 20 (3) (1999) 20–30.
[60] W. Ping, A spatial coupling model for railway turnouts and its application, J. Southwest Jiaotong Univ. 33 (3) (1998) 284–289.
[61] Z. Guo-tang, Method for determining the rigidity of railway track, China Railway Sci. 26 (1) (2005) 1–6.
[62] L. Li-bo, W. Wu-sheng, L. Weixing, Experimental study of static stiffness of ballast, J. Shanghai Railway Univ. 21 (4) (2000) 1–6.
[63] G. Quanmei, Z. Da-shi, Reasonable foundation stiffness range of high speed railway, J. Tongji Univ. (Natural Science) 32 (10) (2004) 390–1393.
[64] D. Guiping, L. Song-liang, L. Yang, Research on reasonable stiffness of the fast-speed railway track, J. East China Jiaotong Univ. 23 Suppl. (2006) 58–62.
[65] C. Xiaoping, W. Ping, Distribution regularity and homogenisation of track rigidity for ballastless turnout, J. Southwest Jiaotong Univ. 41 (4) (2006) 447–451.
[66] W. Ping, L. Xueyi, K. Zhonghou, A study on variation of the vertical rigidity of turnout along the longitudinal direction of track, J. Southwest Jiaotong Univ. 34 (2) (1999) 143–147.
[67] X. Jingmang, W. Ping, X. Dazhen, Study on reasonable fastener stiffness of ballastless turnout's vibration decrease and noise reduction of 350 km/h passenger dedicated line, Appl. Mech. Mater. 105–107 (2011).
[68] L. Xiaoyan, Effects of abrupt changes in track foundation stiffness on track vibration under moving loads, J. Vib. Eng. 19 (2) (2006) 195–199.
[69] H. Dan, X. Jun, Z. Qingyuan, Analysis of effect of track stiffness change on vibration response of high speed train and slab track system, J. Xi'an Univ. Arch. Tech., Natural Science ed. 38 (4) (2006) 559–563.
[70] Z. Wan-ming, C. Cheng-biao, W. Kai-yun, Effect of track stiffness on train Running Behaviour, J. China Railway Soc. 22 (6) (2000) 80–83.
[71] C. Xiaoping, Theories of track rigidity of railway turnouts and their application (Doctor Degree dissertation), Southwest Jiaotong University, Chengdu, 2008.
[72] L. Xiao-yan, Influences of track transition on track vibration due to the abrupt change of track rigidity, China Railway Sci. 27 (5) (2006) 42–45.
[73] C. Cheng-biao, Z. Wan-ming, W. Qi-chang, Research on dynamic performance of train and track at the junction of two different kinds of track structures, J. China Railway Soc. 24 (2) (2002) 79–82.
[74] W. Ping, L. Xueyi, Computing Theories and Design Methods of CWR Turnout, Southwest Jiaotong University Press, Chengdu, 2007.

[75] W. Ping, L. Xue-yi, Analysis of the influences of some parameters on the longitudinal force and rail displacement of CWR turnout, China Railway Sci. 24 (2) (2003) 58−65.
[76] W. Ping, Mechanism of longitudinal force transmission of welded turnouts with different structures, J. Southwest Jiaotong Univ. 38 (4) (2003) 372−374.
[77] W. Ping, H. Shi-shou, Study on the nonlinear theory of welded turnout with swing nose, China Railway Sci. 22 (1) (2001) 84−91.
[78] M. Zhan-guo, Analysis of Longitudinal Forces and Displacement of Rails in Turnouts, China Academy of Railway Sciences, Beijing, 1997.
[79] W. Shu-guo, L. Ji-sheng, Analysis on the temperature force and deformation of large-size continuously welded turnout with finite element method, China Railway Sci. 26 (3) (2005) 68−72.
[80] W. Ping, Study on influences of welded turnout group on displacements and longitudinal forces of rails, J. China Railway Soc. 24 (2) (2002) 74−78.
[81] W. Dan, W. Ping, Effects of stress-free temperature difference on force and displacement of welded turnouts, J. Southwest Jiaotong Univ. 41 (1) (2006) 80−84.
[82] W. Bin, C. Rong, W. Ping, Effects of longitudinal resistance changes of ballast bed on force and displacement of welded turnouts, Railway Eng. 5 (2010) 102−104.
[83] W. Ping, Y. Rong-shan, L. Xue-yi, Analysis on the influence of seamless turnout on large continuous beam bridge, J. Transp. Eng. Inf. 2 (3) (2004) 16−21.
[84] Y. Rong-Shan, Calculation theories and experimental study of longitudinal force of welded turnout on bridge (Doctor Degree dissertation), Southwest Jiaotong University, Chengdu, 2008.
[85] Y. Rong-shan, L. Xue-yi, W. Ping, Analysis of factors influencing longitudinal force of welded turnout on simply supported beam bridge, J. Southwest Jiaotong Univ. 43 (5) (2008) 666−672.
[86] X. Hao, X. Jingmang, D. Xiangyuan, W. Ping, Analysis of influences of the structure of ballastless track on bridge on ballastless turnout, China Railway 3 (2011) 62−64.
[87] X. Hao, W. Ping, Analysis of influence of the support position of simply supported beam bridge of ballast track on welded turnout, Railway Eng. 3 (2011) 90−92.
[88] X. Guihong, X. Hao, W. Ping, D. Feng, Study on regularity of longitudinal interactions between continuous beam bridge on ballastless track and turnout, Railway Eng. 5 (2011) 119−123.
[89] X. Jingmang, C. Rong, Calculating study on longitudinal force of welded turnout on bridge, Railway Eng. 3 (2011) 93−95.
[90] J. Guo, W. Ping, Influences of pier longitudinal stiffness on welded turnout on bridge, Railway Eng. 4 (2011) 27−29.
[91] C. Rong, Coupled vibrations theory of vehicle-turnout-bridge of high-speed railway and its application (Doctor Degree dissertation), Southwest Jiaotong University, Chengdu, 2009.
[92] K.H. Chu, V.K. Garg, A. Wiriyachai, Dynamic interaction of railway train and bridges, Vehicle Syst. Dyn. 9 (4) (1980) 207−236.
[93] M.H. Bhatti, Vertical and Lateral Dynamic Response' of Railway Bridges Due to Nonlinear Vehicle and Track Irregularities, Illinois Institute of Technology, Chicago, IL, 1982.
[94] M.F. Green, D. Cebon, Dynamic response of highway bridges to heavy vehicle loads: theory and experimental validation, J. Sound Vib. 170 (1) (1994) 51−78.
[95] Y.S. Cheng, F.T.K. Au, Y.K. Cheung, Vibration of railway bridges under a moving train by using bridge-track-vehicle element, Eng. Struct. 23 (12) (2001) 1597−1606.
[96] C. Andersson, T. Dahlberg, Wheel/rail impacts at a railway turnout crossing, Proc. Inst. Mech. Eng. Part F-J. Rail Rapid Transit 212 (2) (1998) 123−134.
[97] E. Kassa, C. Andersson, J.C.O. Nielsen, Simulation of dynamic interaction between train and railway turnout, Vehicle Syst. Dyn. 44 (3) (2006) 247−258.
[98] E. Kassa, J.C.O. Nielsen, Dynamic interaction between train and railway turnout: full-scale field test and validation of simulation models, Vehicle Syst. Dyn. 46 (S1) (2008) 521−534.

[99] E. Kassa, J.C.O. Nielsen, Stochastic analysis of dynamic interaction between train and railway turnout, Vehicle Syst. Dyn. 46 (5) (2008) 429–449.
[100] E. Kassa, J.C.O. Nielsen, Dynamic train-turnout interaction in an extended frequency range using a detailed model of track dynamics, J. Sound Vib. 320 (4–5) (2009) 893–914.
[101] G. Schupp, C. Weidemann, L. Mauer, Modelling the contact between wheel and rail within multibody system simulation, Vehicle Syst. Dyn. 41 (5) (2004) 349–364.
[102] C. Xiaoping, W. Ping, C. Rong, G. Likang, Spatial coupling vibration properties of high-speed vehicle-turnout, Sch. Civil Eng., Southwest Jiaotong Univ. 43 (4) (2008) 453–458.
[103] X. Jing-mang, W. Ping, C. Rong, X. Hao, Mechanical properties of high-speed turnout switching and locking device, J. Southwest Jiaotong Univ. 48 (4) (2013) 702–707.
[104] W. Ping, C. Rong, Control circuit analysis and conversion calculation of electric switch, Przegl. Elektrotech. (2012) 53–57 ISSN 0033-2097, R. 88 NR 1b.
[105] X. Jingmang, W. Ping, X. Hao, Improvement and lock calculation of electric switch machine of railway turnout, in: 2nd International Conference on Civil, Architectural and Hydraulic Engineering, 2013, pp. 409–410, 1496–1501.
[106] C. Xiaopei, A study on the switching and its controlling of the switch and nose rails in high-speed turnout (Doctor Degree dissertation), Southwest Jiaotong University, Chengdu, 2008.
[107] M. Xiao-chuan, W. Ping, Analysis on switching force influenced by different forms of rear end of switch rail of turnout No.6 on tramway track, Railway Stand. Des. 58 (7) (2014) 38–40.
[108] P.G.M. Fausto, A digital filter-based approach to the remote condition monitoring of railway turnouts, Reliab. Eng. Syst. Saf. 92 (2007) 830–840.
[109] I. Cedomir, Modeling the turnout switch for calculation the overturning force, Arch. Civ. Eng. 1 (5) (1998) 585–592.
[110] W. Ping, Computation and analysis of the switching force by multipoint traction, Railway Stand. Des. 2 (2002) 22–25.
[111] X. Jingmang, W. Ping, X. Kaize, S. Xiaoyong, Analysis on the dynamic characteristics of turnout switching equipment, J. Railway Sci. Eng. 11 (1) (2014) 29–35.
[112] M. Xiao-chuan, W. Ping, Z. Mengnan, X. Jingmang, Small number rail transformation based on the theory of the finite element analysis, Railway Eng. 3 (2014) 103–106.
[113] C. Xiaopei, L. Chenghui, W. Ping, Effect on the scant displacement of switch rail induced by friction of slide plate, China Railway Sci. 28 (1) (2007) 8–12.
[114] C. Xiao-pei, L. Cheng-hui, Study on controlling the switching force and scant displacement of the point rail of the high speed turnout, J. China Railway Soc. 30 (2) (2008).
[115] Z. Jianyue, Numerical analysis on dynamic behaviour of articulated turnout sleeper in turnout system under wheel load drop, J. Tongji Univ. (Natural Science) 39 (8) (2011) 1155–1160.
[116] X. Wei, L. Liangyu, C. Xiaoping, Composite casing strength analysis of concrete turnout sleeper in speed-raising turnout, Sichuan Constr. 2 (2008).
[117] R. Zun-song, S. Shou-guang, Z. Wan-ming, Analysis of acting force and vibrating characteristics of turnout sleeper in turnout system, J. China Railway Soc. 24 (1) (2002) 65–69.
[118] C. Xiaoping, W. Ping, Y. Yi-nong, The finite element analysis of scissors crossings' hinged concrete turnout sleeper, Railway Eng. 3 (2004) 52–54.
[119] W. Yingying, Analysis of steel turnout sleeper's vibration performance and study of parameter (Master Degree thesis), Southwest Jiaotong University, Chengdu, 2007.
[120] X. Juanjuan, L. Wei, The finite-element analysis of prestressed concrete short turnout sleeper's strength, Railway Eng. 7 (2008) 95–97.
[121] L. Yahang, D. Feng, J. Guo, W. Ping, Design and analysis of a new type of solid guardrail plate, Railway Stand. Des. 5 (2011) 11–13.

[122] L. Liangyu, H. Lihong, X. Wei, Design and research of high-speed rail guardrail plate, Sichuan Constr. 2 (2008).
[123] L. Xincheng, S. Jiang, Simulation on guardrail plate strength of No. 18 turnout of 60 kg/m rail in passenger dedicated line, Railway Eng. 3 (2012) 121–122.
[124] X. Xue-zhong, W. Ke-jian, Exploration on rail fastening for ballastless track of passenger dedicated line, J. Railway Eng. Soc. 2 (2006) 1–4.
[125] Z. Cai-you, W. Ping, Z. Ying, Z. Wei-hua, X. Jie-ling, Theoretical analysis and test for vibration damping fastenings, J. Vib. Shock 31 (23) (2012) 191–196.
[126] China Academy of Railway Sciences, etc. Dynamic Measurement Test Report on No. 18 Ballast Turnout for 250 km/h in Qingdao-Ji'nan Line, 2006.
[127] China Academy of Railway Science, etc. Dynamic Measurement Test Report on No. 18 Ballastless Turnout for 250 km/h in Suining-Chongqing Line, 2007.
[128] China Academy of Railway Science, etc. Dynamic Measurement Test Report on No. 18 Ballastless Turnout for 350 km/h in Comprehensive Test Section in Wuhan-Guangzhou Passenger Dedicated Line, 2009.
[129] W. Ping, C. Rong, Q. Shunxi, Development and application of wheel-set lateral displacement test system in high speed railway turnout zone, Przegl. Elektrotech. (2012) 69–73 ISSN 0033-2097, R. 88 NR 1b.
[130] Y. Wan, Research and design of continuous welded turnout model on bridge (Master Degree thesis), Southwest Jiaotong University, Chengdu, 2006.
[131] Z. Guodong, S. Yang, Z. Xinyang, Y. Rongshan, Experimental design of the model of CWR turnout on bridge in passenger dedicated line, Railway Eng. 1 (2011) 103–105.
[132] Z. Liping, L. Yonggang, Y. Rongshan, Test and simulation on the temperature force of the model of CWR turnout on bridge in passenger dedicated line, Railway Eng. 11 (2010) 135–138.
[133] Z. Xinyang, The model test on temperature force of CWR turnout on bridge (Master Degree thesis), Southwest Jiaotong University, Chengdu, 2010.
[134] Y. Rong-shan, L. Xue-yi, W. Ping, Research on longitudinal force computation theory and experiment of welded turnout on bridge, J. China Railway Soc. 32 (4) (2010) 134–140.
[135] China Academy of Railway Science, etc. Dynamic Measurement Test Report on No. 18 Ballastless Turnout for 350 km/h in Comprehensive Test Section in Zhengzhou-Xi'an Passenger Dedicated Line, 2006.
[136] China Academy of Railway Science, etc. Dynamic Measurement Test Report on Ballast CWR Turnout for 200 km/h on Bridge, 2006.
[137] High-speed Rail Joint Research. Development Report on No. 18 Ballastless Turnout for 250 km/h, 2007.
[138] High-speed Rail Joint Research. Development Report on No. 42 Ballastless Turnout for 350 km/h, 2008.
[139] J. Rongguo, Study on manufacturing technologies of switch rail of high-speed turnout (Master Degree thesis), Southwest Jiaotong University, Chengdu, 2012.
[140] J. Hong-liang, Residual stress tests at rail foot of turnout switch rail in passenger dedicated line, Heat Treat. Met. 36 (10) (2011) 113–115.
[141] J. Hong-liang, Heat treatment process of switch rail for PDL and equipment optimisation, Heat Treat. Met. 36 (10) (2011) 48–54.
[142] W. Shu-qing, Z. Xin-wei, Properties of U74, U71Mn, U75V and U76NbRE rails after slack quenching, Heat Treat. Met. 29 (3) (2004) 12–16.
[143] Z. Yueqing, The Material Performance and Related Technology of Rail, China Railway Publishing House, Beijing, 2005, pp. 83–91.

[144] J. Rongguo, Research on end surface hardness homogenisation in railway turnout of 60 AT rail, Heat Treat. 21 (2011) 36–38.
[145] G. Schleinzer, F.D. Fischer, Residual stress formation during the roller straightening of railway rails, Int. J. Mech. Sci. 43 (10) (2001) 2281–2295.
[146] Z. Wen, Study on theory and application of straightening switch rail of high speed turnout (Doctor Degree dissertation), Southwest Jiaotong University, Chengdu, 2008.
[147] B.E. Varney, T.N. Farris, Mechanics of roller straightening, in: Mechanical Working and Steel Processing Conference Proceedings, 1997, pp. 1111–1121.
[148] Z. Xuebin, Study on rail straightening process for passenger dedicated line, Sichuan Metall. 30 (2) (2008) 23–25.
[149] Z. Nai-hong, Analysis on the mechanical behaviour of the combined vertical-horizontal roller of rail straightener with ANSYS, Sci. Technol. Baotou Steel (Group) Corp. 34 (3) (2008) 15–17.
[150] Z. Chang-qing, Study on transport scheme of Number 42 turnout in PDL, Railway Transp. Econ. 6 (2012) 74–77.
[151] Y. Hong-wei, New laying technology for ballast turnout in high- speed railway, J. Railway Eng. Soc. 1 (2011) 25–30.
[152] Q. Lixiang, Construction management of laying of ballastless turnout in passenger dedicated line, Railway Eng. 8 (2010) 119–121.
[153] X. Shuzhi, Fuzhou-Xiamen railway passenger dedicated line No.42 ballasted turnout laying technology, Railway Eng. 12 (2010) 108–111.
[154] Z. Yong, Research on the control theory and method of construction process quality for ballastless turnout (Doctor Degree dissertation), Southwest Jiaotong University, Chengdu, 2012.
[155] X. Dongzhu, Research on the precise adjustment techniques for double-block ballastless track, J. Railway Sci. Eng. 4 (2009) 51–54.
[156] L. Shihai, G. Jiangang, W. Bo, Static and dynamic adjustment technology for CRTS I double-block ballastless track, Railway Stand. Des. 1 (2010) 80–84.
[157] W. Lin, Study on precision adjustment technology for CRTS I double-block ballastless track, Railway Stand. Des. 1 (2010) 74–79.
[158] W. Weijun, Research on key technology of 3D measurement of track (Master Degree thesis), Nanchang University, 2009.
[159] A. Guodong, Study on technical standard for precise engineering surveying of high-speed railway and its applications, J. China Railway Soc. 32 (2) (2010) 98–104.
[160] B. Ripke, K. Knothe, Simulation of high frequency vehicle-track interactions, Vehicle Syst. Dyn. 24 (Suppl. 1) (1995) 72–85.
[161] J. Oscarsson, T. Dahlberg, Dynamic train/track/ballast interaction computer models and full-scale experiments, Vehicle Syst. Dyn. 28 (Suppl. 1) (1998) 73–84.
[162] Q. Shunxi, W. Pin, W. Zeng, Research and application of fine adjustment system for ballastless track turnouts in passenger dedicated line, Railway Stand. Des. 2 (2010) 36–38.
[163] Q. Shunxi, Study on dynamic analysis and control methods of the geometric irregularity in high-speed turnout (Doctor Degree dissertation), Southwest Jiaotong University, Chengdu, 2012.
[164] L. Lin, Z. Geming, W. Qingwang, C. Xuesong, Control of Track Irregularity of the Wheel-Rail System, Chinese Railway Publishing House, Beijing, 2006.
[165] Shanghai Railway Administration, etc., Jerking of 2# Turnout in Huangdu Station in Beijing-Shanghai High-speed Railway and Preliminary Improvement, 2010.
[166] X. Rui, S. Cheng, Fast pseudo-excitation method in structural non-stationary stochastic response analysis, Chin. J. Comput. Mech. 5 (2010) 822–827.
[167] J.H. Lin, Y.H. Zhang, Chapter 30: "Seismic random vibration of long-span structure" Vibration and Shock Handbook, CRC Press, Boca Raton, USA, 2005.

[168] F. Lu, Q. Gao, J.H. Lin, F.W. Williams, Non-stationary random ground vibration due to loads moving along a railway track, J. Sound Vib. 298 (1−2) (2006) 30−42.
[169] Shanghai Railway Administration, etc., Report on the Investigation and Improvement of Main line Turnout Defects in Hangzhou-Ningbo Passenger Dedicated Line, 2006.
[170] Z. Jiangtao, Theoretical research of three-dimensional plastic flow in rail universal rolling process (Master dissertation), Yanshan University, Qinhuangdao, 2013.
[171] L. Xiubo, W. Weixin, PSD analysis of shortwave irregularity on welded joints, China Acad. Railway Sci. 2 (2002) 26−34.
[172] H.L. Hasslinger, P. Mittermayr, G. Presle, Dynamic behaviours of various track constructions due to traveling loads, Eisenbahningenieur 5 (1994) 42−47.
[173] Z. Jian, W. Changhua, X. Xinbiao, W. Zefeng, J. Xuesong, Effect of unsupported sleepers on sleeper dynamic response, J. Southwest Jiaotong Univ. 2 (2010) 203−208.
[174] A. Lundqvist, Dynamic train/track interaction hanging sleeper, Track Stiffness Variations and Track Settlement, 2005.
[175] J.C.O. Nielsen, A. Igeland, Vertical dynamic interaction between train and track—influence of wheel and track imperfections, J. Sound Vib. (1995).
[176] Ministry of Railways of the People's Republic of China, Specification for Repair of Railway Line, Chinese Railway Publishing House, Beijing, 2004.
[177] F. Lu, D. Kennedy, F.W. Willams, J.H. Lin, Simplistic analysis of vertical random vibration for coupled vehicle-track systems, J. Sound Vib. 317 (2008) 236−249.
[178] C.F. Zhao, W.M. Zhai, Maglev vehicle/guideway vertical random response and ride quality, Vehicle Syst. Dyn. 38 (3) (2002) 185−210.
[179] Z. Caiyou, W. Ping, Q. Shunxi, C. Yang, H. Guoxiang, Detection method for broken rail based on rate of change of strain mode, J. Vib. Meas. Diagn. 32 (5) (2012) 723−729.
[180] Y. Satoh, K. Iwafuchi, Effect of rail grinding on rolling contact fatigue in railway rail used in conventional line in Japan, Wear 9 (2008).
[181] E. Eric, J.K. Magel, The application of contact mechanics to rail profile design and rail grinding, Wear 1 (2002).
[182] A.P. Patra, Maintenance decision support models for railway infrastructure using RAMS & LCC analyses (Doctoral thesis), Luleå University of Technology.
[183] A. Nissen, LCC-Analysis for Switches and Crossings—A Case Study from the Swedish Railway Network, Luleå University of Technology.

Index

Note: Page numbers followed by "*f*" and "*t*" refer to figures and tables, respectively.

C

D

E

F

G

H

I

J

K

L

M

N

O

P

Q

R

S

T

U

V

W

Z